EFCH2 2026

European Fuel Cells and Hydrogen

PIERO LUNGHI CONFERENCE

Book of Proceedings



September **15**th–**17**th 2026
Capri / Italy

ATENA FUTURE TECHNOLOGY

ENEA ITALIAN NATIONAL AGENCY FOR NEW TECHNOLOGIES, ENERGY AND SUSTAINABLE ECONOMIC DEVELOPMENT

Università degli Studi di Napoli Parthenope

CLEAN ENERGY INSTITUTE UNIVERSITY OF CALIFORNIA, IRVINE

EFCH2 2026

European Fuel Cells and Hydrogen

PIERO LUNGHI CONFERENCE

Proceedings

OF THE 12TH EUROPEAN FUEL CELL PIERO LUNGHI CONFERENCE

To Piero Lunghi. We miss you a lot. To you our gratitude for ever.

This book is dedicated to the memory of Piero Lunghi,
creator of the European Fuel Cell Technology and Applications Conference, dear friend and colleague, who prematurely passed away in a car accident on damned November 9, 2007.

Piero made significant contributions in the field of fuel cells in the course of his too short career. He was the leading figure in the formation of the fuel cell research group at the University of Perugia and several activities and research projects initiated by him are still ongoing.
This means that, thanks to Piero, many young people are working in this exciting research field and are coming to Naples to present their results. Therefore, Piero's memory is in the conference name but Piero's contribution is still in the contents of this book.
The memory of our friend Piero, his great personal generosity and energy, survives in our hearts, his contribution and his tenacity survive in the work of young people who carry on his vision throughout the world.

Give them your passion, your strength, and make all necessary effort to realize them. There is no greater satisfaction than seeing one's ideas become reality and become part of the future of our world.
Piero strongly desired this, and constantly followed this through with conviction, passion and dedication.

For a better future, we need young researchers of this kind.

European Fuel Cells and Hydrogen

EFCH2 2026

PIERO LUNGHI CONFERENCE

Capri, Gran Hotel Quisisana
15 > 17 September, 2026

edited by
Viviana Cigolotti, Alessia Piccolo, Gabriele Loreti
2026

ENEA
ITALIAN NATIONAL AGENCY FOR NEW TECHNOLOGIES, ENERGY AND SUSTAINABLE ECONOMIC DEVELOPMENT

Lungotevere Thaon di Revel, 76 / 00196 / Rome

ATENA FUTURE TECHNOLOGY

ENEA ITALIAN NATIONAL AGENCY FOR NEW TECHNOLOGIES, ENERGY AND SUSTAINABLE ECONOMIC DEVELOPMENT

Università degli Studi di Napoli Parthenope

CLEAN ENERGY INSTITUTE UNIVERSITY OF CALIFORNIA, IRVINE

European Fuel Cells and Hydrogen

PIERO LUNGHI CONFERENCE

Organizers



Viviana
CIGOLOTTI
Chairman of the Conference
ENEA



Jack
BROUWER
Chairman of the Conference
University of California Irvine



Elio
JANNELLI
University of Naples
"Parthenope" / ATENA



Adele
PIANESE
ENEA/ATENA



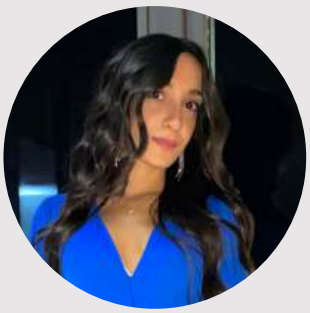
Massimiliano
DELLA PIETRA
ENEA



Silvia
LO CONTE
University of Naples
"Parthenope"



Gabriele
LORETI
ENEA



Alessia
PICCOLO
University of Naples
"Parthenope" / ATENA

EFCH2 2026

European Fuel Cells and Hydrogen

PIERO LUNGHI CONFERENCE

Committee

Australia Rob Dickinson Adelaide University

Austria Günter R. Simader Austrian Energy Agency

Belgium Alessandro Arrigoni JRC

Canada Bruno Pollet Université du Québec à Trois-Rivières

Chile Ana María Ruz Frias Chilean Economic Development Agency (CORFO)

Finland Jari Kiviaho VTT Technical Research Center of Finland

France Paul Lucchese CEA -IEA / Julie Mougin, CEA

Germany Can Remzi Samsun, Forschungszentrum Jülich (FZJ) / Claudio Pistidda, Helmholtz-Zen trum Geesthacht / Mihails Kusnezoff, Fraunhofer-Institut für Keramische Technologien undSysteme IKTS / Nada Zamel, Fraunhofer

Greece Panagiotis Tsiakaras, University of Thessaly / Athanasios Stubos, NCSR Demokritos

Italy Mariagiovanna Minutillo, Università degli Studi di Salerno / Massimo Santarelli. Politecnico di Torino / Antonino Aricò, CNR ITAE / Stefano Campanari, Politecnico di Milano / Giuseppe Spazzafu-mo, EnTraT srls / Giulia Monteleone, ENEA / Adolfo Iulianelli, CNR ITM / Stefano Ubertini, Università della Tuscia / Oreste Tarallo, Università degli Studi di Napoli Federico II / Giuseppina Roviello, Univer-sità degli Sudi di Napoli Parthenope / Domenico Borello, Sapienza Università di Roma

Poland Jakub Kupecki, Institute of Power Engineering – IPE

Portugal Carmen Rangel, LNEG - National Laboratory of Energy and Geology

Spain Emilio Nieto Gallego, Centro Nacional del Hidrógeno (CNH2)

Sweden Martin Andersson, Lund University

Turkey Cigdem Karadag, TUBITAK Marmara Research Center

United Kingdom Ioannis Ieropoulos University of Soton/ Shangfeng Du University of Birmingham

United States of America Yun Wang. University of California Irvine / Feng-Yuan Zhang, University of Tennesse, Knoxville/ Xiao-Dong Zhou, University of Connecticut / Luca Mastropasqua, University of Wisconsin - Madison /

European Fuel Cells and Hydrogen

PIERO LUNGHI CONFERENCE

Capri, Gran Hotel Quisisana
15 > 17 September, 2026

TOPICS

HYDROGEN PRODUCTION
Electrolysis (PEM, Alkaline, AEM, SOEC, PCC, MCEC) | Thermochemical & Photochemical Processes | Biological Hydrogen Production | Low carbon hydrogen (e.g., SMR with CCUS, Nuclear Hydrogen, etc.) | Hydrogen from Biomass and Waste | Water Use and Low Quality Water Electrolysis (e.g. Sea-Water)

HYDROGEN STORAGE AND DISTRIBUTION
Solid Hydrogen Storage (e.g. metal hydrides, MOFs and others) | Gaseous Hydrogen Storage | Liquid and Cryo-Compressed Hydrogen Storage | Hydrogen Infrastructure (Pipelines, Tankers, Trucks) | Hydrogen Blending in Natural Gas Grids | Natural Gas Grid Transformation | Hydrogen Derivatives and Carriers (e.g., ammonia, LOHC, methanol) | Hydrogen Refilling Stations

FUEL CELLS TECHNOLOGIES
Fuel Cells: components, stack, system (PEMFC, SOFC, AFC, MCFC) | Fuel Cells for Transportation (Cars, Buses, Trucks) | Fuel Cells for Heavy Duty & Freight Transport (Trains, Aircraft, Marine) | Fuel Cells for Stationary Power Generation | Portable and Backup Power Applications

HYDROGEN END-USE APPLICATIONS
Hydrogen for Industrial Processes (Steel, Cement, Chemicals) | Hydrogen as Energy Storage Medium (e.g. Hybrid Systems with Renewable Energy) | Sector Coupling and Power-to-X | Next-Generation Hydrogen Fuels (Power-to-fuel) | Hydrogen as a Decarbonization Pathway

HYDROGEN ECONOMY AND SUSTAINABILITY
Life Cycle Assessment (LCA) and Social LCA | Techno-economic assessment (TEA) | Green Hydrogen and Carbon-Free Technologies | Hydrogen's Role in Achieving Climate Targets (Net-Zero Goals) | Hydrogen Hubs and International Trade | Hydrogen Valleys

HYDROGEN POLICY, MARKET, AND BUSINESS MODELS
National and Regional Hydrogen Strategies | Global Hydrogen Supply Chains | Economic Analysis and Market Forecasts | Hydrogen Pricing and Incentives | Hydrogen Safety Codes and Standards

HYDROGEN INNOVATION AND FUTURE TRENDS
Emerging Hydrogen Technologies | Breakthroughs in Catalysts, Electrodes, Membranes | Innovative Diagnostic, Prognostic, and Artificial Intelligence Tools in Hydrogen Systems | Microbial and Bioelectrochemical Technologies

European Fuel Cells and Hydrogen

EFCH2 2026

PIERO LUNGHI CONFERENCE

SPONSORED BY

CalPower www.calpower.it

Duferco Engineering

ErreDue ON-SITE GAS SOLUTIONS

GERG THE EUROPEAN GAS RESEARCH GROUP

pure ENERGY® HYDROGEN

SIAD

SUPPORTED BY

Clean Hydrogen Partnership

Hydrogen Europe Research

H2IT ASSOCIAZIONE ITALIANA IDROGENO

UNDER THE PATRONAGE OF

Ministero dell'Ambiente e della Sicurezza Energetica

MUR Ministero dell'Università e della Ricerca

Città Metropolitana di Napoli

ORGANIZED BY

ATENA FUTURE TECHNOLOGY

ENEA ITALIAN NATIONAL AGENCY FOR NEW TECHNOLOGIES, ENERGY AND SUSTAINABLE ECONOMIC DEVELOPMENT

Università degli Studi di Napoli Parthenope

THE UNIVERSITY OF CALIFORNIA 1868

CLEAN ENERGY INSTITUTE UNIVERSITY OF CALIFORNIA, IRVINE

EFCH2 2026

European Fuel Cells and Hydrogen

PIERO LUNGHI CONFERENCE

Contents

ATENA FUTURE TECHNOLOGY

ENEA ITALIAN NATIONAL AGENCY FOR NEW TECHNOLOGIES, ENERGY AND SUSTAINABLE ECONOMIC DEVELOPMENT

Università degli Studi di Napoli Parthenope

CLEAN ENERGY INSTITUTE UNIVERSITY OF CALIFORNIA, IRVINE



Table of Contents

TOPIC 1. HYDROGEN PRODUCTION 12

Low equivalent weight aquivion® ionomers behaviour in enhanced proton exchange membrane water electrolysis 13

Hydrogen production from recycled aluminum foils and waste: reactivity and kinetic analysis 16

Electrochemists going with the flow: CFD-guided optimization of flow-engineered 3D electrodes and cells for alkaline water electrolysis 19

Seawater electrolysis with integrated brine valorisation: a contribution to the water-energy nexus 22

Characterisation of electrode bubble coverage by electrochemical impedance spectroscopy in an alkaline water electrolysis flow-cell 25

Water Pathways and Impurity Diagnostics in PEM Water Electrolysis 28

Electrochemical characterization of Molten Carbonate Electrolysis Cells: a focus on fuel electrode kinetics and degradation 31

Real-Time Electrolysis Stack Temperature Prediction Using Neural Networks for Industrial PLC Deployment 34

Multi-Mode Electrochemical Transient Characterisation of SOC Short Stacks under Fuel-Flexible/Biogas Operating Conditions 37

Biomass-assisted electrolysis using lignocellulosic feedstock to produce hydrogen 40

EIS-Based Diagnostic Algorithm for State-of-Health Assessment and Degradation Monitoring of SOEC systems 43

Galvanic Pulse-Plating of iridium-ruthenium-alloys as catalyst for PEM water electrolysis 46

Design and Validation of Machine Learning-based Prognostic Algorithm for SOEC durability prediction 49

Development of Performance Factor Analysis Method for Steam Electrolysis by SOEC 52

Techno-Environmental Assessment of Industrial-Scale AEM Electrolysis: The Ansaldo Green Tech case 55

Development of an intensified gasification process for H2-rich syngas production 58

Thermo-Assisted Non-Thermal Plasma Methane Cracking: Prototype Development and First Experimental Insights for CO_2-Free Hydrogen Production 61



Physical Vapor Deposition of thin layers for proton-conducting solid oxide electrolysis cells 64

Performance-degradation oriented multiphysics 0D/3D numerical framework for PEMWE's digital twin applications 67

Efficient urea-assisted water electrolysis at 1.5 a/cm2 for 1100 hours over in-situ produced niooh species 70

Transient Rise of Polarisation-like Resistance During Activation of PEM Water Electrolysers 73

Towards a Standardized Testing Framework for AEM Water Electrolyzers 76

Investigation of the Challenges in Dynamic Operation of Pressurized Alkaline Water Electrolysers 79

Enhancing the Mechanical Durability of Anion Exchange Membranes via Electrospun PVDF Fibers Reinforcement for Water Electrolysis 82

Enhancing alkaline water electrolysys with co-mo layered double hydroxides 85

Integrated Thermochemical Cycles for Carbon-Negative Hydrogen Production 88

Conditional Physics-Informed Neural Network Modelling of PEM Electrolyzer Voltage Dynamics 91

From biowaste to renewable hydrogen: pilot-plant validation and scale-up challenges 94

Toward Sustainable Bio-Inspired Anisotropic Ion Exchange Membranes by Self-Assembly of Bio-Based Solid Polymer Electrolytes 97

Physics-Based One-Dimensional Modelling of a PEM Water Electrolyzer to Quantify Performance Trade-offs of PFAS-Free Membranes 100

Pressurized alkaline electrolyser: technical challenges towards a high-pressure design 103

InnAEM: Innovative Materials for Anion Exchange Membrane Water Electrolysis 106

Surface treatment of stainless steel porous transport layer for oxygen evolution reaction enhancement in an anion exchange membrane electrolyser 109

Towards high-pressure AEM electrolyzer single-cell design through coupled electro–thermo–mechanical modeling 112

Electrochemical analysis of long-term performance of Molten Carbonate Electrolysis Cells under simulated seawater feed 115

Role of reverse Water-Gas Shift Reaction for CO_2 Utilization in Molten Carbonate Electrolysis Cells 118

Optimizing Contact Pressure in PEM Water Electrolyzers for the highest durability: Linking Impedance analysis and DRT to Performance 120

Development of a Flexible Test Bench for Advanced Characterization and Diagnostics of PEM and AEM Electrolyser Stacks 123

Moving Beyond the Limitations of Conventional Alkaline Water Electrolysers for Efficient and Flexible Hydrogen Production 126

A Practical PI Controller Design Approach for DC-DC Power Electronic Converters for Electrolyzer Applications 129

Integration of Proton Conducting Ceramic Electrolysis for hydrogen production in targeted industrial applications 132

Multiphysics Modeling and Optimization of a Membrane-less Supercritical Alkaline Electrolyzer 135

A Scale-Up Platform for Renewable Hydrogen Production Technologies Based on Waste-Derived Biogas and Biomethane 138

Membrane-less Supercritical Water Electrolysis for High-Pressure Hydrogen Production: First Technical Results from the X-SEED Project 141

Scaling PEM Electrolysis: from Materials Innovation to Industrial Manufacturing 144

TOPIC 2. HYDROGEN STORAGE AND DISTRIBUTION 147

Numerical Insights into Transient Hydrogen Tracking in Gas Distribution Networks 148

Dynamic modelling and performance mapping of an integrated hydrogen valley ecosystem: the HySPARK case 151

CFD Assessment of Absorption-Rate-Based Charging Interruption for Thermal Protection and Recovery of an AB_2 Metal Hydride Tank 154

Experimental Investigation of a Lab-Scale Metal Hydride – Phase Change Material Hydrogen Storage System 157

Experimental System for Hydrogen Permeability Testing at High-Pressure 160

Analysis of SOEC-based systems for the production and import of e-NG 163

Geopolymers modification and its hybrid materials for hydrogen storage 166

Kinetic-based and FVM numerical tools for the simulation of Metal Hydride storage tanks coupled with Phase Change Materials 169

H2BIDEA: Experimental and Numerical Evaluation of Structural Integrity and Material Compatibility for 100% Hydrogen Distribution Networks 172

Techno-economic assessment of on-site hydrogen refueling stations based on renewable electricity, biogas, and ammonia pathways 175

Development of Pt-based bimetallic catalyst promoted with Fe, Mn and Co for hydrogen storage and release in LOHC systems 178

C-based materials for solid state hydrogen storage: a new perspective 181

MetroHyVe3: Traceable Metrology for Reliable, Safe and Scalable Hydrogen Refuelling Infrastructure 184

Metrology for Hydrogen and Hydrogen-Natural Gas Mixtures in Gas Networks: Validated Testing Methodologies from the THOTH2 Project 187

Effect of Thermally Grown Oxides on Hydrogen Permeation 190

Evaluation of internal bed temperature in a metal hydride cartridge during hydrogen charging using an experimentally based lumped-parametr model 193

Analysis of the pressure time profile in a liquid hydrogen tank used for ship propulsion ... 196

Predictive operation of a hydrogen refuelling station with scheduled clients 199

Techno-economic optimization of an on-site solar-powered hydrogen refueling station .. 202

Metrology to Support Ammonia Use in Emerging Energy Applications (MetNH3Energy): Validation of the Ammonia Calibration Method 205

Advance H_2 Safety: Material Integrity to Network Resilience drawing on EU Projects (CANDHy, PilgrHYm and SHIMMER) 208

Low-Temperature H_2 Release from Ammonia: Bridging the Ni–Ru Gap in an Electrified Structured Membrane Reactor 210

TOPIC 3. FUEL CELLS TECHNOLOGIES 212

Pinhole growth in PFSA and hydrocarbon membranes under relative humidity cycling 213

Hydrogen Compressor Modeling Using Physics-Informed Surrogates 216

Polydopamine-assisted functionalisation of bacterial cellulose with lignosulfonate as a bio-based ion exchange membrane in fuel cells 219

Test campaign for the proof of funtionality of a pem fuel cell system for regional aircraft applications 222

Concept of a solid oxide electrolysis-molten carbonate fuel cell hybrid system to support a power-to-gas installation 225

Accelerating Solid Oxide Fuel Cell – Gas Turbine Simulations: A Surrogate Modeling Approach 228

Combined thermal management and heat recovery for pemfc-battery hybrid propulsion systems 231

In-situ contact pressure monitoring of PEMFC stack: A new approach 234

Performance and mass transfer evaluation of a single HT-PEM fuel cell with straight and wavy serpentine flow channels using CFD simulation 237

CFD-Based Parametric Optimization of Sinusoidal Flow Fields for High-Temperature PEM Fuel Cells 240

Microstructure–Property Relationships in Digitally Deposited and In-Line Compacted NiO–3YSZ Anode Supports for Solid Oxide Cells 243

Influence of Methanol Reformer Aging on HT-PEMFC Performance under Dynamic Conditions 246

Direct Biomass Fuel Cells for Small-Scale Biomass Utilization 249

Mechanical Testing Investigation of Aqueous Capillary r-GO based Inks for 3D-Printed Electrodes 252

Influence of nominal contact pressure on activation behavior and spatial current redistribution in a pre-doped HT-PEMFC 255

Iron-Induced Degradation and Cation Migration in PFSA Membranes: Spatially Resolved Insights from Segmented Cell Analysis 258

An investigation on the performance of pretreated sPEEK based CCB and CCM MEA for PEMFC operation 261

Integrated On-Board Hydrogen Production and Fuel Cell Systems for Railway Applications: Design and Risk Assessment 264

Digital Twin-Oriented Modeling and Validation of a Fuel Cell Hybrid Electric Propulsion System for Hydrogen-Based Aviation 267

Effect of Air Contact Layer Thickness on Oxygen Transport and Current Density Distribution in Solid Oxide Cells 270

Dynamic Simulation and Optimization of a PEMFC-Battery Fast Ferry on a Real Italian Route 273

Comparing the efficiency of a hybrid ice vehicle fuelled with hydrogen with a fuel cell vehicle, based on a simulation model 276

Performance evaluation of a hybrid energy system of biomass based on solid oxide fuel cell 279



Development and testing of a lightweight two-phase pumped cooling system for aviation fuel cells 282

Electrospun PBI Membranes for HT-PEM Fuel Cells: Phosphoric Acid Uptake, Interaction Mechanisms and Preliminary Single-Cell Assessment 285

Semicrystalline Syndiotactic Polystyrene Membranes for Electrochemical Applications . 288

A Multi-rSOC System for Flexible Energy Management in Data Center Applications: Modeling and Configuration Analysis 291

Impact of Roll-to-Roll Production Technologies on the Cost of PEM Fuel Cell Membrane Electrode Assemblies 294

Electrochemical and morphological analysis of Pt catalyst degradation under maritime-inspired AST for PEMFCs 297

Application of mcfc technology for the decarbonization of italian district heating networks: a case study 300

Interface Engineering in sPPO-Based Hydrocarbon Catalyst-Coated Membranes for PEM Fuel Cells 303

Safe, Fast and Efficient Hydrogen Refuelling for Heavy-Duty Vehicles via a Multiphysics and Data-Driven Approach 306

Nanostructured Pt Catalyst Layers for Low-Loading PEMFCs by Pulsed Laser Deposition and Inverse MAPLE 309

Deep learning model of PEMFC stack degradation under CO contamination 312

Advanced Electrochemical Characterization Methods of Solid Oxide Fuel Cells 315

Impact of High-Energy Neutron Radiation on PEM Fuel Cells in Aviation 318

Ejector Scaling for Marine PEMFC: CFD Modelling and Semi-Empirical Bias Correction from 5 to 200 kW 321

Europy: a modular pemfc multiphysics framework in python/jax/petsc 324

Degradation modelling of the PEMFC system for heavy-duty long-haul applications using semi-empirical modelling approach 327

Computational Model-based Performance Assessment of PFAS-Free Membrane-Electrode Assemblies in PEM Fuel Cells 330

Dimethyl sulphide as a biogas contaminant in SOFCs: experimental characterisation and degradation modelling 333

Advanced In-situ Oxygen Transport Diagnostics for Large Format PEM Fuel Cells 336

1D - 3D heat transfer model for air cooling of hydrogen proton exchange membrane fuel cell 339

Efficient pseudo 2D PEM fuel cell model for integration in multi-stack system 342

Large-scale 3D HTPEM stack simulations: single-cell thermal extrapolation vs. full electrochemistry modelling 345

Fault-Tolerant Operation of a Stacked Interleaved DC-DC Buck Converter for PEM Electrolyzers 348

Fuel-Flexible SOFC-CHP for a Just Hydrogen Transition 351

Thermally Integrated Hydrogen and Electricity Co-generation in a Direct Ammonia-Fueled Solid Oxide Fuel Cell System 354

Estimating Hydrogen, Methanol, and Ammonia Demand for the Deployment of Green Corridors in the Maritime Sector. 357

From natural gas to hydrogen: experimental performance characterization of a solid oxide fuel cell system installed in an airport environment 360

Innovative Manufacturing Processes for Low-Cost, High-Performance SOCs: From Laboratory Results to Industrial Deployment 363

Hot Gas Conditioning and SOFC Systems Coupled to a Steam/Oxygen Fluidized Bed Gasifier Plant 366

STAND UP: Fuel cell–battery power units for heavy-duty applications 369

TOPIC 4. HYDROGEN END-USE APPLICATIONS 372

Electrolyzer Model Detail in Energy System Optimization: Implications for Dispatch and Waste Heat Availability 373

Hierarchical predictive control for coordinated operation of smart prosumers in an energy community 376

Enhancing e-Biomethanol Synthesis from Biomass-Derived Syngas via a LTA-Zeolite Catalytic Membrane System 379

Predictive Energy Management for Hydrogen Fuel Cell Hybrid Trains 382

Integrated Autonomous Hydrogen Energy Systems for Resilience and Humanitarian Crisis Response: A Techno-Economic Assessment 385

Nutrient management in biological methanation reactors: experimental optimization of nutrient formulations and CSTR-TBR comparison 388

Fuel properties and composition of green diesel produced via catalytic deoxygenation of rapeseed oil 391

Novel hydrogen-based technologies for green iron and steel making 394

Integration of green hydrogen production for transport decarbonization into the italian electricity grid: a numerical analysis 397

Hydrogen Energy Storage for Long-Duration Energy Shifting in a Remote Off-Grid Microgrid 400

Green hydrogen-driven *in-situ* biomethanation for methane-enriched biogas production in hybrid PtG configurations 403

Advanced biorefinery platform for renewable h2-based fuels production 406

Mapping Hydrogen Supply Opportunities for Aluminium Decarbonization: Development of a GIS-Based Decision Support Tool 409

Green Methanol Production via SOEC Co-Electrolysis Coupled with Solar Energy: Process Design and Analysis 412

Hydrogen as a Cross-Sector Vector in Advanced Multi-Energy Networks: Use-Case Framework and NZMES Results for Tertiary Buildings 415

Hydrogen Demand Projections and Renewable Power System Sizing for Hard-to-Abate Sectors in the Italian Energy Transition. 418

Preliminary Assessment of a Hydrogen-Powered Pushback Tractor for Ground Handling Decarbonization at Milan Malpensa Airport 421

H2SCORE: An Integrated Hydrogen-Based Architecture for Complex Local Multi-Energy Microgrids 424

Real-Time Optimization of a Hydrogen Based Multi Energy System Using Machine Learning 427

Hydrogen in pathways towards a climate-neutral, circular and competitive European process industry: the AMIGDALA scenario framework 430

TOPIC 5. HYDROGEN ECONOMY AND SUSTAINABILITY 433

Fe-phthalocyanine-derived Fe-N-C electrocatalysts for the Nitrate Reduction Reaction (NO_3RR) 434

HyMantovalley – A Case Study from Italy 437

Environmental performance assessment of catalysts for water electrolysis in the context of the X-SEED project 440

The Best Uses of Green Electrolytic Hydrogen 443

Closing the Hydrogen Emissions Knowledge Gap: the NHyRA Approach 446



A methodological framework for mapping hydrogen value chains: the case of friuli venezia giulia and the north adriatic hydrogen valley 449

The role of hydrogen in Italy's energy transition: effects of carbon budget and of the introduction of nuclear power plants 452

H-PORT: An Integrated Simulation, Safety and Techno-Economic Framework for Hydrogen-Powered Smart Ports 455

Decarbonization of a hard-to-abate process in steel making: effects of measured hydrogen plant performances on the techno-economic feasibility study 458

Optimal green hydrogen generation design for the decarbonization of the steel industry: an Italian case study 461

Mechanical Recovery of Platinum-Based Cathode Catalysts: A Circular Economy Approach for Sustainable and Cost-Effective PEM Technologies 464

Techno-economic modelling of a hydrogen valley in Italy: a multi-scenario analysis of the Levelised Cost of Hydrogen 467

Social Life Cycle Assessment of green hydrogen technologies: a systematic review and commentary from a social science perspective 470

From Scrap to Storage: Life Cycle and Circularity Assessment of $TiFe_{0.80}X_{0.20}$ Alloys for Hydrogen Storage 473

Lessons learned from the PEFCR development process: the case of the Fuel Cells and Hydrogen PEFCR for hydrogen storage devices 476

Qualitative Risk Assessment of Hydrogen Transport and Hydrogen-Fuelled Mobility in Road Tunnel 479

Impacts of the Hydrogen Economy on Global Hydrogen and Air Pollutant Emissions: A Scenario Analysis Using the GAINS Model 482

Advancing Social Life Cycle Assessment for Hydrogen Energy Pathways in Italy's 2050 Transition 485

Advancing the assessment of climate and environmental impacts of a future Hydrogen Economy with the HYDRA project 488

Multi-criteria assessment of green hydrogen value chains for Europe's sustainable transition 491

HySPARK: A Cross-Regional Hydrogen Valley for Airport and Urban Mobility Decarbonization 494



TOPIC 6. HYDROGEN POLICY, MARKET AND BUSINESS MODELS 497

Price-driven optimal grid-connected hydrogen production 498

Standardization Safety and Analytical Protocols for Biomass Hydrogen: the project START-H2 501

CRM content in PEM water electrolysers: a review of catalyst loading, material intensity and temporal trends 504

Applying Hydrogen Safety Lessons to the 2026 Colton Accident 507

Linking hydrogen demand for freight transport and power system decarbonization through spatially resolved energy system modelling 510

Energy system modelling for hydrogen integration in the italian power grid: benchmarking and 2050 scenario analysis 513

Flow measurement traceability for hydrogen in gas networks: an insight into H2FlowTrace project 516

Importing Decarbonisation: The Geopolitics of Italy's Hydrogen Hub Strategy in the Mediterranean 519

Traceable Humidity Measurements Supporting Hydrogen Quality Assurance and Safety Across the Hydrogen Supply Chain 522

Biogas-Fueled Renewable Peak Power and Renewable Hydrogen and Fuel Generation Using Reversible Solid Oxide Electrolysis Cells – potentials on local and national level in Finland 525

The French National Research Program on Low Carbon Hydrogen: Projects and Achievements 528

TOPIC 7. HYDROGEN INNOVATION AND FUTURE TRENDS 530

Research and Innovation Across the Hydrogen Value Chain: current status, main challenges and Future Perspectives 531

Operando SAXS and XAS analyses for PEM fuel cells and water electrolyzers: time-resolved insights about catalyst degradation at a single cell level 534

A Fault Injection Framework for Hydrogen Fuel Cell-Battery Hybrid Trains to Enable Condition-Based Maintenance 537

Redox properties of Azo Dyes determined via quantum chemical methods 540

Anodic biofilm formation under short-circuited conditions of SMFC 543

Feasibility Assessment of Long Short-Term Memory Neural Networks for Electrolyzer Operation Prediction under Start-Stop Conditions 546

Data-Driven Degradation Forecasting for AEM Water Electrolysis 549

From Photovoltaics to Integrated PEC Systems: Hybrid Perovskite Photoanodes with Operando H_2 Analysis 552

H2-SimNet: A Simulation-Based Framework for Data-Driven Monitoring of Hydrogen Networks 555

Electrochemical characterisation of Electrospun Nitrogen-Doped PVDF Hybrid Nanofibers for Bifunctional Metal-Free Electrocatalysts 558

Design and Validation of a Modular Microbial Fuel Cell Stack for Urine Valorization and Energy Harvesting 561

Development of a BioH_2-Biorefinery Through the Integration of Dark Fermentation and Microbial Electrolysis Cells 564

Hydrogen-related pathways in NEST++: reversible conversion, biomass-to-syngas routes, storage monitoring and intelligent control 567

Characterization and Calibration Protocols for Gas Sensors in Hydrogen Systems: Towards Integrated Environmental Monitoring 570

From converter measurements to internal degradation: a converter-oriented method for assessing pem electrolysis cell health 573

Smart and Sustainable Ports Artificial intelligence for cargo logistics and hydrogen terminal tractors 576

EFCH2 2026

European Fuel Cells and Hydrogen

PIERO LUNGHI CONFERENCE

Proceedings

OF THE 12TH EUROPEAN FUEL CELL PIERO LUNGHI CONFERENCE

ATENA FUTURE TECHNOLOGY

ENEA ITALIAN NATIONAL AGENCY FOR NEW TECHNOLOGIES, ENERGY AND SUSTAINABLE ECONOMIC DEVELOPMENT

Università degli Studi di Napoli Parthenope

CLEAN ENERGY INSTITUTE UNIVERSITY OF CALIFORNIA, IRVINE



TOPIC 1. HYDROGEN PRODUCTION



Low equivalent weight aquivion® ionomers behaviour in enhanced proton exchange membrane water electrolysis

Antonino Salvatore Aricò *[a]

* Corresponding author: arico@itae.cnr.it

[a] CNR-ITAE Institute of Advanced Energy Technologies, National Research Council, Via Salita S. Lucia Sopra Contesse 5, 98126, Messina, Italy

Keywords: proton exchange membrane, water electrolysis, radical scavenger, reinforced membrane

Abstract

Given the need for highly efficient and durable membranes for PEM electrolysis, this study compares several short-side-chain Aquivion® membranes with respect to performance and durability. The materials investigated include bare cast polymers, scavenger-enhanced casts, and reinforced films, all integrated into MEAs for hydrogen production. These MEAs were evaluated through polarization curves, electrochemical impedance spectroscopy and 2000-hour durability tests. Complementary techniques, including XRD, XRF, TEM, SEM, and optical microscopy, were employed to assess membrane properties and ionomer dispersion within the catalyst layers. By examining the efficiency and stability of Aquivion® membranes across different configurations, the study identifies strategies to improve polymer electrolytes for PEM water electrolysis and support reliable green hydrogen generation.

Introduction: The transition to clean energy requires efficient storage solutions, and converting surplus renewable electricity into hydrogen via PEM water electrolysis is a promising route, producing high-purity green hydrogen with fast response and compact system design[1-3]. However, large-scale adoption is limited by membrane durability. PEM membranes must combine high proton conductivity with strong chemical and mechanical stability under high-pressure, high-temperature, and high-current-density operation.

Various strategies have been explored to enhance membrane performance, including polymer reinforcement, alternative hydrocarbon-based chemistries and the addition of radical scavengers. Improvements in durability and conductivity have been reported.

Objectives: This study evaluates different Aquivion®-based membranes—bare cast films, radical-scavenger-modified casts (RSP-50), and reinforced films—integrated into MEAs. Performance

was assessed through polarization curves, EIS and 2000-hour durability tests, supported by structural and morphological analyses (XRD, XRF, TEM, SEM, optical microscopy). The aim was to identify the membrane configurations that best enhance efficiency and long-term stability in PEM water electrolysis.

Material and methods: The study describes the materials, preparation procedures, and characterization methods used for developing electrocatalysts, membranes, and membrane–electrode assemblies (MEAs) for PEM water electrolysis. The study describes the preparation and characterization of electrocatalysts, Aquivion®-based membranes, MEAs and their electrochemical testing for PEM water electrolysis.

$Ir_{0.7}Ru_{0.3}O_x$ anode catalyst synthesized by modified Adams fusion methode; 40 % Pt/C cathode catalyst produced via sulphite-complex method.

Four Aquivion® membranes fabricated: two cast (with/without Ce-based radical scavenger) and two e-PTFE-reinforced. All derived from Aquivion® D72-25BS dispersion and cast/dried through a multi-step thermal process. Reinforcement reduced Tg and improved mechanical durability.

Structural, morphological, and compositional analysis were carried out by XRD, XRF, SEM-EDX, TEM, BET, optical microscopy.

Catalyst-coated membranes were produced by ultrasonic spray coating of $IrRuO_x$ (anode) and Pt/C (cathode) inks. The CCMs were hot-pressed at 190 °C. Titanium mesh and carbon cloth were used as GDLs. Performance was assessed before and after durability testing by polarization and EIS measurements (30–90 °C).

Results: This work investigates the physicochemical properties, electrochemical performance, and durability of four Aquivion®-based proton-exchange membranes—C720, C720-RSP-50, R720, and NR720—designed for high-current-density PEM water electrolysis. In-plane proton conductivities at 80 °C ranged between 250–300 mS cm^{-1}, with minimal losses upon incorporation of a CeO_2–silica radical scavenger and more pronounced reductions for conventional e-PTFE reinforcement. Reinforced membranes exhibited significantly improved mechanical strength and reduced dimensional swelling, confirming the beneficial role of structural support. Electrochemical testing in single-cell configuration (5 cm^2, 30–90 °C) demonstrated enhanced performance with increasing temperature, achieving cell voltages as low as 1.87 V at 5 A cm^{-2} for the C720-RSP-50 and R720 membranes at 90 °C. Series resistance dominated high-current operation, with R720 exhibiting the lowest Rs and most favourable Arrhenius behaviour, indicating enhanced ionic transport pathways. Durability assessments at 90 °C and 5 A cm^{-2} for 2000 h revealed moderate voltage degradation rates (39–46 µV h^{-1}), with most losses occurring during the initial 1000 h. Post-test structural analyses (XRD, SEM, TEM) confirmed membrane integrity and only minor catalyst evolution, mainly related to Pt particle growth. Overall, the reinforced R720 membrane emerged as the most balanced candidate,

combining mechanical robustness, high conductivity retention, and stable long-term performance under extreme operating conditions.

Conclusions: Aquivion® membranes show higher conductivity, higher Tg, and better crystallinity than Nafion®, enabling improved PEM electrolysis performance and durability. Ce-based radical scavengers or PTFE reinforcement used in the membrane further enhance chemical and mechanical stability. Both modified membranes achieved 1.87 V at 5 A cm^{-2} (90 °C), corresponding to ~79% efficiency. Fillers slightly improved conductivity by altering membrane morphology. In 2000 h durability tests, reinforced and Ce-modified membranes showed similar stability. Degradation was mainly linked to an initial rise in series resistance, while polarization resistance changed only minimally. Test post analyses revealed no membrane thinning and limited catalyst evolution.

The reinforced membrane, combining robust mechanics with low temperature dependence of Rs, appears the most promising option for high-performance PEM electrolysis.

References

[1] Aricò AS, Siracusano S, Briguglio N, Baglio V, Di Blasi A, Antonucci V. Polymer electrolyte membrane water electrolysis: status of technologies and potential applications in combination with renewable power sources. J Appl Electrochem 2013;43:107–18.

[2] Olabi AG, Abdelkareem MA. Renewable energy and climate change. Renew Sustain Energy Rev 2022;158:112111.

[3] Pani A, Shirkole SS, Mujumdar AS. Importance of renewable energy in the fight against global climate change. Dry Technol 2022;40:2581–2.

Acknowledgment

This research was funded by the European Union – NextGeneration EU from the Italian Ministry of Environment and Energy Security POR H2 AdP MMES/ENEA with involvement of CNR and RSE, PNRR - Mission 2, Component 2, Investment 3.5 “Ricerca e sviluppo sull’idrogeno”, CUP: B93C22000630006



Hydrogen production from recycled aluminum foils and waste: reactivity and kinetic analysis

Veronica Testa[*a,b], Martina Iaia [a], Luca Zannini [a], Marcello Romagnoli [a,b], Paolo Emilio Santangelo [b,c]

* corresponding author: veronica.testa@unimore.it

[a] Università di Modena e Reggio Emilia- Dipartimento di Ingegneria "Enzo Ferrari"

[b] Centro Interdipartimentale di Ricerca e per i Servizi nel settore della produzione, stoccaggio ed utilizzo dell'Idrogeno H2 - MO.RE

[c] Università di Modena e Reggio Emilia - Dipartimento di Scienze e Metodi dell'Ingegneria

Keywords: Dietrich-frühling method, Exothermic Reaction, Hydrogen, Subzero experiments

Abstract

Introduction: Hydrogen is a promising candidate for an energy and economic transition away from fossil fuels due to its low environmental impact and significant potential in energy production, storage, and transportation. In recent years, its industrial applications, such as fuel cells for electricity generation, have expanded. Hydrogen, despite being earth's most abundant element, is typically found bonded to other elements like water and hydrocarbons. Among various methods of hydrogen generation, the reaction between metals and alkaline solutions represents a simple, scalable, and potentially sustainable route [1,2]. The reaction between aluminum and water has been studied for over five decades as a particularly interesting approach due to its potential to benefit from aluminum waste recycling and the large availability of liquid water [3]. It is also widely available, relatively inexpensive, and safe to handle, with non-toxic reaction byproducts. Low energy requirements and low CO_2 emissions compared to conventional methods like steam reforming of hydrocarbons [4] make aluminum and its alloys highly suitable for onboard hydrogen supply in mobile applications. The reaction between aluminum and water ($2Al + 6H_2O \rightarrow 2Al(OH)_3 + 3H_2$) is exothermic but tends not to occur readily due to the formation of a passivating oxide layer on the aluminum surface. Adding promoters, such as NaOH and KOH, is instrumental in facilitating the reaction by preventing oxide layer formation. This makes these techniques attractive for achieving hydrogen yields typically close to or reaching 100% [5].

Objectives: the study investigates hydrogen production from waste aluminum via reaction with aqueous sodium hydroxide solutions (NaOH), focusing on the effects of aluminum surface area, solution concentration, and temperature on reaction kinetics and hydrogen generation efficiency. It also evaluates the feasibility of replacing NaOH with alkaline or acidic solutions derived from food waste streams and digestate, assessing their potential to promote aluminum corrosion and sustain hydrogen production. The research combines theoretical and experimental analyses to compare

reaction performance, kinetics, and hydrogen yield using both conventional reagents and waste-derived solutions.

Material and methods

1. Chemical and microstructural characterization of raw aluminum materials → SEM (Scanning Electron Microscopy, Quanta 200 ESEM FEG by FEI).
2. Assessment of the purity of the aluminum samples → Energy-dispersive X-ray spectroscopy (EDX, INCA Energy 350 Energy Dispersive Microanalysis System by Oxford Instruments) and X-ray diffraction (XRD, X'Pert PRO and Empyrean by Malvern PANalytical).
3. Evaluation of the specific surface area of raw materials → BET analysis (ASAP 2020, Micromeritics).
4. Preparation of NaOH solutions at different molar concentrations (1 – 5 M).
5. Quantification of hydrogen production under different temperature conditions (monitoring by with a K-type thermocouple) → Dietrich–Frühling method (Figure 1); each configuration is repeated six times to enable statistical analysis.
6. Assessment of chemical kinetics → the obtained dataset is used to calculate reaction rates and estimate the Arrhenius parameters, including the pre-exponential factor and activation energy, by correlating hydrogen concentration over time with inverse temperature.
7. Confirmation of reaction completion → XRD and EDX analysis of the byproducts.

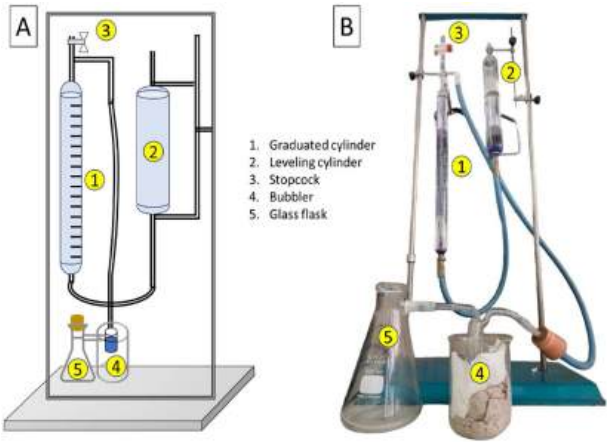


Figure 1 – (A) Schematic experimental apparatus implementing the Dietrich-Frühling method; (B) photo of test rig.

Results

- Hydrogen volume closely matched stoichiometric predictions, with ~1% relative discrepancy.
- Aluminum powder reacted faster than sheets due to higher surface area.
- Increasing solution concentration from 1 M to 5 M accelerated the reaction.
- Temperature strongly influenced kinetics: at 50 °C the reaction was nearly instantaneous, while at −5 to −6 °C it was much slower, clearly showing all three phases.
- Statistical analysis confirmed that temperature, NaOH concentration, and aluminum form significantly affected kinetics.
- Calculated activation energy agreed with literature values.

- XRD and EDX of Byproducts confirmed aluminum hydroxide formation (gibbsite and bayerite), indicating complete reaction.

Conclusions: the study demonstrated that hydrogen production from waste aluminum reacting with NaOH is efficient and predictable, with hydrogen volumes closely matching stoichiometric calculations. Reaction kinetics were strongly influenced by aluminum surface area, NaOH concentration, and temperature, with powdered aluminum and elevated temperatures accelerating hydrogen generation. The work highlights the interplay between surface area, reactant concentration, and temperature in governing reaction kinetics. Moreover, the exploration of waste-derived alkaline or acidic solutions as alternatives to NaOH, along with optimizing aluminum pretreatment, aims to enable sustainable and scalable hydrogen production.

Acknowledgment

This project was funded under the National Recovery and Resilience Plan (NRRP), Mission 04, Component 2, Investment 1.5 – NextGenerationEU, ECS00000033, call for tender n. 3277 dated December 30, 2021, award number: 0001052 dated June 23, 2022. The authors wish to thank M.C. Rossi and C. Sgarlata (Università degli Studi di Modena e Reggio Emilia, Italy) for providing support to the chemical characterization of the samples.

References

[1] J. Uan, C. Cho, K. Liu, Generation of hydrogen from magnesium alloy scraps catalyzed by platinum-coated titanium net in NaCl aqueous solution, Int. J. Hydrogen Energy 32 (2007) 2337–2343. https://doi.org/10.1016/j.ijhydene.2007.03.014.

[2] I. Vishnevetsky, M. Epstein, Production of hydrogen from solar zinc in steam atmosphere, Int. J. Hydrogen Energy 32 (2007) 2791–2802. https://doi.org/10.1016/j.ijhydene.2007.04.004.

[3] H.Z. Wang, D.Y.C. Leung, M.K.H. Leung, M. Ni, A review on hydrogen production using aluminum and aluminum alloys, Renewable and Sustainable Energy Reviews 13 (2009) 845–853. https://doi.org/10.1016/j.rser.2008.02.009.

[4] T. Hiraki, M. Takeuchi, M. Hisa, T. Akiyama, Hydrogen Production from Waste Aluminum at Different Temperatures, with LCA, Mater. Trans. 46 (2005) 1052–1057. https://doi.org/10.2320/matertrans.46.1052.

[5] C.B. Porciúncula, N.R. Marcilio, I.C. Tessaro, M. Gerchmann, Production of hydrogen in the reaction between aluminum and water in the presence of NaOH and KOH, Brazilian Journal of Chemical Engineering 29 (2012) 337–348. https://doi.org/10.1590/S0104-66322012000200014.



Electrochemists going with the flow: CFD-guided optimization of flow-engineered 3D electrodes and cells for alkaline water electrolysis

Kevin Van Droogenbroek*, Ahmed Aissa Berraies, Joris Proost

* corresponding author: kevin.vandroogenbroek@uclouvain.be

Louvain Research & !nnovation Centre for Sustainable Process Engineering (ReC!PE), UCLouvain, Louvain-la-Neuve, Belgium

Keywords: Alkaline water electrolysis, Bubble evacuation, Computational fluid dynamics, Flow distribution

Abstract

Introduction: The role of green hydrogen in the energy transition has been widely recognized by the scientific community and the International Energy Agency (IEA) [1], as it provides a pathway to store and deliver clean and usable energy. Currently, the two most mature technologies for green hydrogen production are alkaline and proton exchange membrane (PEM) water electrolysis. Recent experimental studies conducted in our group have demonstrated that the performance of alkaline water electrolysers (AWE) can be significantly enhanced by incorporating three-dimensional (3D) porous electrodes in a zero-gap cell configuration with forced electrolyte flow [2]. Attempts were made to apply the same methodology (i.e. zero-gap cell with knitted mesh-type spacer and forced flow) to a 6 kW industrial-scale prototype electrolyser installed in our facilities. However, similar performance improvements to those observed at lab scale could not be achieved, mainly due to non-uniform electrolyte distribution in the anodic and cathodic half-cells [3].

Objectives: This work aims to demonstrate how Computational Fluid Dynamics (CFD) simulations, combined with experimental characterization, can be used to optimize both lab- and industrial-scale AWE cells. At lab scale, accurate 3D reconstructions of porous electrodes (i.e. foams or triply periodic minimal surfaces – TPMS – structures) enable the investigation of electrolyte transport from the catalytic layer, where gas is generated, to the porous transport layer (PTL), where gas bubbles are evacuated. Furthermore, numerical simulations provide insights into the performance limitations observed at industrial scale and support the design of improved cell configurations with enhanced flow distribution and electrochemical performance.

Material and methods: Single phase and multiphase flow simulations are performed considering a 30 wt% KOH solution at 80°C as the liquid phase and hydrogen as the gas phase. The discretized continuity and momentum equations are solved using pressure-based solvers implemented in

OpenFOAM and ANSYS Fluent. The corresponding meshing utilities are employed to generate volume meshes of the complex 3D electrode geometries. At larger scale, these porous structures are represented implicitly using the Darcy-Forchheimer approximation. The electrolyte flow rate is imposed at the domain inlet to match experimental operating conditions. In multiphase simulations, a gas flux derived from Faraday's law is imposed at the electrode surface.

Results: As shown in Figure 1, single-phase simulations allow the extraction of lateral velocity profiles within explicit bi-layer structures at lab scale, highlighting electrolyte transport from the catalytic layer towards the PTL. The results indicate that 3D-printed bi-layer TPMS electrodes not only offer greater design flexibility but also promote improved lateral transport, consistent with the enhanced electrochemical performance observed experimentally.

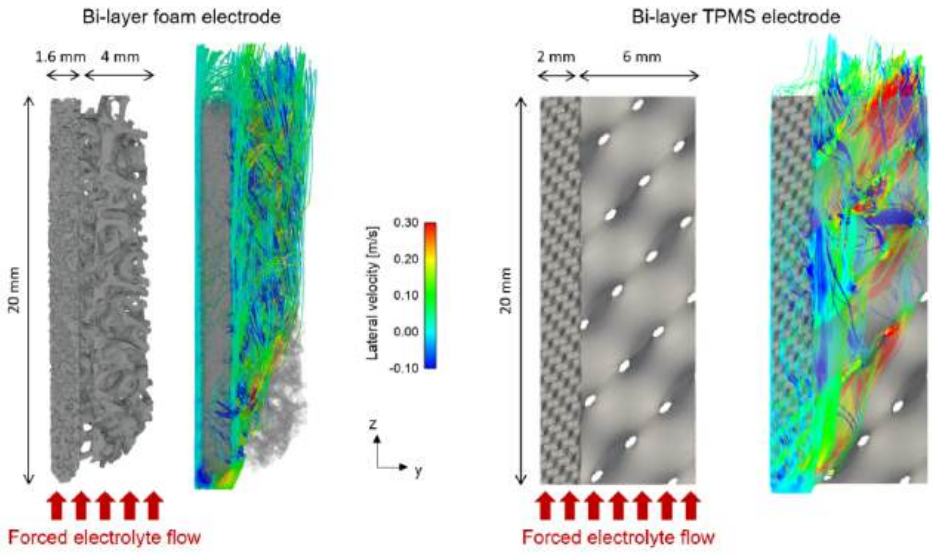


Figure 2: Lateral y-velocity streamlines emitted from the catalytic layer comparing a bi-layer foam (left) and a bi-layer TPMS (right).

These single-phase simulations can be extended to the industrial scale. Figure 2 shows that the use of a 3000 µm foam as PTL results in a more uniform flow distribution within the cell compared to a knitted mesh-type spacer. However, implementing such 3D structures may lead to gas accumulation at the top of the cell. This suggests that current industrial cell designs, characterized by small inlets and outlets, are not optimized for the use of a foam-based PTL, as gas evacuation is hindered.

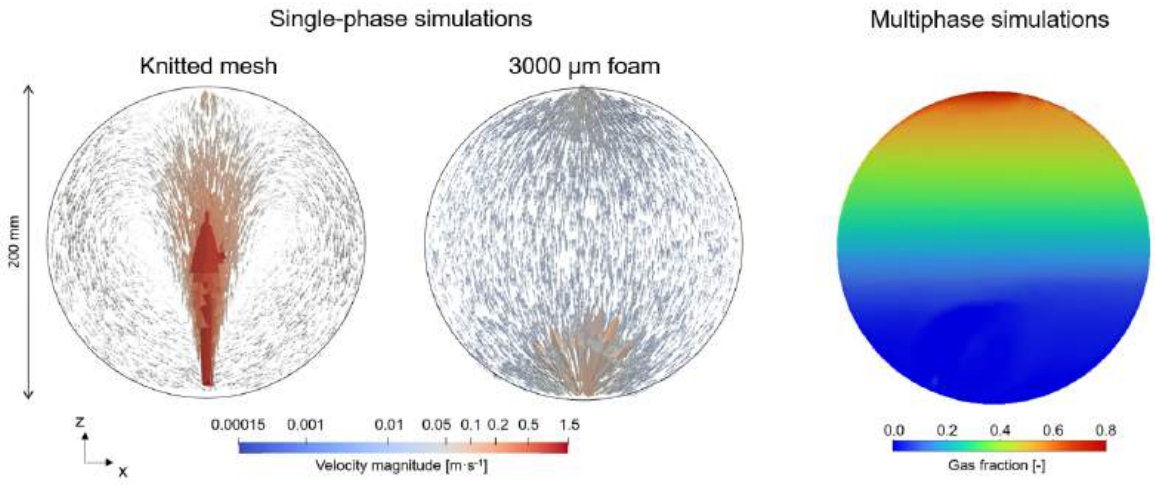


Figure 3: Velocity vectors colored by magnitude comparing a knitted mesh and a 3000 µm foam as PTL (left) and gas fraction profile (right) within industrial cells.

Conclusions: As electrochemists increasingly implement forced electrolyte flow in AWE cells incorporating complex 3D electrodes to enhance bubble removal, CFD simulations become a valuable tool for cell optimization. This approach is applicable at both lab- and industrial-scale, while also revealing the limitations of current cell designs. A paradigm shift in electrolyzer development is therefore required, in which flow fields, gas evacuation pathways, and overall cell architecture are co-designed. In this context single- and multiphase CFD emerge as powerful tools to support a more integrated and performance-driven design strategy.

Acknowledgment

Computational resources have been provided by the supercomputing facilities of the Université catholique de Louvain (CISM/UCL) and the Consortium des Équipements de Calcul Intensif en Fédération Wallonie Bruxelles (CÉCI) funded by the Fond de la Recherche Scientifique de Belgique (F.R.S.-FNRS) under convention 2.5020.11 and by the Walloon Region. Part of this work was performed in the scope of the Regional Walloon PNRR Project "HeCO2", which is gratefully acknowledged.

References

[1] IEA (2024), Global Hydrogen Review 2024, IEA, Paris, Licence: CC BY 4.0.

[2] F. Rocha et al., Proton exchange membrane-like alkaline water electrolysis using flow-engineered three-dimensional electrodes, Nat. Comm., vol. 15, p. 7444, 2024.

[3] K. Van Droogenbroek, C. Georgiadis, B. Scheid and J. Proost, Numerical assessment of flow uniformity and recirculation in a water electrolysis cell with knitted mesh and foam-like electrodes, Chemical Engineering Science, vol. 310, p. 121513, 2025.



Seawater electrolysis with integrated brine valorisation: a contribution to the water-energy nexus

Raphaël Defroyennes*[a], Renaud Delmelle[a], Patricia Luis Alconero[a], Joris Proost[a]

* corresponding author: raphael.defroyennes@uclouvain.be

[a] Louvain Research & !nnovation Centre for Sustainable Process Engineering (ReC!PE), UCLouvain, Louvain-la-Neuve, Belgium

Keywords: Alkaline seawater electrolysis, Desalination, Water-energy nexus.

Abstract

Introduction: The Paris Agreement's 1.5 °C target compels the decarbonisation of energy-intensive sectors — transportation, cement industry, steelmaking and chemical synthesis — via scalable, low-carbon energy carriers [1]. Green hydrogen, generated through renewable-powered water electrolysis, has emerged as a key enabler for this transition. However, its large-scale deployment is hindered by a critical paradox: electrolysis requires substantial freshwater inputs, yet the most solar-rich regions (e.g., the Middle East and North Africa) face acute water scarcity. These regions rely on seawater desalination to meet industrial and agricultural needs, producing hypersaline brine as a byproduct — over 100 million m^3/day globally — which is routinely discharged untreated into marine ecosystems, disrupting salinity gradients and killing local biodiversity [2, 3].

Current electrolysis technologies exacerbate this tension by requiring purified water feedstocks, further depleting freshwater reserves. To address this challenge, this study proposes repurposing desalination brine as an electrolyte for alkaline water electrolysis, thereby transforming a waste stream into a resource while mitigating its environmental impact.

Objectives: This work aims to examine the chemical process for green hydrogen production from desalination brine with a focus on integrating an electrolyser into a seawater desalination workflow. A combined process and energy analysis evaluates the feasibility of this coupling, assessing the operational impact on the desalination unit.

Materials and methods: The energy requirements of the integrated desalination-electrolysis system were assessed via a literature-based analysis, incorporating mean energy consumption values for each unit operation.

Results: The proposed flowsheet (Figure 4) modifies a desalination brine treatment unit by integrating an alkaline electrolyser between the precipitation stage and bipolar membrane electrodialysis (EDBM). In standard plants, reverse osmosis (RO) produces freshwater while discharging brine directly into the sea. Some advanced facilities add three steps: (1) nanofiltration to recover divalent ions, (2) precipitation to remove residual calcium/magnesium and prevent membrane fouling and (3) EDBM to split the brine into NaOH and HCl, reducing its environmental impact. Our adaptation inserts the electrolyser after precipitation, using the ion-rich brine as catholyte and the EDBM-produced NaOH (1–2 M) as anolyte for hydrogen production.

To quantify the benefit of this integration, Table 1 compares the system-level specific energy consumption (SEC) across three configurations. The conventional RO-only process (representing 90% of current installations) discharges untreated brine with a negligible SEC of 0.004 kWh/L_{brine}. The RO with brine treatment without electrolysis (RO + NF + precipitation + EDBM) reaches 14.311 kWh/L_{brine}. The proposed integrated process adds 5 kWh/L_{brine} for the alkaline water electrolysis stage, yielding a total SEC of 19.311 kWh/L_{brine} — a 35% increase over the RO with brine treatment alone. While this represents the highest energy demand, the additional consumption is partly offset by the production of green hydrogen from an otherwise wasted stream, without competing with freshwater resources — a critical advantage in water-scarce regions where desalination is already deployed at scale.

Regarding the operational impact on the EDBM unit, the electrolyser does not significantly modify the brine flow rate entering the EDBM. The Cl^- concentration remains unchanged, as chloride oxidation is avoided to prevent electrode corrosion. The Na^+ concentration increases due to NaOH addition at the anolyte, which enhances ionic conductivity and is expected to moderately reduce EDBM energy consumption. The effect of the resulting pH increase on EDBM performance remains to be experimentally characterised and constitutes a key objective of ongoing work.

Conclusions: This work establishes the feasibility of coupling alkaline electrolysis with seawater desalination brine treatment, offering a dual solution for green hydrogen production and brine valorisation. Although the integrated process exhibits a higher overall SEC (19.311 kWh/L_{brine}) than advanced treatment alone (14.311 kWh/L_{brine}), this additional energy expenditure enables hydrogen production from a waste stream without additional freshwater consumption — directly addressing the water-energy nexus in desalination-dependent regions. The next critical step is to reduce the cell voltage below the chlorine-evolution threshold (1.71 V vs. HER) through improved electrocatalysts, which would further strengthen the case for this integrated approach.

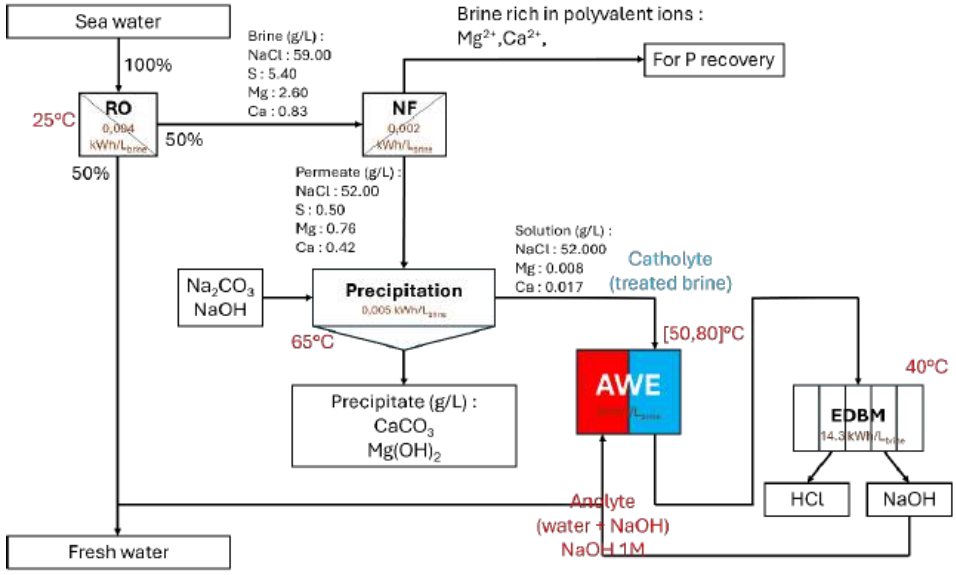


Figure 4 - Adapted desalination process flowsheet with integrated brine valorisation electrolyser.

Table 1 - System-level specific energy consumption across three desalination configurations

Configuration	**Unit operations**	**SEC (kWh/L_{brine})**
Conventional RO	RO	0.004
RO with brine treatment	RO + NF + Precip. + EDBM	14.311
Proposed process	RO + NF + Precip. + AWE + EDBM	19.311

References

[1] U. N. E. Programme, "Paris Agreement," Dec. 2015, [Online]. Available: https://wedocs.unep.org/handle/20.500.11822/20830

[2] E. Jones, M. Qadir, M. T. H. Van Vliet, V. Smakhtin, and S. Kang, 'The state of desalination and brine production: A global outlook', Science of The Total Environment, vol. 657, pp. 1343–1356, Mar. 2019, doi: 10.1016/j.scitotenv.2018.12.076.

[3] J. Eke, A. Yusuf, A. Giwa, and A. Sodiq, 'The global status of desalination: An assessment of current desalination technologies, plants and capacity', Desalination, vol. 495, p. 114633, Dec. 2020, doi: 10.1016/j.desal.2020.114633.



Characterisation of electrode bubble coverage by electrochemical impedance spectroscopy in an alkaline water electrolysis flow-cell

Xavier Pinon*[a,b], Benoit Scheid[b], Joris Proost[a]

* corresponding author: xavier.pinon@uclouvain.be

[a] Louvain Research & !nnovation Centre for Sustainable Process Engineering (ReC!PE), UCLouvain, Louvain-la-Neuve, Belgium

[b] Transfers, Interfaces and Processes, ULB, Brussels, Belgium

Keywords: Electrochemical impedance spectroscopy (EIS), characterisation method, alkaline water electrolysis, bubble

Abstract

Introduction: Alkaline water electrolysis suffers from poor mass transfer at high current densities. Bubble presence within the cell hinders ionic transport and catalytic surface accessibility, thereby decreasing the overall cell efficiency. Therefore, a better understanding and characterisation of bubble behaviour inside a cell will help to improve electrolyser performance[1]. Here, a method based solely on electrochemical measurements allows to obtain the relative bubble coverage fractions at different electrolyte flow rates and compare them with their respective overpotentials.

Objectives: Current-voltage curves (polarisation curves) and electrochemical impedance spectroscopy (EIS) are usually performed to analyse the performance of an electrolyser. This work aims to characterise the bubble-covered surface area fraction based only on these classical electrochemical measurements in order to improve the impact of bubble behaviour under different flow conditions.

Material and methods: An in-house setup and a zero-gap cell were built to conduct the experiments at controlled electrolyte flow rates (0.3 to 1.8 L/min) and 80 °C. The electrodes are both a state-of-the-art 2x2 cm^2 bi-layer nickel foam as published by Rocha *et al.*[1]. Anode and cathode are separated by a Zirfon Perl UTP 500, while a 30 wt.% KOH aqueous solution serves as electrolyte.

Ramp and step chronopotentiometries between 0 and 2 A/cm^2_{geo} are performed on the electrochemical cell. Ramp chronopotentiometry allows to obtain detailed polarisation curves thanks to high data density, while step chronopotentiometries confirm the equivalent response of the electrochemical system between transient and steady measurements, in addition to ensure stabilisation before EIS measurements. 5 rms% of direct current are applied for galvanostatic EIS measurements, with 10 points per decade on a frequency sweep starting at 20 000 Hz and ending at 0.1 Hz.

In polarisation curves, one can distinguish three contributions to the cell voltage (E_{cell}): thermodynamic, kinetic and ohmic. The following equation enables to link cell voltage with current density (j) by summing the three parts[1]:

$$E_{cell} = E_{eq} + b \cdot \log\left(\frac{j}{j_0}\right) + R_{ohm} \cdot j$$

The reversible cell potential E_{eq} is defined by thermodynamics, while the combined Tafel slope b, the non-linear average of the cathodic and anodic exchange current densities j_0, and the area-ohmic resistance R_{ohm} are unknown fitting parameters of the equation.

While comparing polarisation curves measured under different flow rates, b should remain identical as the catalyst is identical. However, j_0 and R_{ohm} should evolve with flow rate since higher flow allows for better evacuation of bubbles, which liberates catalytic surface area and increases electrolyte conductivity. The evolution of j_0 can be related to the electrode surface area fraction masked by attached bubbles (θ), as stated by the following equations for constant Tafel slope[2]:

$$\eta_\theta = b \cdot \log\left(\frac{j}{j_0}\right) = b \cdot \log\left(\frac{I}{A \cdot (1-\theta) \cdot j_{0,free}}\right) = b \cdot \log\left(\frac{j}{(1-\theta) \cdot j_{0,free}}\right)$$

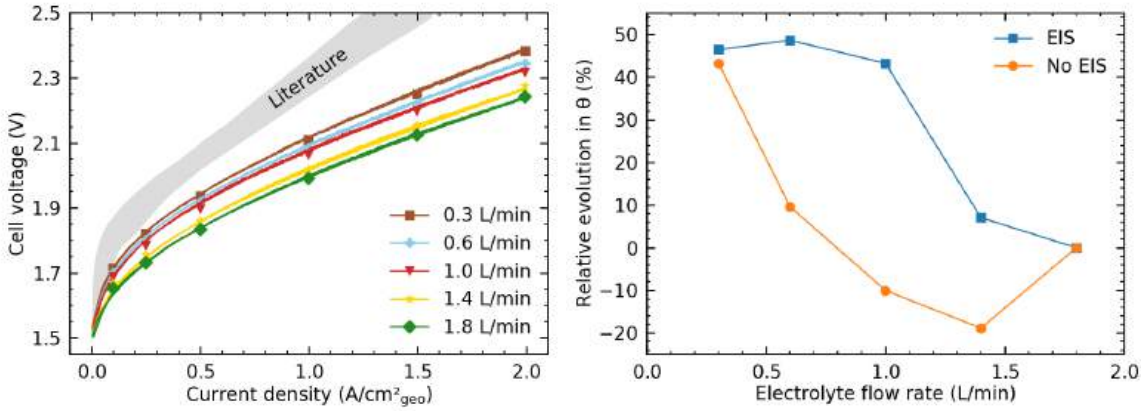
$$\Rightarrow \theta = 1 - \frac{j_0}{j_{0,free}}$$

where I is the current, A is the catalytic surface area of the bubble-free electrode, and $j_{0,free}$ is the non-linear average exchange current density in the case of bubble-free electrodes. Since a completely bubble-free cell is hardly obtained in a zero-gap alkaline water electrolyser, the reference chosen for $j_{0,free}$ is the one most favourable for bubble evacuation, corresponding to the highest flow rate.

To obtain more accurate values for b and j_0, EIS can be used to independently evaluate R_{ohm} at different current densities. A subsequent interpolation of R_{ohm} on the complete current density range during ramp chronopotentiometry therefore allows to improve the fitting results.

Results: In Figure a, the low voltage at high current density due to high bi-layer foam performance published by Rocha *et al.*[1] has been confirmed, as compared to literature operating in similar conditions. In addition, EIS results show strong correlations between area-ohmic resistance, current density and flow rate, confirming the bubble impact. It follows that EIS must be considered before deriving b and j_0 to avoid errors and inconsistencies in θ, as it can be observed in Figure b. From these figures, it can be derived that the 140 mV increase in overpotential at 2 A/cm$^2_{geo}$ for the lowest flow rate of 0.3 L/min originates from a 50 % increase in bubble coverage as compared to the highest flow rate of 1.8 L/min.

(a) (b)



Conclusions: A characterisation method is proposed to describe the relative fraction of catalytic surface area masked by bubbles under different flow rates based solely on electrochemical measurements. Results show that EIS must be performed to accurately estimate the area-ohmic resistance evolution with current density. Finally, bubble removal due to increased electrolyte flow rate is linked to overpotential reduction.

Acknowledgment

This work was supported by the Belgian Regional Walloon project TiNTHyN.

References

[1] Rocha, F. et al. Proton exchange membrane-like alkaline water electrolysis using flow-engineered three-dimensional electrodes. Nat. Commun. 15, 7444 (2024).

[2] Dukovic, J. & Tobias, C. W. The Influence of Attached Bubbles on Potential Drop and Current Distribution at Gas-Evolving Electrodes. J. Electrochem. Soc. 134, 331–343 (1987).



Water Pathways and Impurity Diagnostics in PEM Water Electrolysis

Al-Shabibi, Ruba *[a], Serra, Maria [c], Secchi, Raffaello [b], Martinez-felipe, Alfonso [a]

* Corresponding author: r.alshabibi.25@abdn.ac.uk

[a] *Chemical Processes and Materials Research Group, School of Engineering, Centre for Energy Transition, University of Aberdeen, Just Transition Lab, King's College, Aberdeen, UK*

[b] *School of Engineering, University of Aberdeen, King's College, Aberdeen, UK*

[c] Institut de Robòtica i Informàtica Industrial, CSIC-UPC, C/ Llorens i Artigas 4-6, 08028, Barcelona, Spain

Keywords: Water pathways; water electrolysis; Electrochemical Impedance Spectroscopy.

Abstract

Introduction: Reliable green hydrogen production via water electrolysis depends on effective management of the water pathway from source selection to treatment and delivery to the electrolyser. Candidate water sources, including municipal water, groundwater, rainwater, seawater and wastewater, differ in composition and therefore require different treatment trains to meet PEM water electrolyser inlet specifications; our prior work shows that water source selection drives the required treatment pathway to meet inlet-quality targets, which in turn affects system configuration and practical deployment decisions [1]. PEM water electrolysers experience performance change during operation, which can be observed as shifts in polarisation behaviour [2], and is consistent with broader evidence on degradation processes in low-temperature electrolyser [3]. Meeting water-quality specifications does not guarantee impurity-free operation, and cationic impurities can produce measurable performance effects and diagnostic signatures in polarisation and impedance response [3,4]. Current work is establishing an EIS (Electrochemical Impedance Spectroscopy) test campaign with controlled cationic impurity exposure to quantify water-quality impacts and derive early diagnostic indicators.

Objectives:

(1) Examine representative source-to-treatment water pathways for PEM water electrolysis to produce ultrapure feedwater and compare pathways using MCDA (Multi-Criteria Decision Analysis).
(2) Implement and validate an EIS-based testing methodology to quantify how water quality affects PEM water electrolyser performance and impedance signatures, establishing early diagnostic indicators for operational monitoring.
(3) Develop a controlled, dynamic operational model (PID power tracking, PI temperature regulation) to simulate renewable-driven operation and derive descriptors such as ramp rate and temperature deviation associated with performance changes, to support future degradation-aware modelling.

Material and methods: Representative water pathways are defined by selecting relevant water sources and specifying treatment trains to meet the inlet specifications of low-temperature water electrolysers. Our methodology consists of parameterising water pathways by source characteristics and treatment steps required to meet inlet specifications [1]. Current work is establishing an experimental campaign to quantify water-quality impacts using polarisation curves and EIS. Our EIS methodology includes validity checks, repeatability assessment and artefact mitigation, with model-informed interpretation using equivalent-circuit and Distribution of Relaxation Time (DRT) [3,4]. In this work, we present a preliminary test that includes the

baseline operation followed by controlled exposure to cationic impurities at selected concentrations, with repeated measurements to assess run-to-run consistency. In parallel, a dynamic operational model with control (PID-based power tracking and PI-based temperature regulation) is being developed to simulate renewable-driven operation and derive operating-condition descriptors (e.g., ramp rate and temperature deviation) associated with performance change; EIS and polarisation indicators will provide calibration targets for future degradation-aware models.

Results: Our prior research demonstrates that water source selection drives the treatment steps required for ultrapure water and affects pathway selection and optimisation [1]. Figure 1 presents the MCDA comparison across six water sources, showing that groundwater and municipal water score highest overall, driven by treatment complexity and cost [1]. The literature confirms that meeting inlet specifications does not ensure impurity-free operation, and residual cationic impurities produce measurable performance losses and diagnostic signatures in polarisation and impedance response [3,4]. Figure 2 shows PID (Proportional–Integral–Derivative) power-tracking performance under a simulated renewable-energy input profile, with a ~~steady-state~~ error below 2%. For the EIS baseline measurement (100 kHz–0.1 Hz), the Nyquist plot shows a high-frequency resistance of 347 mΩ. Kramers–Kronig (KK) validation confirms measurement validity, with residuals of root-mean-square (RMS) = 0.42% and χ^2_KK = 1.8×10^{-5}, ahead of the controlled impurity exposure campaign [3,4].

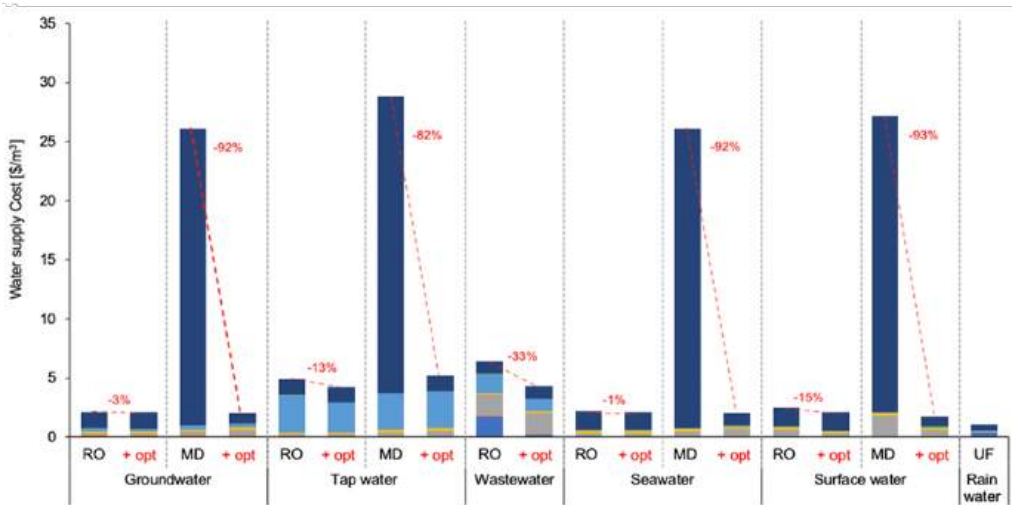


Figure 5. MCDA comparison of six water sources for PEM water electrolysis feedwater pathways, evaluated across technical, economic, and environmental criteria [1].

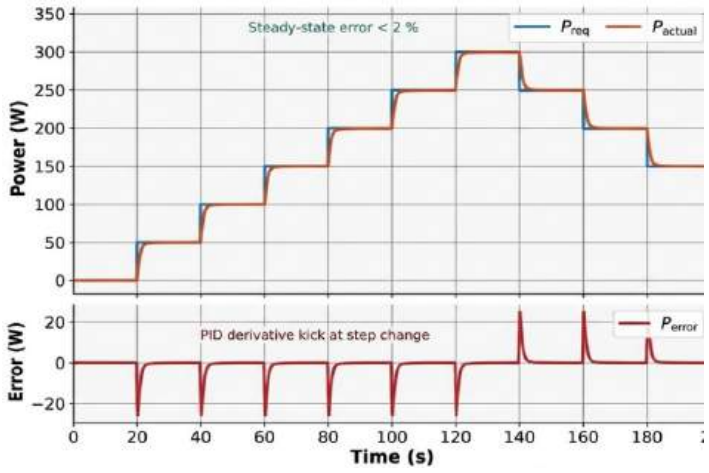


Figure 6.PID power tracking performance under a simulated renewable input profile; steady-state error < 2%.

Conclusions: Key outcomes from our work and the literature can be summarised as follows. First, water pathways matter: source selection and treatment requirements should be treated as core design variables for green hydrogen via water electrolysis. Second, compliance with inlet water specifications does not preclude impurity-driven effects; ionic contaminants remain a critical concern for PEM electrolyser, with cationic impurities particularly performance-relevant and diagnostically observable through polarisation and impedance response. Third, reliable operation under renewable-driven variability requires structured control strategies; our work demonstrates feasible closed-loop power tracking under dynamic renewable input profiles. The novelty of this work is combining dynamic modelling and electrochemical diagnostics to translate water-pathway-driven impurity exposure into degradation-aware operating modes and corrective actions. Polarisation and EIS measurements provide impurity-sensitive signatures. The controlled dynamic operational model defines representative renewable-driven operating profiles. PID-based power tracking and PI-based temperature regulation support stable operation and extraction of operating descriptors for future degradation-aware modelling. Current work is establishing the water-quality exposure campaign and EIS methodology to identify early diagnostic indicators suitable for operational monitoring. Future work will use these indicators to support the development of degradation-aware modelling and will extend the protocol to assess mitigation and recovery strategies, including current-driven recovery behaviour for cation contamination.

References

[1] Peecock A, Al Shabibi R, Haro-Monteagudo D, Martinez-Felipe A. “A new tool to assess the technical, economic, and environmental impacts of green hydrogen generation via water electrolysis using a multi-criteria decision analysis model”, *IJHE,* 2026;198:152750.

[2] Swinton-Blancke R, Al-Shabibi R, et al. “Cloud-Enabled Monitoring and Control of Hydrogen-Based Energy Storage: Challenges and Opportunities”. In: proc. *EFEA* 2025; Newcastle upon Tyne. doi:10.1109/EFEA67685.2025.11385917.

[3] Becker H, Murawski J, Shinde DV, Stephens IEL, Hinds G, Smith G. Impact of impurities on water electrolysis: a review. *Sustain Energy Fuels*. 2023;7:1565–1603.

[4] Padgett E, Adesso A, Yu H, Wrubel J, Bender G, Pivovar B, Alia SM. Performance losses and current-driven recovery from cation contaminants in PEM water electrolysis. *JES*.



Electrochemical characterization of Molten Carbonate Electrolysis Cells: a focus on fuel electrode kinetics and degradation

Fiammetta Rita Bianchi*[a], Silvia Lo Conte[b,c], Barbara Bosio [a]

Massimiliano Della Pietra[b], Elio Jannelli[c], Francesca Santoni[b]

* corresponding author: fiammettarita.bianchi@unige.it

[a] Department of Civil, Chemical and Environmental Engineering, University of Genoa,

via Opera Pia 15, Genoa, 16145, Italy

[b] ENEA - Italian National Agency for New Technologies, Energy and Sustainable Economic Development, via Anguillarese 301, Rome, 00123, Italy

[c] Department of Engineering, University of Naples "Parthenope",

Centro Direzionale Isola C4, Naples, 80143, Italy

Keywords: Molten carbonate electrolysis cell, Performance predictive model, Electrochemical characterization, Durability test

Abstract

Molten carbonate electrolysis is an emerging high-temperature cell technology suitable for efficiently producing hydrogen-rich syngas to use as an energy vector and an intermediate in chemical synthesis. Nevertheless, effective performance at variable working conditions and, above all, in long-term applications is still almost unknown compared to the understanding of molten carbonate fuel cell operation. The research work presents an electrochemical characterization of electrolysis operation performed through both theoretical kinetic investigation and lab-scale testing. The initial sensitivity analysis varying cell working conditions is followed by a durability test under galvanostatic control. The focus is mainly on performance and degradation of the fuel electrode, where a different reaction environment in terms of the fed gas composition may lead to mechanisms specific to the electrolysis cell mode.

Introduction: Molten Carbonate Electrolysis Cells (MCECs) allow hydrogen electrochemical synthesis through water reduction at the fuel electrode; then the produced carbonate ions migrate to the anode, where their oxidation releases oxygen. This is formally the opposite reaction of a fuel cell; nevertheless, previous literature has reported asymmetrical cell behaviour by suggesting specific dependencies and reaction paths for each operation [1], [2], [3]. Preliminary results have showed MCEC competitive energy consumption thanks to high working temperatures and partially possible performance recovery in long-term operation as well [5], [4].

Objectives: The study consists of an investigation of MCEC operation and durability, coupling experimental observations with modelling. The reference cell performance was evaluated at variable working conditions, underlining the main dependencies on anodic and cathodic processes. Specific kinetic parameters were computed, leading to the development of a predictive model of the cell voltage and polarization losses at each side. Consolidated the knowledge of MCEC operation at nominal conditions, a durability test was carried out by monitoring voltage variations over time and focusing, above all, on the fuel electrode degradation where a drop in performance occurred. Following a semi-empirical approach, the model was reviewed to have a preliminary simulation tool for electrolysis cell long-term operation.

Material and methods: The reference samples were circular button cells with a 3 cm^2 active area and composed of state-of-the-art materials. Electrochemical characterization consisted of both polarization curves, distinguishing the measurements between anode and cathode, and EIS analysis performed through a BK Precision 9201 Multi-Range DC Power Supply system and a Solartron SI-1260 analyser coupled to a Solartron SI-1287 module, respectively. Table 1 summarises tested working conditions. The durability test resulted in more than 1000 hours of galvanostatic operation at reference operation, measuring regularly polarization curves and EIS spectra.

Table 2: Working conditions for the sensitivity analysis at cell nominal state (in bold the reference operation).

Temperature [°C]	Fuel electrode feed [vol%]	Oxygen electrode feed [vol%]
620/**650**/680	10/**20** H_2 10/20/30/**40**/50/70 CO_2 10/20/30/**40**/50/70 H_2O 60/50/40/20/**-** N_2	**15** O_2 **30** CO_2 **55** N_2

Cell operation and durability were simulated through a semi-empirical performance predictive model in Python script, formulating electrochemical equations specific for MCECs and deriving from experimental observations some characteristic kinetic parameters. At both electrodes, a mixed reaction-transport control mechanism was supposed, which required combining the Butler-Volmer equation with local material balances. In view of the used experimental setup, an isothermal operation with negligible pressure drops and gas crossover was considered.

Results: The MCEC nominal operation was evaluated at variable working conditions, underlining positive dependencies of the fuel electrode gas composition on both cathodic and anodic overpotentials. Indeed, H_2O and CO_2 can result in limiting reactants of the reduction process; moreover, their evolution can influence the carbonate ion migrating and oxidizing at the anode. On the left, Figure 1 reports the polarization resistances as a function of CO_2 volumetric fraction at the cathodic side. The temperature also favours the cell electrochemical kinetics but to a different extent depending on the gas feed. Looking at the durability test, at the fuel electrode there was a drastic increase of the resistance in the first 400 hours that was followed by a more gradual but continuous

increase up to the end of the test, as shown in Figure 1 on the right through the absolute Degradation Rate (DR) profile.

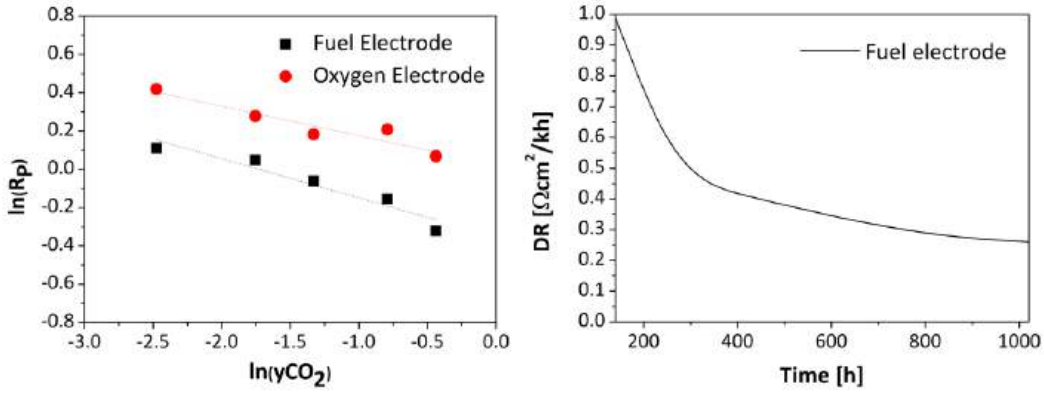


Figure 7: Polarization resistance dependences on CO_2 cathodic composition (left), absolute degradation rate of resistance measured at the fuel electrode (right).

Conclusions: A preliminary analysis of MCEC performance and durability was performed, underlining the influence of the fuel electrode on the whole cell behaviour. Testing resulted in an electrochemical characterization, measuring the voltage at each cell side. In parallel, a predictive semi-empirical model was developed and validated.

Acknowledgment

This research was partially funded by the European Union – NextGenerationEU from the Italian Ministry of Environment and Energy Security, POR H2 AdP MEES/ENEA with the involvement of the CNR and RSE, PNRR - Mission 2, Component 2, Investment 3.5 "Ricerca e sviluppo sull'idrogeno", CUP: I83C22001170006.

References

[1] L. Hu et al., 2015, J. Electrochem. Soc., 162, F1020 (DOI:10.1149/2.0491509jes).

[2] L. Hu et al., 2015, Faraday Discuss., 182, 493 (DOI:10.1039/c5fd00011d).

[3] L. Cardona et al., 2025, Electrochem. Commun., 179, 108023 (DOI:10.1016/j.elecom.2025.108023).

[4] S. Mataloni et al., 2025, J. Power Sources., 652, 237692 (DOI:10.1016/j.jpowsour.2025.237692).

[5] L. Hu et al., 2016, J. Phys. Chem. C., 120, 25, 13427–13433 (DOI:10.1021/acs.jpcc.6b04417).



Real-Time Electrolysis Stack Temperature Prediction Using Neural Networks for Industrial PLC Deployment

Mohsen Gharib*[a, b], Ralf Näke [a], Jakob Schöne [a], Gregor Herz [a], Andreas Richter [a, b]

* Corresponding author

[a] Fraunhofer Institute for Ceramic Technologies and Systems, Winterbergstr. 28, 01277 Dresden, Germany

[b] Institute of Energy Process Engineering and Chemical Engineering, TU Bergakademie Freiberg, Fuchsmühlenweg 9 D, 09599 Freiberg, Germany

Keywords: Electrolysis, Automation, Artificial intelligence, Digital twins

Abstract

Hydrogen is increasingly recognized as a key energy carrier for sustainable energy systems, while electrolysis is considered one of the most promising technologies for its production. This work develops real-time neural network models to dynamically predict the temperature of an electrolysis stack using experimental data from the Thallwitz (Germany) facility. Long short-term memory (LSTM) and feedforward neural networks were trained and validated using separate operational campaigns. The optimized model achieved high predictive accuracy and was implemented in programmable logic controller (PLC)-compatible structured text for real-time execution, demonstrating the feasibility of AI-based predictive monitoring for industrial electrolysis systems.

1. **Introduction** The efficient operation of electrolysis systems is challenging because conventional numerical models, such as Modelica simulations, are computationally intensive and difficult to apply in real-time [1, 2]. While machine learning has been used in different energy systems [3, 4], neural networks for real-time predictive monitoring of electrolysis stacks have not yet been demonstrated. This work addresses this gap by investigating neural networks to predict stack temperature in real-time. Moreover, a future comparison with OpenModelica-based modeling is planned as the next step to evaluate the trade-off between computational efficiency and predictive performance.
2. **Methodology** This study aimed to develop neural-network-based models for real-time temperature prediction of the electrolysis stacks. Initially, key input and output features were identified through a deep analysis of the experimental data. Subsequently, various neural network architectures, including LSTM and feedforward networks, were trained and evaluated using unseen datasets to assess their predictive capabilities. Finally, the optimized model was translated into a PLC-compatible format to evaluate its real-time performance in industrial control applications.

2.1 System definition To ensure model accuracy, we initially defined the system boundaries, selected relevant sensor signals, and specified target variables. Our study leveraged 46 days of operational data from an electrolysis stack in Thallwitz (Germany), comprising approximately 115 sensor signals. A simplified schematic of the stack (see Figure 1).

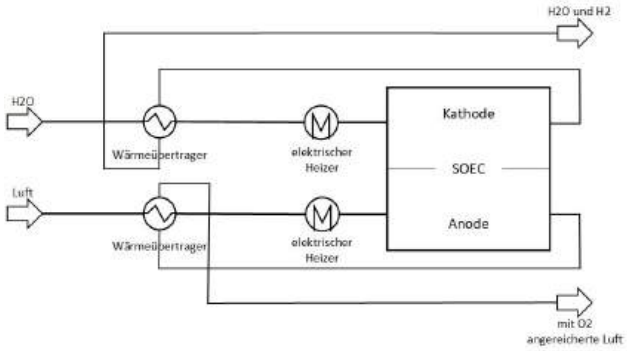


Figure 1: Schematic diagram of the stack system.

2.2 Model development and validation Secondly, we employed iterative hyperparameter tuning to develop the neural networks, thereby balancing predictive accuracy and operational feasibility. The selection of LSTM networks was motivated by their ability to capture temporal dynamics, whereas simpler feedforward networks were tested for lower computational cost, as shown in Table 1.

3. **Results** As shown in Table 1, the analysis of the predictions reveals that LSTM models outperform dense architectures in capturing the dynamic stack temperature behavior as evidenced by lower RMSE values. Specifically, Model 1 reproduces the overall temperature trend; however, increasing the number of neurons to 128 (Model 2) improves prediction accuracy as seen in Figure 2. In contrast, Model 3 (dense layers with 64-32 neurons) exhibits slower and less accurate dynamic responses, highlighting the limitations of feedforward architectures in modeling temporal dependencies. Furthermore, Model 4, which features the same architecture as Model 2 but with fewer input variables, performs worse than Model 2, underscoring the significance of carefully selecting input features.

Table 3: Overview of the best-performing models, including their layer types, number of neurons, and input feature configurations.

Model ID	Layers type	No. of neurons	RMSE (°C)
1	LSTM	64	6.93
2	LSTM	128	2.74
3	Dense	64,32	14.06
4	LSTM	128	7.5

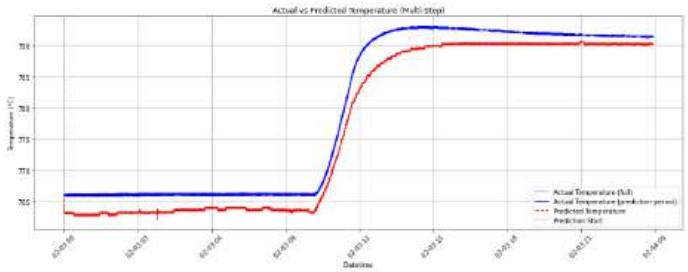


Figure 2: Model 2 (recursive prediction over a single operational day).

However, in addition to predictive accuracy, practical deployment was also investigated. The primary objective of this work was to successfully deploy the neural network model on a PLC. To achieve this, we exported the models' weights and biases from the training environment, translated them into structured text for PLC execution, and functionally validated them to ensure consistency with the offline models. Our findings indicate that LSTM networks are computationally demanding for real-time operation on current standard PLC hardware. In contrast, simpler dense-layer networks facilitate fast computations suitable for continuous predictive control. Therefore, the trade-off between accuracy and deployability must be carefully evaluated for each use case.

Conclusions

This work demonstrates the promising potential of neural network-based models for real-time monitoring of electrolysis systems. Notably, LSTM networks achieved the highest accuracy in predicting the dynamic stack temperature, whereas simpler feedforward networks offered faster computation times, making them suitable for implementation on PLCs. The successful translation and deployment of the trained models on a PLC confirmed the feasibility of integrating AI-based predictions into industrial automation systems.

Acknowledgment This research was supported by the Federal Ministry of Economic Affairs and Energy (03EWS001A).

References

[1] Yin, Ruilin, et al. "Modelica-based multiphysics modeling and multi-timescale dynamic analysis of a 100-kW alkaline water electrolysis system." *Renewable Energy* 253 (2025): 123620. https://doi.org/10.1016/j.renene.2025.123620

[2] Godoy, Vicente Olguín, et al. "An extendible component-based multiphysics model of a single alkaline water electrolysis cell." *International Journal of Hydrogen Energy* 177 (2025): 151399. https://doi.org/10.1016/j.ijhydene.2025.151399

[3] Parsa, Seyed Masoud. "Physics-informed machine learning meets renewable energy systems: A review of advances, challenges, guidelines, and future outlooks." *Applied Energy* 402 (2025): 126925. https://doi.org/10.1016/j.apenergy.2025.126925

[4] Li, Xin, et al. "Hybrid LSTM-heat transfer equation model for key parameter prediction in process industry." *Journal of Physics: Conference Series*. Vol. 3079. No. 1. IOP Publishing, 2025. 10.1088/1742-6596/3079/1/012028



Multi-Mode Electrochemical Transient Characterisation of SOC Short Stacks under Fuel-Flexible/Biogas Operating Conditions

Sadhana Golani*[a], Ute de Haart[a], Dominik Schäfer[a], Remzi Can Samsun[a], Rüdiger-A. Eichel[abc]

* corresponding author: s.golani@fz-juelich.de

[a] Institute of Energy Technologies, Fundamental Electrochemistry (IET-1), Forschungszentrum Jülich, D-52425 Jülich, Germany

[b] Institute of Physical Chemistry, RWTH Aachen University, D-52062 Aachen, Germany

[c] Faculty of Mechanical Engineering, RWTH Aachen University, D-52062 Aachen, Germany

Keywords: Biogas operation, Fuel cell and electrolysis, SOC short stacks, Transient electrochemical characterisation

Abstract

The transition to carbon-neutral energy systems underscores the need to advance solid oxide cell (SOC) technologies capable of fuel-flexible operation, including the use of carbon-containing fuels such as methane and biomass-derived biogas. Although the Jülich F10 short-stack platform demonstrates proven long-term stability, systematic comparisons across multiple operating modes—such as fuel cell, steam electrolysis, and co-electrolysis— investigations under carbon-containing fuel conditions remain limited. Such fuels introduce operational complexities including internal reforming, carbon deposition risks, impurity sensitivity, and localised thermal gradients, all of which influence electrochemical performance and degradation of cells, seals and contact layers.

To address this gap, a comprehensive multi-mode characterisation of a four-layer short-stack is presented under harmonised operating conditions, enabling direct cross-regime performance comparison. Advanced electrochemical impedance spectroscopy (EIS) coupled with distribution of relaxation times (DRT) analysis was employed to resolve mode-specific kinetic and transport contributions. A systematic test campaign was conducted in which fuel composition, cell voltage, and temperature distribution were continuously monitored. The stack exhibited stable voltage behaviour across all conditions, with a moderate but measurable thermal response upon methane addition. Multi-dimensional parameter maps were generated to correlate performance, efficiency, and stability across the operating envelope, identifying optimal utilisation strategies and studying this stack platform as a versatile system for both power generation and energy storage.

Introduction: SOCs are high-efficiency electrochemical devices capable of reversible operation as fuel cells and electrolysers. A key advantage of SOC is its ability to process carbon-containing rich mixtures via internal reforming, making SOC stacks attractive for integration in biogas and power-to-

fuel systems. However, introducing CH_4 and CO_2 into the fuel stream brings significant operational challenges, including carbon deposition, complex thermal management from competing exothermic and endothermic reforming reactions, and increased sensitivity to impurities. At the stack level, these challenges manifest as localised temperature gradients, shifts in electrochemical response, and accelerated degradation. Despite this, stack-level understanding across these modes remain comparatively sparse.

Objectives: To address this, a stepwise approach — progressing from OCV validation and IV characterisation through EIS, DRT analysis, and ECM fitting — across a structured sequence of operating conditions spanning FC, EL, and Co-EL modes at 700, 750, and 800°C. This combined methodology enables direct and consistent mechanistic comparison across all operating modes within a single experimental campaign, providing a unified framework for resolving mode-dependent loss mechanisms in a short stack with focus on Co-EL and biogas.

Experimental: A four-layer Jülich F10 short-stack (F1004-135) with an active area of approximately 80 cm^2 per layer was operated in counter-flow mode; detailed descriptions of the cell and stack design and assembly have been published elsewhere [1,2]. The stack was joined for 100 h at 850 °C, followed by reduction at 800 °C in an H_2/Ar mixture with stepwise increasing hydrogen concentration. Gas flows were regulated by calibrated mass-flow controllers, and stack temperature was monitored at nine positions (T1 – T9), with T5 (stack-centre temperature) serving as the reference. Individual cell voltages were continuously recorded throughout all operating conditions [3]. The performance and diagnosis of the SOC stack was primarily assessed using current-voltage (IV) measurements and EIS, acquired with an EIS system by Zahner Elektrik GmbH (Zennium Pro, PP211) [4].

Results: A continuous overview of stack operating parameters across the test campaign is presented in Figure 1. Cell voltages remained stable throughout all operating conditions, with no evidence of irreversible degradation upon fuel switching under OCV conditions. The transition to co-electrolysis mode produced a characteristic voltage step, consistent with the increased demand of simultaneous H_2O and CO_2 electrolysis. Upon methane addition, a measurable temperature decrease was recorded, consistent with dominant endothermic steam reforming of methane. The thermal response scaled with methane fraction, peaking under simulated biogas conditions (18% CH_4, 12% CO_2, 60% H_2O, 10% H_2) and remained stable without signs of instability. Despite these changes, cell voltages recovered and stabilised at each new operating point, ultimately returning to their initial values by the end of the experiment. Together, these results demonstrate the stack's tolerance to internal reforming conditions and its compatibility with biogas-analogue fuel compositions. Further electrochemical characterisation will be presented in detail at the conference.

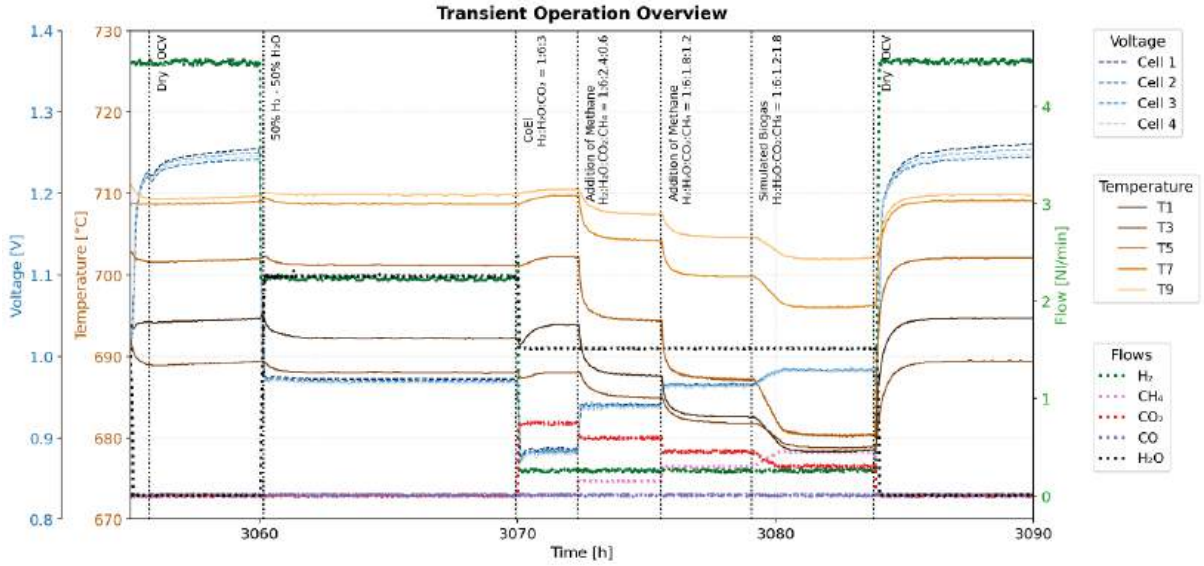


Figure 1: Evolution of cell voltages, stack temperature distribution, and gas flow rates at furnace temperature of 700°C.

Conclusions: The stack demonstrated stable electrochemical performance after only a short transient phase across a wide range of operating conditions, including Co-EL and simulated biogas. The temperature and voltage responses during fuel switching were clearly observed, highlighting the stack's suitability for flexible multi-fuel operation in biogas utilisation.

Acknowledgment: The authors thank all colleagues at Forschungszentrum Jülich GmbH who supported this work. This work was funded by the German Federal Ministry of Research, Technology and Space (BMFTR) within the project "PHOENIX – Launch Space Power-to-X" under the grant number 03SF0775A. Responsibility for the content of this publication lies with the authors.

References

1] N.H. Menzler, F. Tietz, S. Uhlenbruck, H.P. Buchkremer, D. Stöver, Journal of Materials Science. 45 (2010).

[2] L. Blum, S.M. Groß, J. Malzbender, U. Pabst, M. Peksen, R. Peters, I.C. Vinke, Journal of Power Sources. 196, 7175–7181 (2011).

[3] Q. Fang, L. Blum, P. Batfalsky, N. H. Menzler, U. Packbier and D. Stolten, International Journal of Hydrogen Energy, 38(36), 16344–16353 (2013).

[4] D. Schäfer, Q. Fang, L. Blum and D. Stolten, Journal of Power Sources, 433, 126666 (2019).



Biomass-assisted electrolysis using lignocellulosic feedstock to produce hydrogen

Umberto Calice[a,b], Francesco Zimbardi[a], Nadia Cerone[a], Vito Valerio[a]*

** corresponding author:* francesco.zimbardi@enea.it

[a] *ENEA, Dipartimento Tecnologie e Fonti Energetiche Rinnovabili, ss 106, 75026, Rotondella (MT), Italy*

[b] *Università degli studi della Basilicata, 85100 Potenza, Italy*

Keywords: Hydrogen, Biomass, Electrolysis

Abstract

Introduction: Biomass-assisted water electrolysis (BAE) is a sustainable and energy-efficient evolution of conventional water splitting technology. Traditional water electrolysis is often limited by its high operating voltages (>1.8 V) and significant energy consumption (approximately 4.8 kWh/Nm^3 H_2), which impact overall process efficiency. In contrast, BAE replaces the anodic oxygen evolution reaction with the oxidation of organic substrates. This fundamental shift allows for hydrogen generation at much lower cell voltages (≈0.6–0.7 V), effectively reducing the energy demand by up to three times compared to standard methods. The economic viability and efficiency of this process are further enhanced by the diversity of available feedstocks. Ethanol electrolysis, for instance, benefits from an established global supply chain and requires relatively low energy input (1.6–2.3 kWh/Nm3 H2) [1]. Glycerol, a common byproduct of biodiesel production, is another attractive option due to its high hydrogen selectivity and the generation of valuable oxidation co-products [2]. Lignocellulosic biomass stands out as perhaps the most promising source because of its vast abundance and renewable nature. Although its complex structure of cellulose, hemicellulose, and lignin requires pre-treatment to release fermentable sugars, it remains a highly scalable solution. With an estimated production cost of $2.50–$3.50/kg for H_2, it is increasingly competitive with green hydrogen produced via standard electrolysis.

Objectives: In this work, we propose a specific mediated electrochemical approach utilizing phosphomolybdic acid (PMA) for the valorization of lignocellulosic biomass and sideproducts of biorefining these feedstocks. This method couples low-voltage hydrogen generation with the degradation of complex organic matter, transforming raw feedstock into value-added chemicals while maintaining high energy efficiency.

Material and methods: The investigation considered a broad spectrum of lignocellulosic substrates, specifically selected to represent diverse industrial and agricultural waste streams. These included steam-exploded lignin, commercially sourced cellulose and hemicellulose, specialized cellulose

extracted from paper mill sludge, and finely pulverized hazelnut shells. By utilizing such a varied array of feedstocks, the study aimed to demonstrate the versatility of the electrochemical process across different chemical structures found in biomass. Each substrate underwent an oxidative pretreatment in an aqueous environment [3]. This primary stage utilized PMA as a high-efficiency redox mediator at 100 °C. During this thermochemical phase, the organic components of the biomass were oxidized, a reaction that occurred simultaneously with the chemical reduction of the PMA. This interaction is critical as it allows the chemical energy stored within the complex polymeric matrix of the biomass to be transferred to the mediator in the form of stored electrons.

Following the chemical pretreatment, the system transitioned to an electrochemical phase within a H-type electrolysis cell. The previously reduced mediator was introduced to the anodic compartment, where it underwent electrochemical re-oxidation at the electrode surface. Concurrently, at the cathodic interface, protons were reduced to facilitate the evolution of high-purity hydrogen gas. A defining characteristic of this catalytic system is that the phosphomolybdic acid functions as a true mediator, meaning it is not consumed during the reaction but is instead fully regenerated to its original state by the conclusion of the electrochemical cycle, allowing for continuous reuse. The entire integrated process was successfully demonstrated to function at a remarkably low cell potential of 0.7 V versus the Standard Hydrogen Electrode (SHE) at an ambient temperature of 25 °C. To confirm the structural transformation of the organic matter, the research employed advanced analytical techniques. The significant degradation of the biomass substrates following the oxidative pretreatment was verified using Gas Chromatography-Mass Spectrometry (GC-MS), which included specialized analyses following silylation to detect polar intermediates, alongside High-Performance Liquid Chromatography (HPLC) to determine the formation of soluble products. These methods provided a clear chemical fingerprint of the transition from complex polymers to simpler organic fragments. The quantification of the yields was further supported by bulk electrolysis experiments. These were corroborated by electrochemical measurements, including chronoamperometry and Linear Sweep Voltammetry (LSV), which determined the total charge exchanged during the reaction and the specific volume of hydrogen evolved. Furthermore, elemental analysis of the raw materials was conducted to establish a theoretical baseline for the maximum number of electrons available from the total oxidation of each unique substrate. By comparing these theoretical values with the experimental data, the oxidation efficiencies and electron transfer rates for each biomass type were calculated. All controlled electrolysis experiments were maintained at a constant potential of 0.7 V vs SHE.

Results: The energy profile of the system was obtained keeping constant the potential and, from this, an electrical energy consumption of 67 MJ/kg H_2 was calculated. This energy requirement is markedly lower than the demand of conventional water electrolysis systems, which typically operate at significantly higher potentials. This reduction in energy expenditure suggests that the PMA-mediated

approach could serve as a more economically competitive and environmentally sustainable pathway for the production of green hydrogen from renewable waste.

Conclusions: The comprehensive findings derived from this research investigation underscore that the application of PM as a catalytic mediator for the oxidative degradation of complex lignocellulosic structural matrices constitutes a highly sophisticated and advantageous strategy. This methodology is particularly effective because it integrates the high-value transformation of organic waste with the energy-efficient generation of hydrogen gas at remarkably low electrochemical potentials. By successfully coupling these two distinct chemical processes, the system overcomes many of the thermodynamic hurdles that typically affect conventional hydrogen production methods.

Acknowledgment

Work funded by the Italian Ministry of the Environment and Energy Security, program agreement MiTE_ENEA, PNRR - Hydrogen Research - Mission M2-C4 - Investment 3.5: Research and development on hydrogen.

References

[1] Caravaca, A.; Sapountzi, F. M.; de Lucas-Consuegra, A.; Molina-Mora, C.; Dorado, F.; Valverde, J. L. Electrochemical Reforming of Ethanol–Water Solutions for Pure H2 Production in a PEM Electrolysis Cell. Int. J. Hydrog. Energy 2012, 37 (12), 9504–9513. https://doi.org/10.1016/j.ijhydene.2012.03.062.

[2] Coproducing Value-Added Chemicals and Hydrogen with Electrocatalytic Glycerol Oxidation Technology: Experimental and Techno-Economic Investigations | ACS Sustainable Chemistry & Engineering. https://pubs.acs.org/doi/10.1021/acssuschemeng.7b00868 (accessed 2025-05-06).

[3] Electro-Reforming of Biomass Gasification Tar with Simultaneous Hydrogen Evolution, Calice at al., 2026, https://doi.org/10.3390/pr14030444



EIS-Based Diagnostic Algorithm for State-of-Health Assessment and Degradation Monitoring of SOEC systems

Valentino Frasci*[a], Pierpaolo Polverino[a], Bertrand Morel[b], Julien Manzi[b], Luka Žnidarič[c], Jan Pieter Ouweltjes[d], Cesare Pianese[a], Žiga Gradišar[c]

*Corresponding author: vfrasci@unisa.it

[a]Department of Industrial Engineering, University of Salerno, via Giovanni Paolo II 132, 84084, Fisciano (SA), ITALY.

[b]Univ. Grenoble Alpes – CEA/LITEN, 17 rue des Martyrs, F-38054 Grenoble, FRANCE.

[c]Jožef Stefan Institute, Jamova cesta 39, SI-1000 Ljubljana, SLOVENIA.

[d]SolydEra SA, Avenue des Sports 26, CH-1400, Yverdon-les-Bains, SWITZERLAND

Keywords: SOEC degradation; Prognostics and Health Management; Renewable Energy Storage; Electrochemical Impedance Spectroscopy.

Abstract

Introduction: The potential of hydrogen as an energy carrier, coupled with its production from Renewable Energy Sources (RES) via water electrolysis, makes Solid Oxide Electrolyzer Cell (SOEC) fundamental for energy transition [1]. However, their durability is limited by many complex chemical-physical phenomena. For instance, at the electrolyzer cathode side, comprising a porous cermet of nickel and yttria-doped zirconia, nickel oxidation reduces Triple Phase Boundary (TPB) and hinders mass transport [2]. Moreover, the electrolyte can be affected by, e.g., reduced ionic conductivity, due to the formation of insulating layers, and delamination, which can lead to material fractures [3]. These issues can be mitigated by applying diagnostic algorithms to assess components State-of-Health (SoH), enabling suitable control logics to extend the SOEC Remaining Useful Life (RUL). One of the techniques that has recently been applied for on-board monitoring and diagnostics is Electrochemical Impedance Spectroscopy (EIS), which consists of a complex measure of system response to current/voltage stimuli in frequency, enhancing the extraction of significant information on occurring physical phenomena inside the cell, through which it is possible to monitor the overall SoH [4].

Objectives: The aim of this work is to develop an on-board diagnostic algorithm that extracts key information from EIS measurements, such as the evolution of Area Specific Resistance (ASR), performed during long-term tests under different operating conditions. In this way, real-time useful indicators can be provided for evaluating SOEC durability and estimating its RUL under relevant operation.

Material and methods: The experimental data used for training and validation of the diagnostic algorithm have been acquired on reversible six-cell SOEC stack during a 900 h experimental campaign [5], alternating between nominal (NC - 750 °C and 10/90 H_2/H_2O ratio) and faulty conditions: low temperature (LT - 725°C or 690°C), hydrogen inlet starvation (HS - up to 0/100 fuel ratio) and high steam conversion (HSC - reducing total H_2/H_2O inlet keeping 10/90 ratio). To monitor the evolution of the system, EIS measurements have been performed every two hours, for each individual cell. The data have then been processed using a patented algorithm [6, 7] for the automatic identification of the parameters of an Equivalent Circuit Model (ECM). This approach made it possible to overcome the intrinsic limitations of traditional fitting algorithms, ensuring greater robustness and statistical consistency. From the extracted parameters, the ASR is determined as the sum of three distinct resistance contributions: the ohmic resistance (R_Ω), the high-frequency activation resistance (R_{act}) and the low-frequency diffusion resistance (R_{diff}).

Results: Initial NC observations showed an activation period with improved electrical conductivity across all cells, attributed to optimized electrode-interconnect interfaces. Controlled stress scenarios produced distinct electrochemical signatures, which allowed the isolation of specific degradation mechanisms. During the LT tests, R_Ω and R_{diff} increased due to the reduced electrode and electrolyte conductivities.

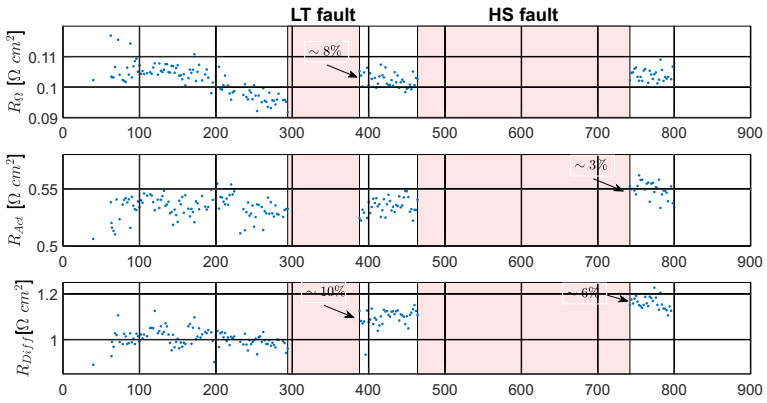


Figure 8: Trends of SOEC cell 1 resistances under nominal condition before and after induce LT and HS faults.

After the LT fault (about 400 hours), the returning to NC revealed electrode delamination, permanently increasing R_Ω and R_{diff} of about 8% and 10%, respectively (Figure 1). HS tests showed no immediate resistance changes; however, subsequent degradation (compatible with Ni oxides formation) triggered by the hydrogen starvation reduced the amount of active triple-phase boundaries and obstructed pores (possibly due to volume expansion caused by the nickel oxidation), increasing R_{act} (3%) and R_{diff} (6%).

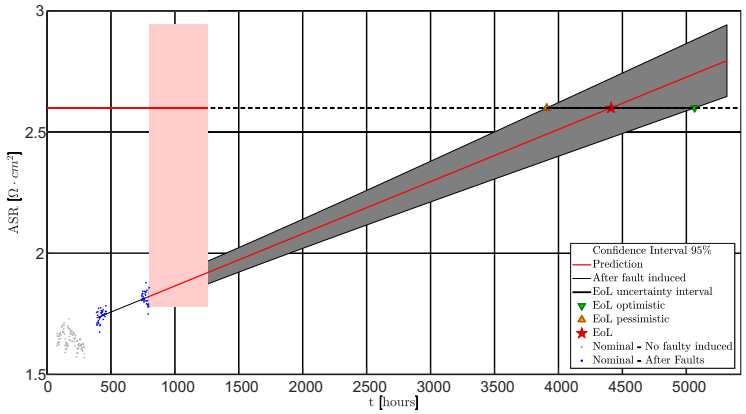


Figure 9: Degradation estimated assuming an ASR EoL value increased by 50%, compared to its initial conditions.

Conversely, HSC tests critically increased R_{diff}, which is ascribed to mass transport issues. Figure 2 shows the predicted ASR of SOEC cell 1 with a 95% confidence interval, assuming nominal operation until End of Life (EoL) and keeping the same constant degradation trend. Assuming an EoL being 50% increased ASR value, the estimated RUL of the cell is 3600 h, with an average deviation of ±600 h.

Conclusions: The proposed EIS-based diagnostic framework was capable of assessing SOEC RUL by leveraging information from periodic EIS measurements, by accurately tracking internal resistances under various faulty conditions. The robust parameters identification algorithm proved highly effectiveness in correlating physical changes to overall performance losses. Ultimately, this methodology provides a reliable tool for predicting stack RUL, enabling the application of real-time control strategies to improve SOEC durability.

Acknowledgment: Part of the presented results have been carried out within the framework of the REACTT project, which have received fundings from the Fuel Cells and Hydrogen 2 Joint Undertaking (now Clean Hydrogen Partnership) under Grant Agreements No 101007175. This Joint Undertaking receives support from the European Union's Horizon 2020 Research and Innovation programme, Hydrogen Europe and Hydrogen Europe Research.

References

[1] Chen et al., Energy Mater. 2025, 5, 500045. DOI: 10.20517/energymater.2024.144.
[2] Cheng et al., J. Power Sources 569 (2023) 232991. DOI: 10.1016/j.jpowsour.2023.232991.
[3] Moçoteguy et al., Int. J. Hydrogen Energy 38(36) (2013) 15887-15902. DOI: 10.1016/j.ijhydene.2013.09.045.
[4] Gallo et al., Applied Energy 279 (2020) 115718. DOI: 10.1016/j.apenergy.2020.115718.
[5] EU Project REACTT, web-page: https://www.reactt-project.eu/.
[6] Petrone et al., European Patent EP3215832A1, WO WO/2016/071801.
[7] On-line web tool for ECM parameters extraction. Link: https://minervas.app/eis/.



Galvanic Pulse-Plating of iridium-ruthenium-alloys as catalyst for PEM water electrolysis

J.Näther*[a], F.Köster[a], R.Muntean, K. Bouzek[c], M. Prokop[c], J.Hüttl[d]

* corresponding author: J.Näther

[a] University of Applied Sciences, Mittweida

[b] Politehnica University, Timisoara

[c] University of Chemistry and Technology, Prague

[d] Fraunhofer IFAM, Dresden

Keywords: iridium plating, PEM-Anode, pulse-plating, ruthenium plating

Short Abstract

This work summarizes the results of pulse plating for the direct loading of PTL (catalystcoated electrode) with iridium/ruthenium catalysts for OER. The focus is on the influence of electrolyte and the parameter set on the alloy composition of the catalyst.

Introduction: One cornerstone for achieving a sustainable energy economy will be the development of efficient and competitive storage systems. Green hydrogen represents a versatile energy carrier that can be used as an alternative fuel or reducing agent in the production of green steel. Polymer Electrolyte Membrane water electrolysis (PEMWE) is already a suitable tool to produce pure hydrogen as energy storage. The paper describes the optimization of different components of existing systems in order to enable the implementation of a cost-effective and sustainable production process, however it is focused on the pulse plating process to decorate the electrodes with catalyst.

Objectives: The main challenge in advancing acidic water electrolysis is to improve the anode, i.e. the oxygen electrode. Due to the slow reaction kinetics, the oxygen evolution reaction (OER) is the limiting partial reaction in the splitting of water into hydrogen and oxygen. This issue is addressed by using noble metal catalysts with high activity for the OER such as iridium or ruthenium. In addition to the catalytic properties, the corrosion resistance of the materials used is also decisive for the longevity of the electrolyzers. The acidic process media and the high anodic potentials make the use of noble metals mandatory. In our approach, the use of precious metals at the anode is to be reduced by improving the catalyst application. The distribution of the catalyst on the surfaces is the key factor in generating a lower electrode loading without compromising performance. Pulse plating technology is used to generate nanoscale iridium particles on the electrodes.

Material and methods: Porous titanium electrodes with a geometric surface of 4cm^2 were fabricated by IFAM in Dresden. The process involves the production of a paper preform with a high filler content (titanium), followed by a debinding process in which the cellulose is completely oxidized, and a

second step for sintering the titanium particles. Reference [1] gives further details of the electrode preparation process. The titanium electrodes were etched in concentrated hydrochloric acid and subsequently exposed to a cathodic potential in 2M sulfuric acid. This pretreatment removes the titanium oxide layer, and the formation of titanium hydrides also prevents the reformation of the oxide layer upon contact with oxygen. The formation of the titanium hydrides is describes in reference [2].

The porous titanium electrodes were loaded with a catalyst using galvanic pulse deposition. The process requires the use of an electrolyte in which both metals are present as complex-bound ions. First, two base electrolytes, such as those used for the monometallic deposition of both metals, were prepared. The ruthenium electrolyte is based on the nitride-bridge complex [3]. To prepare 0.5 liters of base electrolyte, 100 g of sulfamic acid was first adjusted to a pH of 6 using ammonia. Next, ruthenium chloride (0.25 mol metal content) was added, and the solution was boiled under reflux at 100°C for 6 hours. The insoluble residue was filtered off, and the solution was made up to 500mL. The iridium electrolyte is based on the hexabromoiridate complex. To prepare the iridium bulk electrolyte, 0.078 mmol/L sodium hexabromoiridate(III) is dissolved in deionized water along with 100 mmol/L oxalic acid, and the pH is adjusted to 1.8 using sulfuric acid.
For pulse deposition, the two electrolytes were mixed in different ion ratio of $c_{Ru}/(c_{Ir}+c_{Ru})$ and the main process parameters temperature, pH and metal ion concentration and ratio were investigated. A Gamry Interface1001 was used as power source in a three-electrode-setup with Ag/AgCl-reference, inert iridium/ruthenium mixed-oxide anode as counter and the titanium electrodes as working electrodes. Pulse current densities, pulse times and pulse pauses were varied and the influence on the alloy composition investigated. The deposited particles were analyzed using X-ray fluorescence (XRF) and energy-dispersive X-ray spectroscopy (EDX) to determine their chemical composition, and with scanning electron microscopy (SEM) to examine their surface topography and catalyst distribution.

Results: An ion metal ratio of $c_{Ru}/(c_{Ir}+c_{Ru})$ of 2:1 gave good results and a stable process over several experiments. Pulse deposition improved the current efficiency and the distribution of particles on the electrode surface. Figure 1 gives an example of isolated catalyst particles on the titanium surface. The phase analysis showed that a mixed crystal would be deposited. However, by varying the pulse durations, it was also possible to deposit separate iridium and ruthenium phases. First experiments in corrosion testing, catalytic activity for OER and single cell testing showed promising results. However, some experiments have yet to be conducted, and the analysis of all the data is currently in progress.

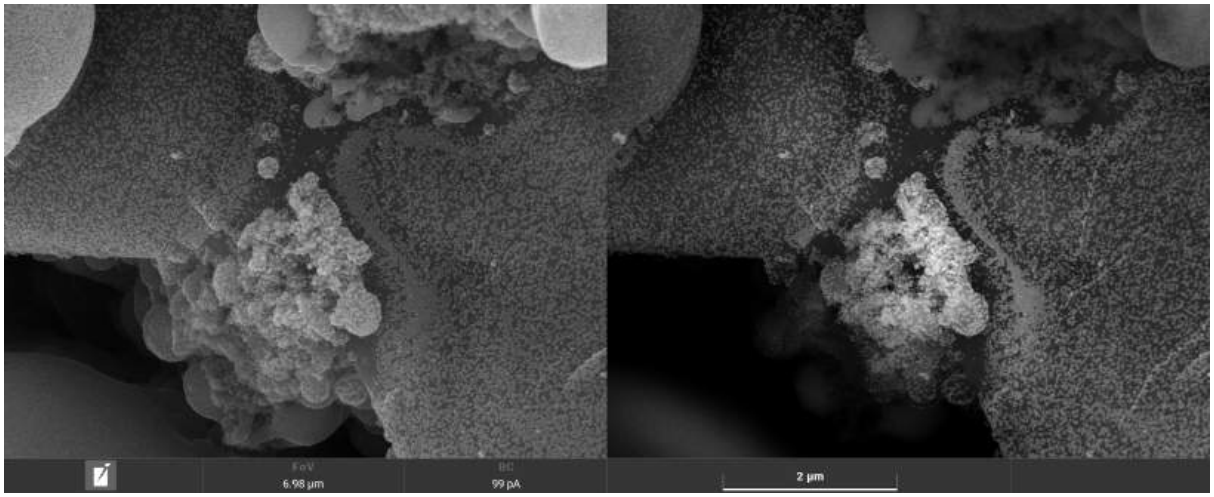


Figure 1 Backscattered electron imaging and secondary electron imaging after deposition

Conclusions: The electrochemical approach of reducing catalytic active metal ions directly on the surface of the porous transport layer can be further improved by the usage of pulse plating. Selecting appropriate parameters allows for an improvement in cathodic current efficiency during the process and enhances the distribution of catalyst particles on the PTL. Furthermore, this is a highly scalable process that could reduce the cost of manufacturing PEM electrolysers.

Acknowledgment: This publication was supported by the project “Development of a Cost-effective anode for PEM water electrolysis” by M-Eranet-program grant number 100687668 and SAB.

References

[1] Andersen, Olaf, et al. "Development of sintered porous titanium paper for electrochemical applications." *European Powder Metallurgy Congress and Exhibition, Euro PM 2018*. 2020.

[2] Bystron, T., Vesely, M., Paidar, M., Papakonstantinou, G., Sundmacher, K., Bensmann, B., ... & Bouzek, K. (2018). Enhancing PEM water electrolysis efficiency by reducing the extent of Ti gas diffusion layer passivation. *Journal of Applied Electrochemistry*, *48*(6), 713-723.

[3] Hydes, P. C. (1980). Electrodeposited ruthenium as an electrical contact material. *Platinum Metals Review*, *24*(2), 50-55.

[4] Böhm, L., Näther, J., Underberg, M., Kazamer, N., Holtkotte, L., Rost, U., ... & Köster, F. (2021). Pulsed electrodeposition of iridium catalyst nanoparticles on titanium suboxide supports for application in PEM electrolysis. *Materials Today: Proceedings*, *45*, 4254-4259.



Design and Validation of Machine Learning-based Prognostic Algorithm for SOEC durability prediction

Alessandro Rinaldi[a], Valentino Frasci[a], Pierpaolo Polverino [*a], Bertrand Morel[b], Julien Manzi[b], Luka Žnidarič[c], Jan Pieter Ouweltjes[d], Cesare Pianese[a], Žiga Gradišar[c]

*Corresponding author: ppolverino@unisa.it

[a] Department of Industrial Engineering, University of Salerno, via Giovanni Paolo II 132, 84084, Fisciano (SA), ITALY.

[b]Univ. Grenoble Alpes – CEA/LITEN, 17 rue des Martyrs, F-38054 Grenoble, FRANCE.

[c]Jožef Stefan Institute, Jamova cesta 39, SI-1000 Ljubljana, SLOVENIA.

[d]SolydEra SA, Avenue des Sports 26, CH-1400, Yverdon-les-Bains, SWITZERLAND

Keywords: SOEC degradation; Prognostics and Health Management; Renewable Energy Storage; Electrochemical Impedance Spectroscopy.

Abstract

Introduction: In the current global energy transition, green hydrogen produced through electrolysis is a promising energy carrier for decarbonization, as it can also be coupled with Renewable Energy Sources (RES) [1]. RES use, e.g., solar and wind energy, introduces operational challenges related to fluctuations and the high unpredictability of electricity availability [2]. To compensate for the mismatch between production and demand, hydrogen serves as an excellent storage means. Among the technologies available in the industrial framework, Solid Oxide Electrolyzer Cells (SOECs) offer a valid solution in terms of efficiency and reliability [3]. However, to enable large-scale deployment, it is necessary to characterize and predict components degradation and fault rates [4].

Objectives: This work aims at developing and validating advanced prognostic algorithms based on Artificial Neural Network (ANN) models to predict the evolution of SOEC stack degradation phenomena and provide highly accurate estimation of the Remaining Useful Life (RUL). The proposed approach aims to overcome the intrinsic limitations of traditional deterministic models, subject to high computational burdens in attempting to capture in real-time the complex non-linearities that govern degradation [5]. Another goal is to predict when the stack will reach an operational status that may be highly inefficient or near to failure, which would be fundamental for design and application of preventive maintenance.

Material and methods: Experimental data have been acquired on a 70-cells SOEC stack during a test campaign conducted at the CEA research center, within the framework of the EU-funded project REACTT [6]. The experimental phase lasted for a total of 1200 hours of uninterrupted operation, and the data (i.e., pressures, temperatures, flow rates, current and voltages) have been acquired using sensors with a sampling frequency of 1 Hz. The data have initially been pre-treated through filtering and standardization, and then divided into three datasets for training, test and validation, respectively. The Nonlinear Autoregressive with Exogenous input (NARX) model has been used for modeling the stack voltage. Afterwards, a Physics-Informed Neural Networks (PINN) has been designed to correct voltage increase prediction over time, taking into account both previous voltage behavior and more detailed information provided by Electrochemical Impedance Spectroscopy (EIS) measurements. Specifically, features from an Equivalent Circuit Model (ECM) are periodically identified upon EIS through a patented algorithm [7], and their trends are used to update the PINN prediction.

Results: The obtained results demonstrate the high accuracy and robustness of the developed predictive algorithms. As shown in Figure 1, the model correctly replicates the trend of the experimental voltage data, as evidenced by the 90 % and 95 % confidence intervals.

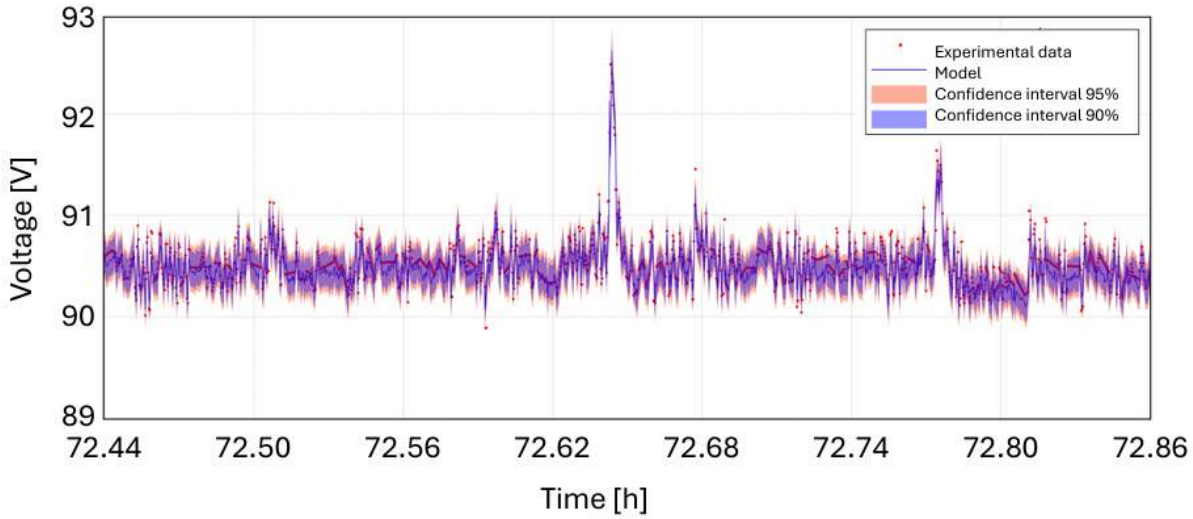


Figure 10: Close up of experimental and modeled stack voltage trends, with 90 % and 95 % of confidence interval.

The algorithm has subsequently been used to predict the stack voltage increase up to its End-of-Life (EoL) criterion. Figure 2 illustrates the projection of the degradation trend over an extended time horizon: at the prediction onset (vertical blue line), the model estimates the progressive increase in stack voltage until it intersects with the predefined critical EoL threshold, which has been assumed to be equal to a 10% increase in voltage compared to that of the stack at the Beginning of Life (BoL). The analysis shows that after approximately 8340 hours of continuous operation under nominal conditions, the stack reaches its critical EoL value, within a range of ±1800 hours (evaluated as the time interval between first and last point above EoL line).

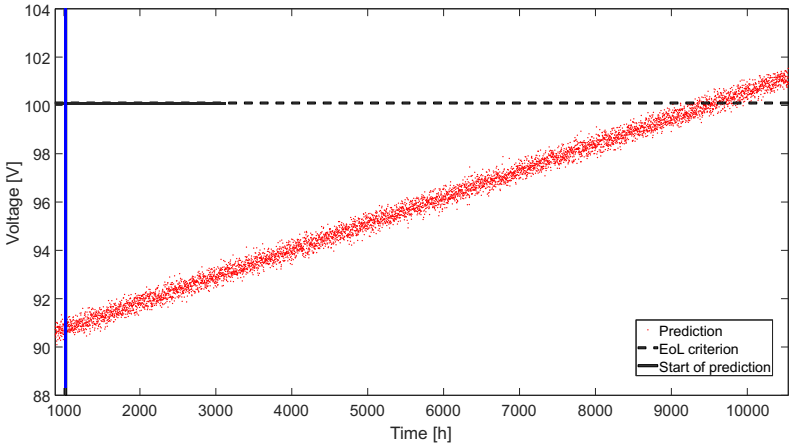


Figure 11: RUL prediction under nominal operating conditions.

Finally, the algorithm's flexibility allows it to be used to simulate alternative operational scenarios: by varying the input setpoints of the model is possible to dynamically recalculate the RUL to assess the impact of different operating conditions.

Conclusions: This methodology gives the final model a high degree of predictive robustness and significantly improves the generalization capacity of the entire system towards abnormal or unexplored operating conditions during the training phase. Overall, the good performance of the algorithm demonstrates that the synergy between the data driven approach and physical constrains provides a robust predictive solution, laying a solid foundation for on-board monitoring and the extension of the lifecycle of industrial SOEC systems.

Acknowledgment: Part of the presented results have been carried out within the framework of the REACTT project, which have received fundings from the Fuel Cells and Hydrogen 2 Joint Undertaking (now Clean Hydrogen Partnership) under Grant Agreements No 101007175. This Joint Undertaking receives support from the European Union's Horizon 2020 Research and Innovation programme, Hydrogen Europe and Hydrogen Europe Research.

References

[1] Du et al., Sustainability 2024, 16(11), 4602. DOI:10.3390/su16114602.
[2] Cosgrove et al., Renewable Energy 211 (2023) 299-307. DOI: 10.1016/j.renene.2023.04.135.
[3] Chen et al., Energy Mater. 2025, 5, 500045. DOI: 10.20517/energymater.2024.144.
[4] Moçoteguy et al., Int. J. Hydrogen Energy 38(36) (2013) 15887-15902. DOI: 10.1016/j.ijhydene.2013.09.045.
[5] Loyola-Gonzalez, IEEE Access 7(1):154096-154113. DOI: 10.1109/ACCESS.2019.2949286.
[6] EU Project REACTT, web-page: https://www.reactt-project.eu/.
[7] Petrone et al., European Patent EP3215832A1, WO WO/2016/071801.

EFCH2 2026 European Fuel Cells and Hydrogen PIERO LUNGHI CONFERENCE
September 15th-17th 2026 Capri / Italy

Development of Performance Factor Analysis Method for Steam Electrolysis by SOEC

Takumi Imabayashi*[a], Takayuki Ozeki[a], Koichi Asano[a], Yoshihiro Mugikura[a]

* corresponding author: imabayashi3814@criepi.denken.or.jp

[a] Central Research Institute of Electric Power Industry (CRIEPI), Kanagawa, Japan.

Keywords: Performance analysis, Overvoltage, SOEC, Steam electrolysis

Abstract: Performance factor analysis method for Solid Oxide Electrolysis Cells (SOECs) was developed by extending a method originally established for Solid Oxide Fuel Cells (SOFCs). The method separates the cell voltage in SOEC mode into open-circuit voltage, internal resistance drop, fuel electrode overvoltage, oxygen electrode overvoltage, and Nernst loss. In this study, a planar single cell was used to determine the applicable range of the method and the parameters required for the method. Based on these examinations, performance factor analysis showed good agreement with experimental data and high accuracy, thereby confirming the validity of this method.

Introduction: Solid Oxide Electrolysis Cells (SOECs) in steam electrolysis can produce hydrogen from steam using electric power at high temperatures. SOECs can achieve lower electrolysis voltages and higher efficiencies compared to other electrolysis technologies. However, the durability of SOEC is insufficient for practical application of SOEC systems. It is necessary to analyze performance factors and degradation factors of SOEC to improve SOEC lifetime. However, quantitative separation of performance factors under practical operating conditions remains challenging.

CRIEPI (Central Research Institute of Electric Power Industry) has developed the original performance evaluation method for SOFC and evaluated many types of SOFC cell stacks by manufacturers in Japan for many years [1, 2]. In this study, the performance analysis method for SOFC has been modified to apply as a performance analysis method for SOEC.

Objectives: A performance factor analysis method for separating overvoltages in SOEC has been developed and validated using a single SOEC cell.

Material and methods: Performance Analysis Method for Steam Electrolysis by SOEC

The cell voltage (V) in SOEC mode can be divided as shown in Eq.(1) into the open-circuit voltage (E, OCV) , internal resistance (IR) drop (η_{ir}), fuel electrode overvoltage (η_{f}), oxygen electrode overvoltage (η_{o}), and Nernst loss (η_{ne}). When the current–voltage (IV) characteristics of the SOEC have an approximately linear relationship, it can be assumed that the cell voltage in SOEC mode can be expressed as Eq. (2). E was calculated based on the Nernst equation shown in Eq. (3), and η_{ir} was determined from experimentally measured values obtained by AC impedance measurements. The fuel reaction resistance and oxygen reaction resistance are expressed by Eqs. (4) and (5), respectively.

The optimal fitting parameters were estimated based on Eqs. (1)–(5). Performance factor analysis was conducted by considering not only the gas flow direction within the cell plane but also the distributions of gas partial pressures and current density under the assumption of equipotential conditions within the cell plane.

$$V = E + \eta_{ne} + \eta_f + \eta_o + \eta_{ir} \quad (1)$$

$$\cong E + \eta_{ne} + (R_f + R_o + R_{ir}) \times J \quad (2)$$

$$E = E^\circ + RT/2F \times \ln\left(P_{H2} \times {P_{O2}}^{0.5} / P_{H2O}\right) \quad (3)$$

$$R_f = f_0 \times {P_{H2}}^{\alpha} \times {P_{H2O}}^{\beta} \quad (4)$$

$$R_o = o_0 \times {P_{O2}}^{\gamma} \quad (5)$$

R_f, R_o: fuel reaction resistance, oxygen reaction resistance [Ω*cm^2],

R_{ir}: internal resistance [Ω*cm^2], J: current density [A/cm^2] ,

E°: standard electromotive force [V], R : gas constant [J/(mol*K)] , T: temperature [K],

F: Faraday constant [C/mol], f_0, o_0: fitting parameters,

α, β, γ: gas partial pressure exponents specific to the cell

Experiments

The tests in this study were conducted by using a planar type of single cell supported by fuel electrode. The cell includes the gas manifold and end separator, same as a stack. This cell was manufactured by MORIMURA SOFC TECHNOLOGY CO., LTD.

Results:

IV Characteristic

The IV characteristic of SOEC under steam electrolysis condition is shown in Fig. 1. A good linear relationship between current density and cell voltage was observed, and the linear fitting showed good agreement with the experimental data. This result supports the assumption of linearity used in the proposed performance factor analysis method and defines the applicable range of the analysis.

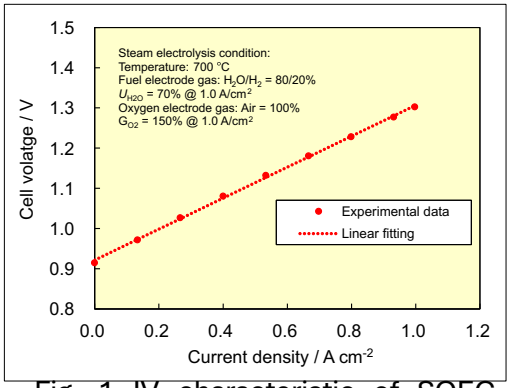


Fig .1 IV characteristic of SOEC under steam electrolysis condition

Gas Partial Pressure Dependence of Fuel and Oxygen Electrode Overvoltages

The gas partial pressure exponents α, β, and γ in Eqs. (4) and (5) must be determined experimentally by analyzing the dependence of electrode overvoltages on gas composition for each cell specification. To determine these exponents, electrode overvoltages were measured while varying the gas partial

pressures. In this analysis, the partial pressures of O_2 at the oxygen electrode, and H_2 and H_2O at the fuel electrode, were varied independently. The overvoltage changes corresponding to variations in O_2 partial pressure at the oxygen electrode, as well as H_2 and H_2O partial pressures at the fuel electrode, were obtained, and the gas partial pressure exponents were determined accordingly.

Performance Factor Analysis

For the performance factor analysis, cell voltages were measured under more than ten different conditions with varying gas compositions and utilizations. A convergence calculation was performed to minimize the error between the experimentally measured cell voltages and those estimated by the performance factor analysis. As a result, the calculated and measured cell voltages were in good agreement, confirming the validity of the performance factor analysis.

The analysis can clarify the dominant performance degradation factors under different operating conditions. This method is useful for investigating degradation factors and guiding strategies for durability improvement.

Conclusions: A performance factor analysis method for SOEC was established by extending a SOFC evaluation approach. The method enables quantitative separation of overvoltage contributions with high accuracy. Experimental validation using a planar single cell demonstrated good agreement between calculated and measured results. This method provides a practical tool for investigating degradation factors and improving SOEC durability.

Acknowledgment

This work is based on results obtained from project, JPNP25002, commissioned by the New Energy and Industrial Technology Development Organization (NEDO).

References

[1] T. Yamamoto et al., *ECS Trans*., **25** (2) 499-508 (2009).

[2] A. Id et al., *ECS Trans*., **103**(1), 1955-1961 (2021).



Techno-Environmental Assessment of Industrial-Scale AEM Electrolysis: The Ansaldo Green Tech case

Vera D'Oriano [a], Stefano Carrozzo [a], Giorgio Orsenigo [a], Valentina Mastronardi [a]

Valeria Tacchino [b], Michela Gallo [c], Adriana Del Borghi [c]

* corresponding author: Vera.Doriano@ansaldoenergia.com

[a] Ansaldo Green Tech, 16152 Genova, Italy

[b] Tetis Institute Srl, Via Zara 33A, 16145 Genova, Italy

[c] Department of Civil, Chemical and Environmental Engineering (DICCA), University of Genoa, Via O. Pia 15, 16145 Genova, Italy

Keywords: AEM Electrolyzer, Green hydrogen, Techno-environmental analysis, LCA

Abstract

Introduction

The rapid growth of Anion Exchange Membrane (AEM) technology in recent years is establishing it as one of the most promising solutions for green hydrogen production, primarily due to its reliance on earth-abundant and cost-effective materials compared to conventional alkaline and Proton Exchange Membrane (PEM) electrolyzers, while maintaining high performance [1]. In this framework, Ansaldo Green Tech (AGT) has successfully entered the market with an industrial-scale 1 MW AEM electrolyzer and is currently advancing the development of multi-MW systems, aimed at accelerating the decarbonization of hard-to-abate industrial sectors. To this end, AGT and Tetis Institute have performed a comprehensive techno-environmental assessment of the 1 MW electrolyzer. The technical evaluation integrates experimental data from laboratory test benches and high-fidelity performance prediction software, while the environmental impact is assessed through a Life Cycle Assessment (LCA) methodology, compliant with ISO 14040-44 international standards [2-3].

Objectives

The present study aims to assess the techno-environmental performance of the AGT 1MW AEM electrolyzer, accounting for a 25-year operational lifetime in a photovoltaic (PV)-coupled configuration. The work focuses on quantifying key technical and environmental indicators identified through an extensive review of international standards [2-5] and scientific literature [6-13], thereby providing a comprehensive overview of the system's viability for large-scale applications. The

technical analysis focuses on stack electrochemical and electrical efficiencies, electrolyzer specific energy consumption and durability, and hydrogen purity. Concurrently, the environmental assessment encompasses a comprehensive set of impact categories, including climate change, resource and water depletion, acidification, eutrophication, and toxicity levels, as well as cumulative energy demand from both renewable and non-renewable sources.

Material and methods

The subject of the study is the AGT 1MW AEM electrolyzer, which comprises the electrochemical stack and the associated Balance of Plant (BoP). A dedicated Excel-based toolbox was developed to harmonize technical and environmental datasets, facilitating a streamlined assessment of the system's performance. Technical performance parameters were calculated using Ebsilon Professional (v.16.0), with the stack's electrochemical behavior calibrated via experimental data from a dedicated test bench campaign. Concurrently, the environmental profile was quantified via LCA using SimaPro (v.10.2), utilizing the Ecoinvent database (v.3.11) for secondary data. To account for site-specific conditions and the configuration of the coupled power plant, a Matlab-based tool was employed to model the stack's operational duty cycle. Finally, these multi-source datasets were integrated within the Excel toolbox to compute the final techno-environmental indicators over the system's operational lifetime.

Results

Preliminary technical and environmental results for the 1 MW AGT electrolyzer coupled with a 4 MW PV plant located in Sicily (Italy) are shown in Table 1. The environmental impact was evaluated using a Functional Unit (FU) of 1 kg of produced hydrogen. The assessment accounts for the entire life cycle of the materials involved, specifically quantifying the Global Warming Potential (GWP), resource depletion, and waste generation. Furthermore, the model incorporates the impacts related to the end-of-life stage, specifically focusing on recycling processes for key stack and BoP components. Preliminary results demonstrate that while PV coupling ensures low carbon operations, the overall environmental footprint, not shown in the table, is dominated by the embodied impacts of stack materials and manufacturing.

Table 1. Preliminary technical and environmental performance indicators

Specific energy consumption (Full Load)	Hydrogen production (Full Load)	Hydrogen purity	Lifetime	GWP total
55 kWh/kgH_2	21 kgH_2/h	99.9%	25 years	4,11 kgCO_{2eq}/kgH_2

Conclusions

The integrated toolbox facilitates a proactive eco-design approach, enabling the optimization of AEM electrolyzer configurations to balance technical efficiency with life-cycle environmental sustainability. This methodology establishes a rigorous framework for the design of sustainable hydrogen systems, effectively bridging technical innovation and efficiency with global decarbonization mandates.

Acknowledgments

This work was funded by the European Union – NextGenerationEU (PNRR-M2C2I5.2), under the IPCEI project "Turnkey electrochemical plants for H2 production".

References

[1] Son, Y.J., et al. (2025) Technology Landscape of Anion Exchange Membrane Water Electrolyzers: Where Are We Today? *ACS Energy Letters,* 10 (7).

[2] ISO 14040:2006 - Environmental management - Life cycle assessment - Principles and framework

[3] ISO 14044:2006 - Environmental management - Life cycle assessment - Requirements and guidelines

[4] ILCD Handbook: General guide for Life Cycle Assessment - Detailed guidance

[5] IPHE, 2023, Methodology for Determining the Greenhouse Gas Emissions Associated With the Production of Hydrogen

[6] Mustapha, F., Guilbert, D., & Gross, B. (2025). Advancements in anion exchange membrane electrolysers: from catalysts to life cycle assessment. *International Journal of Sustainable Energy*, *44*(1)

[7] Pawłowski, A., Żelazna, A., Żak, J. Is the Polish Solar-to-Hydrogen Pathway Green? A Carbon Footprint of AEM Electrolysis Hydrogen Based on an LCA. Energies2023,16, 3702

[8] Schropp, E., Campos-Carriedo, F., Iribarren, D., Naumann, G., Bernäcker, C., Gaderer, M., & Dufour, J. (2024). Environmental and material criticality assessment of hydrogen production via anion exchange membrane electrolysis. Applied Energy, 356, 122247

[9] Shaya, N., Glöser-Chahoud, S. A Review of Life Cycle Assessment (LCA) Studies for Hydrogen Production Technologies through Water Electrolysis: Recent Advances. Energies2024,17, 3968

[10] Wei X., Sharma S., Waeber A., Wen D., Nuggehalli Sampathkumar S., Margni M., Maréchal F., Van herle J., Comparative life cycle analysis of electrolyzer technologies for hydrogen production: Manufacturing and operations, Joule, Volume 8, Issue12, 2024, Pages 3347-3372, ISSN 2542-4351

[11] Ajeeb W., Neto R. C., Baptista P., Life cycle assessment of green hydrogen production through electrolysis: A literature review, Sustainable Energy Technologies and Assessments, Volume 69, 2024, 103923, ISSN 2213-1388

[12] Hassan Q., Zuhair Sameen A., Salman H.M., Jaszczur M., Large-scale green hydrogen production via alkaline water electrolysis using solar and wind energy, International Journal of Hydrogen Energy, Volume 48, Issue 88, 2023, Pages 34299-34315, ISSN 0360-3199

[13] Lee S.A., Kim J., Kwon K. C., Park S.H., Jang H. W., Anion exchange membrane water electrolysis for sustainable large-scale hydrogen production, Carbon Neutralization, Volume 1, Issue 1, June 2022, Pages 26-48



Development of an intensified gasification process for H2-rich syngas production

D. Barisano*[a], F. Nanna[a], A. Villone[a], F. Pietramale[a, b], E. Catizzone[b], M. Migliori[b], S. S. Salman Zadeh Otaghsaraei[a, c], F. Basile[c], A. Fasolini[c], K. Gallucci[d], A. Di Carlo[d], A. A. Papa[d]

* corresponding author: Donatella Barisano, donatella.barisano@enea.it

[a] Centro Ricerche ENEA Trisaia, SS Jonica 106, km 419+500, 75026 Rotondella (MT), ITALY; [b] Università della Calabria, Dipartimento di Ingegneria dell'Ambiente (DIAm), Via P. Bucci - Cubo 44, 87036 Arcavacata di Rende (CS), Italy; [c] Alma Mater Studiorum Bologna, Dipartimento di Chimica Industriale "Toso Montanari", via Bignardi 13, 40129 Bologna, Italy; [d] Università de L'Aquila, Dipartimento di Ingegneria industriale e dell'informazione e di economia, Piazzale Pontieri, 1 Monteluco di Roio, 67100 L'Aquila, Italy

Keywords: Bioenergy, Biohydrogen, Biomass Gasification, Syngas

Abstract

The objective of the work was to study and develop an intensified gasification process to produce biohydrogen from a wide range of residual biomass and biogenic waste fractions. To this purpose, implementations aimed at reducing the contaminant load in the producer gas and enriching the endogenous hydrogen were considered. Both primary (*in-bed*) and secondary (*downstream*) gas upgrading methods, respectively using catalysts and CO_2 sorbents (of low commercial value), were therefore studied. Through collaboration with the Universities of Calabria, L'Aquila, and Bologna, materials specifically tailored to enhance catalytic activity and improve the yield and quality of the producer gas were prepared, characterized, and tested. A bench-scale gasification prototype to integrate the identified innovations and improve process performance was then designed and built.

Introduction: The current situation of international instability provides a new starting point to revive interest and highlight the importance of locally available renewable energy sources. Among these, bioenergy can play a key role, and R&D activities on advanced thermochemical conversion processes offer encouraging prospects for contributing to the goals of the energy transition roadmaps for 2030 and 2050. The gasification of residual biomass feedstocks is widely recognized as one of the most versatile thermochemical processes for their conversion into energy carriers. By producing a gaseous fuel, the process is suitable for use in CHP applications as well as to produce advanced liquid and

gaseous biofuels, including hydrogen. The purpose of the work presented here was to develop a high-efficiency, N_2-free gasification process for the production of a high-quality gas, i.e., low contaminant content (both organic and inorganic) and a high H_2 content (> 50 v-%), suitable for producing bioH_2, as well as advanced energy carriers, such as SNG, MeOH, and Fischer-Tropsch biofuels (e.g. jet fuels, diesel and gasoline).

Objectives: The overall objective of this R&D activity was to study and develop an intensified and scalable gasification process to produce a H2-rich syngas from a wide range of residual biomass and biogenic waste fractions. To this end, considering the fluidized bed gasification technology as the most promising for scalability, main efforts were addressed on the development of advanced materials for *in-bed* gas upgrading and conditioning and on its further refinement downstream. Concordantly, an advanced gasification reactor was designed and realized to test the implementations under fluid dynamic process conditions. An integrated approach, the development of tailored materials, and a gasification prototyping unit are the key features that distinguish this work. Together, these represent the innovative aspects that contribute to advancing the state of the art in the field.

Material and methods: Materials for *in-bed* applications were prepared starting from natural dolomite by calcination and wet impregnation with K_2CO_3 and Fe for enhancing the CO_2 capture capacity and integrate the catalytic effect on the reaction of WGS, respectively. Regarding the materials for downstream use, MgAl-based layered double oxides were used as support for Ni nanoparticles in the presence of other elements (e.g., Co, La). These oxides were synthesized from layered double hydroxides (LDHs) through co-precipitation and subsequently calcined to obtain layered double oxides (LDOs). The above-mentioned materials were prepared in collaboration with University of Calabria, University of L'Aquila and University of Bologna and characterized by using several analytical techniques (e.g. XRD, SEM, EDX, TPR, TGA, BET, Raman spectroscopy). A bench scale facility available at the ENEA-Trisaia Research Center for temperature tests (550÷850 °C) with relevant gas mixture and real syngas was then used for performance screening evaluation. To implement and evaluate the efficacy of the *in-bed* integrated solutions, an advanced gasification reactor combining the stage of gasification with bed materials regeneration was designed and realized in collaboration with University of L'Aquila.

Results: The impregnation of calcined dolomite with K_2CO_3, up to 20 %-wt, resulted in a material with a higher CO_2 capture capacity at higher temperatures than just calcined dolomite. This finding supports the goal of producing materials capable of capturing CO_2 at temperatures exceeding 650 °C, which can then be more effectively integrated with a gasification process typically operating operates

at around 800–850 °C. Iron-enriched calcined dolomite has demonstrated the potential to combine the catalytic activity of Fe toward the WGS reaction with CO_2 capture to produce an H_2 enrichment of over 50 %-v. Among the Ni/MgAl-LDO catalysts, the $Ni_{24}Mg_{56}Al_{20}$ catalyst exhibited good performance and stability after operation with real syngas containing residual organic and inorganic contaminants (CH_4 conversion of 70 % to 62%). Superior overall performance was achieved by adding lanthanum to the material formulation, resulting in a higher and more stable CH_4 conversion than $Ni_{24}Mg_{56}Al_{20}$, i.e. 84% to 77% after operation with real syngas containing residual contaminants.

Conclusions: The activities carried out identified materials for the H_2-enrichment of producer gas from gasification in fluidized bed reactors. For the purposes of the project, the most promising materials for *in-bed* application were found to be dolomite impregnated with 20% (w/w) K_2CO_3 and dolomite enriched with 5% (w/w) iron. For downstream gas upgrading, the activities identified $Ni_9Mg_{64}Al_{26}La_1$ as the material with the best and most stable performance for the reforming of CH_4 present in real syngas, i.e., in the presence of residual organic and inorganic contaminants typical of gasification. Further useful information is expected from the operation of the prototype gasification reactor coupled to the regenerator. The testing will allow for the evaluation of material and process performance under fluid dynamic operating conditions.

Acknowledgment

The research here presented was funded by the European Union – NextGeneration EU from the Italian Ministry of Environment and Energy Security PORH2 AdP MASE/ENEA with involvement of CNR and RSE, PNRR - Mission 2, Component 2, Investment 3.5, Research Operational Plan “Research and development of technologies for the hydrogen supply chain”.

References

[1] Intensified biomass gasification with in-situ enhanced CO2-sorbents for hydrogen production. D. Barisano, F. Nanna, A. Villone, F. Ferrante, A. Di Giuliano, V. Paolucci, K. Gallucci. 32nd European Biomass Conference and Exhibition (EUBCE). 24 - 27 June 2024, Marseille, France.

[2] Study and development of O2/steam gasification in fluidized bed reactor for H2-rich syngas production. D. Barisano, F. Nanna, A. Villone, F. Pietramale, E. Catizzone, S. S. Salman Zadeh Otaghsaraei, F. Basile, K. Gallucci, A. Di Carlo. 33rd European Biomass Conference and Exhibition (EUBCE). 9 - 12 June 2025, Valencia, Spain.

[3] Biomass and biogenic fraction gasification in fluidized bed reactor for H2-rich syngas production. 5th International Symposium on Biomass/Wastes Energy and Environment (BEE). Xi'an, China, September 12-14, 2025.



Thermo-Assisted Non-Thermal Plasma Methane Cracking: Prototype Development and First Experimental Insights for CO_2-Free Hydrogen Production

R. Agostini, O. Corigliano, A. Blasi, N. Lisi, U. P. Laverdura, S. Del Gobbo,

*F. Zimbardi, N. Cerone**

** corresponding author: nadia.cerone@enea.it*

[a] *ENEA, Dipartimento Tecnologie e Fonti Energetiche Rinnovabili, ss 106, 75026, Rotondella (MT), Italy*

Keywords: Hydrogen, Plasma, Methane, Pyrolysis

Abstract: This work investigates a novel thermo-assisted non-thermal plasma (NTP) reactor for methane cracking toward CO_2-free hydrogen production. The objective is to experimentally assess its technical and energy performance. An ad hoc prototype, based on independently controlled AC/DC power supplies, graphitic electrodes, and sub-atmospheric operation, is engineered and instrumented for systematic testing. Experimental campaigns investigate the effects of electrical power, pressure, residence time, and gas composition. Preliminary evaluations indicate CH_4 conversions > 60% and H_2 yields of 45–70%, together with the co-production of structured carbonaceous materials, providing the basis for future reactor optimization and scale-up.

Introduction: Methane pyrolysis enables the direct decomposition into hydrogen and carbon, $CH_4 \rightarrow C(s) + 2H_2$, avoiding carbon dioxide formation, thus eliminating the need for carbon capture and storage. Notably, this process lead to the formation of graphite, carbon black and other functional carbon structures. In this context, NTP cracking introduces mechanisms for CH_4 dissociation by leveraging appropriately generated energetic electrons. These electrons promote the subsequent decomposition of CH_4 into long hydrocarbon chains (C_xH_y), following a pathway from CH_4 to C_2H_2 to C_2H_4 and ultimately to H_2 and C. Unlike conventional processes, such as thermocatalytic systems, where CH_4 decomposition is limited by the high activation energy for C–H bond cleavage [1], NTP combine thermionic electron emission and non-equilibrium electrons acceleration. This enhances CH_4 activation and dissociation, combining thermal and plasma effects. Discharge configuration strongly influences electron energy distribution, reaction kinetics, hydrogen production, and carbon (C) formation pathways [2].

Objectives: This work investigates a novel NTP plasma reactor for CH_4 cracking toward CO_2-free H_2 production, which was properly designed, engineered and setup. The focus is to elucidate the interactions between thermionic emission, plasma electro-physics, and CH_4 decomposition kinetics under controlled plasma conditions, H_2 yield and formation of the carbon structure.

Material and methods: The prototype was conceived with a hybrid configuration that exploits thermionic generation through filament superheating, along with a 'plasma' electrode whose role is to generate the electric field that accelerates electron collision energy. The configuration is therefore designed to exploit both thermal effects (due to filament heating) and plasma effects (glow plasma) for CH_4 dissociation. The reactor is based on independently controlled AC/DC power supplies, AC graphitic electrode, DC electrode, and sub-atmospheric operation, designed and built for systematic testing. The proposed architecture is presented in Figure 12, where side (a) shows the test station along with its ancillary components for testing, while side (b) illustrates the electrode configurations. In this setup, the bottom electrode is responsible for thermionic electron generation and emission, the upper electrode is associated with the generation of the electric field, which serves to accelerate the electrons

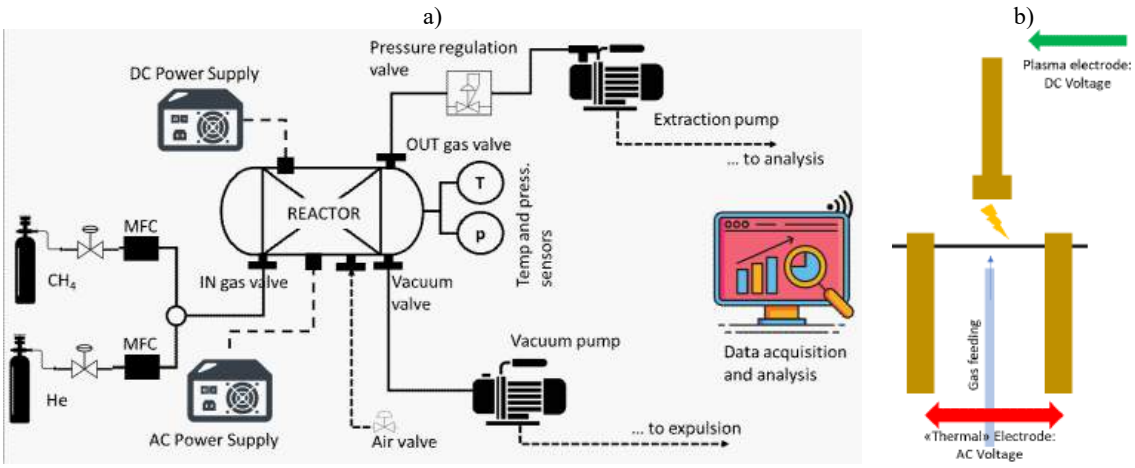


Figure 12. Plasma system at ENEA: test rig a), electrodes configurations b).

The reactor comprises a liquid-cooled stainless-steel chamber with a dedicated Carbon collection section and optical access. Advanced real-time diagnostics, including optical emission spectroscopy, thermal monitoring, and gas analysis, enable direct correlation between plasma characteristics, CH_4 dissociation and H_2 production. Operating at a nominal power of 4.5 kW, with CH_4 and He (the latter as a tracer gas) flow rates up to 1000 sccm and pressures between 0.1 and 1 bar, the system provides a flexible platform to investigate key parameters like, H_2 yield, C_xH_y (mainly acetylene and ethylene) selectivity, CH_4 conversion and specific energy input.

Results: Preliminary results indicate CH_4 conversions > 60% and H_2 yields of 45–75%, together with the co-production of structured carbonaceous materials. Recent studies on plasma-assisted methane cracking report CH_4 conversions ranging 20-70% and H2 yields/selectivities of 40-80%, depending on plasma configuration, power input, pressure, and feed composition [1,2]. Tungsten and graphitic filaments are mutually changed and tested. The results indicate that a smaller filament diameter allows for lower electric current management, thereby reducing electricity costs. Regarding the material, the tungsten filament experiences excessive mechanical deformation during heating, posing a risk of subsequent breakage during processing. In contrast, the graphitic filament proves to be mechanically rigid and generally more stable. During the process, carbon growth increases its cross-sectional area, implying a consequently higher AC electric current draw, experiencing the difficulty for keeping stable and plasma-assisted cracking conditions. Favourable conditions are achieved at 100 torr, a CH_4 flowrate of 150 sccm, and filament temperatures above 2000 °C. Plasma stability is maintained through real-time tuning of the DC power supply, balancing carbon deposition on the filament and limiting electric arc formation. Downstream, Raman spectroscopy analyses indicate the formation of graphitic turbostructures, with the probable presence of nanostructured carbon.

Conclusions: This work demonstrated the feasibility of NTP for CH_4 cracking. Preliminary results showed competitive CH_4 conversions and H_2 yields, together with the formation of valuable carbonaceous materials. These findings provide a solid basis for further optimization of reactor design, plasma stabilization strategies, operating conditions, and overall process performance, supporting future scale-up and technological development.

Acknowledgment

Work funded by the Italian Ministry of the Environment and Energy Security, program agreement MiTE_ENEA, PNRR - Hydrogen Research - Mission M2-C4 - Investment 3.5: Research and development on hydrogen.

References

[1] Frusteri et al., H2 production by methane decomposition: Catalytic and technological aspects, Int J Hydrogen Energy, 2012, 37, 21, pp. 16367-16374, https://doi.org/10.1016/j.ijhydene.2012.02.192

[2] Chen et al., Plasma induced methane conversion: a review on COx-free production of hydrogen, valuable chemicals, and functional carbon materials, EES Catal., 2026, 4, 31, https://doi.org/10.1039/D5EY00054H



Physical Vapor Deposition of thin layers for proton-conducting solid oxide electrolysis cells

Emanuele De Bona *[a], Sandro Zorzi [a], Matteo Bordin [a] Fabio Torazzi [a,b], Vincenzo M. Sglavo [b], Matteo Testi [a]

* Corresponding author: edebona@efbk.eu

[a] Centre of Sustainable Energy, Fondazione Bruno Kessler, Via Sommarive 18, 38123, Trento, Italy

[b] Department of Industrial Engineering, University of Trento, Via Sommarive 9, 38123, Trento, Italy

Keywords: Ceramic Processing, Green Hydrogen, Physical Vapor Deposition, Proton-conducting Solid Oxide Electrolysis Cells

Abstract: The present work reports on the application of Physical Vapor Deposition (PVD) in the production of proton-conducting solid oxide electrolysis cells (P-SOECs). PVD shows promising potential for the realization of non-supporting dense layers, allowing versatile tuning of their chemical composition and precise thickness control. In this work, PVD was used to replace screen printing in the addition of a diffusion barrier layer between the P-SOEC electrodes and electrolyte, with the goal of reducing the overall critical raw material consumption without affecting the cell performance. The barrier layer produced by PVD was 13x thinner than screen printed analogues, resulting in a significant material saving, while preserving the desired microstructure, chemical composition, and barrier effectiveness.

Introduction: Hydrogen is currently considered one of the most promising energy carriers due to its ability to store, transport, and generate green energy. In such context, increasing interest is being devoted to water electrolysis as an alternative to fossil fuels, that still represent the main source of H_2 production. Solid oxide electrolysis cells (SOECs) constitute a fundamental technology in this perspective [1], due to their capacity to work at high temperatures (700–800 °C) therefore increasing the power-to-hydrogen efficiency and lowering the clean H_2 production cost [2].

SOECs are constituted of three main ceramic components: two porous electrodes (anode and cathode), and a dense gas-tight ion-conductive electrolyte. Additionally, a diffusion barrier layer must be applied between the electrolyte and the electrodes to avoid chemical reactions and element interdiffusion during operation. This barrier layer must ideally be chemically inert towards both electrode chemical compositions while allowing ions diffusion (i.e., without hampering the electrochemical performance).

In recent years, Physical Vapor Deposition (PVD) techniques are growing in popularity in SOEC processing thanks to their extreme control on the deposited thin film characteristics, such as density, chemical composition, and crystalline phase [3]. Several authors reported the feasibility of PVD for replacing cell components otherwise produced by wet techniques (screen printing and tape casting) without affecting the cell performance and durability [4–6]. This allowed minimizing the material waste thanks to the absence of the traditional losses associated with wet processing as well as the reduced thickness of the layers needed to fulfil the electrochemical task in the cell assembly.

Objectives: The scope of our research work revolves around the use of PVD for the realization of barrier layers in proton-conducting SOECs (P-SOECs). Our aim is to achieve durable and reliable barrier layers resulting in cell performances comparable to that of state-of-the-art analogues produced by wet processing. This would pave the way to the substitution of wet processing with PVD in the preparation of all the cell non-supporting layers, enhancing the SOEC production process sustainability.

Material and methods: The P-SOECs produced in this work are constituted of:

- supporting $BaZr_{0.8}Y_{0.2}O_{3-\delta}$ (BZY) electrolyte produced by tape casting and sintered at 1650 °C for 2 h in air
- gadolinium-doped Ceria (GDC) barrier layer deposited by PVD at room temperature for 4 h under 90 W in Ar atmosphere
- symmetric $Sr_2Fe_{1.5}Mo_{0.5}O_{6-\delta}$ (SFM) electrodes deposited by screen printing and sintered at 1250 °C for 1 h in air

The integrity and phase composition of the cells was evaluated by SEM, EDX, and XRD. The barrier layer effectiveness is currently being tested in dedicated thermal treatments representative of operative conditions (750 °C in wet air and N_2-H_2). The ingrowth of structural flaws (delamination, cracks) or chemical impurities (secondary phases, elemental migration/interdiffusion) will be assessed by post-mortem SEM, EDS, and XRD characterization. Cells containing the best performing PVD barrier layers will then be tested electrochemically (polarization curves, EIS, durability) and compared to the state-of-the-art.

Results: Figure 1 shows the physico-chemical characterization of the preliminary cell prototypes including a GDC barrier layer. EDS linescan confirms the successful deposition of GDC by PVD (Figure 1-B, bottom), with a reduction of 13x of the layer thickness as compared to screen printing (Figure 1-A, top).

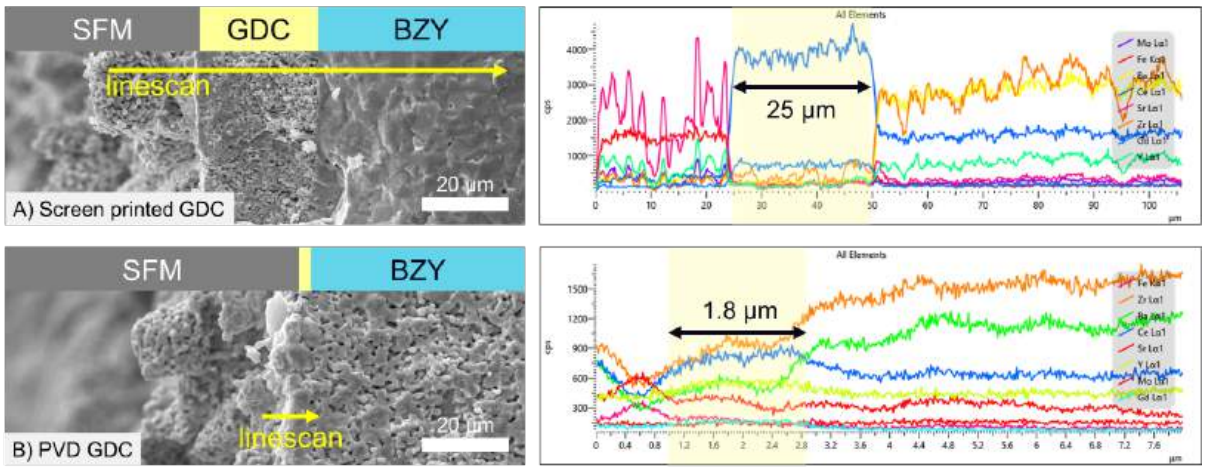


Figure 1: microstructure (SEM images) and elemental distribution (EDS linescan) of two cells with GDC barrier layer deposited by screen printing (A, top) and PVD (B, bottom).

Initial results showed promising stability of the PVD barriers layer under operative conditions (simulated by thermal treatments). Absence of delamination cracks and second phases formation were verified by SEM-EDS after 50 h at 750 °C in static air. At the moment of writing, longer tests (up to 500 h) under wet (3 % steam) air and forming gas (N_2 – 5 % H_2) are ongoing to evaluate the PVD barrier layer long-term durability.

Conclusions: PVD showed promising initial results for replacing screen printing for the preparation of thin ceramic layers for SOEC production. Cells with integrated PVD GDC barrier layer exhibit comparable microstructure as compared to analogues produced by wet processing while significantly reducing the use of critical raw materials. Long-term thermal treatments and electrochemical characterization will validate the durability and performance of PVD cells against state-of-the-art SOECs.

Acknowledgment

H2@TN is funded by the University of Trento (Piano Strategico 2022-2027) and Provincia Autonoma di Trento (Delibera della Giunta Provinciale 2166 – 25/11/2022).

References

[1] Q. Wang, S. Ricote and M. Chen, Electrochimica Acta, 446 (2023) 142101.

[2] M. B. Hanif, S. Rauf, Z. U. Abadeen, K. Khan, Z. Tayyab, S. Qayyum, M. Mosiałek, Z. Shao, C.-X. Li and M. Motola, Matter, 6 (2023) 1782–1830

[3] G. Chasta, Himanshu and M. S. Dhaka, Int. J. Energy Res., 46 (2022) 14627–14658.

[4] F. Buzi, K. Kreka, J. Santiso, L. Rapenne, Z. Sha, J. O. Douglas, F. Chiabrera, A. Morata, M. Burriel, S. Skinner, L. Bernadet, F. Baiutti and A. Tarancón, ACS Appl. Mater. Interfaces, 16 (2024) 43462–43473.

[5] F. Liang, J. Yang, Y. Zhao, Y. Zhou, Z. Yan, J. He, Q. Yuan, J. Wu, P. Liu, Z. Zhong and M. Han, Int. J. Hydrog. Energy, 47 (2022) 36926–36952.

[6] L. Bernadet, F. Buzi, F. Baiutti, J. Segura-Ruiz, J. Dolado, D. Montinaro, M. Torrell, A. Morata and A. Tarancón, APL Energy, 1 (2023) 036101.



Performance-degradation oriented multiphysics 0D/3D numerical framework for PEMWE's digital twin applications

Raffaele Iossa*[a], Piergiovanni Domenighini[a]

*corresponding author: raffaele.iossa@rse-web.it

[a] RSE – Ricerca sul Sistema Energetico S.p.A.

Keywords: degradation analysis, Digital Twin, multiphysics simulation, proton exchange membrane water electrolysis

Abstract

Introduction: PEMWEs (proton exchange membrane water electrolyzers) currently represent the most mature technology for green hydrogen production, due to their commercial level (TRL > 8), high efficiency (up to 85%), high current density (up to 2 A/m^2), compact design, and rapid dynamic response (around 3 minutes to ramping up to full power), which make them well suited for coupling with RES (renewable energy sources) [1]. However, in these conditions, PEMWEs rarely operate under steady-state regime. Instead, they are subjected to intermittent operating profiles characterized by rapid load fluctuations, frequent start–stop cycles, and variable current densities caused by RES variability [2]. In this context, the DT (Digital Twin) concept [3] for PEMWEs applications is widely explored inside the scientific literature. The core is represented by DT's numerical framework where the combination of multiphysics models and numerical approaches together with the historic data acquired by the sensors is aimed at maximizing the efficiency, fault detection, and analysing degradation mechanisms. Despite their promising capabilities, the effectiveness of DTs mostly relies on accurate and computationally efficient models capable of capturing not only the instantaneous performance of the electrolyzer but also predicting the degradation rate of the single components over time, as function of the real-time working parameters.

Objectives: The aim of this work is to develop a multiphysics numerical framework for PEMWEs operating under dynamic conditions, as a first step toward the implementation of a full DT. The proposed framework integrates a 0D multiphysics model, based on the approach proposed in [4], with a high-fidelity 3D CFD-electrochemical model developed in OpenFOAM, based on openFuelCell2 framework [5]. The 0D model is aimed at identifying the optimal operating conditions capable of maximizing system efficiency under both steady and transient operating conditions, while the 3D one is aimed at modelling the PEMWE's stack, analyzing the distribution of the flows inside the channels, the electrode's distribution of electric density, and the temperature gradient inside each cell, as the main precursors of components degradation mechanisms.

Material and methods: The **Figure 13** shows the schematic flow of the developed PEMWE's numerical framework. The steps outside the red dotted square are performed once in a lifetime,

requiring geometric and material properties of the cells' components; the steps inside are continuously performed during PEMWE's operation requiring measured data from sensors, providing analysis and optimized data back to the physical system

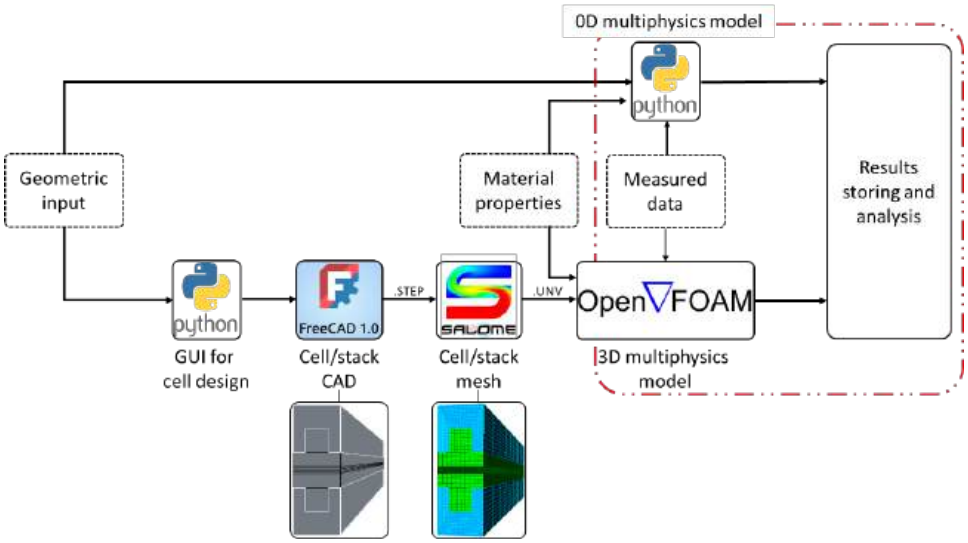


Figure 13 Numerical framework of PEMWE's DT

Once the geometric parameters of the PEMWE's stack/cell are provided through the "*Geometric input"* block, the information are shared with both 0D and 3D model lines. However, on the 3D model line, an in-house script automatically converts the geometric information in a .STEP CAD file, through the FreeCAD software. The meshing phase is then conducted through Salome Mesh software, which .UNV file is used for the 3D multiphysics simulation in OpenFOAM. Due to the significantly lower computational cost of the 0D approach compared to the 3D simulations, the framework combines fast system-level predictions with detailed local multiphysics analyses.

Results: The developed multiphysics numerical framework was tested on the experimental steady state regime data reported in [6], which results are shown in

Figure 14. The 0D model showed good agreement with experimental polarization data, accurately reproducing the global electrochemical performance of the real electrolyzer. At the same time, the 3D CFD-electrochemical simulations provide detailed local information on hydrogen/water flow distributions, temperature gradients, and current density non-uniformities within the cell, highlighting the main operating regions potentially associated with accelerated degradation phenomena.

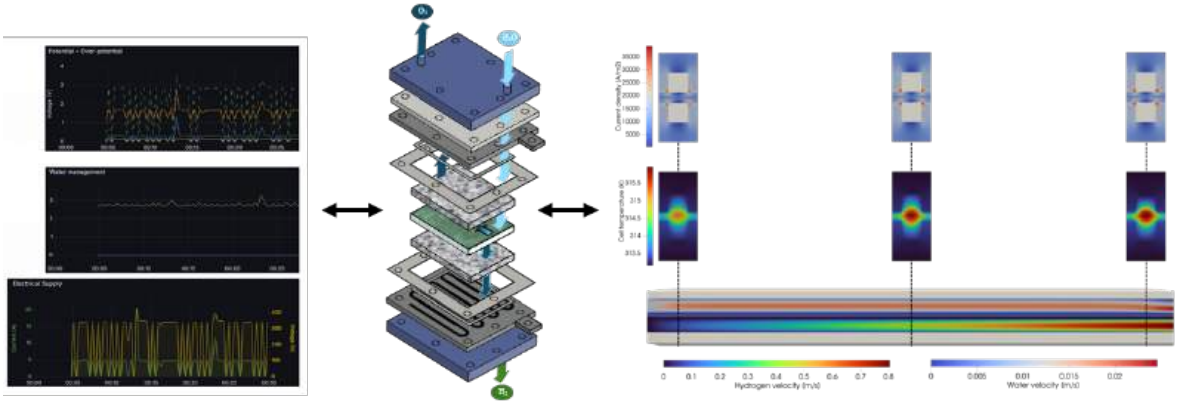


Figure 14 On the left: perfomance curves obtained by 0D model; on the right: 3D multiphysics model results. From the bottom: hydrogen and water velocity [m/s], cell temperature [K], and current density [A/m^2]

Conclusions: A multiphysics 0D/3D numerical framework for PEMWEs operating under dynamic conditions was developed as a first step toward a full Digital Twin implementation. The proposed approach enables both fast system-level analyses and detailed local investigation phenomena, potentially identifying accelerated component degradation. The obtained results demonstrate the potential of the framework for future real-time Digital Twin applications focused on performance optimization and lifetime-oriented PEMWE operation.

Acknowledgment Research activities carried out in the context of the national recovery and resilience plan (pnrr) - mission 2 - component 2 - investment 3.5 "research and development on hydrogen", funded by the european union - next generation eu, and performed in implementation of the operative research program (por) approved by the ministry of ecological transition on 06.27.2022

Funded by the European Union NextGenerationEU

References

[1] C. R. Wang *et al.*, 'Proton Exchange Membrane (PEM) Water Electrolysis: Cell-Level Considerations for Gigawatt-Scale Deployment', *Chem. Rev.*, vol. 125, no. 3, pp. 1257–1302, Feb. 2025, doi: 10.1021/acs.chemrev.3c00904.

[2] B. Endrődi, C. A. Trapp, I. Szén, I. Bakos, M. Lukovics, and C. Janáky, 'Challenges and Opportunities of the Dynamic Operation of PEM Water Electrolyzers', *Energies*, vol. 18, no. 9, Apr. 2025, doi: 10.3390/en18092154.

[3] S. Boschert and R. Rosen, 'Digital Twin—The Simulation Aspect', in *Mechatronic Futures: Challenges and Solutions for Mechatronic Systems and their Designers*, P. Hehenberger and D. Bradley, Eds, Cham: Springer International Publishing, 2016, pp. 59–74. doi: 10.1007/978-3-319-32156-1_5.

[4] Z. Abdin, C. J. Webb, and E. MacA. Gray, 'Modelling and simulation of a proton exchange membrane (PEM) electrolyser cell', *International Journal of Hydrogen Energy*, vol. 40, no. 39, pp. 13243–13257, Oct. 2015, doi: 10.1016/j.ijhydene.2015.07.129.

[5] S. Zhang, S. Hess, H. Marschall, U. Reimer, S. Beale, and W. Lehnert, 'openFuelCell2: A new computational tool for fuel cells, electrolyzers, and other electrochemical devices and processes', *Computer Physics Communications*, vol. 298, p. 109092, May 2024, doi: 10.1016/j.cpc.2024.109092.

[6] Y. Xu, G. Zhang, L. Wu, Z. Bao, B. Zu, and K. Jiao, 'A 3-D multiphase model of proton exchange membrane electrolyzer based on open-source CFD', *Digital Chemical Engineering*, vol. 1, p. 100004, Dec. 2021, doi: 10.1016/j.dche.2021.100004.



Efficient urea-assisted water electrolysis at 1.5 a/cm2 for 1100 hours over in-situ produced niooh species

Panagiotis Tsiakaras1*, Jiaxing Lu2, Costas Molochas1, Angeliki Brouzgou3, Guangfu Qian1,2

*Corresponding authors: tsiak@uth.gr;

1 Laboratory of Alternative Energy Conversion Systems, Department of Mechanical Engineering, School of Engineering, University of Thessaly, 1 Sekeri Street, Pedion Areos 38834, Greece.

2 Guangxi Key Laboratory of Clean Pulp & Papermaking and Pollution Control, School of Light Industry and Food Engineering, Guangxi University, Nanning 530004, China.

3 Laboratory of Hydrogen and Fuel Cell Nanotechnology, Department of Energy Systems, School of Technology, University of Thessaly, 41500, Geopolis, Larisa, Greece.

Keywords: Urea-assisted water electrolysis, lignin-derived carbon, heterojunction catalysis, self-supported structure

Abstract: In order to effectively replace the oxygen evolution reaction (OER) with the urea oxidation reaction (UOR) in water electrolysis systems, the activity and stability of conventional Ni-based catalysts need to be further improved. Here, we developed a self-supported catalyst composed of a FeNi3/Ni2V2O7 heterojunction encapsulated within lignin-derived carbon (LC). The LC@FeNi3/Ni2V2O7 exhibits potentials as low as 1.22 and 1.39 V at 10 and 1000 mA/cm2 for UOR, which are attributed to the selective formation of the active NiOOH species through the synergism between the LC and the heterointerfaces. In addition, the catalyst shows excellent practical potential in a non-membrane electrode assembly, achieving a current density of 1.5 A/cm2 at 1.84 V with a decay of only 100 mV after 1100 hours of operation.

Introduction: Ni-based catalysts activate UOR mainly through the generation of NiOOH species, but their performance and stability are far from ideal. An ideal UOR catalyst should possess excellent stability and selectively activate NiOOH at low overpotentials, favoring UOR against the competing OER during water electrolysis [1]. Ni-based heterostructures can generally cover these demands by appropriately modulating the electronic structure and promoting the selective generation of UOR-active species like NiOOH and Ni2+ [2]. LC can also contribute as a catalyst carrier by enhancing the dispersion of active sites, improving electrical conductivity, and providing anti-corrosion resistance, especially when utilized in self-supporting structures [3]. In this study, a self-supported catalyst composed of a FeNi3/Ni2V2O7 heterojunction encapsulated within LC is proposed for urea-assisted water electrolysis.

Objectives/Innovations: The well-documented ability of heterojunctions to improve the intrinsic activity and stability of Ni-based catalysts towards UOR and the beneficial properties of LC as a catalyst carrier motivated us to set the following objectives:

- Exploiting the synergism between LC and a FeNi3/Ni2V2O7 heterojunction in a self-supported catalyst structure in order to facilitate the selective generation of UOR-active NiOOH species, expose a large active area, and achieve high corrosion resistance.

- Achieving a low potential (<1.9 V) at a high current density of 1.5 A/cm2 in a non-membrane electrode assembly combined with a minimal performance decay after operation for more than 1000 hours.

Methods & Methodology: The LC@FeNi3/Ni2V2O7 catalyst and all control samples were synthesized with a two-step procedure, involving solvothermal treatment followed by calcination. The structure of the as-prepared catalyst was revealed by high-resolution transmission electron microscopy (HRTEM), while the active species on its surface during UOR and OER were elucidated with in-situ Raman spectroscopy. The electrochemical performance of the catalysts was examined in a three-electrode half-cell at 30 oC in an N2-saturated solution (1 M KOH + 0.5 M urea). The practical potential of the catalyst was revealed in a two-electrode cell (6 M KOH + 1 M urea), using LC@FeNi3/Ni2V2O7 as both an anode and a cathode non-membrane electrode. All presented potentials correspond to the reversible hydrogen electrode (RHE) and have been corrected for 90% of the uncompensated ohmic resistance.

Observed Results: The HRTEM images in Figures 1a, b confirm that the as-prepared catalyst consists of distinct FeNi3 and Ni2V2O7 heterointerfaces encapsulated within amorphous LC. The presence of the heterointerfaces on the catalyst surface and their interaction with the LC carrier is expected to enhance electron mobility and increase the density of active sites, thereby accelerating the kinetics of UOR. This argument is supported by the in-situ Raman spectra taken under both UOR and OER operating potentials. As shown in Figures 1c, d, the formation of active NiOOH species on LC@FeNi3/Ni2V2O7 is favored during UOR (onset potential 1.25 V for UOR vs 1.35 V for OER), highlighting the suitability of the proposed catalyst for urea-assisted water electrolysis.

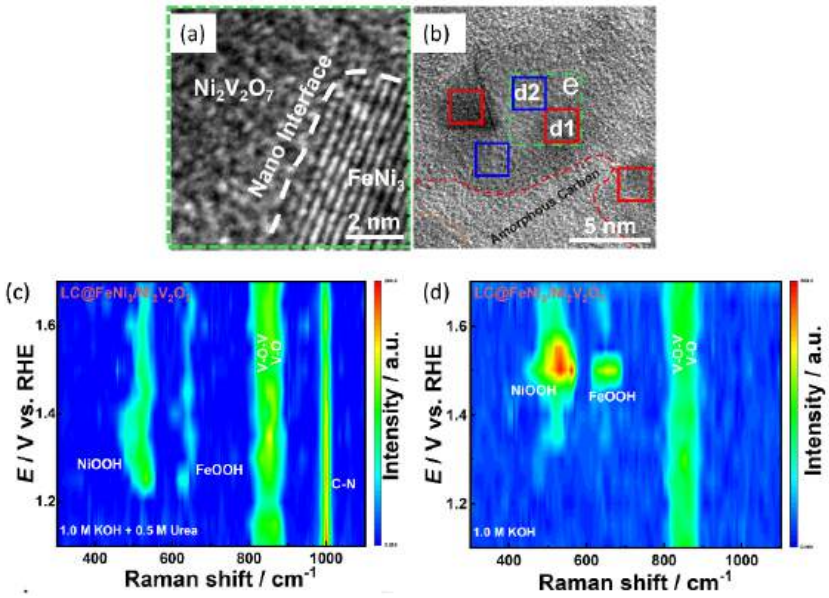


Figure 1. (a-b) HRTEM image of LC@FeNi3/Ni2V2O7 (d1: FeNi3, d2: Ni2V2O7, e: heterointerface); in-situ Raman spectra of LC@FeNi3/Ni2V2O7 for (c) UOR and (d) OER.

Figures 2 a, b show that LC@FeNi3/Ni2V2O7 presents superior UOR performance, exhibiting the lowest potentials (1.23, 1.28, and 1.39 V at 10, 100, and 1000 mA cm−2) and smallest Tafel slope among the compared controlled samples. Notably, LC@FeNi3/Ni2V2O7 displays higher activity than most recently reported UOR catalysts, especially at high current densities (Figure 2c). Finally, the practical potential of

LC@FeNi3/Ni2V2O7 for urea-assisted water electrolysis was examined in a non-membrane electrode assembly, where a potential as low as 1.84 V at 1.5 A/cm2 was achieved combined also with a minimal decay after 1100 hours of continuous operation (Figure 2d).

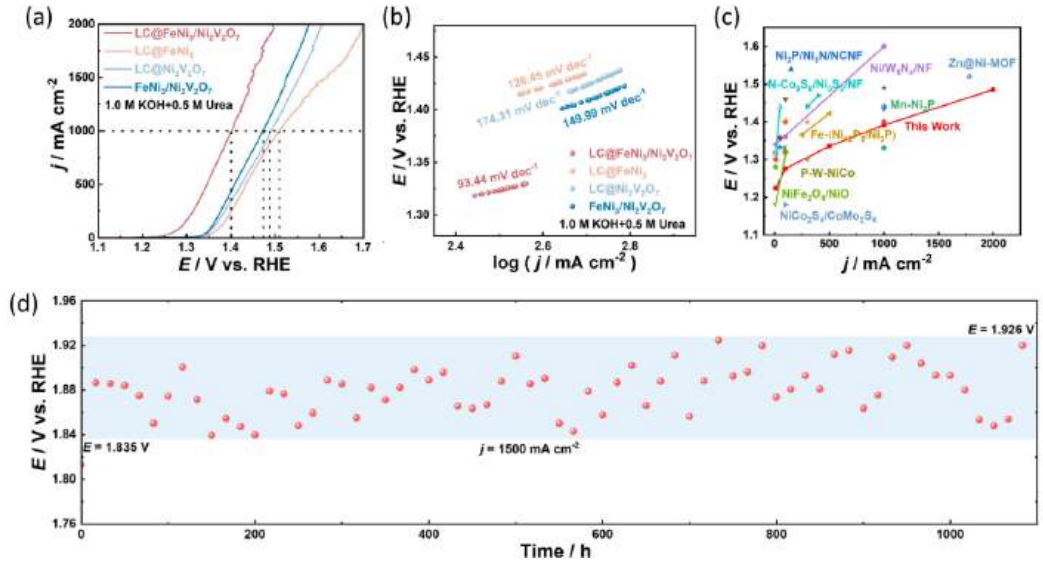


Figure 2. (a) Linear sweep voltammetry curves and (b) Tafel slopes for UOR in a three-electrode half-cell; (c) UOR performance comparison of LC@FeNi3/Ni2V2O7 with recently reported catalysts; (d) Chronopotentiometry at 1.5 A/cm2 for urea-assisted water electrolysis on a non-membrane electrode assembly.

Conclusions: In this study, a self-supported catalyst composed of a FeNi3/Ni2V2O7 heterojunction encapsulated within LC was developed, which achieved excellent UOR activity and stability both in a three-electrode half-cell and in a non-membrane electrode assembly water electrolysis application. The high performance is intrinsically attributed to the selective formation of the active NiOOH species through the synergism between the LC and the heterointerfaces, while the anti-corrosion resistance of LC contributes to the high stability.

Acknowledgments: P. Tsiakaras A. Brouzgou and C. Molochas are grateful for financial support to: 1) the Innovation, Technology Transfer Unit and Entrepreneurship Center "One Planet Thessaly", funded by the Special Account of Research Grants of the University of Thessaly and 2) the “Thessaly 2021 -2027" in the context of Call 49 entitled "Strengthening research infrastructure and equipment of public research bodies based in Thessaly, in the priority areas of RIS3".

References

[1] B. Wu, W. Su, P. Zhu, J. Xu, K. Yuan, L. Li, Y. Chen, Adv. Mater., 37 (2025) e07842.
[2] Q. Li, Y. Wang, T. Pan, Y. Zhu, H. Pang, Sci. China Mater., 68 (2025) 317-340.
[3] L. Li, G. Qian, L. Ge, Y. Wang, X. Cao, J. Li, D. Min, J. Chen, P. Tsiakaras, Chem. Eng. J., (2025) 166556.



Transient Rise of Polarisation-like Resistance During Activation of PEM Water Electrolysers

Andrej Zvonimir Tomić *[a], Frano Barbir [a], Ivan Pivac [a]

* corresponding author: Andrej Zvonimir Tomić, aztomic@fesb.hr

[a] FESB, University of Split, R. Boškovića 32, 21000 Split, Croatia

Keywords: activation, electrochemical impedance spectroscopy, PEM water electrolysis, polarisation resistance

Introduction: Activation of proton exchange membrane (PEM) water electrolyser membrane electrode assemblies (MEAs) is an established conditioning step preceding commercial operation, yet its mechanistic picture remains less systematically documented than for PEM fuel cells [1]. During activation, ohmic membrane resistance decreases, polarisation current increases, and the electrochemically active surface area (ECSA) expands, with all of these changes occurring simultaneously in the same beneficial direction. In this context, the behaviour of the polarisation-like resistance R_p (the non-ohmic, charge-transfer-like component of the electrochemical impedance spectroscopy (EIS) spectrum) is particularly noteworthy in that it moves in the opposite direction to all other activation diagnostics, rising during the conditioning window before collapsing back to or below baseline. This counter-intuitive transient has not been systematically reported for PEM water electrolysers and constitutes the research focus of the present work.

Objectives: The study aims to document and quantify the anomalous transient increase of R_p during the 24-hour activation window of PEM water electrolyser MEAs, to demonstrate that this rise occurs universally across all applied voltage waveforms including constant-voltage protocols, to identify the mechanistic origins of the transient elevation and its subsequent collapse during an idle period, and to examine how the magnitude of the transient scales with the applied waveform parameters.

Material and methods: Eight PEM water electrolyser MEAs (45 cm^2 active area) were each activated for 24 hours with one of seven dynamic voltage waveforms or a constant-voltage reference (1.95 V). The dynamic protocols comprised symmetric and asymmetric square waves (SQ-12, SQ-ASYM, SQ-60), symmetric and asymmetric triangular ramps (TRI-SYM, TRI-ASYM), and a stepped square wave (STEP-24), spanning mean voltages from 1.563 V to 1.950 V and periods from 6 s to 60 s. EIS was recorded at four timepoints, namely before activation (t = 0 h), at the end of activation (t = 24 h), after a performance test (t = 28 h), and following a 16-hour idle interval (t = 44 h). From the Nyquist plot, the high-frequency real-axis intercept R_{HF} (ohmic membrane resistance) and the low-frequency intercept R_{LF} (total impedance) were extracted. The polarisation-like resistance, $R_p = R_{LF} - R_{HF}$, was derived at each timepoint. Complementary diagnostics included polarisation current at 2 V and cyclic

voltammetry (CV) area as an ECSA proxy. Absolute gains $\Delta x_t = x_t - x_0$ were calculated for each diagnostic.

Results: During the 24-hour activation window, all conventional diagnostics improved on every MEA. R_{HF} fell by 1.9 to 7.3 %, polarisation current at 2 V rose by 16 to 34 %, and ECSA expanded by 11 to 43 %. In sharp contrast, R_p increased on every MEA, rising by 12 to 29 % of its initial value (absolute range of +0.0105 to +0.0242 Ω) and moving in the opposite direction to all other diagnostics. Initial R_p values were tightly clustered across all eight MEAs (0.0809 to 0.0871 Ω), indicating a common pre-activation interfacial state. The two largest transients were produced by SQ-60 (+0.0242 Ω, +28.6 %) and SQ-ASYM (+0.0214 Ω, +25.5 %), both waveforms with prolonged or asymmetrically weighted anodic exposure. The smallest transients were observed for STEP-24 (+0.0105 Ω, +12.2 %) and TRI-ASYM (+0.0120 Ω, +13.9 %), the two protocols with the lowest mean voltages in the set. The constant-voltage reference at 1.95 V produced a transient of +0.0188 Ω (+23.2 %), larger than both low-mean dynamic protocols and consistent with its sustained anodic exposure promoting extensive oxide coverage without any cathodic phase to reduce it. Across the dynamic waveforms, the R_p transient magnitude scaled monotonically with applied RMS, so that more energetically demanding protocols produced larger elevations. Importantly, R_p was not meaningfully associated with final current or ECSA gains, confirming that a larger transient does not impair ultimate activation performance. Following the 16-hour idle period, R_p collapsed universally. Three MEAs ended below their initial baseline, with STEP-24 showing the largest downward shift (-0.0043 Ω). The constant-voltage reference retained the largest residual elevation (+0.0068 Ω, +8.4 %), consistent with slower interfacial reorganisation in the absence of potential cycling. By 44 h, R_{LF} had fallen below its initial value on every MEA, confirming that the 24-h R_p peak is a transient phenomenon superimposed on a longer-term improvement trajectory.

Conclusions: The polarisation-like resistance, $R_p = R_{LF} - R_{HF}$, exhibits a universal transient increase during the activation of PEM water electrolyser MEAs that is mechanistically decoupled from the concurrent improvements in membrane resistance, current performance, and ECSA. Importantly, this transient elevation is a fully reversible phenomenon, as R_p collapses universally during the subsequent idle period and by 44 h R_{LF} falls below its initial value on every MEA, confirming that the 24-h R_p peak is superimposed on a longer-term improvement trajectory. On the basis of literature evidence, the rise can then be attributed to the accumulation of transient interfacial species, namely intermediate oxide coverages on the catalyst surface and organic additives migrating from the membrane, which elevate apparent charge-transfer resistance in EIS during the cycling window [2,3]. The subsequent collapse of R_p during idle reflects the flushing of contaminant species and the reduction of accumulated oxide intermediates, consistent with their known reversibility under quiescent conditions [4]. The scaling of the transient peak with applied RMS voltage provides a non-invasive, EIS-accessible indicator of conditioning intensity. This behaviour, which is opposite in direction to all other activation diagnostics,

universally present, and self-resolving, constitutes a previously unreported diagnostic signature of PEM water electrolyser activation that merits routine monitoring during MEA conditioning protocols.

Acknowledgment

The authors acknowledge the support of the Croatian Science Foundation under the project "Advanced diagnostics and prognostics for efficient production and use of green hydrogen - HYTECH" (UIP-2025-02-6150). This research was also partially supported by the project STIM–REI 2.0 (Contract No. PK.1.1.10.0005), funded by the European Union through the European Regional Development Fund–the Operational Programme Competitiveness and Cohesion 2021–2027 (PK.1.1.10).

References

[1] A. Z. Tomić, I. Pivac, F. Barbir, "A Review of Testing Procedures for Proton Exchange Membrane Electrolyzer Degradation," J. Power Sources, vol. 557, 232569, 2023.

[2] D. E. Ramaker et al., "Following ORR intermediates adsorbed on a Pt cathode catalyst during break-in of a PEM fuel cell by in operando X-ray absorption spectroscopy," Phys. Chem. Chem. Phys., vol. 16, pp. 13645-13653, 2014.

[3] N. Zhao et al., "Effects of membrane additives on PEMFC conditioning," ChemistrySelect, vol. 4, no. 43, pp. 12649-12655, 2019.

[4] M. Ruge et al., "Electrochemical oxidation of smooth and nanoscale rough Pt(111): an in situ surface X-ray scattering study," J. Electrochem. Soc., vol. 164, no. 9, pp. H608-H614, 2017.



Towards a Standardized Testing Framework for AEM Water Electrolyzers

Giulia Campolucci*[a], Ottavio Longo[b], Petronilla Fragiacomo[c], Vincenzo Piemonte[a], Valentina Naticchioni*[c]

* Corresponding author: g.campolucci@unicampus.it, valentina.naticchioni@enea.it,

[a] Department of Engineering, Campus Bio-Medico di Roma University, Rome (RM), Italy

[b] Department of Mechanical, Energy and Management Engineering (DIMEG), University of Calabria, Rende (CS), Italy

[c] ENEA, Italian Agency for New Technologies, Energy and the Environment Department of Renewable Energies, TERIN-DEC-H2V-Via Anguillarese, 301-00123 Rome, Italy

Keywords: AEMWE, POLARIZATION CURVE, EIS, TESTING PROTOCOL

Abstract

Anion exchange membrane water electrolyzers (AEMWEs) combine key advantages of alkaline and proton exchange membrane electrolyzers, enabling relatively high current densities (>1 A cm^{-2}) while offering a potentially low-cost solution. However, long-term stability remains a critical challenge to ensure consistent performance during operation. This work presents a unified testing protocol for AEMWEs and demonstrates its implementation using the commercial anion exchange membrane FUMASEP FAA-3 PK-130 membrane. The effect of temperature on the system response is also investigated, showing that higher temperatures enhance both charge transfer and ionic transport processes.

Introduction: *Among current hydrogen production technologies, water electrolysis has gained significant attention as a sustainable solution, enabling net-zero emissions when powered by renewable energy sources [1]. For the large-scale commercialization of green hydrogen, electrolysis systems must be both economically viable and operationally safe. In this context, AEMWEs offer a strategic alternative to both high-cost proton exchange membrane water electrolyzers (PEMWEs) and the corrosive environment of alkaline water electrolyzers (AWEs), enabling the use of non-precious metal catalysts and reducing system costs [2]. Despite significant progress, commercially available AEMs remain insufficient to compete with PEMWEs [3], and the absence of standardized testing protocols critically limits the comparability of laboratory-scale results.*

Objectives: This study aims to establish a standardized and reproducible testing protocol for AEM water electrolysis. As a case study, the commercial FUMASEP FAA-3 PK-130 is evaluated in a 5 cm^2 AEMWE cell, providing a benchmark for future investigations on emerging, non-commercial AEMs.

Additionally, the impact of operating temperature is investigated to assess the potential advantages of high-temperature operation.

Material and methods: A commercial FUMASEP FAA-3 PK-130 membrane was activated by immersion in a 0.5 M KOH solution for 24 hours at room temperature. Commercial stainless steel meshes coated with $NiFe_2O_4$ and NiFeCo are used as anode and cathode, respectively and the cell is assembled using rubber sheet gaskets (thickness 500 um) and stainless steel 316 porous transport layers (PTLs) and closed with a torque force of 3 N*m.

The cell fixture was connected to a Scribner 620 test station and operated at atmospheric pressure. A dry cathode configuration was adopted, while the anode was fed with 0.5 M KOH solution at 50 mL min^{-1}. To prevent the formation of critical H_2 and O_2 concentrations in the outlet streams, N_2 was continuously purged at both electrodes at 30 mL min^{-1}.

Prior to testing, the membrane was conditioned for 50 minutes through five steps of 10 minutes each at increasing current densities (12 - 200 mA cm^{-2}). Polarization curves were recorded at 30 °C, 40 °C, and 50 °C by varying the current density over range of 0-0.5 A cm^{-2}. Electrochemical impedance spectroscopy (EIS) measurements were performed in the frequency range 100 kHz-0.5 Hz under both potentiostatic (0 A) and galvanostatic conditions (0.5 - 2.0 A), applying a 10% current perturbation. Membrane stability was evaluated over 200 hours at a constant current density of 0.3 A cm^{-2}, corresponding to 70% of the maximum stable current density. Polarization curves and EIS measurements were recorded before and after the durability test to evaluate performance at the beginning of life (BoL) and end of life (EoL).

Results: Figure 15 shows that increasing the cell temperature had a negligible effect on cell voltage at low current densities, while at higher current densities operation at 50 °C resulted in the lowest cell potential (2.15 V at 500 mA cm^{-2}), reducing the overall power demand.

EIS indicates that higher temperatures facilitate both electrons and anions transport through the electrolyte and across the membrane (at 100 mA cm^{-2}, the low-frequency resistance (LFR) was 0.128 Ω, compared to 0.139 Ω and 0.157 Ω at 40 °C and 30 °C, respectively.). The membrane durability test demonstrated stable cell operation over 200 hours. Nevertheless, comparison with literature data indicates that further optimization of the cell configuration is required to achieve lower cell voltages.

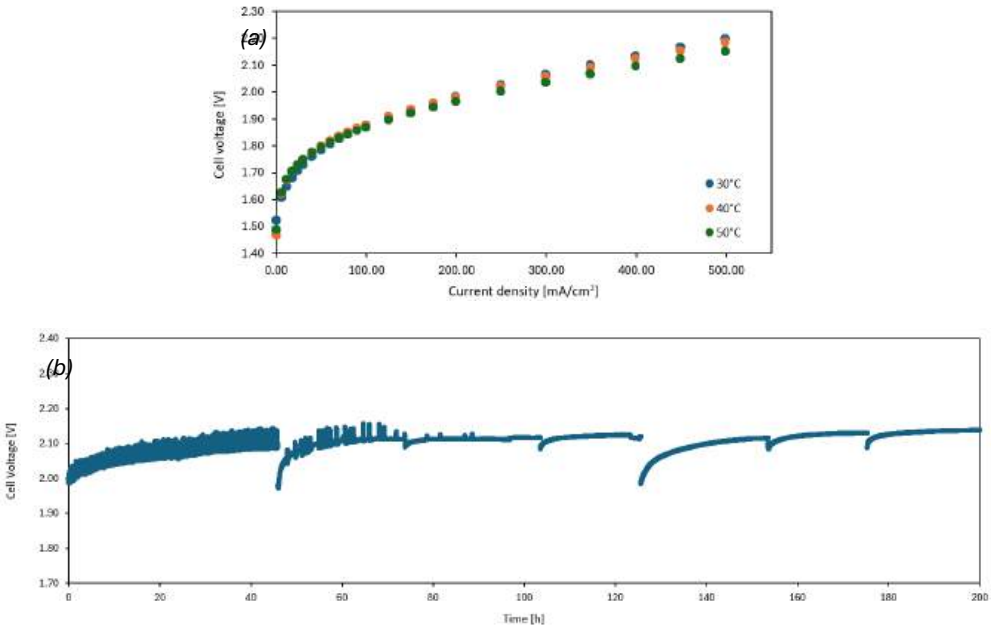


Figure 15. *Polarization curve (0.4 A cm^{-2}) at different operating temperatures (a) and durability test (b)*

Conclusions: This study proposes a standardized testing protocol applicable to different membrane types and cell configurations, whose validity is supported by consistent and reproducible results across the investigated conditions. The findings highlight a beneficial impact of elevated operating temperatures and the results further demonstrate that the commercial FUMASEP FAA3 PK-130 membrane ensures stable operation at low current densities. However, the overall performance remains modest for AEM electrolyzers and still lags behind the benchmarks achieved by PEM systems.

Acknowledgment

ENEA - Italian National Agency for New Technologies, Energy and Sustainable Economic Development for funding (PNRR POR H2).

References

[1] H. Altinisik, C. Celebi, A. Ozden, Y. Devrim, C. Ozgur Colpan, A review on membranes for anion exchange membrane water electrolyzers, Renewable and Sustainable Energy Reviews 226 (2026). https://doi.org/10.1016/j.rser.2025.116277.

[2] Z. Zakaria, S.K. Kamarudin, A review of alkaline solid polymer membrane in the application of AEM electrolyzer: Materials and characterization, Int. J. Energy Res. 45 (2021) 18337–18354. https://doi.org/10.1002/er.6983.

[3] D. Henkensmeier, M. Najibah, C. Harms, J. Žitka, J. Hnát, K. Bouzek, Overview: State-of-the Art Commercial Membranes for Anion Exchange Membrane Water Electrolysis, Journal of Electrochemical Energy Conversion and Storage 18 (2021). https://doi.org/10.1115/1.4047963.



Investigation of the Challenges in Dynamic Operation of Pressurized Alkaline Water Electrolysers

Dirk Ullmer*[a], Davide Grilli [a], Kamal Ghotia[a], Hans Wiggenhauser[a], Fatemeh Razmjooei[a], Syed-Asif Ansar[a]

* corresponding author: dirk.ullmer@dlr.de

a Institute of Engineering Thermodynamics, German Aerospace Center (DLR), Pfaffenwaldring 38-40, 70569 Stuttgart, Germany

Keywords: alkaline water electrolysis, pressurized electrolysis, dynamic operation, renewable energy integration

Abstract

Introduction:

Operating alkaline water electrolysers (AWE) at elevated pressure can advance the pathway for reducing the cost of hydrogen derivative production such as ammonia, synthetic fuels, and other Power-to-X products, as well as for enabling efficient storage and transport of green hydrogen[1]. Pressurized operation offers several benefits, both energetic and economic, including reduced downstream compression requirements, reducing or eliminating the need for bulky, costly and energy-intensive downstream compressors, improved integration into industrial processes, and increased system flexibility.

However, at the same time, operation under elevated pressure introduces significant technical challenges. One of the most critical issues is increased gas crossover through the diaphragm/separator, which can negatively affect the hydrogen purity, and thereby the safety and efficiency of the entire electrolyser system[2]. These effects become even more pronounced under dynamic operation, e.g. with fluctuating power input from renewable energy sources. Therefore, balancing the benefits of pressurized operation with the associated operational and safety limitations is essential for enabling safe and cost-effective large-scale deployment of AWE systems.

Objectives: The presented work aims to improve the understanding of the operational behaviour of AWE stacks under elevated pressure and dynamic load conditions.

The main objectives are:

- Systematic investigation of relevant operating parameters during pressurized operation.
- Experimental evaluation of stacks under elevated pressure and transient renewable-energy-based load profiles.
- Identification of parameter influences on gas purity, efficiency, and operational stability.

- Improvement of the understanding of AWE behaviour under highly dynamic operating conditions.
- Development of optimized operating strategies with respect to gas purity, safety, and efficiency.

Material and methods: For the purpose of this research work, an advanced high-pressure test rig has been designed, built, and qualified for experimental evaluation of alkaline electrolyser stacks.

The test rig enables the operation of stacks at elevated pressure under highly dynamic load conditions. For in-operando analysis of the operating conditions, the testing setup is equipped with measurement devices for electrochemical impedance, gas purity, lye density and -flow rate and temperatures. Electrochemical impedance spectroscopy (EIS) is implemented on both cell and stack level for currents up to 650 A and active cell areas exceeding 1,000 cm^2. The test rig has a flexible electrolyte management, including variation of electrolyte flow rates and separation of anode and cathode electrolyte circuits. It makes fast pressure and temperature transitions possible, as well as operation with defined differential pressure. For the evaluation, standardized JRC test protocols are applied, alongside with renewable energy generation profiles, and specifically developed transient pressure-load protocols. Inline density measurements of the KOH electrolyte are performed using coriolis mass flow meters, enabling early detection of insufficient gas-liquid separation and transient process instabilities.

Results: The experimental work is currently still ongoing. Initial experimental investigations indicate that gas purity represents one of the main limiting factors for pressurised and dynamic operation of alkaline water electrolysers.

The results show that:

- Elevated pressure and transient operating conditions significantly influence gas crossover behaviour, and therefore the admissible operating envelope.
- Separation of anode and cathode electrolyte flows can substantially reduce gas contamination and lower the minimum load point while maintaining safe operating conditions.
- Modification of electrolyte flow rates and pressure management strategies has a measurable impact on gas purity and transient stability.
- Electrochemical impedance spectroscopy provides valuable information regarding performance behaviour and degradation phenomena under dynamic operation for stacks with active areas above 1,000 cm^2.

The ongoing experimental campaign will further quantify the influence of pressure, load gradients, electrolyte circulation, and differential pressure on stack performance, gas quality, and operational stability. The final contribution will include additional experimental data obtained prior to the conference.

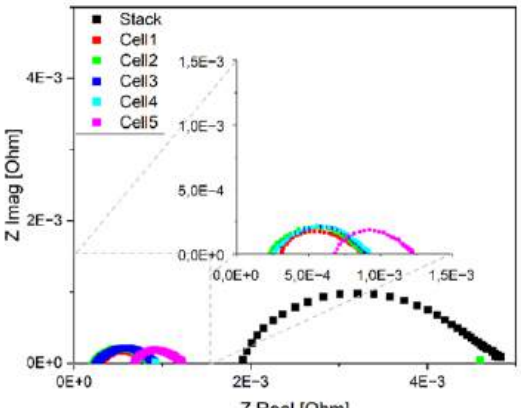


Figure 16: Electrochemical Impedance measurements on a 5-cell stack with 1000 cm² single electrode area at a current density of 0.14 A.cm⁻²

Conclusions: The conducted investigations demonstrate that electrolyte flow management plays a key role in extending the operational window of pressurized AWE under dynamic conditions. In particular, the optimization of electrolyte flow rates and separation of anode and cathode electrolyte circuits can significantly improve gas purity and operational flexibility. The dynamic and pressurized operation requires careful management of pressure gradients and transient operating states to ensure safe operation. Regarding measurement tools, EIS, commonly used for performance evaluation of small-scale cells in various electrochemical applications, also represents a promising diagnostic tool for monitoring performance and degradation of industrial-scale alkaline electrolyser stacks. The generated experimental results contribute to the development of improved operating strategies for future large-scale pressurized AWE systems integrated with fluctuating renewable energy sources.

The ongoing work will provide additional insights into transient high-pressure operation and support the development of safer, more efficient, and more flexible alkaline electrolysis systems for green hydrogen production.

Acknowledgment

This work was financially supported by the project 'Pressurized Efficient Alkaline Electrolyser (PEACE)', funded under the Horizon Europe programme (Grant Agreement No. 101101343) by the Clean Hydrogen Partnership and its members, the German Federal Ministry for Economic Affairs and Energy (BMWE) under the grant number 03EI3053A ('HERA') and the German Federal Ministry of Research, Technology and Space (BMFTR) under the grant number 03HY110B ('H2Giga Degrad-EL3') and 03HY126I (H2Giga AEL4GW).

References

[1] Alfredo Ursúa et al., 2016, Int. J. of Hydrogen Energy, Volume 41, Issue 30;

[2] Jörn Brauns and Thomas Turek, 2023, J. Electrochem. Soc. 170 064510;



Enhancing the Mechanical Durability of Anion Exchange Membranes via Electrospun PVDF Fibers Reinforcement for Water Electrolysis

Davide Damiani*[a], Andrea Fasolini[a], Emanuele Maccaferri[a], Laura Mazzocchetti[a], Giuseppe Nigliaccio[b], Francesco Basile[a]

[a] Dipartimento di Chimica Industriale Toso Montanari, Università di Bologna

[b] ENEA Agenzia nazionale per le nuove tecnologie, l'energia e lo sviluppo economico sostenibile

Keywords: Anion exchange membrane, Electrospinning, Mechanical reinforcement, Poly(vinylidene fluoride).

Abstract:

Anion exchange membrane water electrolysis (AEMWE) is a promising technology for cost-effective green hydrogen production [1]. However, the low mechanical stability of ion-exchange membranes limits their operation at elevated pressures [2]. This study proposes a novel reinforcement strategy using an electrospun nanostructured poly(vinylidene fluoride) (PVDF) backing layer coupled with a commercial AEM (Sustainion X37-50). Through a specific compatibilization process using an ionomer solution, the PVDF mat was successfully bonded to the membrane. The reinforced membrane demonstrated a 60% increase in burst pressure compared to the bare membrane (from 1.0 bar to 1.6 bar) while exhibiting identical electrochemical performance in a redox-flow cell up to 0.5 A/cm^2. The results confirm that the mechanical durability of AEMs can be significantly enhanced without compromising ionic conductivity, paving the way for high-pressure industrial applications [3].

Introduction:

Water electrolysis powered by renewable energy is a primary method for green hydrogen production. Among the available technologies, Anion Exchange Membrane Water Electrolysis (AEMWE) combines the low-cost materials of traditional Alkaline Water Electrolysis (AWE) with the compact design, fast response time, and high efficiency of Proton Exchange Membrane Water Electrolysis (PEMWE). Despite these advantages, the commercialization of AEMWE is hindered by the relatively low mechanical stability of current anion-exchange membranes, especially when subjected to the high pressures required for industrial-scale hydrogen storage and distribution. Enhancing the mechanical properties of these membranes without sacrificing ionic conductivity is therefore a critical challenge. This work introduces an innovative approach to overcome these limitations by reinforcing a commercial AEM with an electrospun, highly porous poly(vinylidene fluoride) (PVDF) microfibrous backing layer.

Objectives: The primary objective of this study is to develop a mechanically robust, chemically stable composite AEM for high-pressure electrolysis. Specific goals include:

- Synthesizing a micro/nanofibrous polymeric support (PVDF) stable in highly alkaline environments (pH 14) with optimal porosity.
- Developing a reliable physical-chemical coupling protocol to seamlessly integrate the PVDF mat with a commercial AEM (Sustainion X37-50).
- Demonstrating that the mechanical reinforcement significantly increases the burst pressure of the membrane.
- Proving that the backing layer does not introduce significant ohmic resistance, thereby preserving the OH^- transport and overall electrochemical performance of the cell.

Material and methods:

- **Materials and Electrospinning:** PVDF was selected for its mechanical robustness and chemical resistance in alkaline environments. Mats with a thickness of ~50 µm were fabricated via electrospinning from a PVDF solution. By optimizing the process parameters, fibers with a longitudinally grooved morphology ("churros") were obtained, maximizing the surface area for mechanical interlocking.
- **Compatibilization and Coupling:** To ensure perfect adhesion, the PVDF mat underwent a compatibilization step. A compatibilizer was deposited onto the PVDF mat (pressed between Teflon sheets to prevent sticking). The compatibilized mat was then coupled to the active commercial Sustainion membrane.
- **Mechanical Testing (Burst Pressure):** To bypass the limitations of standard tensile tests (where water loss alters membrane stiffness), a custom burst pressure set-up was developed. The membrane was clamped, and a constantly increasing gas pressure was applied over a water column until failure or gas permeation occurred.
- **Electrochemical Testing:** Performance was evaluated in a redox-flow cell utilizing 6 M KOH as the electrolyte, with a flow rate of 80 mL/min. Chronoamperometry tests were conducted at 0.1, 0.2, and 0.5 A/cm^2 for 30 minutes each, comparing the bare Sustainion membrane against the PVDF-reinforced composite.

Results:

- **Chemical and Morphological Stability:** The electrospun PVDF mats exhibited complete chemical stability, showing no visible degradation under SEM after 30 days of immersion in pH 14 solutions. The compatibilization process resulted in a homogeneous and easily manageable composite membrane. Following activation in 1 M KOH, the coupled membrane maintained excellent adhesion and structural integrity.

- **Mechanical Enhancement:** The burst pressure tests highlighted a significant mechanical improvement- The chemically compatibilized composite membrane reached a pressure limit 60% higher than the commercial membrane.
- **Electrochemical Performance:** Chronoamperometry tests confirmed that the mechanical reinforcement did not hinder ionic transport. The cell voltages recorded for the PVDF-reinforced membrane were virtually identical to those of the bare Sustainion membrane.

Conclusions: The integration of an electrospun microfibrous PVDF backing layer is a highly effective strategy for overcoming the mechanical limitations of Anion Exchange Membranes in water electrolyzers. The bespoke compatibilization and coupling protocol guarantees a stable, cohesive interface that prevents delamination. The resulting composite membrane achieved a 60% increase in burst pressure resistance while perfectly preserving the electrochemical efficiency and OH^- transport capabilities of the bare membrane. This successful balance between mechanical reinforcement and uncompromised ionic conductivity represents a significant step forward in enabling high-pressure, large-scale AEMWE commercialization.

Acknowledgment

This work has been carried out in the framework of the Operational Research Plan (ROP) on green hydrogen developed by ENEA and funded by the Italian Ministry of Ecological Transition (project code: I83C22001170006) under the National Recovery and Resilience Plan (Mission 2. Investment 3.5) funded by the European Union under the Next Generation EU programme.

References

[1] R. Vinodh, S. S. Kalanur, S. K. Natarajan, and B. G. Pollet, 'Recent Advancements of Polymeric Membranes in Anion Exchange Membrane Water Electrolyzer (AEMWE): A Critical Review', May 01, 2023, *MDPI*. doi: 10.3390/polym15092144.

[2] J. E. Park *et al.*, 'High-performance anion-exchange membrane water electrolysis', *Electrochim Acta*, vol. 295, pp. 99–106, Feb. 2019, doi: 10.1016/j.electacta.2018.10.143.

[3] F. Razmjooei *et al.*, 'Increasing the performance of an anion-exchange membrane electrolyzer operating in pure water with a nickel-based microporous layer', *Joule*, vol. 5, no. 7, pp. 1776–1799, Jul. 2021, doi: 10.1016/j.joule.2021.05.006.



Enhancing alkaline water electrolysys with co-mo layered double hydroxides

Nerea López*[a], Rebeca Simion[a], Jesús Serrano[a], Elisabeth María Roldán-Díaz, Daniel Muñoz-Gil[b], María Luisa Ruiz-González[b], José María González-Calbet[b], Jesús Rodríguez[a].

* Nerea.lopez@cnh2.es

[a] National Hydrogen Center (CNH_2), Puertollano, Spain.

[b] University Complutense of Madrid, Inorganic Chemistry Department, Madrid , Spain.

Keywords: Alkaline water electrolysis, catalytic ink, hydrogen, layered double hydroxides.

Abstract

Co-based layered double hydroxides were investigated as electrocatalysts for alkaline water electrolysis, where their tunable composition and lamellar structure enable improved charge transfer and enhanced catalytic activity toward the oxygen evolution reaction. As a result, these materials demonstrate improved performance compared to conventional benchmarks, highlighting their potential for efficient hydrogen production.

Introduction: Hydrogen is considered one of the most promising energy vectors for the transition toward sustainable and carbon-neutral energy systems due to its high gravimetric energy density and environmentally friendly combustion products. Among the different production methods, water electrolysis powered by renewable energy sources represents a clean strategy for green hydrogen generation. However, the oxygen evolution reaction (OER) remains the main kinetic limitation of the process because of its complex four-electron transfer mechanism of the O–O bond formation, requiring high overpotentials and efficient electrocatalysts. Although RuO_2- and IrO_2-based materials show excellent catalytic performance, their high cost and scarcity strongly limit large-scale industrial applications.[1]

Layered hydroxides have attracted considerable attention as promising electrocatalytic materials due to their tunable composition, high surface area, and flexible lamellar structure. In particular, Co-based layered hydroxides are especially relevant for OER catalysis, as their electronic and structural properties can be effectively tailored through compositional modification and interlayer engineering, leading to improved charge transfer and optimized intermediate adsorption [2][3]. The incorporation of transition-metal species such as molybdenum may provide new opportunities to enhance catalytic activity and simultaneously modulate structural properties of these multifunctional materials for hydrogen-related technologies[4].

Objectives: The present work evaluates Co-based layered double hydroxides (LDHs) as electrocatalysts for alkaline water electrolysis, focusing on their performance in two-electrode cell configurations. This work assesses their practical efficiency, stability, and performance in overall water-splitting applications under realistic operational conditions.

Material and methods: Layered ultrathin Co $(OH)_2$ interleaved with Mo-based oxometallates (Co–Mo-1/0.4 LDH, Co:Mo molar ratio of 1:0.4) was synthesized via a one-pot polyol method adapted from a previously reported procedure [5]. Cobalt (II) chloride hexahydrate and Sodium molybdate tetrahydrate were dissolved in ethylene glycol (1.5 M), followed by the slow addition of NH_3 solution (5 M) until the pH reached 9.5. The resulting mixture was transferred to a Teflon-lined stainless-steel autoclave and heated at 130 °C for 24 h, then cooled to room temperature. The obtained colloidal precipitate was sonicated for 6 h to promote layer exfoliation. Subsequently, the dispersion was centrifuged at 4000 rpm for 5 min, and the recovered solid was washed with water by centrifugation at 21 000 rpm for 5 min until neutral pH was achieved. [6]

For electrochemical characterization, a catalytic ink containing 90 wt% LDH catalyst and 10 wt% Fumion FLN-1005 was prepared in a H_2O: isopropanol (1:2) mixture and homogenized by sonication and mechanical stirring. The ink was spray-deposited onto pre-cleaned Ni200 foam electrodes (5 cm^2) using an airbrush under N_2 at 1 bar.

Physicochemical characterization techniques, such as scanning electron microscopy (SEM) and inductively coupled plasma (ICP) provided insights into the material properties and their correlation with electrochemical characterization (electrochemical impedance spectroscopy (EIS) and cell performance. The catalytic performance was evaluated in AEM flow cell operation (Dioxide materials), with key metrics including overpotential, current density, and long-term stability.

Results: Catalytic inks with different catalyst loadings (1, 2, and 3 mg cm^{-2}) were prepared to evaluate their electrochemical performance. Short-term electrochemical tests revealed that the intermediate catalyst loading of 2 mg cm^{-2} exhibited the best performance.

Although this still requires confirmation, it can be deduced from the SEM images **(Figure 1)** that the 2 mg cm^{-2} electrode presents a dendritic-like morphology, generating additional accessible active sites. The 3 mg cm^{-2} loading exhibits significant catalyst agglomeration with stacked layers, hindering access to the active sites, whereas the 1 mg cm^{-2} loading is insufficient to completely cover the Ni foam, resulting in poor activity.

When compared with a commercial RuO_2 electrode under identical conditions [7], the 2 mg cm^{-2} catalyst showed lower cell voltages, operating at 1.72 V vs 1.86 V at 0.5 A cm^{-2} and 1.95 V vs 2.03 V

at 1 A cm^{-2}, respectively. These differences correspond to a reduction in operating voltage, confirming the superior electrochemical efficiency of the optimized catalyst layer.

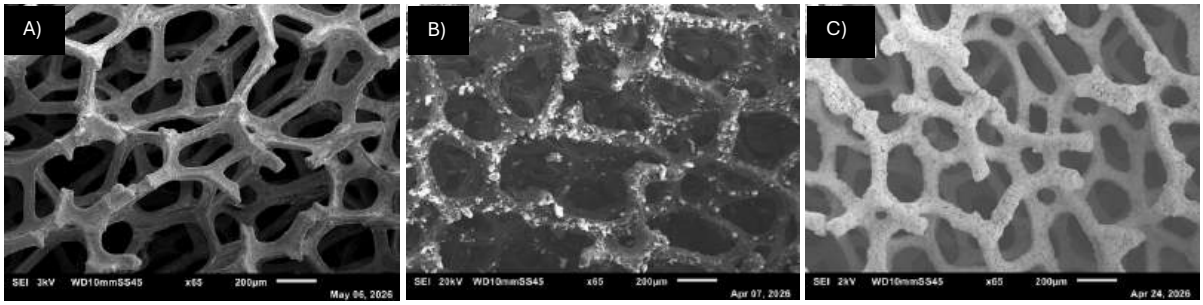


Figure 1: SEM : A) 1 mg/cm² , B) 2 mg/cm² , C) 3 mg/cm²

Conclusions: The present work demonstrates Co-based layered double hydroxides as efficient electrocatalysts for alkaline water electrolysis. The optimized material showed improved performance due to favorable morphology and enhanced active site accessibility, delivering lower operating voltages than a commercial benchmark and indicating improved reaction kinetics and efficiency under practical conditions.

References

[1] S. Kumar, R.Muhammad, S.Kim, J.Yi, K.Son, H.Oh, Adv. Funct. Mater. 2024, 34, 2402513.

[2] F. Lyu, Y.Bai, Q.wang, L.Wang, X.Zhang, Y.Yin, Dalton Trans. 2017, 46, 10545.

[3] A.H.Dorrah, J.-S.Park, A. Palmieri, F.Capasso, Nat. Commun. 024, 16, 3126.

[4] B. Zhang, X. Zheng, O. Voznyy, R. Comin, M. Bajdich, M. García-Melchor, L. Han, J. Xu, M. Liu, L. Zheng, F. Pelayo García De Arquer,C. T. Dinh, F. Fan, M. Yuan, E. Yassitepe, N. Chen, T. Regier, P. Liu, Y.Li, P. De Luna, A. Janmohamed, H. L. Xin, H. Yang, A. Vojvodic, E. H.Sargent, Science 2016, 352, 333.

[5] J. Huang, J. Chen, T. Yao, J. He, S. Jiang, Z. Sun, Q. Liu, W. Cheng, F. Hu, Y. Jiang, Z. Pan, S. Wei, Angew. Chem., Int. Ed. 2015, 54, 8722.

[6] D. Muñoz-Gil, C. Castillo-Blas, D. K. Feler, I. Gómez-Recio, M. Tinoco, A. Querejeta-Fernández, R. González-Prieto, F. Gándara, R. Santos Silva Jr., P. Ferrer, C. Prieto, L. Lajaunie, J. L. Martinez-Peña, M. L. Ruiz-González, J. M. González-Calbet, Adv. Mater. 2025, e12458, https://doi.org/10.1002/adma.202512458.

[7] Z. Zhu, J. Gu, W. Zhao, P. Pei, H. Chang, W. Guo, Y. Wu, J. Kang, Y. Shao, S. Zhao, K. Yao, Nano Energy 2025, 143, 111357.



Integrated Thermochemical Cycles for Carbon-Negative Hydrogen Production

Salvatore F. Cannone*[a], Domenico Ferrero [a], Massimo Santarelli[a]

* corresponding author: salvatore.cannone@polito.it

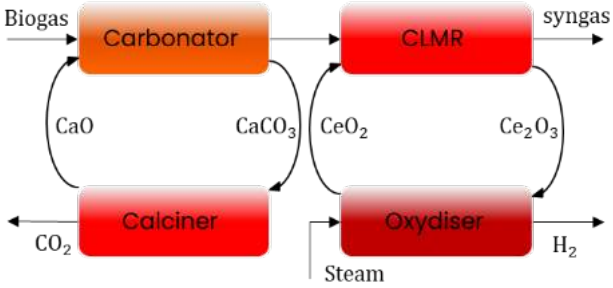
[a] Energy Department, Politecnico di Torino, Corso Duca degli Abruzzi 24, Turin, Italy

Keywords: biogas, calcium looping, chemical looping, thermochemical hydrogen production

Abstract

Introduction: Biogas represents a renewable and dispatchable feedstock for hydrogen production, but its high CO_2 content and the heat demand associated with high-temperature methane conversion limit the overall efficiency of conventional reforming routes. In conventional biogas-to-hydrogen processes, CO_2 separation is typically implemented as an additional downstream unit, increasing process complexity and energy consumption. Thermochemical looping technologies offer an attractive alternative because they can integrate fuel conversion, CO_2 separation, and heat management within the same process architecture. In this context, Calcium Looping (CaL) can be used for upstream CO_2 removal from biogas, while chemical looping methane reforming can convert the remaining methane-rich stream. Ceria-based oxygen carriers are particularly interesting for this purpose because of their reversible oxygen exchange capacity, oxygen mobility, and stability under repeated redox cycles [1-3].

Objectives: This work proposes and assesses an integrated biogas-to-hydrogen process based on four high-temperature reactors: a CaL carbonator for CO_2 capture from biogas, a calciner for sorbent regeneration and CO_2 release, a ceria-based chemical looping methane reformer for syngas production, and a steam oxidiser for reduced-ceria regeneration and direct H_2 production. The process is completed by a two-stage water–gas shift section and pressure swing adsorption for hydrogen purification. The main objective is to identify an optimize operating configuration able to maximize hydrogen production and process efficiency while achieving complete carbon capture through the combined action of CaL, tail gas recirculation, and oxy-fuel combustion.



Methods: The process was evaluated through steady-state process simulation under idealized unit-operation assumptions, including no heat losses and no pressure drops. The Peng–Robinson equation of state was used for gas-phase properties, while rotating equipment was modelled with an isentropic efficiency of 0.75. The ceria loop was described using a dedicated non-stoichiometric thermodynamic framework, in which the gas-phase equilibrium composition was calculated as a function of the oxygen potential imposed by CeO_2–δ. The reduction and oxidation reactors were therefore not represented by a single fixed equilibrium point, but by a transient 0D fixed-bed calculation in which the ceria non-stoichiometry evolves during the redox half-cycle [2-3]. The resulting outlet streams were then obtained as step-averaged compositions. The optimized configuration was selected from reactor-level sensitivity analyses, tail-gas recirculation analisys and heat-integration constraints.

Results: In the optimized configuration, the carbonator operates at 820 °C and 16 bar, achieving high CO_2 capture while maintaining compatibility with the downstream pressure level. The calciner operates at 800 °C and 0.2 bar, exploiting reduced CO_2 partial pressure to decrease the calcination temperature. The ceria reformer operates at 1190 °C and 16 bar, while the steam oxidiser operates at 1210 °C and 16 bar. Heat integration was assessed by pinch analysis using ΔTmin = 20 °C. The PSA tail gas was partially recirculated to the carbonator, and different recirculation ratios were investigated. The selected optimized case corresponds to 50% tail gas recirculation, which provides the best compromise between hydrogen production, carbon capture distribution, and overall efficiency. The system achieves stable conversion performance over the tail gas recirculation range. Methane conversion remains approximately constant between 96 and 97%, while the overall CO conversion across the WGS section is about 93.75%. Increasing tail gas recirculation enhances the amount of CO_2 captured in the CaL carbonator, but its effect on the specific hydrogen yield is limited. In the optimized 50% recirculation case, the CaL section captures approximately 56% of the total carbon available in the process, while the remaining carbon is recovered as a concentrated CO_2 stream from the oxy-fuel combustor.

The energy performance of the optimized configuration is significantly improved compared with the non-optimized case. The cold gas efficiency reaches 85.2%, while the effective thermal efficiency is 80.6%, accounting for the auxiliary electricity demand. The main electrical consumers are biogas and tail gas compression, requiring 7.7 kW, the vacuum pump used to maintain the low CO_2 partial

pressure in the calciner, requiring 1.8 kW, and oxygen production for the oxy-combustion chamber, requiring 4.1 kW. A comparison with other technologies was also investigated.

Conclusions: The proposed CaL–ceria chemical looping process demonstrates the potential for efficient and fully decarbonized hydrogen production from biogas. The optimized configuration, based on 50% PSA tail gas recirculation to the carbonator, achieves complete carbon capture, zero direct specific CO_2 emissions, and high energy efficiency. The integration of CaL with ceria-based chemical looping allows CO_2 separation and hydrogen production to be combined within a thermally integrated process scheme. A key advantage of the configuration is that the CaL and ceria loops are kept as separate solid cycles, avoiding the solid separation challenges typical of sorption-enhanced chemical looping concepts where CaO and oxygen carriers are co-circulated.

The main innovation of the work lies in the integration of upstream CaL CO_2 capture, ceria-based chemical looping methane reforming, steam oxidation for direct hydrogen production, tail gas recirculation, and oxy-fuel combustion for complete carbon recovery. The optimized system reaches 85.2% cold gas efficiency, 80.6% effective thermal efficiency, 100% carbon capture rate, and 0 $kgCO_2/kgH_2$ specific emissions. These results should be interpreted as thermodynamic performance targets and provide the basis for future detailed design of reactors, heat exchangers, and integrated high-temperature heat-transfer solutions.

References

[1] B. Bulfin, M. Zuber, O. Gräub, and A. Steinfeld, “Intensification of the reverse water–gas shift process using a countercurrent chemical looping regenerative reactor,” Chemical Engineering Journal, vol. 461, p. 141896, Apr. 2023, doi: 10.1016/j.cej.2023.141896.

[2] B. Bulfin et al., “Statistical thermodynamics of non-stoichiometric ceria and ceria zirconia solid solutions,” Physical Chemistry Chemical Physics, vol. 18, no. 33, pp. 23147–23154, 2016, doi: 10.1039/C6CP03158G.

[3] M. Zuber, S. Ackermann, and A. Steinfeld, “A fixed-bed reactor for methane dry reforming via a ceria-based redox cycle – modeling and experimental validation,” Front. Energy Res., vol. 13, Jan. 2026, doi: 10.3389/fenrg.2025.1608831



Conditional Physics-Informed Neural Network Modelling of PEM Electrolyzer Voltage Dynamics

Nouhaïla Elkasmi*[a], Maria Serra Prat[a], Carles Batlle Arnau[b]

* corresponding author: nouhaila.elkasmi@estudiantat.upc.edu

[a] Institut de Robòtica i Informàtica Industrial, CSIC-UPC, Llorens i Artigas 4-6, 08028 Barcelona, Spain

[b] Universitat Politècnica de Catalunya, IOC and EPSEVG, Av. V. Balaguer 1, 08800 Vilanova i la Geltrú, Spain

Keywords: *Conditional physics-informed neural networks, Control-oriented modelling, PEM electrolyzers.*

Abstract

Introduction: Proton exchange membrane (PEM) electrolyzers are promising for green hydrogen production under variable renewable electricity, but their voltage dynamics must be predicted accurately for simulation, optimization, and future control-oriented operation. Detailed electrochemical models can capture internal phenomena, but they are often too complex for frequent online prediction. Reduced-order equivalent electrical circuit models provide a practical alternative by representing the dominant transient voltage behaviour with few dynamic states [1,2]. Purely data-driven neural models can be fast, but they often act as black-box approximators and may behave poorly outside the training domain.

Physics-informed neural networks (PINNs) reduce data dependence by embedding governing equations into the training process [3]. However, a standard PINN is usually tied to a fixed problem setup and does not naturally include the control input and initial internal state as conditioning variables [4]. In this work, a conditional physics-informed neural network (CPINN) is developed to represent a family of transient voltage responses of a PEM electrolyzer over a trained short-time interval T_{train}. The model is conditioned on the applied current and initial capacitor voltages and is extended to temperature-dependent prediction by including cell temperature as an additional input.

Objectives: The purpose of this study is to develop a CPINN-based voltage model that combines physical consistency, fast evaluation, and suitability for sequential prediction. The objectives are: (i) to formulate the model from a second-order equivalent electrical circuit; (ii) to train temperature-independent and temperature-dependent CPINNs conditioned on current and initial capacitor voltages; (iii) to evaluate their performance under sequential rollout, operation outside the training range, and direct long-window prediction; and (iv) to assess the effect of increasing the CPINN training period on accuracy and rollout efficiency.

Material and methods: The physical prior is a second-order equivalent electrical circuit with two RC branches, a reversible voltage term, and an ohmic voltage contribution. The internal states are the capacitor voltages U_{c1} and U_{c2}. The terminal voltage is reconstructed as

$$U_{cell}(t) = U_{rev}(T) + U_{c1}(t) + U_{c2}(t) + IR_{\Omega}(T)$$

In the temperature-independent formulation, U_{rev} and R_{Ω} are constant. In the temperature-dependent formulation, U_{rev} follows an affine temperature relation and R_{Ω} is scaled using a temperature-dependent conductivity-inspired expression. The CPINN learns the mappings $(t, I, U_{c1,0}, U_{c2,0}) \rightarrow (U_{c1}, U_{c2}, U_{cell})$ and $(t, I, U_{c1,0}, U_{c2,0}, T) \rightarrow (U_{c1}, U_{c2}, U_{cell})$ for the temperature-independent and temperature-dependent cases. The model is trained over $T_{train} = \alpha \cdot \max(R_1C_1, R_2C_2)$, where α scales the training interval with respect to the dominant RC time constant. Two values are considered, $\alpha = 1$ and $\alpha = 5$, to evaluate the influence of the training interval length on prediction accuracy and rollout efficiency. During prediction, the trained CPINN is evaluated over a prediction window T_w. For sequential rollout, $T_w \leq T_{train}$, and a longer total simulation horizon T_s is obtained by chaining several prediction windows of duration T_w, where the terminal predicted state of one window is used as the initial condition of the next one. Direct long-window prediction with $T_w > T_{train}$ is also tested.

The physics loss includes the differential residuals of the two RC state equations and the algebraic residual enforcing voltage consistency. An optional data loss can also be added when reference voltage are available. The internal states are reconstructed using a hard initial condition embedding, which enforces $U_{c1}(0) = U_{c1,0}$ and $U_{c2}(0) = U_{c2,0}$ by construction. Training is performed using Adam followed by L-BFGS.

Results: The temperature-independent CPINN achieved stable voltage prediction across the evaluated rollout scenarios. In nominal cases within the training range, the terminal-voltage RMSE remained below $10^{-3}V$, with an aggregated in-range RMSE of $7.2828 * 10^{-4}V$. This aggregated value represents the mean performance over rollout cases that remain inside the current, state, and time ranges used during training. Errors increased outside the training range or for $T_w > T_{train}$, but the sequential rollout remained stable.

The temperature-dependent CPINN improved the prediction of voltage dynamics under current and temperature variations. For the $\alpha = 1$ model, the voltage RMSE remained below $10^{-3}V$ in the intended rollout tests, and the long-horizon sequential rollout reached an RMSE of $2.4477 * 10^{-4}V$. This shows that the model can be used repeatedly over several short prediction windows without significant error accumulation.

Direct long-window prediction produced larger errors. For the $\alpha = 1$ temperature-dependent CPINN, using $T_w > T_{train}$ increased the voltage RMSE to $1.6441 * 10^{-2}V$. The $\alpha = 5$ model reduced this direct long-window error to $8.0487 * 10^{-3}V$, showing that increasing T_{train} can reduce the number of rollout calls needed for a total simulation horizon T_s, at the cost of slightly lower short-window accuracy. Figure 1 shows an in-range sequential rollout example for the $\alpha = 5$ model with combined current and temperature variation. The top plot shows that the CPINN voltage prediction closely matches the reference Simulink cell-voltage response. The lower plot shows the imposed current and temperature profiles, which are kept constant within each prediction window.

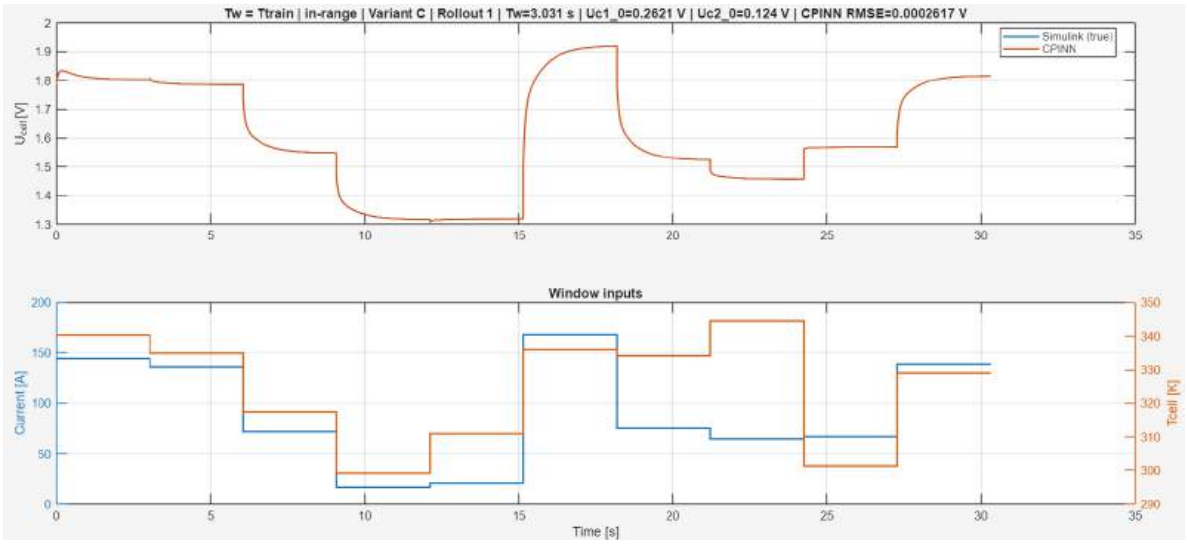


Figure 17: In-range sequential rollout, α = 5, combined current and temperature variation.

Conclusions: The results show that CPINNs are suitable for modelling PEM electrolyzer voltage dynamics over short prediction windows. By conditioning the model on current and initial capacitor voltages, the CPINN represents a family of transient responses rather than a single fixed trajectory. Adding temperature as an additional input extends the surrogate to temperature-dependent voltage behaviour. Direct long-window prediction produced larger errors, confirming that the CPINN should be deployed through sequential rollout instead of direct extrapolation beyond T_{train}. Overall, the proposed contribution is a physically structured, temperature-aware CPINN surrogate suitable for repeated prediction and future optimization or model predictive control applications.

Acknowledgment: This work has been developed as part of the Siemens Energy AI Chair: Energy Sustainability for a Decarbonized Society 5.0 (TSI-100930-2023-5), funded by the Secretary of State for Digitalization and Artificial Intelligence through the ENIA 2022 Chairs call, and co-funded by the European Union-Next Generation EU. This work has also been developed as part of the AVANTE project, supported by the Spanish Ministry of Science, Innovation and Universities and the National Research Agency (PDC2025-165204-C22, financed by MICIU/AEI/10.13039/501100011033).

References

[1] D. S. Falcão and A. M. F. R. Pinto, "A review on PEM electrolyzer modelling: Guidelines for beginners," *Journal of Cleaner Production*, vol. 261, 121184, 2020.

[2] X. Mao, Y. Tian, A. Yang, and G. Zhang, "Identification of Equivalent Circuit Parameters for Proton Exchange Membrane (PEM) Electrolyzer Engineering Models," *IEEE Access*, vol. 12, pp. 15509–15522, 2024.

[3] M. Raissi, P. Perdikaris, and G. E. Karniadakis, "Physics-informed neural networks: A deep learning framework for solving forward and inverse problems involving nonlinear partial differential equations," *Journal of Computational Physics*, vol. 378, pp. 686–707, 2019.

[4] E. A. Antonelo, E. Camponogara, L. O. Seman, E. R. de Souza, J. P. Jordanou, and J. F. Hübner, "Physics-informed neural nets for control of dynamical systems," *Neurocomputing*, vol. 579, 127419, 2024.

EFCH2 2026 European Fuel Cells and Hydrogen PIERO LUNGHI CONFERENCE
September 15th-17th 2026 Capri / Italy

From biowaste to renewable hydrogen: pilot-plant validation and scale-up challenges

E. Tuxans*[a], F. Medina[b], M. Constantí[b], D. Montané[b],
G. Douat[a], C. Bargalló[b], M. Raketh[b] and B. Corzo[a]

* corresponding author: Eudald Tuxans – e.tuxanss@sorigue.com

[a] Innovation Department, Sorigué, Ronda Guinardó, 99. 08041 Barcelona

[b] Chemical Engineering Department, Universitat Rovira i Virgili,

Av. Països Catalans, 26. 43007 Tarragona

Keywords: renewable hydrogen, waste-to-hydrogen, pilot-scale validation, circular economy

Introduction: Renewable hydrogen plays a key role in the transition towards a sustainable energy system, acting as a versatile energy carrier for renewable energy storage and the decarbonization of transport and industry. However, nearly 95% of global hydrogen is still produced from fossil fuels [1]. Although electrolysis is currently the main pathway for renewable hydrogen production, its deployment may be constrained in regions with limited freshwater availability, restricted land for renewable energy installations or high competition for electrical resources. Therefore, alternative and complementary hydrogen production routes are needed.

The conversion of biomass residues into renewable hydrogen offers a promising decentralized pathway, combining hydrogen production with waste valorisation and circular economy principles. This approach may reduce landfill disposal while creating added value from locally available residual streams. Nevertheless, most waste-to-hydrogen technologies remain at early stages of development, and their transition from laboratory to pilot scale involves significant technical and operational challenges. In this context, pilot-scale validation is essential to identify process limitations, implement improvements and define the next steps towards future scale-up and industrial deployment [2].

Objectives: This work aims to assess the pilot-scale transition of a laboratory-validated process for converting pruning residues and organic wastes into ethanol and renewable hydrogen, focusing on the main scale-up challenges, operational improvements and next steps required for further optimization and future industrial deployment.

Material and methods: The proposed system integrates several novel technologies for converting biomass and organic waste into ethanol and renewable hydrogen, as shown in Figure 1.

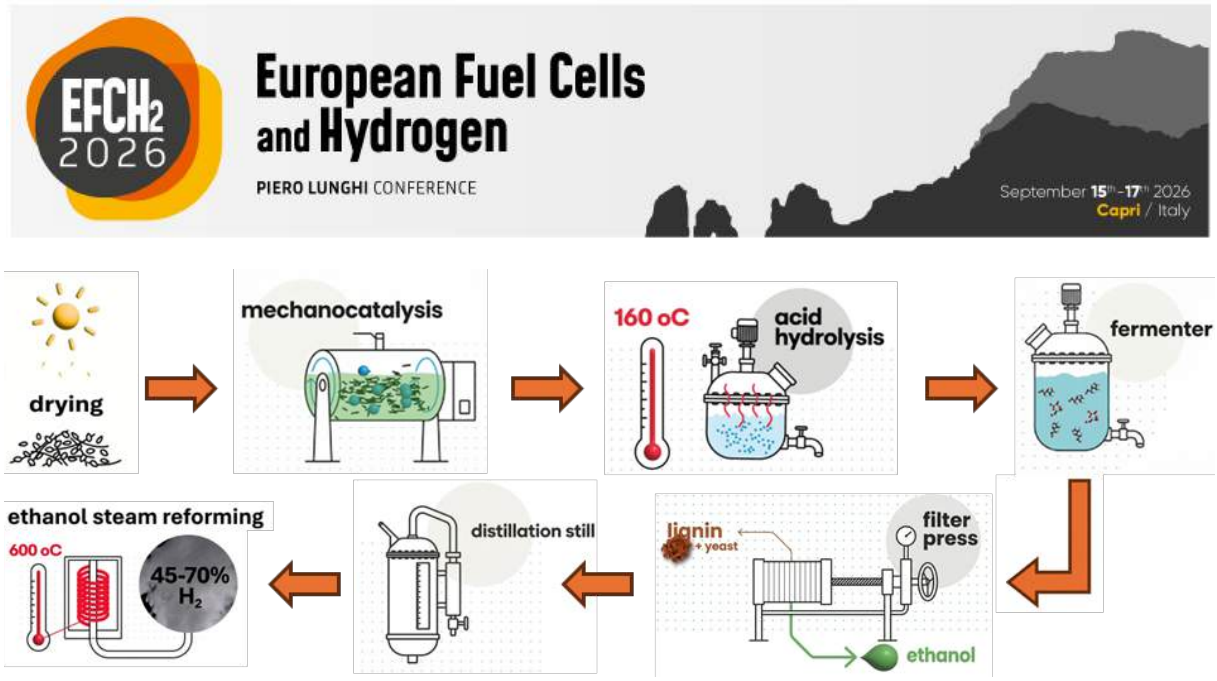


Figure 18. Simplified schematic of the pilot-plant system.

Several operational modifications were required during scale-up, particularly regarding biomass drying and milling. While laboratory tests relied on convection ovens and planetary ball mills, pilot-scale operation required air-drying strategies and drum ball mills, leading to longer processing times and lower particle size homogeneity. Simplified mechanocatalytic approaches were also evaluated at pilot scale, although their performance was unsatisfactory. Hydrolysis, fermentation and downstream operations were adjusted to accommodate larger working volumes and pilot-scale constraints, including longer heating and cooling periods, modified solid–liquid separation systems and adapted distillation conditions. Finally, ethanol-rich streams were converted into hydrogen-rich syngas through steam reforming over a Ni-based catalyst.

Results: The process was transferred from laboratory batches of 6–7 g of waste to pilot-scale batches of approximately 80 kg. All stages were implemented at pilot scale, confirming the technical feasibility of the process chain, although several scale-up challenges were identified.

The main limitation for pruning residues was identified in the mechanocatalysis step. Despite achieving effective particle size reduction at pilot scale (from >5 cm to <350 µm), sugar release during subsequent hydrolysis was lower than in small-scale tests. For bakery waste, hydrolysis reached 627 and 635 g/kg at laboratory and pilot scale, respectively. However, for pruning residues, sugar release decreased from 288 g/kg at laboratory scale to 123 g/kg at pilot scale. These differences were mainly related to the use of a different ball mill with much lower collision energy, which was unable to efficiently promote cellulose-to-glucose hydrolysis.

For pruning residues, lower sugar release at pilot scale limited ethanol production, while bakery waste reached comparable ethanol yields at laboratory and pilot scale (380–386 mL/kg). Bakery residues were blended with pastry wastewater at laboratory, increasing the ethanol production to 480 mL/kg due to a ≈20% increase in soluble sugars during hydrolysis. After solid removal with the press filtration, distillation concentrated the fermentation broth to 17% (w/w) ethanol, meeting the theoretical optimum ratio for the steam reforming unit, which produced hydrogen-enriched gas

containing 45–70% H_2 at both scales. Table 1 summarizes the best results obtained to date at both laboratory and pilot scale.

Table 4. Best results to date at laboratory and pilot scale.

	Sugars (g/kg biowaste)		Ethanol (mL/kg biowaste)			H_2 content in
Biowaste	Pruning r.	Bakery w.	Pruning r.	Bakery w.	Bakery w.*	reforming gas
Laboratory	288	627	160	380	480	69%
Pilot plant	123	635	-	386	-	70%

* Bakery waste blended with pastry wastewater.

Conclusions: The transition from laboratory to pilot scale has been successfully carried out for biowaste valorisation into renewable hydrogen, demonstrating the feasibility of integrating the complete process chain under larger operating conditions. However, mechanocatalysis remains the main bottleneck for biomass residues, mainly due to the lower collision energies generated by the pilot-scale ball mill, which limited downstream processes. Further work should focus on selecting and optimizing higher-energy milling technologies at pilot scale.

Acknowledgment

The VAL2H2 project is funded by the Ministry of Ecological Transition and Demographic Challenge (Ministerio para la Transformación Ecológica y el Reto Demográfico) within the Recovery, Transformation and Resilience Plan (Plan de Recuperación, Transformación y Resiliencia). This project is funded by the European Union (EU) – Next Generation. However, any opinion expressed here are only the author's view, and do not necessarily reflect those of the UE or the European Commission (EC). Neither the EU nor the EC can be considered responsible for these opinions. The authors would like to acknowledge the support of Noguera Renovables, Axpo, and Torre Santamaría.

References

[1] IEA, *Global Hydrogen Review 2024*, IEA, Paris, 2024.

[2] S.C. Wijayasekera, K. Hewage, O. Siddiqui, P. Hettiaratchi, R. Sadiq, Waste-to-hydrogen technologies: A critical review of techno-economic and socio-environmental sustainability, *International Journal of Hydrogen Energy*, 47 (9), 5842-5870, 2022.



Toward Sustainable Bio-Inspired Anisotropic Ion Exchange Membranes by Self-Assembly of Bio-Based Solid Polymer Electrolytes

Gaje Singh [a], Antoine Aynard [a], Christophe Navarro [b], Laurent Billon [a]*

* corresponding author: Laurent.billon@univ-pau.fr

[a] Bio-Inspired Materials group: Functionalities & Self-Assembly, IPREM UMR 5254, Université de Pau et Pays de l'Adour, CNRS, 64000 Pau, France

b ARKEMA, GRL - Specialty Polymer & Additives, 64170 Lacq, France

Keywords: Anisotropic Membrane, Copolymer Self-assembly, Ion Exchange Membrane, Sustainability

Abstract

A new class of bio-inspired polymer membranes was elaborated using block copolymers BCP self-assembly. The BCPs are based on a anion/proton conductive block, paired with a highly hydrophobic monomers derived from biomass, i.e. terpenoid moieties. With either cyclic/ramified linear terpenes, both blocks with high or low glass transition temperatures Tg values were tailored and evaluated for membrane formation. Copolymers were first synthesized via nitroxide-mediated polymerization NMP with BlocBluider from ARKEMA, followed by a post-introduction to introduce the ionic groups, i.e. either for proton or anion exchange membrane. The copolymer composition, as well as the addition of an ionic crosslinker influence the membrane morphologies and properties, i.e. mechanical strength, water uptake or conductivity. The immiscibility between blocks was used as advantage to generate anisotropic segregated domains by creating bio-inspired nano-channels for ion conduction to further boost the through-plane membrane conductivity. Herein, using the bio-inspired strategy, more sustainable anisotropic membranes with up to 50 wt% of renewable bio-sourced carbon and only 15 wt% of Fluorine were tailored with similar features of benchmarked isotropic perfluorinated membranes.

Introduction:

Currently, most of the PEM used in the industry are based of Nafion®-type perfluorosulfonic acid (PFSA) ionomers, consisting of a perfluorinated backbone bearing pendant sulfonic acid moieties forming interconnected clusters within a hydrophobic fluorinated matrix. This isotropic morphology promotes effective water uptake and retention through ionic clustering, ensuring continuous proton-conduction pathways under hydrated conditions. In nature and living cells especially, ionic conductivity arises from highly organized biological membranes. This anisotropic transport is mediated by ion channels maintaining electrochemical gradients essential for cellular function. These designs can attract significant interest for bio-inspired ion exchange membranes with the nanoscale organization of hydrated proton-conducting pathways providing valuable models for next-generation

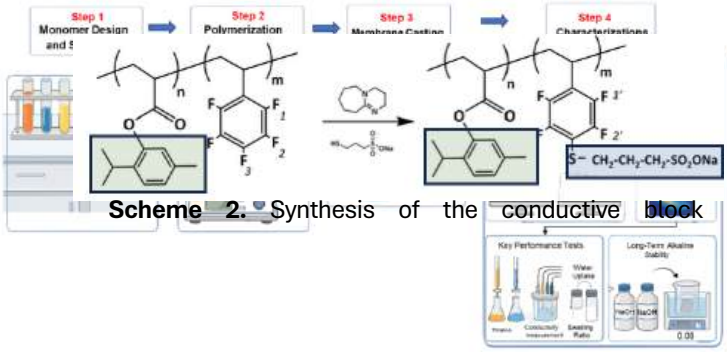
anisotropic synthetic AEMs/PEMs. Block copolymers represent a promising class of copolymers able to be self-assembled in anisotropic structuration, as they offer a unique opportunity to decouple ionic conductivity from mechanical integrity through bio-inspired design of biological membranes. Despite these advantages, most BCP reported to date rely on petro-sourced monomers, limiting their sustainability and long-term relevance. Among bio-based building blocks, terpenes constitute a particularly attractive class of compounds. Naturally produced by plants and widely used in industrial applications, terpenes combine intrinsic rigidity and hydrophobicity with excellent chemical versatility.

Objectives:

In this work, we propose an original block copolymer design that combines conducting block to form nano-channels with a highly hydrophobic terpene-based block for ion exchange membranes driving microphase separation. Beyond demonstrating the feasibility of this sustainable block copolymer approach, i.e. increasing bioresources and decreasing PFAs content, this study wants to highlight how copolymer composition governs membrane morphology and directly impacts ionic conductivity, mechanical robustness, and anisotropic transport properties.

Material and methods:

During this work, 4 different families of block copolymers were designed for proton and anion exchange membranes elaboration following the procedure in Scheme 1. Herein, as example, only bio-based fluorinated proton exchange membrane is showed but similar strategy will be discussed during the $EFCH_2$ 2026 for all designed membranes. The copolymers were synthesized *via* two-step strategy. As example, PolyTerpeneAcrylate-*b*-PolyPentaFluoroStyrene $PTA_{0.66}$-*b*-$PPFS_{0.34}$ (BCP 3) is described with first, ***non-conductive block copolymers,*** i.e. Synthesis of with PTA bio-based block (green) used as macroinitiator (Figure 2 Left), followed by ***Conductive block copolymer by post-modification*** with Para-fluoro/thiol click reaction with sodium 3-mercapto-1-propanesulfonate to modify the non-conductive PPFS block into an ionic conductive one by introducing sulfonic moieties (blue) in Scheme 2 Right.



Scheme 1. Different steps for overall approach of this work

Scheme 2. Synthesis of the conductive block 1.

Results:

Impact of sulfonation on morphology. Before sulfonation, the BCP3 presented a nano organization constituted of *out-of-plane* PPFS cylinders according to its composition (Fig. 1 Left: Atomic Force Microscopy images). After sulfonation, Small Angle X-rays Scattering profiles exhibit a notable shift of the first-order peak towards lower *q* characteristic of a pitch shift from 35 to 70 nm reflecting an increase of the ionic channels volume after sulfonation (Fig. 1b).

The effect of the ionic crosslinking on the mechanical properties of the membrane is shown in Fig 1a. The rheology curves display an increase in extensional viscosity with the extensional strain until a sudden drop reflecting the rupture of the membranes after 100% of elongation.

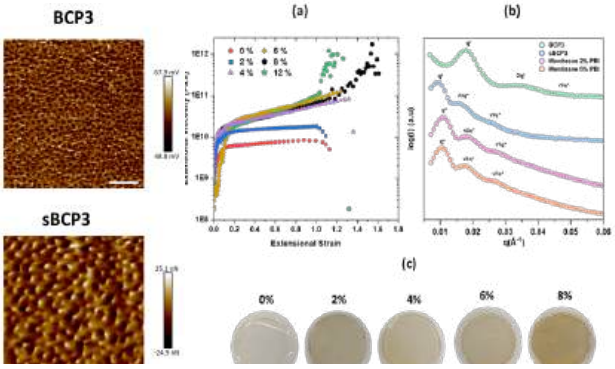
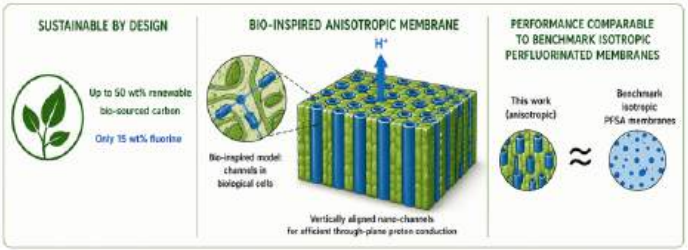


Figure 1. (Left) AFM height images of BCP3 copolymer before (top) and after (bottom) sulfonation, scale bare = 200 nm; (Right) (a) evolution of the extensional viscosity with the extensional strain measured at 100 °C, (b) SAXS profiles (c) photos of BCP3 membranes at different PBI content.

Functional properties of membrane. The BCP3 membrane presents a relatively low WU of 30%, a swelling ratio SR of 5 and an IEC of 1 meq.g^{-1}, similar to Nafion®117 or Aquivion®, as an anisotropic bio-inspired PEM. With *in-plane* conductivity of 35 mS.cm^{-1}, BCP3 behaves differently than Aquivion with 62 mS.cm^{-1}, but displays a similar *through-plane* conductivity value around 3 mS.cm^{-1}.

Conclusions: The resulting bio-inspired membranes exhibit a compelling balance between electrical performance and mechanical stability, making them highly relevant sustainable candidates for next-generation fuel cells and electrolyzers technologies (Scheme 3).



Scheme 3. Bio-inspired self-assembly of block copolymers from bio-based monomers enables sustainable anisotropic membranes with high through-plane conductivity and competitive performances.

Acknowledgment.

The project is supported by E2S UPPA and the Clean Hydrogen Partnership and its members.



Physics-Based One-Dimensional Modelling of a PEM Water Electrolyzer to Quantify Performance Trade-offs of PFAS-Free Membranes

Thomas Dankers *[a], Andreas Podias [a]

* Corresponding author: thomas.dankers@tno.nl

[a] TNO – Netherlands Organisation for Applied Scientific Research

Mobility & Built Environment Unit, Powertrains Research Department

Automotive Campus 30, 5708 JZ, Helmond, the Netherlands

Keywords: PFAS-Free membranes, PEM water electrolysis, physics-based modelling, polarization curve

Abstract: A steady-state, physics-based one-dimensional model of a polymer electrolyte membrane water electrolyzer (PEMWE) is developed by adapting an existing PEM fuel cell framework to electrolysis operation. The model resolves coupled charge, species, and water transport across the membrane–electrode assembly using interface-based boundary conditions and incorporates electrochemical reactions, membrane transport, and operating conditions representative of practical systems. The framework provides a robust and transparent tool for mechanistically assessing membrane-specific performance trade-offs and supports the evaluation and development of PFAS-free membrane concepts in PEM water electrolysis.

Introduction: Polymer electrolyte membrane water electrolysis (PEMWE) is a key technology for green hydrogen production, offering high current density operation and rapid response to dynamic power input. Cell performance arises from tightly coupled electrochemical and transport processes across the membrane–electrode assembly (MEA), including reaction kinetics, charge transport, water management, and two-phase flow. Physics-based modelling has therefore become an essential tool to analyse polarization behaviour and performance losses under realistic operating conditions [1–3].

Recent PEMWE modelling efforts increasingly emphasize the influence of porous transport layers, two-phase effects, and operating conditions on cell efficiency and performance distributions [1,2,4]. However, the majority of existing models remain strongly focused on PFSA/PFAS membrane materials (e.g., Nafion™), for which transport correlations are relatively mature. As interest grows in membrane alternatives beyond PFAS, there is a clear need for model-based tools that can mechanistically assess how changes in membrane transport properties affect PEMWE performance [6].

In this work, a spatially resolved, steady-state one-dimensional PEMWE model is developed by adapting a reference physics-based PEM fuel cell framework by Vetter et al. [7], reformulated for electrolysis operation. The focus is placed on documenting the required model adaptations and demonstrating how the resulting framework can be used to assess performance trade-offs of non-PFSA membranes.

Objectives: The objectives of this study are to:

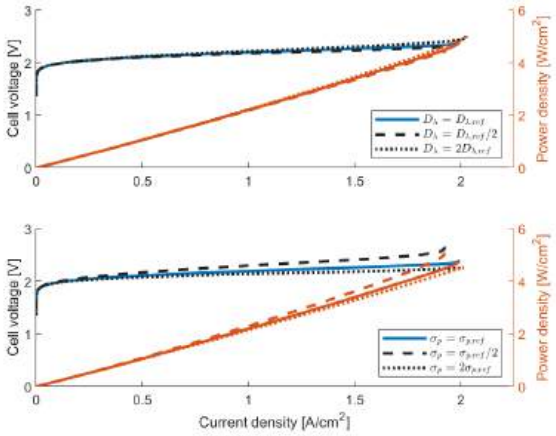
- develop a steady-state, physics-based one-dimensional PEM water electrolyzer model based on a reference PEM fuel cell formulation by Vetter et al. [7], reformulated for electrolysis;
- resolve through-plane coupling of charge and species transport across the MEA using interface-based boundary conditions;
- explicitly identify and document the electrochemical, transport, and operating-condition adaptations required for PEMFC-to-PEMWE conversion;
- establish a consistent parameter set representative of realistic PEMWE operation;
- demonstrate the applicability of the converted framework for studying performance trade-offs associated with PFSA and non-PFSA membrane concepts

Material and methods: A one-dimensional, macro-homogeneous through-plane MEA model is employed, comprising anode PTL, anode catalyst layer, membrane, cathode catalyst layer, and cathode PTL. Charge conservation is coupled with species and water transport using interface-based boundary conditions. The numerical framework and discretization follow the validated PEMFC model of Vetter et al. [7], reformulated for PEM water electrolysis by reversing reactions, transport directions, and boundary conditions.

The oxygen evolution reaction is modeled at the anode catalyst layer and the hydrogen evolution reaction at the cathode. Fully saturated membrane conditions are assumed, with electro-osmotic drag (2.5–3.5) and back-diffusion governing water transport. Liquid water is supplied at the anode, and hydrogen is produced at elevated cathode pressure.

A 125 µm membrane with a reference proton conductivity of 10 S cm^{-1}, and a water diffusivity of 7.0 x 10^{-6} cm^2 s^{-1} at 80 °C is applied. Strongly asymmetric kinetics are used, and high-pressure operation is considered, with anode pressures of 1–30 bar and cathode pressures of 30–80 bar.

Results: The converted PEMWE model is applied using a Nafion-based membrane as the reference case. Simulated polarization curves for a representative PEM water electrolyzer (Nafion NR-211) under typical operating conditions, illustrating the impact of water diffusivity and proton conductivity, are shown in Figure 1. The non-PFAS case exhibits an increased cell voltage at a given current density, indicating a performance penalty primarily associated with increased membrane related losses.



curves for a representative PEM water electrolyzer (Nafion NR-211) under typical operating conditions, illustrating the impact of water diffusivity and proton conductivity.

Because the model resolves spatial distributions across the MEA, these differences can be mechanistically attributed to changes in membrane proton conductivity and water transport behaviour. Reduced conductivity leads to a higher membrane ohmic drop, while altered water transport affects membrane hydration and local reaction environments. The magnitude and qualitative trends of the polarization curves are consistent with recent PEMWE modelling and validation studies reported in the literature [1–4].

Conclusions: A steady-state, one-dimensional physics-based PEM water electrolyzer model was developed through explicit conversion of a reference PEM fuel cell framework. By systematically identifying the required electrochemical, transport, and operating-condition adaptations, the work provides transparency on the PEMFC-to-PEMWE reformulation process.

The converted framework retains the numerical robustness of the original fuel-cell model and enables realistic simulation of electrolyzer operation. Application to PFSA and representative non-PFSA membrane cases demonstrates its suitability as a screening and insight tool for evaluating membrane-related performance trade-offs, supporting membrane development and experimental prioritization.

Acknowledgment: This work was performed within the PROMISERS project framework. The authors acknowledge the contributions of project partners and supporting colleagues.

References

[1] Lettenmeier, P.; Kolb, S.; Stiber, N.; Fallisch, A.; Zielke, L.; Thiele, S.; Gago, A.S.; Friedrich, K.A. *Comprehensive investigation of novel porous transport layers for polymer electrolyte membrane water electrolyzers.* Energy Environ. Sci. 2017, 10, 2521–2533.

[2] Schuler, T.; De Bruycker, R.; Schmidt, T.J.; Büchi, F.N. *Polymer Electrolyte Water Electrolysis: Correlating Performance and Porous Transport Layer Structure – Part I: Physical Modeling.* J. Electrochem. Soc. 2019, 166, F270–F281.

[3] Espinosa-López, M.; Darras, C.; Poggi, P.; Glises, R.; Baucour, P.; Rakotondrabe, A.; Besse, S.; Serre-Combe, P. *Modelling and experimental validation of a 46 kW PEM high-pressure water electrolyzer.* Renew. Energy 2018, 119, 160–173.

[4] Majasan, J.O.; Cho, J.I.S.; Dedigama, I.; Tsaoulidis, D.; Shearing, P.; Brett, D.J.L. *Two-phase flow behaviour and performance of polymer electrolyte membrane electrolysers.* Int. J. Hydrogen Energy 2018, 43, 15659–15672.

[5] Toghyani, S.; Afshari, E.; Baniasadi, E.; Atyabi, S.A. *Thermal and electrochemical analysis of different flow field patterns in a PEM electrolyzer.* Electrochim. Acta 2018, 267, 234–245.

[6] Schalenbach, M.; Tjarks, G.; Carmo, M.; Lueke, W.; Mueller, M.; Stolten, D. *Acidic or alkaline? Towards a new perspective on the efficiency of water electrolysis.* J. Electrochem. Soc. 2016, 163, F3197–F3208.

[7] Roman Vetter, Jürgen O. Schumacher, Free open reference implementation of a two-phase PEM fuel cell model, Computer Physics Communications, Volume 234, 2019, Pages 223-234, ISSN 0010-4655, https://doi.org/10.1016/j.cpc.2018.07.023.



Pressurized alkaline electrolyser: technical challenges towards a high-pressure design

Beatrice Bulzacca[a], Alessandro Guzzini*[a], Emanuela Marzi[b], Giuseppe Nigliaccio[b], Marco Pellegrini[a], Cristina Renzi[b], Cesare Saccani[a]

* corresponding author: alessandro.guzzini2@unibo.it

[a] Department of Industrial Engineering, University of Bologna, Viale del Risorgimento 2, 40136 Bologna (BO), Italy.

[b] ENEA, TERIN-DEC-H2V, via dei Mille 21, 40121, Bologna, Italy.

Keywords: energy transition, hydrogen, alkaline electrolysis, pressurized electrolyser

Abstract

Current research is focused on developing innovative solutions to improve the performance of state-of-the-art water electrolysis technologies. Increasing the operating pressure to high values represents another important challenge. Recent European calls, for example, have set targets requiring operating pressures above 30 bar(g) for alkaline water electrolyzers. To address this challenge, the "*LA1.1.2 PNRR PorH2*" project investigated the technical issues associated with high-pressure operation and designed both cell and stack prototypes. This paper presents the main results obtained from thermomechanical and fluid-dynamic simulations and provides key recommendations for future research activities.

Introduction: Although hydrogen has recently experienced a golden age, interest in hydrogen technologies appears to have cooled in recent years. This trend can be attributed to several factors, including the complexity of permitting procedures, the high capital and operating costs that are often not compensated by adequate incentive schemes, and the relatively low efficiency of the overall value chain, from production to end use. These factors contribute to investments that are either unprofitable or characterized by long payback periods. Reducing costs and improving efficiency inevitably require dedicated research and development activities. The most recent Strategic Research and Innovation Agenda (SRIA) identifies several key performance indicators related to efficiency, cost, reliability, and material utilization that must be achieved to support the widespread deployment of hydrogen technologies [1]. Recently, renewed interest has emerged within the scientific community regarding high-pressure operation of water electrolysis systems. High-pressure operation can reduce the compression work, decrease the number of compressor stages required, or even eliminate the need for downstream compression in low-pressure applications. Several attempts to increase the operating pressure of alkaline electrolyzers have been reported in literature [2–5]. Among them, recent studies conducted at Brandenburg University of Technology Cottbus–Senftenberg demonstrated a medium-scale (55 kW) prototype designed to operate at pressures up to 60 bar(g). However, the

absence of commercially available solutions suggests that the additional design complexity has not yet been sufficiently compensated by the associated benefits. Consequently, future research should focus on low-TRL innovative concepts capable of simplifying system design while simultaneously improving overall performance.

Objectives: The current work aims to summarize the main findings obtained from the design of a single cell and a stack prototype of alkaline water electrolyser. To minimize the mechanical stress on the frame, a pressure vessel was considered to contain the components.

Material and methods: Several aspects and constraints have taken into account during the design of the prototype. First, fluid-dynamic simulations were performed in Ansys Fluent R2025 software to evaluate the flow and the temperature profiles. Bubble size distribution based on operating pressure was considered to account for the effect of operating pressure. Thermomechanical simulation was performed with FEA Nastran software to evaluate the mechanical stresses experienced from the main components. Linear static analysis was performed when no large movements and no yielding occur. Non-linear static analysis was adopted for other cases.

Results: Focusing on fluid-dynamic analysis, the effect of cell design was investigated. For example, hydrogen volume fraction at the cathode side at a pressure of 60 bar(g) was shown in Figure 19. The inlet and outlet channels are not perfectly positioned at the top and the bottom of the cell, but an offset was imposed. This condition is responsible for a more complex fluid dynamic compared to what would occur in the case of perfectly aligned ducts. However, the result confirms an increase in hydrogen concentration towards the outlet reaching values close to 80%. Figure 20 shows the results of thermomechanical simulation considering AISI 316L as material of the frame. Plastic materials were also simulated because of their convenience in terms of lower costs and ease of manufacturing compared to metallic ones. However, the analysis confirms their greater difficulty in dissipating heat to the surrounding environment compared to metallic materials.

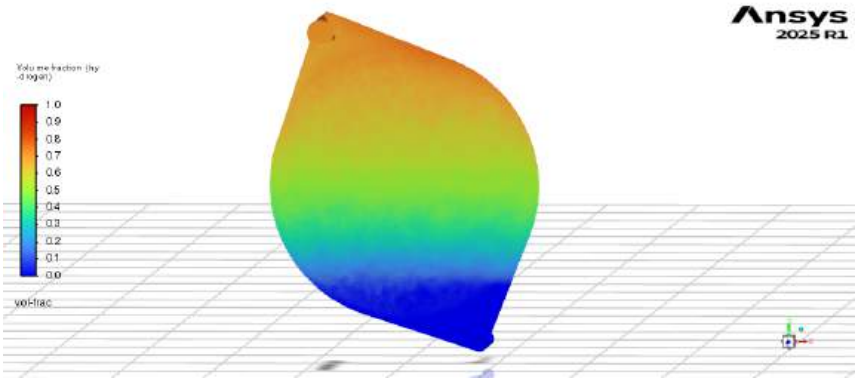


Figure 19. Hydrogen volume fraction on the cathode side for an operating pressure of 60 bar(g).

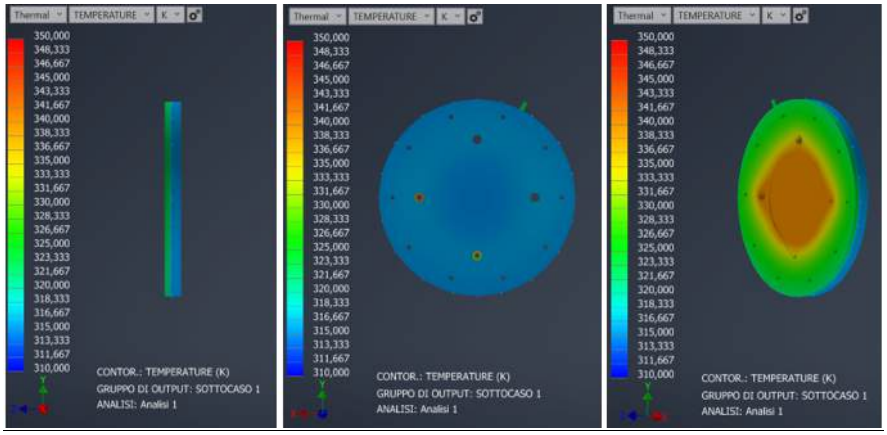


Figure 20. Results of the thermomechanical simulation for AISI 316L.

Conclusions: An alkaline cell and stack prototypes have been designed for the operation at relatively high-pressures. However, further research is still required. First, commercial sealing solutions require high contact pressures to minimize leakage rates under high operating pressures. This requirement may result in large forces, leading to the need for bolts and Belleville spring complex configurations. Second, the adoption of plastic materials for the frame could be hindered by the cost. Therefore, the frame design should be optimized to reduce material waste during manufacturing. Third, the pressure vessel is also a critical component. Although steel is currently the most widely used material, its overall weight and cost may represent significant barriers. On the other hand, even though lighter materials such as carbon fiber have already been certified for high-pressure hydrogen applications, their applicability and suitability for this specific application have not yet been fully verified.

Acknowledgment

This research was funded by the European Union – NextGeneration EU from the Italian Ministry of Environment and Energy Security POR H2 AdP MMES/ENEA with involvement of CNR and RSE, PNRR - Mission 2, Component 2, Investment 3.5 "Ricerca e sviluppo sull'idrogeno".

References

[1] Clean Hydrogen Joint Undertaking. Strategic Research and Innovation Agenda 2021-2027.

[2] Metkon S.A. 1985. Apparatus for the electrolysis of solutions. US 4758322.

[3] von Hoerner-System GmbH. 1996. Electrolysis cell block assembly installed within high pressure pipe. DE 4418999 C2.

[4] Shug CA. 1998. Operational characteristics of high-pressure high efficiency water hydrogen electrolysis. Int J Hydrogen Energy, 23, 1113–20.

[5] Kuleshov, V.N., Kurochkin, S.V., Udris, E.Y. 2020. High-pressure alkaline water electrolyser of coaxial configuration, J. Phys. Conf. Ser., 1683, 5.

European Fuel Cells and Hydrogen
PIERO LUNGHI CONFERENCE
September 15th-17th 2026
Capri / Italy

InnAEM: Innovative Materials for Anion Exchange Membrane Water Electrolysis

Miryam Gulino [a, b], Davide Principe[a,b], Teo Martin[b], Marco Martino[b], Anna Paola Panunzi [b], Marta Feroci[a], Maria Assunta Navarra[a], Valentina Naticchioni[b]*

* Corresponding author: valentina.naticchioni@enea.it

[a] Department of Basic and Applied Sciences for Engineering (SBAI), Sapienza University, Rome, Italy
[b] *ENEA, Italian National Agency for New Technologies, Energy and Sustainable Economic Development – Energy Technologies and renewable Sources Department Hydrogen and New Vectors Laboratory- TERIN-DEC-H2V, Via Anguillarese, 301-00123 Rome, Italy*

Keywords: AEMWE, Materials, Electrocatalysts, Membranes

Abstract

The transition toward a green hydrogen economy is hindered by the cost and technological limitations of current electrolysers. This research aims to develop a next-generation membrane electrode assembly (MEA) through a synergistic design strategy. Cobaltite-type perovskite electrocatalysts with reduced or no critical metals were synthesized and employed for their alkaline stability and activity. In parallel, per- and polyfluoroalkyl substances (PFAS)-free polybenzimidazole (PBI)-based ion-solvating membranes were manufactured by electrospinning to achieve high ionic conductivity. The materials were chemically, physically, and electrochemically characterized for joint application in Anion Exchange Membrane Water Electrolysis (AEMWE) for sustainable green hydrogen production (Figure 1).

Introduction: Electrocatalysts and membranes are key materials determining performance, cost, and sustainability in AEMWE. Replacing noble-metal catalysts with non-noble alternatives and fluorinated polymers with fluorine-free materials, represents a major challenge for this technology. Although benchmark catalysts such as Pt, RuO_2 and IrO_2 exhibit excellent activity, their cost and scarcity hinder large-scale deployment, motivating the search for transition-metal-based alternatives. Among these, perovskite-structured electrocatalysts (ABO_3) are promising due to their compositional flexibility, which enables activity tuning through targeted doping, and their structural stability [1]. In parallel, fluorine-free PBI-based membranes represent a promising route toward durable and conductive anion exchange membranes [2].

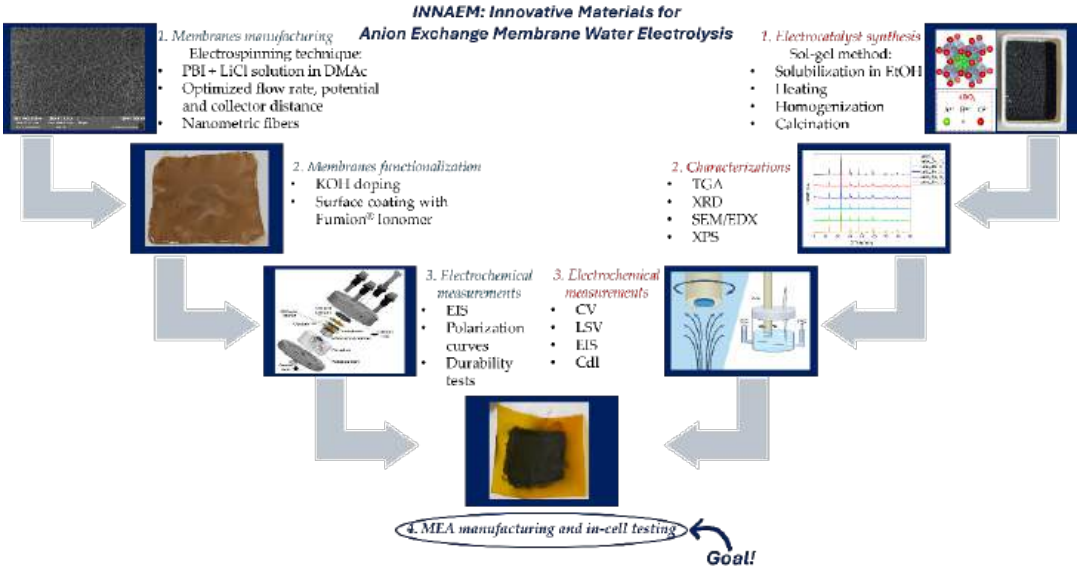


Figure 21: Workflow of the integrated approach adopted for the development of innovative materials.

Objectives: This work aims to address the lack of integrated strategies for AEM water electrolysis by simultaneously developing advanced electrocatalysts and anion exchange membranes. The project focuses on perovskite-structured (ABO_3) electrocatalysts and PBI-based ion-solvating membranes (ISMs), with the goal of integrating them into innovative MEAs and validating their performance at prototype scale.

Material and methods: Lanthanum–cobalt perovskite electrocatalysts B-site doped with fourth-period metals (Zn, Fe, Ni, Cu, Mn) were synthesized by sol–gel method at 70 °C using metal nitrates, citric acid and ethanol. The gels were calcined at 1100 °C for 6 hours to obtain the oxide phases. Thermal behaviour was studied by TGA, while crystal structure and morphology were characterized by XRD and SEM–EDX. Oxygen Evolution Reaction (OER) activity was evaluated by LSV and CV using a rotating disk electrode in 1.0 M KOH. PBI-based membranes were prepared by electrospinning of a 16 wt% commercial PBI solution. The membranes (τ≈50 μm) were washed in DI water, doped with KOH solutions at different concentrations and their alkali doping level (ADL) was determined. After coating with a thin Fumion® ionomer layer, the membranes were characterised by ATR-FTIR, SEM, optical microscopy, mechanical tests, air permeability and ionic conductivity. The best-performing membrane was then integrated into a 2 cm^2 MEA and tested in a lab-scale AEMWE cell by impedance spectroscopy, polarization curves, and 150 h galvanostatic operation.

Results: Crystalline and homogeneous microstructures were successfully obtained for all the doped cobaltite-based perovskites. XRD patterns revealed good agreement between experimental and simulated curves, suggesting that doping cations occupy the B sites of the perovskite structure. Onset potentials ranged from 1.6 to 1.8 V. Among samples, the Mn doped perovskite showed the best electrochemical performances, while the absence of reduction peaks confirmed the absence of

reducible oxide species (Figure 2a). Fibrous PBI membranes (d ≈ 150 nm) were successfully electrospun. Their high porosity allowed to reach ADL values up to 6 KOH molecules per PBI repeating unit. The ionomer coating turned the membranes into impermeable to KOH, water and air. Conductivity values (NaCl 0.5 M, RT) as high as 6.20 ± 0.44 mS cm^{-1} were achieved. In-cell test showed promising performance (Figure 2b) and stability, with a very low increase of 0.3 mV/h.

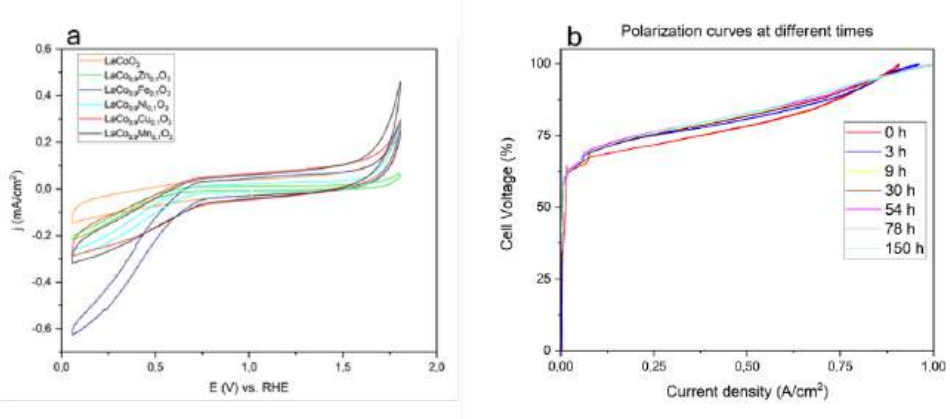


Figure 22: a) CV curves of the different doped perovskite electrocatalysts in 1M KOH; b) Polarization curves of a PBI AEM doped with KOH at different times.

Conclusions: Noble metals free electrocatalyst were successfully synthetised and the effect of different dopants on the perovskite structure and the resulting electrochemical properties were evaluated, identifying Mn as the best one of them. In parallel, novel PBI AEMs were manufactured through the employment of the electrospinning technique combined with surface coating, achieving conductivity values and electrochemical performances comparable to commercial benchmarks. Next step will be the integration of these two materials in an optimized MEA and their testing in a 5 cm^2 test station.

Acknowledgment: This research was supported by the POR H2 - W.P. 3.1 – LA 3.1.1 “Sviluppo di processi per la produzione di membrane a conduzione protonica ad alta temperatura” and LA 3.1.3 “Sviluppo di elettrocatalizzatori basati su metalli e leghe di metalli M/C a elevata area superficiale,” and by the “Avvio alla Ricerca 2026” Grant from Sapienza University of Rome.

References

[1] F. Hadji, M. Omari, and M. Mebarki, “Boosting the electrocatalytic activity of lanthanum cobaltite ceramic through Zn doping for the oxygen evolution reaction”, Ceram Int, vol. 49, no. 15, pp. 25405–25413, Aug. 2023.

[2] D. Henkensmeier, W.-C. Cho, P. Jannasch, J. Stojadinovic, Q. Li, D. Aili and J. O. Jensen, “Separators and Membranes for Advanced Alkaline Water Electrolysis,” Chem. Rev., vol. 124, no. 10, pp. 6393-6443, 2024.



Surface treatment of stainless steel porous transport layer for oxygen evolution reaction enhancement in an anion exchange membrane electrolyser

Stefan Edinger[a], Helena Kern[a,b], Janine Lichtenberger[a], Martin Krammer[a], Jürgen Fleig[b],

Rachmat Adhi Wibowo*[a]

*corresponding author: rachmat.wibowo@ait.ac.at

[a] AIT Austrian Institute of Technology, Power and Renewable Gas s,
Giefinggasse 2, 1210, Vienna, Austria

[b] Institute of Chemical Technologies and Analytics, TU Wien,
Getreidemarkt 9, 1060 Wien, Austria

Keywords: anion exchange membrane electrolyser, catalyst, hydrogen, Nickel oxyhydroxide

Abstract

Introduction: Ni-based compounds, such as Ni-alloys, CoPi, NiMoFe, $NiFeO_xH_y$, $CoFeSeO_x$, and FeCo, have been studied for OER catalysts due to their low OER overpotential [1,2]. It was reported that Ni-based OER catalysts can also be prepared by a direct, in-situ growth on a stainless steel through solution-processed surface treatments [3-6], which is an attractive synthesis route for developing an OER catalyst for the anion exchange membrane electrolyser (AEMEL). A stainless steel possesses elemental compositions consisting of Fe, Ni, and Cr, which can be the source for growing a Ni-based catalyst layer. When it is implemented as a porous transport layer (PTL) in an AEMEL, it also exhibits high conductivity, which reduces the overall electrolyser resistance, leading to higher electrolyser voltage at the same applied current density. Moreover, the growth of an in-situ OER catalyst layer directly on a stainless steel can also enhance the charge transport during AEMEL operation [3].

Objectives: This study aimed to develop a durable Ni-based OER catalyst through the direct growth of a Ni-based catalyst thin layer on stainless steel by alkaline immersion for AEMEL application.

Material and methods: The stainless steel felts, or SSFs, of 316 type (SS316, Bekaert Currento PTL SS-71/260, Belgium) were used. The surface treatment of the SSF was done by immersing the SSF in an alkaline solution composed of 0.133 M $(NH4)_2S_20_8$ and 2 M NaOH at room temperature at various immersion times. The as-immersed SSF structure was studied using a scanning electron microscope at 5 kV accelerating voltage (SEM, Carl Zeiss, Germany). A Raman spectroscopy (Horiba, Germany) from 400 – 5000 cm^{-1} using a 532 nm laser wavelength at a power of 1 mW was also utilised to analyse the surface-activated felts.

The electrochemical behaviour of the as-immersed SSF was investigated by performing cyclic voltammetry (CV) and electrochemical impedance spectroscopy (EIS) using 1 M KOH as the electrolyte. A three-electrode electrochemical cell was used, employing a reversible hydrogen electrode (RHE) (Gaskatel, Germany), the as-immersed SSF working electrode, and Pt-Ti counter electrodes. The solution resistance, R, between the working electrode and reference electrode was determined using the high-frequency intercept of the EIS Nyquist plots fitted using RelaxIS software. The potential values throughout this contribution were iR-corrected. The as-immersed felts were cut into a 4.84 cm^2 area, and were integrated into an AEMEL cell (Dioxide Materials, USA) as the anode. The cathode was a sputtered Ni_4Mo layer with a nominal thickness of 200 nm on a 4.84 cm^2 carbon paper. An anion exchange membrane (Orion, USA) with an area of 16 cm^2 separated the anode and the sputtered Ni_4Mo, forming a membrane-electrode assembly (MEA). A polarisation curve was obtained through a series of chronopotentiometry measurements, each maintained for 5-10 min. Subsequently, the current was maintained at 1210, 2410mA, 3630, and 4840 mA for 4 8 min.

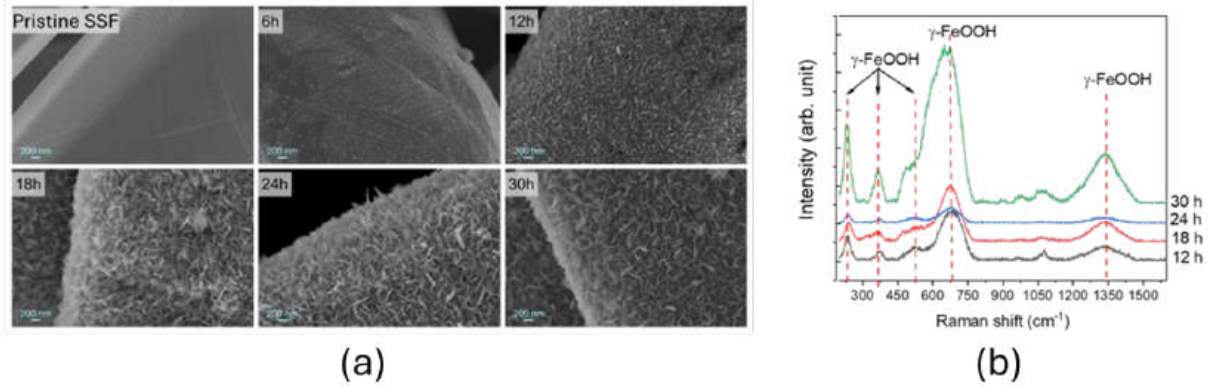
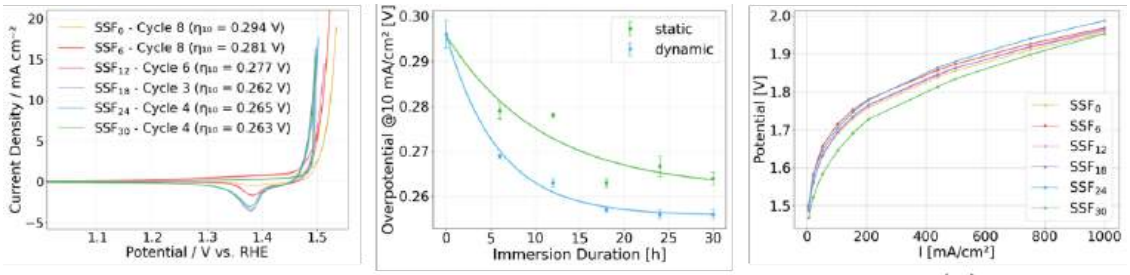


Figure 1. (a) SEM images of the pristine and immersed SSFs as a function of immersion time. (Right) The corresponding Raman shifts of the pristine and immersed SSFs.

Results: In-depth microscopic analysis of the as-immersed SSF. reveals that the immersion at different times promotes a uniformly grown lamellar structure, starting from a small randomly distributed nuclei-like feature after 6 hours of immersion, to a fully grown lamellar structure after 30 hours of immersion, as seen in Figure 1(a). Raman spectroscopy structural analysis, presented in Figure 1(b) suggests that the lamellar structure consists of the FeOOH phase. The cyclic voltammograms of the as-immersed felts reveal a systematic OER current density shift towards lower overpotential, measured at 10 mA/cm^2. It is worth noting that the CV results also represent a typical Ni oxidation-reduction behaviour, which implies that the SSF surface may be enriched by $Ni(OH)_2$, which is a typical active catalyst towards OER (Figure 2(a)). This finding has been confirmed by XPS experiments (not shown). Figure 2(b) shows the quantitative progressive OER overpotential decrease as a function of alkaline immersion time taken from the CV measurement. The overpotential continuously declines towards 0.265 V as the alkaline immersion is extended to 30 hours, due to the extensive growth of the lamellar structure that provides more catalytically active sites for OER. We

found that the progress of the OER overpotential decline reaches a plateau within 24 – 30 hours of immersion time. An optimisation of alkaline immersion of SSF with a simple stirring was sufficient to bring the OER overpotential down to 0.255 V, as also shown in Figure 2(b). A polarisation test demonstrates that at 1 A/cm^2, the AEMEL can operate at 1.85 V using the 30-hour immersed SSF as the anode and OER catalyst (Figure 2(c)).

Figure 2. (a) CV tests for the "blank" or pristine SSF and immersed SSF at various immersion times. The dotted red line marks the 10 mA/cm^2 reference for determining OER overpotential. (b) The



overpotential trend as a function of immersion time from the CV data on the Left, measured at 10 mA/cm^2.(c) Polarisation results of the AEMEL.

Conclusions: As a summary, the alkaline immersion leads to a surface modification of the SSF surface into a lamellar structure with the main phase of FeOOH and a small amount of $Ni(OH)_2$ as a secondary phase. Despite it being the main phase, the FeOOH is well known to be not catalytically active species. Nevertheless, the small amount of $Ni(OH)_2$ phase in the lamellar structure has an indication to play an important role in reducing the SSF overpotential, making the SSF exhibit high OER catalytic activity, as seen in the CV as well as AEMEL polarisation tests.

Acknowledgment. The project is partially supported by the Clean Hydrogen Partnership and its members, under the ENDURION project, Grant Agreement No. 101192485, as well as the Austrian FFG HyCentA COMET Center project.

References

[1] Charles C. L. McCrory, et al., J. Am. Chem. Soc. 137, 4347−4357, 2015.

[2] Peugeot et al., Joule 5, 1281–1300, 2021

[3] H. Schäfer, et al, Energy Environ. Sci., 8, 2685, 2015.

[4] H. X. Zhong, J. Wang, F. L. Meng, X. B. Zhang, Angew. Chem. Int. Ed. 55, 9937–9941.2016.

[5] F. S. Yu, F. Li, L. C. Sun, Int. J. Hydrogen Energy 41 (10), 5230–5233, 2016.

[6] S. N. Sampathkumar, T.B. Ferriday, P.H. Middleton, J. Van Herle, Electrochemistry Communications 146, 107418, 2023.



Towards high-pressure AEM electrolyzer single-cell design through coupled electro–thermo–mechanical modeling

Martina Prastaro*[a], Hosein Parsayan[a], Mohsen Mansourkiaei[a], Leonardo Catalano[a], Domenico Ferrero[a], Massimo Santarelli[a], Giuseppe Nigliaccio[b], Cristina Renzi[b]

*Corresponding author: Martina Prastaro

[a]Department of Energy (DENERG), Politecnico di Torino, Turin, Italy

[b]ENEA – Italian National Agency for New Technologies, Energy and Sustainable Economic Development, Bologna Research Centre, Bologna, Italy

Keywords: Anion exchange membrane electrolysis, Single-cell design, High pressure analysis, Multiphysics modeling

Abstract

Introduction: Anion exchange membrane water electrolysis is a promising route for green hydrogen production, particularly for pressurized operation with potentially non-critical materials. However, high-pressure AEM cell design requires the simultaneous control of electrochemical performance, heat generation, sealing reliability, and mechanical stress. Since polarization curves alone cannot describe local current-density distribution, temperature gradients, compression uniformity, and sealing-critical regions, coupled electrochemical, thermal, and mechanical analysis is needed to support the transition from single-cell studies toward multi-cell configurations.

Objectives: This study develops a coupled three-dimensional electro–thermo–mechanical model of a high-pressure AEM water electrolysis cell. The model reproduces a planar rectangular zero-gap cell inspired by the NREL high-pressure low-temperature electrolysis hardware [1], including the membrane–electrode assembly, porous transport layers, catalyst layers, bipolar plates, sealing regions, and metallic compression structure. The selected architecture combines reinforced sealing with a triple-serpentine flow-field layout, providing a scalable and pressure-compatible design concept for high-pressure operation [2].

Material and methods: The modeling framework integrates Secondary Current Distribution, Porous Electrode formulation, Heat Transfer in Solids, and Solid Mechanics in COMSOL Multiphysics. The electrochemical model resolves ionic/electronic potentials, charge-transfer kinetics, and porous-electrode current distribution in homogenized porous domains. Heat generation from activation and ohmic losses is coupled with conductive heat transfer, while the mechanical model evaluates deformation, pressure distribution, and von Mises stress under clamping and operating pressure. Concentration overpotentials, detailed two-phase flow, and fully resolved channel fluid dynamics are not explicitly included. Simulations are performed at 70 °C, 30 bar, with 1 M KOH electrolyte and 25 cm^2 active area. Electrochemical results are compared with published AEMWE polarization data,

while thermal and mechanical fields are benchmarked against published numerical and finite-element studies.

Results: The predicted current density increases from 0.049 A cm^{-2} at 1.5 V to 1.24 A cm^{-2} at 2.2 V, falling within the selected AEMWE literature performance envelope [3]. The current-density field is mainly through-plane, as expected for a zero-gap architecture, with localized intensification near inlet and edge regions. The thermal analysis predicts a membrane-centered temperature maximum of approximately 360 K, consistent with dominant ionic ohmic heating, with smooth gradients toward porous layers and metallic components. Agreement with published thermal models is observed in terms of maximum-temperature location and spatial gradient distribution [4]. The mechanical analysis shows that the applied clamping load (~20.86 kN) produces von Mises stress levels of the order of 10 MPa in the membrane and structural components, consistent with comparable finite-element literature results [5]. The deformation field is symmetric and stable, while gasket and porous-layer pressure distributions highlight the role of compression uniformity in sealing reliability, contact resistance, and durability.

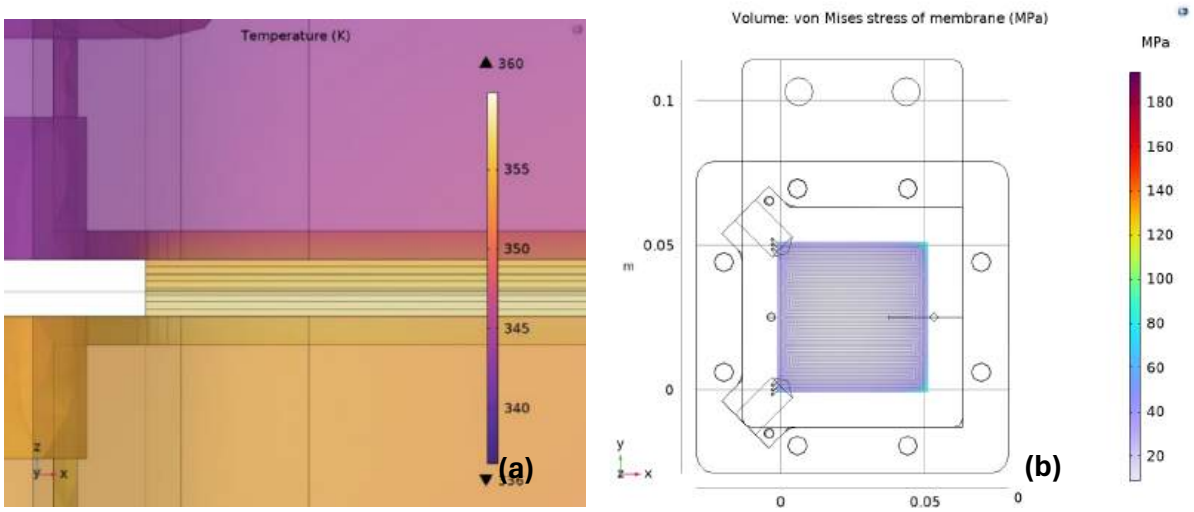


Figure 1. *Representative results from the coupled electro–thermo–mechanical model: (a) temperature distribution showing a membrane-centered maximum and (b) von Mises stress distribution in the membrane under cell compression.*

Conclusions: The main innovation of this work is a design-oriented multiphysics modeling workflow linking electrochemical performance, heat generation, and mechanical reliability within a unified framework. By resolving local current-density, temperature, deformation, and compression fields, the model identifies critical regions that cannot be detected from global polarization curves alone, enabling the assessment of trade-offs between electrochemical performance, high-pressure operation requirements, and mechanical integrity. Although concentration overpotentials, detailed

two-phase flow, hydration-dependent membrane conductivity, and nonlinear porous-media compression are not explicitly included, the dominant steady-state electrochemical, thermal, and mechanical phenomena governing high-pressure AEM operation are consistently captured. Overall, the coupled electro–thermo–mechanical model provides an engineering basis for the design and optimization of high-pressure AEM water electrolysis cells.

Acknowledgment

This work has been carried out within a collaboration between Politecnico di Torino and ENEA.

References

[1] Wrubel, J. A., Ware, S., Schaffer, C., Allen, M., Klein, E., Rice, R., Engtrakul, C. and Bender, G., NREL 25-cm^2 high-pressure low-temperature electrolysis cell hardware (open source), NREL Data Catalog, National Renewable Energy Laboratory, Golden, CO, 2023, DOI: 10.7799/2205626.

[2] Loh, A., Li, X., Sluijter, S., Shirvanian, P., Lai, Q. and Liang, Y., Design and scale-up of zero-gap AEM water electrolysers for hydrogen production, Hydrogen, 4 (2023), 257–271, DOI: 10.3390/hydrogen4020018.

[3] Delp, E., Mishra, R. and Wagner, E., Evaluation of complex multiphysics phenomena at gas diffusion electrodes during high-pressure water electrolysis with AEMs, Scientific Reports, 15 (2025), 24866, DOI: 10.1038/s41598-025-05216-5.

[4] Bock, R., Karoliussen, H., Seland, F., Pollet, B. G., Thomassen, M. S., Holdcroft, S. and Burheim, O. S., Measuring the thermal conductivity of membrane and porous transport layer in proton and anion exchange membrane water electrolyzers for temperature distribution modeling, International Journal of Hydrogen Energy, 45 (2020), 1236–1254, DOI: 10.1016/j.ijhydene.2019.01.013.

[5] Ozdemir, S. N., Taymaz, I., San, F. G. B. and Okumuş, E., Performance assessment and optimization of the PEM water electrolyzer by coupled response surface methodology and finite element modeling, Fuel, 365 (2024), 131138, DOI: 10.1016/j.fuel.2024.131138.



Electrochemical analysis of long-term performance of Molten Carbonate Electrolysis Cells under simulated seawater feed

Silvia Lo Conte*[a,b], Alessia Gwis[c], Fiammetta Rita Bianchi[c], Massimiliano Della Pietra[b], Francesca Santoni[b], Alfredo Zingone[b], Barbara Bosio[c], Elio Jannelli[a]

* corresponding author: silvia.loconte@uniroma1.it

[a] Department of Engineering, University of Naples "Parthenope",

Centro Direzionale Isola C4, Naples, 80143, Italy

[b] ENEA - Italian National Agency for New Technologies, Energy and Sustainable Economic Development, via Anguillarese 301, Rome, 00123, Italy

[c] Department of Civil, Chemical and Environmental Engineering, University of Genoa,

via Opera Pia 15, Genoa, 16145, Italy

Keywords: Electrochemical characterization, Fuel electrode degradation, Molten carbonate electrolysis cell, Seawater electrolysis

Abstract: Seawater electrolysis results in a promising solution for green energy production by minimising the freshwater footprint, but salt contamination drastically penalises the performance after a few working hours. Molten carbonate electrolysis cells have been investigated due to their higher impurity tolerance, performing a preliminary comparison of long-term operation under steam derived from demineralised water and synthetic seawater.

Introduction: Water electrolysis is widely recognized as a key technology for sustainable hydrogen production; however, current systems mainly rely on freshwater resources. Considering that less than 1% of the Earth freshwater is readily accessible at an affordable cost, while seawater accounts for approximately 97.5% of the global water reserves, the direct utilization of seawater represents an attractive alternative [1]. Nevertheless, low-temperature seawater electrolysis faces several challenges, including corrosion phenomena, electrode and membrane degradation caused by dissolved ions, competition between the oxygen evolution and chlorine evolution reactions, and the formation of insoluble precipitates that can compromise long-term operation. Significant research efforts have been devoted to developing more robust electrode materials and cell architectures [2,3]. Despite few available studies, high-temperature electrolysis technologies, such as Solid Oxide Electrolysis Cells (SOECs) and Molten Carbonate Electrolysis Cells (MCECs), are considered promising alternatives due to their potential tolerance to contaminants and reduced susceptibility to chloride-related issues [4]. Despite these advantages, the operation of molten carbonate cells with seawater-derived feeds remains largely unexplored.

Objectives: The present work investigates the durability of MCECs operated with synthetic seawater-derived steam as an alternative steam source for hydrogen production. The study aims to assess the impact of seawater-derived species on fuel electrode performance by comparing long-term operation under synthetic-derived steam and demineralized water feeding conditions. Particular attention is devoted to the evolution of electrochemical performance and degradation phenomena through voltage monitoring and impedance analysis. The final objective is to identify the main degradation mechanisms associated with synthetic seawater operation and provide preliminary insights into the feasibility of seawater-fed high-temperature electrolysis in molten carbonate systems.

Material and methods: Durability tests were performed on laboratory-scale MCECs composed of state-of-the-art materials (3 cm^2 active area). Two independent durability campaigns were carried out under galvanostatic conditions: a reference test using demineralized water and a second test employing synthetic seawater as the steam source. The cells were operated at 650 °C with a fuel electrode gas composition of 40/40/20 mol% $H_2O/CO_2/H_2$ and a total flow rate of 200 Nml min^{-1}, while the oxygen electrode was supplied with 15/30/55 mol% $O_2/CO_2/N_2$. In the seawater configuration, the cathodic feed was generated by bubbling a dry H_2/CO_2 mixture through a thermostated three-necked bottle filled with synthetic seawater. Synthetic seawater was prepared by dissolving a commercial sea salt mixture in demineralized water to reproduce the average salinity of natural seawater, corresponding to approximately 38 PSU. Cell and single electrode performance was periodically evaluated through polarization curves and EIS analysis, using a BK Precision 9201 Multi-Range DC Power Supply and a Solartron SI-1260 frequency response analyser coupled with a Solartron SI-1287 electrochemical interface, respectively.

Results: The reference durability test with demineralized water lasted for more than 1000 h, whereas the test under synthetic seawater-derived steam was limited to slightly over 500 h due to the observed higher voltage increase. To compare their degradation behaviour, Figure 1 (left) reports the absolute Degradation Rate (DR) of the fuel electrode operating voltage at 100 mA cm^{-2} that confirms a progressive loss of performance. In the reference cell, the voltage shows a nearly continuous increase throughout the test duration but with a decreasing rate up to 400 h, where the degradation rate almost stabilizes. In contrast, the cell operated with synthetic seawater exhibits a significantly higher degradation rate during the whole lifetime. Its non-monotonic trend indicates a complex evolution of the degradation mechanisms, with an initial attenuation, followed by a progressive increase and a subsequent quasi-steady regime. Both high- and low-frequency contributions are conditioned (Figure 1 right), indicating that degradation should affect both charge transfer and mass transport processes. This behaviour may be associated with microstructural changes of the fuel electrode, such as partial pore blockage, as well as possible modifications of the electrolyte composition due to the presence of Sodium and Potassium species derived from the synthetic seawater, which can influence electrolyte conductivity and electrode wettability [5].

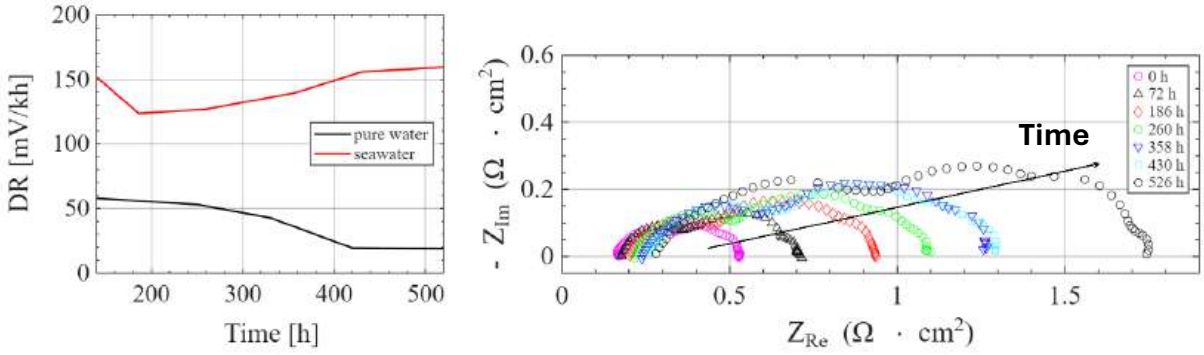


Figure 23. Absolute degradation rate of fuel electrode voltage at 100 mA cm^{-2} (left), EIS measurements at OCV performed on the fuel electrode fed with seawater (right).

Conclusions: A preliminary assessment of MCEC durability under synthetic seawater shows a higher degradation rate compared to conventional demineralized water feeding cells. Electrochemical analyses reveal a progressive increase in both ohmic and polarization losses at the fuel electrode, suggesting its microstructure degradation. These results provide a first experimental basis for evaluating the feasibility, limitations and degradation mechanisms associated with seawater-derived feeding in MCECs.

Acknowledgment

This research was partially funded by the European Union – NextGenerationEU from the Italian Ministry of Environment and Energy Security, POR H2 AdP MASE/ENEA with the involvement of the CNR and RSE, PNRR - Mission 2, Component 2, Investment 3.5 "Ricerca e sviluppo sull'idrogeno", CUP: I83C22001170006.

References

[1] Gleick, Peter H., et al. *The World's Water Volume 7: The Biennial Report on Freshwater Resources*. Island press, (2012).

[2] Tong, Wenming, et al. *Nature Energy* 5.5 (2020): 367-377.

[3] Mishra, Arti, et al. *Fuel* 361 (2024): 130636.

[4] Luo, Xing, et al. *International Journal of Hydrogen Energy* 48.28 (2023): 10359-10367.

[5] Bodén, Andreas, et al. *Journal of The Electrochemical Society* 155.2 (2008): B172-B179.

EFCH2 2026 European Fuel Cells and Hydrogen PIERO LUNGHI CONFERENCE
September 15th-17th 2026 Capri / Italy

Role of reverse Water-Gas Shift Reaction for CO_2 Utilization in Molten Carbonate Electrolysis Cells

Simone Mataloni*[a], Silvia Lo Conte[b,c], Massimiliano Della Pietra[c], Nicola Verdone[a]

* corresponding author: simone.mataloni@uniroma1.it

[a] Sapienza University of Rome, Department of Chemical Engineering Materials and Environment, Via Eudossiana 18, 00184 Rome, Italy

[b] Department of Engineering, Parthenope University of Naples, Centro Direzionale Isola C4, Naples, 80143, Italy

[c] Department of Energy Technologies and Renewable Sources, Laboratory for Hydrogen and new Energy Vectors (TERIN-DEC-H2V), ENEA Italian National Agency for Energy, New Technologies and Sustainable Economic Development, R.C. Casaccia, Rome, Italy

Keywords: CO_2 utilization, Molten Carbonate Electrolysis Cell, reverse Water-Gas shift.

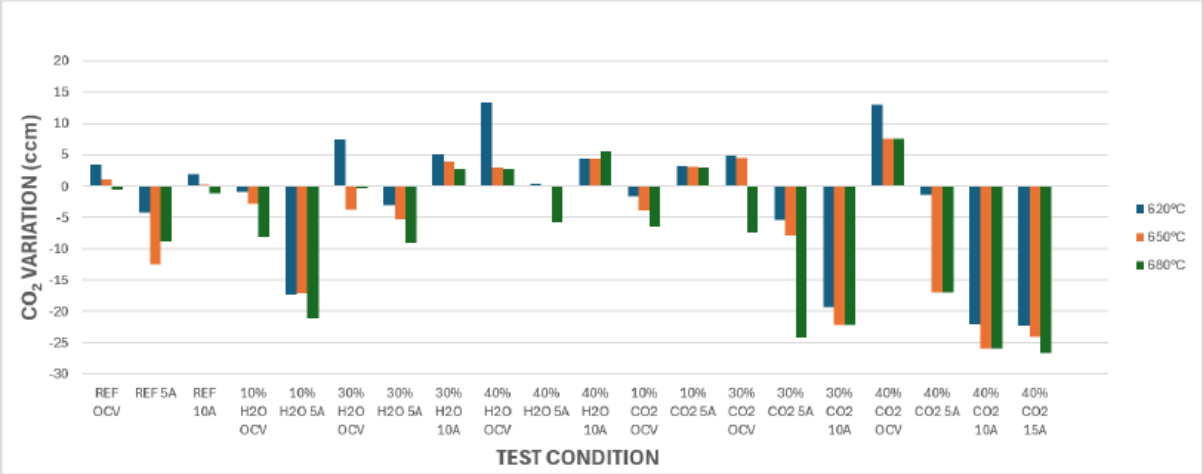


Figure 24. Variaton of CO_2 content after rWGS reaction in different test conditions

Introduction: Molten Carbonate Electrolysis Cells (MCECs) are emerging as promising technologies for high-temperature CO_2 utilization and conversion and hydrogen production. Under typical operating conditions for water and CO_2 co-electrolysis, chemical reactions such as the reverse water gas shift (rWGS) may significantly affect gas composition and apparent CO_2 conversion.

Objectives: This work aims to isolate and quantify the purely chemical contribution of rWGS reaction under conditions representative of MCEC operation, with the objective of improving the understanding and optimization of CO_2 utilization pathways in molten carbonate systems.

Material and methods: An experimental campaign was carried out on a laboratory-scale single molten carbonate cell operated at three high temperature (620-650-680 °C), without applying any electrical load. To decouple chemical effects from electrochemical phenomena, synthetic gas

mixtures were fed to the cell to simulate inlet compositions corresponding to different water and CO_2 co-electrolysis operating points. A systematic parametric analysis was performed by varying steam and CO_2 concentrations over a wide range representative of MCEC conditions. The outlet gas composition was continuously monitored using an N-DIR infrared gas analyzer, allowing quantitative evaluation of CO, CO_2, H_2 concentrations and direct assessment of rWGS reaction extent.

Results: The experimental results demonstrate that rWGS reaction contribute to gas composition changes under molten carbonate conditions. Reaction extents were found to slightly depend on temperature over the the investigated range. Quantifiable deviations between inlet and outlet CO_2 concentrations confirm the active role of chemical reactions in CO_2 consumption in MCEC environment. Was found that rWGS can lead to an increase of utilization of CO_2 up to 50% in simulated high current condition while producing up to 20% surplus of CO_2 in other conditions. This can significantly affect MCECs co-electrolysis efficiency, depleting or increasing reactants availability. Based on the experimental data, effective reaction rates and thermodynamic parameters were derived for conditions representative of high-temperature co-electrolysis operation.

Conclusions: By isolating the chemical contribution of rWGS reactions, this study provides essential experimental insight into CO_2 utilization mechanisms in molten carbonate electrochemical cells. The results highlight the need to explicitly account for chemical kinetics when evaluating CO_2 conversion efficiency in MCECs and related technologies. The derived kinetic information supports improved modeling and operational strategies aimed at maximizing CO_2 utilization, contributing to the development of high-temperature electrochemical systems within net-zero CO_2 emission and carbon capture and utilization frameworks.

Acknowledgment: This research was funded by the European Union - NextGenerationEU from the Italian Ministry of Environment and Energy Security, POR H2 AdP MEES/ENEA with involvement of CNR and RSE, PNRR - Mission 2, Component 2, Investment 3.5 "Ricerca e sviluppo sull'idrogeno", CUP: I83C22001170006

References

[1] S. Mataloni, S. Lo Conte, M. Della Pietra, F. Santoni, A. Zingone, and N. Verdone, "Effect of operating conditions on Molten Carbonate Electrolysis Cell performance: an experimental study," J. Power Sources, vol. 652, Oct. 2025, doi: 10.1016/j.jpowsour.2025.237692.

[2] E. Audasso, K. I. Kim, G. Accardo, H. S. Kim, and S. P. Yoon, "Investigation of molten carbonate electrolysis cells performance for H2 production and CO2 capture," J. Power Sources, vol. 523, Mar. 2022, doi: 10.1016/j.jpowsour.2022.231039.



Optimizing Contact Pressure in PEM Water Electrolyzers for the highest durability: Linking Impedance analysis and DRT to Performance

Mohsen Mansourkiaei*[a], Fatemeh Firouzi[a], Mariem Jnina[b], Massimo Santarelli [a]

*Corresponding author: Mohsen Mansourkiaei

[a] Department of Energy (DENERG), Politecnico di Torino, Turin, Italy

[b] LERMA, International University of Rabat, 11100 Sala Al Jadida, Morocco

Keywords: Cell Compression, Distribution of relaxation times (DRT), Electrochemical impedance spectroscopy (EIS), PEM electrolysis

Abstract

Introduction: Proton exchange membrane water electrolysis (PEMWE) is a promising technology for green hydrogen production due to its high efficiency, compact design, and excellent compatibility with renewable energy sources. The performance and durability of PEMWEs are influenced by several factors, including cell design, material selection, and operating conditions such as temperature, pressure, and water flow rate. Among these parameters, cell contact pressure is a critical assembly parameter, as it directly affects interfacial contact resistance, mass transport phenomena, and electrochemical reaction kinetics. Nevertheless, despite its critical role in cell operation, the influence of contact pressure on PEMWE degradation and long-term durability remains insufficiently understood [1], [2], [3].

Objectives: This study aims to optimize cell contact pressure for enhanced PEMWE performance and durability while elucidating the electrochemical mechanisms governing performance losses and degradation. Through the combined analysis of polarization behaviour, voltage degradation, electrochemical impedance spectroscopy (EIS), and Distribution of Relaxation Times (DRT), the work seeks to establish mechanistic relationships between contact pressure and the interfacial, kinetic, and mass-transport phenomena governing long-term cell operation.

Material and methods: Experiments were conducted using a flexible PEM/AEM electrolyser test station able to reach 150°C and 30 bars. Cells were tested in a Baltic Fuel Cells quickCONNECT qCf FC25/125LC 8bar-Ely fixture, which allows precise control of cell contact pressure. Two experimental campaigns were performed to investigate the influence of contact pressure on PEM water electrolyzer performance and durability. In the first campaign, a membrane electrode assembly (MEA) comprising a Nafion membrane with 3 mg cm^{-2} Pt and 3 mg cm^{-2} Ir catalyst loadings was evaluated under contact pressure levels of 2.4, 3.4, 4.4, and 5.0 bar, corresponding to a cumulative degradation testing duration of 253 h. In the second campaign, an MEA consisting of a Nafion 115 membrane, a 1 mg cm^{-2} Pt anode

catalyst, and a 2 mg cm^{-2} Ir cathode catalyst was employed. Tests were performed at 60 °C and 1 bar cathode pressure under four contact pressure levels: 2.4, 3.4, 4.4, and 4.9 bar. For each contact pressure, a degradation test of approximately 70 h was conducted at a current density of 1 A cm^{-2}, corresponding to a cumulative testing duration of approximately 300 h. Electrochemical characterization was performed before and after each pressure step during this degradation test using polarization curves and electrochemical impedance spectroscopy (EIS). In addition, Distribution of Relaxation Times (DRT) analysis was carried out to assess the influence of contact pressure on electrochemical loss mechanisms and degradation processes.

Results: In the first experimental campaign (ca. 250 h on a 3 mg cm^{-2} Pt / 3 mg cm^{-2} Ir MEA), contact pressure significantly influenced PEMWE durability and electrochemical behaviour. The highest degradation rate was observed at 2.4 bar (0.76 mV h^{-1}), whereas substantially lower degradation rates were obtained at 3.4 and 4.4 bar (0.16 and 0.17 mV h^{-1}, respectively). Increasing the pressure to 5.0 bar resulted in a higher degradation rate (0.38 mV h^{-1}).

In the second experimental campaign (300 h on a 1 mg cm^{-2} Pt / 2 mg cm^{-2} Ir MEA), a similar dependence on contact pressure was observed. The degradation rate decreased from 0.922 mV h^{-1} at 2.4 bar to 0.349 and 0.336 mV h^{-1} at 3.4 and 4.4 bar, respectively, reaching a minimum value of 0.234 mV h^{-1} at 4.9 bar. In addition, increasing contact pressure resulted in lower operating voltages, indicating improved electrochemical performance. EIS measurements showed a gradual decrease in both ohmic and charge-transfer resistances, with R_s decreasing from 1.21 to 1.13 Ω·cm^2 and R_{ct} decreasing from 0.84 to 0.73 Ω·cm^2 between 2.4 and 4.9 bar. Conversely, the mass-transport resistance exhibited only minor variations. These findings suggest that the performance improvement and reduced degradation at higher contact pressures were primarily associated with reduced contact resistance and kinetic losses [1], [4], [5].

Overall, both experimental campaigns demonstrate that contact pressure is a critical parameter governing PEMWE performance and durability, with an optimal pressure range identified between approximately 3.4 and 4.9 bar depending on the MEA configuration.

Conclusions: The main innovation of this work is the integration of durability analysis with the EIS, and DRT diagnostics to establish a mechanistic relationship between contact pressure and PEMWE degradation mechanism. These findings provide practical guidelines for cell assembly and stack design and demonstrate the value of advanced impedance-based diagnostics for optimizing the long-term operation of PEM water electrolyzers.

Through the combined use of polarization curves, long-term degradation testing, EIS, and DRT analysis, optimal compression windows were identified for different investigated cells. Within the identified ranges, the cells exhibited the best compromise between performance, electrochemical losses, and durability. The results show that insufficient compression increases interfacial contact

resistance and accelerates voltage degradation, while excessive compression may introduce transport limitations despite lower ohmic losses. DRT analysis provided additional resolution of the underlying electrochemical processes, enabling the differentiation of contact, kinetic, and mass-transport phenomena and their evolution during aging. [1], [2], [6].

References

[1] E. Borgardt *et al.*, 'Impact of clamping pressure and stress relaxation on the performance of different polymer electrolyte membrane water electrolysis cell designs', *Int. J. Hydrogen Energy*, vol. 44, no. 42, pp. 23556–23567, Sep. 2019, doi: 10.1016/j.ijhydene.2019.07.075.

[2] S. H. Frensch, A. C. Olesen, S. S. Araya, and S. K. Kær, 'Model-supported characterization of a PEM water electrolysis cell for the effect of compression', *Electrochim. Acta*, vol. 263, pp. 228–236, Feb. 2018, doi: 10.1016/j.electacta.2018.01.040.

[3] T. Srour *et al.*, 'On the contact resistance between the anode and the porous transport layer in a proton exchange membrane water electrolyzer', *Int. J. Hydrogen Energy*, vol. 58, pp. 351–361, Mar. 2024, doi: 10.1016/j.ijhydene.2024.01.134.

[4] U. Rost *et al.*, 'A novel advanced test system for polymer electrolyte membrane water electrolysis based on hydraulic cell compression', *Fuel Cells*, vol. 22, no. 6, pp. 284–289, Dec. 2022, doi: 10.1002/fuce.202200068.

[5] O. F. Selamet and M. S. Ergoktas, 'Effects of bolt torque and contact resistance on the performance of the polymer electrolyte membrane electrolyzers', *J. Power Sources*, vol. 281, pp. 103–113, May 2015, doi: 10.1016/j.jpowsour.2015.01.162.

[6] E. Cruz Ortiz, N. van Treel, S. Koch, S. Vierrath, and M. Bühler, 'The effect of compression on PEM Electrolyzer membrane electrode Assemblies', *J. Power Sources*, vol. 614, Sep. 2024, doi: 10.1016/j.jpowsour.2024.235018.



Development of a Flexible Test Bench for Advanced Characterization and Diagnostics of PEM and AEM Electrolyser Stacks

Manuel Anselmo*[,a], Luca Sità[a], Marco De Campo[a], Oriol H. Galceran[a], Stefano Barberis[a]

* corresponding author: Manuel Anselmo – manselmo@bluenrev.com
a BluEnergy Revolution Soc. Coop. – Via Greto Di Cornigliano 6 – 16152 Genova - Italy

Keywords: stack characterization, AEM, PEM, test bench

Abstract

This work presents the design and realization of a versatile laboratory-scale test bench developed by BluEnergy Revolution for the characterization and validation of PEM and AEM electrolyser stacks in the power range of approximately 1 kW. The system has been specifically conceived to provide a flexible and highly instrumented environment for testing next-generation electrolysis technologies and supporting both research and industrial development activities.

Introduction: The rapid deployment of water electrolysis technologies is a key enabler for the large-scale production of renewable hydrogen. Among the available solutions, particularly looking at green hydrogen production and coupling with renewables, Proton Exchange Membrane (PEM) and Anion Exchange Membrane (AEM) electrolysers are attracting increasing interest due to their potential for high efficiency and operational flexibility. However, the development and industrialization of these technologies require advanced experimental platforms [1] capable of accurately evaluating stack performance, durability and degradation mechanisms under realistic operating conditions [2]. Advanced experimental infrastructures capable of reproducing realistic operating conditions and providing detailed diagnostic information are essential for understanding degradation mechanisms [3] and supporting technology development, also privileging simple operability and design [4]. The proposed test bench aims to do so via a "simple design" aiming to perform proper testing but limiting the number of components and the cost/complexity of the system.

Objectives: This work presents the design and realization of a flexible laboratory-scale test bench developed by BluEnergy Revolution for advanced characterization of PEM and AEM electrolyser stacks in the power range of approximately 1 kW (up to 1,5 kW). The objective is to provide a highly instrumented platform supporting research, technology validation and industrial development.

Material and methods: The facility was developed using a modular architecture allowing rapid adaptation to different stack configurations. Independent control of temperature, pressure and flow rates is available on both anodic and cathodic sides. For AEM systems, dedicated electrolyte preparation, conditioning and monitoring units guarantee accurate electrolyte management during experimental campaigns.

The acquisition system continuously records electrical and process parameters including voltage, current, power consumption, temperatures, pressures, flow rates and hydrogen production indicators. Advanced diagnostic tools include Cell Voltage Monitoring (CVM) and Electrochemical Impedance Spectroscopy (EIS). CVM provides real-time information on individual cell behaviour and voltage distribution, while EIS enables detailed investigation of charge-transfer phenomena, ohmic contributions and mass transport limitations.

Since the preliminary design phase, particular attention was devoted to minimizing system complexity and reducing the number of components required (to reduce costs as well as data acquisition), while maximizing flexibility and overall functionality.

The system incorporates indeed most of the process components within a transparent plastic enclosure (Figures below) The enclosure is appropriately ventilated to ensure the dilution of any potential hydrogen leaks, which is continuously monitored by a dedicated hydrogen sensor. The enclosure can be opened to allow installation of the stack and its connection through two anodic and two cathodic ports. Components located outside the enclosure include the electrical control panel, the power supply unit, liquid storage tanks (with the exception of the feed tank, which will be installed inside the enclosure), the nitrogen cylinder, and the chiller.





Figure 1 – BER AEM/PEM flexible test bench

One of the main aspects investigated by BER team, concerned the management of a pressurized anode circuit that has been tackled via a proportional control valve (Bürkert component) equipped with an adjustable orifice. By regulating the orifice opening, the upstream pressure can be controlled, thereby setting the pressure of the gas-liquid mixture. This approach enables the effective operation of the gas-liquid separator at atmospheric pressure. As a result, only one automatic back-pressure regulator is required instead of two, leading to a significant reduction in both system cost and operational complexity. The proposed configuration allows operation of both the anode and cathode either at atmospheric pressure or under controlled pressure conditions, up to 6 bar on the anode side and up to 15 bar on the cathode side, thus enabling the proposed test bench to be used with different type of stacks and different type of pressurization. From a safety perspective, no automatic nitrogen inerting in the event of power loss is foreseen in order to limit the internal process volumes and, in the event of an emergency, any potentially hazardous gas mixtures would be rapidly diluted. Conversely, the uncontrolled release of nitrogen into the process lines was considered to introduce greater risks than benefits. According to the current design, the control software will nevertheless provide the capability to inject nitrogen into the process lines depending on the selected operating mode and specific testing requirements.

Results: The test bench allows operation under a wide range of anodic and cathodic conditions, including independently controlled temperatures, flow rates and pressure levels. For AEM systems, the platform incorporates automatic electrolyte preparation, conditioning and monitoring functionalities, enabling accurate control of electrolyte composition and operating parameters throughout the experimental campaign. The modular architecture of the facility allows rapid adaptation to different stacks configurations and operating strategies. A key feature of the platform is the implementation of advanced diagnostic tools (based on GRAFANA environment) for in-depth electrochemical analysis via EIS and CVM. The datasets that could be generated (voltage, temperature. Pressure…) support performance mapping, efficiency evaluation, durability assessment and supports the development of data-driven approaches for stack optimization and predictive maintenance The availability of high-resolution operational also provides a valuable basis for digital twin development and advanced control strategies both for PEM and AEM technologies, operating in atmospheric and pressurized electrodes conditions.

Conclusions: The proposed facility represents an advanced experimental infrastructure for the characterization of low-power electrolyser stacks and bridges the gap between laboratory-scale component testing and larger pilot-scale demonstrations. The combination of flexible operating conditions, automated process management and advanced diagnostic capabilities provides valuable support for technology developers, research organizations and industrial stakeholders involved in the development of next-generation hydrogen production systems.

References

[1] Michel Suermann et al., High pressure polymer electrolyte water electrolysis: Test bench development and electrochemical analysis, International Journal of Hydrogen Energy, Volume 42, Issue 17, https://doi.org/10.1016/j.ijhydene.2017.01.224.

[2] Qiucheng Xu et al. Anion Exchange Membrane Water Electrolyzer: Electrode Design, Lab-Scaled Testing System and Performance Evaluation, EnergyChem, Volume 4, Issue 5, 2022, https://doi.org/10.1016/j.enchem.2022.100087.

[3] Jon Aizpuru et al., A Systematic Benchmarking of PEM Electrolyser Degradation: Towards a standardised methodology for experimental degradation campaigns, International Journal of Hydrogen Energy, Volume 224, 2026, https://doi.org/10.1016/j.ijhydene.2026.154448.

[4] Florian Berg et al. , Evaluation of simplified test rig for high throughput screening of proton exchange membrane water electrolysis components, International Journal of Hydrogen Energy, https://doi.org/10.1016/j.ijhydene.2025.03.210.



Moving Beyond the Limitations of Conventional Alkaline Water Electrolysers for Efficient and Flexible Hydrogen Production

Fatemeh Razmjooei,[a]* Dirk Ullmer, [a] Davide Grilli, [a] Kamal Ghotia, [a] Akshata Barge,[a] Hans Julian Wiggenhauser,[a] Syed Asif Ansar[a]

* Corresponding author: Fatemeh.Razmjooei@dlr.de

[a] Institute of Engineering Thermodynamics, German Aerospace Center (DLR), Pfaffenwaldring 38-40, 70569 Stuttgart, Germany

Keywords: alkaline water electrolysis, transient operation, gas purity, operational strategy

Abstract

The global need for decarbonisation has elevated electrolysers as a key technology for large-scale hydrogen production powered by renewable energy. Alkaline water electrolyser (AEL) owing to its high maturity and independence from expensive precious-based metal electrodes and components, has emerged as a viable and scalable solution for large-scale industrial hydrogen production. Conventional AELs is suitable for steady-state operation but mainly faces two major issues; limited part-load range due to an increased gas impurity at low loads and limited current density. In addition, degradation mechanisms and degradation rates under realistic operating conditions such as wide range of operating current and fluctuating loads, remain not yet fully understood, and thus necessitate further research. Addressing these challenges is essential for the effective integration of AELs into renewable energy systems. This is achieved through implementation of advanced components at stack and system level, enabling operation beyond the performance limits of conventional systems. Additionally, the degradation behavior is systematically investigated under both steady-state and dynamic operating conditions. Based on the experimental findings, optimized operating strategies are proposed to mitigate degradation while maintaining high-performance. Furthermore, through optimized operational strategies developed based on transient modeling and system-level optimization approaches, strategies are proposed to significantly reduce gas impurity levels particularly at low loads.

Introduction: Conventional stack components, system design and operating strategies will not be able to fully support the effective integration and operation of AEL technology in future energy systems based on renewable resources. Advancing beyond the conventional technologies require the development of next-generation AEL systems capable of maintaining high efficiency, safety, and durability across a wide range of harsh operating conditions. Current AEL technologies have mostly been developed for steady-state operation and are typically suitable for low current density operation (0.2-0.4 A cm^{-2}).[1] As the share of intermittent renewable electricity continues to increase, AEL systems are expected to be able to perform under highly dynamic and demanding conditions. Under

such circumstances, maintaining high efficiency, operational stability, and system safety become even more challenging. A significant limitation arises at high loads, where degradation becomes an issue and at low-load operation, where increased gas crossover can negatively affect overall system performance and safety.[2] As a result, conventional AEL systems and their operating strategies are no longer sufficient to fully exploit the potential of AEL technology in future energy systems. Therefore, developing next-generation AEL systems, which could be capable of maintaining high efficiency, safety, and durability under particularly harsh and intermittent conditions requires extensive research and developments across all system components. This includes improved stack/system components, enhanced system architectures, and optimized operating strategies that enable efficient and reliable operation. Achieving these advancements will significantly expand the operational flexibility of AEL systems and accelerate their integration into renewable energy infrastructures, going towards more resilient, efficient, and reliable hydrogen energy solutions. Therefore, finding and investigating the critical parameters that facilitate the advancement of conventional AEL toward next generation AEL technology is highly demanded and important. Particular attention is given to the improved efficiency and durability of AEL while ensuring increased reliability and safety under fluctuating operating conditions.

Objectives: The presented work aims to investigate and develop strategies for advancing conventional AEL systems toward next-generation AEL technologies capable of operating efficiently, reliably, and safely under dynamic conditions associated with renewable energy sources. The main objectives are: efficiency improvements, improved durability and lifetime and optimised dynamic operation.

Material and methods: For the purpose of this research work, various AEL test benches up to kW-scale equipped with electrochemical impedance spectroscopy (EIS) devices and gas purity sensors were employed to experimentally and systematically investigate the performance of AEL stacks and their cell under various operating conditions. To further understand the system behavior under transient operation, the modeling platform Transient Electrochemical Model for Process and Energy Systems (TEMPEST) was utilized to analyze the dynamic response of the AEL system. The combination of experimental testing and modeling enabled a comprehensive assessment of the AEL performance under dynamic operation.

Results: The efficiency of the AEL was enhanced through the implementation of advanced components along with optimized operational strategies, enabling operation beyond the performance limits of conventional systems. The degradation behavior was systematically investigated under both steady-state and dynamic operating conditions, including operation at minimum and maximum current densities as well as under severe load fluctuations representative of renewable-energy-driven applications. Based on the experimental findings, optimized operating strategies were developed and proposed to mitigate degradation while maintaining high-performance operation. In parallel, a simulation was developed to investigate the transient behavior of conventional AEL systems, with

particular emphasis on low-load operation where gas crossover and gas purity issues become critical. Through control-oriented and system-level optimization approaches, strategies were proposed to significantly reduce gas impurity levels.

Conclusions: The results demonstrated that the efficiency of the AEL can be significantly enhanced through the implementation of advanced components along with optimized operational strategies (74 to 76% at 70 and 80 °C). These improvements enabled operation at high current densities while maintaining low cell voltages, thereby increasing the overall energy efficiency of the system. Furthermore, it was found that through optimizing the system design and operational parameters, high gas purity and safe operating conditions can be achieved. The influence of key operating parameters on the degradation behavior of advanced AEL was systematically investigated over a wide range of operating conditions. EIS measurements were extensively employed to evaluate performance degradation and identify the dominant degradation and performance loss mechanisms under different operating conditions. This analysis enabled the separation and quantification of various loss contributions during operation. Based on these findings, optimized operating conditions were proposed to mitigate degradation while maintaining stable operation under fluctuating power inputs. In addition, the results showed that appropriate control strategies and optimized system design can effectively suppress gas crossover and impurity formation. The proposed control and system-level optimization strategies provide a practical pathway toward the deployment of highly efficient, reliable AEL systems compatible with renewable energy sources.

Acknowledgment: This work was financially supported by different project. 'Pressurized Efficient Alkaline Electrolyser (PEACE)', funded under the Horizon Europe programme (Grant Agreement No. 101101343) by the Clean Hydrogen Partnership and its members, the German Federal Ministry of Research, Technology and Space (BMFTR) under the grant number 03HY110B ('H2Giga Degrad-EL3') and 03HY126I (H2Giga AEL4GW). NEXTAEC, European Union's Horizon 2020 research and innovation action programme (Grant Agreement No. 862509).

References

[1] S. F. Amireh. et al., Journal of Power Sources 560 (2023) 232629.

[2] H. Fang. et al., International Journal of Hydrogen Energy 232 (2026) 154988.

European Fuel Cells and Hydrogen
PIERO LUNGHI CONFERENCE
EFCH2 2026
September 15th-17th 2026
Capri / Italy

A Practical PI Controller Design Approach for DC-DC Power Electronic Converters for Electrolyzer Applications

S. Di Girolamo*[a], A. Sferlazza[b], A. Accetta[a], M. Pucci[a], M. Luna[a]

* corresponding author: silviadigirolamo@cnr.it

[a] National Research Council, Institute of Marine Engineering. Italy

[b] University of Palermo, Department of Engineering. Italy

Keywords: electrolyzer, PI controller, power electronic converter, root locus

Abstract

Introduction: Electrolyzers are typically interfaced with the grid through a two-stage power conversion system consisting of an active rectifier (to convert AC to DC, establishing a DC bus) and a DC-DC converter (to reduce the voltage level). Usually, the output current of the DC-DC converter is controlled using proportional-integral (PI) controllers to modulate the hydrogen flow rate. However, such controllers require proper tuning because their performance is highly sensitive to their parameters. Although several PI tuning methods are available in the literature, the most widely used design procedure consists of: 1) deriving the converter small-signal transfer function around the rated operating point; 2) analyzing its Bode plots; 3) selecting the controller poles and zeros to achieve the desired crossover frequency ω_c and phase margin m_ϕ; and 4) verifying the gain margin m_g, repeating the process if necessary [1]. Since this method relies on trial-and-error iterations, it can be time-consuming, motivating the development of more practical and straightforward PI tuning techniques.

Objectives: This work proposes a practical PI controller design approach for power electronic converters in electrolyzer applications. Unlike conventional methods, the proposed procedure avoids trial-and-error tuning, making the design process simpler and faster. It identifies ranges of controller parameters that guarantee closed-loop stability, allowing the designer to select specific values according to performance requirements such as phase margin, overshoot, and settling time. The approach is described and validated using the Stacked Interleaved Buck Converter (SIBC) presented in [2], a topology featuring zero output-current ripple, which helps extend electrolyzer lifetime. Please refer to [2] for the schematic and the open-loop model of the SIBC.

Material and methods: As shown in [2], the state-space model of the open-loop converter is expressed by:

$$\begin{aligned} \dot{x} &= Ax + Bu \\ y &= Cx + Du \end{aligned} \qquad (1)$$

where the input vector $u = [V_{in}\ V_i]$ encompasses the DC bus voltage V_{in} and the electrolyzer reversible voltage V_i, which acts as a disturbance term. The output vector is $y = i_{out}$, whereas $x = [i_{Lp} \quad i_{Ls} \quad v_{Cp} \quad v_{Cs} \quad v_{C1}]$ is the state vector. An extended closed-loop state-space model is derived by augmenting the system with the PI controller dynamics, rather than considering the open-loop converter. The tracking error is defined as $e(t) = I^*\text{-}y$, where I^* denotes the reference current for the electrolyzer stack. The integral state evolves according to $\dot{\xi} = I^* - Cx - Du$, and the PI control law is defined as $d = K_P(I^* - y) + K_I\xi$.

By defining the augmented state vector $z = [x \quad \xi]^T$, the state-space model of the extended closed-loop system has the structure of (1) with different expressions for matrices $\{A, B, C, D\}$ and input vector u. The matrices elements include the controller gains K_P and K_I as free design parameters. This formulation captures the interaction between converter dynamics, controller action, and load behavior. The augmented closed-loop model is characterized by six eigenvalues, and a root locus analysis in the MATLAB environment allows us to compute their trajectories as functions of K_P and K_I. Such trajectories can be plotted and analyzed to derive PI design guidelines.

Results: The analysis of the global eigenvalue trajectories for all modes shows that the system exhibits a dominant slow real pole near the origin ($\lambda_1 \approx -0.7$), a secondary faster real pole ($\lambda_2 \approx -2$), and a dominant complex-conjugate pole pair ($\lambda_{3,4} \approx -300 \pm j2 \cdot 10^4$); two additional fast real poles are located far in the left half-plane, approximately at ($\lambda_5 \approx -600$) and ($\lambda_6 \approx -10^4$), and therefore have a negligible influence on the closed-loop transient response and stability boundaries. The poles λ_1 and λ_2 exhibit intermediate dynamics with a dependence on both K_P and K_I, as shown in Figs. 1 and 2. The remaining dominant behavior is associated with a complex-conjugate eigenvalue pair, whose trajectory is strongly affected by K_P, as shown in Fig. 3. As K_P increases, these poles move significantly in the complex plane and ultimately determines the stability boundary and oscillatory characteristics of the closed-loop system. On the other hand, the two real poles λ_1 and λ_2 cannot ever move to the right halfplane. The parametric eigenvalue analysis confirms that the proportional gain K_P is the primary tuning parameter governing closed-loop stability, whereas the integral gain K_I mainly influences the slow real poles (λ_1 and λ_2), shifting them toward more negative values and improving low-frequency convergence with limited effect on the oscillatory modes.

Based on these observations, a sequential tuning strategy is adopted. First, K_P is constrained to ensure an adequate stability margin by maintaining the dominant complex-conjugate pair sufficiently far from the imaginary axis. The resulting feasible region in the (K_P, K_I) plane enables the selection of K_I values that maximize the displacement of the slow pole toward the left-half plane while preserving sufficient damping of the dominant complex pole pair. Thus, it is possible to minimize the settling time t_a, which is directly related to the modal decay rate according to $t_a = {}^{1}/_{|\sigma|} \cdot \ln({}^{1}/_{\varepsilon})$, where $\sigma = -Re(\lambda)$ and ε denote the prescribed settling tolerance. With reference to the chosen case study, from Fig. 4, the real part of $\lambda_{3,4}$ is null for $K_P = 1 \cdot 10^{-3}$. A stability margin of 6 dB is considered, thus limiting the range for K_P to [0; $5 \cdot 10^{-4}$]. This choice corresponds to considering only a slice of the surface shown in Fig. 1, for which the maximum allowed value for $|\sigma|$ is 0.61 and is obtained with $K_P = 0$. To avoid nulling the proportional action, it is worth considering the neighborhood of $|\sigma| = 0.61$, thus further narrowing the range for the PI coefficients. If $|\sigma| = 0.6$ is chosen, the following PI coefficients are obtained: $K_P = 1 \cdot 10^{-4}$ and $K_I = 1.5 \cdot 10^{-3}$. This value of $|\sigma|$ corresponds to a 5% settling time of 5 seconds ($\varepsilon = 0.05$ and t_a=5 s). The closed-loop converter response with the designed PI controller for a stepwise current reference variation was simulated in Simulink. The corresponding waveforms are reported in Fig. 4. As the figure shows, the closed-loop system is stable, and all the design constraints are respected.

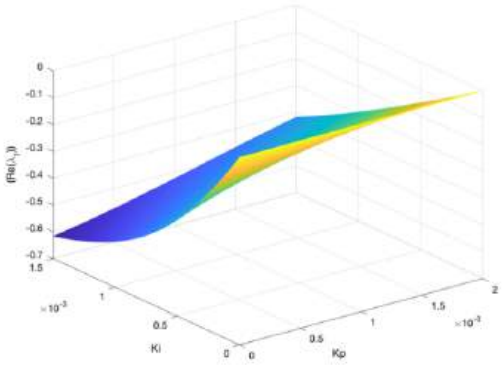


Figure 1. 3D plot showing the variation of $Re(\lambda_1)$ as a function of K_P and K_I

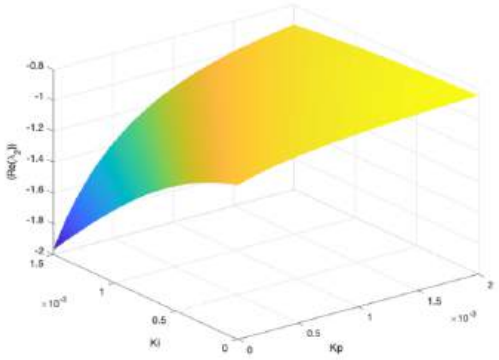


Figure 2. 3D plot showing the variation of $Re(\lambda_2)$ as a function of K_P and K_I

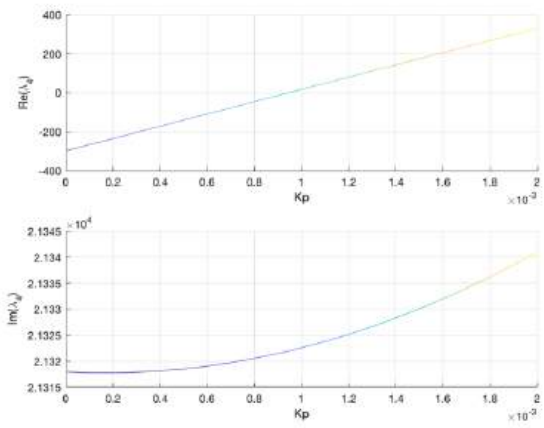


Figure 3. 2D plots of $Re(\lambda_{3,4})$ abs($Im(\lambda_{3,4})$) as a function of K_P. Such quantities do not vary with K_I

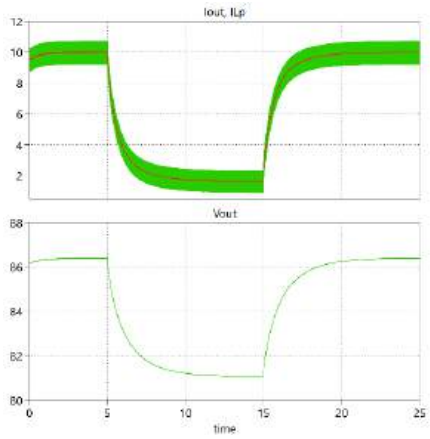


Figure 4. Response of the SIBC controlled by the designed PI regulator: output current, main inductor current, and output voltage waveforms

Conclusions: The proposed PI controller design technique is not based on a trial-and-error approach; thus, it is simpler and faster than the classic PI design technique. It has been applied to a DC-DC converter for electrolyzers and validated in simulation.

Acknowledgment: This research was funded by NextGenerationEU, POR H2 AdP MEES/ENEA with involvement of CNR and RSE, PNRR – Miss. 2, Comp. 2, Invest. 3.5 “Ricerca e sviluppo sull’idrogeno”.

References

[1] H. W. Fung, Q. G. Wang, and T. H. Lee, “PI Tuning in Terms of Gain and Phase Margins,” Automatica, vol. 34, no. 9, pp. 1145-1149, Sept. 1998.

[2] D. Guilbert, D. Sorbera, G. Vitale, “A stacked interleaved DC-DC buck converter for proton exchange membrane electrolyzer applications: Design and experimental validation”, International Journal of Hydrogen Energy, vol. 45, no. 1, pp. 64-79, 2020.



Integration of Proton Conducting Ceramic Electrolysis for hydrogen production in targeted industrial applications

M. Minutillo[a,c], V. Cigolotti[b,c], S. Di Micco[d], F. Romano*[a]

* corresponding author: fabiromano@unisa.it

[a] Department of Industrial Engineering, University of Salerno, Italy

[b] ENEA - Italian National Agency for New Technologies, Energy and Sustainable Economic Development, Italy

[c] ATENA Future Technology, Naples, Italy

[d] Department of Engineering, University of Naples Parthenope, Napoli, Italy

Keywords: hydrogen, proton-conducting ceramic electrolyzer, hard-to-abate sectors, technical performance analysis.

Abstract: This study investigates the application of an innovative Proton-Conducting Ceramic Electrolysis (PCCEL) system within three hard-to-abate industrial sectors: steel mill, ammonia plant, and oil refinery.

Introduction: The PCCEL is an innovative electrolyzer ideal for producing hydrogen to be used in industrial contexts, as operating at 30 bar significantly reduces downstream compression energy requirements. Furthermore, because it utilizes medium-temperature heat for water vaporization, it can seamlessly integrate with industrial waste heat sources to achieve high efficiencies in energy conversion.

Objective: The aim of this study is to evaluate the integration and optimal sizing of a PCCEL system to meet the demands of three industrial sectors, identifying the configuration that maximizes operating advantages.

Material and methods: The analysis of the PCCEL system integration is carried out considering the operating conditions and performance (Table 1) estimated by the thermo-electrochemical model developed under the Protostack project [1].

Table 1. Operating data and performance of the PCCEL system developed under the Protostack project.

Parameters	Values	Parameters	Values
PCCEL Operating Temperature (°C)	600 [2][a]	PCCEL stack electrical consumption (kWh/kg)	38.2 [b]
PCCEL Operating pressure (bar)	30 [3][a]	Faradaic efficiency (%)	92 [2] [b]
Steam utilization (%)	80 [b]	PCCEL degradation rate (% per 1,000h)	1.2 [b]
Water recirculation (%)	20 [b]	System operating hours (h)	8,000 [4] [a]

[a] Values fixed [b] Values assumed/declared

The PCCEL system is sized according to the hydrogen requirements of the three industrial sectors under consideration, using literature-derived data [5],[6],[7]. These data are summarized in Table 2,

which outlines the annual operating hours, industrial process outputs (steel, ammonia, and crude oil), and corresponding hydrogen demands for each plant. Because comparing the declared operating hours of the PCCEL with those of the industrial processes highlights a clear mismatch, the analysis is structured around two distinct operating scenarios to address this: *synchronized operation* (scenario 1) and *decoupled operation* (scenario 2).

Table 2. Operating hours, industrial process outputs and hydrogen requirements of three case studies.

Plant type	Steel mill	Ammonia plant	Oil refinery
Plant operating hours (h/y)	8,760	4,380	8,760
Industrial process output type	steel	Ammonia	Crude oil
Industrial process output amount ton/h (ton/y)	114.15 (1,000,000)	98.2 (430,000)	1,301 (11,400,000)
H2/process output ratio (ton H_2/ton fuel)	0.06	0.178	0.057
H2 demand ton/h (ton/y)	6.80 (59,547)	17.4 (76,359)	7.40 (64,824)

The first scenario aligns the PCCEL system's operating hours directly with the downstream industrial process. Conversely, the second scenario allows the electrolyzer to operate according to its optimal technical specifications, targeting 8,000 h/y. Another key aspect is evaluating the industrial waste heat available to facilitate water vaporization in the PCCEL. Since quantifying this highly variable thermal potential is challenging, a sensitivity analysis is conducted by varying the percentage of recovered heat relative to the total steam demand (0%, 25%, 50%, 75% and 100%). This approach allows for estimating the net energy savings across different integration scenarios.

Results: Table 3 presents the PCCEL system capacity and the corresponding operating results, in terms of hydrogen production, oxygen production, and water consumption, for each industrial process and operating scenario.

Table 3. PCCEL system integrated in three case studies.

	Steel mill		**Ammonia plant**		**Oil refinery**	
	Scenario 1	Scenario 2	Scenario 1	Scenario 2	Scenario 1	Scenario 2
PCCEL Size MW	259	284	665	364	282	309
H2 Production ton/h (ton/y)	6.80 (59,547)	7.44 (59,547)	17.4 (76,359)	9.53 (76,359)	7.40 (64,824)	8.10 (64,824)
O2 Production ton/h (ton/y)	54.0 (472,747)	59.1 (472,747)	138 (606,218)	75.8 (606,218)	58.7 (514,640)	64.3 (514,640)
Demineralized H2O ton/h (ton/y)	62.0 (543,186)	68.0 (543,186)	159 (696,544)	87.1 (696,544)	67.5 (591,321)	73.9 (591,321)
Sweep steam ton/h (ton/y)	15.2 (133,078)	16.6 (133,078)	39.0 (170,650)	21.3 (170,650)	16.5 (144,871)	18.1 (144,871)

From an energy perspective, Table 4 summarizes the results regarding electricity consumption and heat recovery, based on the sensitivity analysis performed on the percentage of available industrial waste heat. Consequently, it also reports the fuel consumption (natural gas) of the boiler required to vaporize the water for the electrolyzer. It can be noted that if no thermal integration is realized (0%

recovery), the external thermal energy demand is 358,605 MWh/y, 459,851 MWh/y, and 390,384 MWh/y for the steel plant, ammonia plant, and oil refinery, respectively.

On the other hand, if the entire heat demand can be supplied internally, fossil fuel consumption can be reduced to zero. This avoids associated CO2 emissions, enabling deep decarbonization of these hard-to-abate sectors. Specifically, the avoided CO2 emissions amount to 30,455 t/y, 39,053 t/y, and 33,154 t/y, respectively.

Table 4. Supplied external thermal energy and fuel consumption based on heat recovery.

	Steel mill	Ammonia plant	Oil refinery
PCCEL system electric consumption (MWh/y)	2,272,980	2,912,711	2,474,402
Thermal recovery Percentage	**Supplied external thermal energy (MWh/y) / Boiler fuel consumption (ton/y)**		
0 %	358,605 / 30,455	459,851 / 39,053	390,384 / 33,154
25%	268,954 / 22,841	344,888 / 29,290	292,788 / 24,865
50%	179,303 / 15,227	229,925 / 19,527	195,192 / 16,577
75%	89,651 / 7,614	114,963 / 9,763	97,596 / 8,288
100%	0	0	0
Thermal recovery Percentage	**CO2 avoided (ton/y)**		
100%	83,751	107,396	91,172

Conclusions: All three sectors show strong potential, although ammonia production best aligns with PROTOSTACK technology by simultaneously offering suitable waste heat, compatible process temperatures, and high hydrogen pressure demands.

Acknowledgment: PROTOSTACK project has received support from the European Union's Horizon 2020 Research and Innovation Program, Hydrogen Europe, and Hydrogen Europe Research. Grant agreement 101101504

References

[1] F. Romano "Techno-Economic and Environmental Analysis of innovative Proton-Conducting Ceramic Electrolyzers for sustainable hydrogen production - https://hdl.handle.net/11367/160458".

[2] E. Vøllestad *et al.*, "Mixed proton and electron conducting double perovskite anodes for stable and efficient tubular proton ceramic electrolysers," *Nat. Mater.*, vol. 18, no. 7, pp. 752–759, Jul. 2019, doi: 10.1038/s41563-019-0388-2.

[3] "Protostack project - https://protostack.eu/objectives."

[4] "CLEAN HYDROGEN PRODUCTION PATHWAYS REPORT 2024. https://hydrogeneurope.eu/wp-content/uploads/2024/06/2024_H2E_CleanH2ProductionPathwaysReport.pdf"

[5] A. Bhaskar et al. "Decarbonizing primary steel production: Techno-economic assessment of a hydrogen based green steel production plant in Norway," *J. Clean. Prod.*, vol. 350, May 2022, doi: 10.1016/j.jclepro.2022.131339.

[6] H. Nami et al. "Green ammonia production using current and emerging electrolysis technologies," *Renewable and Sustainable Energy Reviews*, vol. 199, Jul. 2024, doi: 10.1016/j.rser.2024.114517.

[7] "SARAS GROUP - Half year financial report https://www.saras.it/sites/default/files/documents_attachments/interim-report-as-of-30th-june-2024.pdf".



Multiphysics Modeling and Optimization of a Membrane-less Supercritical Alkaline Electrolyzer

Arash Nemati *[a], Giovanna Massobrio [b], Anna Testolin [c], Francesco Cartasegna [c], Alessandro Narri [c], Marian Garcia [d], Pau Bosch [d], Leonardo Cognigni [e], Henrik Lund Frandsen [a]

* corresponding author: arnem@dtu.dk

[a] Danmarks Tekniske Universitet (DTU), Department of Energy Conversion and Storage, Denmark

[b] SNAM S.p.A., Italy

[c] Industrie De Nora S.p.A. (IDN), Italy

[d] Acondicionamiento Tarrasense (LEITAT), Spain

[e] Particular Materials S.r.l. (PMat), Italy

Keywords: Supercritical water electrolysis, membrane-less, CFD, gas mixing.

Abstract

This work highlights the modeling and simulation-guided optimization of an innovative membrane-less alkaline water electrolyzer developed to operate at supercritical water conditions (>374°C, >220 bar). Eliminating the conventional physical membrane minimizes transport and ohmic resistances, curtails investment capital, and produces highly pressurized green hydrogen streams (>200 bar) directly without post-production mechanical compression. Utilizing 2D and 3D CFD multiphysics architectures implemented in COMSOL v6.3, a rigorous parametric investigation was executed targeting electrolyte flow profiles, inter-electrode gap spacing, fluid flow dynamics, and asymmetric distribution strategies. The computational results demonstrate that fluid flow velocities safely mitigate flammability cross-over risks at the critical hydrogen outlet stream.

Introduction:

While water electrolysis is critical for global decarbonization, conventional systems suffer from severe thermodynamic penalties stemming from high activation overpotentials, interfacial resistances, and energy-intensive post-production mechanical compression. The Horizon Europe X-SEED project circumvents these limitations by introducing a membrane-less alkaline electrolyzer engineered for supercritical water conditions (>374°C, >220 bar). Operating within the supercritical regime fundamentally alters the fluid's thermophysical properties—accelerating charge-transfer kinetics, drastically lowering electrolyte resistivity, and directly generating high-pressure H_2 (>200 bar) to eliminate auxiliary downstream compression stages.The defining architecture omits a physical

separator to minimize transport resistance, reduce critical raw material dependencies, and mitigate long-term degradation mechanisms. Because product isolation relies entirely on fluid dynamics rather than a structural barrier, rigorous multi-scale computational modeling is mandatory to establish convective containment pathways and guarantee that gas cross-over remains safely below established flammability thresholds.

Objectives:

This research aims to design a membrane-less supercritical alkaline electrolyzer using advanced numerical modeling. The specific objectives are to:

1. Develop a 2D/3D multiphysics model simulating fluid dynamics, heat transfer, species transport, and electrochemical kinetics under supercritical conditions.
2. Conduct sensitivity analyses on electrode spacing, flow rates, and asymmetric feeding to prevent reactant starvation and mitigate gas cross-over risks.

Material and methods:

COMSOL Multiphysics models coupled Navier–Stokes/Brinkman flow, Nernst–Planck transport, Butler–Volmer kinetics, and heat transfer. Sensitivity analyses investigated electrolyte molarity, electrode spacing, flow rate, asymmetric flow distribution, and diffusion coefficients [1-2]. A critical concern in membrane-less supercritical electrolyzers is the potential mixing of hydrogen and oxygen due to the absence of a membrane, which poses a significant risk of hydrogen combustion [3] which is investigatred in this study.

Results: Parametric evaluations established that the electrolyte volumetric flow rate dictates both product gas cross-over dynamics and local mass transport at the electrode interfaces. Multi-scale CFD simulations at a cell potential of 2.0 V demonstrate that the mass fraction mixing ratio (x = H2 / (H2 + O2)) at the primary H2 outlet remains consistently above the upper flammability limit (UFL = 0.54) and outside the risky zone for both 4 mm and 8 mm electrode spacings. While reducing the volumetric flow rate enhances diffusive mixing, the convective velocity profile maintains a safe margin above the UFL, confirming effective gas separation at the product header. Conversely, the O2 outlet exhibits heightened susceptibility to cross-over contamination, with the mixing ratio crossing the lower flammability limit (LFL = 0.03) at symmetrical flow regimes below 8.5L/h for the 4 mm gap configuration. This threshold behavior occurs because lower bulk flow rates suppress the convective velocity boundary layer along the electrodes without restricting molecular gas diffusion, driving cross-over flux toward the opposite channels. Furthermore, this symmetrical operational envelope is strictly bound by severe mass transport limitations within the 1 M NaOH electrolyte; at 8.5 L/h, intense electrochemical consumption outpaces convective replenishment, inducing severe hydroxyl (OH^-)

starvation close to electrode which drops local ionic conductivity, escalates overpotentials, and introduces severe risks of catalytic degradation.

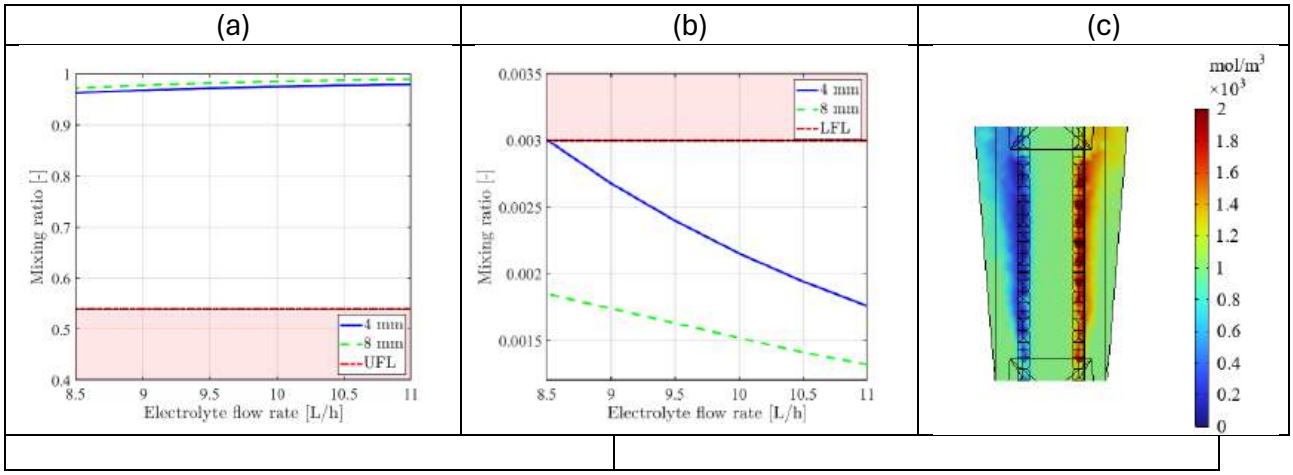


Figure 25. H_2 and O_2 mixing ratio based on mass fraction at a) H_2 outlet and b) O_2 outlet based on mass fraction ratios at 2V. c) OH concentration at 8.5 L/h.

Further investigations are carried out on the effect of asymmetric flow distribution on the electrodes to tackle this problem which helps to reduce the flow rate to 5 L/h.

Conclusions: This work presents a comprehensive multiphysics modeling framework validating the operational capabilities of the membrane-less supercritical water electrolyzer developed for the X-SEED project. The numerical evaluations indicate that balancing high convective flow with gas diffusion is key to ensuring intrinsic system safety. Adopting a tight 4 mm electrode spacing and 1 M NaOH electrolyte layout permits a reliable performance. Furthermore, implementing an asymmetric flow strategy successfully eliminates localized anode starvation risks, lowering the safe minimum fluid loop threshold to 5 L/h.

Acknowledgment: This work has been done in the context of the X-SEED project, with Grant Agreement number 101137701. The project is supported by the Clean Hydrogen Partnership and its members. Co-funded by the European Union. Views and opinions expressed are however those of the author(s) only and do not necessarily reflect those of the European Union or the Clean Hydrogen Partnership. Neither the European Union nor the granting authority can be held responsible for them.

References

[1] S. Kraft, F. Vogel, Industrial & Engineering Chemistry Research, 56(16), pp. 4847-4855, 2017.

[2] X. Zhao, H. Jin, Applied Thermal Engineering, 171, p. 114941, 2020.

[3] R.W. Ring, J.E. Stott, C. Hales, 3rd IAASS Conference Proceedings, No. M09-0064, 2008.



A Scale-Up Platform for Renewable Hydrogen Production Technologies Based on Waste-Derived Biogas and Biomethane

Daniele Micale*[,a], Pietro Giovanni Santori[a], Giordano Ghisu[a], Stefano Mezzavilla[a], Amedeo Agosti[a], Pere Margalef Valldeperez[a]

*corresponding author: daniele.micale@snam.it

[a] Snam S.p.A., Via Vezza d'Oglio 6, 20136 Milan (Mi), Italy

Keywords: open-innovation test bed, renewable hydrogen, technology scale-up, waste-to-hydrogen

Abstract

Introduction: The deployment of low-carbon hydrogen technologies at industrial scale remains challenged by several technical, economic, and regulatory barriers. While low-carbon hydrogen is often associated with water electrolysis powered by renewable electricity, alternative biological production pathways based on the thermochemical conversion of sustainable feedstocks, such as biogas and biomethane, can provide complementary solutions for accelerating hydrogen deployment and valorising waste-derived resources. Despite the significant progress achieved by innovative hydrogen production technologies at laboratory scale, their transition towards commercial implementation is often hindered by high capital expenditure requirements, lengthy permitting procedures, site availability constraints, and the complexity of integrating novel processes into industrial environments.

As a result, many promising technology providers face substantial obstacles in demonstrating and validating their solutions under representative operating conditions, slowing down technology maturation and market adoption.

To address these challenges, in the context of the H_2Shift project [1], we are developing an innovative demonstration platform in Legnano (Italy), conceived as a ready-to-use infrastructure for testing, validating, and scaling up hydrogen production technologies based on renewable gaseous feedstocks generated through the treatment of municipal and organic waste streams.

Objectives: The proposed Technology Platform, conceived as an integrated testing and validation environment to support the transition of innovative technologies, aims to address both technological and non-technological barriers that currently limit the large-scale deployment of renewable hydrogen production systems of biological origin. By providing a pre-permitted and fully integrated testing infrastructure, the project seeks to reduce the time, costs, and complexity typically associated with the transition from laboratory-scale demonstrations to commercial applications by bridging the gap between research, demonstration, and market implementation. The platform is designed to enable technology providers to validate innovative solutions under real operating conditions, generating

reliable performance data related to hydrogen yield, process efficiency, operational flexibility, and system reliability.

Furthermore, the facility aims to evaluate the impact of feedstock variability on process performance and to support the development of scalable hydrogen production pathways capable of contributing to Europe's decarbonisation objectives.

Material and methods: The facility integrates feedstock conditioning, shared utilities, dedicated testing areas, gas cleaning, and hydrogen purification technologies to convert biogas and biomethane into renewable hydrogen. The plant is designed as a flexible and modular platform capable of accommodating different process configurations and technology solutions, ranging from biogas reforming to biomethane pyrolysis. To ensure the validation of technologies under industrially relevant conditions, the facility is designed to process up to 25 Nm^3/h of biogas or 20 Nm^3/h of biomethane, operating at pressures of up to 14 barg, while hosting hydrogen production prototypes with an installed electrical power of up to 100 kW.

Feedstocks originating from the waste treatment facility are subjected to dedicated pre-treatment stages for contaminant removal before entering the hydrogen production section. Downstream purification units enable the production of hydrogen suitable for industrial and energy applications.

A comprehensive monitoring system has been implemented to collect operational data related to feedstock quality, hydrogen yields, process efficiency, energy consumption, and system reliability. The generated dataset will support the evaluation of technology performance under representative industrial operating conditions.

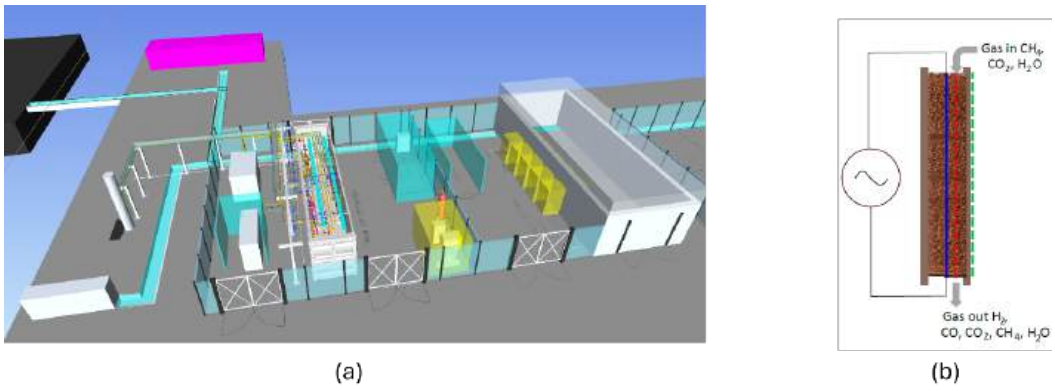


Figure 26 (a) 3D model of the Technology Platform; (b) Schematic representation of the eSMR reactor.

Results: The platform, whose 3D model is shown in Figure 1(a), is currently under construction and will soon host its first demonstration campaign based on an electrified Steam Methane Reforming (eSMR) technology, schematized in Figure 1(b), jointly developed by Snam and Politecnico di Milano [2]. The pilot will process biogas and biomethane derived from organic waste streams to produce

renewable hydrogen while assessing the technical performance of electrified reforming under representative industrial operating conditions.

Beyond the initial demonstration, the facility is intended to become a long-term testing hub for innovative hydrogen and carbon management technologies. Its modular nature is expected to facilitate the integration of future technology providers. In particular, the facility will host future demonstration activities within the Horizon Europe projects COUPLED [3] and ELEKTRA [4], enabling the validation of advanced processes for renewable fuel production, carbon utilization, process electrification, and hydrogen generation. Through these successive testing campaigns, the platform will provide a unique environment for technology developers to bridge the gap between laboratory research and industrial deployment.

Conclusions: The facility addresses one of the major challenges of the hydrogen sector: enabling the transition of innovative technologies from laboratory-scale development to industrial implementation. By providing a pre-permitted and fully integrated testing infrastructure, the platform significantly reduces the technical, economic, and regulatory barriers that typically slow down the scale-up of novel hydrogen production processes.

The first demonstration of the eSMR technology will provide valuable insights into renewable hydrogen production from waste-derived biogas and biomethane, while future campaigns under the COUPLED and ELEKTRA projects will further expand the scope of the platform towards carbon utilization and industrial electrification applications.

As a result, the platform is expected to evolve into a reference European infrastructure for the validation and acceleration of emerging hydrogen technologies, supporting both technology providers and the broader deployment of low-carbon energy solutions in line with European decarbonisation objectives.

Acknowledgment: This work has received funding from the European Union's Horizon Europe Research and Innovation Programme through the projects H2SHIFT – Services for Hydrogen Innovation Facilitation and Testing (Grant Agreement No. 101137953), COUPLED – CO_2 Utilisation Process via Looping tEchnology Demonstration (Grant Agreement No. 101235724), and ELEKTRA – Advanced Electrification of Key Industrial Reactions (Grant Agreement No. 101294850).

References

[1] H2SHIFT - https://h2shift.eu/

[2] Ambrosetti M., et al. 2023, WO/2023/062591

[3] COUPLED - https://www.coupled-horizoneurope.eu/

[4] ELEKTRA - https://www.elektraproject.eu/



Membrane-less Supercritical Water Electrolysis for High-Pressure Hydrogen Production: First Technical Results from the X-SEED Project

G. Massobrio[1], P. Bosch-Jimenez[2], M. Garcia[2], S. Martínez-Crespiera[2], A. Ramunni[3], A. Testolin[3], F. Cartasegna[3], L. Cognigni[4], A. Nemati[5]

[1]Snam spa, Italy

[2]Leitat technological center, Spain

[3]Industrie De Nora SPA, Italy

[4]Particular Materials SRL, Italy

[5] Danmarks Tekniske Universitet, Denmark

Keywords: Supercritical Water Electrolysis, Membrane-less Electrolysis, High-Pressure Hydrogen, Catalyst Development, Circular Economy, Wastewater Valorisation, Multiphysics Modelling.

Abstract

Introduction: Renewable hydrogen is expected to play a pivotal role in achieving climate neutrality, enabling large-scale integration of renewable energy and the decarbonization of hard-to-abate sectors. However, meeting future hydrogen demand will require not only a massive scale-up of electrolyser capacity, but also the development of next-generation electrolysis technologies combining higher efficiency, lower cost, and improved sustainability [1].

The X-SEED project [2] (eXperimental Supercritical ElEctrolyser Development), funded by the Clean Hydrogen Partnership under Horizon Europe, addresses these challenges through the development of an innovative membrane-less alkaline electrolyzer operating under supercritical water conditions (>374°C and >220 bar). The technology aims to directly produce high-purity hydrogen at pressures above 220 bar while reducing electrochemical losses, simplifying system architecture, and increasing component lifetime.

Objectives: The main objective of X-SEED is to develop and validate a novel supercritical water electrolysis concept capable of delivering highly efficient and sustainable hydrogen production. Specific objectives include:

1. Develop and validate a membrane-less electrolyser operating under supercritical water conditions, capable of producing high-pressure hydrogen while ensuring safe separation of hydrogen and oxygen without the use of membranes.
2. Design, model and optimize single-cell and short-stack architectures through advanced CFD and multiphysics simulations, identifying operating conditions that maximize efficiency and product separation.

3. Develop and characterize catalyst-coated electrodes based on earth-abundant materials, suitable for operation under extreme temperature and pressure conditions.
4. Investigate the behaviour of alkaline electrolytes under subcritical and supercritical conditions through dedicated experimental facilities and conductivity measurements, generating the data required for cell design and performance optimization.
5. Demonstrate circularity approaches for hydrogen production technologies by recovering strategic metals from industrial wastewaters and converting them into electroactive catalyst materials, reducing dependence on virgin raw materials and critical resources.
6. Assess the technical, environmental and economic potential of the technology, supporting its future scale-up as a competitive alternative to conventional alkaline and PEM electrolysis systems.

Material and methods: The project combines advanced modelling, material development, component testing, and stack validation activities. Novel catalytic materials and electrode architectures have been designed and experimentally assessed for operation at supercritical temperature and pressure conditions. In parallel, dedicated experimental facilities were developed to characterize electrolyte behaviour under supercritical conditions, while customized equations of state for electrolyte mixtures were developed in collaboration with an external partner to accurately describe thermophysical properties and support the simulation activities. Multiphysics and CFD simulations have been used to optimize fluid dynamics, mass transfer, gas separation, and electrochemical performance within the cell. Experimental campaigns have focused on evaluating electrochemical behaviour, gas separation efficiency, materials durability, and thermal management under supercritical water conditions. In parallel, sustainability, techno-economic, and market analyses have been conducted to evaluate the long-term industrial potential of the technology and identify promising application sectors.

Results: During the first two years, significant progress has been achieved across all technical activities. A total of 24 catalyst formulations were synthesized and characterized, including perovskite-based materials produced through electrospinning and continuous hydrothermal flow synthesis routes. The catalyst development activities also validated the use of three industrial wastewater streams as alternative raw material sources. Several catalyst formulations achieved the project electrochemical targets, namely HER overpotentials below 100 mV at 10 mA cm^{-2} and OER overpotentials below 150 mV at 10 mA cm^{-2}, while supporting the long-term objective of reaching current densities above 3 A cm^{-2} at cell voltages below 1.8 V. Furthermore, catalyst characterization demonstrated specific surface areas of up to 25.8 $m^2 g^{-1}$ for CHFS-derived materials and 18.1 $m^2 g^{-1}$ for electrospun catalysts, exceeding the project target of 10 $m^2 g^{-1}$. A dedicated reactor for conductivity measurements under high-temperature and high-pressure conditions was successfully designed and validated, enabling the acquisition of experimental conductivity data for different electrolyte compositions under subcritical and supercritical conditions. Conductivity measurements

of 0.1 M NaOH identified a maximum conductivity of 45.1 mS cm^{-1} at 340°C and 145 bar, providing key input data for model calibration and operating condition definition. Modelling confirmed the feasibility of the membrane-less concept and enabled optimization of the cell architecture, reducing the electrode gap from 8 mm to 4 mm. Simulations demonstrated safe operation above 200 bar, achieving >99% hydrogen recovery and >99.9% purity, with stable operation at current densities up to 2.9 A cm^{-2}. Results also showed that further design improvements are needed to maintain these performances at lower flow rates. Future design improvements will therefore focus on enhancing gas separation performance while reducing the electrolyte flow demand, ultimately lowering balance-of-plant requirements, reducing heating and cooling duties, and improving overall process efficiency. Modelling and experimental activities enabled the development of an optimized membrane-less cell architecture and a preliminary 5-cell stack design. In parallel, market and process assessments were carried out to identify key application sectors and evaluate the integration of the electrolyser within the overall hydrogen production system.

Conclusions: X-SEED is demonstrating the potential of membrane-less supercritical water electrolysis as a promising alternative to conventional hydrogen production technologies. The project has already delivered important advances in catalyst development, electrolyte characterization, cell design, and process modelling, while integrating sustainability and circularity considerations from the early stages of technology development. Ongoing work will focus on the validation of the electrolyser under supercritical operating conditions and on the optimization of cell and stack performance, providing the basis for the future scale-up of a new generation of efficient and sustainable hydrogen production systems.

Acknowledgments: This work has received funding from the Clean Hydrogen Partnership under the Horizon Europe programme through the X-SEED project (Grant Agreement No. 101137701). The authors gratefully acknowledge the contribution of INRiM (Istituto Nazionale di Ricerca Metrologica), in particular Alberto Albo, for the development of the equations of state and the related support in modelling the thermophysical properties of electrolyte mixtures under supercritical conditions, and prof. Massimo Santarelli.

References

[1] https://www.iea.org/reports/global-hydrogen-review-2022

[2] https://www.xseedproject.eu/

[3] https://patentscope.wipo.int/search/en/detail.jsf?docId=WO2026133249&_cid=P11-MR3JQK-20141-1



Scaling PEM Electrolysis: from Materials Innovation to Industrial Manufacturing

Katherine Ayers* [a], Luke Dalton [a], Chris Capuano [a], Eliot Littlefield [a]

[a] Nel Hydrogen US, Wallingford, CT

Keywords: PEM electrolysis; manufacturing scale-up; system integration

Abstract

Proton exchange membrane (PEM) water electrolysis has been mature as a technology for decades (1), with use in high reliability applications such as life support on submarines and space stations. However, these applications were typically smaller scale (kW) and lower volume (dozens of units), which do not require a high level of manufacturing maturity. In contrast, reaching gigawatt scale requires practical improvements in manufacturing methods and system design to be economical. To get there, new levels of fundamental understanding, focused on processing and design, are critical.

Introduction: Hydrogen is a feed source to many chemical applications, including fertilizer and hydrocarbon fuels (2), as well as a possible energy vector itself. Currently these applications are mainly served by hydrogen derived from fossil fuels, due to the high cost of producing hydrogen via electrolysis. Proton exchange membrane (PEM) electrolyzers are well suited for pairing with renewable electricity to produce low carbon hydrogen because they can operate at high current density, respond quickly to changing power input, and pair effectively with renewable electricity. Still, reducing the cost of low carbon hydrogen requires much higher global production of electrolyzers, from components to systems.

This talk will discuss how manufacturing science and system-scale engineering can be combined to support the scale-up of PEM electrolysis, with emphasis on component production, automated assembly, stack design, and system integration for larger electrolyzer installations. The challenges in driving implementation speed while balancing cost will also be discussed.

Objectives: Manufacturing scale-up requires increases in production capacity, moving from thousands of cell equivalents per year toward megawatt-scale annual output. The mindset in experimental design also has to change accordingly. Predicting the right conditions from the lab scale is not simple, but large trials at scale are very costly, so a balance is needed between lab methods that can approach formulations that will work at scale with refinement in relevant equipment and quantities.

Electrolysis is also not just a cell or a stack. Component and stack improvements must also be translated into complete electrolyzer systems. As active area, stack size, and manufacturing volume

increase, design choices across electrochemical, mechanical, and electrical subsystems become more closely linked and have to be co-optimized.

Materials and Methods: Nel Hydrogen has invested millions of dollars in research and equipment towards increasing scale and decreasing cost. In PEM electrolyzer stacks, the majority of the cost is the materials; therefore, automation is not used as much to decrease labor cost as it is to decrease material usage. Moving to higher precision fabrication methods enables thinner layers and higher yields.

At the system level, rectifier integration, fluid distribution, thermal management, and gas-liquid separation affect performance, reliability, and manufacturability. Parameters such as the number of cells per stack, stacks per plant, and system layout influence how electrolyzer installations scale from approximately 10 MW to 100 MW-class plants.

Results: As an example, the membrane electrode assembly (MEA) fabrication relied largely on batch-based and labor-intensive methods with limited process control. More recent manufacturing approaches include continuous fabrication methods such as roll-to-roll (R2R) coating and automated processing. These methods can improve coating consistency, support thinner catalyst layers and lower precious metal loading, and increase production throughput when the processes are well controlled.

Figure 1 summarizes the evolution of MEA fabrication from manual, batch-scale processing to automated, roll-to-roll production, with emphasis on material utilization and process control. Hand spread electrodes were by necessity very thick in order to fill a template uniformly. However, much of the catalyst was just acting as a scaffold and was not actually required for catalytic activity. Roll to roll methods can precisely fabricate much thinner layers, allowing higher catalyst usage and lower platinum group metal loadings. But getting there requires complete requalification of materials, formulations, and process conditions. Electrodes have to produce the same results thousands of times; a 1% failure in a research lab does not sound large, but is catastrophic in production.

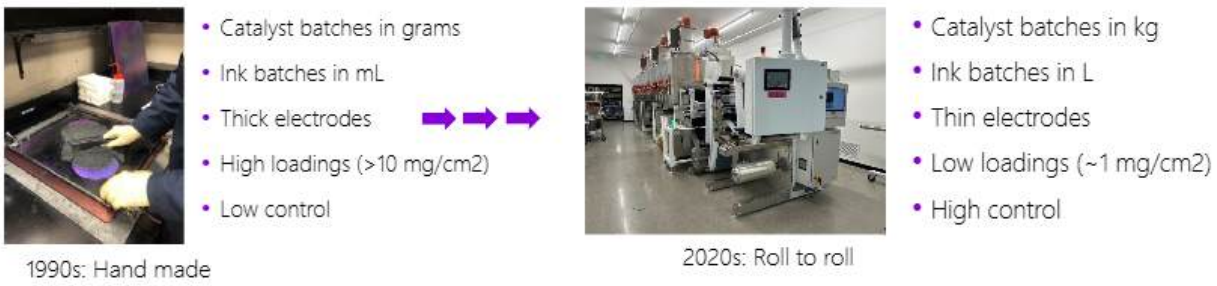


Figure 1.: Evolution of MEA manufacturing processes from manual fabrication to automated roll-to-roll production, highlighting reductions in catalyst loading and improvements in process control

Figure 2 shows the progression of electrolyzer system size from kilowatt-scale units to multi-megawatt installations. As the systems have scaled, the cost of the balance of plant relative to the hydrogen output has decreased substantially (3). For example, a 5 MW balance of plant is less than 10x the cost of a 200 kW balance of plant, but produces roughly 25x the amount of hydrogen.



Figure 2: Progression of PEM electrolyzer systems from kilowatt-scale units to multi megawatt-scale plants

Conclusions:

Cost reductions for PEM electrolysis are expected to depend on a combination of higher process yield and more efficient assembly methods. Producing meters of electrodes per minute means that characterization has to happen equally fast, to prevent producing significant waste. Finally, precision and repeatability take on completely new magnitudes. Investing in these areas needs to happen at the right pace and right time for the market. At the same time, system optimization has to follow new stack platforms, to get to the targets needed.

Acknowledgements:

The authors acknowledge CERL grant W9132T-22-2-0018 and DOE grants DE-EE0008848, DE-EE0009238 and DE-EE0011302 for funding the manufacturing development discussed in this paper.

Bibliography

(1) Applications and Development of High Pressure PEM Systems", F. Mitlitsky, B. Myers, A. Weisberg, A. Leonida, LLNL 1999, https://www.osti.gov/servlets/purl/9866
(2) International Energy Agency. Global Hydrogen Review 2026. IEA, Paris, 2026
(3) DOE Hydrogen Program Record 24005, "Clean Hydrogen Production Cost Scenarios with PEM Electrolyzer Technology", M. Hubert et al, 2024, https://www.hydrogen.energy.gov/docs/hydrogenprogramlibraries/pdfs/24005-clean-hydrogen-production-cost-pem-electrolyzer.pdf?sfvrsn=8cb10889_1



TOPIC 2. HYDROGEN STORAGE AND DISTRIBUTION

EFCH2 2026 European Fuel Cells and Hydrogen PIERO LUNGHI CONFERENCE
September 15th-17th 2026 Capri / Italy

Numerical Insights into Transient Hydrogen Tracking in Gas Distribution Networks

Michele Francesconi*[a], Lorenzo Busi[b], Michele Meazzini[b],Carlo Carcasci [a]

* Corresponding author email: michele.francesconi@unifi.it

[a] University of Florence, Department of Industrial Engineering, Via di Santa Marta 3, 50139

[b] Centria S.r.l., via I. Cocchi, 14, 52100 Arezzo

Keywords: Gas distribution network, Hydrogen blending, Preissmann scheme, Transient flow

Abstract

Introduction: Hydrogen blending in existing natural gas infrastructures introduces strong compositional gradients, as hydrogen and natural gas differ markedly in molecular weight, compressibility, and calorific value [1]. Under operational disturbances, these contrasts generate propagating pressure and concentration waves that significantly influence hydraulic response and delivered gas composition. While transient modelling frameworks are widely employed for transmission-scale systems, most implementations treat hydrogen transport as predominantly advection-driven and rely on fully implicit discretization schemes. The impact of scheme-dependent numerical diffusion on hydrogen tracking accuracy, however, remains insufficiently quantified, particularly in short distribution networks, where limited transport distances reduce cumulative effects, and comprehensive quantitative analysis remains scarce.

Objectives: This work aims to quantify numerical-model-induced bias in transient hydrogen transport across two representative scales: a controlled long high-pressure pipeline and a real-world radial distribution network. The implicitness parameter is systematically varied within its stability region to evaluate its impact on front propagation and concentration dynamics under identical operating conditions. Bias is assessed through specific Quantities of Interest (QoIs), including peak concentration and arrival times, and quantified via the normalized root-mean-square error (NRMSE), computed with respect to the injected hydrogen profile X_{H2}^{inj}.

$$NRMSE = \sqrt{\frac{1}{N}\sum(X_{H2}^{obs} - X_{H2}^{inj})^2} \Big/ \max\left(X_{H2}^{inj}\right) - \min(X_{H2}^{inj}) \quad (1)$$

allowing consistent comparison across discretization schemes and spatial resolutions.

Material and methods: Hydrogen–natural gas transport is modelled through a transient one-dimensional compressible-flow formulation applied to each pipeline, with nodal coupling enforcing global mass conservation and instantaneous mixing [2]. The Preissmann box scheme [3] is adopted as the reference four-point space–time discretization of the governing PDEs, with spatial weight ϕ and

temporal weight θ. For a generic scalar variable $y(x,\ t)$, the temporal derivative evaluated at the midpoint of the box is approximated as:

$$\left(\frac{\partial y}{\partial t}\right)_M \approx \frac{(1-\phi)\left(y_i^{t+1}-y_i^t\right)+\phi\left(y_{i+1}^{t+1}-y_{i+1}^t\right)}{\Delta t} \quad (2)$$

While the spatial derivative is written as:

$$\left(\frac{\partial y}{\partial x}\right)_M \approx \frac{(1-\theta)\left(y_{i+1}^t-y_i^t\right)+\theta\left(y_{i+1}^{t+1}-y_i^{t+1}\right)}{\Delta x} \quad (3)$$

Two complementary case studies are analyzed (see Figure 1). A 25 km Single-Inlet Single-Outlet (SISO) configuration isolates discretization effects under controlled boundary conditions, while a real-world radial distribution network (Arezzo (IT), 11.84 km, 503 nodes) evaluates their system-level propagation. Both systems are assessed using a Courant-number constrained discretization, with minimum resolutions of Δx = 10 m and Δt = 300 s, and complemented by a grid-sensitivity analysis. Grid sensitivity is evaluated across fine (F), medium (M), and coarse (C) resolutions, while unstable configurations (I) are identified outside the admissible stability region. Within this framework, the temporal weighting parameter θ is varied over its feasible stability range (0.55-1.0) [4], and key quantities of interest, as described in the objectives, as well as the computational cost, are systematically evaluated. Lastly, a composite Global score is defined as the arithmetic average of sign-consistent normalized QoI, enabling the aggregated ranking of discretization schemes

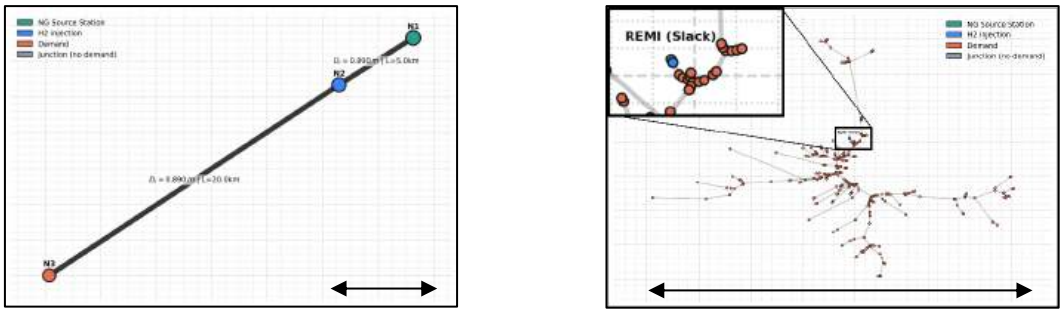


Figure 1. Left panel: two-pipe case study; right panel: real-world NG network case study.

Results: The temporal weighting parameter θ directly controls numerical diffusion. Lower θ values systematically outperform more implicit formulations in the global multi-metric ranking. The configuration θ = 0.55 achieves the highest global score (0.982), preserving peak hydrogen concentration (9.81%) and maintaining accurate arrival time (ETA ≈ 11 h). Increasing θ progressively damps the concentration peak and alters transient timing, confirming that excessive implicitness degrades front fidelity over long transport distances. The θ = 0.55 configuration remains the best-performing scheme both with and without added spatial diffusion. Introducing physical diffusion ([5]) does not modify the ranking and only slightly increases the NRMSE (from 0.016 to 0.0255), indicating limited sensitivity within this range. However, the low-diffusion configuration exhibits a minor trailing

concentration artifact, leaving a small residual wake behind the propagating front. This effect does not significantly affect global error metrics but reflects reduced numerical damping. When applied to the short radial Arezzo distribution network, numerical-model biases are considerably attenuated compared to the SISO case. Inter-scheme deviations are markedly lower than in the SISO case, with normalized errors on the order of 10^{-3}–10^{-2}. The $\theta = 0.55$ configuration continues to provide the most consistent transient tracking, both with ($D_{xx} = 5.65 \times 10^{-4}$) and without diffusion (D_{xx}=0), although performance differences between schemes are substantially compressed. The relatively short pipe segments, high flow velocities, and absence of looped paths limit hydraulic residence time and restrict cumulative diffusion, preventing progressive bias amplification. Under these conditions, spatial resolution becomes comparable to, or more influential than, temporal weighting in governing local solution accuracy. These findings should be regarded as indicative and require further validation under alternative flow regimes and meshed network configurations.

Conclusions: Transient hydrogen tracking bias is predominantly controlled by the temporal weighting parameter θ. For identical spatial grids and boundary conditions, increasing θ enhances artificial numerical diffusion, attenuating concentration peaks and distorting arrival times. In contrast, moderately implicit Preissmann-type configurations provide a more accurate compromise between stability and transient fidelity. In the Arezzo radial network, short residence times and limited pipe lengths restrict cumulative diffusion, resulting in only marginal propagation bias. These findings suggest that temporal discretization is critical in long transport scenarios, while its impact becomes scale- and topology-dependent in distribution systems. Large-scale experimental validation, based on hydrogen tracing at strategically selected network nodes, will be essential to verify model reliability and confirm the robustness of the proposed discretization approach under real operating conditions.

References

[1] M. Chaczykowski, F. Sund, P. Zarodkiewicz, and S. M. Hope, “Gas composition tracking in transient pipeline flow,” Journal of Natural Gas Science and Engineering, 2018.

[2] Z. Zhang, I. Saedi, S. Mhanna, K. Wu, and P. Mancarella, “Modelling of gas network transient flows with multiple hydrogen injections and gas composition tracking,” IJHE, vol. 47, no. 4, pp. 2220–2233, 2022.

[3] A. Preissmann, “Propagation of surges in open channels and pipes,” in Proceedings of the International Association for Hydraulic Research Congress, 1961.

[4] M. Urh and M. Pantoš, “Gas composition tracking feasibility using transient finite difference θ-scheme model for binary gas mixtures,” IJHE, vol. 49, pp. 1319–1331, 2024.

[5] M. Francesconi, N. Taddeucci, M. Riccardi, L. Busi, M. Meazzini, M. Pagliai, G. Cardini, and C. Carcasci, “Multiscale assessment of gravity-induced stratification for hydrogen blending applications in gas networks,” IJHE, vol. 196, p. 152605, 2025.



Dynamic modelling and performance mapping of an integrated hydrogen valley ecosystem: the HySPARK case

Jarosław Milewski*[a], Arkadiusz Szczęśniak[a], Aliaksandr Martsinchyk[a], Katsiaryna Martsinchyk[a], Olaf Dybiński[a]

* corresponding author: jaroslaw.milewski@pw.edu.pl

[a] Warsaw University of Technology, Faculty of Power and Aeronautical Engineering, Institute of Heat Engineering, 21/25 Nowowiejska Street, 00-665 Warsaw, Poland

Keywords: hydrogen valley, dynamic modelling, hydrogen logistics, hydrogen refuelling station, digital twin

Abstract

Introduction: Hydrogen valleys combine production, storage, transport, refuelling and end-use assets that must be operated as one coordinated system rather than as isolated units. This requires modelling environments able to represent time-varying interactions between generation, trailer logistics, station inventory and user demand. In the HySPARK project, this challenge is addressed for the Mazovian Hydrogen Valley, linking the Włocławek hydrogen production hub with hydrogen refuelling stations (HRSs), Warsaw Chopin Airport mobility applications and an industrial ammonia off-taker. The present work develops a conceptual and numerical framework for a valley-scale performance map and future digital-twin deployment, consistent with recent hydrogen-valley and hydrogen-system modelling studies [1-3].

Objectives: The objective was to develop and verify a coherent system-level model of the HySPARK ecosystem covering not less than 90% of the identified hydrogen-valley entities. Specific goals were to represent major production, storage, transport and end-use assets in a common environment; quantify hydrogen generation, utilisation and consumption over time; verify interactions between production hubs, multiple-element gas container (MEGC) trailer logistics, HRS operation and final users; and provide a modelling basis for the future Mazovian Hydrogen Valley Energy Planner.

Material and methods: Mathematical models were developed for hydrogen production facilities, transportation and distribution infrastructure, HRS operation and consumption sectors. The model was implemented as a discrete-time simulation environment in which each physical asset is represented by a digital node with a unique tag. Static parameters, including capacities, efficiencies, thresholds, locations and economic data, were separated from dynamic operating states, including current inventory, active refuelling sessions, trailer loads, station status and vehicle position. This registry-based architecture enabled synchronised propagation of state changes at each simulation step. The model portfolio included Włocławek hydrogen hubs, MEGC trailers, HRSs, buses, heavy-duty vehicles, towing tractors and an ammonia off-taker. Representative scenarios were simulated to evaluate station inventory behaviour, refuelling events, buffer utilisation, trailer dispatch and coupling between mobility demand and industrial withdrawal. The formulation follows the need for spatially and temporally explicit hydrogen-system models identified in recent reviews and optimisation studies [3-7].

Results: The developed framework generated a system-level performance map covering the major HySPARK assets and reproduced realistic hydrogen-flow interactions across the valley. At the airport HRS, the model captured the combined effect of on-site storage and trailer-based buffering under demand from buses, towing tractors and additional non-contracted users. Vehicle-level simulations reproduced repeated discharge and refuelling cycles, which translated directly into time-varying station demand. For the production layer, the flexible Hub 2 model showed that a 5 MW-class electrolyser coupled with a 5 t hydrogen buffer can absorb intermittent trailer-filling events while sustaining quasi-continuous hydrogen supply to ammonia production through threshold-based electrolyser control. The Hub 1 model confirmed a different operating philosophy of a large industrial hydrogen source, where ammonia demand dominates and trailer loading acts as a secondary but strategically important sink. The main model outputs are summarised in Table 1.

Table 1. Summary of key model outputs for the HySPARK hydrogen-valley modelling framework.

Model layer	Representation in the framework	Main output / result
System scope	Digital-node registry for production, storage, transport, HRSs and end-use assets.	Coverage of >90% of identified valley entities and a coherent valley topology.
Hydrogen flows	Time-resolved mass balances between Włocławek hubs, MEGC trailers, HRSs and users.	Stable, mass-conserving propagation of production, delivery, inventory and consumption.
Refuelling operations	Airport HRS with on-site storage, trailer buffer, buses, towing tractors and additional users.	Inventory trajectories and refuelling-cycle patterns suitable for station scheduling.
Production layer	Hub 2: 5 MW-class electrolyser with 5 t buffer; Hub 1: industrial hydrogen source dominated by ammonia demand.	Threshold-based dispatch, trailer-filling logic and coupled industrial withdrawal representation.
Planning value	Separate static asset registry and dynamic state registry prepared for scenario updates.	Basis for hydrogen allocation, routing, storage assessment and digital-twin integration.

Conclusions: The HySPARK modelling environment provides a robust basis for analysing integrated hydrogen-valley operation at both asset and ecosystem levels. The framework captures transient interactions between production, storage, transport and demand while remaining transparent and extensible through the separation of static and dynamic registries. The obtained performance map confirms that the conceptual design can be translated into an operational planning tool supporting hydrogen allocation, trailer routing, storage assessment and scenario evaluation. The same architecture is suitable for future connection to live operational data, enabling progression from offline simulations toward a digital twin of the Mazovian Hydrogen Valley.

Acknowledgment

This project is supported by the Clean Hydrogen Partnership under Grant Agreement No. 101192536.

References

[1] Rosén S., Göransson L., Taljegård M., Lehtveer M. Modeling of a "Hydrogen Valley" to investigate the impact of a regional pipeline for hydrogen supply. Front. Energy Res. 12, 1420224 (2024). doi:10.3389/fenrg.2024.1420224.

[2] Romano V., Marocco P., Gandiglio M., Santarelli M. Modelling a small-scale hydrogen valley: optimisation under techno-economic and environmental perspectives. Int. J. Hydrogen Energy 191, 152172 (2025). doi:10.1016/j.ijhydene.2025.152172.

[3] Bozzolo Lueckel F.B., Monaghan R.F.D., Lynch M. Hydrogen supply chain modelling at energy system scale: a review. Renew. Sustain. Energy Rev. 210, 115218 (2025). doi:10.1016/j.rser.2024.115218.

[4] Riera J.A., Lima R.M., Knio O.M. A review of hydrogen production and supply chain modeling and optimization. Int. J. Hydrogen Energy 48(37), 13731-13755 (2023). doi:10.1016/j.ijhydene.2022.12.242.

[5] Blanco H., Leaver J., Dodds P.E., Dickinson R., García-Gusano D., Iribarren D., Lind A., Wang C., Danebergs J., Baumann M. A taxonomy of models for investigating hydrogen energy systems. Renew. Sustain. Energy Rev. 167, 112698 (2022). doi:10.1016/j.rser.2022.112698.

[6] Welder L., Ryberg D.S., Kotzur L., Grube T., Robinius M., Stolten D. Spatio-temporal optimization of a future energy system for power-to-hydrogen applications in Germany. Energy 158, 1130-1149 (2018). doi:10.1016/j.energy.2018.05.059.

[7] Samsatli S., Samsatli N.J. A multi-objective MILP model for the design and operation of future integrated multi-vector energy networks capturing detailed spatio-temporal dependencies. Appl. Energy 220, 893-920 (2018). doi:10.1016/j.apenergy.2017.09.055.



CFD Assessment of Absorption-Rate-Based Charging Interruption for Thermal Protection and Recovery of an AB_2 Metal Hydride Tank

Andrej Markovic[a,*], Massimiliano Renzi[a]

* corresponding author: andrej.markovic@student.unibz.it

[a] Faculty of Engineering, via Bruno Buozzi 1

Free University of Bozen - Bolzano,

Bozen - Bolzano, Italy

Keywords: AB_2 metal hydride, absorption-rate, CFD modelling, thermal management strategy

Abstract

Introduction

Metal hydrides are attractive solid-state hydrogen storage materials due to their high volumetric hydrogen density, improved safety, and operation at moderate pressures and temperatures compared with compressed or liquefied hydrogen storage systems [1]. Among them, composition-tailored AB_2-type Laves phase alloys are particularly relevant for practical storage applications because they can operate under favourable pressure and temperature conditions, while their thermodynamic and kinetic properties can be adjusted through alloy composition [2,3]. Their use in low-temperature hydrogen storage and fuel cell-related systems has also been widely considered [4,5]. However, heat transfer often limits the charging performance of metal hydride tanks [6,7]. Hydrogen absorption is exothermic: if the generated heat is not removed effectively, the hydride temperature increases, the equilibrium pressure rises, and the absorption driving force decreases. As a result, hydrogen may continue to be supplied, while the bed is thermally suppressed and exhibits reduced hydrogen uptake. Since direct measurement of the internal temperature is difficult in practical tanks, this work uses a transient Computational Fluid-Dynamic (CFD) model to evaluate whether the absorption-rate response can support charging interruption criteria and thermal recovery strategies for the investigated storage tank.

Objectives

The objective of this work is to assess, using transient CFD modelling, whether the absorption-rate response can serve as a practical indicator for defining charging interruption periods in an AB_2 metal hydride storage tank. The study relates the reduction in hydrogen uptake rate to the coupled effects of temperature rise, equilibrium pressure increase, and progressive hydride loading during charging. A further objective is to evaluate whether temporary interruption of the hydrogen supply can enable thermal recovery of the hydride bed. As the bed cools, the absorption driving force may be partially restored, allowing the tank to accept hydrogen at a higher rate once charging is resumed. In this way,

the proposed approach is investigated not only as a thermal protection measure, but also as a potential strategy for improving the practical charging behaviour of the tank.

Material and methods

A transient CFD model of the metal hydride storage tank was implemented in ANSYS Fluent. The hydride bed was represented as a porous medium, while hydrogen absorption was modelled using user-defined source terms coupled with the local pressure, temperature, and hydride loading. The data on the thermo-chemical properties of the hydride, as well as the detailed geometrical properties of the enclosure and the bottle, are based on a real system available in the premises of the University. The spatially integrated gas-phase mass sink was used to determine the instantaneous hydrogen absorption rate, whereas the corresponding energy source accounted for the heat released during absorption. Two charging cases were simulated: continuous pressure-driven charging and charging with temporary hydrogen supply interruption based on the absorption-rate response. In the interruption scenario, the hydrogen supply was stopped when the absorption rate decreased below a predefined threshold and resumed after a thermal recovery period.

Results

Detailed temperature, absorption rate and heat fluxes contours are obtained for a scenario based on a real system and adopting real operating characteristics and parameters. For continuous charging, the results show that the process is limited by heat transfer rather than hydrogen supply. Local hot regions develop within the hydride bed, causing the maximum temperature to exceed the manufacturer-recommended limit, while the average bed temperature remains significantly lower. The absorption rate decreases due to the combined effects of temperature rise, increased equilibrium pressure, and progressive hydride loading. This confirms that internal heat transport is the dominant limitation during charging. For the interruption-based strategy, stopping the hydrogen supply suppresses absorption heat generation and allow the bed to cool. This reduces the equilibrium pressure, partially restore the absorption driving force, and enables renewed hydrogen uptake after charging is resumed, supporting safer operation and complete use of the storage capacity.

Conclusions

This study confirms that the charging performance of metal hydride tanks is strongly affected by internal heat transfer limitations. Under continuous charging, reaction heat leads to local hot spots, which may become unfavourable for the hydride material if the recommended temperature limit is exceeded. The absorption-rate response is shown to be a practical indicator of reduced hydrogen uptake capability. Temporary interruption of the hydrogen supply can suppress heat generation and allow thermal recovery of the bed, thereby partially restoring the absorption driving force after cooling. Although such interruptions increase the total charging time, they can support safer operation and more complete use of the available storage capacity. Therefore, absorption-rate-based charging

interruption represents a promising strategy for thermal protection and improved charging control in metal hydride storage systems. On the basis of the results of this analysis, novel geometries and solutions to enhance and optimize the thermal fluxes are proposed to boost charging and discharging rates of metal hydrides, including phase change materials.

Acknowledgment

This research was supported by the project LabGPT (EFRE1090), cofinanced by the European Union within the Regional Development Fund (ERDF) Programme 2021-2027.

References

[1] B. Sakintuna, F. Lamari-Darkrim, M. Hirscher, "Metal hydride materials for solid hydrogen storage: A review," International Journal of Hydrogen Energy, vol. 32, no. 9, pp. 1121–1140, 2007. https://doi.org/10.1016/j.ijhydene.2006.11.022

[2] V. A. Yartys, M. V. Lototskyy, "Laves type intermetallic compounds as hydrogen storage materials: A review," Journal of Alloys and Compounds, vol. 916, article 165219, 2022. https://doi.org/10.1016/j.jallcom.2022.165219

[3] A. Hariyadi, S. Suwarno, R. V. Denys, J. Bellosta von Colbe, T. O. Sætre, V. Yartys, "Modeling of the hydrogen sorption kinetics in an AB2 laves type metal hydride alloy," Journal of Alloys and Compounds, vol. 893, article 162135, 2022. https://doi.org/10.1016/j.jallcom.2021.162135

[4] M. V. Lototskyy, I. Tolj, L. Pickering, C. Sita, F. Barbir, V. Yartys, "The use of metal hydrides in fuel cell applications," Progress in Natural Science: Materials International, vol. 27, no. 1, pp. 3–20, 2017. https://doi.org/10.1016/j.pnsc.2017.01.008

[5] J. Bellosta von Colbe, J.-R. Ares, J. Barale, M. Baricco, C. Buckley, G. Capurso, N. Gallandat, D. M. Grant, M. N. Guzik, I. Jacob, E. H. Jensen, T. Jensen, J. Jepsen, T. Klassen, M. V. Lototskyy, K. Manickam, A. Montone, J. Puszkiel, S. Sartori, D. A. Sheppard, A. Stuart, G. Walker, C. J. Webb, H. Yang, V. Yartys, A. Züttel, M. Dornheim, "Application of hydrides in hydrogen storage and compression: Achievements, outlook and perspectives," International Journal of Hydrogen Energy, vol. 44, no. 15, pp. 7780–7808, 2019. https://doi.org/10.1016/j.ijhydene.2019.01.104

[6] M. Afzal, R. Mane, P. Sharma, "Heat transfer techniques in metal hydride hydrogen storage: A review," International Journal of Hydrogen Energy, vol. 42, no. 52, pp. 30661–30682, 2017. https://doi.org/10.1016/j.ijhydene.2017.10.166

[7] V. K. Kukkapalli, S. Kim, S. A. Thomas, "Thermal Management Techniques in Metal Hydrides for Hydrogen Storage Applications: A Review," Energies, vol. 16, no. 8, article 3444, 2023. https://doi.org/10.3390/en16083444



Experimental Investigation of a Lab-Scale Metal Hydride – Phase Change Material Hydrogen Storage System

Marco Maggini*[a], Gebregziabihier T. Ayenew[a], Andrea L. Facci[a], Viviana Cigolotti[b], Stefano Ubertini[a]

* corresponding author: marco.maggini@unitus.it

[a] Department of Economics, Engineering, Society and Business Organization, Tuscia University, Largo dell'Università 01100 Viterbo (Italy)

[b] Department of Energy Technologies and Renewable Sources (TERIN), ENEA C.R. Casaccia, 000123 Rome, Italy

Keywords: energy storage, hydrogen technologies, metal hydrides, phase change materials, renewable energies

Abstract

Although hydrogen compression to very high pressures (up to 800 bar) or its liquefaction are mature technologies, the storage into metal hydrides (solid-state storage) emerges as a relevant low-pressure, high-density alternative to physical-based storage. The present work investigates the absorption and desorption of hydrogen into and from the Hydralloy C5 alloy. A comparison is made between an air-based cooling and a passive thermal management through phase change materials. Results show that the complete absorption requires 180 s while as much as 1 g of hydrogen can be absorbed or desorbed (corresponding to approximately 0.67 kW of average charge power). The temperature ranges from -5°C to 48 °C when the storage pressure is set to 20 bar.

Introduction: Hydrogen storage into Metal Hydrides (MH) can significantly lower the storage pressure and maintenance or safety costs and issues. Nonetheless, their thermal management is not trivial, since the absorption reaction is strongly exothermic and the desorption is endothermic **[1]**. Therefore, an efficient heat management system is necessary for this technology to be competitive with state-of-the-art compression. As opposed to active systems (e.g., heat exchangers) passive HMS's do not require external energy supplies and therefore do not reduce the round-trip efficiency of the storage system. The usage of Phase Change Materials (PCM), in this context, thus increases the round-trip efficiency of the hydrogen supply chain while allowing for safe storage of hydrogen **[2]**.

Objectives: The goal of the work is to experimentally investigate the charge/discharge cycling of the hydralloy C5 MH during the absorption and desorption cycles while the lab-scale canister is immersed respectively in still air and in a paraffin-based phase change material.

Material and methods: The hydralloy C5 powder (159.61 g) is inserted into a 1in, 20-cm long steel tube. Both ends are constrained with Teflon and double gaskets, to ensure leak-proof sealing. One cap is drilled for a 1/8in BSPG threading, while an adapted is used to shift to a compression-type sealing. The filling coefficient for the tube is 50%, to leave more than enough space for the powder to expand after the absorption of hydrogen starts. Two one-way 1 micron filters are located after the BSPG-compression adapter, to ensure separate ways for the absorption and desorption lines. One mass flow meter is located between the HP hydrogen bottle and the MH canister to measure the instantaneous mass flow rate and the total flow mass in and out of the tube. We use two K-type thermocouples to measure the tube surface temperature in two different locations while the tube is held horizontally. The data is analyzed in real-time on a dedicated LabView program, which monitors mass flow rate, total mass flow, temperature and pressure. The estimated absorbed fraction of hydrogen is calculated as $m_{abs}^{H_2} = m_{tot}^{H_2} - m_g^{H_2}$, where $m_{tot}^{H_2}$ and $m_g^{H_2} = pV/R_{H_2}T$ are the total mass flow rate as measured by the mass flow meter and the gaseous amount of hydrogen inside the tube, respectively.

Results: The absorbed mass of hydrogen increases rapidly with time during a very brief initial phase, when the temperature of the hydride is relatively low (see **Fig. 1**). As the temperature increases, the kinetics of the reaction slows down, as well as the hydrogenation. The total amount of absorbed mass then rapidly stalls and continues at a very low pace. Four cycles are needed to reach complete activation of the powder, i.e., good pulverization of the powder and good penetration of the hydrogen gas through the powder surface. Therefore, cycle 1 reaches a maximum of ~ 0.65 g of hydrogen, while cycle 5 reaches a maximum of ~ 1 g of hydrogen. Correspondingly, the tube temperature reaches a maximum of $\sim 40 \div 48$ °C for cycle 1 and cycle 5, respectively. In air, the heat exchange with the surrounding environment is very slow, thus we suggest immersing the MH tube inside a PCM for passive thermal management or coupling it with an heat exchanger to increase effectiveness at the expense of the round-trip efficiency. By adding the PCM around the MH tube, the H2 capacity increases to 1.22 g (+ 20.7%, see **Fig. 2**, cycle #4). This is due to the better capacity of the MH to dispose of the hydrogenation heat. Correspondingly, the absorption peak temperature reduces to 38°C/41°C and desorption lower temperature increases to -5°C/+9°C.

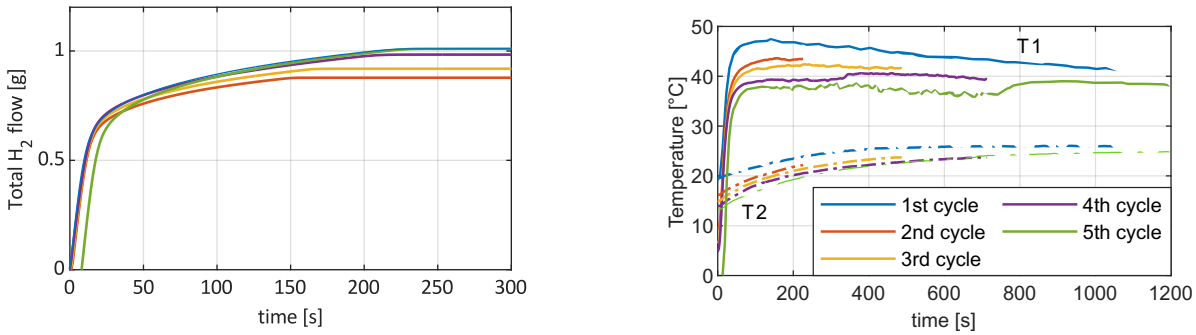


*Figure 27: hydrogen mass (**left**) and surface temperature of the tube (**right**) during the absorption cycle in air.*

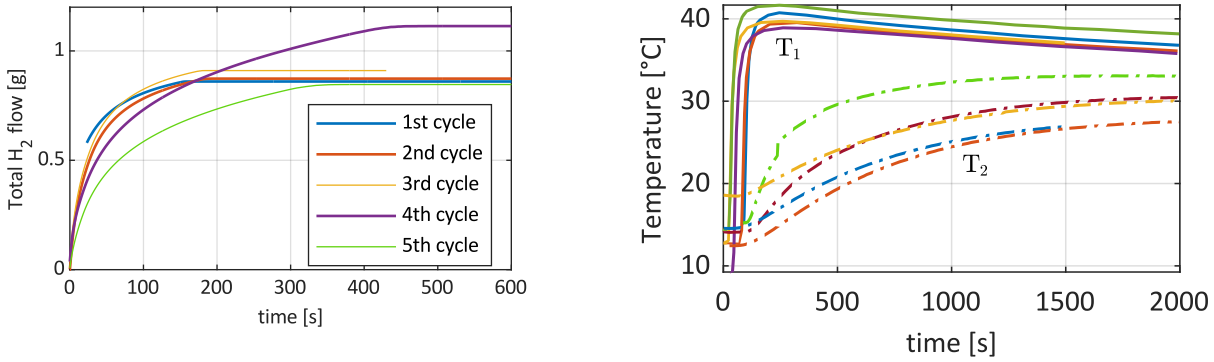


*Figure 28: hdyrogen mass (**left**) and surface temperature of the tube (**right**) during the absorption cycle with PCM.*

Conclusions: Integrating paraffin as passive thermal management in metal hydride tanks mitigates temperature spikes (keeping them between 38°C and 41°C), which increases hydrogen storage capacity by 20.7% (from 1.01 g to 1.22 g). The system, at an equal volumetric energy density (330 kWh/m^3), operates at a pressure 6 times lower than compressed gas (2 MPa vs 12.2 MPa), offering superior safety.

Acknowledgment

This research was funded by: (i) the European Union – NextGeneration EU from the Italian Ministry of Environment and Energy Security POR H2 AdP MASE/ENEA with involvement of CNR and RSE, PNRR - Mission 2, Component 2, Investment 3.5 "Ricerca e sviluppo sull'idrogeno". (ii) The European Union - NextGenerationEU. Award Number: Project code PE0000021, Concession Decree No. 1561 of 11.10.2022 adopted by Ministero dell'Università e della Ricerca (MUR), CUP I53C22001450006, according to attachment E of Decree No. 1561/2022, Project title "Network 4 Energy Sustainable Transition—NEST. (iii) ECS 0000024 Rome Technopole, CUP B83C22002820006, National Recovery and Resilience Plan (NRRP) Mission 4 Component2Investment 1.5, funded by the European Union—NextGenerationEU

References

[1] M. Maggini, G. Falcucci, A. Rosati, S. Ubertini, A. L. Facci, J. of En. Storage, 93 2024

[2] H. El Mghari, J. Huot, L. Tong, J. Xiao, Int. J. of H. Energy, 45 2020, 14922–14939



Experimental System for Hydrogen Permeability Testing at High-Pressure

Andrea Dei Sommi*[a,b], Maria Federica De Riccardis*[b], Corradino Sposato[b], Giuseppe Montesano[b], Francesco Grandizio[b], Francesca Lionetto[a], Alfonso Maffezzoli[a]

* corresponding author: andrea.deisommi@unisalento.it, federica.dericcardis@enea.it

[a] Department of Engineering for Innovation, University of Salento, Lecce, Italy

[b] ENEA, Italian National Agency for New Technologies, Energy and Sustainable Economic Development, Energy Technologies and Renewable Sources Department, Italy

Keywords: polymer composites, hydrogen storage, gas permeability

Abstract: This work presents a custom high-pressure system for measuring the gas permeability of polymeric and composite materials suitable for hydrogen storage applications. The development of efficient and safe hydrogen storage technologies is critical to the transition towards a carbon-neutral economy, particularly for advanced Type V pressure vessels, where the composite structure must provide both mechanical strength and gas barrier. The experimental apparatus was developed in accordance with the CSA/ANSI CHMC 2:19 standard. The system consists of a dual-chamber configuration separated by the test specimen. The setup enables permeability measurements under gas pressures up to 40 MPa. Several polymeric and composite materials were investigated, including polycarbonate (PC), poly(ether-ketone-ketone) (PEKK), carbon fiber-reinforced PEKK (C/PEKK), and carbon fiber-reinforced epoxy (C/EPOXY). Preliminary tests were carried out at up to 10 MPa using helium to simplify handling and improve safety. Gas transmission was quantified by using an optical bubble sensor that had been preliminarily calibrated through a syringe pump. Among the tested materials, the C/PEKK composite exhibited the lowest permeability, demonstrating superior barrier performance compared with the other samples investigated. The developed setup proved capable of accurately evaluating low gas permeation in polymer and composites.

Introduction: The global effort to achieve a carbon-neutral economy is intensifying in order to reach net-zero carbon dioxide emissions by 2050. Attaining this target relies on the widespread adoption of green hydrogen as a key energy carrier [1]. However, critical challenges remain, particularly in developing storage technologies that are both economically viable and energy efficient, and in establishing safe and robust infrastructure for hydrogen transport. The selection of appropriate materials for storage applications is inherently complex, as it requires achieving an optimal balance between safety requirements, cost considerations, and overall economic feasibility [2]. Regarding gas hydrogen storage strategies, the most advanced configuration of composite pressure vessels corresponds to Type V systems. However, despite their potential, the manufacture of these vessels and the mitigation of gas permeation present numerous challenge [3].

Objectives: A custom system was designed and implemented to measure hydrogen permeability at high pressures. The system was then tested and the gas barrier properties of various polymer and composite materials were investigated under different test conditions.

Material and methods: The list of analyzed polymer and composite samples is reported in Table 1. All the samples had a diameter of 78 mm and a thickness ranging from 50 µm to 3.1 mm. The composite samples were manufactured by using hot pressing at a temperature of 380 °C and a pressure of 0.7 MPa for poly(ether-ketone-ketone) with carbon fibers (C/PEKK) and vacuum-bag-only process at a temperature of 120 °C for epoxy resin with carbon fibers (C/EPOXY).

Table 1. Tested polymer and composite materials.

Material	Details	Sample thickness	Label
Polycarbonate	commercial; density = 1.2 kg/m^3	3.0 mm	PC
Poly(ether-ketone-ketone)	film form; density = 1.3 kg/m^3	50 µm	PEKK
Poly(ether-ketone-ketone) + carbon fibers	composite laminate; polymer weight fraction = 34%	3.1 mm	C/PEKK
Epoxy resin + carbon fibers	composite laminate; polymer weight fraction = 38%	1.0 mm	C/EPOXY

The permeability testing system (Figure 1a) was designed in conformity with the CSA/ANSI CHMC 2:19 standard [4]. The test chamber was located inside a climate chamber to control the temperature and the relative humidity. It consisted of two volumes that are separated by the sample under test. The sample acted as a barrier to gas transmission between the high-pressure hydrogen volume (up to 40 MPa) and the volume at atmospheric-pressure volume. The equilibrium value of the leakage rate, which was equal to the slope of the linear portion of the plot of transmitted volume vs time, can be used to calculate the permeability value *P*:

$$P = \frac{Q \cdot t}{\Delta p \cdot A} \quad \left[\frac{\mathrm{m}^3 \cdot \mathrm{m}}{\mathrm{m}^2 \cdot \mathrm{s} \cdot \mathrm{Pa}}\right]$$

where Q (m^3/s) was the leakage rate, t (m) the sample thickness, Δp (Pa) the pressure difference, and A (m^2) the permeation area.

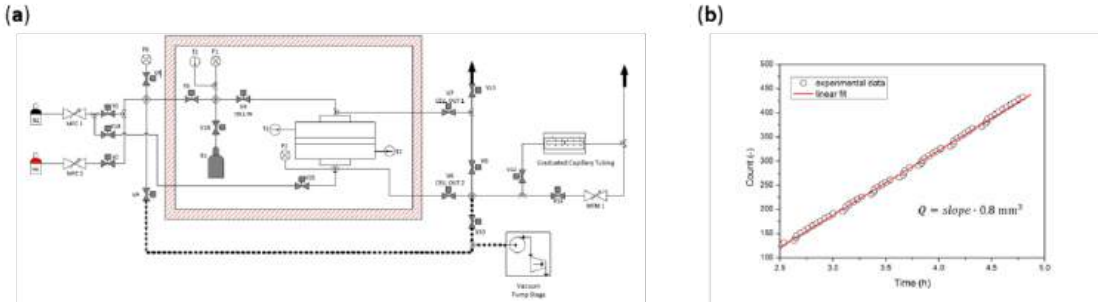


Figure 1. (**a**) Permeability testing system and (**b**) plot of bubble count over time for PC sample.

Results: To measure the amount of gas transmitted through the sample, the effectiveness of various configurations was evaluated. For low-permeability materials, an optical bubble sensor was used as more sensitive than a mass flow meter. The optical sensor was calibrated using a controlled-infusion syringe pump, and an average bubble volume of 0.80 mm^3 was estimated. In this study, helium was used for the preliminary tests, with a maximum pressure of 10 MPa applied up to 48 h. Figure 1b shows the permeation data at equilibrium. The observed trend is representative of all samples. The C/PEKK sample produced the best permeability results, revealing a permeability of $2.0 \cdot 10^{-18}$ $(m^3 \cdot m)/(m^2 \cdot s \cdot Pa)$. The test pressure and permeability values are summarized in Table 2.

Table 2. Testing pressure and permeability results.

Label	Pressure (MPa)	Leakage rate (m^3/s)	Permeability ($m^3 \cdot m/(m^2 \cdot s \cdot Pa)$)
PC	3	$3.0 \cdot 10^{-11}$	$1.7 \cdot 10^{-17}$
PEKK	1	$2.7 \cdot 10^{-10}$	$8.1 \cdot 10^{-18}$
C/PEKK	10	$1.1 \cdot 10^{-11}$	$2.0 \cdot 10^{-18}$
C/EPOXY	5	$2.6 \cdot 10^{-11}$	$3.0 \cdot 10^{-18}$

Conclusions: A permeability testing system capable of conducting hydrogen tests at a maximum pressure of 40 MPa has been designed and built. The system performed well in preliminary tests conducted with helium at pressure of up to 10 MPa. The composite C/PEKK was the most effective. Future work will include conducting hydrogen tests at higher pressure levels.

Acknowledgment: This research was funded by the European Union Next Generation EU from the Italian Ministry of Environment and Energy Security, POR H2 AdP MEES/ENEA with involvement of CNR and RSE, PNRR- Mission 2, Component 2, Investment 3.5 “Ricerca e sviluppo sull’idrogeno”, CUP: I83C22001170006.

References

[1] Mekonnin AS, Wacławiak K, Humayun M, Zhang S, Ullah H. Hydrogen Storage Technology, and Its Challenges: A Review. Catalysts 2025;15:260. https://doi.org/10.3390/catal15030260.

[2] Panigrahi PK, Chandu B, Motapothula MR, Puvvada N. Potential Benefits, Challenges and Perspectives of Various Methods and Materials Used for Hydrogen Storage. Energy and Fuels 2024;38:2630–53. https://doi.org/10.1021/acs.energyfuels.3c04084.

[3] Air A, Shamsuddoha M, Gangadhara Prusty B. A review of Type V composite pressure vessels and automated fibre placement based manufacturing. Compos B Eng 2023;253:110573. https://doi.org/10.1016/j.compositesb.2023.110573.

[4] CSA/ANSI CHMC 2:19 (R2024) | Codes & Standards - Purchase | Product | CSA Group 2026. https://www.csagroup.org/store/product/2427320/?srsltid=AfmBOoplqfKTfahTpCk4v1WDqQnTU9F_cjTB-nL5iwHX3bj7qbZVRKTl (accessed May 21, 2026).

EFCH2 2026 European Fuel Cells and Hydrogen PIERO LUNGHI CONFERENCE
September 15th-17th 2026 Capri / Italy

Analysis of SOEC-based systems for the production and import of e-NG

Alberto Cammarata*[a], Victor Martinez Guija[a], Stefano Campanari[a]

* corresponding author: alberto.cammarata@polimi.it

[a] Department of Energy, Politecnico di Milano - Milan, Italy

Keywords: SOEC, power-to-gas, methanation, e-NG

Abstract

Power-to-gas (P2G) processes allow to convert renewable electricity into hydrogen and then to synthetic methane (also known as electric methane, e-NG), enabling its use as drop-in fuel in the existing natural gas infrastructure. This work presents a process modelling and preliminary economic assessment of Solid Oxide Electrolysis (SOEC) based P2G systems producing e-NG, including detailed mass and energy balances of the proposed process and a preliminary economic analysis focusing on the costs of producing e-NG in North Africa and transporting the gas *via* pipelines to Italy.

Introduction: Clean energy carriers derived from hydrogen, such as methane, ammonia and methanol, can play a key role in the energy transition to a decarbonized economy: (i) they can be produced as 'e-fuels' using clean electricity in regions with abundant renewable energy sources and transported overseas by ships or pipelines; (ii) they can be used for medium- and long-term energy storage, overcoming the limitations of other types of energy storage systems like batteries [1], and (iii) they act as 'drop-in' fuels, taking advantage of existing infrastructures and established utilization technologies [2]. Synthetic natural gas (SNG or e-NG) can be produced *via* the Sabatier reaction (Eq. 1), a strongly exothermic process typically carried out at 200-550°C and about 30 bar:

$$4H_2 + CO_2 \rightarrow CH_4 + 2H_2O \qquad (1)$$

The required hydrogen can be produced from water and electricity through high-temperature SOEC electrolysis, exploiting heat produced by the Sabatier reaction to produce steam [3]. CO_2 can be sourced from fossil-based industrial processes, whereas the overall CO_2 cycle is not fully closed unless CO_2 is re-captured at the e-NG utilization stages (depending on the carbon capture rates); alternatively, biogenic CO_2 or direct air capture (DAC) can be used to achieve a fully net-zero process, with different impacts in terms of energy consumption and costs [4].

Objectives: This work presents a thermodynamic analysis of the integrated SOEC and methanation process for producing e-NG, with detailed mass and energy balances, and a preliminary economic analysis for the case of producing e-NG in North Africa and transporting the gas to Italy *via* pipelines.

Methods and assumptions: The SOEC employs cathode recirculation to increase the inlet H_2 fraction at 50%, to avoid nickel reoxidation, with single-pass steam utilization factor U_{H_2O} = 60%, and global steam utilization (including recirculation) of 80%. SOEC inlet streams are preheated at 700°C by heat recovery complemented

by electric heaters, since the SOEC is operated at the thermoneutral voltage (1.3 V). The air flow rate is set to limit the O_2 fraction at SOEC outlet to a maximum of 40%, to avoid risks of metal degradation by high-temperature oxidation. Hydrogen produced is then pressurized to 30 bar in an intercooled compressor, while CO_2 is assumed for simplicity to be available at 30 bar; they feed, in proportion 4:1, three Sabatier reactors arranged in series with intercooling. Heat produced by the reactions is used to produce steam for the SOEC, and the produced e-NG is finally compressed to 70 bar for pipeline injection. The system size matches a 500 MW_{el} electrolyzer (DC power), in line with recent large-scale projects [5]. Other assumptions include 5 MW_{th} heat loss and 30 mbar pressure loss in the SOEC, operating with 97% DC/AC conversion efficiency; 1 bar pressure loss across the reactors; compressors and blowers adiabatic, mechanical, and electric efficiency equal to 80%, 98%, and 98%, respectively. System mass and energy balances are solved with Aspen Plus® using Peng-Robinson correlations for the fluid thermodynamic properties; Sabatier reactors are simulated at chemical equilibrium. The levelized cost of e-NG (€/MWh_{th}) is estimated according to Eq. 2, assuming 20 years lifetime, 7% discount rate and 8000 equivalent operating hours to calculate the capital recovery factor (CRF). The calculation includes the specific cost of electricity c_{el} (35 €/MWh_{el}), system efficiency η, a pipeline tariff cost ($c_{transport}$) of 7.9 €/MWh_{th} [6], a cost of CO_2 of 70 €/t (compatible with long-term estimations for DAC systems [4]), and annual O&M costs equal to 2% of the investment cost (C_{inv}).

$$LCOeNG = \frac{C_{inv} \cdot CRF}{\dot{Q}_{e-NG}^{LHV} \cdot h_{eq}} + \frac{c_{el}}{\eta} + c_{transport} + \frac{c_{CO_2} \cdot \dot{m}_{CO_2}}{\dot{Q}_{e-NG}^{LHV}} + \frac{C_{O\&M}}{\dot{Q}_{e-NG}^{LHV} \cdot h_{eq}} \quad (2)$$

The cost of equipment is calculated assuming 1500 €/kW_{el} for the SOEC, 200 €/kW_{th} (specific to the produced e-NG) for the methanation system [7], and additional models for the cost of compressors and low-temperature heat exchangers [8]. The overall bare module cost is then increased by 50% to include contingencies, fees, site preparation, auxiliary facilities in the total investment cost C_{inv} [9].

Results: Figure 1 shows the system configuration and simulation results for the e-NG production system.

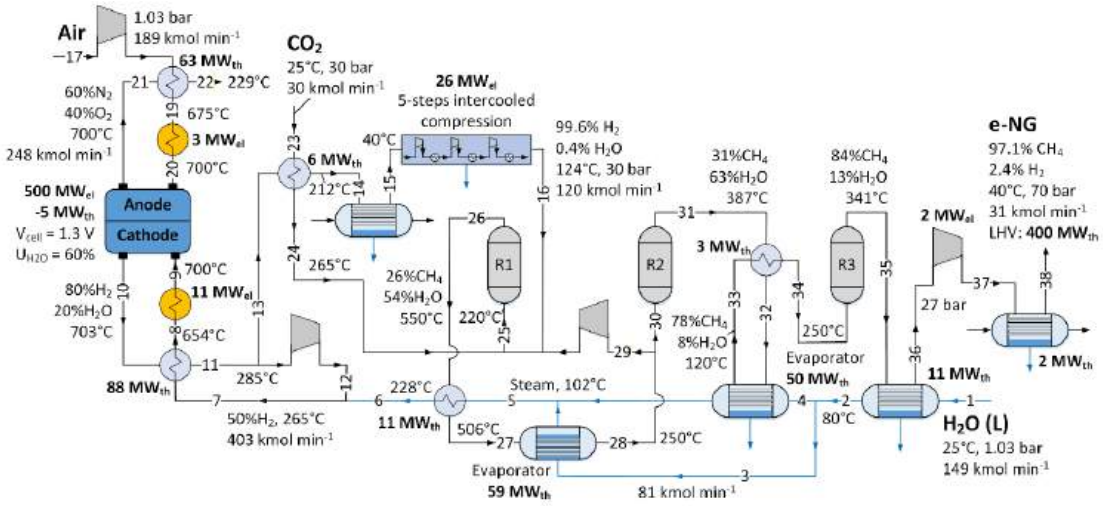


Fig. 29 – Simulation results for the SOEC-based e-NG production plant (blue lines represent H_2O streams).

The produced e-NG has a high methane content and a residual H_2 amount compatible with the thresholds allowed in several European countries [10]. The overall system electricity consumption is equal to 70.1 MJ $kg^{-1}_{e\text{-}NG}$, equivalent to 71.6% energy efficiency η (from electricity to e-NG LHV).

Figure 2 shows that the SOEC system represents the largest share of the plant cost (left); the overall investment cost and the electricity cost account for a combined 75% of the LCOeNG (right), whereas costs related to CO_2, O&M, and gas transport contribute for nearly 11%, 7.5% and 7% respectively. The final calculated levelized cost of e-NG is 119 €/MWh_{th}, suggesting that CAPEX and OPEX reduction or incentives are necessary to enhance the economic feasibility of the concept.

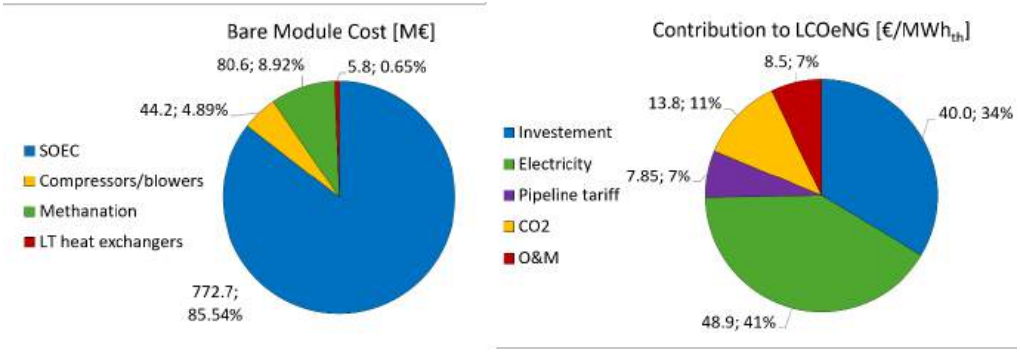


Fig. 30 – Breakdown of equipment cost (left; referred to a 500 MWel SOEC) and levelized cost of e-NG (right).

Conclusions: A thermodynamic analysis of an integrated SOEC and methanation process for producing e-NG shows the possibility to achieve a system electricity consumption of 70.1 MJ kg^{-1}, equivalent to 71.6% energy efficiency (LHV basis). A preliminary economic analysis for the case of producing e-NG in North Africa and transporting the gas to Italy *via* pipelines, assuming a SOEC specific cost of 1500 €/kW and a cost of electricity of 35 €/MWh_{el}, yields a levelized costs of e-NG equal to 119 €/MWh_{th}, suggesting areas of potential cost reduction or the necessity of incentives to improve the concept economic feasibility.

References

[1] Environmental and Energy Study Institute. Energy Storage. 2019.

[2] Zwaan B Van Der, Detz R, Meulendijks N, Buskens P. Renewable natural gas as climate-neutral energy carrier ? Fuel 2022;311:122547. https://doi.org/10.1016/j.fuel.2021.122547.

[3] Qi M, Park J, Stephen R, Kim J, Liu Y, Moon I. Continuous and flexible Renewable-Power-to-Methane via liquid CO2 energy storage: Revisiting the techno-economic potential. Renew Sustain Energy Rev 2022; https://doi.org/10.1016/j.rser.2021.111732.

[4] Fasihi M, Olga E, Breyer C. Techno-economic assessment of CO2 direct air capture plants. J Clean Prod 2019;224:957–80. https://doi.org/10.1016/j.jclepro.2019.03.086.

[5] Tree Energy Solutions. Projects for the production of e-NG. 2026 n.d. https://tes-h2.com/projects (accessed May 21, 2026).

[6] TRANSMED s.p.a. Key Contractual Terms and Conditions of the Gas Transportation Agreement. 2025.

[7] Lefebvre J, Friedemann M, Manuel G, Graf F, Bajohr S, Reimert R, et al. Renewable Power-to-Gas: A technological and economic review. Renew Energy 2016; doi.org/10.1016/j.renene.2015.07.066.

[8] Martinez Guija V. MSc thesis: Techno-Economic Analysis of an SOEC-based System for the Production of e-NG and Different Options for its Export to Italy. 2025.

[9] Nosherwani SA, Neto RC. Techno-economic assessment of commercial ammonia synthesis methods in coastal areas of Germany. J Energy Storage 2021; doi.org/10.1016/j.est.2020.102201.

[10] European Network of Trasmission System Operators for Gas. Gas Quality Monitoring Network, 2024.



Geopolymers modification and its hybrid materials for hydrogen storage

Md Akram Hossain*[a], Tero Luukkonen[a], Satu Ojala[b]

* corresponding author: Akram Hossain, akram.hossain@oulu.fi

[a] Fibre and Particle Engineering Research Unit, University of Oulu, Finland

[b] Environmental and Chemical Engineering, University of Oulu, Finland

Keywords: Adsorption, Geopolymers, Hydrogen storage, sol-gel

Abstract

Introduction: Hydrogen (H_2) is one of the most promising energy carriers but its storage as gas or liquid is challenging due to the low density of compressed gas (23 kg/m^3 at 27 °C and 350 bar) or liquid H_2 (71 kg/m^3 at -252 °C and 1 bar) and related leakage, boil-off losses, and safety issues [1,2]. Consequently, H_2 has low energy per unit volume (~10 MJ/L for liquid H_2) but tremendously high energy per unit weight (143 MJ/kg) [2]. Thus, reversible solid-state storage under realistic conditions (U.S. Department of Energy conditions: ≤ 12 bar pressure and temperature of -40 to +60 °C) would be beneficial especially in fuel cell vehicles [3]. However, the challenge of the current solid-state storage materials is mainly low storage capacity, which should be 6.5 wt.% of hydrogen as defined by the U.S. Department of Energy (DoE) conditions [3]. We explore geopolymers as new hydrogen storage materials. The abundant literature on zeolite-based hydrogen storage [4] indicates that geopolymers show highly potential due to e.g., their more energy efficient preparation, simple modification possibilities, and co-existence of micro- and mesopores. Geopolymers are amorphous zeolite-like aluminosilicates consisting of 3D network of $[SiO_4]^{4-}$ and $[AlO_4]^{5-}$ tetrahedra [5]. It is expected that geopolymers have better and practically relevant hydrogen (H_2) storage performance in comparison to for example zeolites (one of the most actively studied H_2 storage medium) due to their amorphous structure and open nano-scale porosity. Geopolymers with a wide range of compositions, additives, and post-synthesis modifications will be studied. They are all evaluated comprehensively for H_2 storage considering the required conditions (pressure and temperature), storage capacity, kinetics of adsorption/desorption, thermodynamics, and long-term performance. Geopolymers are completely unexplored materials for hydrogen storage. There are some preliminary scientific publications available that provide proof-of-concept, but the area is largely unexplored [6,7]. Geopolymers have the potential to be practically interesting and commercially competitive materials for this application.

Objectives:

- To develop geopolymer compositions or composite/hybrid materials for hydrogen storage.
- Thoroughly evaluate hydrogen storage capacity, operational conditions (temperature and pressure), adsorption/desorption kinetics, thermodynamics, and long-term use.
- To understand the connection between the key material characteristics affecting the hydrogen storage properties.

Material and methods: $Al(NO_3)_3{\cdot}9H_2O$, $Ca(NO_3)_2{\cdot}4H_2O$, colloidal silica, NaOH, 1M HCl, 3M HCl, $Co(NO_3)_2{\cdot}6H_2O$, and $Ni(NO_3)_2{\cdot}6H_2O$. A series of geopolymer compositions with different ratios of Si-Al-Na-Ca of 1:1:1:0 to 20:1:1:21 synthesized by using sol-gel method [8]. The geopolymers obtained are characterized by N_2 adsorption/desorption analyzer, XRF, XPS, and DRIFT. The best-performing materials are exposed with 1 M and 3 M HCl to induce dealumination for improving the porosity. All materials were characterized for H_2 adsorption/desorption (i.e., H_2 storage capacity and kinetics) at different pressure and temperature by using an isorb-HP100 volumetric gas dosing analyzer. The characterization of materials enables to determine the linkage between the materials properties of geopolymers and H_2 storage performance.

Results: As the overall observing results, Ca-free geopolymers achieved better hydrogen adsorption capacity than Ca-containing ones. The hydrogen adsorption capacity was increased by increasing the Si/Al ratio, increasing the specific surface area, and increasing the total pore volume. Compared with zeolites, geopolymer represents better hydrogen adsorption performance. The maximum hydrogen adsorption capacity of 0.6 wt.% at -20 °C and 100 bar was achieved for the unmodified Ca-free geopolymers with composition of $Si_{20}Al_1Na_1$. After the modification of 1 M HCl the hydrogen adsorption capacity increased to 0.7 wt.% at -20 °C and 100 bar.

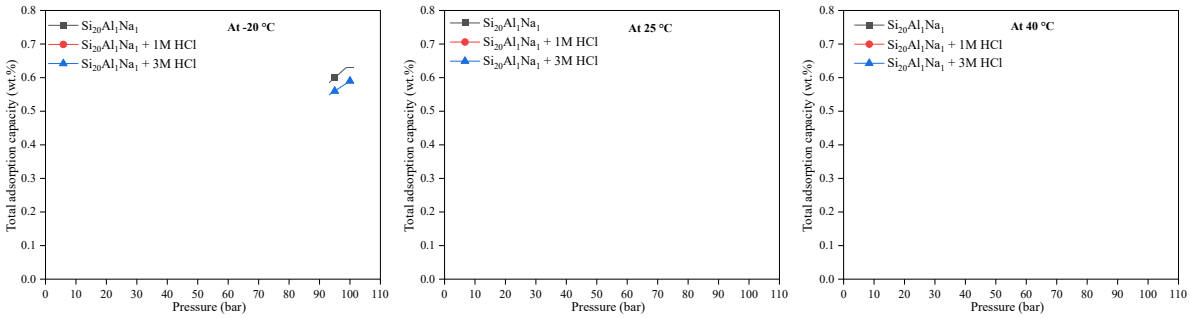


Fig. 1. Total adsorption capacity of Si20Al1Na1 and treated with 1 M and 3 M HCl at -20 °C, +25 °C, and +40° C and pressure up to 100 bar.

Conclusions: The results of this study provide a correlation between geopolymer compositions and hydrogen adsorption performance which can be used as a guideline for developing the geopolymer-based hydrogen storage materials in the future.

Acknowledgment

I would like to acknowledge the University of Oulu and the Technology Industries of Finland for financially supported my work.

References

[1] M.R. Usman, Hydrogen storage methods: Review and current status, Renew. Sustain. Energy Rev. 167 (2022) 112743. https://doi.org/10.1016/j.rser.2022.112743.

[2] I.A. Hassan, H.S. Ramadan, M.A. Saleh, D. Hissel, Hydrogen storage technologies for stationary and mobile applications: Review, analysis and perspectives, Renew. Sustain. Energy Rev. 149 (2021) 111311. https://doi.org/10.1016/j.rser.2021.111311.

[3] https://www.energy.gov/eere/fuelcells/doe-technical-targets-onboard-hydrogen-storage-light-duty-vehicles, n.d., n.d.

[4] B. Taşğın, J. Ryšavý, T. Sangeetha, W.-M. Yan, Hydrogen Storage in Zeolites: A Mini Review of Structural and Chemical Influences on Adsorption Performance, Green Energy Fuel Res. (2025). https://doi.org/10.53941/gefr.2025.100005.

[5] J.L. Provis, G.C. Lukey, J.S.J. Van Deventer, Do Geopolymers Actually Contain Nanocrystalline Zeolites? A Reexamination of Existing Results, Chem. Mater. 17 (2005) 3075–3085. https://doi.org/10.1021/cm050230i.

[6] E.A. Yatsenko, B.M. Goltsman, V.I. Parshukov, Analysis of suitability of TPP ash-slag waste as materials for hydrogen fuel storage, Int. J. Hydrog. Energy 47 (2022) 3906–3917. https://doi.org/10.1016/j.ijhydene.2021.10.272.

[7] C.H. Rüscher, Boronhydride-Geopolymer Composites, J. Ceram. Sci. Technol. (2017). https://doi.org/10.4416/JCST2017-00051.

[8] B. Walkley, R. San Nicolas, M.-A. Sani, J.D. Gehman, J.S.J. Van Deventer, J.L. Provis, Synthesis of stoichiometrically controlled reactive aluminosilicate and calcium-aluminosilicate powders, Powder Technol. 297 (2016) 17–33. https://doi.org/10.1016/j.powtec.2016.04.006.



Kinetic-based and FVM numerical tools for the simulation of Metal Hydride storage tanks coupled with Phase Change Materials

V. K. Krastev*[a], P. Proia [a], G. Falcucci[a]

* corresponding author: krastev@dii.uniroma.it

[a] Enterprise Engineering Department, University of Rome "Tor Vergata", 00133 - Rome (Italy)

Keywords: LBM, FVM, Metal Hydrides, Phase Change Materials

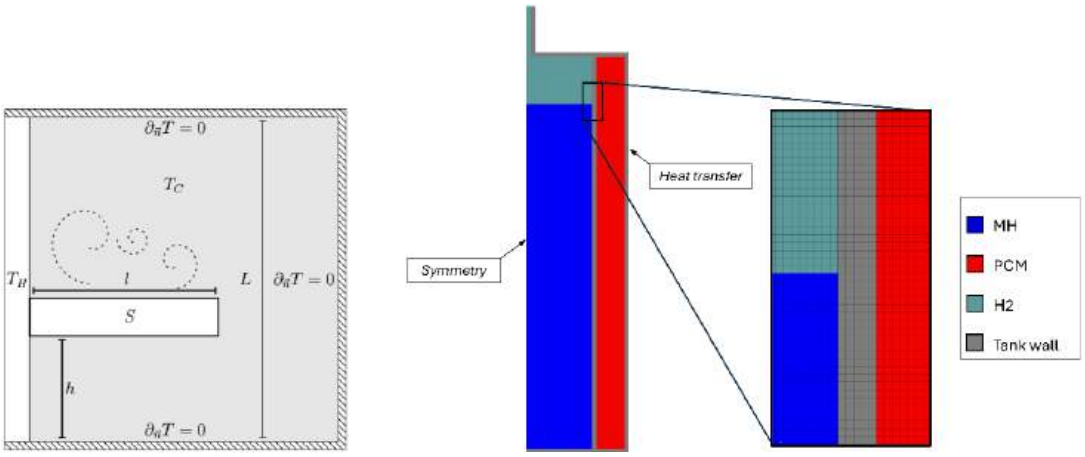
Abstract

Introduction: From a techno-economic perspective, Metal Hydrides (MHs) have been recently recognised as capable of exceeding 1.2 to 4.7 times the volumetric storage density of compressed hydrogen at 170–350 bar, while reducing system footprint by up to 65% and keeping comparable specific storage costs [1]. Nonetheless, this potential is essentially hindered by two major bottlenecks: i) MH production costs and ii) the heat transfer limitations related to the highly exothermic/endothermic nature of the chemical reactions that take place during hydrogenation/dehydrogenation [2]. To address the latter, passive thermal control through Phase Change Materials (PCMs) has been identified as an attractive option due to its relative ease of implementation and potential energy savings [3], [4], [5]. Various multidimensional approaches have already been applied to model coupled MH-PCM transient operation, often based on the Finite Volume or Finite Element methods [3], [6]. Although generally successful in terms of accuracy, most of these approaches suffer from relatively poor computational efficiency, essentially due to the large variation in time scales between the fast hydrogen filling/discharge and the slow PCM melting/solidification process. Thus, a research gap clearly emerges in balancing fidelity and efficiency to develop practical design and optimization tools for MH-based storage systems.

Objectives: The present work has two main objectives: i) compare state-of-the-art FVM with the kinetic-based Lattice Boltzmann Method (LBM) for the simulation of MH-PCM systems, with a special focus on the PCM melting/solidification dynamics; ii) assess full MH-PCM modelling against different reduced-fidelity approaches. The main expected outcome is to derive insights and guidelines to improve efficiency in MH-PCM simulation, without sacrificing essential details in engineering-related performance parameters.

Material and methods: The computational analysis is split into two parts. The first one is dedicated to PCM melting/solidification in a standard square-cavity test case, with and without a single fin for heat transfer enhancement (Fig. 1a). The second part starts from a previous hydrogen discharge simulation campaign based on a jacket-type MH-PCM reactor (Fig 1b), introducing simplified

constant-temperature and constant-power boundary conditions at the MH-PCM interface and then comparing reduced-fidelity and detailed modelling results. For further information on the FVM and LBM modelling framework, the reader is redirected to references [3] and [7], respectively.



(a) (b)

Figure 31 *– a) square cavity test-case for analysis of the PCM melting/solidification: melting starts from the hot wall at the left and then develops up to complete melting of the PCM medium; b) schematics of the reference jacket-type cylindrical MH-PCM reactor used in the reduced-fidelity modeling assessment.*

Results: Figure 2 shows preliminary results from Part 1 of the proposed analysis. PCM melting simulations are performed for a Rayleigh number equal to 10^7, at two different Stefan numbers. The nondimensional melting time $\hat{t}_m$ is used as the main performance indicator and is evaluated as the ratio between finned and finless full-melting physical times. The finned configuration has a single fin place half-height and with a half-width length, compared to the cavity characteristic dimension *L*. Notably, results exhibit very similar trends for FVM and LBM, with a reduction of about 6-7% in $\hat{t}_m$, passing from *St* = 1 to *St* = 10. Furthermore, the absolute difference between FVM and LBM is well within 2%.

Conclusions: The results shown above reveal that kinetic-based approaches are on-par with FVM in terms of PCM melting modelling accuracy and thus potentially well-suited for full MH-PCM simulation. Further results are in the process of being produced for both Parts 1 and 2 of the study described above.

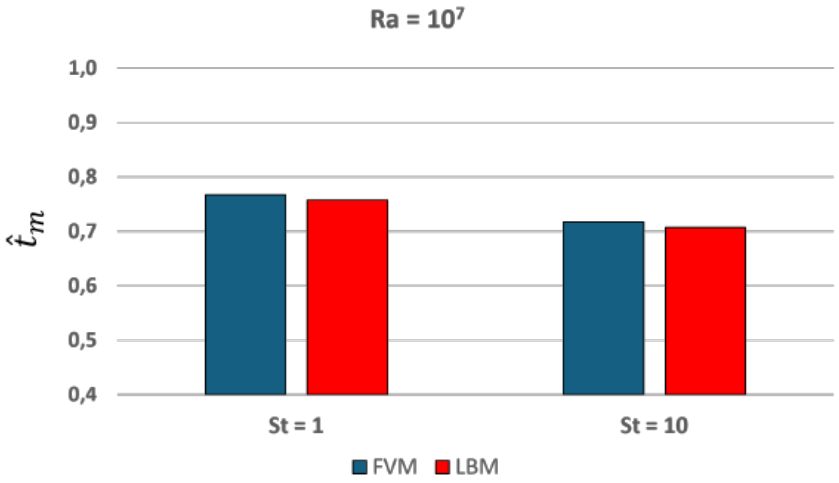


Figure 32 – *Preliinary PCM melting results at Ra = 10^7. Normalised melting time is expressed as the ratio of finned vs finless cavity simulation cases.*

References

[1] X. Wang, P. Peng, M. D. Witman, V. Stavila, M. D. Allendorf, and H. M. Breunig, "Technoeconomic Insights into Metal Hydrides for Stationary Hydrogen Storage," *Advanced Science*, vol. 12, no. 21, Jun. 2025, doi: 10.1002/advs.202415736.

[2] V. K. Kukkapalli, S. Kim, and S. A. Thomas, "Thermal Management Techniques in Metal Hydrides for Hydrogen Storage Applications: A Review," *Energies (Basel).*, vol. 16, no. 8, Apr. 2023, doi: 10.3390/en16083444.

[3] L. Bartolucci and V. K. Krastev, "On the Thermal Integration of Metal Hydrides with Phase Change Materials: Numerical Simulation Developments towards Advanced Designs," in *SAE Technical Papers*, SAE International, 2022. doi: 10.4271/2022-24-0018.

[4] A. P. Shrivastav, P. K. Kanti, G. Mohan, and M. P. Maiya, "Design and optimization of metal hydride reactor with phase change material using fin factor for hydrogen storage," *J. Energy Storage*, vol. 77, Jan. 2024, doi: 10.1016/j.est.2023.109975.

[5] M. Maggini, A. L. Facci, G. Falcucci, and S. Ubertini, "Increasing the Metal-Hydride Power Density Using Phase-Change Materials, Advanced Thermal Supports, and Expanded Graphite Nano-Particles," *Energies (Basel).*, vol. 19, no. 1, Jan. 2026, doi: 10.3390/en19010185.

[6] T. Alqahtani, S. Mellouli, A. Bamasag, F. Askri, and P. E. Phelan, "Thermal performance analysis of a metal hydride reactor encircled by a phase change material sandwich bed," *Int. J. Hydrogen Energy*, vol. 45, no. 43, pp. 23076–23092, Sep. 2020, doi: 10.1016/j.ijhydene.2020.06.126.

[7] P. Proia, M. Sbragaglia, and G. Falcucci, "Melting with natural convection with heterogeneous heating sources," *Appl. Therm. Eng.*, vol. 257, Dec. 2024, doi: 10.1016/j.applthermaleng.2024.124089.



H2BIDEA: Experimental and Numerical Evaluation of Structural Integrity and Material Compatibility for 100% Hydrogen Distribution Networks

Unai De Francisco Vargas*[a], Maria Jesus Juan [a], Daniel Cuadrado Inclán[b], Josu Aramburu Chopitea[b]

* corresponding author: Unai De Francisco Vargas

[a] affiliation: TECNALIA, Basque Research and Technology Alliance (BRTA), Mikeletegi Pasealekua 2, 20009 Donostia / San Sebastián, Gipuzkoa, Spain

[b] affiliation: NORTEGAS ENERGÍA DISTRIBUCIÓN, S.A.U., Plaza Euskadi, 5 – Planta 23, 48009, Bilbao, Bizkaia, Spain

Keywords: Hydrogen Embrittlement, Modelling, Component Testing, Structural Integrity

Abstract

Introduction: Decarbonizing industrial "Hydrogen Valleys" requires transitioning distribution infrastructure from natural gas blending to 100% H_2. This shift introduces critical technical challenges, primarily the lack of standardized procedures and Hydrogen Embrittlement (HE), which reduces the ductility of ferritic steels. To bridge the gap between theoretical standards (e.g., ASME B31.12) and utility operations, the H2BIDEA project is developing the H2TESTLAB, a high-pressure demonstrator for evaluating components under real operational conditions (up to 30 bar, 100% H_2). Unlike static tests, H2TESTLAB validates complex scenarios such as supply-demand balancing and "under-load" operations (e.g., hot tapping). A key feature is the dynamic autoclave, which enables the testing of real-world components with service defects (e.g., weld porosity, scratches) rather than ideal laboratory specimens.

To support this demonstrator, this work integrates an experimental-numerical framework: quantifying HE susceptibility in Grade B steel via Slow Strain Rate Testing (SSRT) and Fracture Toughness (J–R curves), and developing a high-fidelity Phase-Field numerical model incorporating Kocks-Mecking plasticity. Results confirm that Grade B steel is compatible with 40 bar H_2 service, with the weld metal being the most critical region. The numerical model showed excellent agreement (deviation < 4%) with experimental data, providing a validated tool for predicting failure in defective components. Together, these tools establish a certified pathway for the safe transition to 100% hydrogen infrastructure.

Objectives: The main objective of this work is to ensure the structural integrity of Grade B steel for 100% H_2 distribution at 40 bar. Specific objectives include: (i) Operational validation: To design and implement the H2TESTLAB and its dynamic autoclave to evaluate component damage tolerance and validate "in-load" operational procedures; (ii) to quantify the susceptibility to HE in the base metal (BM), weld metal (WM), and heat-affected zone (HAZ) using SSRT and fracture toughness tests; (iii) to develop a validated numerical model coupling H_2 diffusion, elastoplasticity (Kocks-Mecking), and Phase-Field fracture to determine safety margins.

Material and methods:

Material: Grade B steel pipes (nominal thickness 12.7 mm) with circumferential welds. *Experimental Setup:*

1. **Dynamic Autoclave:** A modular bypass system integrated into the H2TESTLAB. The design evolved to a certified stainless steel pressure vessel to maintain ATEX certification. Monitoring is performed via ultrasonic testing.
2. **SSRT (ASTM G142):** Specimens with notches ($k_t \approx 3.3$) were tested at a strain rate of 10^{-6} s^{-1} under 40 bar H_2 to determine the Ratio of Notched Tensile Strength (RNTS).
3. **Fracture Toughness (ASTM E1820):** Compact Tension (CT) specimens were pre-cracked by fatigue. The J-integral and critical stress intensity factor K_{IH} were measured.

Numerical Modelling: A Phase-Field model was implemented in Abaqus using UEL and UMAT subroutines. The model couples: (i) **Diffusion:** Fickian flow driven by chemical potential gradients, including hydrostatic stress effects; (ii) **Plasticity:** A Kocks-Mecking (KM) model describing dislocation density evolution, with H_2 concentration (C) linearly affecting the initial flow stress σ_0; (iii) **Fracture:** A degradation function where the critical fracture energy $G_c(C)$ decreases exponentially as H_2 concentration increases.

Results:

Material Compatibility: SSRT results yielded RNTS values of 0.90 (BM), 0.91 (WM), and 0.91 (HAZ). All values are significantly above the 0.5 threshold defined by ANSI/CSA CHMC-1, implying the material can be used for hydrogen distribution.
Fracture Toughness: All regions exceeded the ASME B31.12 minimum requirement of $K_{IH} > 55$ MPam$^{0.5}$. The weld metal was identified as the most vulnerable region ($K_{IH} \approx 59.6$ MPam$^{0.5}$), while the HAZ showed the highest resistance. SEM analysis confirmed a transition from ductile dimpled rupture in air to transgranular cleavage in H_2.
Numerical Validation: The Phase-Field model reproduced experimental SSRT stress-strain curves (Figure 1) with deviations in σ_{uts} and plastic strain ε_{pl} below 4%. The simulated J–R curves matched

the experimental initiation point ($J_{0.2}$=56 N/mm predicted vs. 51 N/mm experimental), successfully capturing the onset of unstable crack growth.

Dynamic Autoclave: The final design ensures safety through N_2 inertisation of the autoclave volume where the component is tested and certified pressure relief valves, providing a validated environment for testing "acceptable" service defects (porosity, scratches, bumps, weld defects, ...).

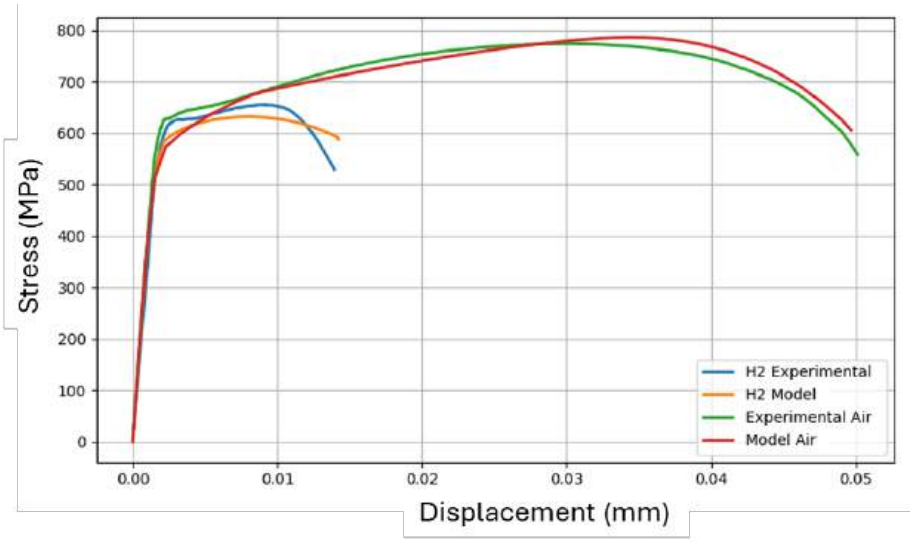


Figure 33: Stress-strain curves for the WM SSRT specimens, both in air and in H_2.

Conclusions: The integrated experimental-numerical framework confirms that Grade B steel is structurally suitable for 100% H_2 distribution at 40 bar. While the weld metal is the most susceptible region, it remains within safe regulatory limits. The developed Phase-Field model, calibrated with SSRT and J-integral data, is now a validated tool for predicting failure loads in real-world piping defects, reducing the need for exhaustive physical testing. The Dynamic Autoclave provides a critical link between lab-scale specimens and full-scale infrastructure, ensuring that the transition to green hydrogen valleys is grounded in quantified safety margins.

Acknowledgment: This work was carried out within the framework of the HAZITEK H2BIDEA project, funded by the Basque Government through the SPRI (Basque Business Development Agency), with the collaboration of NORTEGAS and TECNALIA.

References

[1] Mandal et al., "Computational predictions of weld structural integrity in hydrogen transport pipelines," Int. J. Hydrogen Energy, 2024.



Techno-economic assessment of on-site hydrogen refueling stations based on renewable electricity, biogas, and ammonia pathways

D. Lanni*[a,b], G. Di Cicco[a,b], A. Perna[a,b], A. Agresta[c], M. Della Pietra[c], V. Cigolotti[d]

* corresponding author: davide.lanni@unicas.it

[a] Department of Civil and Mechanical Engineering, University of Cassino and Southern Lazio, Cassino, Italy

[b] European University of Technology EUt+, European Union

[c] DTE-PCU-SPCT, ENEA R. C. Casaccia, Rome, Italy

[d] TERIN-PSU-ABI, ENEA Portici, Portici, Italy

Keywords: hydrogen refueling stations; power-to-hydrogen; biogas; ammonia

Abstract

This work presents a comparative techno-economic assessment of on-site hydrogen refueling stations (HRSs) developed within the Italian PORH$_2$ project. Renewable-based (Power-to-Hydrogen), biogas-based (Biogas-to-Hydrogen), and ammonia-based (Ammonia-to-Hydrogen) production pathways were investigated under both on-grid and off-grid operating conditions for different station capacities. The analysis was performed through a Life Cycle Costing approach. The results identify the most economically competitive configurations and quantify the impact of plant scale and grid connection on HRS profitability.

Introduction

Hydrogen is expected to play a major role in the decarbonization of the transport sector, particularly for applications requiring high energy density and fast refueling. In this context, on-site HRSs can reduce hydrogen transportation requirements while increasing operational flexibility. Several hydrogen production pathways have been proposed, including renewable-powered electrolysis, biogas reforming, and ammonia cracking, each characterized by different technical and economic performances [1–3].

Objectives

The objective of this work is to compare different on-site hydrogen production pathways for HRS applications and identify the most economically competitive configurations under both on-grid and off-grid operating conditions. Three station capacities were considered, corresponding to hydrogen

demands of 200, 500, and 1000 kgH_2/day. Figure 1 shows the layouts of the different analyzed configurations.

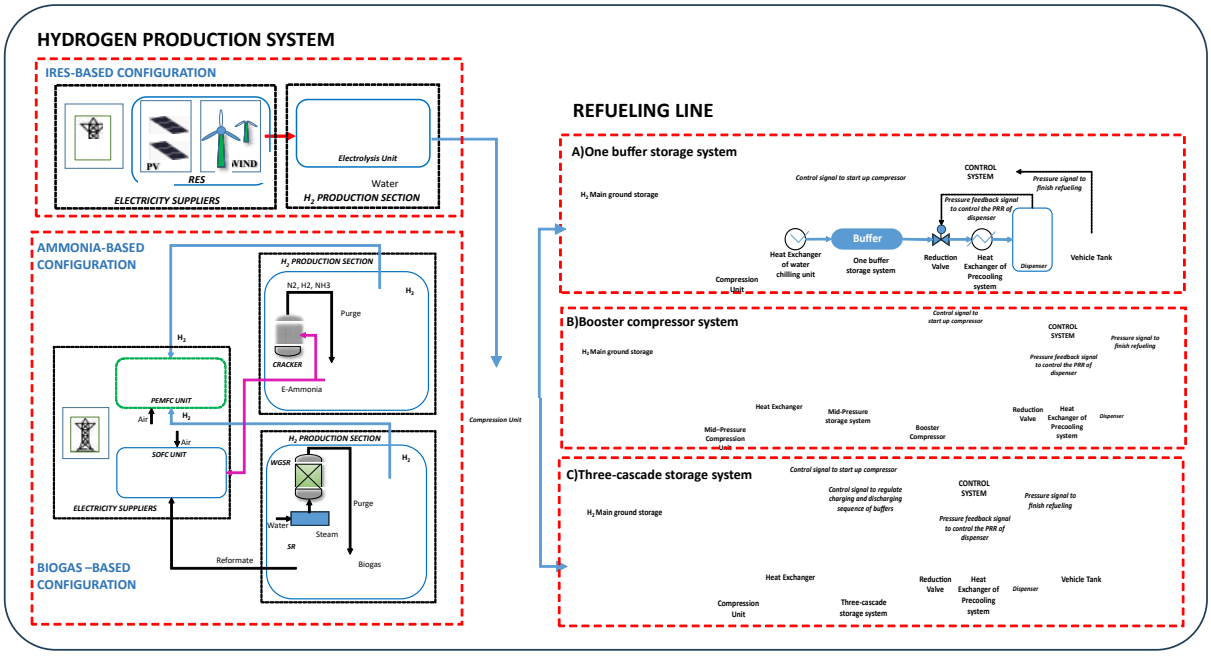


Figure 1. Layouts of the analyzed HRSs based on Power-to-Hydrogen, Biogas-to-Hydrogen, and Ammonia-to-Hydrogen pathways.

Material and methods

Three hydrogen production pathways were investigated: Power-to-Hydrogen (PtH) through water electrolysis powered by photovoltaic, wind, or hybrid renewable systems; Biogas-to-Hydrogen (BtH) through steam reforming (SR) and autothermal reforming (ATR); and Ammonia-to-Hydrogen (AtH) through ammonia cracking coupled with hydrogen purification via Pressure Swing Adsorption (PSA) or membrane separation (MEM), and integrated with PEMFC or SOFC systems in off-grid configurations.

Three refueling-line layouts were preliminarily assessed: one buffer system, booster system, and three-cascade storage system. For renewable-based systems, a multi-objective optimization framework implemented in MATLAB and modeFRONTIER was adopted to identify the optimal plant configuration. For biogas- and ammonia-based systems, the optimal operating conditions were identified by maximizing hydrogen production and minimizing specific energy consumption. Economic performance was assessed through a Life Cycle Costing methodology considering CAPEX, OPEX, replacement costs, and hydrogen revenues over a 20-year lifetime. The main KPIs were the Levelized Cost of Hydrogen (LCOH), Net Present Value (NPV), Profitability Index (PI), and Discounted Payback Period (DPBP).

Results: The three-cascade storage system was selected as the reference refueling line layout owing to its lower energy consumption, improved storage utilization, and higher reliability.

The economic analysis highlighted a systematic improvement in performance with increasing station size, resulting in lower LCOH and DPBP values and higher NPV and PI values.

For on-grid configurations, ammonia-based systems achieved the best overall performance. For the SMALL station, AtH_MEM was the most competitive configuration, with LCOH = 8.41 €/kgH_2, DPBP = 12 years, NPV = 2.93 M€ and PI = 1.82. For the MEDIUM station, AtH_MEM further improved its performance, reaching LCOH = 7.33 €/kgH_2, DPBP = 7 years, NPV = 11.0 M€ and PI = 2.70. For the LARGE station, although BtH_ATR achieved the lowest hydrogen production cost (LCOH = 7.02 €/kgH_2), AtH_PSA exhibited the best overall economic profile, combining DPBP = 7 years, NPV = 22.9 M€, and PI = 2.81. Among the renewable-based configurations, PtH_Hybrid consistently outperformed the standalone PV and wind alternatives, achieving LCOH values of 8.81, 8.16, and 7.97 €/kgH_2 for the SMALL, MEDIUM, and LARGE stations, respectively. However, PtH systems generally remained less competitive than the best-performing AtH configurations.

Off-grid configurations showed lower economic attractiveness, particularly at small scale. For the SMALL station, all configurations exhibited marginal or negative profitability, with BtH_SR representing the best option (LCOH = 10.62 €/kgH_2, NPV = 0.05 M€, PI = 1.01). For the MEDIUM station, BtH_SR clearly emerged as the preferred solution, achieving LCOH = 8.60 €/kgH_2, DPBP = 14 years, NPV = 6.77 M€, and PI = 1.52. The same trend was observed for the LARGE station, where BtH_SR reached LCOH = 8.09 €/kgH_2, DPBP = 8 years, NPV = 24.0 M€, and PI = 2.50, significantly outperforming the ammonia-based off-grid alternatives.

Conclusions: The results demonstrate that plant scale strongly affects HRS economic viability. On-grid configurations provide the best overall economic performance, with ammonia-based pathways emerging as the most competitive option, whereas biogas-based systems become economically preferable under off-grid conditions. Among PtH solutions, hybrid configurations outperformed standalone PV and wind systems.

Acknowledgment: This research was funded by the European Union - NextGenerationEU from the Italian Ministry of Environment and Energy Security, POR H2 AdP MEES/ENEA with involvement of CNR and RSE, PNRR - Mission 2, Component 2, Investment 3.5 "Ricerca e sviluppo sull'idrogeno", CUP: I83C22001170006.

References

[1] C. Blazquez-Diaz, Int. J. Hydrogen Energy 44, 495–510 (2019).

[2] A. Perna, M. Minutillo, S. Di Micco, E. Jannelli, Energies 15, 2 (2022).

[3] D. Lanni, G. Di Cicco, M. Della Pietra, V. Cigolotti, A. Perna, Proc. EEEIC 2024 (2024).



Development of Pt-based bimetallic catalyst promoted with Fe, Mn and Co for hydrogen storage and release in LOHC systems

J. Aguilera[a*], C. Tardío[a], C. Montes[a], N. Garcia-Mancha, R. Campana[a], E. Nieto[a]

[a] Centro Nacional del Hidrógeno, Prolongación Fernando El Santo, s/n, 13500 Puertollano, Spain.

Keywords: cobalt, iron, LOHC, manganese.

Abstract

Introduction

Hydrogen is considered one of the most promising energy carriers for the transition towards a low-carbon economy. Among the available storage technologies, Liquid Organic Hydrogen Carriers (LOHCs) offer high safety, long-term stability and compatibility with existing fuel infrastructures. Dibenzyltoluene (DBT) is one of the most promising LOHCs owing to its high hydrogen storage capacity (6.2 wt%), low toxicity and commercial availability. Hydrogenation and dehydrogenation of DBT require highly active noble-metal catalysts, typically based on Pt, Pd, Rh or Ru. [1]. However, the high cost and limited availability of these metals hinder the large-scale deployment of LOHC technology [2].

In this work, Fe, Mn and Co were investigated as secondary metals to promote Pt/Al_2O_3 catalysts with the aim of reducing noble metal requirements while improving catalytic performance in both hydrogenation and dehydrogenation reactions.

Objectives

Pt and Mn/Fe/Co bimetallic catalysts supported on alumina exhibit high efficiency in the dehydrogenation of H18-DBT, highlighting the relevance of incorporating non-noble secondary metals in LOHC systems due to their low cost, wide availability, and enhanced sustainability.

Material and methods

Perhydro-dibenzyltoluene (H18-DBT) and dibenzyltoluene (H0-DBT) were supplied by Solutia Europe SPRL, Ghent, Belgium. Al_2O_3 support, was purchased from Thermo-Fischer Scientific Int, Madrid, Spain; $Mn(NO_3)_2 \cdot 4H_2O$ by Chem-Lab, Zedelgem, Belgium; and $Co(NO_3)_2 \cdot 6H_2O$ by Chem-Lab, Kandel, Germany.
$H_2PtCl_6 \cdot 6H_2O$ (37.5 wt% of Pt) and $Fe(NO_3)_3 \cdot 9H_2O$ were bought from Merck
KGaA, Darmstadt, Germany. All gases were supplied by Air Products and Chemicals.

Catalysts were prepared by wet impregnation and characterised by N_2 physisorption and H_2 pulse chemisorption (Micromeritics, 3Flex).

The activity of the catalysts in the hydrogenation stage was evaluated in a 600 mL autoclave reactor (Parr, Type 4568), whilst for the dehydrogenation stage, a system comprising mainly a spherical flask,

a heating plate (Heildolph, Hei-PLATE Mix Heat Expert) and a flowmeter (Alicat, MW-2SLPM-D-DB9M) was used.

Results

This study evaluates the effect of different Pt bimetallic catalysts containing other non-precious metals: Fe, Mn and Co. The catalysts were synthesised by wet impregnation, as was done with the Ni bimetallic catalysts in previous studies [2]. In addition, the effect of the loading of the second metal was investigated; to this end, the Pt loading was kept constant at 0.25 wt%, while the loadings of Fe, Mn and Co varied between 0.1, 0.25 and 0.5 wt%.

Once synthesised, the performance of the Pt monometallic catalyst was compared with that of all the bimetallic catalysts mentioned, in both hydrogenation and dehydrogenation reactions (Figure 1). In dehydrogenation (Figure 1.a), the bimetallic catalysts exhibited higher degree of dehydrogenation (DoD) values, outperforming that achieved by the Pt monometallic catalyst. Furthermore, it is observed that as the loading of the secondary metal increases, the efficiency of the catalyst improves. This behaviour is attributed to electronic modifications induced by the secondary metals. The formation of Pt alloys with these metals weakens the interaction between Pt and the H* species generated following the breaking of C–H bonds, facilitating the desorption of the generated species. Furthermore, the H* can migrate towards Fe, Mn or Co oxides present in the catalyst, where they are stabilised and released as H_2, keeping the availability of Pt active sites and improving the catalytic stability. In contrast, in hydrogenation test (Figure 1.b), hydrogen activity decreased for all bimetallic catalysts, particularly at higher secondary- metal loadings. This effect is due to the fact that alloying Pt with any of these three secondary metals weakens the Pt–H_2 interaction, hindering the dissociation of the H–H bond as well as Pt's affinity for H0-DBT.

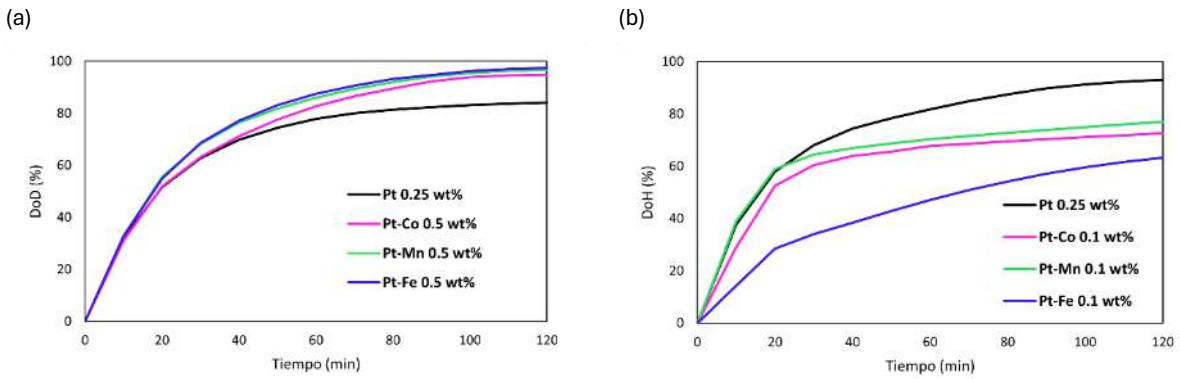


Figure 1. Comparison of the best performing bimetallic catalysts in hydrogenation and dehydrogenation with the Pt monometallic catalyst.

Conclusions

The incorporation of Fe, Mn or Co significantly enhances the dehydrogenation performance of Pt/Al_2O_3 catalysts, although at the expense of hydrogenation activity. These findings highlight the importance of tailoring metal–metal interactions and metal oxides formation to optimise catalyst performance

depending on the targeted LOHC process. The use of non-precious metals represents a promising strategy towards more sustainable and economically viable LOHC catalysts.

Acknowledgment

This research has been co-funded by the Centre for Industrial Technological Development (CDTI) and with European funds from the Recovery and Resilience Facility, under the 2021 call for proposals of the MISIONES Programme, within the framework of the State Programme to Catalyse Innovation and Business Leadership, part of the State Plan for Scientific Research, Technology and Innovation 2021–2023, with the support of the Ministry of Science and Innovation, as part of the GreenH2Pipes project (Hydrogen (H2) generation by electrolysis, its injection into the natural gas network and its transport using liquid carriers), file number MIG-20211014, and the Complementary Plan for Renewable Energy and Hydrogen under the Recovery, Transformation and Resilience Plan, funded by the European Union —Next Generation EU— (grant no. C17.I01.P01).

References

[1] Barthos, R., Lónyi, F., Shi, Y., Szegedi, A., Vikár, A., Solt, H., Novodárszki, G. Catalytic aspects of Liquid Organic Hydrogen Carrier Technology. Catalysts, 15, 427 (2025).

[2] Rodríguez, J., García-Mancha, N., Campana, R., Tardío, C. Catalytic role of nickel in hydrogen storage and release using dibenzyltoluene as a liquid organic hydrogen carrier. Energies, Submitted.



C-based materials for solid state hydrogen storage: a new perspective

C. Milanese*[a], Sara Paraboschi,[a] Alessandro Girella[a], Valentina Benazzi[a], Giacomo Magnani[b], Daniele Pontiroli[b], Mauro Riccò[b], Brigida Alfano[c], Maria Lucia Miglietta[c]

* corresponding author: Chiara Milanese

[a]Pavia Hydrogen Lab, C.S.G.I. & Chemistry Department, Università di Pavia, Italy

[b]Nanocarbon Laboratory, DSMFI, Università di Parma, Italy

[c]ENEA C.R. Portici, Energy Technologies and Renewable Sources Department, Naples, Italy

Keywords: activated carbon, biochar, fullerides, solid state hydrogen storage

Abstract

Introduction: The implementation of environmentally green materials is essential in materials chemistry to ensure a fair and ethical transition to net zero. Carbon-based materials, such as activated carbon, graphene, carbon nanotubes, and recently Mxenes, have been extensively studied for hydrogen storage [1,2] and in general for energy storage (electrodes for supercapacitors and batteries) [3-5] and analytical green applications (adsorbents for water purification, selective removal of pollutants [6,7]) thanks to to their high surface area, tunable pore size, versatile surface chemistry, with possibility of decorating and functionalising, scalability, and high chemical and thermal stability. Concerning hydrogen storage, the reported gravimetric capacities are very promising, namely up to 6.0 wt% H_2 [1,2,8], but the working conditions for efficient and reversible cycling (cryogenic temperatures for graphene based- and activated carbon materials, working in physisorption mode, [1,2] or higher than 300°C for fullerenes [8], mainly acting with a chemisorption mechanism) are still far from practical applications. In recent years, our research groups have started a joint systematic investigation on C-based materials [9-16] with the dual purpose to explore the effect of both the different C sources and doping strategies on the hydrogen storage mechanism and performance of the materials. The first focus was on alkali cluster-intercalated fullerides [9, 12-16], consisting in crystalline nanostructures in which positively charged alkaline and alkaline-earth metal clusters are ionically bonded to negatively charged C_{60} molecules, forming charge-transfer salts. For the first time in literature, we explore the possibility to intercalated simultaneously Na and Li in the fullerite structure, with promising storage efficiency results [12,14]. The price of C_{60} being quite high for large scale practical applications, our attention moved to biochar [10], the carbon side-product in the pyrolysis/gasification of residual waste biomasses, that started to receive a widespread attention in the field of energy-storage thanks to its inexpensiveness, porous structure (inherited from biomass precursors), and excellent chemical stability. Biochar can be converted into activated carbon (materials with specific surface area > 1000m^2/g) through a chemical treatment with bases giving a

new cost-effective and environmentally friendly carbon material whose physico-chemical characteristics can be tuned for improving the gas sorption efficiency.

Objectives: the aim of the work is to find innovative materials for solid state hydrogen storage with properties as close as possible with respect to the international targets, demonstrating the value of the C-based materials in this field, and their tunability and efficiency, in the frame of low cost and circular economy backgrounds.

Material and methods: Li_6C_{60}, $Na_xLi_{6-x}C_{60}$ ($0 \leq x \leq 6$) and $M_xLi_6C_{60}$ were synthesized by mixing commerical C_{60} and lithium (or the respective LiM_x alloys, where M = Pd, Pt or Ni and x = 0.17 and 0.07 and 0.11 respectively) by 30 Hz frequency high energy ball milling in a Fritsch Mini-Mill Pulverisette23 for 30 min (10 min turns, each separated by 5 min cooling). $Na_xLi_{6-x}C_{60}$ ($0 \leq x \leq 6$) materials were prepared from the $Li_{6-x}C_{60}$ materials by thermal reaction with Na azide in the suitable stoichiometry [12,14]. The air sensitivity of the samples required their preparation and storage under strict oxygen and moisture free condition (Ar with less than 1 ppm O_2 and H_2O).

Biochar were prepared by pyrolysis of different agrifood or textile wastes, previously dried and reduced in powders or small pieces, at 650 °C for 6 h under nitrogen flux. Activated carbon was obtained by mixing biochar with KOH at different weight ratio (from 1:2 to 1:6), heating at 700 °C for 6 under nitrogen flux, washing the obtained powder with HCl and distilled water up to pH = 7 and drying in oven at 55°C overnight [10]. The materials have been analysed after the different preparation steps by X-ray diffraction, Raman and IR spectroscopy, thermogravimetry and calorimetry. The H_2 storage performance were evaluated by manometric analysis.

Results: Concerning the fullerites, by manometric and thermal analyses it has been proved that C_{60} covalently and reversibly binds up to 5.5 wt% H_2 at 260°C/320°C and 50 bar/1 bar for absorption/desorption, thanks to the catalytic effect of the intercalated alkali clusters. The destabilizing effect of Na in the co-intercalated $Na_xLi_{(6-x)}C_{60}$ compounds leads to an improvement of the hydrogen-sorption kinetics by about 70%, together with a decrease in the desorption enthalpy from 62 kJ/mol H_2 to 44 kJ/mol H_2. The addition of Ni, Pt and Pd nanoparticles to Li fullerides increases up to 5.9 wt% H_2 the absorption performance and of about 35 % the absorption rate.

Concerning activated carbon, pyrolysis and activation strategies have been optimized, allowing us to obtain materials (from rice bran and wood residues) with specific surface area up to 2500 m^2/g, gravimetric capacity up to 4.5 wt % H_2 (30 seconds for adsorption and 1.5 min for full desorption at 77K - Figure 1). Thermodynamic analysis and kinetics modelling are under development to fully characterize the physico-chemistry of the materials.

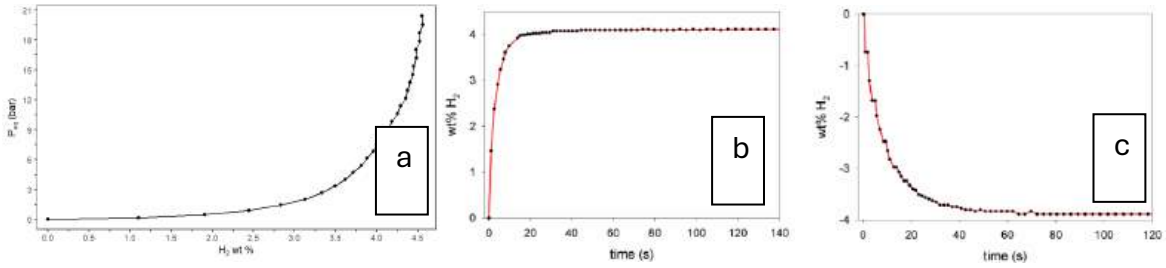


Figure 1: Pressure – Composition Isotherm curve at 77 K and up to 22 bar (a), kinetics adsorption and desorption curves (b and c) at 77 K and 10 bar/vacuum for activated carbon (KOH:C ratio 6:1) from rice bran

Conclusions: Different allotropes of C are able to chemisorb (fullerites) or physisorb (activated carbon) hydrogen with promising sorption performance concerning the gravimetric capacity and kinetics. The working temperature are still far from practical applications. Work is in progress to improve the sorption performance and optimize the working temperatures by intercalating with metals (Na, Li, and transition metals) and doping the C surface with transition metals and/or oxides.

Acknowledgment

The authors acknowledge the funds from MASE (Nanostrutture Carboniose da Scarti Agricoli per l'Accumulo di Idrogeno allo Stato Solido - CIRCOLARE RSH2A_000015).

Finanziato dall'Unione europea NextGenerationEU
MINISTERO DELL'AMBIENTE E DELLA SICUREZZA ENERGETICA

References

[1] RSC Appl. Interfaces 2025,2, 25-55, doi: 10.1039/D4LF00215F; [2] Energies 2025, 18(15), 3958, 10.3390/en18153958; [3] ACS Appl. Energy Mater. 2025, 8, 17155−17179, 10.1021/acsaem.5c03095; [4] Chemical Physics Letters 2019, 731, art. no. 136607, 10.1016/j.cplett.2019.136607; [5] Electrochimica Acta 2017 250, pp. 212-218, 10.1016/j.electacta.2017.08.049; [6] Journal of Chromatography Open 2026, 9, 100287, 10.1016/j.jcoa.2025.100287; [7] Green Analytical Chemistry 2025, 15, 100298, 10.1016/j.greeac.2025.100298; [8] Proceedings of the 2001 DoE Hydrogen Program Review, NREL/CP-570-30535; [9] J. Mater. Res. Bull. 2020, 126, art. no. 110848, 10.1016/j.materresbull.2020.110848; [10] 30th European Biomass Conference and Exhibition Proceedings 2022, pp. 895 – 901, ISBN: 978-88-89407-22-6; [11] Int. J. Hydrogen Energy 2018, 43 (34), 16766-16773, 10.1016/j.ijhydene.2018.03.210; [12] Int. J. Hydrogen Energy 2017, 42 (35), 22544-22550, 10.1016/j.ijhydene.2017.02.182; [13] Carbon 2017, 120, pp. 77-82, 10.1016/j.carbon.2017.05.025 [14] Phys. Chem. Chem. Phys. 2017, 19 (33), pp. 21980-21986, 10.1039/c7cp04353h



MetroHyVe3: Traceable Metrology for Reliable, Safe and Scalable Hydrogen Refuelling Infrastructure

V. Fernicola*[a], R.Cuccaro [a], R. Nobakht [a], T. Bacquart[b]

* corresponding author: V. Fernicola

[a] Istituto Nazionale di Ricerca Metrologica, Torino, Italy

[b] National Physical Laboratory, Teddington, London TW11 0LW, UK

Keywords: hydrogen refuelling stations; fuel quality; flow metrology; online sensors; traceability; legal metrology; fuel cell electric vehicles; ISO 14687; EN 17124; OIML R139.

Abstract

Introduction: Hydrogen refuelling stations (HRS) for fuel cell electric vehicles (FCEVs) represent a technically demanding measurement environment, combining high-pressure dispensing (up to 87.5 MPa), transient compressible high-velocity flow, rapidly varying thermodynamic states, safety-critical operation in potentially explosive atmospheres, and a legal-metrology requirement for delivered-mass accuracy. Fuel cells are also sensitive to trace-level contaminants (water, oxygen, nitrogen, ammonia, sulphur compounds, hydrocarbons), making conformance with ISO 14687 and EN 17124 a continuous measurement challenge.

Current metrological frameworks were largely developed for light-duty vehicles; the transition to heavy-duty mobility introduces flow rates up to 18 kg/min, delivered masses above 100 kg, and networks where extended verification downtime is economically incompatible with commercial operation. MetroHyVe3 addresses these gaps.

Objectives: MetroHyVe3 – "Metrology for Hydrogen Vehicles'3" (EPM project 24GRD11) – links primary standards, deployable verification units, online sensor methods, and contaminant occurrence studies into a coherent traceability framework for HRS , structured around four interconnected pillars.

Pillar 1 – High-flow hydrogen quantity metrology

At flow rates up to 18 kg/min and masses above 100 kg per fill, gravimetric primary standards become impractical. MetroHyVe3 investigates traceability routes via master-meter skids, parallel Coriolis configurations, and critical-flow Venturi nozzles (CFVN), quantifying the additional uncertainty from surrogate-fluid (water, nitrogen) calibration and assessing compatibility with OIML R139 error limits.

Pillar 2 – Integrated field verification of quantity and quality

Separate site visits for flow-meter verification and fuel-quality sampling impose substantial station downtime. MetroHyVe3 develops mobile integrated verification units combining a traceable flow standard with a validated sampling system in a single deployment, and validates sample representativeness under realistic HRS conditions.

Pillar 3 – Online monitoring and deployable sensor calibration

Laboratory sampling provides only retrospective, discrete snapshots; contamination events are often transient and station-specific, making online monitoring essential. MetroHyVe3 develops traceable, deployable calibration methods for field sensors and analysers targeting H_2O, O_2, N_2, NH_3, and trace organics, characterising response time, detection limit, cross-sensitivity, and drift under representative station conditions.

Pillar 4 – Contaminant occurrence from emerging supply chains

As hydrogen production diversifies – electrolysis, carriers (LOHC, NH_3), underground storage, grid injection – the contaminant profile at the nozzle may include species not fully covered by current specifications. MetroHyVe3 conducts probability-informed screening and real-world sampling (ammonia, toluene, ions, microbiological markers), generating a dataset linking contaminants to supply-chain elements and concentration ranges for future ISO 14687 / EN 17124 revisions.

Measurement Methodology: The methodology is grounded in the principle that deployable hydrogen infrastructure requires traceability chains that remain valid under field conditions, not only in controlled laboratory environments. Table 1 summarises the metrological issues addressed, the approach adopted, and the targeted outputs for each pillar.

Table 5: MetroHyVe3 methodological framework.

Metrological issue	MetroHyVe3 approach	Targeted output
High-flow mass delivery (up to 18 kg/min, 87.5 MPa)	Master meter skids, CFVN, parallel Coriolis configurations; surrogate-fluid (N_2, H_2O) calibration with transfer uncertainty budgets	Traceable calibration route for heavy-duty dispenser verification; compat. with OIML R139
Representativeness of fuel-quality samples	Validated sampling systems, calibrated laboratory analysis, inter-laboratory comparisons	Documented sampling procedures demonstrably linked to EN 17124 / ISO 14687 compliance evidence
Field monitoring of trace contaminants (H_2O, O_2, N_2, NH_3, organics)	Transportable optical and electrochemical gas standards; on-site sensor validation protocols	Fit-for-purpose field calibration procedures for online HRS analysers
Emerging contaminants from new supply chains	Probability-informed screening; real-world sampling at electrolysers, carriers and grid injection points	Evidence datasets for standards revision (EN 17124, ISO 14687) and quality-control plans

All four pillars share a systematic GUM-compliant uncertainty analysis. For Pillar 1, the key question is whether surrogate-fluid calibration uncertainty is compatible with OIML R139 error limits. For Pillars 2–3, the central requirement is sample representativeness. For Pillar 4, absence-of-evidence conclusions must be accompanied by quantified detection-probability thresholds.

Results: MetroHyVe3 is expected to deliver: (i) traceable high-flow quantity measurement services with surrogate-fluid uncertainty budgets; (ii) mobile integrated HRS verification units (quantity + quality, single visit, OIML R139 compliant); (iii) field calibration methods for hydrogen quality sensors and analysers; and (iv) a probability-informed contaminant occurrence dataset supporting future revision of ISO 14687 and EN 17124.

Heavy-duty hydrogen mobility demands stations with high throughput and availability; master-meter-based verification and combined quantity-quality checks directly reduce the operational downtime that is otherwise incompatible with commercial refuelling networks.

On the safety side, H_2 leak sensors must operate reliably under ATEX conditions; MetroHyVe3 characterises commercial and emerging sensors in representative environments, generating evidence for safety certification and future monitoring strategies. The contaminant occurrence dataset supports both standards revision and quality-control plan design for station operators.

Conclusions: MetroHyVe3 delivers an integrated metrology framework for HRS, covering quantity, quality, safety and emerging supply-chain contaminants. Its four pillars – high-flow traceability, integrated mobile verification, deployable sensor calibration, and contaminant occurrence datasets – provide practical tools for station operators, legal metrology bodies and standards organisations. The project supports the scale-up of hydrogen mobility from current light-duty HRS towards the high-throughput, heavy-duty networks the hydrogen economy requires.

Acknowledgment: This work is supported by the European Partnership on Metrology project 24GRD11 MetroHyVe3; the authors acknowledge all consortium partners and stakeholders.

No. 101101540), funded by the Clean Hydrogen Partnership and supported by the European Union, Hydrogen Europe and Hydrogen Europe Research.

References

[1] MetroHyVe3 Consortium, “Metrology for Hydrogen Vehicles 3 – Joint Research Protocol,” 24GRD11, European Partnership on Metrology, version April 2025.

[2] ISO 14687:2025, “Hydrogen fuel quality – Product specification,” ISO, Geneva.

[3] OIML R 139:2018, “Compressed gaseous fuel measuring systems for vehicles,” OIML, Paris.



Metrology for Hydrogen and Hydrogen-Natural Gas Mixtures in Gas Networks: Validated Testing Methodologies from the THOTH2 Project

Alessandro Guzzini[a], Pawel Kulaga[b], Vito Fernicola[c], Diana Enescu[c], Denis Smorgon[c], Rugiada Cuccaro[c], Matteo Robino[d], Ludovico Mazzocco*[e]

*Corresponding author: L. Mazzocco

[a] Università degli Studi di Bologna (UNIBO), Via Zamboni 33, 40126 Bologna, Italy
[b] INIG, Lubicz 25 A, 31-503 Krakow, Poland
[c] INRIM, Strada delle Cacce 9, 10135 Torino, Italy
[d] SNAM, Via Vezza d'Oglio 6, 20139 Milano, Italy
[e] European Gas Research Group (GERG), Rue du Commerce 31, 1000 Bruxelles, Belgium

Keywords: Gas grids; Hydrogen measurement; Metrology; Testing methodologies

Abstract

Introduction:Ensuring adequate measurement performance is a prerequisite for the large-scale uptake of hydrogen and hydrogen-natural gas blends (H_2NG), both to strengthen confidence in the use, of H_2NG and pure H_2 in existing infrastructure, and to accelerate the decarbonisation of the energy sector. The project "*Novel Methods of Testing for Measurement of Natural Gas and Hydrogen Mixtures"* (THOTH2) aimed to develop, validate, and disseminate new methods, protocols, and test facilities for assessing the metrological performance of measuring devices installed in gas distribution and transmission networks when operating with H_2NG mixtures.

Objectives: The share of hydrogen in the global energy mix is projected to increase substantially, potentially accounting for up to 12 % of total energy demand by 2050 [1]. Evidence indicates that both transmission and distribution pipelines can accommodate certain hydrogen volume fractions - depending on material specification and other site-specific factors. For example, data on the hydrogen effect on gas meters is not always aligned, especially among gas meters' technologies [2]. So, further experimental evidence is needed to confirm the hydrogen threshold for existing measuring devices installed in the gas grids, so as to provide additional data to the state-of-the-art to update existing standards [3].

Material and methods: A three-step testing approach was adopted to address the range of measuring devices relevant to the gas grid: (i) *validation tests*, ensuring measurement traceability and fit-for-purpose uncertainty; (ii) *limit tests*, aimed at determining the H_2 concentration thresholds at which measurement accuracy is adversely affected; and (iii) *ageing tests*, assessing long-term durability under representative operating conditions.

Starting from the identification of the measuring devices currently installed in the NG grids, data were collected for each major category of grid component, with the objective of identifying the hydrogen tolerance limits of gas meters as a function of meter type, operating conditions, and H_2 content based on available literature and manufacturers' know-how.

Multiple meter technologies were tested and cross-compared across participating laboratories, followed by formal methodology validation and systematic characterisation of measurement performance at varying H_2 volume fractions. The number of tests to be performed and the Key Performance Indicators (KPIs), the characteristics of the installed devices from Work Package (WP1) and the availability of testing infrastructures from WP3 are the input. A preliminary list of measuring devices to be tested was then proposed and, basing on the manufacturers' feedback, the devices were included or not in the final testing list.

Results: The principal outcome of THOTH2 is the definition and experimental validation of novel testing methodologies applicable to state-of-the-art gas metering instrumentation in H_2NG service. The devices were identified through the analysis of the data provided by gas transmission and distribution system operators (TSO and DSO). For example, aggregated data on transmission gas meters technologies and sizes (G) provided by THOTH2 TSOs is reported in Table 1. As shown, turbine gas meters are the most installed technology followed by rotary and ultrasonic devices in the size G160 - G1000.

Table1. Aggregated data of transmission gas meters' size and technology installed in THOTH2 TSOs grids.

	SIZE G															
	≤16	25	40	65	100	160	250	400	650	1000	1600	2500	4000	6500	>6500	
	Qmax - Sm3/h															
TECHNOLOGY	< 25	40	65	100	160	250	400	650	1000	1600	2500	4000	6500	10000	> 10000	TOTAL
TURBINE	0.0%	0.01%	0.2%	2.1%	5.1%	8.4%	14.0%	11.3%	10.8%	8.8%	6.0%	4.7%	1.3%	0.4%	0.01%	73.2%
ROTARY PISTON	0.5%	1.1%	0.9%	2.8%	2.4%	2.2%	1.5%	0.7%	0.3%	0.1%	0.0%	0.0%	0.0%	0.0%	0.0%	12.3%
ULTRASONIC	0.0%	0.0%	0.003%	0.003%	0.5%	0.3%	0.6%	0.4%	1.0%	0.1%	0.3%	0.6%	0.4%	0.9%	1.6%	6.6%
DIAPHRAGM	7.4%	0.4%	0.1%	0.03%	0.01%	0.0%	0.0%	0.0%	0.0%	0.0%	0.0%	0.0%	0.0%	0.0%	0.0%	7.9%
CORIOLIS	0.0%	0.0%	0.0%	0.00%	0.00%	0.0%	0.0%	0.0%	0.0%	0.01%	0.0%	0.01%	0.01%	0.0%	0.0%	0.01%

Other devices are currently installed along the network. The presence of trace water in the natural gas flow is detrimental because of the risk of water condensation and hydrate formation downstream large pressure reductions, the reduction of the heating value, and the reaction with other components. The water trace in natural gas is measured to prevent or reduce the risks mentioned above. The allowable limit on water content is generally set at 0.08-0.096 g/m^3. Pressure transmitters, on the other hand, measure the operating pressure that is needed for billing purposes. The devices used for the purpose are indicated in Figure 1. As shown, few technologies cover almost the entire market. For example, piezoresistive sensors cover more than 83%.

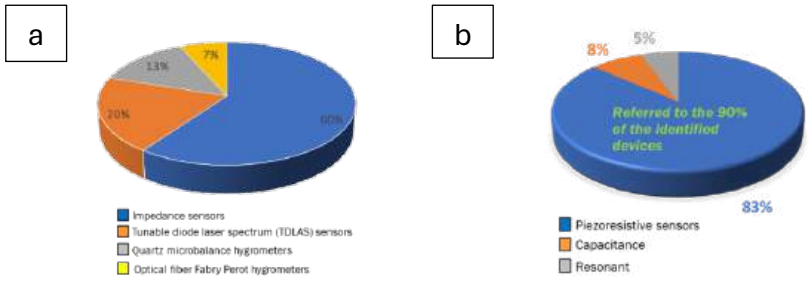


Figure1. Data of trace water humidity sensors (a - left) and pressure transmitters (b - right) in THOTH2 TSOs grids.

The project contributes to the development of new correction algorithms for measurement consistency between reference values and the indications of calibrated gas meters, addressing a recognised gap in the availability of volume conversion algorithms for H_2NG mixtures with H_2 content exceeding 10 % vol. Furthermore, the project provides a substantial experimental dataset - encompassing H_2NG mixtures up to 100 % H_2 - that constitutes a scientific basis for informing the revision of existing metering standards and drafting new technical guidelines.

Conclusions: The main outcomes of THOTH2 include the review, update and filling of gaps in the normative and standard frameworks covering H_2NG blends and pure H_2 measurements in the gas infrastructure, and more scientific knowledge/experience about the performances of the existing devices in H_2NG mixtures and pure H_2: all crucial topics, as shown from the interest raised during the participation at the Emerging Fuels Symposium [4]. Consequently, THOTH2 will have a positive impact on unlocking the potential of gas networks to transport hydrogen, allowing faster decarbonization.

Acknowledgment: The THOTH2 project has received funding from the Clean Hydrogen Partnership under Grant Agreement N°101101540.

References

[1] IRENA, 2022. *Global Hydrogen Trade to Meet the 1.5°C Climate Goal*.

[2] Guzzini, A., Pellegrini, M., Saccani, C., Dudek, A., Gajec, M., Król, A., Kulaga, P. Gislon, P. Cigolotti, V., Robino, M., Enescu, D., Fernicola, V.C., Smorgon, D., Maury, R., Gaiardo, A., Valt, M., Polak, D., Bissig, H., Hydrogen in natural gas grids: prospects and recommendations about gas flow meters, Int. J. Hydrogen Energy, Vol. 86, pp 343-362, 2024.

[3] Gislon, P., Cerone, N., Cigolotti, V., Guzzini, A., Pellegrini, M., Saccani, C., Robino, M., Carrubba, T., Cigni, A., Enescu, D., Fernicola, V., Dudek, A., Gajec, M., Kułaga, P., Maury, R., Rayana, F.B., Hydrogen blending effect on fiscal and metrological instrumentation: A review, Int. J. Hydrogen Energy, Vol. 67, pp 1295-1307, 2024.

[4] Robino M., Ballesteros M. Novel methods of testing for measurement of natural gas and hydrogen mixtures. Paper presented at the Emerging Fuels Symposium, Orlando, United States, 2023.



Effect of Thermally Grown Oxides on Hydrogen Permeation

M. Pelucchi[a], B. Alfano[b]*, L. Gritti[a], R. Rosa[a], M. Cabrini[a]

[a] University of Bergamo, Department of Engineering and Applied Sciences, Dalmine, Italy

[b] ENEA-Italian National Agency for New Technologies, Energy and Sustainable Economic Development, Portici, Italy

*** corresponding author: brigida.alfano@enea.it**

Keywords: Hydrogen permeation, Thermally grown oxides, Hematite, Magnetite

Abstract

Hydrogen–steel interactions are a key concern for the safe implementation of hydrogen infrastructures. While material qualification typically focuses on bulk properties, surface conditions, particularly thermally grown iron oxides, may significantly affect hydrogen uptake and transport. This study investigates the influence of oxide layer position, composition, and oxidation time on hydrogen permeation in a ferrite-pearlite low-alloy carbon steel. Thin oxide layers were produced by thermal oxidation in air at 250 °C for different exposure times and characterised by Raman spectroscopy to assess the relative amounts of hematite (Fe_2O_3) and magnetite (Fe_3O_4). Hydrogen permeation tests were performed using a modified Devanathan-Stachurski cell, enabling preservation of the oxide layers, with the oxide positioned either on the charging or detection side to evaluate its effect on hydrogen transport.

Introduction

Hydrogen permeation in steels is governed by both bulk diffusion and surface electrochemical reactions, which can be significantly affected by thermally grown oxide layers. Previous studies have reported that these oxides reduce hydrogen permeation, although the relative influence of oxide thickness and phase composition remains controversial. Moreover, conventional electrochemical permeation tests may alter or degrade the oxide layer under cathodic charging conditions, potentially masking its actual contribution [1-3]. To overcome this limitation, the present study employs a modified experimental configuration that preserves oxide integrity, allowing a systematic evaluation of the effects of oxide position and phase composition on hydrogen permeation behaviour.

Materials and Methods

Ferrite–pearlite low-alloy carbon steel specimens were thermally oxidised in air at 250 °C for different exposure times, and the resulting oxide layers were characterised by Raman spectroscopy. Hydrogen permeation tests were performed using a modified Devanathan–Stachurski cell in two configurations, with the oxide layer positioned either on the hydrogen charging or detection side (Figure 1). Hydrogen permeation transients were recorded to determine the apparent diffusion coefficients.

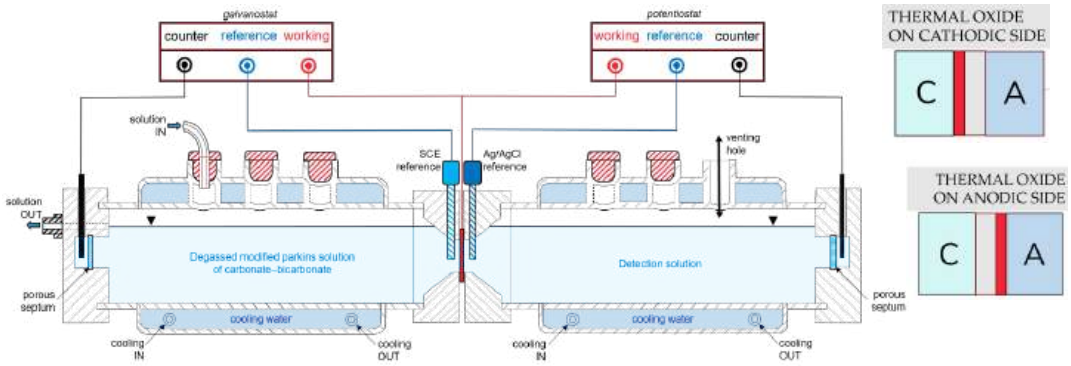


FIGURE 1. Modified Devanathan-Stachurski permeation cell showing the two experimental configurations: oxide layer on the charging side and oxide layer on the detection side.

Hydrogen permeation current density was continuously monitored and apparent diffusion coefficients were determined from permeation transients.

Results and Discussion

Hydrogen permeation behaviour strongly depended on the position of the thermally grown oxide layer. When the oxide was exposed to the charging side, permeation was comparable to that of unoxidised specimens due to oxide degradation under cathodic charging, as confirmed by Raman spectroscopy. In contrast, when the oxide was located on the detection side, it remained stable and significantly reduced the measured hydrogen permeation current, while the apparent diffusion coefficient remained essentially unchanged, indicating that the oxide mainly affects surface electrochemical reactions rather than bulk hydrogen diffusion. A clear correlation was found between oxide phase composition and permeation behaviour (Figure 2): hematite-rich oxides, formed after short oxidation times, produced the lowest permeation currents, whereas magnetite-rich oxides allowed higher hydrogen fluxes. These results demonstrate that oxide phase composition has a greater influence on hydrogen permeation than oxide thickness, highlighting the importance of considering oxide chemistry, in addition to thickness, when evaluating the barrier effect of thermally grown oxides.

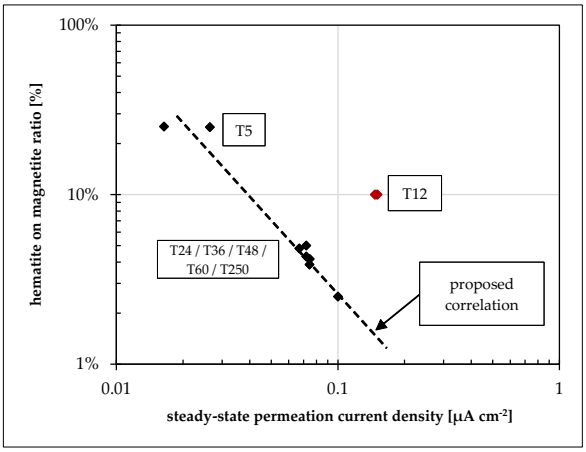


FIGURE 2. Relationship between hematite-to-magnetite ratio and apparent steady-state hydrogen permeation current density.

Conclusions

The results of this study demonstrate that thermally grown oxide layers can significantly influence the hydrogen permeation behaviour of carbon steels, although their effect strongly depends on their position during testing and on their phase composition. When the oxide layer is exposed to cathodic charging conditions, its influence is negligible because the oxide rapidly degrades, leading to a permeation response comparable to that of unoxidized steel. In contrast, oxide layers located on the detection side remain stable throughout the experiment and produce a marked reduction in the measured hydrogen permeation current density.

The experimental findings further indicate that this reduction is mainly associated with surface electrochemical phenomena rather than changes in bulk hydrogen diffusion, as the apparent diffusion coefficient remains within the same order of magnitude for all investigated conditions. Among the oxide characteristics examined, phase composition appears to be the dominant factor controlling permeation behaviour. In particular, oxide layers with a higher hematite-to-magnetite ratio exhibit lower hydrogen permeation currents, whereas no clear correlation is observed between permeation behaviour and oxide thickness.

Overall, these results highlight the importance of considering not only the presence of surface oxides but also their composition when evaluating the suitability of steels for hydrogen applications. The findings suggest that hematite-rich oxide layers may contribute to limiting hydrogen transport and should therefore be considered during material qualification and the design of components intended for hydrogen service.

Acknowledgment

This research was funded by the European Union – NextGeneration EU from the Italian Ministry of Environment and Energy Security POR H2 AdP MMES/ENEA with involvement of CNR and RSE, PNRR - Mission 2, Component 2, Investment 3.5 "Ricerca e sviluppo sull'idrogeno", CUP: I83C22001170006

References

[1] Manolatos P.; Jerome M.; Duret-Thual C.; Le Coze J., The electrochemical permeation of hydrogen in steels without palladium coating. Part I: Interpretation difficulties. Corrosion Science. Novembre 1995;37(11):1773–83. doi:10.1016/0010-938X(95)00079-Y

[2] Casanova T., The Influence of an oxide layer on hydrogen permeation through steel. Corrosion Science. 1996; 38.

[3] Song RH.; Pyun S.; Oriani RA., The hydrogen permeation through passivating film on iron by modulation method. Electrochimica Acta. Gennaio 1991;36(5–6):825–31. doi:10.1016/0013-4686(91)85280-K



Evaluation of internal bed temperature in a metal hydride cartridge during hydrogen charging using an experimentally based lumped-parametr model

Scipione D'Avino[a,b], Luigi Sequino[c], Agnese Magno[c], Elio Jannelli[a,b], Giovanni Di Ilio*[a,b]

* corresponding author: giovanni.diilio@uniparthenope.it

[a] University of Naples "Parthenope", Naples, Italy

[b] ATENA s.c.a.r.l., Naples, Italy

[c] Institute of Sciences and Technologies for Sustainable Energy and Mobility, Naples, Italy

Keywords: experimental lumped-parameter model, hydrogen storage, metal hydrides

Abstract: The temperature of the hydride bed plays a central role in the thermal management of metal hydride (MH) tanks, as it directly affects hydrogen (H_2) absorption/desorption kinetics and usable storage capacity. However, direct access to the hydride bed temperature is not available during operation, and only external quantities can typically be measured. This work presents an approach for estimating the internal bed temperature profile of a flat MH cartridge during H_2 charging by means of a lumped-parameter (LP) model based on experimental measurements. The resulting temperature profiles are validated against those obtained from a three-dimensional finite element model (FEM).

Introduction: MHs enable compact H_2 storage at moderate pressures and near-ambient temperatures, making them attractive when these features are prioritised over gravimetric capacity [1]. The H_2 absorption and desorption processes, however, are strongly exothermic and endothermic, respectively; in both cases, inadequate thermal management negatively affects the reaction rate and limits the usable storage capacity [2]. The key thermal state is the internal temperature of the MH bed, rather than the external wall temperature. During charging, the low effective thermal conductivity of the bed causes internal heat accumulation, leading to temperature peaks that are higher and occur earlier than at the surface. Since internal measurements are intrusive and poorly representative, especially during the initial transient, a methodology is needed to estimate the bed temperature from accessible external measurements, thus supporting the thermal assessment and management of MH storage systems.

Objectives: This work aims to assess the validity of a LP model developed to determine the representative internal temperature of the hydride bed by using external experimental measurements as input data. The model is applied to a commercial MH cartridge during H_2 charging and uses accessible quantities, including wall temperature, heat flux, H_2 flow rate, and pressure. This allows the

decoupling between the external surface response and the estimated internal thermal state to be quantified.

Material and methods: The considered tank is a MyH2®SLIM350 cartridge filled with Hydralloy C5, with a nominal H_2 storage capacity of 30 g. The tank has a planar layout, composed of 12 cylindrical hydride-containing elements enclosed in an aluminium casing. Since the internal layout is not directly accessible, the cartridge was reconstructed in CAD to estimate the masses and volumes of the aluminium casing and hydride regions, as well as the free gas volume and bed porosity. The thermophysical properties of Hydralloy C5 were taken from literature [3]. Experimental charging tests were performed at 30 bar using the setup shown in Figure 34. The experimental campaign was designed to provide the input data required by the model, namely the external surface temperature field reconstructed by infrared thermography and supported by local thermocouple temperatures, total heat flux exchanged at the cartridge surface, H_2 pressure, and inlet H_2 mass flow rate.

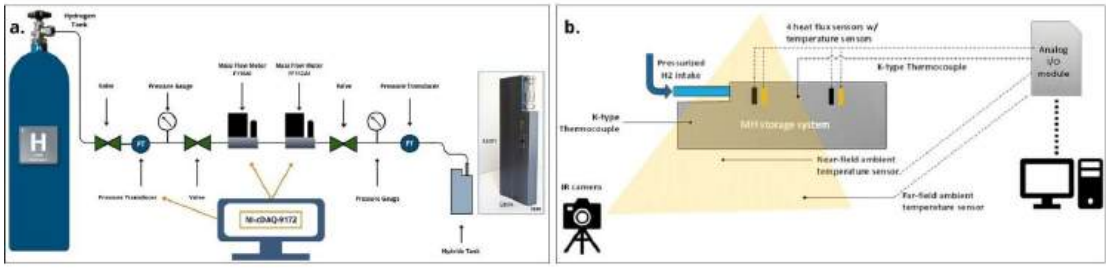


Figure 34. Schematic representation of the experimental setup.

These quantities were used as input data for a LP thermal model. The model assumes a representative spatially uniform temperature for the MH bed, and a uniform aluminium casing temperature, taken as the average surface temperature reconstructed from thermographic data. The specific heat capacity of the hydride bed is evaluated as a function of H_2 concentration, also accounting for the corresponding porosity variation during absorption. The absorbed H_2 mass is obtained by combining the inlet H_2 flow measured by the mass flow meter with the gaseous H_2 mass estimated from pressure and free volume. The corresponding reaction heat rate is then determined from the reaction enthalpy. The internal bed temperature (T_{MH}) is then determined from the following global energy balance:

$$m_{MH}\, c_{p,MH}\, \frac{dT_{MH}}{dt} + m_{AL}\, c_{p,AL}\, \frac{dT_{AL}}{dt} = \dot{Q}_{react} - \dot{Q}_{ext} \qquad (1)$$

where $\dot{Q}_{ext}$ is obtained from the measured surface heat flux. The methodology was applied consistently to repeated charging tests, and the resulting temperature profiles were compared with 3D finite element simulations.

Results: The results are reported in Figure 35 for an illustrative charging test. The figure compares the average internal temperature of the MH bed estimated by the LP model with the average external surface temperature of the cartridge, and with the corresponding values obtained from the FEM

simulation. An example of the surface temperature field acquired by infrared thermography at a selected time instant is shown in the same figure.

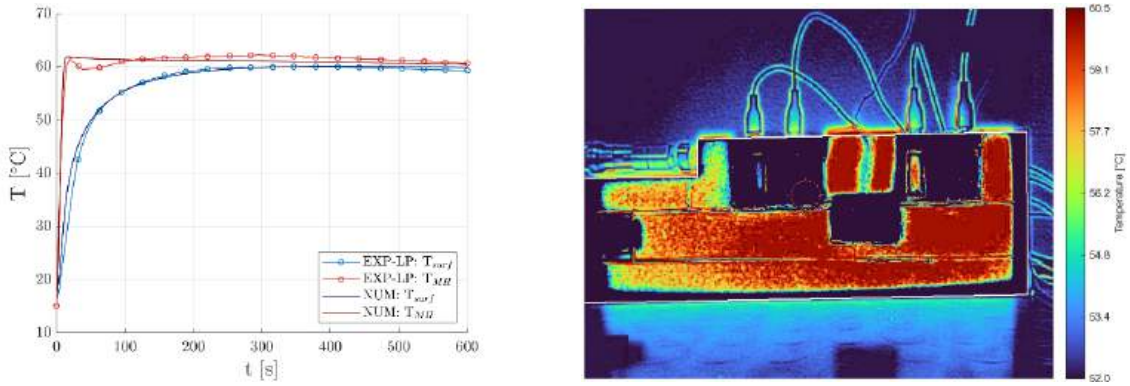


Figure 35. Comparison of internal and external temperature profiles from LP model and FEM simulation (left), and surface temperature field from infrared thermography at 200 s from the start of the test (right).

The LP model provides temperature trends consistent with the numerical simulation. In both cases, the internal bed temperature is higher than the external surface temperature, confirming the presence of a non-negligible thermal resistance between the hydride material and the aluminium casing. This behaviour is mainly related to the low effective thermal conductivity of the hydride powder, which limits heat transfer from the reacting bed toward the cartridge surface. A clear temporal shift is also observed, with the internal temperature peak occurring before the corresponding surface temperature maximum. This is consistent with the heat generation occurring inside the hydride bed during H_2 absorption and the subsequent heat propagation toward the external casing. These results highlight that surface measurements alone may underestimate the actual thermal conditions experienced by the hydride material, especially during transient operation.

Conclusions: The internal MH temperature is a more physically relevant indicator than the external casing temperature, as it directly reflects the thermo-kinetic conditions governing H_2 absorption and desorption. By estimating this quantity from external measurements, the proposed methodology supports a more effective assessment of thermal management strategies and their ability to control the hydride bed conditions.

Acknowledgment: This research was supported by MASE under grant n. RSH2A_000029, CUP:F57G25000270006 “DRAGON iDruri peR La Gestione dell'idrOgeNo “in the frame of PNRR-M2C2-3.5.

References

[1] C. Drawer et al., J Energy Storage 2024, doi: 10.1016/j.est.2023.109988

[2] V.K. Kukkapalli et al., Energies 2023, doi:10.3390/en16083444

[3] J.A. Puszkiel et al. Int J Hydrogen Energy 2025, doi:10.1016/j.ijhydene.2025.03.161.



Analysis of the pressure time profile in a liquid hydrogen tank used for ship propulsion

Michela ZANELLI [a], Diego MICHELI [b], Stefano MALABOTTI [a], Michele CAPOBIANCO [a], Stefano QUATTRINI [c], Rodolfo TACCANI [b, *]

* corresponding author

[a] CENERGY S.r.l., Trieste, Italy

[b] Department of Engineering and Architecture, University of Trieste, Italy

[c] Viking Hydrogen AS, Oslo, Norway

Keywords: Liquid hydrogen, ship, boil off management, decarbonization

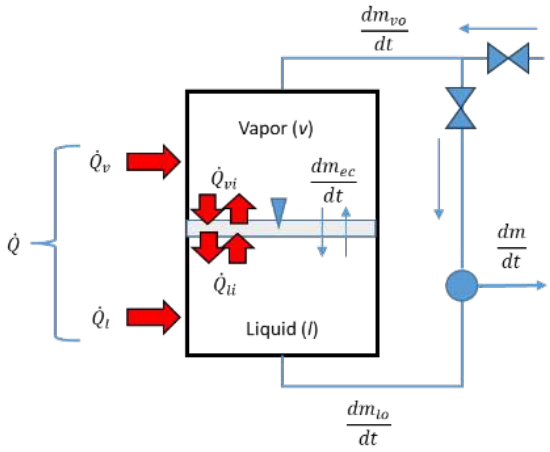
Abstract

Introduction. In the decarbonization of shipping, green hydrogen is considered one of the potential alternative fuels that offers the possibility to cut CO_2 local emission. In order to increase the energy density, for deep sea ships, liquid hydrogen (LH_2) is considered one of the most mature options. A relevant technical challenge in liquid hydrogen storage and transport to deal with is managing boil-off gas (BOG), which is formed by unavoidable heat leakage into cryogenic tanks. In closed systems, BOG is accumulated and this leads to pressure and temperature increase, requiring effective strategies to extend the holding time and ensure operational safety. For this reason, it is important to be able to accurately predict tank internal conditions so that operations can be carried out safely and the BOG can be properly managed. This paper presents the applications of a computational model to forecast the pressure profile in a LH_2 tank of a ship over a typical sailing profile. The computational model has already been presented by the authors in a previous work [1], where four numerical models were compared for simulation of the self-pressurization phase of LH_2 tanks; the best performing model has been selected to be used in this following work.

Objectives. The overall aim of the work is to provide a numerical tool able to help in managing LH_2 tanks for the maritime transport sector, dealing with a generic navigation profile: self-pressurization phase at full tank, possible pressure setting through an evaporator, fuel withdrawal, BOG management, and self-pressurization phase at empty tank. The main objective of this paper is to investigate the tank pressure profile over the normal service of the ship. This information is important to define the pressure build up circuit operation and allows to avoid over-pressurization or under-pressurization in the tank. It is also helpful to track the fuel consumption and its availability over time.

Material and methods. The numerical model applied in this work is the Subcooled Liquid and Superheated Vapor and interface in thermal equilibrium Model (SLSVM). This model is based on references found in scientific literature [2] and validated with other references with both LH_2 [3] [4] [5]

and LN_2 [6] [7]. This model is developed in MatLab and is zero-dimensional, with 3 zones, see Figure 1, in which no thermal gradient in single-phase volumes is considered.



More sophisticated models can be found in the scientific literature, but the focus is not only the accuracy of the results of the model, but also the computational effort, since the model has to be used for an entire navigation profile with an extent of multiple days. The model is applied to describe the tank behaviour in a cruise ship sailing for short periods of time in particular sensitive areas where no CO_2 emissions are allowed. The considered power profile includes both the propulsion power and the hotel load.

Figure 36. Schematic of the tank model SLSVM.

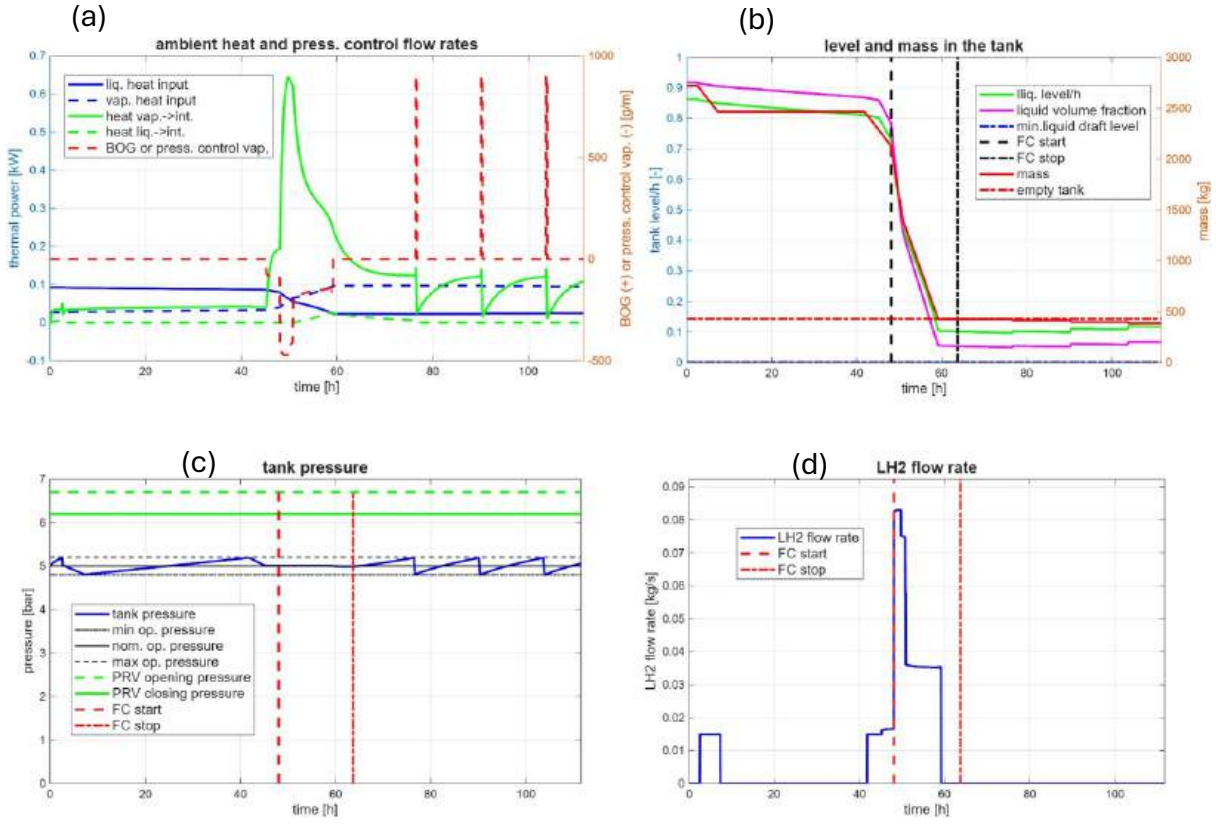


Figure 37. Time profile of main tank operating thermodynamic variables.

Results. The following ghaphs are examples of how the model can be used to simulate different ship operating profiles assuming different initial conditions and control strategy.

Figure 2 shows the main operating thermodynamic variables time profile estimated over 110 hours of operation of a horizontal cylindrical tank of 49.8 m^3 volume. In figure 2.a is reported the time profile of

the heat input through the tank wall, distinguished between liquid and vapor phases, and the heat exchanged at the interface between the phases. In figure 2.b the LH_2 mass and level in the tank is shown. In particular, it is highlighted the reduction of these variables during the operation of the fuel cell, from 48 to 63 hours. In figure 2.c the pressure management strategy is shown: pressure is maintained constant during the fuel cell operation, while the pressure is maintained in a set range when the fuel cell is not operating. In figure 2.d the hydrogen flow rate is indicated; it is due to the operation of the fuel cell and also for the pressure management.

Conclusions. This work shows how the simulation model can be used for the operation of LH_2 system applied to ship propulsion. In particular, the simulation model developed allows to foresee the pressure and mass level inside the tank starting from different initial conditions and with different operating profiles. Moreover, the model can be used with different geometry of the tank and also with multiple tanks.

The model will be validated with new experimental data in the following phases of the research.

Acknowledgment. This work has been partly funded by the Horizon Europe Project sHYpS – sustainable HYdrogen powered Shipping – Grant Agreement 101056940.

References

[1] M. Zanelli, D. Micheli, S. Malabotti, M. Capobianco, R. Taccani, «Comparison of simulation models for the self-pressurization time profile forecast of liquid hydrogen storage tanks for maritime sector», International Journal of Hydrogen Energy, article in Press.

[2] H. Wang, B. Wang, Q. Pan, Y. Wu, L. Jiang, Z. Wang e Z. Gan, «Modeling and thermodynamic analysis of thermal performance in self-pressurized liquid hydrogen tanks», International Journal of Hydrogen Energy, vol. 47, 2022.

[3] N. T. Van Dresar, C. Lin e M. M. Hasan, «Self-Pressurization of a Flight Weight Liquid Hydrogen Tank: Effects of Fill Level at Low Wall Heat Flux», NASA, 30th Aerospace Sciences Meeting and Exhibit, 1992.

[4] L. Hastings, R. Flachbart, J. Martin, A. Hedayat, M. Fazah, T. Lak, H. Nguyen e J. Bailey, «Spray Bar Zero-Gravity Vent System for On-Orbit Liquid Hydrogen Storage», NASA/TM-2003-212926, 2003.

[5] E. Lan, S. Shi, W. Ji e M. Ishii, «Modeling and simulation of cryogenic propellant tank pressurization in normal gravity», Applied Thermal Engineering, vol. 236, 2024.

[6] F. Perez, S. Z. Ghafri, L. Gallagher, A. Siahvashi, Y. Ryu, S. Kim, S. Kim, M. Johns e E. May, «Measurements of Boil-off Gas and Stratification in Cryogenic Liquid Nitrogen with Implications for the Storage and Transport of Liquefied Natural Gas», Energy, vol. 222, 2021.

[7] M. Seo e S. Jeong, «Analysis of self-pressurization phenomenon of cryogenic fluid storage tank with thermal diffusion model», Cryogenics, vol. 50, 2010.



Predictive operation of a hydrogen refuelling station with scheduled clients

Pol Cardona*[a], Carlos Ocampo-Martinez[b], Maria Serra Prat[a]

* corresponding author: pol.cardona@upc.edu

[a] Institut de Robòtica i Informàtica Industrial, CSIC-UPC, Llorens i Artigas 4-6, 08028 Barcelona, Spain

[b] Automatic Control Department (ESAII), Universitat Politècnica de Catalunya – BarcelonaTECH, Av. Diagonal, 647, 08028 Barcelona, Spain

Keywords: Hydrogen refuelling stations, Hybrid model predictive control, Lexicographic optimization.

Abstract

Introduction: Recently funded by the Ministerio de Ciencia, Innovación y Universidades, the future expansion of this work will be carried out through an international collaboration among four institutions: the Universitat Politècnica de Catalunya (Spain, lead), California State University, Los Angeles (USA), the University of Calabria (Italy), and the Marie and Louis Pasteur University (France). Each institution will contribute distinct expertise in hydrogen-infrastructure operations and technology, enabling the project to address international variations, technical challenges, and deployment pathways across regions. The operation of an on-site Hydrogen Refuelling Station (HRS) is not a trivial control problem. The operator manages two energy vectors, electricity and hydrogen, and must satisfy numerous logic-based rules and physical constraints while handling nonlinear dynamics across the hydrogen subsystems. Moreover, refuelling is a complex event-triggered process: dispensers usually lack compression capabilities, so a positive pressure gradient must exist between the station source tank and the vehicle on-board storage, which requires carefully sequenced depletion of the cascaded storage tanks. In previous works, these behaviours were captured with a Mixed Logical Dynamical (MLD) model of a real HRS under development [1], and a Lexicographic Hybrid Model Predictive Control (L-HMPC) framework was designed on top of it [2], where incommensurable objectives (refuelling readiness, energy efficiency, economic benefit) are ranked by a strict priority ordering. However, that framework assumes vehicle arrivals as unknown, and the controller must sustain readiness against an unknown demand profile at all times. In practice, the demand of an HRS serving Heavy Duty Fuel-cell Vehicles (HDFVs) fleets can be booked in advance in certain operational scenarios, and such commitments are valuable information for the controller. This work presents the integration of booked clients into the lexicographic HMPC design: each accepted booking enters the optimization as a set of algebraic constraints, and the solver dynamically reserves a refuelling pattern for each client while its service is guaranteed by hard constraints.

Objectives: The purpose of this study is to extend the L-HMPC framework of [2] with a booking-aware module and to assess its operational behaviour in a controlled simulation. The objectives are: (i) to integrate booked clients into the lexicographic HMPC as algebraic constraints; (ii) to show how the solver dynamically reserves and reassigns a depletion pattern per client over the prediction horizon while service commitments are enforced as hard constraints; (iii) to show the flexibility of the resulting proactive strategy under low photovoltaic (PV) availability, where the controller keeps the compressors off and compresses only the required hydrogen,

just before each arrival, in contrast to conventional rule-based strategies; and (iv) to expose the conservativeness introduced by the equilibrium-pressure abstraction.

Material and methods: The case study is a pilot HRS, comprising a PV system, a battery, a bidirectional grid connection, an electrolyzer with a buffer gasometer, three compression stages (C*i*), a cascaded high-pressure storage bank of four tanks at 500 bar (T3*i*), a 1000 bar hydrogen storage tank (T4) plus a portable interchangeable tank at 500 bar (MEGC), and a single 350 bar dispenser serving HDFVs. The plant is modelled in the MLD framework [1], so hydrogen flows, pressure thresholds, valve logic and event-triggered refuelling are captured in a linear mixed-integer structure. Two controllers cooperate, as in [2]: a supervisory L-HMPC (10-minute sampling, 12-hour horizon) manages production, storage allocation and the energy strategy in non-refuelling mode, and an event-triggered HMPC (with 1-minute sampling time) governs tank sequencing during refuelling. Within the supervisory layer, a refuelling event is abstracted as a one-shot algebraic operation over a *pattern*: an ordered sequence of at most two high-pressure sources whose mass transfers resulting from pressure equalization determine the mass each cascade step can transfer to the vehicle. A pattern is feasible for a client when its total transferable mass covers the requested mass. Each accepted booking forces the activation of one Boolean selector per pattern at its scheduled arrival time slot: exactly one feasible pattern must be selected, and the corresponding depletion per-step masses are subtracted from the predicted tank states at the next time slot. Since these constraints are hard, an accepted booking cannot be dropped by the optimizer, and the infeasibility of a new request constitutes its rejection signal. The receding horizon lets the solver reassign the selected pattern of each client at every step, as long as all commitments remain satisfied. It is important to highlight that the equilibrium-pressure abstraction assumes full pressure equalization at every cascade step, and therefore the model subtracts more mass than each client actually demands. The simulation scenario consists of a six-hour-long operation during a winter day with low PV generation and with partially depleted high-pressure tanks as initial conditions. It is also considered a predefined schedule of booked clients with overlapping booking windows.

Results: Figure 1 summarizes the closed-loop behaviour. The upper panel shows the pattern reserved at the notified arrival time for each booked client along its booking window, from request to arrival: the solver reassigns the reserved tanks repeatedly as the predictions evolve and the arrival time gets closer, while every commitment remains feasible and all clients are served at their scheduled arrival even with the reassignments and new, previously unknown, bookings being managed simultaneously. The middle panel relates compressor operation with PV availability. The controller concentrates compression in the remaining PV window, keeps the compressors mostly off during the dark period, and completes each preparation with short bursts that end one minute before every arrival, moving just the sufficient mass into the tanks of the reserved pattern. This contrasts with typical rule-based strategies, which fill each tank as fast as possible in a predetermined order regardless of the energy context. The lower panel shows the tank states of charge: the 1000 bar tank T4 is raised from to 97% before at the first arrival, depleted, and rebuilt only to the 54% needed by the last client.

Conclusions: This work presented the integration of booked clients into a lexicographic hybrid predictive control design for an on-site Hydrogen Refuelling Stations (HRSs). Bookings enter the optimization as algebraic constraints, the solver dynamically reserves a refuelling pattern per client, and service is guaranteed by hard constraints under the assumption of linear HRS dynamics. The simulation results illustrate the flexibility of the proactive strategy: under low photovoltaic availability, the controller delays compression and prepares only the amount of hydrogen required in the reserved pattern shortly before each arrival. However, the equilibrium-pressure abstraction subtracts more mass than each client demands, which is over-conservative and can turn fulfillable requests into rejections. Future work will address the mitigation of this over-subtraction, the characterization of the model mismatch, and linearization methods for HRS dynamics grounded in real operation, considering not only the thermodynamic nonlinearities but also strongly operation-driven behaviours such as hydrogen venting, hydrogen losses and settle times of equipment such as electrolysers and

compressors, together with the detection and prediction of such behaviours from operational data. Moreover, in the search for proactive optimization-based policies that consider information from the demand side, such as public transport systems or operators with fully or partially automated supply chains, the prognostics of component failure from operational data, through approaches such as information fusion, and predictive maintenance should be considered within the same optimization-based framework; for model-based approaches such as the one proposed here, this requires expanding the current control-oriented model.

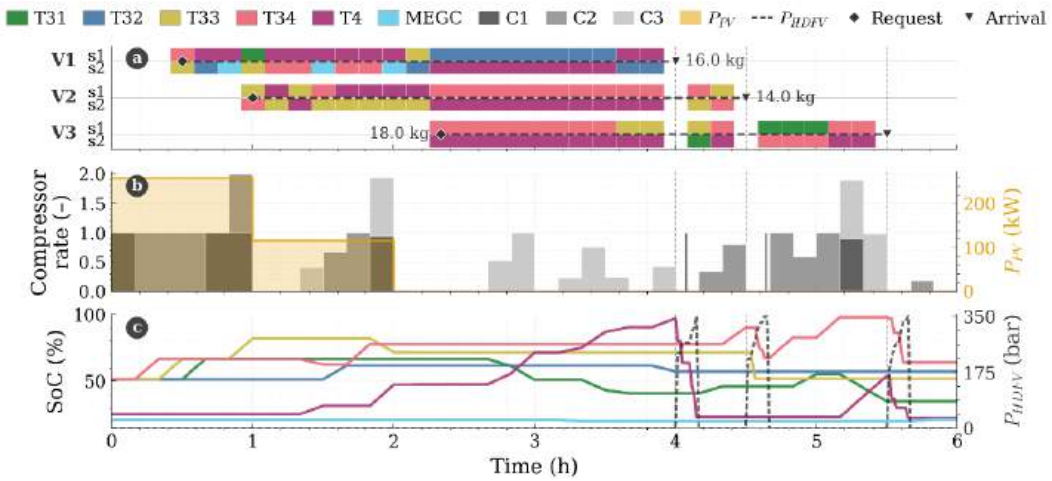


Figure 38: a) Booked pattern for the moment of arrival of each client (Vx), detailing each tank selected for each step (sX) of the pattern; b) compressors rate and photovoltaic power input to the microgrid; c) dynamic evolution of the high-pressure tanks State-of-Charge (SoC) and the HDFVs clients pressures in bar during refuelling.

Acknowledgment: Work funded by CSIC, MICIU, I-Link call 2025 (CSIC/I-LINK2025/ILINK25160) and SEAMLESS (PID2023-148840OB-I00, MCIN/AEI/10.13039/501100011033/FEDER, UE).

References

[1] P. Cardona et al., "Mixed logical dynamical modelling of renewable hydrogen refuelling stations for the design of optimization-based operational schemes", *Applied Energy*, 2025. doi:10.1016/j.apenergy.2025.126037.

[2] P. Cardona et al., "Optimization-based operation of a hydrogen refuelling station: lexicographic hybrid predictive control with multi-arrival readiness and opportunistic priority-level skipping", under review, 2026. Preprint: https://ssrn.com/abstract=6773789.



Techno-economic optimization of an on-site solar-powered hydrogen refueling station

Pierpaolo Vigliotti[a], Simona Di Micco [a], Mariagiovanna Minutillo[a], Giovanni Di Ilio*[a]

* corresponding author: giovanni.diilio@uniparthenope.it

[a] University of Naples "Parthenope", Naples, Italy

Keywords: Hydrogen refueling station; LCOH; Solar energy; Techno-economic optimization

Abstract: This work presents the techno-economic optimization of an on-site solar-powered hydrogen refueling station (HRS). The aim is to identify the station configuration and operating strategy that minimize the total cost while ensuring the required refueling service. The optimization is carried out in two coupled stages. First, the storage and distribution section layout is optimized; then, the production section is optimized by sizing the PV plant and battery storage. For the production section, two approaches are considered, namely without and with specific constraint imposed on grid dependence. Overall, the optimized HRS configurations achieve a levelized cost of hydrogen (LCOH) of 7.4 and 8.1 €/kgH_2, with a renewable energy share (RES) of 76.4% and 80.7% in the two cases, respectively.

Introduction: HRSs are a key element of the hydrogen (H_2) supply chain, as their design and operation directly affects both technical performance and the final cost of H_2 delivered to users [1]. An on-site HRS is a complex system integrating renewable power generation, electrolysis, H_2 compression, multi-level storage, dispensing and thermal management. The sizing and operation of these components are strongly interdependent [2]. Moreover, PV intermittency introduces additional challenges related to grid dependence and possible battery integration. Therefore, the optimization of both station layout and operating strategy is essential to reduce the LCOH while ensuring reliable refueling operation and an effective use of renewable energy.

Objectives: The objective of this work is to perform the optimal design of an on-site solar-powered HRS, including the production, storage and distribution sections, while providing an exhaustive economic assessment. The study investigates how the management strategy of the storage and refueling process affects the technical and economic performance of the station. The analysis also assesses the impact of battery storage on renewable energy use, grid dependence and LCOH.

Material and methods: The HRS is designed to supply 180 kgH_2/day, corresponding to 36 vehicles per day, with 5 kg of H_2 delivered to each vehicle having a nominal on-board storage pressure of 700 bar (Figure 39). Hydrogen is produced by a PEM electrolyzer operating for 10 consecutive hours at a constant rated power of 990 kW and a constant specific energy consumption of 55 kWh/kgH_2. To maximize solar electricity use, electrolyzer operation starts each day when PV generation first becomes available. The storage section consists of a cascade system composed of low-, medium- and high-pressure storage levels, operating at 400 bar, 650 bar and 900 bar, respectively. Compressors transfer H_2 between the different storage levels, while a pre-cooling system reduces H_2 temperature before dispensing.

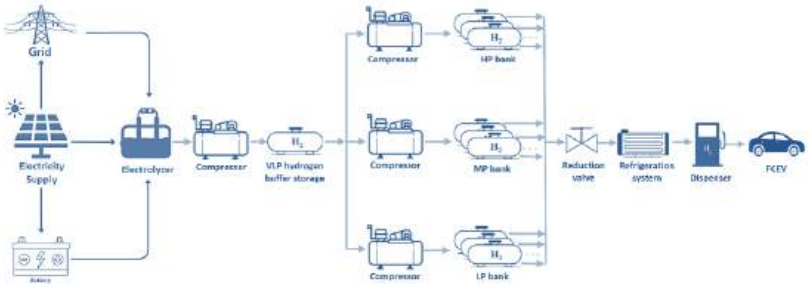


Figure 39. Schematic representation of the investigated HRS.

The proposed operating strategy is based on simultaneous vehicle refueling and storage reintegration, allowing more efficient use of the available high-pressure storage capacity and avoiding unnecessary storage oversizing. A switching algorithm is implemented to assign priority to the storage level involved in the refueling process and to manage the reintegration of the remaining tanks. The optimization procedure is divided into two steps (Figure 40). First, the storage and distribution section is optimized by defining the compressor mass flow rates. This step is performed through a grid-search approach supported by surrogate optimization. The resulting energy profile is then used to size the PV plant and the battery of the production section through a second optimization procedure, based on the same approach. Within this production-side optimization, two cases are investigated: 1) no specific constraint is imposed on grid dependence, i.e. the optimizer minimizes the total cost without penalizing electricity imports from the grid; 2) a soft constraint based on the annual grid fraction is introduced in the objective function to increase renewable self-consumption and reduced grid dependence.

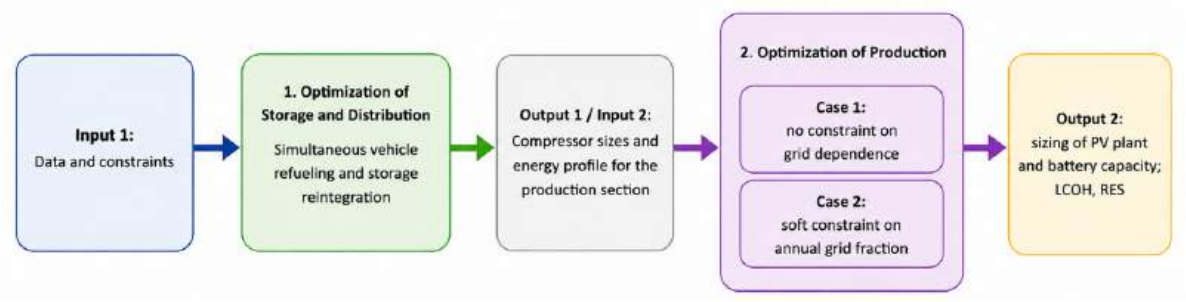


Figure 40. Flowchart of the two-stage optimization procedure.

The economic assessment is carried out over a 20-year lifetime and includes CAPEX, OPEX, replacement costs, grid electricity costs, electricity export revenues and oxygen revenues.

Results: The optimization of the storage and distribution section identifies increasing compressor mass flow rates with the storage pressure level, meaning that compressor size progressively increases from the unit feeding the low-pressure line to the one feeding the high-pressure line, as shown in Table 6. As far as the production section is concerned, in both considered cases, the PV field reaches the upper bound of the investigated range, with an installed peak power of 3 MW. This indicates that oversizing the PV plant with respect to the electrolyzer nominal power might be convenient: a large PV field increases renewable H_2 production under low irradiance conditions and allows surplus electricity to be exported to the grid and remunerated (Table 7). Without grid-dependence penalization, the optimizer selects a negligible battery capacity, since battery investment, maintenance and replacement costs are not compensated by the savings obtained from shifting PV surplus. Conversely, when the soft constraint is introduced, the optimizer includes a

limited battery capacity, which reduces grid imports and increases the local use of PV electricity (Figure 41). Depending on the battery presence, the RES for H_2 production ranges from 76.4% to about 80.7%.

Table 6. Optimized compressor sizes for the HRS.

Component	Mass flow rate (g/s)	Rated power (kW)
LP compressor	1.66	9.7
MP compressor	2.04	14.8
HP compressor	2.36	20.0

Table 7. Optimized production-side configuration and annual energy balance.

Parameter	CASE 1	CASE 2
PV peak power (kW)	3000	3000
Battery capacity (kWh)	0	700
Annual HRS load (MWh)	3767	3767
Annual PV production (MWh)	4832	4832
Energy imported from grid (MWh)	929	728
Energy exported to grid (MWh)	1986	1765
Renewable energy share (%)	**76.4**	**80.7**

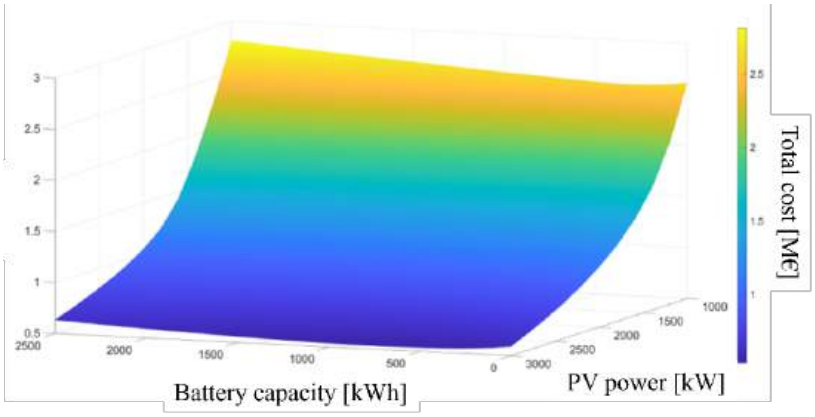


Figure 41. Grid-search of production section with penalty factor: PV power and battery capacity vs total HRS cost.

The corresponding LCOH is 7.4 €/kgH_2 for the unconstrained grid-dependence case and 8.1 €/kgH_2 for the grid-penalized case, respectively. A sensitivity analysis was also performed by reducing the H_2 selling price from approximately 14 €/kgH_2 to 9 €/kgH_2 and assuming a 30% CAPEX reduction scenario. Under these assumptions, the LCOH decreases to 5.6–6.1 €/kgH_2.

Conclusions: The optimized HRS configuration confirms the feasibility of on-site solar H_2 production for mobility applications. The proposed strategy improves storage utilization and reduces unnecessary oversizing. Results show a clear trade-off between minimum H_2 cost and reduced grid dependence, while sensitivity analysis highlights the key role of CAPEX reductions in improving economic feasibility.

References

[1] M. Genovese et al., J. Energy Storage 61, 106758 (2023), doi:10.1016/j.est.2023.106758

[2] L. Wu et al., Int. J. Hydrog. En. 52, 1577-91 (2024), doi:10.1016/j.ijhydene.2023.09.164



Metrology to Support Ammonia Use in Emerging Energy Applications (MetNH3Energy): Validation of the Ammonia Calibration Method

Florbela A. Dias[a], Joana Constantino[a], Cristina Palma[a], Tamara Sarac[*b]

* Corresponding author: Tamara Sarac

[a] Instituto Português da Qualidade, I.P. (IPQ), Rua António Gião 2, 2829-513 Caparica, Portugal

[b] European Gas Research Group (GERG), Rue du Commerce, 31, Brussels 1000, Belgium

Keywords: ammonia, calibration, energy vector, metrology.

Abstract

Introduction: Ammonia (NH_3) is emerging as a key molecule in the global energy transition, both as a carbon-free hydrogen carrier and as a potential fuel for maritime transport and power generation. Ammonia offers significant advantages for the large-scale transport and storage of renewable hydrogen due to its high volumetric energy density and established global infrastructure. However, the widespread deployment of ammonia-based energy systems requires reliable and traceable measurements to ensure safety, operational efficiency, environmental compliance and market confidence across the entire value chain.

European policy frameworks such as REPowerEU, REFuelEU and FuelEU Maritime highlight the urgent need for a robust metrological infrastructure to support the safe and reliable deployment of ammonia in these emerging applications.

Objectives: The European Partnership on Metrology (EPM) project MetNH3Energy - "Metrology to Support Ammonia Use in Emerging Applications" - brings together 26 partner institutions from 15 countries, coordinated by PTB (Germany), and addresses the measurement challenges associated with the production, transport, storage and utilisation of ammonia as an energy vector. The project aims to establish the metrological infrastructure necessary for ammonia-based energy applications by developing traceable measurement solutions for fuel quality assessment, flow metering, custody transfer, leak detection and emissions monitoring.

Material and methods: The project combines laboratory investigations, field testing and metrological analysis to evaluate measurement technologies under representative operating conditions. Activities include the development of reference materials for ammonia quality assessment and emissions measurements, the investigation of calibration methods for gaseous and liquid ammonia flow meters, the assessment of sensor performance and degradation in ammonia-rich environments, and the development of advanced optical sensing techniques for real-time monitoring of ammonia and combustion-related emissions. Particular attention is given to establishing traceability, quantifying

measurement uncertainties and assessing the transferability of calibration approaches required for future industrial deployment.

The Reference Gas Laboratory (LGR) of the Instituto Português da Qualidade (IPQ), Figure 1, participates in Work Package 1 of MetNH3Energy, being responsible for the preparation and certification of NH_3 reference gas mixtures in air matrix in the range of (5 to 30) µmol/mol, and for contributing to emission monitoring standards. This work presents the calibration of NH_3 reference gas mixtures performed at LGR/IPQ according to ISO 6143, using a first-order linear adjustment with three certified reference gas standards at nominal mole fractions of 25 µmol/mol, 503 µmol/mol and 1001 µmol/mol.

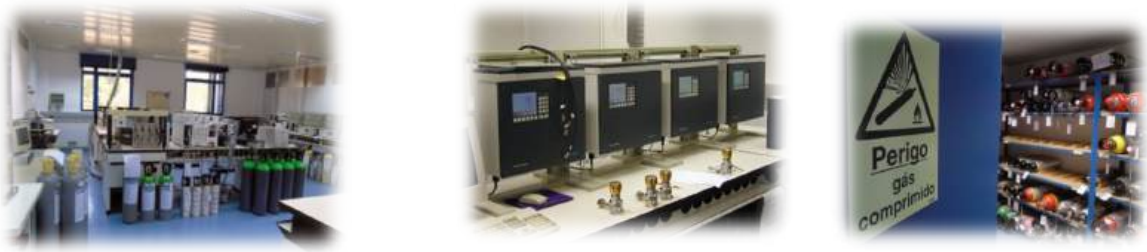


Figure 1: Certification Laboratory

The validation of the NH_3 calibration method was carried out over three consecutive measurement days using the normalised error (*En*) statistical criterion, together with repeatability and reproducibility studies performed in accordance with ISO 5725-2.

Results: All En values obtained were within the acceptance criterion $|En| \leq 1$, confirming full statistical compatibility between the results obtained at LGR/IPQ and the certified reference values. The repeatability and intermediate precision components were found to be well below the calibration uncertainty at all three concentration levels, demonstrating the robustness and stability of the measurement procedure (Table 1).

These results support the establishment of new Calibration and Measurement Capabilities (CMCs) for NH_3 reference gas mixtures at IPQ, to be submitted to the BIPM Key Comparison Database (KCDB) and contribute to the metrological infrastructure being developed within MetNH3Energy for ammonia quality assessment and emission monitoring.

Table 1. Summary of mean calibration results and uncertainty components (normalised error, repeatability and intermediate precision) for the three NH_3 reference standards.

Cylinder	Nominal (µmol/mol)	Mean Result (µmol/mol)	*En* range	s_r (µmol/mol)	s_R (µmol/mol)
D326534	25.0	25.0 ± 0.8	-0.2 to +0.1	0.059	0.116
D350676	503	520 ± 12	+0.6	0.363	0.640
D350678	1001	982 ± 22	-0.4 to -0.3	0.898	1.837

Conclusions: The measurement capabilities being developed within MetNH3Energy provide essential foundations for standardisation, regulatory acceptance and industrial uptake of ammonia-based energy technologies. The validated NH_3 calibration method at LGR/IPQ constitutes a concrete contribution to this framework, ensuring traceable and reliable reference gas mixtures for ammonia quality assessment and emission monitoring. Overall, the project contributes to the establishment of a harmonised measurement framework that will support the safe and efficient integration of ammonia into future hydrogen and clean energy value chains.

Acknowledgment

This work was carried out within the European Partnership on Metrology (EPM) project MetNH3Energy, which received funding from the European Union through EURAMET.

References

1. REPowerEU, (accessed 24 July 2026).
2. ReFuelEU aviation - Mobility and Transport - European Commission, (accessed 24 July 2026).
3. Decarbonising maritime transport – FuelEU Maritime - Mobility and Transport, (accessed 24 July 2026).
4. Qu, Z. et al., MetNH3Energy — Metrology to Support Ammonia Use in Emerging Applications. JRP Protocol v16_Protocol_P1.2, European Partnership on Metrology, EURAMET, 2024.
5. ISO 6143:2025. Gas analysis — Comparison methods for determining and checking the composition of calibration gas mixtures. International Organisation for Standardisation, Geneva, 2025.
6. Dias, F. A., Palma, C., Costa, C. J., Preparation of Multicomponent Mixtures to Support Carbon Metrology. *Measurement – Elsevier* **2025**, 239, 115453.
7. Dias, F. A., Palma, C., Costa, C. J., Multicomponent Mixtures - Stability Study to Support Carbon Metrology. *J Electrical Electron Eng* **2025**, 4(4), 01-09
8. JCGM 100:2008. Evaluation of measurement data — Guide to the expression of uncertainty in measurement (GUM). Joint Committee for Guides in Metrology, 2008.
9. ISO 5725-2:2019. Accuracy (trueness and precision) of measurement methods and results — Part 2: Basic method for the determination of repeatability and reproducibility of a standard measurement method. International Organisation for Standardisation, Geneva, 2019.
10. Search KCDB https://www.bipm.org/kcdb/ (accessed 24 July 2026).



Advance H_2 Safety: Material Integrity to Network Resilience drawing on EU Projects (CANDHy, PilgrHYm and SHIMMER)

Robert Judd[a], Ludovico Mazzocco*[a], Vanesa Gil[b], Magali Polo[c], Martin Fossen[d]

* corresponding author: L.Mazzocco

[a] European Gas Research Group (GERG), Rue du Commerce 31, 1000 Bruxelles, Belgium

[b] Aragon Hydrogen Foundation (FHa), Parque Tecnológico Walqa, Ctra. N-330a, km 566, 22197 Cuarte, Huesca, Spain

[c] NATRAN, 6 Rue Raoul Nordling, 92270 Bois-Colombes, France

[d] SINTEF, Strindvegen 4, 7034 Trondheim, Norway

Keywords: Hydrogen embrittlement; Hydrogen safety; Material integrity; Network resilience

Abstract

Introduction: Hydrogen is expected to play a central role in Europe's decarbonisation strategy, supporting the transition toward climate neutrality by 2050. A major challenge in this transition is the repurposing of existing natural gas infrastructure for hydrogen transport and distribution. While gas networks have demonstrated high levels of reliability and safety over decades of operation, hydrogen introduces new technical and safety concerns due to its specific physical and chemical properties. Hydrogen embrittlement, leakage risks, and the uncertain behaviour of legacy materials under hydrogen exposure are among the key issues affecting the integrity and resilience of gas networks. Ensuring safe operation is therefore a prerequisite for large-scale hydrogen deployment and for maintaining public confidence in future hydrogen systems.

Objectives: This work examines how hydrogen safety can be advanced through a comprehensive understanding of material integrity and network resilience, drawing on the experience and outcomes of major European research initiatives. The main objective is to identify how existing gas infrastructure can be safely adapted for hydrogen transport while supporting the development of harmonised standards, risk assessment methodologies, and operational best practices. Particular attention is given to the common contributions of the CANDHy, SHIMMER, and PilgrHYm projects in addressing hydrogen compatibility and safety challenges across European gas networks.

Material and methods: The analysis is based on a comparative review of the technical approaches and expected outcomes of the three Horizon Europe projects. CANDHy focuses on the integrity assessment of non-steel metallic materials commonly found in low-pressure gas distribution

systems. Through harmonised testing methodologies under realistic operating conditions, the project generates reproducible data on hydrogen tolerance and degradation mechanisms. SHIMMER addresses the broader challenge of safe hydrogen integration into multi-gas networks by mapping the readiness of European transmission and distribution infrastructure, assessing risks related to hydrogen blending, and developing methods for gas quality tracking, transient management, and operational safety. PilgrHYm complements these efforts by establishing a pre-normative framework for high-pressure hydrogen transport pipelines, including extensive testing of representative pipeline steels, welds, and heat-affected zones to support future European standards.

Results: The three projects collectively demonstrate that hydrogen safety is intrinsically linked to infrastructure integrity, material compatibility, and network-wide resilience. Their combined outcomes are expected to provide validated scientific data, improved risk assessment methodologies, and harmonised guidance for operators, regulators, and standardisation bodies. Together, they contribute to reducing uncertainties regarding hydrogen embrittlement, component lifetime, leakage behaviour, and operational reliability across both transmission and distribution systems.

Conclusions: The transition from natural gas to hydrogen cannot be achieved without a robust safety framework capable of ensuring infrastructure reliability and public acceptance. CANDHy, SHIMMER, and PilgrHYm share a common objective: enabling the safe and resilient repurposing of Europe's gas networks for hydrogen transport through scientific evidence, harmonised methodologies, and pre-normative research. Their complementary contributions represent a critical step toward the development of reliable European hydrogen infrastructure and the successful implementation of the energy transition.

Acknowledgment: Funding from the Clean Hydrogen Partnership under the relatives Grant Agreements N° 101111893, N° 101111888 and N° 101137592, CANDHy, SHIMMER and PilgrHym are gratefully acknowledged.



Low-Temperature H_2 Release from Ammonia: Bridging the Ni–Ru Gap in an Electrified Structured Membrane Reactor

C. Falchetta[1], E. Meloni[1], V. Palma[1]*

* corresponding author: vpalma@unisa.it

[1] University of Salerno, Department of Industrial Engineering (DIIN), UNISA, Fisciano (SA), Italy.

Keywords: Ammonia cracking, Electrified structured reactors, Hydrogen release, Pd membranes

Abstract

Introduction: Ammonia is considered one of the most promising hydrogen carriers due to its high hydrogen content, established storage and transport infrastructure, and carbon-free nature. Its use as an H_2 vector for fuel-cell-based power generation, however, requires efficient on-demand hydrogen release together with effective separation from unconverted ammonia and other components of the cracking stream. High ammonia conversion is therefore particularly important to minimize residual NH_3, while selective H_2 separation is required to provide a high-purity hydrogen stream suitable for downstream utilization. Achieving these targets at relatively low temperature remains a major technological challenge. Lowering the operating temperature is desirable to reduce thermal requirements and facilitate integration of the H_2 release unit with downstream energy-conversion systems, but conventional Ni-based catalysts suffer from limited low-temperature activity compared with Ru-based formulations.

Objectives: This work investigates an electrified structured reactor integrating a Ni-based catalyst supported on an open-cell SiC foam with a hydrogen-selective supported Pd membrane. The proposed concept combines efficient electrical heating[1], structured catalysis and continuous H_2 removal, with the dual objective of intensifying low-temperature ammonia decomposition and simultaneously recovering a high-purity H_2 stream. Particular attention is devoted to determining whether selective H_2 removal can promote Ni activity beyond the conventional thermodynamic equilibrium shift and thereby narrow the low-temperature performance gap between Ni- and Ru-based catalytic systems.

Material and methods: The reactor employs open-cell SiC foams as structured catalyst supports, coated with a Ni-based catalytic formulation and electrically heated to provide efficient and localized heat supply to the endothermic ammonia cracking reaction. A supported Pd-based membrane, consisting of a thin dense Pd layer deposited on a porous ceramic support, is integrated within the catalytic zone for selective in-situ H_2 extraction. The effects of reaction temperature, pressure, space velocity, feed composition and membrane operating conditions were investigated. The membrane

was also tested in ammonia-containing streams to assess its H_2 permeation stability. Particular attention was devoted to the relationship between H_2 recovery and ammonia conversion.

Results: The electrified structured reactor showed effective ammonia decomposition over the Ni-based catalyst, with conversion strongly affected by temperature, space velocity and feed composition. Integration of the Pd membrane resulted in a marked enhancement of NH_3 conversion, particularly in the low-temperature kinetically limited region. By progressively increasing H_2 recovery, ammonia conversion increased from approximately 30% in the absence of membrane-assisted separation to values as high as ~96% at ~429 °C, corresponding to an H_2 recovery of approximately 88%.

At these H2 removal degree, the effect of Ni catalytic activity promotion enables the system to approach the low-temperature conversion levels typically reported for Ru-based catalysts.

At the same time, the Pd membrane provides selective H_2 recovery from the $NH_3/N_2/H_2$ reaction environment, combining reaction intensification and hydrogen purification within a single reactor architecture. The integrated system also exhibited electrical energy efficiencies approaching 80%, further supporting its potential for compact and efficient H_2 release from ammonia.

Conclusions: Selective hydrogen removal can simultaneously address two critical requirements for the use of ammonia as a hydrogen carrier for downstream fuel-cell systems: high conversion at reduced temperature, minimizing residual NH_3 in the reactor outlet, and one-step selective recovery of a high-purity H_2 stream. Moreover, H_2 removal provides an additional kinetic benefit by alleviating hydrogen inhibition of the Ni catalyst, substantially narrowing the conventional low-temperature performance gap between Ni- and Ru-based systems. The integration of electrification, structured Ni/SiC catalysis and Pd-based membrane separation therefore represents a promising strategy for compact, energy-efficient and on-demand H_2 release from ammonia, with potential integration with downstream fuel-cell systems.

References

[1] E. Meloni, G. Iervolino, V. Palma, “Highly-efficient hydrogen production through the electrification of OB-SiC nickel structured catalyst: Methane steam reforming and ammonia cracking as case studies,” Int. J. Hydrogen Energy 65 (2024) 42–49. https://doi.org/10.1016/j.ijhydene.2024.03.349.



TOPIC 3. FUEL CELLS TECHNOLOGIES



Pinhole growth in PFSA and hydrocarbon membranes under relative humidity cycling

Mina Bahraminasab*a, David Sedarsky a

* corresponding author: minaba@chalmers.se

a Department of Mechanics and Maritime Sciences, Chalmers University of Technology, Göteborg, Sweden

Keywords: membrane, relative humidity, PEM fuel cell, pinhole growth

Abstract

Proton exchange membrane fuel cells (PEMFCs) are a promising technology due to their high efficiency and low operating temperature. However, the membrane lifespan is one of the major barriers that hinders their widespread commercialization. Mechanical stress is an important degradation mechanism, which can be significantly accelerated by relative humidity (RH) cycling, contributing to membrane thinning, crack formation, and pinhole growth. Most mechanical durability studies have focused on perfluorosulfonic acid membranes (PFSA) such as Nafion, however, due to high cost and environmental concerns, there is a renewed interest in non-fluorinated hydrocarbon membranes, such as sulfonated poly (ether ether ketone) (SPEEK) and sulfonated polysulfone (SPSU). In this work, a mechanical degradation model is developed to investigate the relative humidity cycling that induced pinhole growth in Nafion, SPEEK, and SPSU membranes. The results show that the SPSU membrane exhibits approximately two times greater pinhole growth than Nafion under the same RH cycling. The degradation is driven by the pronounced plastic deformation in the wet state and generates high residual tensile stress during dehydration. In contrast, the SPEEK membrane remains in the elastic regime throughout the entire cycle. These findings reveal that higher yield strength alone does not guarantee improved mechanical stability. Excessive stiffness can amplify stress accumulation in constrained hydrated membranes.

Introduction: One of the key factors limiting the durability of proton exchange membrane fuel cells (PEMFCs) is membrane degradation induced by unavoidable relative humidity (RH) fluctuations [1]. At high RH the membrane experiences compressive stress due to in-plane physical constraints and clamping pressure. Consequently, when this stress exceeds the yield strength, the membrane undergoes plastic deformation. As RH decreases, the plastically deformed membrane attempts to shrink, generating tensile stress which accelerates the growth of microscopic pinholes [2]. Currently, high manufacturing costs and environmental concerns of perfluorosulfonic acid (PFSA) membranes, such as Nafion, are prompting a shift toward non-fluorinated hydrocarbon membranes like sulfonated poly (ether ether ketone) (SPEEK) and sulfonated polysulfone (SPSU) [3]. Although higher stiffness is typically believed to improve mechanical resilience, current analyses indicate that an increased

modulus may amplify stress accumulation under restricted swelling conditions [4]. Consequently, mechanical durability cannot be evaluated solely based on yield strength, while, the combined effects of stiffness, swelling strain, plasticity, and stress must be considered.

Objectives: The aim of this study is developing a mechanical degradation model to comparatively analyse Nafion, SPEEK, and SPSU membranes. The approach uses a Rice–Tracey void growth formulation to quantify pinhole evolution and combines isotropic swelling with elastoplastic stress–strain behavior based on the von Mises criterion. The model builds on established mechanical degradation frameworks, ensuring consistency with the literature [2], while extending the analysis to hydrocarbon membranes.

Material and methods: We present a model developed in Siemens Simcenter Amesim to simulate membrane mechanical degradation under RH cycling. In the model, the domain lies in the X–Y plane and the membrane is fully constrained in the in-plane direction. The swelling of the membrane and the stress–strain response are isotropic. The clamping pressure is applied uniformly on the membrane surface. To evaluate plastic deformation, the von Mises equivalent stress is defined. A continuum plasticity-based model combined with the Rice–Tracey formulation is used to describe and quantify pinhole growth under swelling-driven cyclic stresses.

Results: The results show different degradation behaviors for the investigated membranes under RH cycling. Figure 1 (a) illustrates that Nafion shows a moderate evolution of pinhole growth, reaching a normalized radius (R/R_0) of about 3.2, whereas SPEEK remains in the elastic regime for the duration of the cycles. However, Roshanzamir et al. showed that under hygrothermal conditions, SPEEK exhibits a tendency toward brittle behavior. They showed that both tensile strength and Young's modulus increase with prolonged exposure to high temperatures and RH cycling, while its toughness is significantly reduced, making the material more susceptible to brittle failure [4]. Conversely, SPSU has the most severe pinhole growth evolution, reaching a normalized radius (R/R_0) of about 6.8, nearly twice that of Nafion, despite experiencing similar swelling strain in the wet state to SPEEK. This significant difference is due to the high dry Young's modulus of SPSU (1150 MPa) [5] compared to both Nafion (250 MPa) [ref] and SPEEK (700 MPa) [6]. This elevated stiffness generates larger stresses under swelling, leading to plastic deformation and accelerated void growth. The severe mechanical vulnerabilities of pristine SPSU highlight the need to improve its structure. Yang et al. successfully mitigated these structural weaknesses by creating a highly compact polymeric network that restricts free volume and achieves a better balance in stiffness [7].

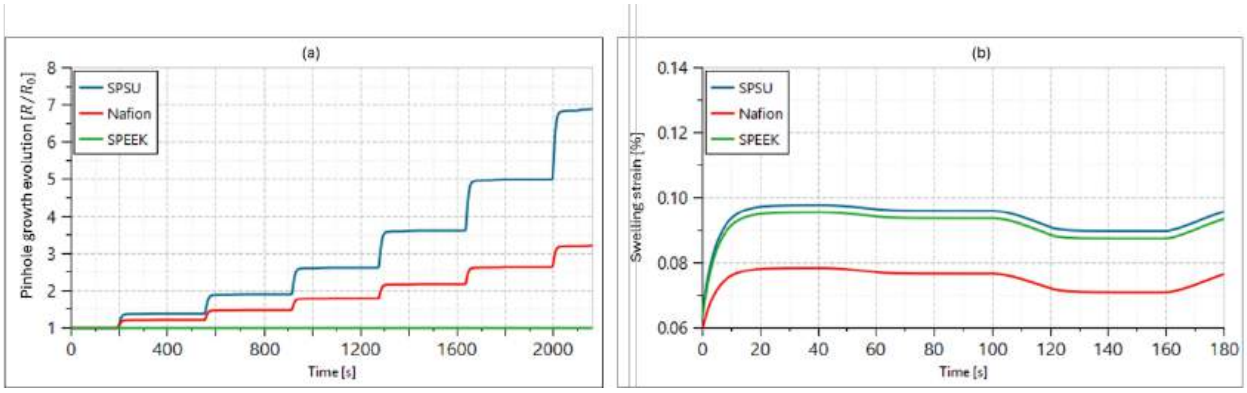


Figure (1) the plot show pinhole growth evolution (a), and swelling strain (b) in three different membranes

Conclusions: This study shows the critical role RH cycling in the membrane mechanical degradation. The results indicate that SPSU membranes are highly susceptible to pinhole growth due to severe plastic deformation during hydration and high residual tensile stress during dehydration. Nafion exhibits moderate degradation, while SPEEK remains within the elastic regime under the studied conditions. These findings show that high yield strength alone is insufficient to ensure durability, as excessive stiffness can intensify stress accumulation in constrained membranes. Therefore, balancing stiffness, swelling behavior, and plasticity is essential for designing mechanically stable membranes.

Acknowledgment: The Competence Centre TechForH2 is hosted by Chalmers University of Technology and is financially supported by the Swedish Energy Agency (P2021-90268) and the member companies Volvo, Scania, Siemens Energy, GKN Aerospace, PowerCell, Oxeon, RISE, Stena Rederier AB, Johnsson Matthey and Insplorion.

References

[1] Borup, R., Meyers, J., Pivovar, B., et al. (2007). Scientific aspects of polymer electrolyte fuel cell durability and degradation. Chemical Reviews, 107(10), 3904–3951.

[2] Kusoglu, A., & Weber, A. Z. (2014). A mechanistic model for pinhole growth in fuel-cell membranes during cyclic loads. Journal of The Electrochemical Society, 161(8), E3311.

[3] Haragirimana, A., et al. (2021). [Full article title]. International Journal of Hydrogen Energy, 46.

[4] Mirfarsi, S. H., et al. (2018). Study of mechanical degradation of sulfonated poly(ether ether ketone) membrane using ex-situ hygrothermal cycles. Journal of Power Sources, 401, 73–84.

[5] Martinez-Morlanes, M. J., et al. (2021). Sulfonated polysulfone/TiO2(B) nanowires composite membranes as polymer electrolytes in fuel cells. Polymers, 13(12), 2030.

[6] García-Salaberri, P. A. (2023). 1D two-phase, non-isothermal modeling of a proton exchange membrane water electrolyzer: An optimization perspective. Sustainable Materials and Technologies, 38, e00727.

[7] Yang, X., et al. (2018). A graphene oxide polymer brush based cross-linked nanocomposite proton exchange membrane for direct methanol fuel cells. RSC Advances, 8(28), 15740–15753.



Hydrogen Compressor Modeling Using Physics-Informed Surrogates

Niklas Nickig*[a], Matthias Bahr [a]

* corresponding author: n.nickig@zbt.de

[a] The Hydrogen and Fuel Cell Center (ZBT), Carl-Benz-Straße 201, 47057 Duisburg, Germany

Keywords: Surrogate Modeling, Dimensionless Coefficients, Thermodynamic State-Dependency, Real-Time Performance Prediction

Abstract

Introduction: Centrifugal compressors and blowers are essential components within hydrogen energy systems, especially for fuel cell applications and hydrogen recirculation loops. Nevertheless, the computational demands of intricate fluid dynamic simulations impede the ability to perform real-time performance predictions and system-level optimization. This study proposes a physics-informed surrogate modelling methodology that integrates dimensionless flow coefficients with polynomial fitting, thereby providing precise and computationally efficient predictions in hydrogen environments.

Objectives:

1. Computational efficiency: A surrogate model reduces computational overhead compared to CFD-based approaches, making it suitable for dynamic system simulation and control applications in hydrogen fuel cell systems.

2. Physics-informed and state dependency: Nitrogen accumulation in the anode of the fuel cell system leads to varying specific heat capacities and gas densities, leading to significant deviations in performance predictions if the model lacks corresponding thermodynamic correlations. Therefore, a physics-informed approach that explicitly accounts for the thermodynamic state enables robust simulation of compressors and blowers in hydrogen applications, unlike purely empirical models that fail under varying conditions.

3. Dual-Type Architecture: The generic model framework supports both blower and compressor implementations through trait-based abstraction, facilitating code reuse and consistent physics across different machinery types.

4. Buildable as functional mock-up unit (FMU): The FMU standard is a well-supported interface for simulation software, and thus a key necessity for integration in the resident simulation suite, AVL CruiseM.

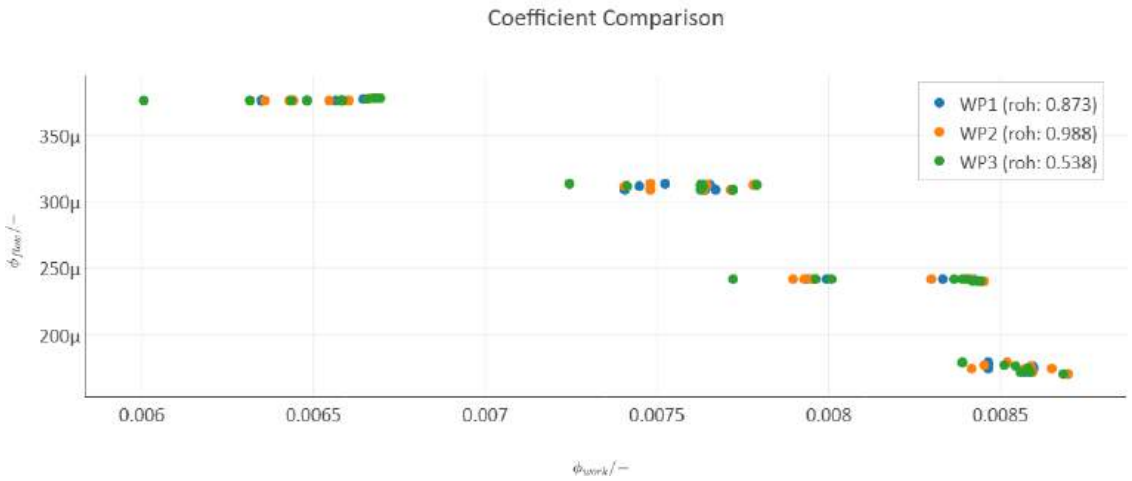


Figure 42: Comparison between 3 different gas mixtures (working points: WP) with 4 different speed lines in the dimensionless characteristic map (Φ_{flow} and Φ_{work})

Material and methods: The model employs a physics-informed surrogate approach for centrifugal flow machines [1], utilizing dimensionless coefficients (Φ_{flow} and Φ_{work} [Figure 42]) derived from experimental or CFD-generated characteristic maps. The coefficients are calculated by $\Phi_{\mathrm{flow}} = \dot{\mathrm{V}}/(\mathrm{A} \cdot \mathrm{u})$ and $\Phi_{\mathrm{work}} = 2 \cdot \Delta \mathrm{h}_{\mathrm{is}} / \mathrm{u}^2$. These maps, consisting of rotational speed, pressure characteristics, and mass or volume flow rate data, are processed to compute the dimensionless work coefficient Φ_{work} based on isentropic enthalpy changes and peripheral velocity. In contrast, Φ_{flow} is calculated from volumetric flow normalized by impeller geometry and speed. A multivariate polynomial regression fits [2] basis functions to establish relationships between angular velocity, Φ_{work}, and Φ_{flow}, enabling interpolation across operating points. The model incorporates thermodynamic state dependence through a gas-state structure, accounting for variable gas properties such as density, specific heat capacity, and composition, and supports both blower and compressor configurations via trait-based abstraction in Rust, thereby ensuring computational efficiency for real-time simulations in hydrogen systems. The model is integrated into the simulation environment in AVL CruiseM and evaluated and tested in a fuel cell system simulation.

Results: The model demonstrates high accuracy in predicting centrifugal compressor and blower performance, achieving mean deviations of less than 5% relative to the source data across a wide range of operating conditions in hydrogen systems. Regardless of the amount of data and runtime, the model requires approximately 180 ns for a calculation [Figure 43] and, thanks to its implementation in Rust, does not exhibit runtime spikes caused by garbage collection.

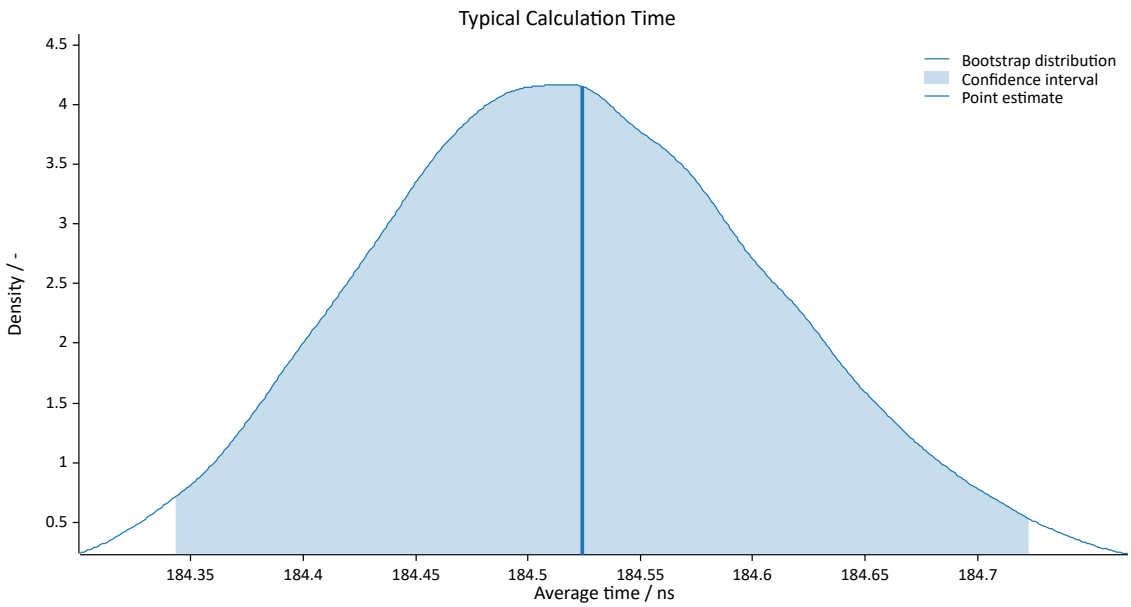


Figure 43: Typical Benchmark results across 20 billion calculations

Conclusions: *This work demonstrates that a physics-informed surrogate model can accurately predict the performance of centrifugal compressors and blowers in hydrogen systems while maintaining extremely low computational effort. By combining dimensionless flow coefficients with polynomial regression, the model achieves low prediction errors when compared with the sauce data while maintaining a fast calculation time. The explicit incorporation of thermodynamic state dependency enables reliable performance estimation even under changing gas compositions, such as nitrogen accumulation in hydrogen recirculation loops. Additionally, the Rust-based, trait-oriented architecture enables flexible implementations for both compressors, blowers, and other flow machines, approaching well suited for real-time simulation and control of hydrogen energy systems.*

Acknowledgment:

Many thanks to AVL for providing software and technical support.

Funded by NRW Innovationsagentur project H2Extend 2.0 (EFRE-20800250)

References

[1] Nachtigal, P., Kentschke, T., and Seume, J. R. (October 7, 2022). "Experimentally Validated Design of an Anode Recirculation Blower for Polymer-Electrolyte-Membrane Fuel Cells Under Variable Fluid Composition." ASME. *J. Eng. Gas Turbines Power*. December 2022; 144(12): 121014, https://doi.org/10.1115/1.4055667

[2] https://github.com/geo-ant/varpro



Polydopamine-assisted functionalisation of bacterial cellulose with lignosulfonate as a bio-based ion exchange membrane in fuel cells

Sara Zdovc*, Maša Hren, Selestina Gorgieva

* corresponding author: Sara Zdovc

Faculty of Mechanical Engineering, University of Maribor, Slovenia

Keywords: bacterial cellulose, ion exchange membrane, lignosulfonate, polydopamine

Abstract: This work presents the fabrication of bio-based membranes composed of bacterial cellulose (BC) functionalised with polydopamine (PDA) and lignosulfonate (LS) for potential fuel cell (FC) applications. Structural and chemical analyses confirmed successful membrane modification while preserving the crystalline structure of cellulose. The modified membranes exhibited an approximately 160-fold increase in ionic conductivity compared to pristine BC, demonstrating the potential of PDA/LS-functionalised BC as a promising and sustainable membrane material for FC applications.

Introduction: The growing demand for sustainable energy technologies has intensified the search for environmentally friendly materials for FC applications. Proton exchange membrane fuel cells (PEMFCs) and microbial fuel cells (MFCs) require membranes with high proton conductivity, low fuel permeability, and good mechanical and chemical stability. Although commercial perfluorosulfonic acid membranes exhibit excellent performance, their high cost and environmentally demanding synthesis limit broader application. BC is a promising bio-based material [1] due to its high purity, nanofibrillar structure, mechanical robustness, and high water retention capacity. However, native BC lacks the ionic functional groups necessary for efficient proton transport. PDA offers a versatile surface modification platform [2] due to its catechol and amine groups, enabling strong adhesion and further functionalisation. LS, derived from lignin, contain sulfonic acid groups that can facilitate proton transport [3]. While LS-only modification was not successful in preliminary tests, we investigated the PDA-assisted modification of BC with LS as a sustainable approach to introduce proton-conducting domains in stable, bio-based proton exchange membranes for PEMFC and MFC applications.

Objectives: The objective of this study is to develop LS-functionalised BC membranes with PDA pre-activation for use as ion exchange membranes in FC systems.

Materials and methods: BC membranes were produced using modified Hestrin-Schramm (HS) medium and *Komagataeibacter europaeus* LMG 1521, purified in 0.5 M NaOH, autoclaved, and stored fully hydrated. Tris buffer (p.a., Carl Roth), dopamine hydrochloride, and lignosulfonic acid sodium salt

(Sigma-Aldrich) were used for membrane functionalisation. Milli-Q water was freshly prepared and used in all experiments.

BC discs (25 mm) were treated with dopamine (DA) solutions (0.25, 0.5, and 1.0 mg mL^{-1}) prepared in 10 mM TRIS buffer (pH 8.0), while the lignosulfonate (LS) concentration was kept constant (1 mg mL^{-1}). Three modification regimes were applied (Fig. 1a): PDA treatment only (BC-0.25PDA, BC-0.5PDA, BC-1PDA), simultaneous DA/LS addition (BC-0.25PDA-LSt0, BC-0.5PDA-LSt0, BC-1PDA-LSt0), and delayed LS addition after 3 h PDA pre-treatment (BC-0.25PDA-LS-t3, BC-0.5PDA-LS-t3, BC-1PDA-LS-t3). After 24 h shaking at 100 rpm, samples were rinsed with Milli-Q water and dried at room temperature. ATR-FTIR spectra were recorded using a Perkin-Elmer Spectrum One spectrometer with a Golden Gate ATR accessory in the range 4000–650 cm^{-1}. XRD measurements were performed on a Bruker Siemens D5005 diffractometer using Cu-Kα radiation over a 2θ range of 5-70°. Through-plane ionic conductivity (σ) was determined by electrochemical impedance spectroscopy (EIS) using an SP-50e potentiostat (BioLogic, France). Membrane resistance was obtained from Nyquist plots, and conductivity was calculated considering membrane thickness and electrode area.

Results: The FTIR spectra of all membranes (Fig. 1b) display the characteristic bands of cellulose, including O–H stretching (~3600-3000 cm^{-1}), C-H stretching (~2900 cm^{-1}), and bands at ~1430-1450 cm^{-1} and ~1160-1030 cm^{-1} associated with C-H bending and C-O-C vibrations. In all PDA-modified samples, an additional band appears around ~1525 cm^{-1}, attributed to aromatic C=C vibrations of PDA. The XRD pattern of pure BC shows characteristic cellulose I reflections at 2θ ≈ 14.5°, 16.5°, and 22.5°, corresponding to the ($1\bar{1}0$), (110), and (200) planes (Fig. 1c). These reflections remain after modification, indicating that the crystalline structure of BC is preserved. The commercial LS sample displays a predominantly amorphous profile with several sharp diffraction peaks, likely originating from crystalline salt-related or inorganic residues. These peaks are also observed in LS-containing composites, confirming its presence. The pristine BC membrane shows very low ionic conductivity (2.25 x 10^{-4} mS cm^{-1}). The highest conductivity among PDA-only samples is observed for BC-0.25PDA (3.45 x 10^{-3} mS cm^{-1}), representing approximately a 15-fold increase compared to pristine BC, while incorporation of LS further enhances conductivity, most probably due to the introduction of sulfonate groups acting as proton-conducting sites. The highest conductivity is observed for BC-0.25PDA-LSt0 (3.57 x 10^{-2} mS cm^{-1}), corresponding to an approximately 160-fold increase compared to pristine BC. The stability of the composites arises from interactions between components, likely involving H-bonding between BC hydroxyl groups and PDA catechol groups, as well as π-π and electrostatic interactions between PDA and LS.

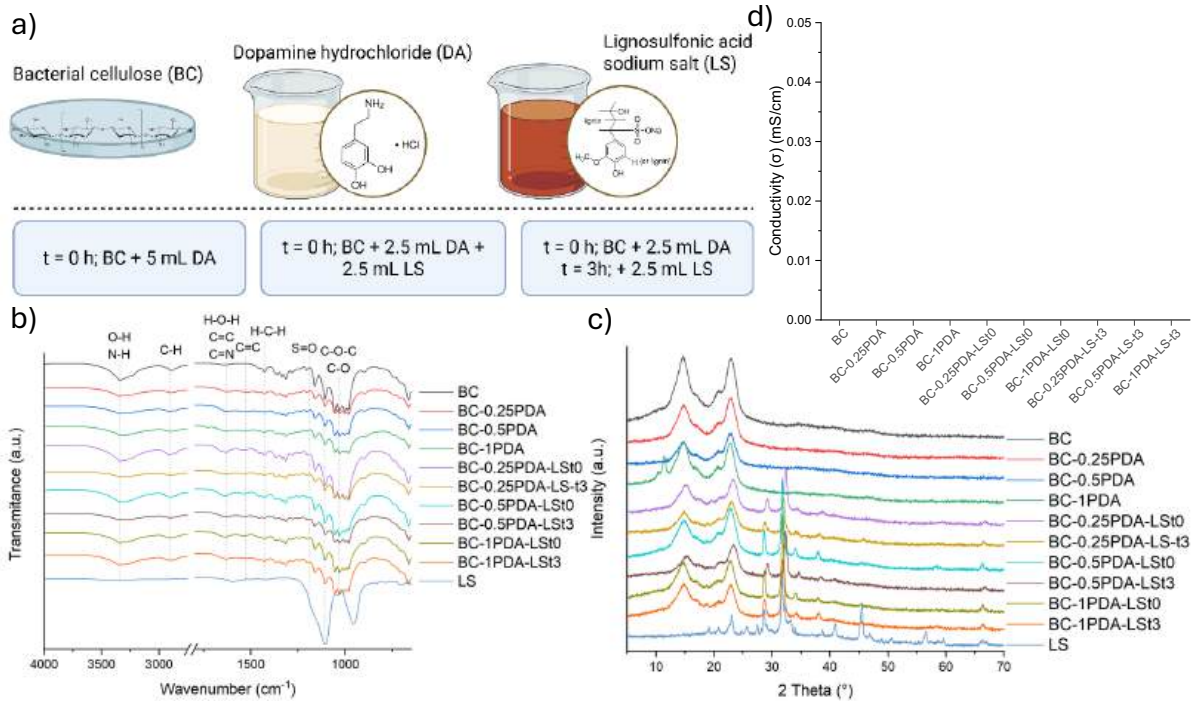


Figure 1. a) Tentative preparation scheme, b) ATR-FTIR, c) XRD and d) ionic conductivity data for the BC membranes, prior and after modification with PDA and LS.

Conclusions: BC membranes were successfully functionalised with LS through PDA-assisted coupling, forming a stable composite. Spectroscopic and structural analyses confirmed the incorporation of PDA and LS while preserving the BC crystalline structure. The presence of LS significantly improved ionic conductivity, with the highest value observed for the BC-0.25PDA-LSt0 membrane (3.57 x 10^{-2} mS cm^{-1}), representing an approximately 160-fold increase compared to pristine BC. For a more comprehensive understanding of the structure-property relationships and proton transport mechanisms, additional characterisation techniques in FC set-up are envisaged.

Acknowledgment: The authors acknowledge the financial support from the Slovenian Research and Innovation Agency (ARIS) through projects J2-50086, Z2-60175, N2-0388, and the Young Researcher Programme within the Textile Chemistry and Advanced Textile Materials Programme (P2-0118).

References

[1] S. Zdovc, M. Hren, and S. Gorgieva, "Bacterial nanocellulose-based composite membranes for fuel cells applications," *J. Power Sources*, vol. 665, 2026, 239045.

[2] P. Samyn, "Polydopamine and Cellulose: Two Biomaterials with Excellent Compatibility and Applicability," *Bioengineered*, vol. 12, 2021, pp. 1345–1361.

[3] C. Vilela et al., "Flexible nanocellulose/lignosulfonates ion-conducting separators for polymer electrolyte fuel cells," *Nanomaterials*, vol. 10, 2020, p. 1713.



Test campaign for the proof of funtionality of a pem fuel cell system for regional aircraft applications

Cornelie Bänsch*[a], Kai Sommer[a], Oliver Thalau[a], Milan Lieser[a]

* Corresponding author: cornelie.baensch@dlr.de

[a] German Aerospace Center (DLR), Institute of Engineering Thermodynamics, Pfaffenwaldring 38-40, 70569 Stuttgart, Germany

Keywords: multi-stack fuel cell system, PEMFC for aircraft applications, MW fuel cell powertrain

Abstract

Introduction:

More and all-electric aircraft concepts have gained increasing attention within the last decades in terms of decarbonization of the aviation sector (see e.g. [1,2]). Given the beneficial specific energy density of hydrogen fuel cell systems compared to battery-only concepts, hydrogen-electric propulsion systems are considered to be feasible for regional aircraft [3,4]. However, for the realization of such systems fuel cell power in the MW range is required. The test environment BALIS of the German Aerospace Center [5,6] provides test fields and corresponding units under test, namely liquid hydrogen storage, fuel cell system, e-drive and battery, for experimental investigation of fuel cell-based powertrains with MW power.

Objectives:

In this work the results of a test campaign within the BALIS fuel cell test field with a multi-stack fuel cell system (MFCS) of around 800 kW maximum power is presented. The aim of the experiments is the proof of functionality of the MFCS architecture for the application in a hybrid-electric propulsion system for regional aircraft applications.

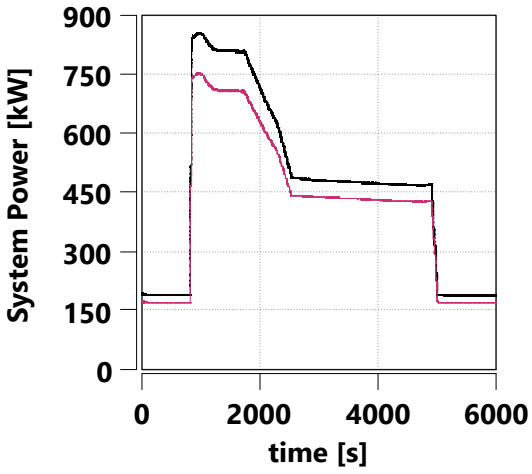
Experimental setup and methods:

The MFCS applied in this work consists of eight fuel cell modules, which include the PEM stack and BoP components (PS-100, PowerCell, P_{gross} = 120 kW, P_{net} = 100 kW, I_{max} = 420 A). Two modules are connected in series to form a so-called string and 4 strings are connected in a parallel, converter-free configuration. Hence, all fuel cell strings of the MFCS are operated at the same voltage level. The test campaign is divided into three test blocks: steady-state, transient and failure mode tests. During the first test block polarization curves are measured for the separate strings and the full system. In addition, the potential of regeneration procedures and rearrangement of single modules to improve the system performance is investigated and the degradation over the whole test campaign is monitored. During the second test block the system performance at different current ramps and aviation-relevant load profiles is investigated. During the third test block failures like insufficient

coolant flow or anode over- and under-pressure are systematically induced at string level and the system response is analyzed.

Results:

During the first test block, the polarization curve measurements of the four strings revealed significant performance differences leading to a variation of the maximum string output power of 4 %. In full system operation, a system maximum power output of 790 kW was obtained. By rearranging the modules within the strings, the voltage levels of the different strings could be converged at maximum power leading to an increase of the system power by 7 % to 848 kW.
During the second test block, a stable operation of the MFCS at different current ramps was observed ranging from 40 A/s to 160 A/s, which was determined to be the ramp limit of the full system due to system-internal current variances. A stable power output of the MFCS was also observed during application of aviation-relevant load-profiles with a duration of 55 to 103 min. An exemplary profile with 103 min duration is shown in Figure 2. In this profile, a peak power of 855 kW_{gross} and 754 kW_{net} during takeoff and a hydrogen consumption of 44.9 kg throughout the full mission was obtained.
Figure 2: Measured power output of the MFCS under a flight-relevant load profile; black: gross power output; red: net power output.



During the third test block, the actual limits for a system shutdown are determined. The shutdowns are mostly dependent on the fuel cell module internal controller settings. Nevertheless, the tests can give first insights in the module reaction under failure mode scenarios and the implications for the high voltage system of an electrical powertrain.

Conclusions:

With the presented test campaign, the MFCS could be proven to be functional for the considered load demands. Significant improvements could be achieved by an optimized arrangement of the modules in the converter-free architecture. Apart from the performance requirements, however, no other aviation-relevant requirements were considered conclusively. Further development with regard to specific power density, system efficiency and altitude operability are necessary in order to qualify the

technology for regional aircraft applications. In terms of integration of the MFCS into the full powertrain system the integration of a DCDC converter has to be considered to match the voltage levels of energy supply system and e-drive. In this regard, a modular system being able to control the voltage levels of the different strings separately should be investigated.

Acknowledgment

Funding: The project is supported by the Clean Aviation Joint Undertaking and its members in the framework of Grant Agreement n° 101102020 – AMBER.

Funded by the European Union. Views and opinions expressed are however those of the author(s) only and do not necessarily reflect those of the European Union or Clean Aviation Joint Undertaking. Neither the European Union nor the granting authority can be held responsible for them.

References

[1] K. Dahal, S. Brynolf, C. Xisto, J. Hansson, M. Grahn, T. Grönstedt, M. Lehtveer, Techno-economic review of alternative fuels and propulsion systems for the aviation sector, *Renew. Sustain. Energy Rev.* **151** (2021) 111564. doi: 10.1016/j.rser.2021.111564

[2] H. Schefer, L. Fauth, T. H. Kopp, R. Mallwitz, j. Friebe, M. Kurrat, Discussion on Electric Power Supply Systems for All Electric Aircraft, *IEEE Access* **8** (2020) 84188. doi: 10.1109/ACCESS.2020.2991804

[3] R. Ahluwalia, X. Wang, A. Shah, M. G. Lauer, P. J. Ansell, Fuel cells for single-aisle regional aircraft: System configuration, performance and cost, *Int. J. Hydrog. Energy* **159** (2025) 150568.

[4] M. Schröder, F. Becker, C. Gentner, Optimal design of proton exchange membrane fuel cell systems for regional aircraft, *Energy Convers. Manag.* **308** (2024) 118338.

[5] K. Sommer, B. Ni., J. Weiss, O. Thalau, C. Bänsch, Performance analysis of a megawatt fuel cell-based electric powertrain for regional aircraft (2025) 11th European Conference for AeroSpace Sciences, Rome. doi: 10.13009/EUCASS2025-202

[6] Weiss, J., Diarra, D., Sommer, K., Ni, B., Thalau, O., Bänsch, C., Methodological approach of the BALIS test fields fuel cell, battery and e-drive, (2024) Deutsche Luft- und Raumfahrtkonferenz, Hamburg. doi: 10.25967/630212



Concept of a solid oxide electrolysis-molten carbonate fuel cell hybrid system to support a power-to-gas installation

Jarosław Milewski[*a], Janusz Zdeb[b], Arkadiusz Szczęśniak[a], Aliaksandr Martsinchyk[a], Jakub Kupecki[c,d,e], Olaf Dybiński[a]

* corresponding author: jaroslaw.milewski@pw.edu.pl

[a] Warsaw University of Technology, Faculty of Power and Aeronautical Engineering, Institute of Heat Engineering, 21/25 Nowowiejska Street, 00-665 Warsaw, Poland

[b] TAURON Wytwarzanie S.A., Promienna 51, 43-603 Jaworzno, Poland

[c] Institute of Power Engineering, 01-330, Warsaw, Mory 8, Poland

[d] Center for Hydrogen Technologies (CTH2), Institute of Power Engineering, Augustówka 36, 02-981 Warsaw, Poland

[e] National Fuel Cell Research Center (NFCRC), University of California, Irvine, Engineering Laboratory Facility, Irvine, CA 92697-3550, United States

Keywords: CO2 capture, molten carbonate fuel cell, power-to-gas, solid oxide electrolysis, methanation

Abstract

Introduction: Renewable power-to-gas (P2G) converts surplus electricity into storable methane by water electrolysis followed by CO2 methanation, enabling use of existing gas-grid infrastructure [1,2]. A typical route, however, couples alkaline electrolysis with amine scrubbing, which creates two efficiency bottlenecks: high electricity demand for H2 production and a thermal penalty for solvent regeneration [3,4]. Molten carbonate fuel cells (MCFCs) can transport carbonate ions from the cathode to the anode, thereby concentrating CO2 from flue gas while producing DC electricity [5,6]. Solid oxide electrolysis (SOE), operated with steam at high temperature, can lower the electric energy input for hydrogen production and is thermally compatible with MCFC operation [3].

Objectives: This work proposes and evaluates a hybrid SOE-MCFC configuration for a P2G installation producing synthetic natural gas (SNG). The concept replaces the amine CO2 capture unit with an MCFC module and the alkaline electrolyzer with an SOE module. Because both devices operate at elevated temperature and use DC current, the design also considers direct thermal coupling and partial electric supply of the SOE by the MCFC. The key objective is to reduce external electricity use per unit of SNG, remove the CO2-capture heat penalty, and simplify balance-of-plant equipment. A simplified process scheme is shown in Fig. 1.

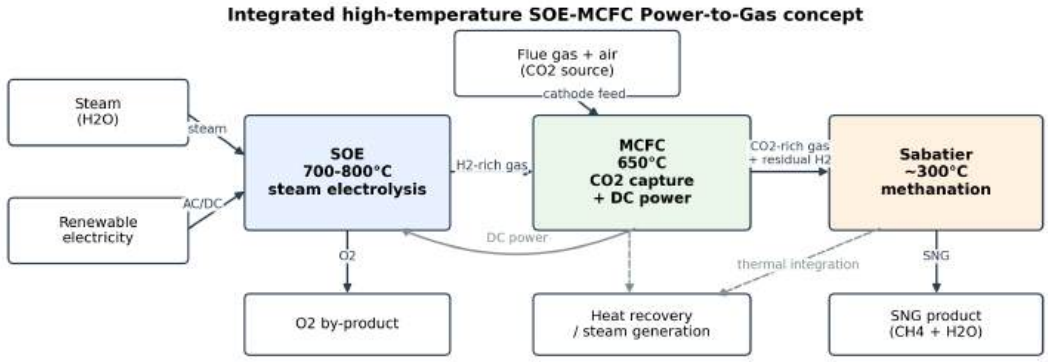


Fig. 1. Conceptual scheme of the proposed high-temperature SOE-MCFC system integrated with a Sabatier reactor for SNG production.

Material and methods: A design-level steady-state model was built for preliminary feasibility analysis. The system consists of an SOE operating at 700-800 °C, an MCFC at 650 °C, and a Sabatier reactor at about 300 °C. The methanation reaction was modelled as CO2 + 4H2 -> CH4 + 2H2O with high CO2 conversion. Ideal reactions were assumed at this stage, while performance indicators were taken from the authors' MCFC experiments and literature data for P2G, methanation and SOE operation. The molar balance links three subsystems: steam electrolysis generates H2 and O2; a hydrogen-rich stream supports MCFC anode operation while the cathode receives flue gas mixed with air; concentrated CO2 from the MCFC and H2 from the SOE are then fed to the methanation reactor. The model compares the proposed configuration with a reference P2G installation using alkaline electrolysis and MEA capture, considering H2-production electricity, CO2-separation energy, product purity, CO2 conversion and integration benefits.

Results: Preliminary calculations indicate that SOE replacement decreases the electricity requirement for hydrogen from about 50 to 39 kWh/kg H2, a reduction of approximately 22%. Hydrogen purity remains above 99.9%. For CO2 separation, the reference MEA unit requires about 3.9 MJ/kg CO2 of thermal energy, whereas the MCFC-based route provides a net electrical output during capture, represented in the model as approximately -4 MJ/kg CO2. CO2 purity increases from 96.7% to above 99%, and separation efficiency remains close to 89%. Methanation performance is preserved, with CO2 conversion maintained at about 95%. The proposed DC coupling reduces external electrical demand because part of the SOE load can be supplied by the MCFC. Thermal integration is also favourable: the hot SOE outlet can be routed toward the MCFC anode without additional preheating, and heat recovered from high-temperature streams can support steam generation or reactor temperature control. Compared with the reference layout, the MCFC route avoids solvent circulation, reboilers and large liquid-handling equipment, which improves modularity and facilitates scale-up by adding electrochemical modules.

Conclusions: The hybrid SOE-MCFC configuration can improve P2G operation by combining CO2 capture, hydrogen production and methanation in an integrated high-temperature system. At preliminary design level, it reduces the H2-production electricity demand by about one quarter relative to alkaline electrolysis, eliminates the conventional CO2-capture heat penalty, and adds useful DC power. The concept is therefore attractive for compact and modular SNG production coupled with

industrial or power-plant flue gas streams. Further work will validate the assumptions using operational data from the pilot-scale TENNESSEE installation and will optimize heat exchange, current matching, transient operation and control strategy.

Acknowledgment

This work was supported by the National Centre for Research and Development under grant no. WPC3/2022/29/IMPRESSION/2025.

References

[1] M. Götz et al., Renewable Power-to-Gas: A technological and economic review, Renewable Energy 85 (2016) 1371-1390. doi:10.1016/j.renene.2015.07.066.

[2] S. Rönsch et al., Review on methanation - From fundamentals to current projects, Fuel 166 (2016) 276-296. doi:10.1016/j.fuel.2015.10.111.

[3] M.A. Laguna-Bercero, Recent advances in high temperature electrolysis using solid oxide fuel cells: A review, Journal of Power Sources 203 (2012) 4-16. doi:10.1016/j.jpowsour.2011.12.019.

[4] G.T. Rochelle, Amine scrubbing for CO2 capture, Science 325 (2009) 1652-1654. doi:10.1126/science.1176731.

[5] T.A. Barckholtz et al., Molten carbonate fuel cells for simultaneous CO2 capture, power generation, and H2 generation, Applied Energy 313 (2022) 118553. doi:10.1016/j.apenergy.2022.118553.

[6] J. Milewski, J. Lewandowski, Separating CO2 from flue gases using a molten carbonate fuel cell, IERI Procedia 1 (2012) 232-237. doi:10.1016/j.ieri.2012.06.036.



Accelerating Solid Oxide Fuel Cell – Gas Turbine Simulations: A Surrogate Modeling Approach

P. Köhler*[a], O. Frotscher[a], A.-L. Schaller[a], M. Richter[a]

* corresponding author: koehler@ift.uni-hannover.de

[a] Leibniz University Hannover, Institute of Thermodynamics,
An der Universität 1, 30823 Garbsen (Germany)

Keywords: Aircraft propulsion, Solid Oxide Fuel Cell – Gas Turbine Hybrid, Surrogate Modeling, Symbolic Regression

Abstract

Introduction: Global aviation is economically and culturally vital, contributing approximately 4.5% to EU GDP. However, its rising climate impact necessitates a shift from conventional kerosene-powered engines toward innovative decarbonization technologies [1,2]. While sustainable aviation fuels (SAF) offer near-term improvements, fuel cells enable significantly higher efficiency levels [2]. Due to their high technology readiness level, proton exchange membrane fuel cells (PEMFCs) are widely studied, achieving efficiencies of around 50% when accounting for the thermal management system [3,4]. Alternatively, solid oxide fuel cells (SOFCs) offer even higher efficiencies, especially when coupled with a gas turbine (GT) system. These hybrid SOFC-GT systems can exceed 60% efficiency by utilizing exergy-rich waste heat within the downstream turbine. Furthermore, such systems leverage proven GT technology and offer high fuel flexibility, including the use of ammonia or hydrocarbons. However, given their high operating temperatures (>600 °C), they require effective heat integration while taking into account the weight of the system and the SOFC [5].

Objectives: A key design challenge is to understand the behavior and operational constraints of the SOFC in the hybrid system to ensure system feasibility within technical and physical limits. Typically, for a detailed calculation of the temperature profiles within the SOFC, as one of the crucial parameters, one- or multidimensional models are used. However, their dependence on numerous parameters makes them computationally intensive and hinders numerical optimization. To reduce computing time, the present study compares machine- learning-based surrogate models - specifically artificial neural networks (ANN) and symbolic regression. These models are evaluated with respect to their suitability for system-level simulations and their predictive accuracy for cell voltage, operating temperatures, and air demand (oxygen utilization).

Material and methods: The surrogate models are based on a modified 1D-SOFC model from [6], which was previously used in system-level studies [7]. Artificial neural networks were trained in Python using the *Scikit-learn* and *Optuna* packages, while symbolic regression was implemented via

the Thermodynamics-informed Symbolic Regression (TiSR) framework [8,9]. To evaluate these methods, the coefficient of determination

$$R^2 = 1 - \frac{\sum_{i=1}^{n}(y_i - \hat{y}_i)^2}{\sum_{i=1}^{n}(y_i - \bar{y})^2}$$

was compared for cell voltage, SOFC outlet temperature, and the oxygen utilization required to maintain a 150 K temperature difference between the inlet and outlet.

Results: Preliminary findings indicate high accuracy in reproducing cell voltage, maximum SOFC solid-state temperature (PEN), and the oxygen utilization required to maintain a certain temperature difference between inlet and outlet of the fuel cell. The achieved R^2 values all exceed 0.99 (Figure 1). For both methods, the largest deviation occurs in the predicted oxygen utilization, while the Symbolic Regression achieves a maximum deviation of ±7%, the neural network shows a deviation of ±10%. Voltage prediction deviations are ±2% for both surrogate models, and less than ±1% for the solid-state temperature. Notably, the trained surrogate models generate results almost instantaneously, whereas the original 1D model takes several minutes, yielding significant savings in computation time.

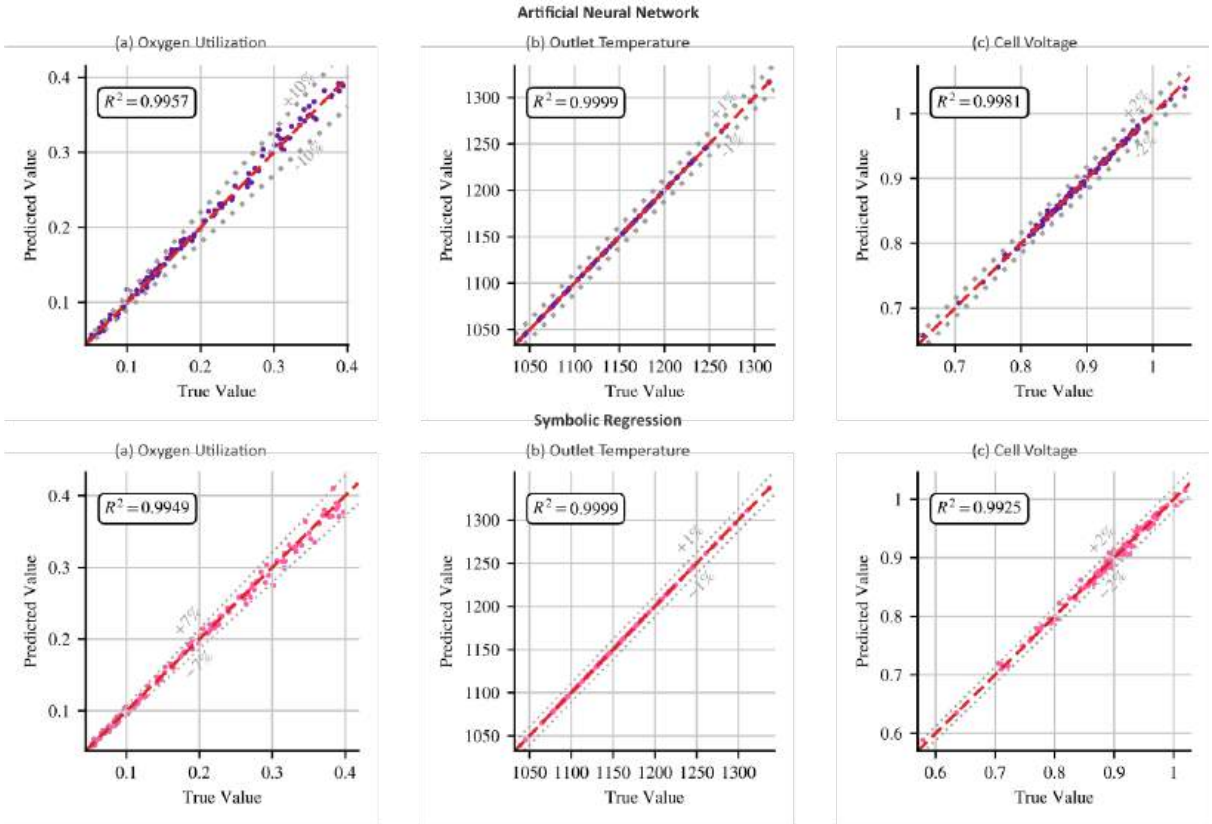


Figure 44: Comparison between the prediction accuracy of Artificial Neural Networks and Symbolic Regression

Conclusions: Machine learning-based surrogate models enable precise prediction of SOFC parameters, with deviations within the studied range ranging from less than 1% to 10%. While

preliminary results indicate that both neural networks and symbolic regression achieve high predictive accuracy, neural networks suffer from their 'black-box' nature, which obscures the underlying functional form. In contrast, symbolic regression - a method rarely applied in this field - offers distinct advantages, particularly for system integration. Beyond producing physically interpretable equations, symbolic regression allows for seamless implementation. Unlike black-box models that require complex software interfaces, the derived equations can be directly embedded into the simulation environment. Consequently, the development of more accurate symbolic-regression-based surrogate models is ongoing, with further research focusing on quantifying their influence on overall system behavior. At the system level, especially the influence of the used surrogate models regarding the aircraft propulsion studies and the differences in, e.g., efficiency and component sizes, need to be investigated.

Acknowledgment: The development of TiSR was funded by the Deutsche Forschungsgemeinschaft (DFG, German Research Foundation) within the Priority Programme SPP 2331 (Machine Learning in Chemical Engineering) - Project number 466528284.

The authors would like to acknowledge Cagatay N. Dagli for the continues work on multi-dimension SOFC models.

References

[1] Air Transport Action Group (ATAG) (2025). https://atag.org/industry-topics/supporting-economic-social-development (accessed on 18 April 2025).

[2] Fuel Cells and Hydrogen 2 Joint Undertaking (2020). Publications Office of the European Union. https://doi.org/10.2843/471510

[3] Peyrani, G.; Marocco, P.; Gandiglio, M. et al. (2025). eTransportation. https://doi.org/10.1016/j.etran.2025.100408

[4] Nozinski, M.; Meyer, P.; Delony, F. et al. (2026). Aerospace. https://doi.org/10.3390/aerospace13030243

[5] Ferrari, M.L.; Damo, U.M.; Turan, A. et al. (2017). Wiley. https://doi.org/10.1002/9781119039044

[6] Hollmann, J.; Kabelac, S. (2023). Energies. https://doi.org/10.3390/en16237827

[7] Köhler, P.; Hollmann, J.; Taissir, A. et al. (2026). Aerospace. https://doi.org/10.3390/aerospace13030263

[8] Martinek, V.; Frotscher, O.; Richter, M. et al. (2025). Zenodo. https://doi.org/10.5281/zenodo.15100641

[9] Martinek, V.; Frotscher, O.; Richter, M. et al. (2023). arXiv. https://doi.org/10.48550/arXiv.2309.02805



Combined thermal management and heat recovery for pemfc-battery hybrid propulsion systems

N. Bianco[a], F. Caruso[a], M. Di Somma[a], M. Iasiello[a], C. Menale*[b], F. Ortenzi[b], M Sicignano[a]

* corresponding author: carla.menale@enea.it

[a] Dipartimento di Ingegneria Industriale, Università degli Studi di Napoli Federico II, Piazzale Tecchio 80, 80125, Napoli, Italy

[b] Dipartimento Tecnologie Energetiche e Fonti Rinnovabili, ENEA Centro Ricerche Casaccia, Via Anguillarese 301, 00123, Roma, Italy

Keywords: Proton Exchange Membrane Fuel Cells, Thermal management system, Heat recovery, Hydrogen fuel cell vehicles

Abstract: This study presents a comprehensive predictive model for an urban bus powered by a PEM fuel cell and a Li-ion battery pack. By integrating a Nernst-based thermodynamic model with a first-order Thevenin battery model, the study evaluates thermal energy recovery from both power sources. The model was validated against experimental data and simulated using real-world driving cycles from Rome's public transport system. Preliminary results indicate a thermal recovery efficiency of approximately 70% for the fuel cell stack. Ultimately, this work provides a framework for multi-objective optimization to enhance energy efficiency and sustainability in heavy-duty mobility.

Introduction: To meet global energy demands and neutralize transportation emissions—which account for 29% of fossil fuel consumption—sustainable mobility has become a structural requirement [1]. Hydrogen and PEMFCs are the leading technologies for this transition, offering superior range and faster refueling compared to standard BEVs [2].

Technically, managing the waste heat produced by PEMFCs is critical for safety and durability. Furthermore, integrating thermal energy recovery from both fuel cells and battery packs can significantly boost efficiency. Ultimately, optimizing this heat management is essential for reducing costs and meeting long-term sustainability goals.

Objectives: The objective is to derive a comprehensive predictive model for an energy system that drives a bus, based mainly on a PEM fuel cell and a Li-ion pouch cell battery pack. This predictive model, to be extensively validated, will be used to simulate different scenarios based on typical drive cycles, including also multi-objective optimization to maximize aspects like the round-trip efficiency while accounting for constraints or other objectives like the bus weight or the usage of non-fossil energy carriers.

Material and methods: In this work, a thermodynamic model of a PEMFC for an electric urban bus was developed. The thermodynamic model of the PEMFC was based on the Nernst model, through which the polarization curve and power output of the cell were obtained and validated, comparing them to experimental data available in the literature. The experimental validation is shown in Fig. 1 using data from Chen et al. [3]. This model was then used to consider different thermal management system strategies, starting from data obtained from real driving simulations of the ATAC public transport system in Rome, with the aim of quantifying the recoverable waste heat from the PEMFC and assessing its potential reuse. Additionally, a battery model, including a thermal analysis for potential heat recovery, is included in the predictive model.

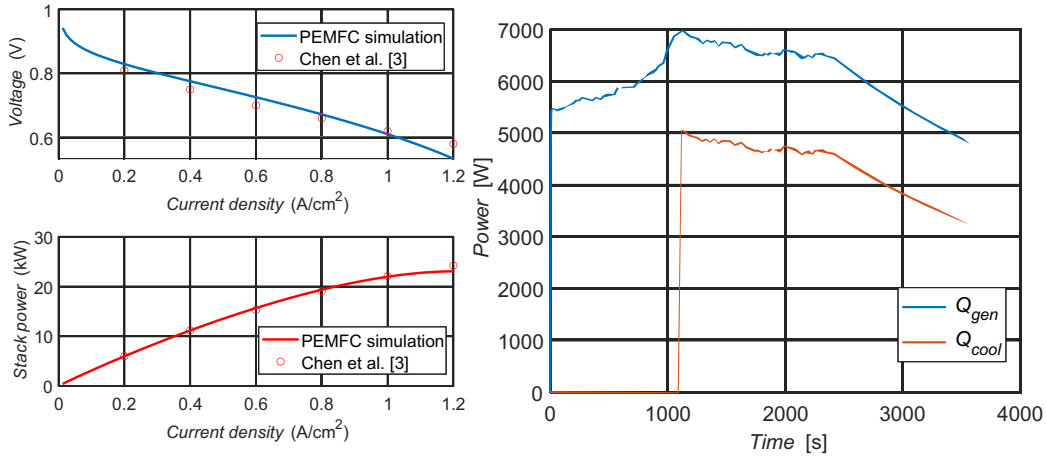


Figure 1 – Comparison of the fuel cell electrical model with experimental data from [3] (left); heat generation and cooling terms as a function of time, highlighting when the cooling system is activated (right).

Results: Preliminary results for the predictive model are presented in this section. The potential heat power recoverable from the fuel cell is shown in Fig. 1. This parameter is computed based on stack current density, voltage, and the chemical reaction of the hydrogen fuel integrated within the model. Additionally, the same figure presents the cooling heat power, calculated by assuming an inlet coolant temperature of 30 °C and an outlet temperature equal to the cell temperature. It is evident from the figure that the coolant starts circulating only after approximately 1000 seconds, which is when the stack temperature approaches the target of 75 °C. Notably, these results indicate a thermal recovery efficiency, specifically the fraction of heat available for recovery, of about 70%. For the preliminary tests, the battery is modeled as a Li-ion pouch cell. The total resistance, included in the heat generation term, is computed using a first-order Thevenin model. This model accounts for internal, activation, and concentration polarization resistances, along with the open-circuit voltage and concentration polarization capacity to capture transient effects. Fig. 2 shows the heat generated by a single elementary cell, serving as a baseline to compute temperature evolution through models such as the Cauer model.

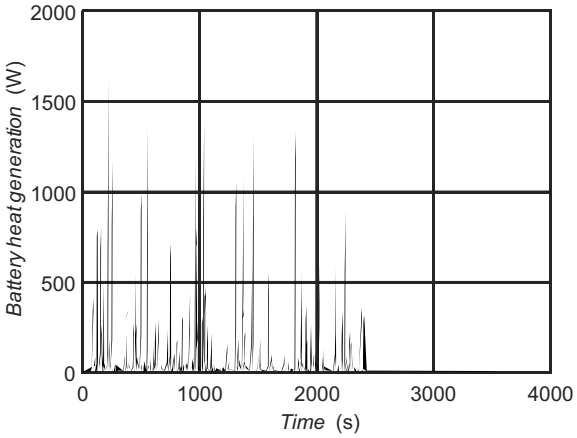


Figure 2 – Battery heat generation term as a function of time

Conclusions: This contribution provides a comprehensive model for fuel cell heat recovery that accounts not only for the heat generated by the fuel cell stack but also integrates the waste heat originating from the battery pack.

Acknowledgment

This research was funded by the European Union - NextGenerationEU from the Italian Ministry of Environment and Energy Security, POR H2 AdP MEES/ENEA with involvement of CNR and RSE, PNRR - Mission 2, Component 2, Investment 3.5 "Ricerca e sviluppo

sull' idrogeno"

References

[1] Mousavi, S. B., & Ahmadi, P. (2026). Enhancing the performance of hybrid battery-fuel cell electric buses: Optimal component sizing, thermal systems effect, and power source durability. Journal of Energy Storage, 149, 120104

[2] Wahab, A., Prakash, R., Schopen, O., Esch, T., & Shabani, B. (2025). Thermal management of fuel cell-battery electric vehicles: Challenges and solutions. Applied Energy, 387, 125635

[3] Chen, X., Long, S., He, L., Wang, C., Chai, F., Kong, X., ... & Tu, Z. (2022). Performance evaluation on thermodynamics-economy-environment of PEMFC vehicle power system under dynamic condition. *Energy Conversion and Management*, *269*, 116082.



In-situ contact pressure monitoring of PEMFC stack: A new approach

Vasanth Parthasarathy*

* corresponding author: Vasanth Parthasarathy

Lecturer-Researcher, Mechanical Engineering Department, Hanze University of Applied Sciences, Groningen, The Netherlands

Keywords: contact pressure, electrical contact resistance, Fuel cells, pressure sensor

Abstract

In the energy transition, Hydrogen utilisation and production are the major focus amongst scientist, engineers and all commercial sectors. Fuel cells(Hydrogen utilisation) and Electrolyser(Hydrogen production) are stacked with cells based on required rated voltage and specifications. The major challenge during stacking is to maintain designed contact pressure. This contact pressure is responsible for contact resistance(ohmic losses) in the entire stack assembly. There are several ways to stack the cells, generally the cells are placed with tie-rod and the torque is given on end plates(on tie-rod and nuts) using Wrench. Another way, could be to use a press-machine to compress the pre-assembled stack and tighten (lock) with tie-rod and nuts. The research question here is "whether the contact pressure is distributed evenly between the cells through end plates?". For this question, its necessary to first monitor the applied stacking pressure. In this research paper, a new methodology is proposed by placing a pressure sensor called flexiforce Sensors placed at the end plates and at the cells (bipolar plate) showed pressure variation during the assembly. In conclusion, within the scope of this research, a pressure sensor technique is successfully attempted (lab-scale) at Hanze UASLab to monitor in-situ contact pressure felt by the stack. This method could be a valuable and effective procedure during stack assembly for manufacturers of any type of fuel cell stack and electrolyser stack. Subsequently, the accurate measurement of contact pressure could be useful information to map/ contour contact resistance in the cells. Moreover, the localised contact resistance estimation is a two fold advantage. One, to calculate ohmic losses wherein the stack performance could be calculated and the other advantage is to guess heat generation spots in the cells. From the literature, it is evident that local current density spots on fuel cells are related to hot spots(heat generation) and this could be valuable information for cell degradation.

Introduction: There is limited / (or) no literature for in-situ measurement of contact pressure and hence the title of this article includes " A new approach". The keywords for literature search used are the following, contact pressure, PEMFC clamping force, in-situ contact pressure PEM, and stack assembly. But there are research paper available for optimising stacking pressure and effects of contact pressure on cell/stack performance. A complete review on clamping load and its effect on cell performance is analysed [1]. A detailed posteriori of experiments on contact pressure and modelling studies have been developed [2]. However, contact pressure is not measured with pressure

sensor during assembly and stack in operation. There are several pressure sensors and flexi force pressure sensors [3] are selected based on its easy to install, many specification to suit the torque and importantly and its dimensions and size that can be mounted in PEM stack. Therefore, in this article, a new methodology has been attempted to measure in-situ contact pressure.

Objectives: to measure in-situ contact pressure felt by the cells during stacking (assembly) and its proposed new methodology using pressure sensor.

Methodology: (a)Experiments are conducted using flexi-force placed at required position in the stack and force applied by Torque wrench with bolts-nut(tie rod) and hydraulic press. Flexi force is calibrated using know weight as shown in Figure 1. The data is monitored live and collected from software (exported to excel). (b) Design of Experiments: Calibrated sensors are placed at the end plate of anode and cathode side, and one at the middle of the stack(placed between bipolar plates). (c) The cells are stacked with end plates and the tie rod is inserted through the end plates. Torque is applied on the nut using torque wrench by following the sequence. This sequence ensures uniform load on the stack and the torque is stopped when sensors show designed pressure. Another method of applying contact pressure is shown in Figure 2. The designed pressure is applied using hydraulic press on the stack and checked / monitored using the sensors. The tie rod is then inserted through the end plate and tightened with nuts to lock the stack clamping load. This attempt could be considered as a first generation methodology to monitor the pressure during the stacking and in operation. Figure 2 (insert) shows a dummy fuel cell stack made of wooden sheets and foam. Due to confidentiality from stack supplier, only the conceptual picture is shown with minimum details.

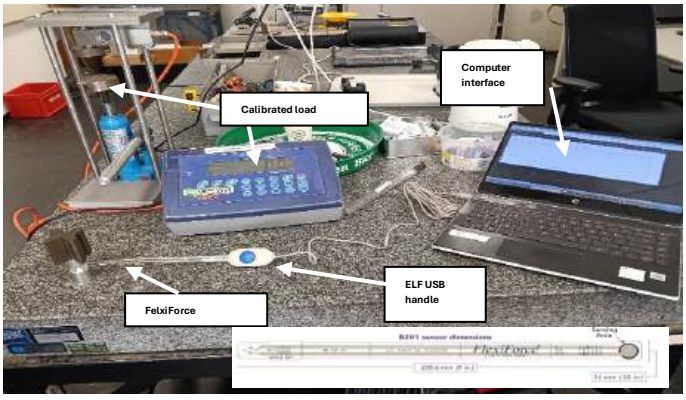


Figure 1. Pressor sensor calibration

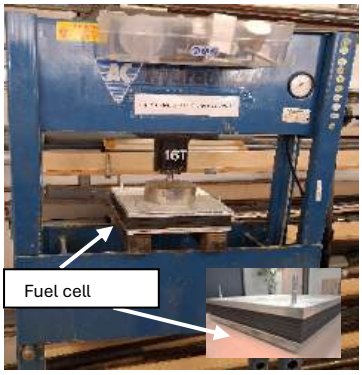


Figure 2 Stack and Hydraulic press

Results and Discussion: The applied dynamic load on the stack is monitored during assembling and shown in Figure 3. The data shown are typical and not exact values due to NDA of the stack supplier. It is observed that the response to the load applied by both torque wrench and hydraulic press is dynamic. It means, the cell experiences compression and expansion at the local area. This may further be researched to understand the contact pressure distribution and could be analysed for contact resistance.

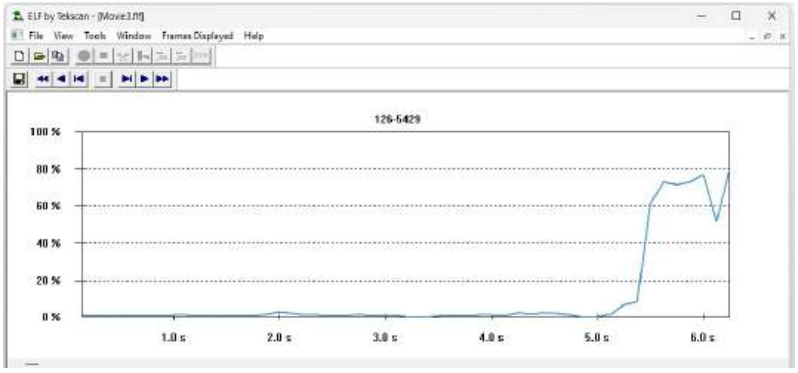


Figure 3 A snapshot of pressure variation during stacking using torque wrench

Conclusion: A new attempt has been made to measure in-situ contact pressure during stack assembly and fuel cell operation. The experiment conducted showed a clear proof that clamping pressure at the end plate recorded variation confirming the movement of the plate while following the torque sequence between bolts.

Acknowledgment: The author initiated this idea at Centre for Fuel Cell Technology (CFCT), ARCI, India (2011-2013) under the guidance of Dr. K S Dhattathreyan and Dr. R Rajalakshmi. The author would like to thank ARCI. Hanze UAS, Mechanical engineering department and colleagues are acknowledged for their support and this research on Energy Transition is disseminated to students at Hanze as a part "Research to curriculum" LO(Learning outcome). Thanks to Rene Wit, Double Energy and EnTranCe team. Makerspace, Hanze UAS is appreciated for Fuel cell model fabrication. EnTranCe-Hanze is acknowledged for design of experiments and Michel, Workshop-Hanze Mechanical engineering is acknowledged for Hydraulic press experiment.

References :

[1] Effect of Clamping Load on the Performance of Proton Exchange Membrane Fuel Cell Stack and Its Optimization Design: A Review of Modeling and Experimental Research, Wei Zhang, Cheng-wei Wu, https://doi.org/10.1115/1.4026070

[2] Contact pressure in the proton exchange membrane fuel cell: Development of analytical models based on experimental investigation and a posteriori design of experiments, L. Marcelli , D. Chamoret , E. Mancini, X. François , Y. Meyer , D. Candusso, https://doi.org/10.1016/j.jpowsour.2024.235158.

[3] Force Measurement System | FlexiForce ELF System | Tekscan, https://www.antratek.nl/



Performance and mass transfer evaluation of a single HT-PEM fuel cell with straight and wavy serpentine flow channels using CFD simulation

Mahmoud M. Abdelkader*[a, b], E. D'Alessio [a], F. Donato[b], G. Agati[c], D. Borello[c]

* mahmoudmohamed.abdelkader@uniroma1.it

[a] Dept. of Astronautical, Electrical and Energy Engineering, Sapienza University of Rome, Rome, Italy

[b] Dept. for Energy Technologies, ENEA, Italian National Agency for New Technologies, Energy and Sustainable Economic Development, Rome, Italy

[c] Dept. of Mechanical and Aerospace Engineering, Sapienza University of Rome, Rome, Italy

Keywords: HT-PEM Fuel cell, CFD, straight and wavy serpentine channels, Flow field design.

Abstract

This study presents a comparative analysis of the electrochemical performance and mass transfer characteristics of High-Temperature Proton Exchange Membrane Fuel Cells (HT-PEMFCs) utilising three distinct channel geometries: a conventional straight channel and two wavy channel configurations with wavelengths of 4 mm and 8 mm, respectively. Using three-dimensional computational fluid dynamics (CFD), the study evaluates the impact of channel design on species distribution, pressure drop, and current density distribution. The numerical model is validated against the polarization curve presented on BASF Celtec© P1100 W factsheet for the commercial membrane electrode assembly (MEA). The results, obtained for stoichiometric ratios of 1.2 and 2 at the anode and cathode, a temperature of 160 °C, and a pressure of 101325 Pa, reveal that a wavy serpentine configuration with a wavelength of 4 mm slightly outperforms the straight serpentine in terms of power density. It showed a 3.6% increase in current density at 0.44 V, whereas the wavy serpentine with a wavelength of 8 mm showed a 1.5% improvement.

Introduction: Flow channel design plays a vital role in the uniformity of reactant distribution and proper pressure difference profiles between anode and cathode in fuel cells. Many channel shapes have been studied, including serpentine and parallel designs. Serpentine design improves reactant distribution, but increases pressure drop. Parallel configuration exhibits a lower pressure drop, but it generally lacks reactant uniformity [1]. Serpentine design exhibits better coolant distribution and stable operating temperature. In addition, a multi-pass design may lead to lower pressure loss [2]. Computational fluid dynamics (CFD) is a robust tool for investigating the performance of PEMFCs [3]. A comparison between straight parallel channels and sinusoidal channels of various wavelengths has been investigated [4]. The study showed enhanced diffusion and convection with an optimal wavelength of 4.8 mm. Another study investigated zigzag configuration with different bending angles (from 5 to 45) and different numbers of bends (3 to 9). It showed that the zigzag configuration outperformed the conventional straight channel, with a 7-bend and 45-degree zigzag channel as an optimal design [5]. A new study examined the difference between parallel serpentine and parallel wavy channels [6]. It showed a 37.8 % increase in power density in wavy channels compared to parallel channels. They demonstrated that parallel wavy channels were capable of maintaining a pressure difference across the membrane lower than its threshold. Introducing new configurations, like wavy serpentine channels, is expected to enhance overall performance. To address the limited understanding of wavy serpentine flow fields, this study compares a conventional design [7] against two sinusoidal configurations (λ

≈ 4 mm and 8 mm). Implemented in a phase-shifted arrangement, these geometries aim to enhance heat and mass transfer while improving mechanical support for the PBI membrane to mitigate mechanical degradation.

Numerical Model: A three-dimensional, steady-state, non-isothermal CFD framework was developed using ANSYS Fluent, utilizing User-Defined Functions to capture the complex multiphysics of the PEMFC. The model solves the conservation equations for mass, momentum, energy, charge, and species transport. Electrochemical kinetics, specifically Hydrogen Oxidation at the anode and Oxygen Reduction at the cathode, are represented as volumetric source terms governed by the Butler-Volmer equation. The model parameters were calibrated against experimental data within the activation and ohmic regions, following the methodology outlined in [8]. The laminar flow equations are resolved using a SIMPLEC pressure-based solver with a first-order upwind discretization scheme. To ensure numerical fidelity, grid independence studies were conducted, and convergence was rigorously monitored based on reactant consumption and current balance between the anode and cathode [9].

Case Description: The three cells adopted in this study have similar dimensions for channels and ribs cross-section, but differences exist in the shape of the flow field design. The baseline geometry presents straight channels (wavelength $\lambda = \infty$) serpentines; meanwhile, the other two geometries use wavy channels with wavelengths $\lambda = 4$ mm and 8 mm, as shown in Figure 1-c. Conventional straight channels typically result in a channel-over-channel alignment, leaving the MEA unsupported across the channel span. Under transmembrane pressure differences, this lack of support leads to localized membrane deflection and high tensile stress at the rib edges, accelerating mechanical degradation. Conversely, the wavy channel design facilitates a staggered, channel-over-rib alignment as shown in Figure 1-c. This configuration provides continuous mechanical backing to the MEA, preventing deflection, minimizing tensile stress, and substantially improving the mechanical stability and lifespan of the fuel cell. The active area of the membrane electrode assembly (MEA) in the computational domain of 45 cm^2. The MEA is assumed to be composed of a 0.05 mm membrane, a 0.015 mm catalyst layer, and a 0.36 gas diffusion layer on both electrodes. This study considers a steady state simulation with a laminar flow (Re = 128). The study fixes the temperature of 160 °C at the external wall of the flow field plates. The inlet reactant gases are at 120 °C. It assumes thermal insulation at the lateral wall of the MEA and plates. The mass flow rate is calculated at a reference current of 1 A/cm2, ambient pressure of 101325 Pa, and no relative humidity at the anode and cathode, and a stoichiometric ratio of 1.2:2 at the anode and cathode, respectively. The fuel at the anode is composed of hydrogen and air at the cathode. The computational domain is composed of approximately 8 million cells to capture relevant physical phenomena.

Results: The numerical model is validated against the polarization curve presented on BASF Celtec© P1100 W factsheet [10], as shown in Figure 1-a. This curve was obtained under slightly different conditions, namely, the stoichiometric ratios (1.2/2 for anode/cathode) were kept constant on the entire current density range. This partly explains the better agreement that can be seen close to the reference current density adopted in the present study. The power density curves shown in Figure 1-b show that the wavy serpentine configuration has a slightly higher performance than the straight channel by 3.6 % at a voltage of 0.44 V. The wavy serpentine of wavelength 4 mm minimally outperforms the wavy serpentine of wavelength 8 mm by 2% at a voltage of 0.44 V.

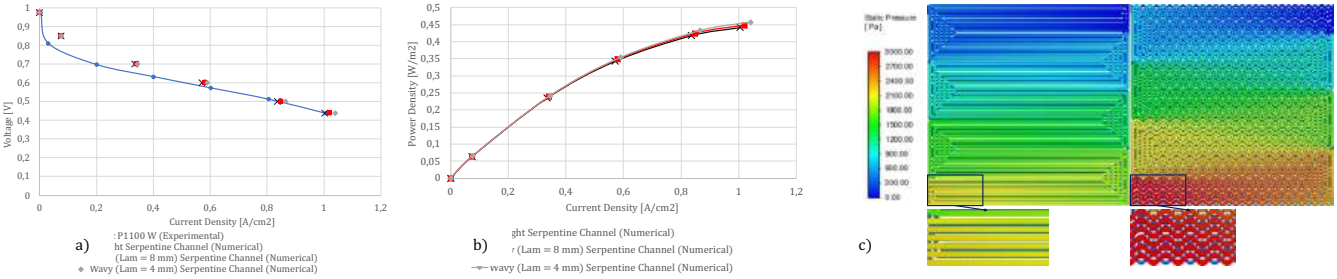


Figure 1: (a)- Numerical vs experimental polarization curves. (b)- Power density curves for the three cells. (c)- Pressure distribution on flow channels for straight and wavy configurations, consequently.

Conclusions: This study demonstrates that wavy serpentine flow channels enhance HT-PEMFC performance, yielding up to a 3.6% increase in current density compared to conventional straight channels. This slight increase may be due to the lower channel/rib ratio of the wavy serpentine configuration compared to the straight serpentine one. Furthermore, the wavy geometry creates a staggered channel-over-rib alignment that provides continuous mechanical support to the MEA.

References

[1] S. T. Bunyan, H. A. Dhahad, D. S. Khudhur, and T. Yusaf, "The Effect of Flow Field Design Parameters on the Performance of PEMFC: A Review," Jul. 01, 2023, *Multidisciplinary Digital Publishing Institute (MDPI)*. doi: 10.3390/su151310389.

[2] M. Ahmed and X. Shusheng, "Comprehensive review of serpentine flow fields for effective thermal management of proton exchange membrane fuel cell," Nov. 15, 2024, *Elsevier Ltd*. doi: 10.1016/j.heliyon.2024.e39793.

[3] E. D'Alessio, M. M. Abdelkader, F. Donato, G. Agati, and D. Borello, "Flow Field Optimization for HTPEM Fuel Cells: A Comparative Study of Serpentine-Parallel and Wavy Flow Channels," 2025.

[4] R. Kaiser, C. Y. Ahn, Y. H. Kim, and J. C. Park, "Performance and mass transfer evaluation of PEM fuel cells with straight and wavy parallel flow channels of various wavelengths using CFD simulation," *Int. J. Hydrogen Energy*, vol. 51, pp. 1326–1344, Jan. 2024, doi: 10.1016/j.ijhydene.2023.05.025.

[5] M. Li, L. Fu, H. Lin, J. Liu, and X. Zhang, "Wave flow field design optimization for enhanced performance of high-temperature PEM fuel cells," 2025. [Online]. Available: https://ssrn.com/abstract=5385761

[6] E. D'Alessio, M. M. Abdelkader, F. Donato, G. Agati, G. Monteleone, and D. Borello, "CFD analysis of sinusoidal flow fields for High Temperature PEM Fuel Cells: Balancing electrochemical performance and mechanical safety," *Int. J. Hydrogen Energy*, vol. 224, p. 154473, Apr. 2026, doi: 10.1016/j.ijhydene.2026.154473.

[7] V. K. Krastev, M. Baldelli, L. Bartolucci, F. Donato, M. Kheir Rouz, and V. Mulone, "Optimal cathode design of a single high temperature PEM fuel cell: A computational study," *Int. J. Hydrogen Energy*, vol. 142, pp. 80–89, Jun. 2025, doi: 10.1016/j.ijhydene.2025.05.346.

[8] E. D'Alessio, R. M. van Ginkel, F. Donato, G. Agati, and D. Borello, "Accuracy estimation of a CFD multiphysics approach to study a mixed parallel and serpentine flow channels PEM fuel cell," in *Journal of Physics: Conference Series*, Institute of Physics, 2024. doi: 10.1088/1742-6596/2893/1/012076.

[9] T. Bednarek and G. Tsotridis, "Issues associated with modelling of proton exchange membrane fuel cell by computational fluid dynamics," *J. Power Sources*, vol. 343, pp. 550–563, 2017, doi: 10.1016/j.jpowsour.2017.01.059.

[10] "Celtec MEAs. Membrane electrode assemblies for high temperature PEM fuel cells."



CFD-Based Parametric Optimization of Sinusoidal Flow Fields for High-Temperature PEM Fuel Cells

E. D'Alessio*[a], B. Paul[a], M. M. Abdelkader[a], G. Agati[a], F. Donato[b], D. Borello[a]

*emanuele.dalessio@uniroma1.it

[a] Sapienza University of Rome, Rome, Italy

[b] ENEA, Italian National Agency for New Technologies, Energy and Sustainable Economic Development, Rome, Italy

Keywords: HT-PEMFC; Sinusoidal flow field; Multiphysics CFD; Parametric geometry optimization

Abstract: Sinusoidal flow fields have recently been shown to enhance electrochemical performance in High-Temperature PEM Fuel Cells (HT-PEMFCs) while keeping the transmembrane pressure differential within the mechanical safety limits of phosphoric acid-doped PBI membranes. However, to the best of the authors' knowledge, no systematic parametric optimization of sinusoidal channel geometry has yet been reported for HT-PEMFCs. This work presents an automated CFD-based framework, driven by a Julia controller, for the parametric optimization of sinusoidal HT-PEMFC flow fields over five geometric variables: channel width, channel height, rib width, wave amplitude, and wave period. The framework integrates parametric CAD and mesh generation, CFD simulation via a calibrated three-dimensional steady-state multiphysics model, and iterative optimization logic, with dual objectives of maximizing current density and satisfying the PBI membrane burst pressure constraint. A baseline geometry has been defined, a mesh independence study performed, and a first polarization curve generated, yielding a current density of 0.699 A/cm^2 at 0.6 V. These preliminary results confirm the operability of the automated pipeline; the full parametric campaign is currently underway.

Introduction: High-Temperature Proton Exchange Membrane Fuel Cells (HT-PEMFCs) are enabling technologies for clean and efficient energy conversion, offering high tolerance to CO impurities, simplified water management, and compatibility with reformed hydrogen fuels at operating temperatures of 120–180 °C [1,2]. Within this framework, bipolar plate flow field design is a critical multi-objective problem: it must maximise reactant distribution and current density while controlling hydraulic resistance [3]. The mechanical characteristics of phosphoric acid-doped polybenzimidazole (PBI) membranes impose a particularly stringent constraint on HT-PEMFC flow field design. PBI membranes exhibit tensile strengths of only 1.5–5.0 MPa at high doping levels — an order of magnitude lower than Nafion — and are susceptible to creep deformation and structural failure under sustained anode-to-cathode pressure differentials [4]. Conventional serpentine flow fields, while effective in promoting under-rib convection, routinely generate transmembrane pressure differences that approach or exceed the safety limit of commercial PBI-based MEAs [5,6]. Sinusoidal ("wavy") channel geometries represent a promising compromise architecture. The curvature of the sinusoidal path induces centrifugally-driven secondary flows (Dean vortices) that continuously sweep fresh reactant toward the Gas Diffusion Layer (GDL), enhancing mass transport and current density without the excessive pressure drops of serpentine designs [7,8]. D'Alessio et al. [9] demonstrated that wavy channels outperform a hybrid serpentine-parallel baseline in HT-PEMFCs — achieving up to 35% higher peak power density — while maintaining the transmembrane pressure differential within the mechanical safety limit of the Celtec® P1100W MEA [6]. However, those results were obtained for a small set of discrete geometric configurations. To the best of the authors' knowledge, no systematic parametric optimisation of sinusoidal channel geometry has been reported for HT-PEMFCs, accounting for the coupled effects of channel width, channel height, rib width, wave amplitude, and wave period on both electrochemical performance and membrane mechanical safety. The present work addresses this gap through an automated high-throughput CFD framework that continuously maps the five-dimensional sinusoidal design space under these coupled constraints. The multiphysics model relies on the data-driven calibration of electrochemical parameters established in [9] to ensure a reliable baseline for geometric comparison.

Objectives: This work develops an automated CFD framework to optimise sinusoidal HT-PEMFC flow channels across five geometric parameters: channel width, channel height, rib width, wave amplitude, and wave period. The investigation focuses on:

- Quantifying the individual and coupled effects of the five parameters on current density and transmembrane pressure differential, mapping the performance–safety trade-off surface of the sinusoidal design space.
- Identifying the channel geometry that simultaneously maximises current density and satisfies the burst pressure constraint of the Celtec® P1100W MEA [6].
- Extracting compact design indications for sinusoidal bipolar plate architectures in HT-PEMFCs.

Numerical model: The simulations are carried out with the three-dimensional, steady-state, non-isothermal CFD model presented in [9], to which the reader is referred for the full governing equations and implementation details. The framework, implemented in ANSYS Fluent with User-Defined Functions, solves the coupled conservation equations for mass, momentum, energy, species transport, and electric charge across the bipolar plates, Gas Diffusion Layers (GDLs), Catalyst Layers (CLs), and PBI membrane. Porous-media transport is accounted for through a Darcy-Forchheimer source term with Bruggeman-corrected effective diffusivities. Electrochemical kinetics are modelled via the Butler-Volmer equation, and the protonic conductivity of the PA-doped PBI membrane follows the empirical correlation of Ma et al. [10], capturing the dependence on temperature and phosphoric acid doping level. The electrochemical parameters were calibrated against the experimental data of Ubong et al. [11] and validated with a maximum relative error below 1%; the same calibrated parameter set is adopted here without modification.

Case Description: The baseline geometry is a reduced-area adaptation of the sinusoidal HT-PEMFC configuration presented in [9], retaining the same wave amplitude and period. The cell consists of three anode and three cathode sinusoidal channels with a total active length of 56.4 mm and a width of 10.0 mm. In the baseline configuration, anode and cathode are geometrically symmetric: channel width 2.0 mm, rib width 1.0 mm, and channel height 1.0 mm on both sides. The only difference between the two electrodes is a π-phase shift in the sinusoidal path. The MEA comprises a 0.05 mm PBI membrane, 0.015 mm catalyst layers, and 0.36 mm GDLs. During the optimisation, all five geometric parameters — channel width, channel height, rib width, wave amplitude, and wave period — are varied independently for anode and cathode, so the optimal configuration may result in an asymmetric anode/cathode layout. A mesh independence study was performed on the baseline geometry using five structured hexahedral grids ranging from 43K to 1.15M elements. The relative error in current density at 0.6 V with respect to the finest mesh was 3.66% (43K), 1.23% (108K), 0.27% (367K), and 0.36% (812K); pressure values at monitored locations showed similarly limited sensitivity above 367K elements. The 367K mesh was therefore selected as the best compromise between accuracy and computational cost and is adopted throughout the parametric campaign.

Preliminary results: An automated optimization framework has been developed in Julia to drive the full simulation loop: geometric parameter definition, parametric CAD and mesh generation, CFD execution, and performance evaluation for the next iteration. A schematic of the workflow is shown in Fig. 1a. The framework was first applied to the baseline wavy geometry described above (Fig. 1b), yielding the polarization curve shown in Fig. 1c. At the reference operating voltage of 0.6 V, the baseline configuration produces a current density of 0.699 A/cm^2, in line with the performance range reported in [9]. These first data confirm that the automated pipeline drives the solver to convergence across the full voltage range and is ready to systematically explore the five-dimensional sinusoidal design space.

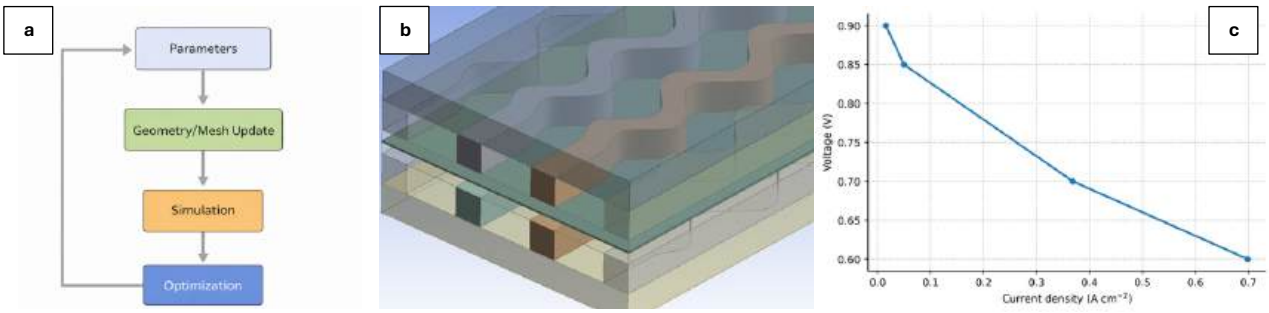


Fig. 1 - Automated optimisation framework and first results for the baseline sinusoidal HT-PEMFC geometry.

References

[1] S.S. Araya, F. Zhou, V. Liso, S.L. Sahlin, J.R. Vang, S. Thomas, X. Gao, C. Jeppesen, S.K. Kær, "A comprehensive review of PBI-based high temperature PEM fuel cells," International Journal of Hydrogen Energy, vol. 41, no. 46, pp. 21310–21344, 2016. DOI: 10.1016/j.ijhydene.2016.09.024

[2] R. Haider, Y. Wen, F. Ma, D.P. Wilkinson, L. Zhang, X. Yuan, S. Song, J. Zhang, "HTPEMFC: progress in advanced materials and key technologies," Chem Soc Rev, vol. 50, 2021. DOI: 10.1039/D0CS00296H

[3] Y. Wang, X. Liao, G. Liu, H. Xu, C. Guan, H. Wang, H. Li, W. He, Y. Qin, "Review of flow field designs for polymer electrolyte membrane fuel cells," Energies, vol. 16, no. 10, p. 4207, 2023. DOI: 10.3390/en16104207

[4] D. Aili, D. Henkensmeier, S. Martin, B. Singh, Y. Hu, J.O. Jensen, L.N. Cleemann, Q. Li, "Polybenzimidazole-based high-temperature polymer electrolyte membrane fuel cells: New insights and recent progress," Electrochemical Energy Reviews, vol. 3, no. 4, pp. 793–845, 2020. DOI: 10.1007/s41918-020-00080-5

[5] G. Falcucci, E. Jannelli, M. Minutillo, S. Ubertini, "Fluid dynamic investigation of channel design in high temperature PEM fuel cells," Journal of Fuel Cell Science and Technology, vol. 9, no. 2, p. 021014, 2012. DOI: 10.1115/1.4005628

[6] J. Song, "BASF Stack Handbook: How to Build, Test, and Diagnose High Temperature PEM Fuel Cell Stacks with Celtec® P1100W," BASF Fuel Cell, Inc., n.d.

[7] R. Kaiser, C.-Y. Ahn, Y.-H. Kim, J.-C. Park, "Performance and mass transfer evaluation of PEM fuel cells with straight and wavy parallel flow channels of various wavelengths using CFD simulation," International Journal of Hydrogen Energy, vol. 51, pp. 1326–1344, 2024. DOI: 10.1016/j.ijhydene.2023.05.025

[8] L. Wei, Y. Zhang, Z. Tu et al., "Performance investigation of proton exchange membrane fuel cell with Dean flow channels," Energy Technology, vol. 10, no. 11, p. 2100851, 2022. DOI: 10.1002/ente.202100851

[9] E. D'Alessio, M.M. Abdelkader, F. Donato, G. Agati, G. Monteleone, D. Borello, "CFD analysis of sinusoidal flow fields for High Temperature PEM Fuel Cells: Balancing electrochemical performance and mechanical safety," International Journal of Hydrogen Energy, vol. 224, p. 154473, 2026. DOI: 10.1016/j.ijhydene.2026.154473

[10] Y.-L. Ma, J.S. Wainright, M.H. Litt, R.F. Savinell, "Conductivity of PBI membranes for high-temperature polymer electrolyte fuel cells," Journal of The Electrochemical Society, vol. 151, no. 1, p. A8, 2003. DOI: 10.1149/1.1630037

[11] E.U. Ubong, Z. Shi, X. Wang, "Three-dimensional modelling and experimental study of a high temperature PBI-based PEM fuel cell," Journal of The Electrochemical Society, vol. 156, no. 10, p. B1276, 2009. DOI: 10.1149/1.3203309



Microstructure–Property Relationships in Digitally Deposited and In-Line Compacted NiO–3YSZ Anode Supports for Solid Oxide Cells

D.N. Boccaccini*[a,g], M. Cannio[b], S. Molin[c], B. Lemieszek[c], E. Mercadelli[d], A. Gondolini[d], A. Sanson[d], E. Paradisi[a], R. Taurino[e,f], V. Testa[a,f,g], M. Iaia[a], L. Zannini[a], Marcello Romagnoli[a,g]

* corresponding author: dino.boccaccini@unimore.it

[a] Dipartimento di Ingegneria "Enzo Ferrari", Università degli studi di Modena e Reggio Emilia

[b] Resoh Solutions SRL, Italy

[c] Advanced Materials Center, Faculty of Electronics, Telecommunications and Informatics, Gdansk University of Technology, Gdansk, Poland

[d] Institute of Science, Technology and Sustainability for Ceramic, Consiglio Nazionale delle Ricerche (ISSMC-CNR), Italy

[e] Department of Industrial Engineering, University of Florence, Italy

[f] National Interuniversity Consortium of Materials Science and Technology (INSTM), Italy

[g] Centro Interdipartimentale di Ricerca e per i Servizi nel Settore della Produzione, Stoccaggio e Utilizzo dell'Idrogeno H2 – MO.RE. Università degli Studi di Modena e Reggio Emilia, Modena, Italy

Keywords: Anode support, digital deposition, dry powder processing, solid oxide cells

Abstract: Dry powder processing represents a promising solvent-free alternative to conventional tape casting for the fabrication of anode-supported solid oxide cells (SOCs). In this work, porous NiO–3YSZ anode supports were fabricated by uniaxial pressing of powder mixtures containing NiO, ready-to-press 3YSZ, and graphite as a pore former, at pressures between 150 and 600 kg/cm^2, followed by sintering at 1315 °C. The influence of compaction pressure on shrinkage, porosity, mechanical strength and electrical conductivity after reduction was systematically investigated. Porosity decreased from 54.2% to 50.7% with increasing pressure. The biaxial flexural strength (normalized to V_eff = 1 mm^3) ranged between 35–40 MPa, without a clear pressure dependence, as differences fall within the experimental scatter (≈12% standard deviation). Reduced Ni–3YSZ composites exhibited improved electronic conductivity for higher compaction levels, confirming enhanced percolation of the metallic Ni phase. Laboratory-scale uniaxial pressing was used as a model system to investigate microstructure–property relationships relevant to the proposed in-line digital dry powder route. The results provide key insights into process–structure–property relationships governing dry-manufactured SOC supports and demonstrate the technological potential of scalable digital dry processing routes.

Introduction: Solid oxide cells (SOCs) operate at high temperatures (typically 600–1000 °C) and enable efficient electrochemical energy conversion in both fuel cell and electrolysis modes. Among planar configurations, anode-supported architectures are widely adopted due to their mechanical robustness and optimized gas transport[1]. The anode support plays a critical multifunctional role: it

must provide mechanical integrity, ensure interconnected porosity for fuel diffusion, and allow the formation of a continuous metallic Ni network after reduction[2]. Conventional manufacturing methods such as tape casting involve solvent-based processing and shrinkage typically exceeding 20%, increasing complexity and limiting compatibility with emerging digital manufacturing approaches[3][4]. Dry powder deposition combined with in-line pressing represents an attractive alternative, enabling solvent-free fabrication, reduced shrinkage and potential integration in continuous production lines[3][5]. In the present study, laboratory compaction was employed to isolate and quantify the microstructure–property relationships relevant to this digitally controlled dry powder route. The effects of compaction pressure on microstructure, mechanical reliability and electronic conductivity remain to be clarified. This work addresses these aspects through an integrated microstructural, mechanical and electrical investigation.

Objectives: The study aims to evaluate the influence of compaction pressure (150–600 kg/cm^2) on porosity, shrinkage, mechanical strength and electronic conductivity of NiO–3YSZ anode supports, and to compare their behavior with dense 8YSZ substrates while assessing compatibility with future SOC architectures.

Material and methods A powder mixture consisting of NiO (nickel oxide, 56.0 wt%), ready-to-press 3YSZ (3 mol% yttria-stabilized zirconia, ZrO_2 + 3 mol% Y_2O_3, 24.0 wt%) and graphite (C, 20.0 wt%) as pore former was uniaxially pressed into disk-shaped samples (Ø 25 mm and Ø 40 mm) at 150, 300, 450 and 600 kg/cm^2. Thermal treatment consisted of debonding at 900 °C for 4 h followed by sintering at 1315 °C for 15 h. Shrinkage and density were determined geometrically (theoretical density 6.47 g/cm^3). Mechanical characterization was performed using ring-on-ring biaxial flexural testing (Zwick Z050). Electrical conductivity of reduced Ni–3YSZ pellets was measured using the van der Pauw method in wet hydrogen (50 ml·min^{-1}) from room temperature to 900 °C. Nickel volume fraction after reduction was corrected considering oxygen loss and final porosity. Anode-supported semicells were fabricated by screen printing NiO–8YSZ functional anode and 8YSZ electrolyte layers onto pressed supports, followed by cofiring. The processing route was also tested by fabricating dense 8YSZ electrolytes, with the long-term objective of enabling electrolyte-supported SOC configurations.

Results: Anode supports for SOCs typically require a minimum porosity of 30–40% in the reduced state to ensure sufficient gas transport to electrochemically active sites [1]. Total porosity of the as-sintered, unreduced samples decreased from 54.2 ± 0.7% (150 kg/cm^2) to 50.7 ± 0.5% (600 kg/cm^2), remaining above this threshold before reduction. Linear shrinkage after sintering decreased from 10.9% to 9.5% with increasing pressure.

Mechanical behavior: The biaxial flexural strength (normalized to V_eff = 1 mm^3) ranged between 35–40 MPa, without a statistically significant pressure dependence, as variations fall within the experimental scatter (≈12% standard deviation). In contrast, dense 8YSZ electrolyte substrates

exhibited significantly higher strength (265 ± 30 MPa normalized to V_eff = 1 mm^3). Both results are in agreement with previous work [6].

Electrical conductivity: Reduced Ni–3YSZ samples compacted at higher pressure showed higher electronic conductivity and improved stability between heating and cooling cycles. This indicates enhanced metallic Ni percolation at higher compaction levels. At 900 °C, the electrical conductivity of reduced Ni–3YSZ samples increased from ~412 S/cm (300 kg/cm^2) to ~625 S/cm (600 kg/cm^2), corresponding to an enhancement of approximately 50%, confirming improved metallic Ni percolation at higher compaction pressures.

Conclusions: Dry pressing of NiO–3YSZ mixtures enables controlled fabrication of porous anode supports with porosity between 50–54%. Porosity and shrinkage decrease with increasing compaction pressure, while the biaxial flexural strength, normalized to an effective volume V_eff = 1 mm^3, remains in the range 35–40 MPa without exhibiting a statistically significant dependence on pressure, as the observed differences fall within the experimental scatter (≈12% standard deviation). Higher compaction pressure enhances the electronic conductivity after reduction due to improved metallic Ni connectivity. Dry powder processing therefore offers a solvent-free and scalable alternative for SOC manufacturing, enabling microstructural control while maintaining mechanical reliability and functional performance.

Acknowledgment: The authors acknowledge CNR-ISSMC (Faenza) for mechanical and thermal characterization activities and Gdansk University of Technology for electrical conductivity measurements. The work was performed within Contract EM-2025/01, with the support of *Incubatore di Imprese innovative* del Politecnico di Torino (I3P S.c.p.a.).

References

[1] A. Hauch et al., Science, 370 (6513), 2020, doi:10.1126/science.aba6118.

[2] T. Suzuki, S. Sugihara, T. Yamaguchi, H. Sumi, K. Hamamoto, and Y. Fujishiro, “Effect of anode functional layer on energy efficiency of solid oxide fuel cells,” *Electrochem. commun.*, vol. 13, no. 9, pp. 959–962, Sep. 2011, doi: 10.1016/J.ELECOM.2011.06.011.

[3] A. Chaparro *et al.*, “Non-Conventional and Advanced Sustainable Manufacturing Technologies for Fuel and Electrolytic Cells,” 2025.

[4] R. Singh *et al.*, “Advances in additive manufacturing of fuel cells: A review of technologies, materials, and challenges,” *Sustainable Materials and Technologies*, vol. 43, Apr. 2025, doi: 10.1016/J.SUSMAT.2025.E01317.

[5] Boccaccini Dino *et al.*, “Novel Dry Powder Processing Routes for Porous Anode Supports in Solid Oxide Electrochemical Cells,” in *11TH EUROPEAN FUEL CELL PIERO LUNGHI CONFERENCE*, G. Balint, B. Antala, C. Carty, J.-M. A. Mabieme, I. B. Amar, and A. Kaplanova, Eds., Viviana Cigolotti, Alessia Piccolo, Gabriele Lore, 2025, pp. 440–442.

[6] D. N. Boccaccini *et al.*, “Influence of Porosity on R-Curve Behaviour of Tetragonal Stabilized Zirconia,” *Ceramics 2022, Vol. 5, Pages 533-549*, vol. 5, no. 3, pp. 533–549, Sep. 2022, doi: 10.3390/CERAMICS5030040.



Influence of Methanol Reformer Aging on HT-PEMFC Performance under Dynamic Conditions

Emilija Todorovski*[a], Filip Todorovski [a], Mitja Mori [a], Andrej Lotrič [a], Mihael Sekavčnik [a]

* corresponding author: emilija.todorovski@fs.uni-lj.si

[a] University of Ljubljana, Faculty of Mechanical Engineering

Keywords: HT-PEMFC, reformate composition, reformer aging, system-level coupling

Abstract

Introduction: High-temperature proton exchange membrane fuel cells (HT-PEMFCs) are well suited for integration with methanol steam reformers (MSR) due to their tolerance to reformate impurities and simplified water management [1]. In such coupled systems, fuel cell performance is directly governed by the composition of the reformate gas, which typically contains hydrogen diluted with CO_2 and residual CO. A key challenge arises from reformer aging, which leads to gradual catalyst deactivation and changes in reformate composition, particularly in CO concentration. As a result, the fuel cell is exposed to a continuously evolving anode feed, rather than a constant gas composition. However, most studies investigate HT-PEMFC performance under fixed reformate compositions, which do not reflect realistic system operation [2]. This limits the understanding of degradation mechanisms in coupled systems. In this work, the influence of reformer aging on HT-PEMFC performance under dynamic reformate conditions is investigated, focusing on the interaction between changing fuel composition and cumulative cell degradation.

Objectives: The objective of this study is to investigate the impact of reformer aging on HT-PEMFC performance under dynamic reformate conditions, with emphasis on system-level coupling between fuel processing and electrochemical conversion. The study aims to:

- Simulate reformer lifetime evolution through stepwise variation of reformate gas composition, reflecting realistic changes in CO content
- Evaluate HT-PEMFC performance degradation under dynamically changing anode feed conditions during start-stop operation
- Compare fuel cell response across different stages of reformer aging, identifying trends in voltage decay and performance loss

Material and methods: All experiments were performed using a Greenlight G60 test station. Reformate mixtures were simulated by controlled blending of H_2, CO_2, CO and H_2O while methanol slip was not considered in this study. The H_2 fraction was kept constant, and variations in CO

concentration were introduced at the expense of CO_2 to represent reformer aging. A post-doped PBI-based membrane electrode assembly (MEA) supplied by Blue World Technologies was used, with an active area of 45 cm^2. To simulate realistic system operation, a start-stop cycling protocol was applied, as described in [3]. Performance characterization was conducted every 10 cycles, including polarization curves and electrochemical impedance spectroscopy (EIS) measurements. All diagnostic measurements were performed at a cell temperature of 160 °C, with stabilization at 0.3 A cm^{-2} prior to acquisition. Reformer aging was represented through stepwise variation of CO concentration during cycling from 2% to 1%. Independent sequences were defined to simulate two reformer lifetimes, each consisting of a progressive change in reformate composition over 70 cycles.

Results: The influence of reformer aging on HT-PEMFC performance was evaluated under dynamically changing reformate composition, using DRT peak evolution (Figure 45) and normalized performance losses (Figure 46). During the simulation of the first reformer's lifetime (cycles 1–70), the CO concentration decreases from 2% to 1%, while voltage losses increase approximately linearly. This indicates that degradation is primarily governed by start-stop cycling effects rather than reformate composition. The simultaneous decrease in ohmic resistance (ΔR) suggests improved membrane conductivity, likely due to initial MEA conditioning and acid redistribution. In contrast, the dominant increase in P3 indicates a progressive deterioration of transport-related processes, associated with structural changes in the electrode and gas diffusion layers.

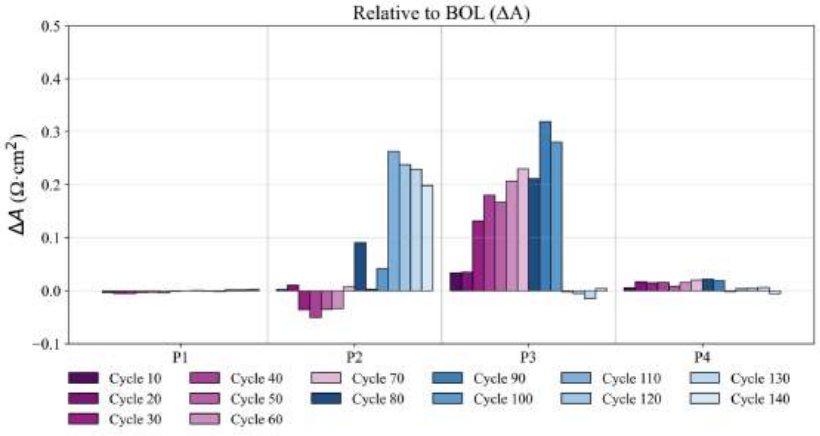


Figure 45: DRT peak evolution during cycles (relative to beginning of life-BOL)

In the second reformer lifetime (cycles 70–140), the same CO trajectory is repeated, but the system response differs significantly. P3 reaches its maximum at high CO levels and subsequently decreases with decreasing CO, indicating that transport limitations become increasingly coupled to CO concentration. At the same time, degradation shifts toward intrinsic electrochemical processes, with increasing R and P2, indicating membrane degradation and deterioration of ORR kinetics. The concurrent rise in OCV loss further confirms cumulative cell degradation. Despite these effects, the voltage at 0.3 A cm^{-2} remains relatively stable and even improves with decreasing CO.

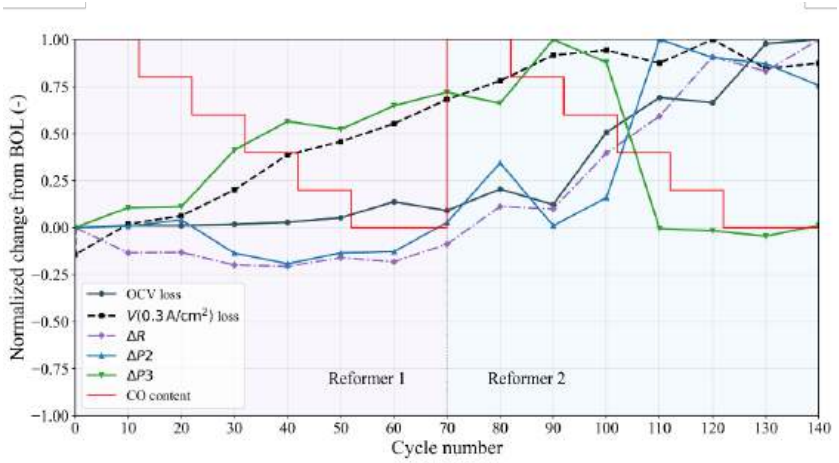


Figure 46: Normalized evolution of OCV, V(0.3 A cm^{-2}), R, P2, P3 and CO vs cycle

Conclusions: The results show that HT-PEMFC degradation is most pronounced during the initial 70 cycles, after which the degradation rate stabilizes. While dynamic reformate composition influences transport losses and short-term performance, the overall degradation is dominated by cumulative cycling effects. The observed differences in response under identical CO trajectories highlight the importance of system history. Future studies should directly compare dynamic and constant reformate compositions under identical start-stop protocol to isolate the contribution of fuel variability to degradation mechanisms.

Acknowledgment

The authors acknowledge financial support from Slovenian Research and Innovation Agency (research core fundings No. P2-0401) and thank Blue World Technologies for providing the MEAs used in this study.

References

[1] E. Todorovski, F. Todorovski, A. Lotrič, M. Mori, B. Likozar, S.J. Andreasen, M. Sekavčnik, Fuel Processing Technology 278 (2025) 108350.

[2] E. Todorovski, F. Todorovski, M. Sekavčnik, M. Mori, A. Lotrič, Electrochim. Acta (2026) 148676.

[3] F. Todorovski, E. Todorovski, M. Sekavčnik, M. Mori, A. Lotrič, Electrochim. Acta (2025) 147254.

EFCH2 2026 European Fuel Cells and Hydrogen
PIERO LUNGHI CONFERENCE
September 15th-17th 2026
Capri / Italy

Direct Biomass Fuel Cells for Small-Scale Biomass Utilization

Makoto KAWASE *[a], Yoshinobu Nakao [a]

* corresponding author: Makoto KAWASE

[a] Central Research Institute of Electric Power Industry (JAPAN)

Keywords: Direct biomass fuel cell, Molten carbonate, Carbon, Volatile matter

Abstract: To utilize unused biomass hindered by transportation costs, we propose and investigate direct biomass fuel cells (DBFCs) as a compact and efficient power generation technology. DBFCs directly feed solid or carbonized biomass into the cell's reaction zone, enabling direct electrochemical conversion of solid carbon and volatiles into electricity. Experiments at 700 °C using coconut shell–activated carbon achieved a power density exceeding 170 mW cm^{-2} and a single-cell efficiency of 31.8% (HHV). A system analysis indicates that a hybrid DBFC–gas engine configuration can achieve an overall electrical efficiency of approximately 40%.

Introduction: In recent years, increasing efforts toward carbon neutrality have led to the construction of biomass power plants. However, a large amount of biomass remains unused due to transportation costs. To effectively utilize such resources, small-scale, low-cost, and high-efficiency power generation systems are required. We propose direct biomass fuel cells (DBFCs) as a technology that can enable such a system (Fig. 1) [1]. A defining feature of DBFCs is that solid or carbonized biomass is fed directly into the cell's reaction zone, enabling direct electrochemical conversion of both solid carbon and volatiles into electricity. In addition, gasification reactions occur in the reaction chamber, producing combustible gases. By utilizing these combustible gases in combination with other power generation devices, a higher overall electrical efficiency can be achieved. In this study, the power generation system is discussed based on experimental results obtained using coconut shell-activated carbon as the fuel.

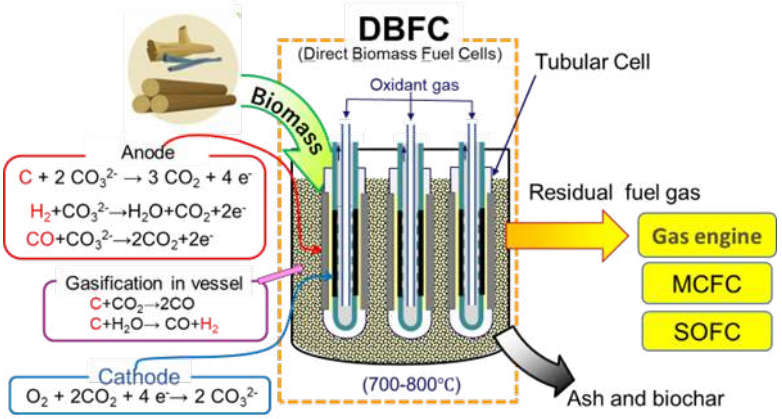


Fig.1 Schematic illustration of DBFCs

Materials and Methods:

Figure 2 shows a schematic diagram of the experimental apparatus and an external photograph of the cell used in this study. In the tubular DBFC used in the experiment, the anode in contact with the solid carbon fuel is a porous material composed mainly of Ni, the cathode in contact with the oxidant gas is a porous material composed mainly of NiO, the electrolyte is a carbonate salt ($(Li_{0.6}/Na_{0.4})_2CO_3$) with a melting point of 500 °C, and a porous electrolyte plate made from $LiAlO_2$ powder is impregnated with electrolyte. The method for fabricating the fuel cell was the same as in previous reports [1-2]. Furthermore, a small amount of carbonate ($(Li_{0.6}/Na_{0.4})_2CO_3$) was added (weight ratio 100:2) to ensure contact between the solid carbon fuel and the electrode. Solid carbon fuel was added periodically via a hopper at the top of the device. When woody biomass is used as the fuel, water vapor is generated during pyrolysis. To simulate this condition, coconut shell–activated carbon (UES Co., Ltd., KD-GW; particle size 20–50 mesh) was used as the solid carbon fuel, and humidified N_2 was supplied to the fuel side. The N_2 flow rate was 26 mL min^{-1}. A mixture of $N_2/O_2/CO_2$ (55/15/30 vol.%) was supplied to the cathode side at a flow rate of 150 mL min^{-1}. All experiments were conducted at an operating temperature of 700 °C.

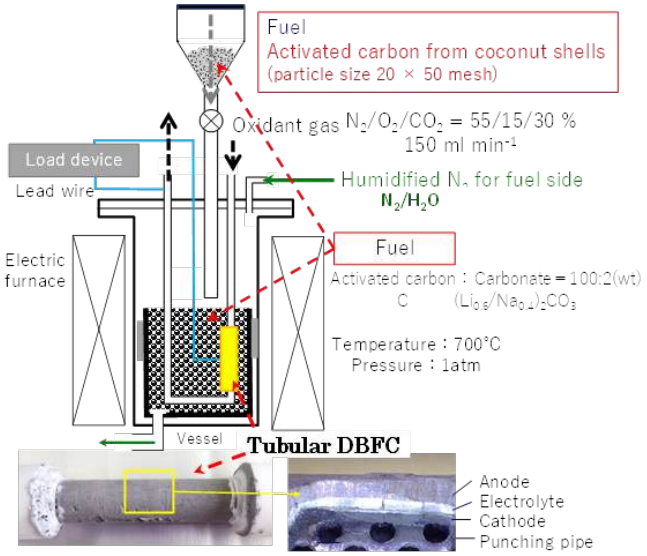


Fig.2 Schematic illustration of experimental apparatus and photograph

Results:

Basic performance of the DBFC

Figure 3 shows the current-voltage (I-V) characteristics and the corresponding power density. At a current density of 251 mA cm^{-2}, the cell exhibited a high voltage, with the power density at that time exceeding 170 mW cm^{-2}. Moreover, based on data listed in table 1, the single-cell power generation efficiency was estimated to be 31.8% (HHV).

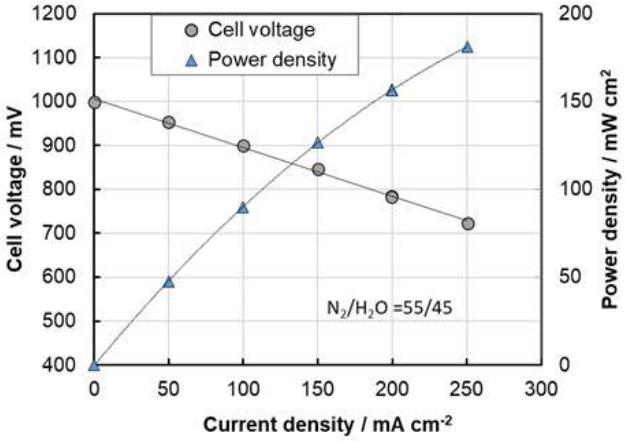


Fig. 3 Polarization and power density curves

Table 1 Cell voltage and anode outlet gas composition at 251 mA cm^{-2}, as shown in Figure 3.

Temperature [°C]	Current density [mA cm^{-2}]	N_2 for fuel side [mL min^{-1}]	Cell voltage [mV]	Anode outlet gas composition [%]				
				H_2	CO	CO_2	CH_4	N_2
700	251	26	723	10.3	15.7	28.9	0.1	45.0

Estimation of System Efficiency

As shown in Table 1, combustible gases were discharged as anode exhaust gas. Assuming a system (Fig. 4) in which this gas is utilized by a small-scale gas engine, a thermodynamic and mass balance analysis was conducted. The results indicate that an electrical efficiency of approximately 40% can be achieved.

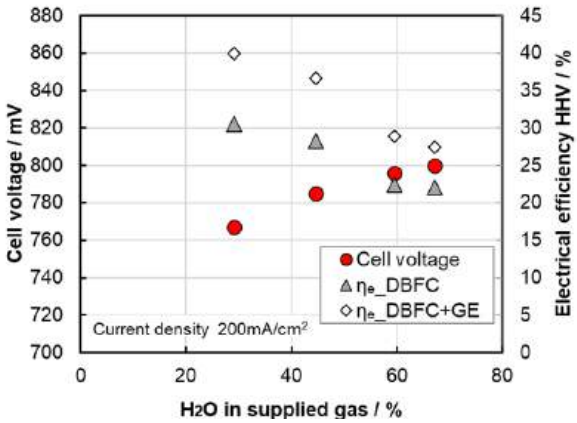


Fig. 5 Effect of steam content on the cell voltage and electrical efficiency

In addition, the effect of steam content on the cell voltage was investigated by simulating the moisture contained in biomass, and the electrical efficiency was estimated (Fig. 5). As the steam content increases, gasification reactions are enhanced, leading to higher concentrations of combustible gases and an increase in the output voltage. However, it was found that the overall power generation efficiency decreases with increasing moisture content.

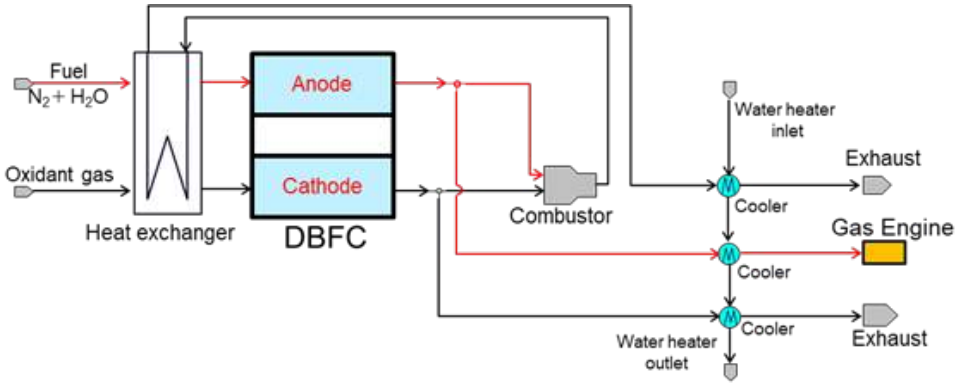


Fig. 4. Illustration of a DBFC–gas engine power generation system.

References

[1] M. Kawase, A. Ido. J. Power Sources., 642, 236880 (2025)

[2] A. Ido, M. Kawase. J. Power Sources., 449, 227483 (2020)



Mechanical Testing Investigation of Aqueous Capillary r-GO based Inks for 3D-Printed Electrodes

Milaki, E.[a], Li, B.[b], Brouzgou, A. *[a], Vlassopoulos, D.[b&c]

[a] Laboratory of Hydrogen and Fuel Cell Nanotechnology, Department of Energy Systems, School of Technology, University of Thessaly, 41500, Geopolis, Larisa, Greece

[b] Institute of Electronic Structure and Laser (IESL), Foundation for Research and Technology Hellas (FORTH), 70013 Heraklion, Greece

[c] Department of Materials Science and Engineering, University of Crete, 70013 Heraklion, Greece

Keywords: 3d-printed electrodes, aqueous-inks, graphene-based materials, rheological characteristics

Abstract: The rheological properties of reduced graphene oxide (r-GO) aqueous capillary inks were investigated for direct ink writing (DIW) of 3D-printed electrodes. DIW inks require optimized viscosity for controlled extrusion and shape retention after deposition. Increasing graphene concentration improved structural stability, while excessive concentrations reduced flowability and printability. Among the formulations tested, 15 wt% r-GO, 8 wt% CMC, and 2 vol% 1-octanol provided the best balance between fluidity and structural integrity, making it suitable for reliable electrode printing.

Introduction: Fuel cells suffer from various potential losses, some of which are attributed to the electrocatalytic activity of the materials. For this reason, various novel nano-catalysts as well as preparation methods for electrodes have been investigated, optimizing their internal structure and reducing their polarization losses. Compared to the conventional preparation methods , 3D-printed electrodes enable complicated structures with special sizes and shapes that improve electrodes performance and efficiency. 3D printing processing typically involves several steps: (i) preparation of the printable materials, (ii) design of the structures using 3D modelling software, (iii) the printing process, and (iv) post processing procedure. DIY is the most preferable additive manufacturing technique for managing graphene-based inks to prepare the special electrode architecture [1, 2]. DIY permits not to use molten polymers during the printing process , however the formulation of inks with high content of graphene still remains a challenge. This study focuses on capillary inks, a novel class of extrudable inks that reduce post-processing requirements. Capillary bridges formed by a secondary liquid matching the particle surface tension provide the yield stress and shear-thinning behavior required for printing. Here, aqueous r-GO capillary inks for DIW electrode fabrication are investigated. Due to the hydrophobic nature of r-GO, ink formulation remains a significant challenge [3].

Experimental procedure: The rheological characteristics of aqueous inks with different compositions (r-GO, cellulose, octanol, water) were investigated. Our protocol involved variable amplitude and

constant frequency measurements were performed to examine initially the influence of cellulose and then that of r-GO, on the change in the values of the dynamic storage modulus (G´) and the loss modulus (G´´). Cellulose helps improving the shear-thinning behavior of the ink and is a renewable and compatible agent. 1- Octanol is an ideal structural agent helping the formulation to keep its shape after printing.

Results: Studying the strain amplitude sweep and frequency sweep of different formulations, we observed that at lower percentage of cellulose 4wt% and 6wt%, G´´ >G´, indicating mainly viscous behavior.

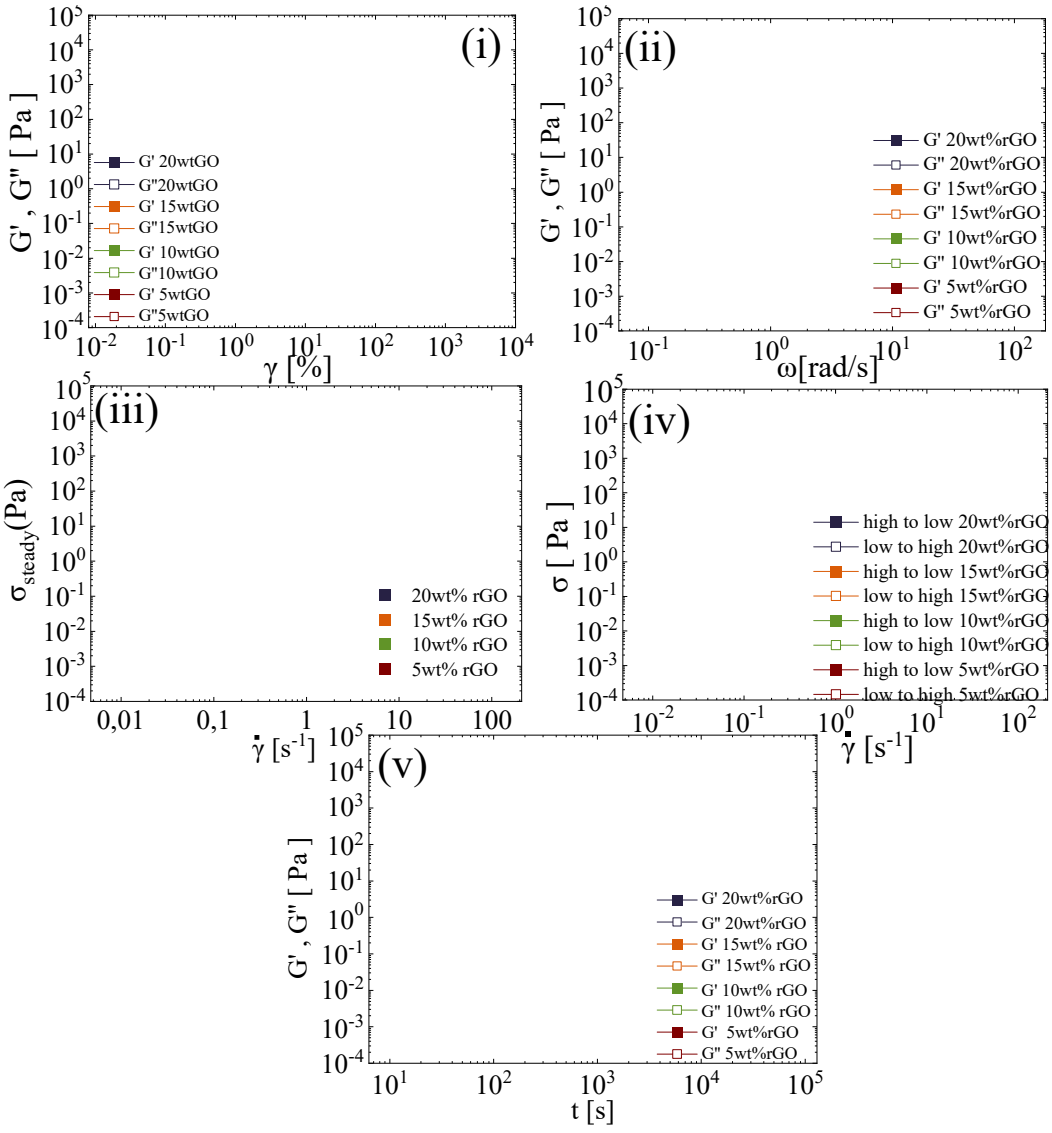


Figure 1. (i) change of the dynamic storage (G´) and loss (G´´) moduli in relation to the oscillatory shear strain amplitude (γ),(ii) angular frequency (ω), (iii) steady shear stress curve as a function of shear rate (γ̇), (iv) shear stress (σ) as a function of increasing and decreasing shear rate values (γ̇), in combination with the shear stress curve of diagram (iii), (v) change in G´ and G´´ with respect to time.

However, 8wt% CMC, also exhibited viscous behaviour, but with a significant increase in the values of the moduli. Subsequently, keeping the sample with 8wt% CMC we studied the effect of r-GO in capillary aqueous inks (92wt%H2O/8wt% CMC/x(x=5, 10, 15 20) wt% rGO/ 2vol% 1-octanol. As can be observed in Fig.1, the behavior of the 5 and 10wt% r-GO samples is viscous-dominated across the entire range of strains and frequencies, indicating a weak 3D network and low structural coherence.

The 15 wt% r-GO sample ensures excellent structural coherence and stability, indicating sufficient fluidity for smooth extrusion as well as sufficient elastic response that allows shape retention after deposition. It also exhibits strong pseudoplastic (shear thinning) behavior and rapid recovery of the structure (reversibility), with almost complete overlap of the curves for increasing and decreasing shear rates, as well as excellent temporal stability. The 20 wt% r-GO sample exhibits a reduced range of linear viscoelastic response, making it sensitive to changes during extrusion and deposition, leading to difficulty in controlling the printing process and possible loss of precision in the geometry and stability of the printed structure.

Conclusions: The ink composition 92wt% H_2O/8wt% CMC/15wt% rGO and 2vol% 1-octanol emerges as the most suitable for the 3D printing of fuel cell electrodes, as it combines an ideal balance between printability and structural integrity. It also presents quite satisfactory reversibility in shear, while at the same time ensures reliable and predictable behavior during printing, thus covering the basic requirements for the 3D printing of functional electrodes with complex microstructures.

Acknowledgment: We acknowledge support by the Hellenic Foundation for Research and Innovation (HFRI) under the HFRI Greece 2.0 Basic Research Financing Action (Horizontal support of all Sciences) Sub-action II Funding Projects in Leading-Edge Sectors and the research project "THUNDER" (Thermal stimuli-responsive 3D printed electroactive polymer nanocomposites towards 4D “programmable” geometries) (Project ID Number: 15515).

References

1. Polychronopoulos, N.D. and A. Brouzgou, Catalysts, 2024. 14(2): p. 110.
2. Poompiew, N., A.J. Román, P. Potiyaraj, and C. Aumnate, Journal of Power Sources, 2026. 662: p. 238810.
3. Tagliaferri, S., G. Nagaraju, A. Panagiotopoulos, M. Och, G. Cheng, F. Iacoviello, and C. Mattevi, ACS nano, 2021. 15(9): p. 15342-15353.



Influence of nominal contact pressure on activation behavior and spatial current redistribution in a pre-doped HT-PEMFC

Filip Todorovski*[a], Emilija Todorovski [a], Mihael Sekavčnik[a], Mitja Mori[a], Andrej Lotrič[a]

* corresponding author: filip.todorovski@fs.uni-lj.si

[a] University of Ljubljana, Faculty of Mechanical Engineering, Slovenia

Keywords: HT-PEMFC, nominal contact pressure, break-in, segmented current distribution, DRT analysis

Abstract

Introduction: High-temperature proton exchange membrane fuel cells (HT-PEMFCs) require an initial activation period to stabilize phosphoric acid distribution and electrochemically active interfaces before reliable performance evaluation. While nominal contact pressure is commonly reported for post-doped membrane electrode assemblies, typically around 0.75 MPa, corresponding information for pre-doped MEAs is often missing despite potentially higher sensitivity to mechanical assembly conditions [1]. As a result, the influence of nominal contact pressure on activation-induced spatial current redistribution and post-break-in electrochemical behaviour of pre-doped HT-PEMFCs remains insufficiently understood [2], [3]. Because local current non-uniformity formed during activation may influence the initial state from which degradation develops, understanding this early-stage behaviour is important for representative durability studies.

Objectives: This study aims to evaluate the influence of nominal contact pressure on activation-induced current redistribution and post-break-in electrochemical behaviour of a pre-doped HT-PEMFC using segmented current monitoring, polarization curves, EIS, and distribution of relaxation times (DRT) analysis.

Material and methods: Three p-PBI carbon paper-coated BASF Celtec-P 2200 N MEAs (45 cm^2, 770 µm) were assembled under nominal contact pressures of 0.85, 0.55, and 0.30 MPa and tested on a Greenlight Innovation Greenlight G60. Break-in was performed at 160 °C and 0.2 A/cm^2 for 50 h with anode/cathode stoichiometries of 1.25/2.5. Polarization curves were recorded down to 0.5 V after break-in. EIS was conducted at 0.4 A/cm^2 using a Gamry Reference 3000 (5 mV, 0.01 Hz–1 kHz) and evaluated by DRT analysis. Segmented current was monitored using an S++ Current Scan plate.

Results: During the 50 h activation period, nominal contact pressure strongly influenced voltage stability and current redistribution (Fig. 1). At 0.85 MPa, the voltage level remained 2.8% higher than at 0.55 MPa and 3.3% higher than at 0.30 MPa, while mean segmented current stayed stable and CV remained low (~23%), indicating homogeneous activation. At 0.55 MPa, moderate voltage decay was accompanied by minor current redistribution and a slight CV decrease, suggesting gradual

stabilization. In contrast, 0.30 MPa showed a similar relative voltage decay to 0.85 MPa, but with increasing mean segmented current and a pronounced CV rise after 20 h (>30%), indicating progressive spatial non-uniformity.

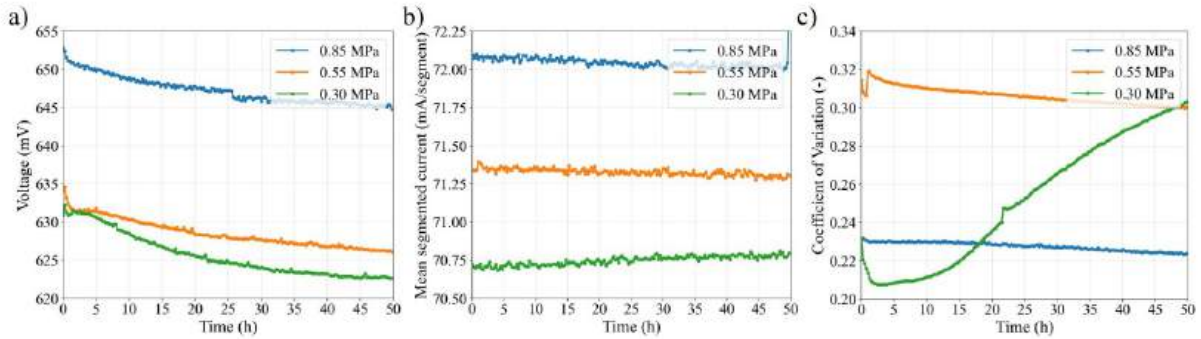


Fig. 1: Evolution of electrochemical and segmented-current characteristics during activation at different nominal contact pressures: (a) Voltage evolution during 50 h activation at constant operating conditions; (b) Mean segmented current evolution during activation; (c) CV of segmented current during activation

Spatial segmented current analysis confirmed that lower nominal contact pressure intensified local current redistribution during activation (Fig. 2). At 0.85 MPa, the inlet/outlet ratio remained highest and nearly stable, while the center/edge ratio and 2D FFT high-frequency fraction changed only slightly, indicating uniform activation. At 0.55 MPa, all spatial descriptors evolved gradually, suggesting moderate redistribution without pronounced localization. In contrast, 0.30 MPa showed the strongest redistribution: the center/edge ratio decreased continuously after ~20 h, accompanied by a temporary increase in high-frequency fraction, indicating growing spatial heterogeneity likely related to local contact pressure differences.

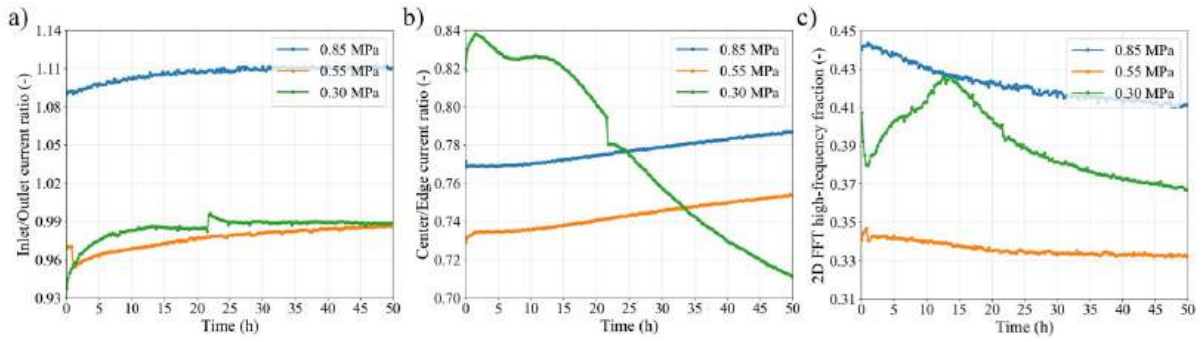


Fig. 2: Quantitative descriptors of spatial segmented current redistribution during 50 h activation under different nominal contact pressures: (a) inlet/outlet current ratio, (b) center/edge current ratio, and (c) 2D FFT high-frequency fraction

Post-activation electrochemical characterization confirmed superior performance at higher nominal contact pressure (Fig. 3). Polarization curves showed consistently higher voltages at all current densities for 0.85 MPa, while 0.30 MPa exhibited the lowest performance. DRT analysis revealed that decreasing contact pressure increased ohmic resistance and P1 contribution, whereas P3 decreased progressively. The higher ohmic resistance indicates less effective interfacial contact under lower

compression, while the disappearance of P4 at lower pressures suggests modified transport-related response after activation.

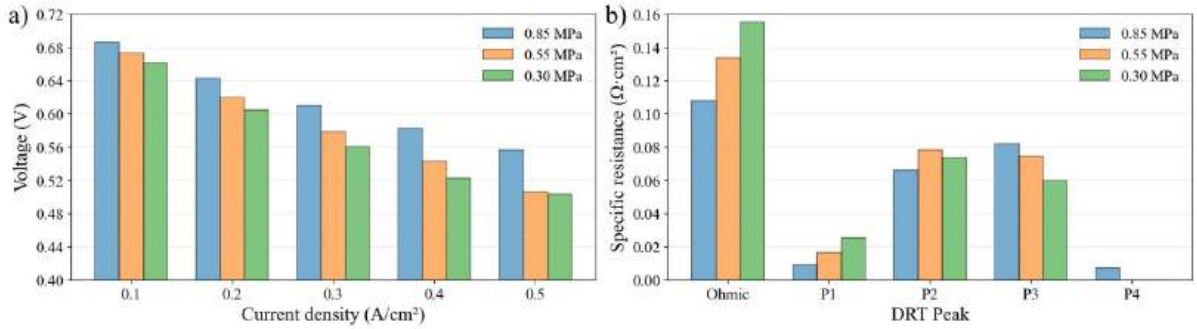


Fig. 3: Post-activation electrochemical characterization: (a) Voltage extracted from polarization curves recorded after break-in procedure; (b) Comparison of DRT-derived peak resistances after break-in

Conclusions: The results demonstrate that nominal contact pressure strongly governs activation uniformity and post-break-in electrochemical response in pre-doped HT-PEMFCs. Higher contact pressure (0.85 MPa) ensured more homogeneous activation and superior initial performance, whereas lower pressures promoted spatial heterogeneity and increased ohmic losses. Interestingly, these contact-pressure levels correspond to previously reported start–stop degradation behaviour under identical assembly conditions [1], where 0.85 MPa showed the highest voltage loss after 70 cycles (ΔV=127.67 mV), while 0.55 and 0.30 MPa exhibited substantially lower degradation (ΔV=21.07 and 18.05 mV), suggesting that favourable activation conditions may not directly correspond to optimal durability under dynamic operation.

Acknowledgment: The authors acknowledge financial support from Slovenian Research and Innovation Agency (research core fundings No. P2-0401)

References

[1] F. Todorovski, E. Todorovski, M. Sekavčnik, M. Mori, and A. Lotrič, "Electrochemical assessment of contact pressure effects on durability of high-temperature proton exchange membrane fuel cells under dynamic operation," *Electrochim. Acta*, p. 147254, Aug. 2025, doi: 10.1016/j.electacta.2025.147254.

[2] A. Diedrichs, M. Rastedt, F. J. Pinar, and P. Wagner, "Effect of compression on the performance of a HT-PEM fuel cell," in *Journal of Applied Electrochemistry*, Kluwer Academic Publishers, Nov. 2013, pp. 1079–1099. doi: 10.1007/s10800-013-0597-3.

[3] A. Zucconi, J. Hack, R. Stocker, T. A. M. Suter, A. J. E. Rettie, and D. J. L. Brett, "Challenges and opportunities for characterisation of high-temperature polymer electrolyte membrane fuel cells: a review," *J. Mater. Chem. A Mater.*, vol. 12, no. 14, pp. 8014–8064, 2024, doi: 10.1039/D3TA06895A.



Iron-Induced Degradation and Cation Migration in PFSA Membranes: Spatially Resolved Insights from Segmented Cell Analysis

M. Vincenot[a], Z. Gomez[b], A. El Kaddouri*[a], J. Dillet[a], F. Dubelley[b], C. Bas[2], J. Durst[c], O. Lottin[a]

*corresponding author: assma.el-kaddouri@univ-lorraine.fr

[a] Université de Lorraine, CNRS, LEMTA, F-54000 Nancy, France

[b]Univ. Grenoble Alpes, Univ. Savoie-Mont Blanc, CNRS, Grenoble INP, LEPMI, 38000 Grenoble, France

[c]SYMBIO, 10 rue Specia, 69190 Saint-Fons, France

Keywords: PEMFC durability, PFSA membrane degradation, cation contamination, segmented cell analysis

Abstract

Metallic cation contamination significantly limits the durability of proton exchange membrane fuel cells (PEMFCs). Iron cations (Fe^{2+}/Fe^{3+}), originating from bipolar plate corrosion, replace protons in PFSA membranes, reducing proton conductivity and altering transport properties [1]. This effect is strongly dependent on hydration and is further coupled with radical generation via Fenton-type reactions, accelerating membrane degradation [2]. In this work, the impact of controlled Fe^{2+} contamination on PFSA-based membrane electrode assemblies (MEAs) is investigated using a segmented cell enabling spatially resolved diagnostics [3]. The results reveal strong performance losses, spatial heterogeneities, and dynamic cation redistribution.

Introduction:

The durability of PEMFCs remains a key challenge for their deployment in heavy mobility applications [4]. Among degradation mechanisms, cationic contamination is particularly critical, as metallic cations such as Fe^{2+} or Fe^{3+} compete with protons for sulfonic acid sites in PFSA membranes, leading to reduced conductivity and increased resistance and modify the water management [1]. This effect is amplified under low humidity due to the dependence of proton transport on water-mediated mechanisms [5].

In addition to transport limitations, iron cations promote chemical degradation through radical formation, causing polymer chain scission and membrane thinning [2]. Furthermore, cations redistribute dynamically within the membrane electrode assembly (MEA) through diffusion and electromigration processes, among others, leading to spatially heterogeneous degradation. However, these local effects remain poorly captured by conventional global measurements.

Objectives:

This study aims to investigate the impact of Fe^{3+} contamination on PFSA-based MEAs using spatially resolved diagnostics, in order to quantify performance losses, identify transport limitations, and analyse cation redistribution. Particular attention is given to the transition from reversible ionic effects to irreversible degradation mechanisms (steric hindrance vs. chemical attack, membrane failure…).

Material and methods:

Reinforced PFSA membranes were contaminated with Fe^{3+} solutions with R ratios (cation/sulfonic site ratio) of 0.1 and 0.5, respectively, by contaminating either the entire membrane or only half of the membrane… The membranes were assembled into MEAs with 0.3 $mgPt \cdot cm^{-2}$ electrodes using CCB (catalyst-coated backing) process.

Electrochemical characterization was performed in a $25cm^2$ segmented cell (Figure 1), enabling spatially resolved measurements. Tests were conducted at 80 °C under varying humidity (30 - 50 - 70%) and pressure (1-2-3 bar), using polarization curves and electrochemical impedance spectroscopy. Accelerated stress conditions were applied to investigate degradation under intermediate conditions (50% RH, 2 bar) by cycling both the humidity and load.

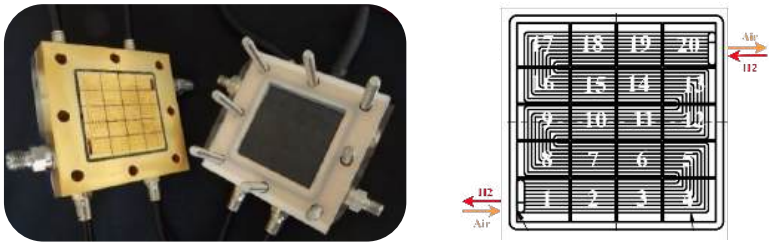


Figure 1. Photo of the segmented cell (left) and schematic representation of the segments and gas flow (right).

Results:

Fe^{3+} contamination leads to a clear degradation of electrochemical performance, which increases with cation concentration. This degradation is primarily associated with a reduction in proton conductivity, reflected by an increase in high-frequency resistance, particularly under low relative humidity conditions.

At higher contamination levels (R = 0.5), voltage losses extend across the entire current density range, with strong impacts at low humidity, highlighting the sensitivity of ionic conduction to hydration. Spatially resolved measurements reveal pronounced heterogeneities, with reduced current densities in contaminated regions and partial propagation to adjacent areas, indicating cation redistribution within the MEA through diffusion and electromigration.

Under accelerated stress conditions, the system evolves toward more pronounced and potentially irreversible degradation. This includes further performance decay over time, possible deterioration of

membrane conductivity, and emerging links between high-frequency resistance and membrane aging. However, structural degradation remains limited, suggesting that performance losses are initially dominated by physicochemical effects (cation-induced transport and kinetic limitations) rather than mechanical failure, at least in the tested operating conditions.

Overall, the results highlight a dominant "hindrance" effect at early stages - where cations hinder ionic and reactive pathways - followed by a transition toward long-term degradation mechanisms under sustained operating conditions.

Conclusions:

Fe^{2+} contamination induces spatially heterogeneous degradation in PEMFCs through coupled transport and chemical mechanisms. Initial performance losses are governed by reversible ionic effects, while prolonged operation leads to irreversible degradation driven by radical-induced membrane damage and catalyst deterioration. Spatially resolved diagnostics reveal cation redistribution and local degradation phenomena that are not accessible with conventional methods. These results highlight the importance of controlling contamination and improving durability strategies for PEMFC systems.

Acknowledgment

This work was carried out within the ANR DeliCat project (ANR-22-CE05-0031), in collaboration between LEMTA, LEPMI, and SYMBIO. The authors acknowledge the technical teams for their support. The authors also thank Kévin Mozet from Métro'NRJ – LEMTA (Université de Lorraine-CNRS – https://lemta.univ-lorraine.fr/).

References

[1] B. Kienitz et al., J. Electrochem. Soc. 158 (9) (2011) B1175. doi:10.1149/1.3610986.

[2] T. Tsuneda, Sci. Rep. 10 (2020) 18144. doi:10.1038/s41598-020-74646-0.

[3] J. Dillet et al., J. Power Sources 195 (9) (2010) 2795–2799. doi:10.1016/j.jpowsour.2009.10.103.

[4] D. Madhav et al., Energies 17 (5) (2024) 998. doi:10.3390/en17050998.

[5] K. Hongsirikarn et al., J. Power Sources 195 (21) (2010) 7213–7220. doi:10.1016/j.jpowsour.2010.05.005.



An investigation on the performance of pretreated sPEEK based CCB and CCM MEA for PEMFC operation

G. Etienne*[a], A. El Kaddouri*[a], J. Mainka[a], J. Dillet[a], S. Brimaud[b] and O. Lottin[a]

* corresponding author: guillaume.etienne@uniiv-lorraine.fr / assma.el-kaddouri@univ-lorraine.fr

[a] Université de Lorraine, CNRS, LEMTA, F-54000 Nancy, France

[b] Zentrum für Sonnenenergie und Wasserstoff Forschung Baden-Württemberg, Ulm, Germany

Keywords: PEMFC performance, Hydrocarbon ionomer membrane, sulfonated poly(ether ether ketone) (sPEEK), CCM/CCB MEA

Abstract

Current PEMFC systems for heavy-duty transportation are based on PerFluoroSulfonic Acid (PFSA) ionomers in both the electrodes and the membrane. Despite their high chemical stability and proton conductivity, efforts aim to develop alternatives to PFSA to reduce cost competitiveness and the dependence on fluorine-based materials because of environmental concerns, prompting research into alternative materials. Sulfonated poly(ether ether ketone) (sPEEK) is a promising alternative due to its attractive thermal and mechanical properties. Although its lower proton conductivity and chemical stability remain challenging. Nevertheless, recent studies showed that optimized pretreatment can enhance nanophase separation, improving proton conductivity [1] and overall fuel cell performance [2], although these improvements during fuel cell operation have been observed under an oxygen atmosphere. In light of these considerations, the present work aims to further assess the potential of sPEEK-based membranes in fuel cell applications.

Introduction:

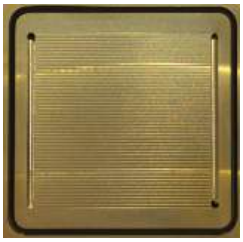
PEMFC systems are currently based on PFSA ionomers because of their high chemical stability and proton conductivity. However, efforts are underway to replace them due their cost and the environmental concerns. Sulfonated poly(ether ether ketone) (sPEEK) is considered a promising alternative, although it exhibits lower proton conductivity and chemical stability. Nevertheless, optimized pretreatment have been shown to significantly improve its performances, making it interesting for fuel cell applications.

Objectives:

Therefore, this work aims to evaluate the performance of a pretreated sPEEK membrane under various operating conditions, after a pretreatment based on previous studies [1,2]. The performance of a Catalyst Coating Backing (CCB) Membrane Electrode Assembly (MEA) as well as home-made Catalyst Coating Membrane (CCM) MEA prepared using the same pretreated sPEEK, were compared to a MEA with a PFSA-based membrane (NR211).

Material and methods

Fuel cell tests were performed using a 25 cm^2 single cell with a straight-channel flow field, operated under various operating conditions (temperature, pressure, inlet relative humidity, and air stoichiometry).



Straight parallel channels	
No. of channels	50
Anode depth	0.15 mm
Cathode depth	0.25 mm

Figure 47. Straight parallel channels cell geometry used for the study.

Fuel cell performances were evaluated by polarization curve and Electrochemical Impedance Spectroscopy (EIS). Commercial Fumapem® E730 and NR211 membranes were used as sPEEK and PFSA reference, respectively. CCB MEA were assembled by hot-pressing using Gas Diffusion Layer (GDE). For sPEEK-based MEA, a PFSA ionomer overcoat was added to GDE to ensure adhesion between the membrane and the electrodes. sPEEK-based CCM MEA were home-made according to the process described in a previous study [3]. Prior to assembly, sPEEK membranes were subjected to a "*standard*" pretreatment recommended by the supplier and a "*nanostructured*" pretreatment developed in previous studies [2].

Results

After optimizing the compression rate and conditioning step, *nanostructured* sPEEK-based CCB MEA were evaluated under various operating conditions (temperature, gas pressure, inlet relative humidity (RH), and air stoichiometry). No significant performance was observed at 95°C due to poor proton conductivity, despite the wide RH range tested (30-70%). In contrast, the best results were obtained at 70°C, highlighting a compromise between improved gas diffusion and membrane conductivity at higher temperatures, and reduced MEA hydration state. The nanostructuring of sPEEK results in significantly improved performance under air and low to moderate gas inlet RH (30-50%), due to more efficient water utilization, particularly in comparison with *standard* sPEEK. Electrochemical Impedance Spectroscopy (EIS) measurements further revealed superior cathode operation for the MEA based on *nanostructured* sPEEK, suggesting that both the membrane and the membrane-electrode interface may play a key role in cathode operation. Additional comparison with a PFSA-

based CCB MEA (NR211) showed comparable performance overall, with slightly lower voltage at low current densities but improved performance at higher current densities.

In a second stage, the performance of *nanostructured* sPEEK-based CCM and optimized CCB MEA was compared. The CCM configuration showed better performance up to medium current densities, whereas the CCB MEA performed better at higher current densities. These results suggest that the ionomer overcoat on the GDE may act as a resistive layer, reducing fuel cell performance at low current densities, while helping to maintain proton conduction and performance at high current densities.

Conclusions

These results demonstrate that an appropriate pretreatment enables sPEEK to operate under air and relatively low humidity conditions, contrary to common assumptions, with fuel cell performance comparable to that of NR211. In addition, this study demonstrates that operation of an sPEEK-based CCM under air/H_2 is feasible, with performance comparable to that of CCB MEAs fabricated with identical sPEEK or PFSA membranes. Furthermore, the results reveal a significant influence of MEA fabrication, with the PFSA ionomer overcoat having a strong impact on PEMFC performance that is highly dependent on the operating setpoints.

Acknowledgment

This study was carried out within the framework of the PEMFC95 project. The PEMFC95 project was funded by “France 2030 " operated by the French National Research Agency (grant ANR-22-PEHY-0005). The authors also thank Kévin Mozet from Métro’NRJ – LEMTA (Université de Lorraine-CNRS – https://lemta.univ-lorraine.fr/).

References

[1] H. Mendil-Jakani, I. LOPEZ, V. H. Mareau, and L. Gonon, ‘Optimization of hydrophilic/hydrophobic phase separation in sPEEK membranes by hydrothermal treatments’, Phys Chem Chem Phys, vol. 19, May 2017, doi: 10.1039/C7CP00087A.

[2] M. Daoudi et al., ‘Impact of sulfonated poly(ether ether ketone) membranes pretreatments on their physicochemical properties and fuel cell performances’, J. Polym. Sci., vol. 61, no. 9, pp. 761–776, 2023, doi: 10.1002/pol.20220649.

[3] M. S. Ripa, L. Jörissen, M. Hölzle, and S. Brimaud, ‘Catalyst Ink Solvent Composition and its Impact on Polarization of Proton Exchange Membrane Fuel Cells Under Hydrogen/Air Operation’, J. Electrochem. Soc., vol. 172, no. 5, p. 054513, May 2025, doi: 10.1149/1945-7111/add9d6.



Integrated On-Board Hydrogen Production and Fuel Cell Systems for Railway Applications: Design and Risk Assessment

Maria Portarapillo*, Maria Turco, Almerinda Di Benedetto

* corresponding author: maria.portarapillo@unina.it

Department of Chemical, Materials and Production Engineering, University of Naples Federico II, P.le Tecchio 80, 80125, Naples, Italy

Keywords: Alcohols Oxidative Steam Reforming, Ammonia Cracking, Fuel Cell, Energy Self-Sustainability in railway Systems

Abstract and Introduction: Due to the progressive decarbonization of the transport sector and the limitations of electrification for non-electrified railway lines, hydrogen-based technologies are emerging as a promising alternative to conventional diesel systems. However, their implementation requires the development of efficient, compact and safe solutions for hydrogen production, storage and utilization. Among the available technologies, proton exchange membrane fuel cells (PEMFCs) are particularly suitable for mobile applications due to their high efficiency and operational flexibility. High-temperature PEM fuel cells (HT-PEMFCs), operating in the range of 120-200 °C, offer additional advantages such as improved reaction kinetics, higher tolerance to CO and simplified water management. To overcome the challenges associated with high-pressure hydrogen storage, the in-situ production of hydrogen from alternative liquid carriers (e.g., methanol, ethanol, glycerol and ammonia) has been proposed as a safer and more practical solution for on-board railway applications.

Objectives: The aim of this work is to evaluate the feasibility of an integrated on-board railway traction system based on hydrogen production and utilization via HT-PEM fuel cells. Different hydrogen storage strategies are investigated, including liquid carriers such as methanol, ethanol, glycerol and ammonia, coupled with hydrogen production through oxidative steam reforming (OSR) or ammonia decomposition. The systems are assessed in terms of volume, weight and energy self-sufficiency, and compared with a reference configuration based on compressed hydrogen storage at 350 bar. The analysis is carried out for a representative railway application with a total traction power of 628 kW, assuming integration of the entire system within a single traction unit. A quantitative risk assessment is also performed using both empirical models and PHAST software, allowing a comprehensive comparison of the different storage and hydrogen production solutions.

Material and methods: The energy self-sufficiency of the integrated system was evaluated using Aspen Plus®, considering heat integration between the preheating, reaction and cooling stages. The heat released by the fuel cell and by product stream cooling was compared with the thermal demand required for reactant vaporization and preheating, to assess the feasibility of autothermal operation. The system was preliminarily designed for a total electrical output of 628 kW, supported by

appropriately sized Li-ion batteries, while the HT-PEMFC efficiency was assumed to be 50% based on literature data. Reactor and catalyst sizing were performed using kinetic data from the literature ([1], [2], [3]), with the catalyst volume scaled by a factor of 10 to account for dilution and quasi-isothermal operation. The total reactor volume was estimated as 2-3 times the catalyst bed, including void fraction and auxiliary components. Storage system dimensions were determined based on hydrogen production yields ([1], [2], [3]), while fuel cell volume was estimated using commercial specifications. A quantitative risk assessment (QRA) was carried out using both traditional empirical models [4], [5] and PHAST software, enabling a comparative evaluation of accident scenarios and model predictions for the different hydrogen storage solutions.

Results: The electrical system, based on HT-PEM fuel cells and Li-ion batteries, was dimensioned by simulating the Brescia-Edolo railway line using conventional train kinematics equations [6]. A battery capacity of 400 kWh was selected to meet peak power demands, while the fuel cell system was sized according to the average power requirement. For the reference case with compressed hydrogen storage at 350 bar, the total system weight is approximately 20 tons, with about 50% attributed to Type IV storage tanks, highlighting the significant impact of high-pressure storage on system design. In contrast, systems based on liquid hydrogen carriers show reduced weight and improved compactness: methanol and ammonia configurations reach approximately 14 tons, while ethanol requires about 17 tons. Glycerol-based systems are not suitable for on-board applications due to the large system volume, which approaches the maximum capacity of the train carriage, and the high CO content in the reformate, requiring additional purification units and further increasing system complexity. All the remaining configurations are compatible with railway constraints in terms of volume and allowable weight. The use of liquid fuels stored at near-ambient conditions represents a safer and more practical alternative to high-pressure hydrogen storage. Although the presence of reforming by-products (e.g. CO, CO_2, N_2) slightly affects fuel cell performance [7], hydrogen-rich reformate (>50%) can be directly utilized in HT-PEMFC systems with limited efficiency penalties.

From a safety perspective, significant differences emerge among the considered fuels. Ethanol exhibits the lowest risk index, with pool fire as the main hazard, while methanol and ammonia are primarily associated with toxic dispersion scenarios. Hydrogen, instead, shows a higher explosion potential under accidental release conditions. Overall, the ranking of the different solutions strongly depends on the fuel production pathway: ethanol represents the safest option, followed by methanol and ammonia, while hydrogen storage shows higher risk levels due to pressurized conditions. Comparison between empirical models and PHAST simulations highlights notable discrepancies in some scenarios, confirming the importance of adopting a multi-model approach for reliable risk assessment.

Conclusions: The sizing and integrated assessment of on-board hydrogen production systems coupled with HT-PEM fuel cells for the Brescia-Edolo railway line demonstrate the technical feasibility of alternative hydrogen carriers such as methanol, ethanol and ammonia. All the investigated

configurations can achieve autothermal operation, eliminating the need for external heat supply. By combining design constraints and safety analysis, ethanol-based systems emerge as the most promising solution, offering the best compromise between system integration, operational safety and overall performance. These results highlight the potential of in-situ hydrogen production as a viable pathway for the development of sustainable and safe railway propulsion technologies.

Acknowledgment

This study was carried out within the MOST – Sustainable Mobility National Research Center and received funding from the European Union Next-GenerationEU (PIANO NAZIONALE DI RIPRESA E RESILIENZA (PNRR) – MISSIONE 4 COMPONENTE 2, INVESTIMENTO 1.4 – D.D. 1033 17/06/2022, CN00000023). This manuscript reflects only the authors' views and opinions, neither the European Union nor the European Commission can be considered responsible for them.

References

[1] S. J. Kim, T. S. Nguyen, J. Mahmood, and C. T. Yavuz, "Sintering-free catalytic ammonia cracking by vertically standing 2D porous framework supported Ru nanocatalysts," Chem. Eng. J., vol. 463, no. March, p. 142474, 2023, doi: 10.1016/j.cej.2023.142474.

[2] S. Bac, S. Keskin, and A. K. Avci, "Recent advances in materials for high purity H2 production by ethanol and glycerol steam reforming," Int. J. Hydrogen Energy, vol. 45, no. 60, pp. 34888–34917, 2020, doi: 10.1016/j.ijhydene.2019.11.237.

[3] L. Selva Roselin and H. W. Chiu, "Production of hydrogen by oxidative steam reforming of methanol over Cu/SiO2 catalysts," J. Saudi Chem. Soc., vol. 22, no. 6, pp. 692–704, 2018, doi: 10.1016/j.jscs.2017.12.001.

[4] D. A. Crowl and J. F. Louvar, Chemical and Process Safety. 2002. doi: 10.1021/op3003322.

[5] Center for Chemical Process Safety (CCPS), Guidelines for Chemical Process Quantitative Risk Analysis, 2nd Edition. 1999.

[6] Joshua Peli, "APPLICAZIONE DELLE FUEL CELL PER L'ALIMENTAZIONE DI VEICOLI FERROVIARI," Politecnico Milano, 2018.

[7] T. Guan, P. Alvfors, and G. Lindbergh, "Investigation of the prospect of energy self-sufficiency and technical performance of an integrated PEMFC (proton exchange membrane fuel cell), dairy farm and biogas plant system," Appl. Energy, vol. 130, pp. 685–691, 2014, doi: 10.1016/j.apenergy.2014.04.043.



Digital Twin-Oriented Modeling and Validation of a Fuel Cell Hybrid Electric Propulsion System for Hydrogen-Based Aviation

Christian Simone*[a], Marco Sorrentino [a]

* Corresponding author: Tel: +39-347-089-9671; e-mail address: csimone@unisa.it.

[a] Department of Industrial Engineering, University of Salerno, via Giovanni Paolo II 132, Fisciano (SA), 84084, Italy.

Keywords: Proton Exchange Membrane Fuel Cell, Lithium-ion Battery, Digital Twin, Model-Based Approach, Regional Aircraft

Introduction: Fuel cell (FC) hybrid-electric aircraft represent a highly promising pathway toward zero-emission aviation [1]. The seamless integration of the proton-exchange membrane fuel cell system (PEMFCS), the battery pack, and their auxiliary systems is crucial for optimal power management within the powertrain. To streamline this process, digital twins (DTs) allow for rapid and accurate preliminary analyses relying on model-based approaches [2]. Moreover, since strict operational constraints are essential to extend the powertrain lifetime, a physics-aware tool is pivotal for technology deployment [3]. While recent studies offer fast dynamic models for aviation fuel cells, they often neglect full powertrain integration [4]. Furthermore, the limited availability of experimental data concerning hydrogen systems significantly hinders the development of reliable DTs [5]. Consequently, a critical gap remains for a comprehensive framework capable of ensuring system-level simulation and physical fidelity.

Objectives: This study aims to develop a scalable multi-physics model of an FC-hybrid unit tailored for aviation applications, leveraging a hierarchical modeling approach. Specifically, a physics-based PEMFCS model is employed to overcome the scarcity of experimental data, generating the dataset required to identify a reduced-order model suitable for DT-oriented simulations.

Material and methods: The proposed hierarchical approach consists of developing a physics-based model of the PEMFCS and subsequently deriving its corresponding reduced-order model. Experimental data from [6] were utilized to identify an offset voltage (V_{off}) and update the polarization curve (described in eq (1) according to [7]) of a model available within the MATLAB/Simscape environment.

$$V_{cell} = E_0 - V_{act} - V_{Ohm} - V_{conc} - V_{off} \quad (1)$$

V_{cell} represents the actual cell voltage and E_0 is the standard potential, while the subsequent terms denote the activation, ohmic, and concentration voltage drops, respectively. The identification of this updated polarization curve yielded a more accurate physics-based PEMFCS model, overcoming the ideal assumptions of the original framework by accounting for minor losses associated with the offset voltage [7]. Following the hierarchical strategy, a reduced-order model based on the efficiency-driven structure proposed by [8] was identified using a dataset generated through the physics-based one. This

reduced-order PEMFCS model was then integrated into a comprehensive simulation framework alongside the battery pack model and the control logic block. The former consisted of a 2-RC dynamic model, parameterized using hybrid pulse power characterization (HPPC) test data and validated against driving cycles from an extensive open-source dataset [9]. The mathematical formulation of this model is given by eq (2):

$$V_{batt}(t) = OCV(t) - I_{batt}(t) \cdot R_0 - I_{batt}(t) \cdot R_1 \cdot \left(1 - e^{-\frac{t}{\tau_1}}\right) - I_{batt}(t) \cdot R_2 \cdot \left(1 - e^{-\frac{t}{\tau_2}}\right) \quad (2)$$

Here, V_{batt} and I_{batt} are the battery voltage and current, respectively. OCV is the open-circuit voltage, R denotes the internal resistances and τ the time constants, modeling both the short- and long-term transient polarization dynamics. The resulting DT-oriented framework, whose electric scheme is represented in Figure 48, was tested and validated using a representative flight mission profile for a regional aircraft [10]. Finally, the resulting PEMFC power demand profile was fed back into the physics-based PEMFCS model to extract electric variables for validation, as well as physical variables to ensure constraint compliance.

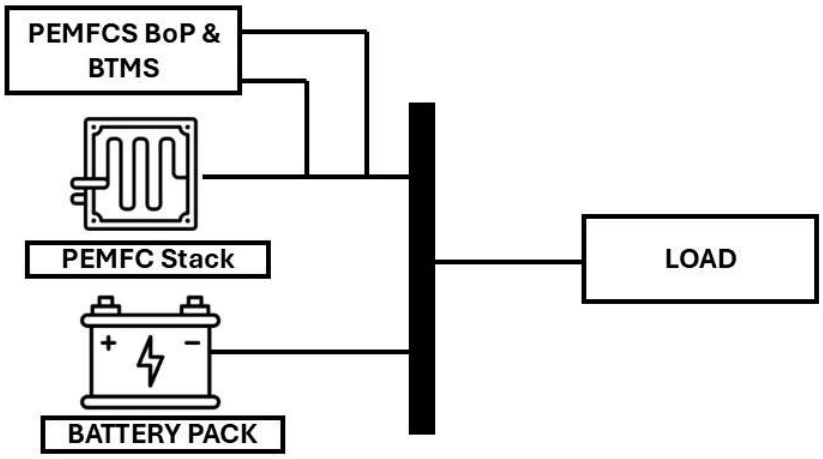


Figure 48: Electric scheme of the modeled FC-based hybrid unit. The PEMFC stack and the battery pack are the main electrochemical devices. The electrical connections, which are associated with respective power fluxes, are highlighted.

Results: Simulation results comparing the electric variables of the PEMFCS physics-based model with the efficiency-driven one show an average error of 0.63% for voltage and 0.50% for current, demonstrating the effectiveness of the hierarchical approach and ensuring the reliability of the reduced-order model to be implemented within the DT-oriented framework. Moreover, the developed simulation framework exhibits a power split behavior for both the PEMFCS and the battery that qualitatively aligns with [10], where the cell parameters were different for both devices thus not allowing a quantitative comparison. Finally, the physical variables extracted via the detailed PEMFCS model confirmed strict compliance with operational constraints throughout the flight, apart from deviations during the start-up

phase, which aligns with [3]. Overall, the robustness of the presented methodology is supported by these outcomes.

Conclusions: In this work, a scalable DT-oriented modeling framework for aviation FC-hybrid powertrains has been established. Overcoming the challenge of experimental data scarcity, this tool represents a crucial enabler for next-generation aviation technologies. Indeed, it paves the way for future model-based design and control, providing a robust foundation for the constrained optimization of flight performance, fuel economy, and the operational lifetime of fuel cell-based aircraft.

Acknowledgment

The University of Salerno is kindly acknowledged for the support provided in the development of this work.

References

[1]. Marksel, M., and Prapotnik Brdnik, A. Maximum Take-Off Mass Estimation of a 19-Seat Fuel Cell Aircraft Consuming Liquid Hydrogen. Sustainability. Volume 14, article no. 8392, 2022. https://doi.org/10.3390/su14148392.

[2]. Aliberti, P., Simone, C., Addesso, P., De Piano, G., Donsì, F., Galdi, A., Maritato, L., Pantani, R., Pianese, C., Polverino, P., Postiglione, F., and Sorrentino, M. Fuel cells in aviation: challenges to power the future of flight. Energy Convers. Manag. X. Volume 29, article no. 101426, 2026. https://doi.org/10.1016/j.ecmx.2025.101426.

[3]. Bove, G., Aliberti, P., Simone, C., and Sorrentino, M. Multilevel Control Strategy Design and Optimization for Fuel Cell Hybrid Heavy-Duty Vehicles. SAE Technical Paper. article no. 2025-24-0107, 2025. https://doi.org/10.4271/2025-24-0107.

[4]. Dotzauer, N. A. Dynamic Modeling of Fuel Cells for Applications in Aviation. Eng. Proc. Volume 90, article no. 68, 2025. https://doi.org/10.3390/engproc2025090068.

[5]. Ramírez-Cruzado, A., Ramírez-Peña, B., Vélez-García, R., Iranzo, A., and Guerra, J. Data from Experimental Analysis of the Performance and Load Cycling of a Polymer Electrolyte Membrane Fuel Cell. Data. Volume 5, article no. 47, 2020. https://doi.org/10.3390/data5020047.

[6]. Lohse-Busch, H., Duoba, M., Stutenberg, K., Iliev, S., Kern, M., Richards, B., Christenson, M., and Loiselle-Lapointe, A. Technology Assessment of a Fuel Cell Vehicle: 2017 Toyota Mirai. Technical Report, U.S. Department of Energy, June 2018. https://www.osti.gov/biblio/1460541.

[7]. Arsie, I., Di Domenico, A., Pianese, C., and Sorrentino, M. Modeling and Analysis of Transient Behavior of Polymer Electrolyte Membrane Fuel Cell Hybrid Vehicles. J. Fuel Cell Sci. Technol. Volume 4, pp. 261–271, 2007. https://doi.org/10.1115/1.2743071.

[8]. Aliberti, P., Minneci, M., Sorrentino, M., Cuomo, F., and Musto, C. Efficiency-based modeling of aeronautical proton exchange membrane fuel cell systems for integrated simulation framework applications. *Energies*. Volume 18, no. 4, article no. 999, 2025. https://doi.org/10.3390/en18040999.

[9]. Kollmeyer, P., Naguib, M., and Skells, M. LG 18650HG2 Li-ion Battery Data. Mendeley Data. V2, 2020. https://doi.org/10.17632/b5mj79w5w9.2.

[10]. HECATE. Hybrid Electric regional Aircraft distribution Technologies. Project Website, https://hecate-project.eu/; 2025 [accessed 11 May 2026].



Effect of Air Contact Layer Thickness on Oxygen Transport and Current Density Distribution in Solid Oxide Cells

I. Chowdhury, S. Zhang, R. C. Samsun, R.-A. Eichel

Institute of Energy Technologies (IET-1), Forschungszentrum Jülich GmbH, 52428 Jülich,
i.chowdhury@fz-juelich.de

Keywords: Solid Oxide Cells (SOCs), Hydrogen, Electrochemistry, Modeling

Solid oxide cells (SOCs) are electrochemical devices used for efficient energy conversion and hydrogen production. They can operate as solid oxide fuel cells (SOFCs) for electricity generation or as solid oxide electrolysis cells (SOECs) for hydrogen production. Because of their high operating temperature, SOCs offer high efficiency and fuel flexibility. However, strong gradients of physical parameters and non-uniform current density inside the cell can accelerate material degradation and reduce cell lifetime [1]. Transport processes in SOCs depend strongly on the geometry of the cell layers. One important component is the air contact layer (ACL), which connects the air electrode to the interconnect ribs. This layer distributes electrical current and provides a path for oxygen transport from the air channel to the electrode. Therefore, ACL thickness can influence both oxygen availability and the current density distribution inside the cell. In practical stack designs, reducing ACL thickness can lower material usage and cost. However, if the layer becomes too thin, oxygen transport may be limited, and strong local current peaks may appear. These effects can influence both cell performance and durability. In this work, the influence of ACL thickness on oxygen transport and current density distribution is investigated for both SOFC and SOEC operation.

Methods and Methodologies: A 3D Multiphysics modeling framework in COMSOL Multiphysics was developed to simulate transport processes and electrochemical reactions inside a planar SOC. The modeling approach and geometric parameters are adopted from a previous study [3], and the same experimental operating conditions of stack F1004-67 are used in this study. The model includes the main cell components: metallic interconnect (MIC), fuel support, fuel electrode, electrolyte, air electrode, and ACL [3]. Air channels and ribs are also included in the geometry. The model simultaneously solves the governing equations for mass transport of gaseous species, momentum transport, ionic and electronic charge transport, and electrochemical reactions at the electrodes. Transport of concentrated species is modeled using Maxwell-Stefan equation, and Knudsen diffusion is incorporated in the model via an effective diffusion coefficient [3]. A linear expression of electrochemical kinetics is used from a previous study [3]. All physical processes are fully coupled within a 3D finite-element framework, allowing simultaneous solution of multiphysical transport and electrochemical phenomena. The governing equations are discretized using the finite element method, and steady-state solutions are obtained using a fully coupled nonlinear solver implemented in COMSOL. The model is used to evaluate spatial distributions of current density, oxygen partial pressure, and oxygen pressure drop across ACL.

Observed Results: The investigation is done on a planer solid oxide cell as shown in Figure 1(a) with a counterflow arrangement. The simulations show that the ACL thickness strongly affects current density distribution during SOFC operation. For a cell design with a 100 µm ACL thickness, noticeable lateral variations in current density occur due to the presence of the air channel, as shown in Figure 1(b). Electrical current cannot pass through the air channels and therefore concentrates near the rib edges. This results in local current density peaks near ACL as indicated by the red dotted circles in Figure 1(b).

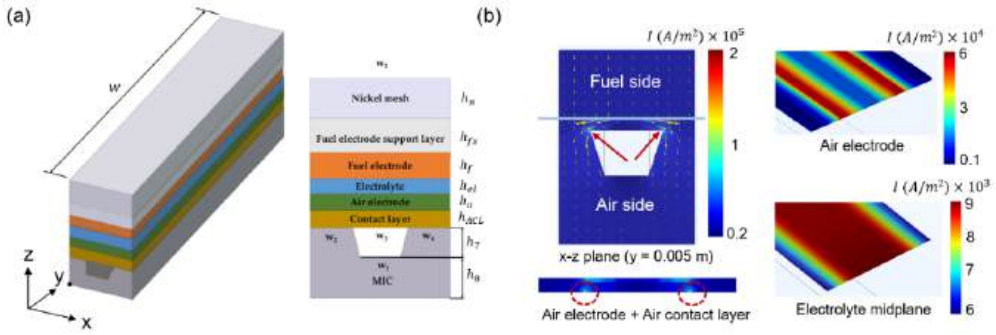


Figure 1: (a) 3D and 2D geometry of a planar solid oxide cell. b) Current density distribution in x-z plane (y = 0.005 m), air electrode, ACL and at the electrolyte mid-plane for SOFC operation at a mean current density of $i = 8000\ A/m^2$ and ACL thickness of $h_{ACL} = 100\ \mu m$

These peaks can reach up to two orders of magnitude higher than the applied current density near the ribs, as shown in Figure 1(b). During SOFC operation, internal current flows from the fuel side to the air side through the electrolyte, air electrode, and ACL (refer Figure 1(b)). The mean current density at the electrolyte mid-plane remains consistent with the cell voltage. However, local current density increases by roughly one order of magnitude at the air electrode and by an additional order at the ACL, due to the electrical obstruction created by the air channel (refer Figure 1(b)). Increasing ACL thickness improves current density uniformity at the electrolyte mid-plane. A thicker ACL provides a larger path for lateral current distribution, reducing the propagation of local peaks toward the electrolyte.

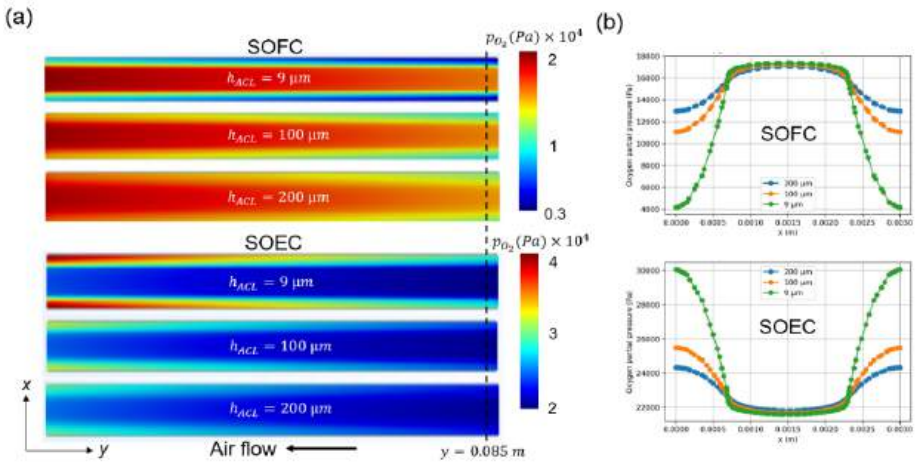


Figure 2 : (a) O_2 partial pressure distribution at ACL in SOFC and SOEC operation ($I = 4000\ A/m^2$) for different ACL thicknesses ($h_{ACL} = 9\ \mu m$, $100\ \mu m$ and $200\ \mu m$), and b) Variation of O_2 partial pressure at ACL in the lateral direction close to the entrance (y = 0.085 m) of air

Oxygen transport also depends on ACL thickness, as shown in Figure 2(a). For thinner layers, oxygen supply to regions above the ribs is limited. As shown in Figure 2(b), during SOFC operation with a thin

ACL, the region near the air entrance can reach an oxygen partial pressure as low as 0.04 atm. For 9 µm ACL configuration, oxygen partial pressure approaches zero in some areas at a mean current density of 6000 A/m^2, resulting in a limitation on current density. For an operating current density of 8000 A/m^2, the ACL thickness should be above 60 µm to avoid oxygen starvation. A recommended ACL thickness for safe SOFC operation is found to be above 100 µm. Despite these variations in current distribution, overall cell performance changes only slightly with ACL thickness, because the electrolyte dominates the total ohmic resistance, which is much higher than the electrical resistance of the ACL. The oxygen pressure drop across the ACL increases with current density due to higher oxygen flux. For a fixed current density (e.g., 6000 A/m^2), the pressure drop also increases with ACL thickness, following Fick's law. While this increases vertical diffusion resistance, it allows oxygen to spread laterally. Consequently, a thicker ACL improves lateral oxygen distribution, supporting a more uniform current density. For SOEC operation, the effect of ACL thickness is much smaller. The current density distribution remains fairly uniform across different ACL thicknesses, with lateral fluctuations of around 100–200 A/m^2, compared to 2000–3000 A/m^2 in SOFC mode. This is because oxygen is produced at the electrode during electrolysis, so reaction sites do not experience oxygen shortages. Simulations show that the oxygen partial pressure remains above 0.2 atm throughout the electrode region (see Figure 2(b)), preventing oxygen starvation even with a thin 9 µm ACL. While oxygen distribution improves slightly with thicker ACLs, the effect on current uniformity is minimal. Overall, a thin ACL in SOEC operation does not impose any current density limitations.

Summary: This study provides a detailed numerical analysis of how the ACL influences oxygen transport and current distribution in SOCs. A key outcome is the identification of a minimum ACL thickness required to prevent oxygen starvation during SOFC operation. ACL thickness above 100 µm is recommended for safe SOFC operation. This finding offers a practical design guideline for improving current density uniformity and enhancing cell durability. A comparison of SOFC and SOEC operation with respect to ACL thickness sensitivity indicates that SOFC performance is strongly affected by ACL thickness due to oxygen starvation and current density limitations. In contrast, SOEC operation is much less sensitive, with no oxygen starvation issues, as oxygen is generated directly at the triple phase boundary (TPB) sites. This difference suggests that ACL thickness requirements can be optimized based on the intended operating mode. Finally, the developed 3D Multiphysics modeling framework provides a useful tool for evaluating design parameters and guiding the development of more reliable and cost-effective SOC systems. Future studies could extend this framework to investigate thermal effects and transient operations.

Acknowledgements: The authors like to acknowledge Shangzhe Yu for providing detailed modeling parameters. This work was funded by the German Federal Ministry of Research, Technology and Space (BMFTR) within the project "PHOENIX – Launch Space Power-to-X" under the grant number 03SF0775A.

References:

1. Z. Wu, et al., *Chemical Reviews*, 125(4), 2184-2268 (2025)
2. Y. Ma, et al., *Journal of Power Sources*, 655, 237876 (2025)
3. S. Yu, et al., *Energies*, 16(9), 3827 (2023)



Dynamic Simulation and Optimization of a PEMFC-Battery Fast Ferry on a Real Italian Route

Giuliano Agati*[,a], Domenico Borello[a], Luca Cedola[a], Giulio Lo Re[a], Franco Rispoli[a], Paolo Venturini[a]

* corresponding author: giuliano.agati@uniroma1.it

[a] Department of Mechanical and Aerospace Engineering, Sapienza University of Rome, 00184, Rome, Italy

Keywords: Fast ferries, Hydrogen propulsion, PEMFC-battery powertrain, Techno-economic optimization

Abstract: This study presents a route-based dynamic simulation and techno-economic optimization framework for the design of PEMFC-battery fast ferries. The methodology integrates vessel dynamics, component sizing, rule-based energy management, and degradation-aware lifecycle cost assessment in a unified framework. The approach is applied to the Airone Jet, a 36.5 m high-speed catamaran operating on the Napoli-Capri route. For the analysed mission, the optimization identifies a feasible cost-optimal PEMFC-battery architecture with a nominal fuel-cell power of 1171.93 kW, a battery capacity of 2021.43 Ah, and a specific cost of 17.79 €/km. The results highlight the strong influence of battery mass, duty cycle, and component replacement costs on the final optimum.

Introduction: The maritime sector is under increasing pressure to reduce greenhouse gas and pollutant emissions, especially in short-sea passenger transport, where ferries operate on repetitive missions and in environmentally sensitive coastal areas. In this context, hydrogen-based propulsion is attracting growing interest, since PEM fuel cells can enable zero-emission operation at the point of use and can be effectively coupled with batteries to manage load fluctuations and peak power demand. Recent studies have addressed the topic from different perspectives, including broad retrofit pathways for shipping decarbonization [], real-world demonstration of hydrogen-powered ferries [2], preliminary retrofit-oriented design and layout studies for PEMFC-battery vessels [3], and techno-economic analyses of hydrogen-based fast ferries [4,5]. However, the available literature is still fragmented. Most existing studies focus on demonstration, retrofit feasibility, or static architecture comparisons, while less attention has been devoted to integrated tools that directly couple route-based vessel dynamics, powertrain sizing, energy management, and degradation-aware techno-economic assessment for PEMFC-battery fast ferries.

Objectives: This work develops and applies a dynamic simulation and techno-economic optimization framework for the design of a PEMFC-battery fast ferry on a real route. The Napoli-Capri case study is used to identify the cost-optimal hybrid architecture while accounting for vessel dynamics, onboard mass, energy management, component degradation, and replacement costs over the system lifetime.

Models and numerical details: A general MATLAB-based dynamic simulation and optimization framework was used to size hybrid marine powertrains for assigned vessel missions. Starting from route characteristics, vessel data, and sea-state conditions, the tool computes the propulsion power demand through a time-resolved vessel dynamic model, sizes the onboard components, simulates their operation through a rule-based Energy Management System (EMS), verifies mission feasibility, and evaluates the cost function within a surrogate-assisted optimization loop. Here, the framework is applied to the Airone Jet, a 36.5 m high-speed catamaran operating on the Napoli-Capri route. The analysis is restricted to PEMFC-battery configurations, with hydrogen storage iteratively updated according to the simulated mission demand. The optimization identifies the cost-optimal architecture by accounting for fuel-cell sizing, battery capacity, onboard hydrogen requirement, total powertrain weight, and lifetime replacement costs.

Results: Table 1 summarizes the cost-optimal PEMFC-battery configuration obtained for the Napoli-Capri route. The optimal solution is characterized by a nominal fuel-cell power of 1171.93 kW and a battery capacity of 2021.43 Ah, yielding a specific cost of 17.79 €/km. As expected, the battery mass (28 t) is significantly higher than both the fuel-cell system mass (2.0 t) and the hydrogen storage mass (3.6 t), showing that onboard electrochemical storage plays a major role in the system-level design. Moreover, the predicted 3 battery replacements and 4 fuel-cell replacements over the lifetime confirm that degradation and replacement costs are non-negligible drivers of the techno-economic optimum.

Table 8. Optimal sizing results for the PEMFC-battery fast ferry on the Napoli-Capri route.

Parameter	Symbol	Value	Unit
FC nominal power	$P_{\text{nom,FC}}$	1171.93	kW
Battery capacity	C_{batt}	2021.43	Ah
Battery mass	m_{batt}	28.0	t
Fuel-cell system mass	m_{FC}	2.0	t
Hydrogen storage mass	$m_{\text{H}_2\text{,storage}}$	3.6	t
Battery replacements	$N_{\text{repl,batt}}$	3	-
Fuel-cell replacements	$N_{\text{repl,FC}}$	4	-
Specific cost	C_{spec}	17.79	€/km

The power profile of the optimal solution (Figure 1a) shows that the PEMFC operates as a quasi-steady onboard generator, while the battery covers the most demanding phases of the round-trip mission. This confirms the role of the fuel cell as a range extender operated close to a stable working point, and of the battery as the main power buffer within the rule-based EMS, enabling the system to handle rapid

load variations while limiting fuel-cell degradation. The SOC evolution (Figure 1b) further highlights the demanding duty cycle of the battery: although the mission is successfully completed, the minimum SOC drops to about 0.02, indicating intensive battery utilization during the most critical phases.

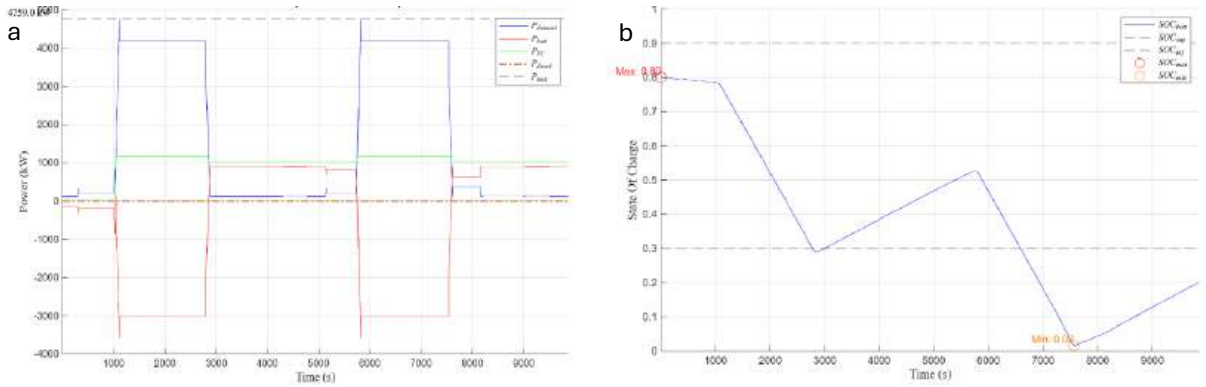


Figure 49.Simulated power demand, onboard power split (a), and battery SOC (b) for the optimal PEMFC-battery fast-ferry solution.

Conclusions: A dynamic simulation and techno-economic optimization framework was developed for the design of PEMFC-battery fast ferries on real routes. For the Napoli-Capri case study, the method identified a feasible cost-optimal architecture and highlighted the strong influence of degradation and replacement costs on the final design. Future work will focus on extending the analysis to different hydrogen refuelling frequencies in order to assess their impact on the optimal hybrid configuration.

Acknowledgment: This work was carried out within the MIMIT-funded AIRONE 5.0 project (Hybrid Vessel for High-Speed Maritime Transport), Project code: F/350062/01-03/X60. The authors gratefully acknowledge Alilauro S.p.A. and Lauro.it for their technical support.

References

[1] A.A. Kondratenko *et al.*, "Existing technologies and scientific advancements to decarbonize shipping by retrofitting," *Renewable and Sustainable Energy Reviews*, 212 (2025), 115430.
[2] E. Van Sickle *et al.,* "MV Sea Change: The first commercial 100% hydrogen fuel cell passenger ferry in the world," *International Journal of Hydrogen Energy*, 105 (2025), 389-404.
[3] G. Di Ilio *et al.,* "Towards the design of a hydrogen-powered ferry for cleaner passenger transport," *International Journal of Hydrogen Energy*, 95 (2024), 1261-1273.
[4] D. Melideo, U. Desideri, "The use of hydrogen as alternative fuel for ship propulsion: A case study of full and partial retrofitting of roll-on/roll-off vessels for short distance routes," *International Journal of Hydrogen Energy*, 50 (2024), 1045-1055.
[5] M. Mojarrad, *et al.,* "Technical and cost analysis of zero-emission high-speed ferries: Retrofitting from diesel to green hydrogen," *Heliyon*, 10 (2024), e27479.



Comparing the efficiency of a hybrid ice vehicle fuelled with hydrogen with a fuel cell vehicle, based on a simulation model

Fernando Ortenzi*[a], Dario Aliberti[b], Carla Menale[a], Francesco Vitiello[a]

* Corresponding author: fernando.ortenzi@enea.it

[a] ENEA Italian National Agency for Energy, New Technologies and Sustainable Economic Development, C.R. Casaccia, Rome, Italy;

[b] Max Racing Team

Keywords: Hydrogen, fuel cells, Internal combustion engines, vehicle

Abstract: The aim of this paper is to compare the performances, in terms of efficiency, of hybrid internal combustion engine vehicles fueled with hydrogen and fuel cell vehicles. The potential advantages, in using the ICEs, in a parallel hybrid powertrain, even if its efficiency is lower than fuel cell one, are the more efficient transmission efficiency, due to the fact that the engine is directly connected to the wheel through a gearbox, that has traditionally a very high efficiency, while the storage system help the engine when its efficiency is very low, recovering also energy during regenerative brakes. A fuel cell vehicle is generally a series hybrid vehicle, where the fuel cell has a higher efficiency than ICE, but the energy conversion from fuel cell to the electric motor has a lower efficiency. The expected result of this comparison is that the ICE hydrogen fueled can recover the great part of the efficiency Gap with a higher powertrain efficiency. The study has been made using an in-house simulation code written in ENEA, using as input data the characteristics of two different vehicles, with their electric subsystems (battery storage, electric motors, converters etc.) control strategies running fixed driving cycles (e.g. the WLTC driving cycle) and comparing the fuel consumption and efficiency.

Introduction: The rapid growth of the global vehicle fleet, together with strict decarbonization policies such as the EU *Fit for 55* packages, poses major technological, economic and geopolitical challenges. Full electrification is constrained by high vehicle costs, supply-chain dependencies on non-European manufacturers, employment impacts, and life-cycle CO_2 emissions associated with battery production. These issues are particularly critical for heavy-duty and long-range vehicles, where battery mass and charging requirements remain limiting factors.

Within this framework, hybrid powertrains powered by hydrogen are investigated as a transitional and potentially long-term solution. Hydrogen enables near-zero tank-to-wheel emissions while preserving much of the existing industrial know-how related to internal combustion engines. The study compares two hydrogen-based hybrid configurations through simulation:a Fuel Cell Hybrid Electric Vehicle (FC-HEV) with a series architecture and a Hydrogen Internal Combustion Engine Hybrid Electric Vehicle (H_2-ICE-HEV) with a parallel architecture.

Objectives: The objective is to assess whether a hydrogen-powered ICE hybrid can achieve efficiency levels comparable to fuel-cell-based hybrids and thus represent a viable alternative for sustaining ICE technology in a low-emission future.

Methodology: All analyses are performed using Vehicle Sim [1] [2], an in-house simulation code developed at ENEA in Visual Studio. The software evaluates vehicle performance over standard driving cycles with user-defined time resolution, accounting for vehicle mass, aerodynamics, drivetrain characteristics, energy storage systems and auxiliary loads. Both fuel cells and internal combustion engines are represented by three-dimensional efficiency maps (efficiency vs. load and speed). Simulations are conducted on the WLTC class 3b driving cycle, representing light-duty vehicles. To ensure comparability between configurations, all simulations are performed under charge-sustaining (battery ΔSOC ≈ 0) conditions, achieved by repeating ten consecutive cycles and analyzing the final ones.

Results: a comparison of both powertrains is reported in Figure 50: the primary sources of power (FC in FCEV vehicle and the ICE in the H2-ICE vehicle) have a totally different behavior; more smoothed for FC, where all the transients have been covered by battery, while for the ICE is opposite, with ICE that participates also during unsteady conditions.

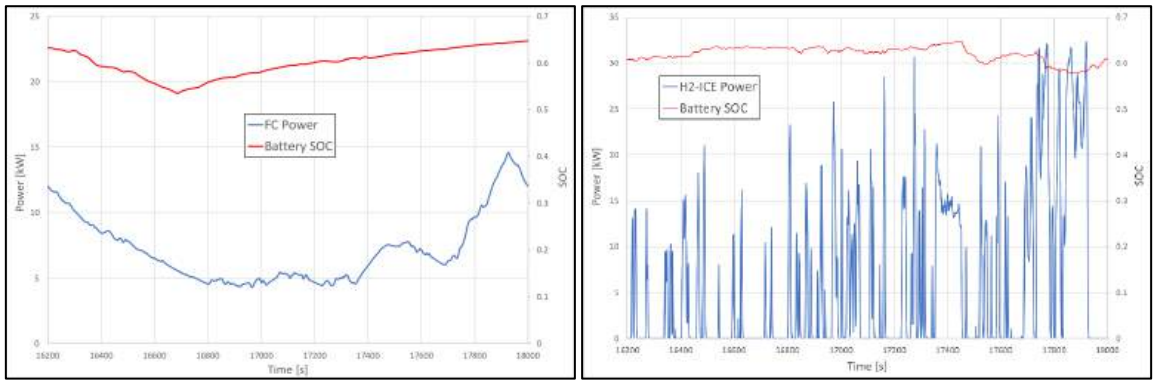


Figure 50 comparison between the two technologies in terms of Power (FC vs ICE)

Simulation results show charge-sustaining operation with SOC variations limited to ~0.01%. Graphs of ICE power, electric motor power and battery power illustrate coordinated energy flows, with the ICE compensating for regenerative braking phases and battery recharging. The peak ICE power (~32 kW) and average power (~18 kW) align with WLTC requirements.

The final comparison (Figure 51) considers the optimized FC-HEV configuration (30 Ah battery, Load Follow with 20% cut-off) against the H_2-ICE-HEV. The FC-HEV achieves a slightly higher overall vehicle efficiency (34.8%) compared to the H_2-ICE-HEV (31.8%), corresponding to an efficiency gap of about 9%.

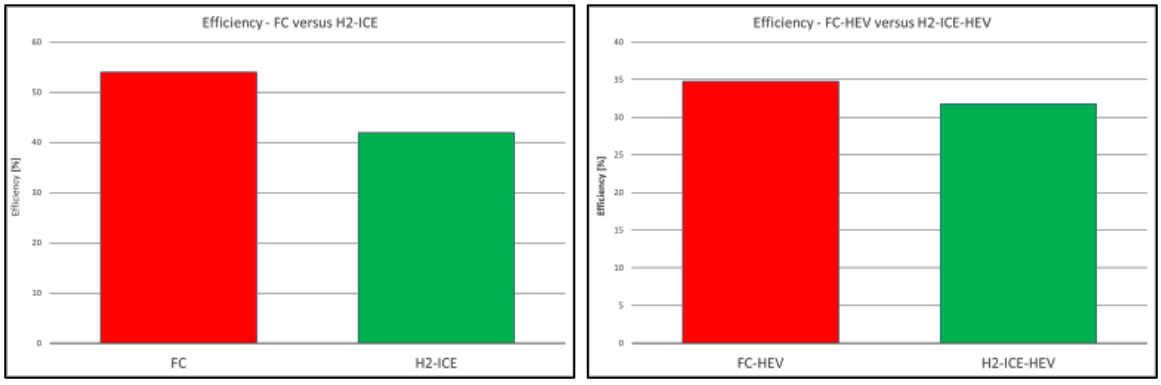


Figure 51 Efficiency of FC vs H2-ICE (left) and TTW efficiency of FC-vehicle vs H2-ICE vehicle (right)

While the fuel cell exhibits much higher peak efficiency than the hydrogen ICE, the series configuration of the FC-HEV imposes multiple energy conversion losses (converter, battery, motor). Conversely, the parallel architecture of the H_2-ICE-HEV benefits from direct mechanical coupling to the wheels with gearbox efficiencies close to 98%, partially compensating for the lower engine efficiency. Graphical comparisons highlight how architectural simplicity can offset lower component efficiency, resulting in comparable tank-to-wheel performance.

Conclusions:

The study demonstrates that hydrogen-based hybrid vehicles, both fuel-cell and ICE-powered, can achieve high efficiency levels compatible with future low-emission targets. The FC-HEV offers maximum efficiency, while the H_2-ICE-HEV shows competitive performance.

With further advances such as variable compression, turbocharging, improved combustion control, combustion chamber insulation etc., H_2-ICE efficiency could be significantly enhanced, strengthening its competitiveness in the transition toward sustainable mobility.

References

[1] C. Villante; M. Anatone; A. De Vita; F. Ortenzi; E.M. Ursitti. A New Parallel Hybrid Concept for Microcars: Propulsion System Design, Modeling and Control. SAE Technical Paper 2019-24-0246. Warrendale, PA, USA, 2019.

[2] F. Ortenzi; N. Andrenacci; M. Pasquali; C. Villante, On the Hybridization of Microcars with Hybrid UltraCapacitors and Li-ion Batteries Storage Systems, Energies 2020.



Performance evaluation of a hybrid energy system of biomass based on solid oxide fuel cell

Patsias A.[a], Ipsakis, D.[*b], Molochas, C.[c], Brouzgou, A.[*a]

* corresponding author: dipsakis@tuc.gr; amprouzgou@uth.gr

[a] *Laboratory of Hydrogen and Fuel Cell Nanotechnology, Department of Energy Systems, School of Technology, University of Thessaly, 41500, Geopolis, Larisa, Greece*

[b] *School of Production Engineering and Management, Technical University of Crete, 73100 Chania, Greece*

[c] *Laboratory of Alternative Energy Conversion Systems, Department of Mechanical Engineering, School of Engineering, University of Thessaly, Volos 38303, Greece*

Keywords: process simulation, solid oxide fuel cell, hybrid energy system, biogas fuel

Abstract. Current direct biogas-fed SOFC systems suffer from coke formation, which can be mitigated by recycling the anode and cathode off-gases. Additionally, recirculation leverages flow properties such as pressure and temperature, thereby reducing the energy requirements for heat exchangers and compressors. In this study, a process simulation was conducted in Aspen HYSYS across four scenarios: without recirculation, with anode off-gas recirculation, with cathode off-gas recirculation, and with combined anode and cathode off-gas recirculation. According to the simulation results, the configuration without recirculation and the one with cathode off-gas recirculation exhibit similar electrical efficiencies. In contrast, anode off-gas recirculation increased the system's electrical efficiency from 50% to 70% and improved fuel utilization to approximately 99%.

Introduction: Generating electricity from biogas is one of the most efficient and reliable methods for utilizing organic waste. However, the most common technologies currently used for biogas combustion, such as internal combustion engines and gas turbines, exhibit low efficiency. Biogas-fed SOFCs offer an alternative technology that directly converts the fuel's chemical energy, achieving electrical efficiencies of 60–80% (LHV). Furthermore, the overall efficiency of combined heat and power (CHP) generation can reach 80–90% through heat recovery [1, 2]. Existing biogas-fed SOFC systems suffer from carbon deposition, which clogs the anode pores, obstructs gas flow, and causes a rapid drop in performance [3]. A viable approach to mitigating carbon deposition is the recirculation of anode and cathode off-gases back to their respective inlets [4]. To this end, this study investigates novel internal reforming strategies and identifies scenarios that lead to increased energy efficiency and operational flexibility.

Objectives: This study represents the initial phase of a broader research project focused on integrating SOFC technologies with conventional biomass-based processes, specifically anaerobic digestion. To this end, the following objectives are established.

- To develop a process flow diagram for combined heat and power (CHP) production using an SOFC system.
- To simulate the process in Aspen HYSYS and identify operational scenarios that lead to increased energy efficiency and operational flexibility.

Methodology: Figure 1 illustrates the simulation of a biogas-fed SOFC with and without recirculation control. Four distinct scenarios are analyzed: i) no recirculation in either the anode or cathode, ii) recirculation limited to the anode, iii) recirculation limited to the cathode, and iv) recirculation applied to both the anode and cathode. The analysis is based on the following assumptions: the SOFC operates at 800 °C; the initial feed stream is mixed with the recirculated flow in a mixer to recover unreacted methane (CH_4) and the hydrogen (H_2) produced at the anode; and all potential methane reforming reactions are taken into account. [5]; in the scenario where the system fully utilizes recirculation, the RCY1-GAS stream is identical to the RCY1-GAS-TO-MIX1 stream; methane conversion is the same for all scenarios. At the cell's operating temperature of 800 °C, the literature specifies a steam-to-carbon (S/C) ratio of 2 to prevent carbon deposition; therefore, the model was developed by maintaining this constant ratio [6]. The latter stream is directed to the mixer along with the biogas feed, completing the cell's anode loop. Moreover, the O_2 stream is initially introduced, alongside the cathode recirculation flow (RCY2-AIR), into a mixer, after which the combined air stream is compressed and preheated. The oxygen stream is then routed to a cooler and subsequently to a water separator to remove any moisture present in the air.

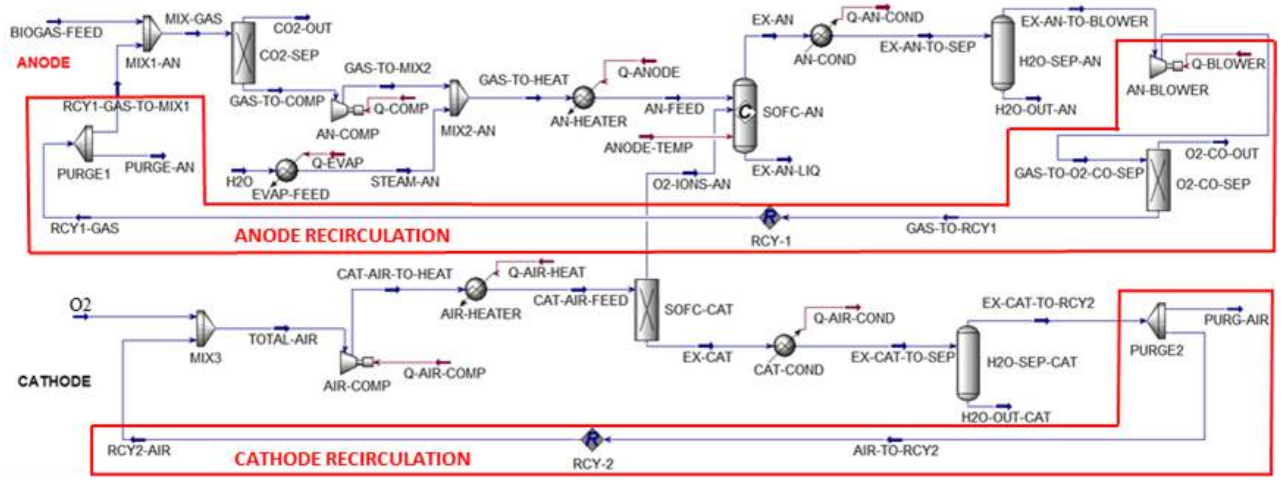


Figure 1. Aspen Hysys V10 flow diagram of a biogas fed-SOFC.

Results & Discussion: Table 1 presents the stream properties from four simulations conducted at varying recirculation rates with fixed feed flow rates. In all scenarios, a constant fresh CH_4 input ensures that variations in the anode inlet composition are solely attributed to the recirculation rate. Additionally, it is assumed that when recirculation is not utilized, the exhaust gases can be safely discharged into the environment at an appropriate temperature, following carbon monoxide (CO) purification. As demonstrated in Table 1, the implementation of anode recirculation leads to an increase in $U_{f,\,sys}$ which consequently enhances the output current. In contrast, cathode-only recirculation does not affect either the electrical efficiency or the $U_{f,\,sys}$; therefore, the performance observed in Scenario IV aligns with these expectations. Anode recirculation significantly enhances electrical efficiency, raising it from approximately 50% to around 70%, while $U_{f,\,sys}$ approaches nearly 99%.

Table 9. Results from the four adopted recirculation scenarios.

Scenario I (without recirculation)

CH_4 conversion (%)	Electrical efficiency $n_{el, sys}$ (%)	$U_{f, sys}$ (%)
85.0	54.6	75.8
75.0	47.6	66.1
65.0	41.0	56.9
Scenario II (anode recirculation)		
85.0	70.8	98.3
75.0	70.5	97.9
65.0	70.0	97.2
Scenario III (cathode recirculation)		
85.0	54.6	75.8
75.0	47.6	66.1
65.0	41.0	56.9
Scenario IV (anode & cathode recirculation)		
85.0	70.8	98.3
75.0	70.5	97.9
65.0	70.0	97.2

This increase in electricity production is attributed to the recirculation of unreacted hydrogen present in the anode-off gas. Furthermore, introducing hydrogen into the fresh methane feed stream helps prevent catalyst deactivation caused by carbon deposition.

Conclusions: The implementation of recirculation enables the recovery of unreacted methane and hydrogen present in the anode exhaust stream .An increase in the anode recirculation rate leads to a higher methane concentration at the SOFC inlet, consequently elevating the oxygen demand at the cathode.The higher fuel consumption resulting from enhanced methane utilization leads to increased electricity production.

Acknowledgments.: The research is conducted in the operating framework of the University of Thessaly Innovation, Technology Transfer Unit and Entrepreneurship Center "One Planet Thessaly", under the "University of Thessaly Grants for Scientific Publication Support" action and is funded by the Special Account of Research Grants of the University of Thessaly. Mr P.T, M.C. and Asst. Prof. B.A. are grateful to the "Thessaly 2021 -2027" in the context of Call 49 entitled "Strengthening research infrastructure and equipment of public research bodies based in Thessaly, in the priority areas of RIS3".

References

1. Ma, C.; Yu, H.; Monticone, G.; Ma, S., Wang, L. Techno-economic evaluation of biogas-fed SOFC systems with novel biogas purification and carbon capture technologies. *Renewable Energy* 2024, *235*, 121302.
2. Athanasiou, C.; Drosakis, C.; Booto, G.K., Elmasides, C. Economic feasibility of power/heat cogeneration by biogas–solid oxide fuel cell (SOFC) integrated systems. *Energies* 2022, *16*, 404.
3. Brouzgou, A.; Demin, A., Tsiakaras, P., Interconnects for solid oxide fuel cells, in: Advances in medium and high temperature solid oxide fuel cell technology, Springer, 2016, pp. 119-153.
4. Park, Y.J.; Min, G., Hong, J. Optimal method for the anode exhaust gas recycling of atmospheric solid oxide fuel cell-combined heat and power systems. *Journal of Power Sources* 2023, *567*, 232970.
5. Escudero, M.J.; Yeste, M.P.; Cauqui, M.Á., Muñoz, M.Á. Performance of a direct methane solid oxide fuel cell using nickel-ceria-yttria stabilized zirconia as the anode. *Materials* 2020, *13*, 599.
6. Wu, W.; Zhou, Z.; Wu, W.-T.; Wei, L.; Hu, C.; Li, Y.; Yang, Y.; Li, Y., Song, Y. Optimization studies of intake parameters for direct internal reforming solid oxide fuel cell. *International Journal of Hydrogen Energy* 2024, *79*, 60-72.



Development and testing of a lightweight two-phase pumped cooling system for aviation fuel cells

Henk Jan van Gerner [*,a], Georg Mühlthaler [b] and Marcus-Benedict Buntz [c]

* corresponding author: henk.jan.van.gerner@nlr.nl

[a] NLR-Royal Netherlands Aerospace Centre, 1059 CM Amsterdam, The Netherlands

[b] Airbus Commercial Aircraft, 22335 Hamburg, Germany

[c] Aerostack GmbH, 72581 Dettingen, Germany

Keywords: cooling, fuel cell, pump, two-phase

Introduction: Hydrogen-powered fuel cells are the preferred energy source for electric aircraft. For aircraft application, it is of upmost importance to reduce the mass of the fuel cell cooling system. For this reason, a novel lightweight two-phase pumped cooling system is being developed in the EU funded BRAVA project. This system uses the evaporation of methanol (the term 'two-phase' refers to the phase transition of the fluid from liquid to vapor), which can result in a mass saving of 1600 kg for a 100 passengers aircraft with four engines compared to a conventional liquid ethylene glycol water (EGW) cooling system [1].

Objectives: The project has two main objectives:

1. Built and test a lightweight two-phase pumped cooling system with 240 kW cooling capacity. This system uses electric heaters to emulate the heat load of a fuel cell system
2. Built and test a small (few kW) fuel cell stack that is cooled with a two-phase cooling (2-PC) system in order to demonstrate the compatibility of 2-PC with a fuel cell stack

Material and methods: The 240 kW system has been designed with NLR's cooling system analysis tool [2]. Figure 52 shows the calculated temperatures in a 240 kW 2-PC system with methanol as coolant. The input parameters for the model are indicated with red text, while the output is in black text. The mass flow is chosen such that 30% of the liquid flow is evaporated in the evaporator. Liquid is pumped to the evaporators, where it absorbs the waste heat from the fuel cells. As a result, the liquid temperature quickly rises until it reaches the saturation temperature, after which the liquid starts to evaporate and the temperature no longer rises. Instead, the vapor mass fraction increases along the evaporator. The liquid/vapor mixture then flows to the air-cooled condensers where it condenses back into liquid. The total mass of the cooling system (pump, fluid, tubing and air heat exchanger) is just 33 kg. Figure 53 shows a CAD drawing of the system, while Figure 54 shows a photo. The system has a liquid flowmeter, an air flowmeter and four sight glasses with cameras to monitor the flow. The fluid pressure is measured at 7 locations and a d*p* sensor is used to measure the air pressure drop over the heat exchanger.

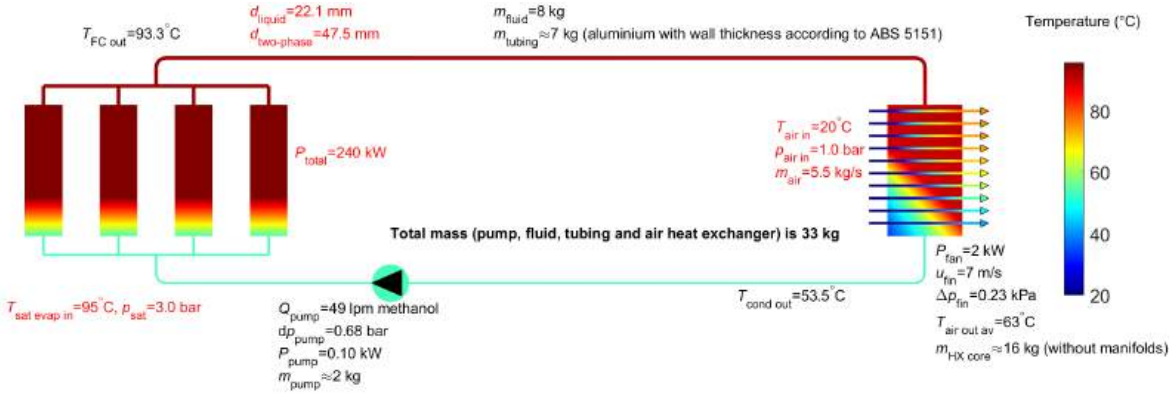


Figure 52 Calculated temperatures in the 240 kW system.

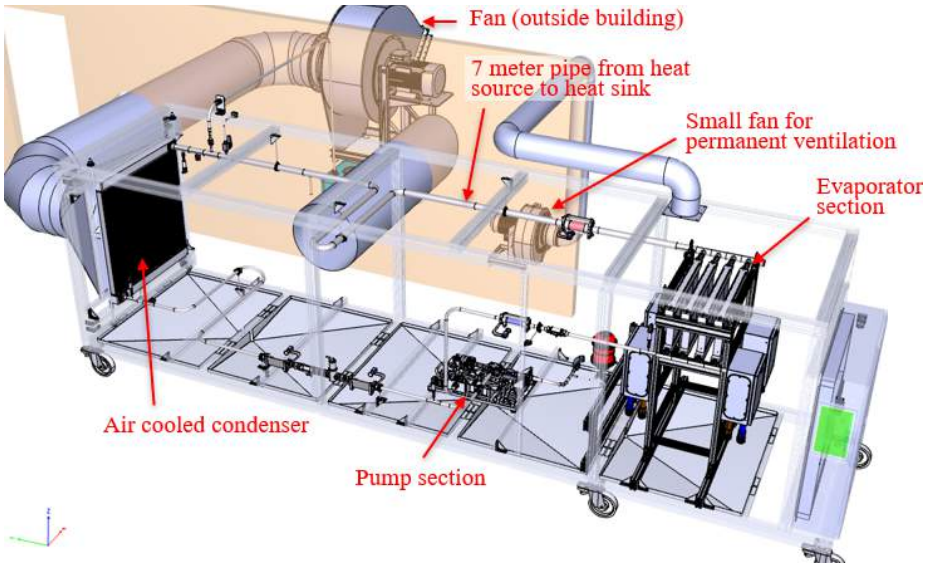


Figure 53 CAD drawing of the 240 kW system.

Results: As an example of a test result, Figure 55 shows the measured temperatures at 40 locations in the evaporator blocks while the heat load is varied from 240 kW to 120 kW and 60 kW and the fluid temperature is controlled (the dashed green line indicates the setpoint for the fluid temperature) to different values between 65°C and 100°C. The 240 kW cooling system uses electric heaters to emulate the heat load of a fuel cell and the total thermal mass of the evaporator section is similar to a fuel cell stack with 240 kW capacity. As a result, the thermal response time will be similar. In order to investigate if two-phase cooling with methanol works with a functional fuel cell, tests were caried out with two-phase cooling of an Aerostack fuel cell stack with 9 cells, see Figure 56 of a photo of an fuel cell test bench at Aerostack with a dedicated 2-PC system. All tested operating conditions showed stable operation and good cell voltages homogeneity. At system maximum power condition, approximately 3 kW of waste heat is generated by the fuel cell stack which is cooled by the 2-PC system.

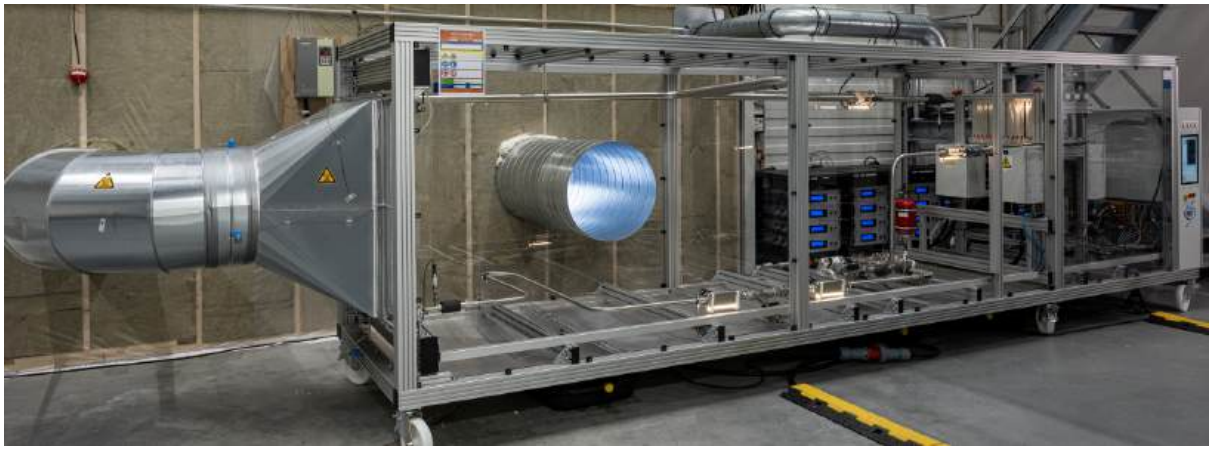


Figure 54 Photo of the 240 kW system.

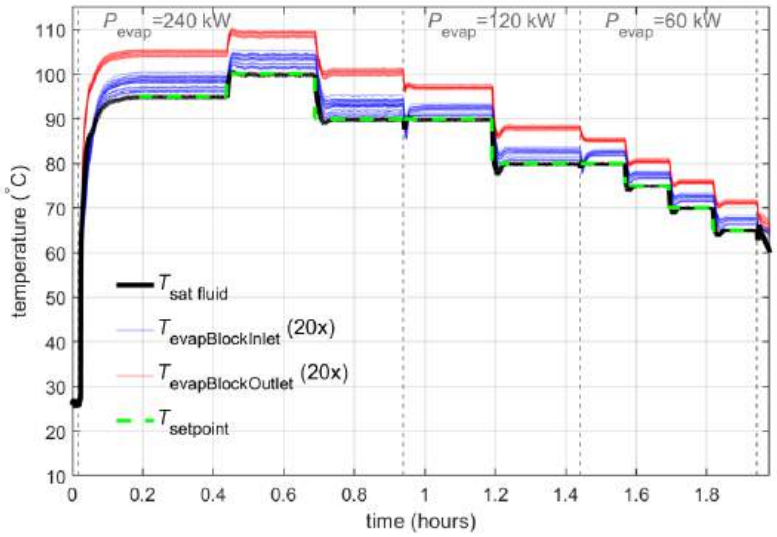


Figure 55 Measured temperatures in the evaporator blocks with varying heat load



Figure 56 Fuel cell test bench with 2-PC

Conclusions: The successful tests with the 240 kW two-phase cooling system and two-phase cooling of a functioning fuel cell successfully verified the feasibility of this new technology.

Acknowledgment: This BRAVA project is funded by the European Union's Horizon program under grant agreement number 101101409. This publication reflects the authors' views. Neither the European Union nor the Clean Hydrogen Joint Undertaking can be held responsible for them.

References:

[1] H. van Gerner, T. Luten, W. Resende, G. Mühlthaler and M. Buntz, "System Analysis and Comparison Between a 2 MW Conventional Liquid Cooling System and a Novel Two-Phase Cooling System for Fuel Cell-Powered Aircraft," Energies, 2025.

[2] H. van Gerner and N. Braaksma, "Transient modelling of pumped two-phase cooling systems: Comparison between experiment and simulation," in 46th International Conference on Environmental System, Vienna, Austria, 2016.



Electrospun PBI Membranes for HT-PEM Fuel Cells: Phosphoric Acid Uptake, Interaction Mechanisms and Preliminary Single-Cell Assessment

Emmanuel De Gregorio[a*], Carlo De Luca[c], Valentina Naticchioni[b], Viviana Cigolotti[b], Claudio Ferone[a], Elio Jannelli[a], Oreste Tarallo[c], Giuseppina Roviello[a]

* corresponding author: emmanuel.degregorio@phds.uniparthenope.it

[a] Department of Engineering, University of Naples "Parthenope", Centro Direzionale, Isola C4, 80143 Napoli, (Italy)

[b] Department of Energy Technologies and Renewable Sources (TERIN), ENEA, Via Anguillarese 301, 00123, Roma

[c] Department of Chemical Sciences, University of Naples Federico II, Complesso Universitario di Monte Sant'Angelo, via Cintia, 80126, Napoli, (Italy)

Keywords: Polybenzimidazole, HTPEM-FC, Acid Impregnation, Electrochemistry

Abstract

Electrospun polybenzimidazole membranes were prepared from a commercial PBI solution and investigated as proton-conducting electrolytes for high-temperature proton-exchange membrane fuel cells. The membranes were impregnated with phosphoric acid through a dedicated protocol based on different acid concentrations and treatment temperatures. The acid uptake process was analyzed through kinetic and thermodynamic approaches in order to clarify the interaction between phosphoric acid and the electrospun PBI network.

Preliminary single-cell tests performed at 160 °C confirmed the feasibility of using the acid-doped electrospun membranes under HT-PEMFC operating conditions. Galvanostatic electrochemical impedance spectroscopy revealed a progressive decrease in high-frequency resistance with increasing current density. This behavior suggests a gradual in situ conditioning of the membrane–electrode assembly, likely associated with acid redistribution, improved interfacial contact, and enhanced proton transport during operation, rather than a fully stabilized initial MEA state. These preliminary results indicate that electrospun PBI membranes are promising candidates for HT-PEMFCs, although dedicated activation protocols and further durability testing are required.

Introduction: Polybenzimidazole-based membranes doped with phosphoric acid are among the most established materials for HT-PEMFC operation in the 120-180 °C range because they combine thermal stability with the ability to conduct protons under low-humidity [1] or nominally dry conditions [2]. Within this framework, electrospun PBI membranes [3] are particularly attractive because their nanofibrous morphology offers high surface area, interconnected porosity, and tunable architecture,

all of which can affect acid impregnation and transport properties [4]. However, the same open fibrous structure that favors acid uptake can also make the impregnation process more complex, since acid distribution, acid retention, and local membrane morphology may depend strongly on treatment concentration, temperature, and exposure time [5]. For this reason, understanding the kinetics and thermodynamics of phosphoric acid uptake is essential not only to maximize proton conductivity but also to control the balance between membrane stability and electrochemical performance in real cell conditions.

Objectives: The objective of this work was to develop electrospun PBI membranes from a commercial PBI solution, referred to as S26, and to assess their suitability as electrolytes for HT-PEMFC operation at 160 °C.

The specific aims were:

- to optimize the electrospinning process and obtain homogeneous PBI fibrous membranes;
- to develop a controlled phosphoric acid impregnation protocol based on acid concentration and treatment temperature;
- to investigate the kinetic and thermodynamic features of acid uptake;
- to evaluate preliminary single-cell performance under HT-PEMFC conditions;
- to use galvanostatic electrochemical impedance spectroscopy to follow the evolution of the high-frequency resistance during operation.

Material and methods: Electrospun membranes were produced from a commercial PBI solution used as the precursor dope for electrospinning. After optimization of the processing conditions, uniform and reproducible fibrous membranes were obtained and used for the subsequent phosphoric acid impregnation study. Membranes of around 100 µm thick, were imbibed through an impregnation protocol that was developed by exposing the electrospun PBI membranes to different phosphoric acid solutions at different temperatures, with the aim of modulating acid uptake and clarifying the effect of operating variables on membrane loading. The interaction between acid and membrane was then analyzed through kinetic and thermodynamic approaches in order to infer the nature of the adsorption/uptake process and preliminary fuel cell tests were carried out in a single-cell HT-PEMFC configuration at 160 °C. The electrochemical measurements reported here must be considered preliminary feasibility tests rather than fully optimized performance data. GEIS measurements were performed during cell operation to monitor the evolution of the ohmic contribution, and special attention was paid to the change in HFR as a function of current density.

Results: The optimized electrospinning conditions enabled the preparation of stable and homogeneous PBI membranes suitable for post-treatment with phosphoric acid. From the kinetic and

thermodynamic analysis, the acid-membrane interaction appeared to be sufficiently strong to support the use of these electrospun membranes as HT-PEM electrolytes, while still remaining dependent on the selected operating window. Preliminary single-cell tests at 160 °C revealed promising behavior, confirming the feasibility of the electrospun PBI membranes under HT-PEMFC conditions. At the same time, the GEIS response showed a progressive decrease in HFR with increasing current density, which is consistent with a gradual *in situ* conditioning of the membrane-electrode assembly during operation rather than with a fully activated initial state. This trend supports the interpretation that proton transport pathways and acid redistribution improve under load, even in the absence of a dedicated pre-activation step.

Conclusions: Electrospun PBI membranes were successfully prepared and impregnated with phosphoric acid through a controlled treatment protocol. The combined analysis of acid uptake, kinetics, and thermodynamics provides useful information on the interaction between phosphoric acid and the fibrous PBI network. Preliminary single-cell tests at 160 °C demonstrate the feasibility of these membranes as HT-PEMFC electrolytes. The decrease in high-frequency resistance observed during galvanostatic impedance measurements suggests that the MEA undergoes progressive in situ conditioning during operation. This effect is likely related to acid redistribution and improvement of proton-conducting pathways and interfacial contact under current load. Electrospun PBI membranes thus represent promising candidates for HT-PEMFC applications. Future work should focus on defining a safe and reproducible activation protocol, optimizing acid loading and retention, and assessing long-term durability under steady-state and dynamic operating conditions.

References

[1] Araya, S.S., et al., International Journal of Hydrogen Energy, 41(46), 21310-21344, 2016

[2] Vang, J.R., et al., International Journal of Hydrogen Energy, 39(17), 14959-14968, 2014

[3] De Gregorio, E., et al., Polymers, 17(12), 1594, 2025

[4] Boaventura, M., et al., International Journal of Hydrogen Energy, 35, 11649-11660, 2010

[5] De Gregorio, E., et al., ACS Applied Energy Materials, 9(2), 938-952, 2026



Semicrystalline Syndiotactic Polystyrene Membranes for Electrochemical Applications

Alessandra Laperuta[a*], Emmanuel De Gregorio[a], Carlo De Luca[b], Claudio Ferone[a], Elio Jannelli[a], Oreste Tarallo[b], Giuseppina Roviello[a]

* corresponding author: alessandra.laperuta@phds.uniparthenope.it

[a] Department of Engineering, University of Naples "Parthenope", Centro Direzionale, Isola C4, 80143 Napoli, (Italy)

[b] Department of Chemical Sciences, University of Naples Federico II, Complesso Universitario di Monte Sant'Angelo, via Cintia, 80126, Napoli, (Italy)

Keywords: Polyelectrolyte membranes, Solid-state sulfonation, Syndiotactic polystyrene, Electrochemistry

Abstract

This work investigates the potential use of sulfonated semicrystalline syndiotactic polystyrene (sPS) films as a hydrocarbon-based proton-exchange membrane. Commercial films were sulfonated in the solid state, enabling preferential functionalization of amorphous domains while preserving crystalline regions. This approach allows tuning of ion exchange capacity (IEC) and water uptake (WU) while maintaining high crystallinity that will limit swelling and improve stability under hydrated conditions.

Introduction

Proton-exchange membrane fuel cells require electrolytes with high conductivity, chemical stability, controlled WU, and mechanical durability. PFSA ionomers are benchmarks, but cost and environmental concerns drive interest in hydrocarbon-based alternatives. A key issue in these systems is the coupling between IEC and WU: increasing sulfonation enhances conductivity but leads to excessive swelling and mechanical degradation. Controlling the spatial distribution of ionic groups while preserving structural stability is therefore essential. sPS, a semicrystalline polymer with high stability and rich polymorphic behavior, offers a promising platform. Its δ co-crystalline phase forms nanometric cavities, enabling selective sulfonation of the amorphous phase: in this way, crystalline domains act as physical cross-links to limit swelling, while the sulfonated amorphous phase provides proton-conducting pathways [4–5].

Objectives

This work aims to develop highly conductive and mechanically durable hydrocarbon-based PEMs using extruded commercial sPS films by:

- establishing a reproducible procedure for converting commercial sPS films into homogeneous δ co-crystalline membranes by solvent treatment;
- performing selective solid-state sulfonation of the amorphous domains targeting varying degrees of sulfonation;
- evaluating the impact of the preserved crystalline regions on the membrane's swelling behavior, water management, and mechanical robustness;
- correlating the resulting IEC and WU with the electrochemical performance and proton conductivity of the membranes.

Material and methods

Crystalline α-form sPS films (50 μm) were converted into δ co-crystalline phase via solvent-induced crystallization with toluene at room temperature for several days. The obtained membranes were then sulfonated in the solid state at 40 °C for 2–24 h (Figure **1**) by using a bulky sulfonating agent (C_{12} lauroyl sulfate) synthesized from lauric acid and chlorosulfonic acid (1.6 molar ratio) diluted to 20% v/v in chloroform. This bulky sulfonating agent limits functionalization to the amorphous phase, preventing diffusion into crystalline domains. The degree of sulfonation was determined by acid–base titration. WU was measured after equilibration in deionized water, while in-plane and through-plane swelling were used to assess anisotropy and dimensional stability. The semicrystalline structure of the obtained samples was then assessed by WAXD (Wide Angle X-ray Diffraction).

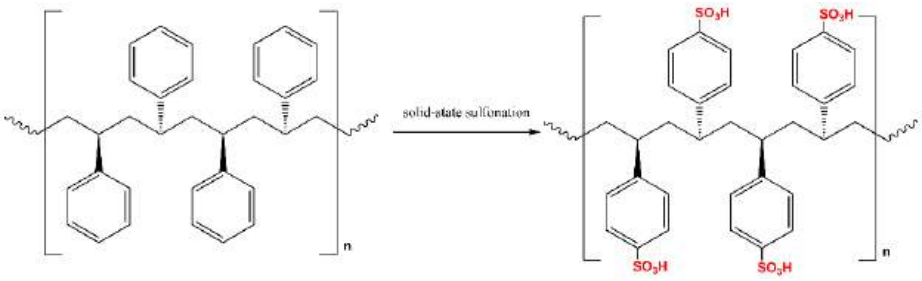


Figure 1: Schematic representation of the sulfonation reaction

Results

Solid-state sulfonation procedure was utilized to produce semicrystalline sulfonated sPS (s-sPS) membranes, which exhibited tunable IEC and WU properties (Table **1**). Increasing sulfonation time led to higher functionalization, confirming reaction time as an effective control parameter. Despite chemical modification, the membranes retained significant crystallinity, indicating that sulfonation occurs mainly in the amorphous domains. The crystalline regions act as physical cross-links, strongly influencing hydration behavior. Unlike fully amorphous sulfonated polymers, which often exhibit excessive swelling and mechanical degradation, s-sPS membranes show limited dimensional expansion, even at relatively high IEC. This combination of tunable IEC, controlled WU, and controlled

swelling suggests that semicrystalline s-sPS membranes can partially decouple ionic conductivity from mechanical instability, a key requirement for hydrocarbon-based proton-exchange membranes in electrochemical applications.

sample	w_0 (g)	V_{NaOH} (mL)	w_{wet} (g)	IEC (mol/g)	WU (%)
1	0.0394	13.3	0.1158	2.95	194
2	0.0379	13.5	0.1115	3.12	194
3	0.0389	14.5	0.1125	3.26	189
4	0.037	14.4	0.1151	3.41	211
5	0.0387	14.2	0.1214	3.21	214
6	0.0382	17.8	0.1142	4.08	199
7	0.0381	13.1	0.1121	3.01	194

Table 1: Characteristic properties of a set of 50 µm sPS membranes upon 5h 30' sulfonation

Conclusions

Solid-state sulfonation of δ co-crystalline sPS enables the preparation of semicrystalline PEMs with controlled hydrophilicity and improved dimensional stability. The bulky C_{12} lauroyl sulfate sulfonating agent is able to selectively functionalizes the amorphous phase while preserving crystalline domains. This feature enables balanced ionic transport and stability: the sulfonated amorphous phase provides WU and proton conduction, while the crystalline phase acts as a physical network that limits swelling, thus mitigating the typical trade-off between high IEC and dimensional stability in hydrocarbon membranes. These semicrystalline s-sPS membranes are promising fluorine-free, low-cost candidates for electrochemical applications.

Acknowledgment

We gratefully acknowledge Idemitsu Kosan Co., Ltd. for providing the commercial XAREC™ sPS extruded films. Financial support from Regione Campania is gratefully acknowledged through the programme "Dottorati di ricerca innovativi con caratterizzazione industriale", A.A. 2025/2026, Ciclo XLI, DGR n. 261/2025, Regione Campania, Avviso Pubblico "Dottorati di ricerca innovativi con caratterizzazione industriale" – PR Campania FSE+ 2021/2027 – Priorità 2 Istruzione e Formazione – Obiettivo specifico ESO 4.7 – Azione 2.g.4, CUP I61I25000320007.

References

[1] K. A. Mauritz, R. B. Moore, Chem. Rev. 2004, 104, 4535–4586. DOI: 10.1021/cr0207123.

[2] K. D. Kreuer, J. Membr. Sci. 2001, 185, 29–39. DOI: 10.1016/S0376-7388(00)00632-3.

[3] G. Guerra, et al Macromolecules 1990, 23, 1539–1544. DOI: 10.1021/ma00207a050.

[4] A. Borriello, et al. Chem. Mater. 2009, 21, 3191–3196. DOI: 10.1021/cm900632r.

[5] M.M. Schiavone et al. Membranes 2019, 9, 136. DOI: 10.3390/membranes9110136.



A Multi-rSOC System for Flexible Energy Management in Data Center Applications: Modeling and Configuration Analysis

Luigi Margutti*[a], Lorenzo Tulipani[b], Daniele Penchini[b], Giovanni Cinti [a]

* corresponding author: luigi.margutti@dottorandi.unipg.it

[a] University of Perugia, Department of Engineering, Via G. Duranti 93, 06125 Perugia, Italy

[b] SolydEra SpA, viale Trento 115/117, 38017 Mezzolombardo, Italy

Keywords: Prime power, Data centers, rSOC, System modeling

Abstract: The global energy transition necessitates efficient storage solutions to manage renewable intermittency. This study explores the application of reversible Solid Oxide Cell (rSOC) technology as a sustainable prime power alternative for energy-intensive data centers. Utilizing a multi-unit system architecture, this research models 10 rSOC modules integrated via Aspen Plus and calibrated using experimental data to accurately represent electrochemical and thermodynamic behaviour. Different operating configurations are investigated: hydrogen production or power generation mode.

Introduction: The energy transition requires decarbonization and high renewable integration, but their intermittency makes energy storage essential for grid stability and flexibility. Hydrogen has emerged as a key energy vector due to its capability for long-term energy storage and reconversion into electricity when needed [1]. Among hydrogen technologies, solid oxide cells (SOC) are particularly attractive due to their high efficiency and reversibility: the same device can operate as a solid oxide fuel cell (SOFC) to produce electricity or as a solid oxide electrolyzer (SOE) to produce hydrogen [2]. At the same time, the exponential growth of digital services has significantly increased the number and size of data centers, which are highly energy-intensive and require reliable prime power systems. By 2026, data centers energy consumption is expected to reach 620–1050 TWh, nearly double 2022 levels, mainly driven by AI-based services [3]. This study extends the modeling of single rSOC units to a multi-unit system, where different modules are optimized for different operating modes. The system is designed to operate flexibly under varying demand conditions, making it suitable for data center prime power applications.

Objectives: The objective of this work is to develop and analyze a multi-rSOC system capable of flexible operation between hydrogen production and power generation. Efficiency, thermal integration and flexibility of the system are assessed to evaluate it as a prime power energy source for data centers.

Material and methods: The system consists of 10 rSOC modules integrated with heat exchangers, H_2 storage, recirculation systems and other BoP components. The rSOC module, developed by SolydEra S.p.A., is derived by the product PM-X. Its core is a stack of 100 planar solide oxide cells, operating between 700 and 750°C, producing 9.6 kW under nominal conditions in fuel cell mode, while also enabling thermal energy recovery. Figure 57 depicts the efficiency and thermal power of a single module.

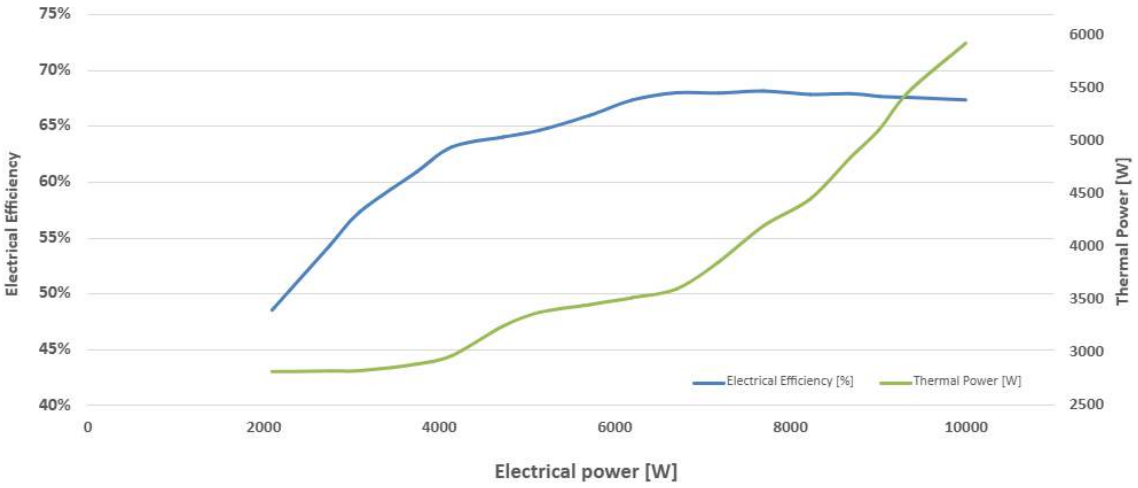


Figure 57: Efficiency and Thermal Power of a PM-X module.

Each module can operate either in SOFC or SOE mode depending on system requirements. A detailed Aspen Plus model of the integrated multi-unit rSOC system is developed, using a modular flowsheet, which includes mass and energy balances, thermodynamic property calculations and custom electrochemical blocks. Cell electrochemical performances are derived from experimental data and implemented through correlations between current density, voltage, lifetime and operating conditions. Different system configurations are analyzed. For example, all units operate in SOE mode when there is no power demand from the data center, thereby maximizing hydrogen production. In another configuration, all rSOC units operate in SOFC mode, with H_2, CH_4 or an H_2-CH_4 blend, to satisfy peak energy demand.

Results: The operating voltage in SOE mode is linked to the thermal management strategy and directly influence the optimal operating window. Operating below or above the thermoneutral voltage leads to endothermic or exothermic behaviour. Moreover, stack degradation causes an increase in cell voltage at constant current, resulting in unavoidable efficiency losses and a trade-off between operation stability and inlet energy consumption. The electrochemical model evaluates voltage, in both fuel cell and electrolyzer modes, as a function of current density, temperature, fuel utilization and stack degradation. These effects are included in the system model for rSOC unit definition, highlighting a strong asymmetry between SOFC and SOE mode. In SOFC operation, the stack typically works at V=0.8 V, delivering about 9.6 kW while consuming 0.47 kg/h of H_2, with U_f=0.8. In SOE mode, assuming

comparable power levels and operation near thermoneutral voltage, the current decreases and H_2 production is limited to 0.23 kg/h. However, SOE mode can sustain higher current densities due to more favourable high-temperature kinetics and improved tolerance to thermal gradients. At higher currents, such as I=195 A, internal ohmic heating supports thermal balance, increasing power absorption to about 26 kW and raising H_2 production up to 0.72 kg/h, nearly double the amount required for a SOFC in the previously described operating condition.

Conclusions: This work presents a comprehensive analysis of a multi-rSOC system for flexible energy management, a promising low-emission alternative for data center prime power systems. The integration of multiple units operating in different modes enables efficient coupling between hydrogen production and power generation. Although SOE appears less productive under strict equal-power assumptions, its operational flexibility at higher current densities enables higher hydrogen throughput, emphasizing the importance of thermo-electrochemical coupling in rSOC system design.

Acknowledgment

This research was partially supported by the ERASMUS+ project “H2Excellence”, Grant Agreement number 101104447.

References

[1] Welder L, Stenzel P, Ebersbach N, Markewitz P, Robinius M, Emonts B, et al. Design and evaluation of hydrogen electricity reconversion pathways in national energy systems using spatially and temporally resolved energy system optimization. Int J Hydrogen Energy 2019;44. https://doi.org/10.1016/j.ijhydene.2018.11.194.

[2] Mogensen MB, Chen M, Frandsen HL, Graves C, Hansen JB, Hansen K V., et al. Reversible solid-oxide cells for clean and sustainable energy. Clean Energy 2019;3. https://doi.org/10.1093/ce/zkz023.

[3] Takci MT, Qadrdan M, Summers J, Gustafsson J. Data centres as a source of flexibility for power systems. Energy Reports 2025;13. https://doi.org/10.1016/j.egyr.2025.03.020.

European Fuel Cells and Hydrogen
PIERO LUNGHI CONFERENCE
September 15th-17th 2026
Capri / Italy

Impact of Roll-to-Roll Production Technologies on the Cost of PEM Fuel Cell Membrane Electrode Assemblies

Jakob Hog [a], Linda Ney [a], Ulf Groos*[a]

* corresponding author: ulf.groos@ise.fraunhofer.de

[a] Fraunhofer Institute for Solar Energy Systems ISE

Keywords: PEM Fuel Cells, techno-economic assessment, roll-to-roll manufacturing

Abstract

Introduction: The high manufacturing cost of proton exchange membrane (PEM) fuel cells (FC) remains a primary obstacle to their widespread adoption. The membrane electrode assembly (MEA), particularly the catalyst coated membrane (CCM), persists as one of the central cost factors. This study examines the cost implications from catalyst ink mixing and roll-to-roll (R2R) coating processes, such as slot die coating (SDC) and rotary screen printing (RSP) to R2R production of a 7 layer MEA (CCM with sub-gaskets and gas diffusion layers (GDL) on anode and cathode) (Figure 1). Additionally, continuous (con) and intermittent (int) coating modes are compared.



Figure 1: Industrial machinery for MEA production research at Fraunhofer ISE

Objectives: The goal is to develop a comprehensive techno-economic model to identify key cost drivers along the production chain and to support informed decisions on process routes and MEA designs when scaling up PEM fuel cell production.

Material and methods: The study employs a Total Cost of Ownership (TCO) framework where the TCO of a CCM is determined by the sum of Cost of Ownerships (COO) of each production step i (Eq. 1):

$TCO = \sum_{i=1}^{N} COO_i$ (equation 1)

Each COO follows the SEMI E35 standard (Eq. 2), comprising fixed costs F, recurring costs R, and scrap costs S, divided by lifetime L, throughput TP, total utilization TU, and product yield PRY.

$COO = \frac{F+R+S}{L*TP*TU*PRY}$ (equation 2)

The modeled process chain includes: (1) ink mixing, (2) coating and drying of the CL on decal, and (3) transfer of anode and cathode CL onto a membrane. All assumptions are based on the Generic Stack cell design (Figure 2).

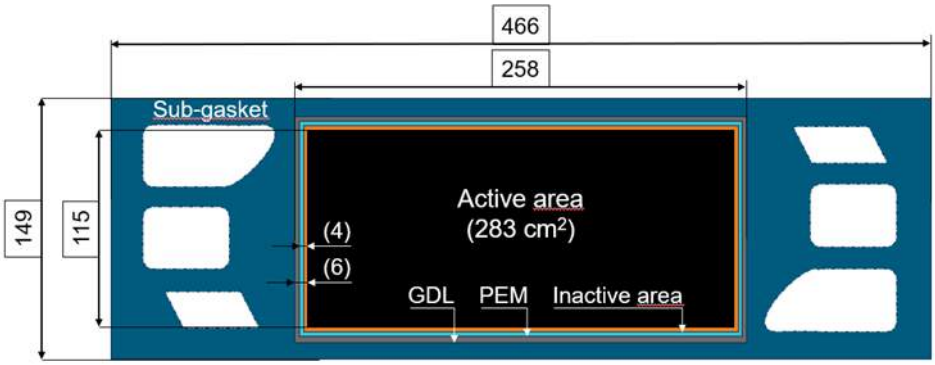


Figure 2: Generic Stack cell design with key production parameters

Manufacturing tolerances differ by coating method. SDC usually covers the full membrane with CL. Down the process line the CL is cut and framed into sub-gaskets, which leads to losses of active CL. Thus, concepts for intermittent coating like intermittent SDC and RSP produce gaps in machine direction, reducing material waste. In today's production, yield is a major issue. To evaluate the effect in contrast to machinery investments, especially for quality control, yield losses between 40% and 3% were evaluated. Therefore, already at relatively low production volumes, investments to increase yield pay off. A Monte Carlo simulation was performed for each scenario using a Gaussian distribution (±30% at 6σ) on the ten most influential cost parameters to assess robustness.

Results: RSP inks require more than 5 times longer drying times than SDC inks due to the high-boiling-point of their solvents. Inks prepared for RSP use ethylene glycol, 1,2-propanediol, while low-boiling-point solvents, namely, 1-propanol/water, are used for SDC. Already with a 250 m batch length, consumables and waste materials have approximately 50% share of the MEA costs (Figure 3). Since material costs dominate at high throughput, further cost reduction is limited with current materials. On the other hand, already for low volumes, equipment costs become insignificant when using industrial pilot plants.

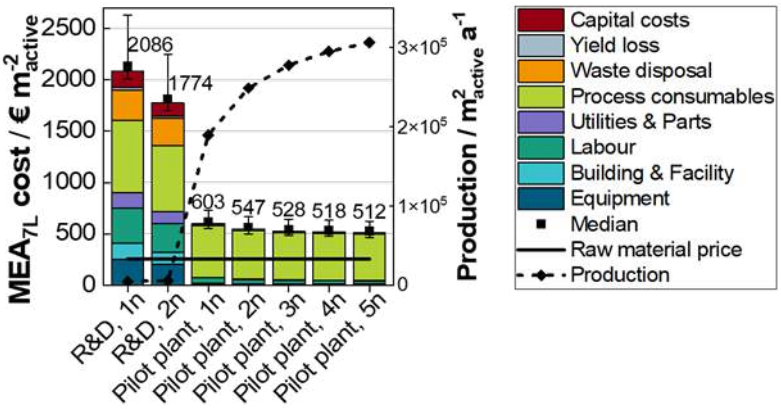


Figure 3: Cost breakdown for R&D and pilot production for batch lengths from 250 m substrate rolls (1n) to 1,250 m (5n)

Conclusions: Intermittent SDC and RSP enable tighter tolerances, reducing inactive CL area and material waste —a key lever for cost reduction. Process direction rotation (0° → 90°) increases the number of CLs per roll width and throughput, though membrane waste improvement is modest. Optimizing cell design to match supply-roll dimensions is identified as a further lever. While not yet cost-differentiated, RSP offers unique potential for structured in-plane coatings that may improve CL performance—a benefit not captured by cost models alone. On the other hand, stable process operation with open ink processing systems has to be realized. At industrial scale, 90% of consumable costs stem from MEA materials. Future work must target performance improvements through new materials and cell designs to break the material-cost floor and enable widespread fuel cell deployment.

Acknowledgment: This work was funded by the German BMV of the project H2GO: R2MEA.

References

[1] Hog, J., Matali Goya, D., Wild, J., Ney, L., Zamel, N. Techno-Economic Assessment of Manufacturing Membrane Electrode Assemblies for PEM Fuel Cells: Focus on Coating Technologies, Fuel Cells 26, 1, https://doi.org/10.1002/fuce.70058



Electrochemical and morphological analysis of Pt catalyst degradation under maritime-inspired AST for PEMFCs

Sara Tamburello*[a], Marco Russo Cirillo [b], Yurii Yakovlev[c], Iva Matolínová[c], Rodolfo Taccani[b], Andrea Coraddu [a], Marco Bogar[b], Linder van Biert[a]

* corresponding author: s.tamburello-1@tudelft.nl

[a] Department of Maritime & Transport Technology, TU Delft, The Netherlands

[b] Department of Engineering and Architecture, University of Trieste, Trieste, Italy

[c] Department of Surface and Plasma Science, Faculty of Mathematics and Physics, Charles University, Prague, Czech Republic

Keywords: PEMFC, catalyst degradation, accelerated stress test, CV, SAXS, WAXS

Abstract: A previously developed AST designed to reproduce transient operating conditions representative of passenger ferry operation was applied to a 2-cell PEMFC stack to investigate early-stage Pt catalyst degradation. Cyclic voltammetry measurements showed a progressive decrease in ECSA during 200 hours of operation, while post-mortem SAXS and WAXS analyses revealed a consistent Pt particle and cluster growth. Results highlight the value of combined electrochemical and morphological analyses for interpreting Pt catalyst degradation under application-relevant operating conditions.

Introduction: Polymer Electrolyte Membrane Fuel Cells (PEMFCs) represent a promising solution for the decarbonisation of the maritime sector, particularly for small- and medium-sized vessels such as tugs and passenger ferries [1]. However, understanding durability under application-relevant operating conditions remains essential for reliable long-term deployment. Catalyst degradation is one of the primary causes limiting system lifetime, leading to a progressive loss of electrochemically active surface area (ECSA) and performance decay [2]. Several accelerated stress test (AST) protocols have been developed to investigate Pt catalyst degradation. However, application-specific durability protocols for maritime PEMFC systems are still scarce in the current literature. In our recent work, we proposed a methodology to evaluate the degradation of PEMFC membrane electrode assemblies (MEAs) under a novel load cycle designed to mimic the transient operation of a passenger ferry [3]. Results showed measurable catalyst layer degradation under the considered transient load profile, with the most pronounced ECSA decrease occurring during the initial stages of operation. Therefore, further experimental investigations, including post-mortem analyses of Pt nanoparticle morphology, are required to better understand the rapid early-stage degradation under application-specific operating conditions observed in our previous study.



Objectives: In this work, we replicate the AST protocol presented in [3] on a 2-cell stack with self-fabricated MEAs to investigate degradation behaviour during the early stages of operation. The protocol is applied for 200 hours, and cyclic voltammetry (CV) is repeated every 40 hours to evaluate ECSA with a higher time frequency compared to our previous work. Post-mortem analysis of the samples is performed via small-angle and wide-angle X-ray scattering (SAXS and WAXS) to investigate Pt morphological changes and check the degree of homogeneity of degradation.

Material and methods: Two 25 cm^2 MEAs were fabricated by ultrasonic spraying coating a Pt/Vulcan catalyst ink onto Nafion® NR211 membranes using a CNC-controlled system, achieving Pt loadings of 0.5 mg/cm^2 at the cathode and 0.1 mg/cm^2 at the anode, as detailed in [4]. The MEAs, assembled with Sigracet 29BC gas diffusion layers, were tested in a short-stack under galvanostatic control for 200 hours following the previously introduced protocol [3]. SAXS and WAXS patterns were recorded ex situ from the two aged MEAs by means of laboratory equipment (Xenocs XEUSS 2.0, SAXS detector: Dectris Pilatus3 R 300K, WAXS detector: Dectris Pilatus3 R 100K, wavelength: 1.54 Å). Each MEA was measured at three points: hydrogen inlet (point A), hydrogen outlet (point C), and centre (point B), to evidence any possible inhomogeneities in degradation.

Results: As shown in Fig. 1 a) – 1 b), CV measurements show a peak reduction in the hydrogen adsorption/desorption region (0.05-0.4 V), indicating a decline in Pt surface activity, which was evaluated with ECSA calculations. As reported in Fig. 1 c), ECSA varied from an initial value of ~40 m^2/g_{Pt} to ~30 m^2/g_{Pt} for both MEAs after 200 hours of AST, in line with our previous results. SAXS patterns, shown in Fig. 2 a), show a shift of the bump corresponding to Pt nanoparticles (which can be found around 1 nm^{-1}) for aged samples, indicating a change of average particle size with respect to pristine conditions. No changes can be noticed between the two samples and between the three different measurement points, showing homogeneous degradation. Particle size distributions (PSD), shown in Fig. 2. B), are obtained by fitting SAXS patterns with an analytical model within the range of 0.05 nm^{-1} and 4 nm^{-1}, where catalyst nanoparticles were modelled as a set of spheres following the Shultz distribution and aggregated into small clusters. The mean particle mean diameter D_P increased from 2.33 ± 0.01 nm in pristine conditions to an average of 2.9 ± 0.01 nm for both MEAs, while the average particle cluster diameter increased from 7.96 ± 0.02 nm to 11.56 ± 0.07 nm. The particle geometrical specific area decreased from 30.06 m^2/g_{Pt} in pristine conditions to an average of 24.07 m^2/g_{Pt} for both MEAs after the AST, representing a reduction consistent with the electrochemically observed ECSA evolution. WAXS patterns show a shift of diffraction angle, indicating a compression or strain of the metallic crystalline lattice that might be attributed to Pt oxides formation, since the fuel cell reached potentials above 0.8 V, at which Pt oxidation is well known to take place. The WAXS-derived average crystalline size increased from 5.27 nm to 8.2 nm, which is roughly in agreement with the percentage variation of SAXS-derived aggregate size.

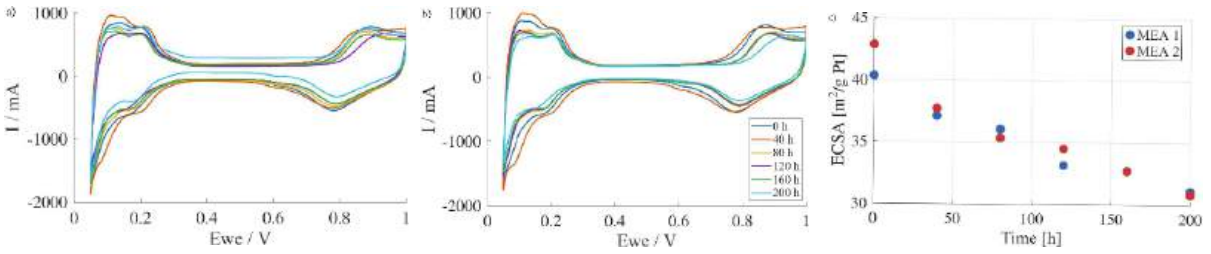


Figure 58. *CV measurements for MEA 1 (a) and MEA 2 (b) over the AST, and corresponding ECSA trend (c).*

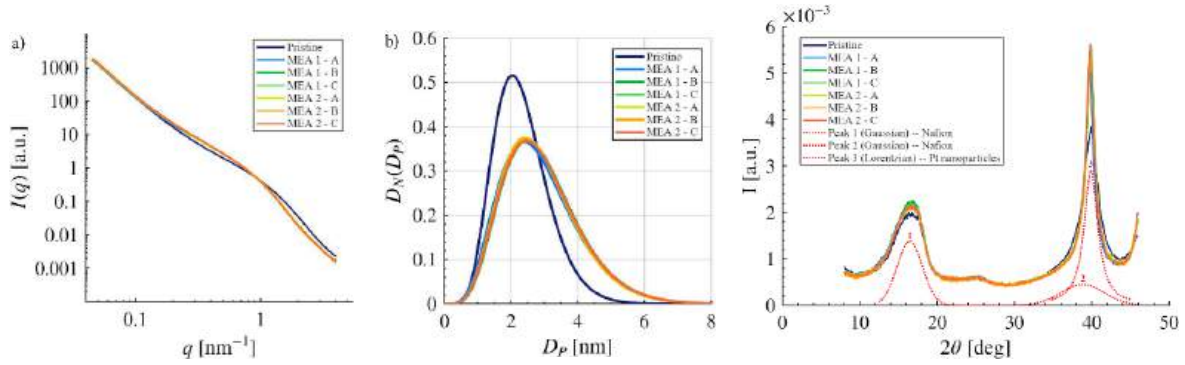


Figure 59*. Evolution of SAXS patterns (a), SAXS-derived PSD (b), and WAXS patterns (c) before and after the AST for MEA 1 and MEA 2, at 3 different spatial points of measurement (A: H_2 inlet, B: mid-way, C: H_2 outlet).*

Conclusions: This study investigates Pt catalyst evolution under the proposed load-transient AST. Post-mortem SAXS and WAXS analyses indicated Pt particle and cluster growth during the test, consistent with the observed ECSA decrease. The agreement between electrochemical and morphological observations supports the interpretation of the dominant degradation pathways occurring during the early stages of the AST observed in our studies.

Acknowledgment: This research is part of the project SEANERGETIC (with project number KICH1.KICH1.21.003) funded by the Dutch Research Council. The authors acknowledge the CERIC-ERIC Consortium for access to experimental facilities and Alessandra Del Giudice for her support with SAXS and WAXS measurements at the Sapienza University of Rome.

References

[1] S. Tamburello, L. van Biert, A. Coraddu, Durability and prognostic modelling of low-temperature polymer electrolyte membrane fuel cells in maritime applications: A review, Energy Conversion and Management: X (2026) 101576.

[2] I. Laghryb, M. Malki, N. Y. Steiner, C. D. Barrett, H. El Kadiri, Catalyst degradation in proton exchange membrane fuel cells: Mechanisms, investigation techniques, and predictive modelling, International Journal of Hydrogen Energy 145 (2025) 496–507.

[3] S. Tamburello, M. R. Cirillo, Y. Yakovlev, I. Matolínová, R. Taccani, A. Coraddu, M. Bogar, L. van Biert, Preliminary methodology assessment for PEMFC durability testing in transport applications, Electrochimica Acta (2026) 148267

[4] Y.V. Yakovlev, Y.V. Lobko, M. Vorokhta, J. Nováková, M. Mazur, I. Matolínová, V. Matolín, Ionomer content effect on charge and gas transport in the cathode catalyst layer of proton-exchange membrane fuel cells, J. Power Sources 490 (2021) 229531.



Application of mcfc technology for the decarbonization of italian district heating networks: a case study

Mattia Baiguini[a], Michele Doninelli[a], Andrea Stecchini[b], Gianni Martinazzoli[b], Abdelrahman Mostafa[b], Gioele Di Marcoberardino*[a]

* Corresponding author: gioele.dimarcoberardino@unibs.it

[a] Università degli studi di Brescia, DIMI, Via Branze 38, 25123, Brescia, Italy

[b] A2A S.p.A., Via Lamarmora 230, Brescia, 25124, Italy

Keywords: CO_2 capture; District Heating decarbonization; Molten Carbonate Fuel Cell; Techno-economic analysis.

Abstract

Introduction: District heating (DH) currently accounts for approximately 10% of global building heat demand, with significantly higher penetration in Europe. However, 90% of global DH supply is still based on fossil fuels [1]. A2A is committing to identifying technologies for the decarbonization of its energy production assets, with particular attention to reducing CO_2 emissions from small scale power plant. In this context, the Molten Carbonate Fuel Cell (MCFC) technology has been identified as a possible solution for CCS. MCFCs are high-temperature electrochemical devices that convert the chemical energy of fuels directly into electricity, while simultaneously enabling CO_2 separation [2]. By transporting carbonate ions through a molten electrolyte, MCFCs consume CO_2 from flue gases at the cathode and release it as a concentrated stream at the anode, simplifying carbon capture.

Objectives: The objective is to assess the feasibility of MCFC integration in existing DH systems through a representative case study coupling an MCFC with a CHP internal combustion engine for simultaneous CO_2 capture, electricity generation, and heat production.

Material and methods: The methodology combines process modelling and preliminary economic assessment to evaluate the integration of MCFC technology within the DH network located in northern Italy.

The flue gas stream, from the existing CHP NG-fed ICE, is first characterized in terms of mass flow rate, temperature, and composition. A simplified 0D model of the MCFC is then developed in Aspen Plus, using literature-based assumptions and electrochemical relations to describe cell performance [3] [4]. The model accounts for the main operating parameters of the cell, enabling the estimation of voltage, current density, power output, and CO_2 transfer across the cell. The overall system (Figure 60) is analysed by integrating mass and energy balances, allowing the evaluation of key performance indicators (Table 10).

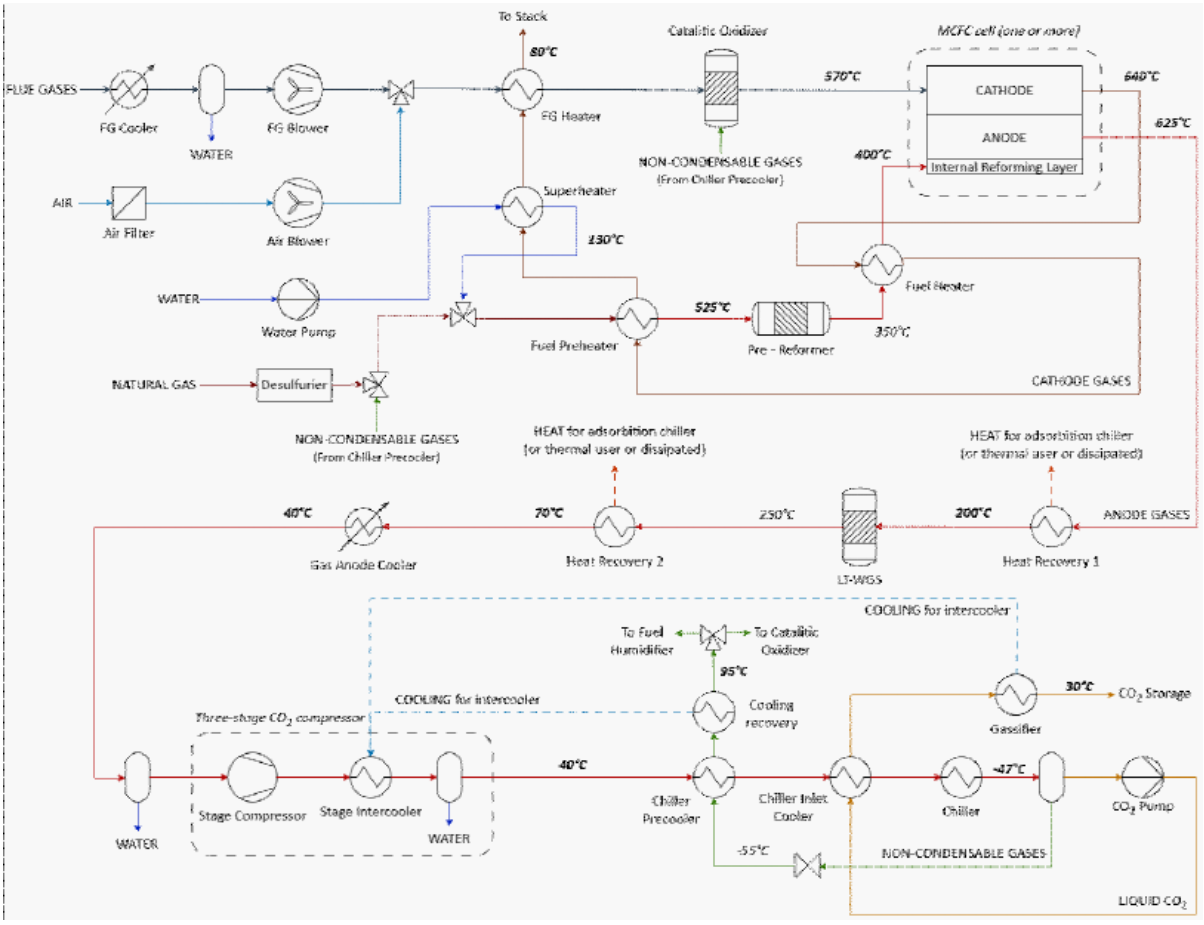


Figure 60: Layout of the MCFC system

Table 10: Main key performance indicators adopted in this work.

Efficiency	Formula	Indicator	Formula
Electric (MCFC)	$\eta_{el} = \frac{\dot{W}_{MCFC} \cdot \eta_{alt} - \sum \dot{W}_{BoP}/\eta_{alt}}{\dot{m}_{NG} LHV_{NG}}$	**CCR**	$CCR = \frac{\dot{m}_{CO_2,c}}{\dot{m}_{CO_2,c} + \dot{m}_{CO_2,e}}$
Thermal (MCFC)	$\eta_{th} = \frac{\dot{Q}_{MCFC}}{\dot{m}_{NG} LHV_{NG}}$	**Specific Emission**	$e_{CO_2} = \frac{\dot{m}_{CO_2,e}}{E_{EE} + E_{TH}}$

From an economic perspective, the analysis is based on simplified cost correlations and literature data, considering the main cost items associated with the MCFC system and its integration within the existing plant [5]. The main objective is to evaluate the increase of the cost of heating considering production of all DH network.

Results: The analysis was carried out by varying the installed MCFC capacity (1.5–3 MW), the fuel and CO_2 utilization factor. The MCFC electrical efficiency ranges between 25% and 29%, while the combined system (ICE + MCFC) reaches overall efficiencies up to 78-79% when thermal recovery is included. The additional electrical output provided by the MCFC is up to 1.2 MW, while the recoverable

thermal power is in the range of 1.76 MW. The CCR is around 72-90% and se_{CO_2} are reduced below 70 gr/kWh, a 70% reduction comparing the standard ICE. The integration of MCFC technology leads to an increase of the cost of heating of 10-30% comparing base scenario. However, the additional cost associated with MCFC integration can be distributed over the entire heat production of the network. The resulting increase in the heat tariff remains below 1 €/MWh in all the analysed scenarios.

Conclusions: MCFC integration offers a promising route for decarbonizing district heating networks, with limited system-level cost impact when distributed over large-scale heat production.

Acknowledgment

"This work is carried out in collaboration with the R&D unit of A2A S.p.A. for the identification of technologies for the decarbonization of its main emission-generating sectors (CCGT and WtE), through the development of renewable sources and CCUS technologies."

References

[1] H. Böhm, S. Moser, S. Puschnigg, A. Zauner, Power-to-hydrogen & district heating: Technology-based and infrastructure-oriented analysis of (future) sector coupling potentials, Int. J. Hydrogen Energy 46 (2021) 31938–31951. https://doi.org/10.1016/j.ijhydene.2021.06.233.

[2] M. Cassir, A. Meléndez-Ceballos, A. Ringuedé, V. Lair, Molten carbonate fuel cells, Compend. Hydrog. Energy Hydrog. Energy Convers. Vol. 3 3 (2016) 71–87. https://doi.org/10.1016/B978-1-78242-363-8.00003-7.

[3] S. Campanari, P. Chiesa, G. Manzolini, CO2 capture from combined cycles integrated with Molten Carbonate Fuel Cells, Int. J. Greenh. Gas Control 4 (2010) 441–451. https://doi.org/10.1016/J.IJGGC.2009.11.007.

[4] H. Ghezel-Ayagh, Pilot Test of Novel Electrochemical Membrane System for Carbon Dioxide Capture and Power Generation (Final Report), (2018). https://doi.org/10.2172/1484012.

[5] J. Spendelow, T. Nguyen, C. Houchins, K.E. Martin, D. Papageorgopoulos, DOE Hydrogen and Fuel Cells Program Record Title: Medium-scale CHP Fuel Cell System Targets Originator, (2011).



Interface Engineering in sPPO-Based Hydrocarbon Catalyst-Coated Membranes for PEM Fuel Cells

Carlo De Luca*[a,c], Emmanuel De Gregorio[b,c], Immacolata Manco[a], Giuseppina Roviello[b], Claudio Ferone[b], Elio Jannelli[b], Viviana Cigolotti[c], Valentina Naticchioni[c], Martina Butori[d], Björn Eriksson[d], Rakel W. Lindström[d], Oreste Tarallo[a]

* corresponding author: carlo.deluca2@unina.it

[a] University of Naples Federico II, Department of Chemical Sciences, Complesso Universitario di Monte Sant'Angelo, 80126 Naples (Italy)

[b] University of Naples Parthenope, Department of Engineering, Centro Direzionale Isola C4, 80133 Naples (Italy)

[c] ENEA - Italian National Agency for New Technologies, Energy and Sustainable Economic Development, Via Anguillarese 301, 00123 Rome (Italy)

[d] KTH Royal Institute of Technology, Department of Chemical Engineering/Applied Electrochemistry, SE-100 44 Stockholm (Sweden)

Keywords: Catalyst-coated membranes, Hydrocarbon ionomers, PEM fuel cells, Sulfonated poly(phenylene oxide).

Abstract

Here, an in-house sulfonated PPO is reported as a dual hydrocarbon platform for spray-coated PEMFC catalyst-coated membranes, operating as both membrane and catalyst-layer ionomer. The fully sPPO-based architecture improved polarization performance and reduced ohmic/interfacial losses, highlighting effective membrane–electrode integration while identifying mechanical robustness as the remaining durability challenge.

Introduction

The performance of a proton exchange membrane fuel cell (PEMFC) is governed by the membrane–electrode assembly (MEA), where the membrane and catalyst layers must jointly ensure proton transport, gas separation, electronic insulation and electrochemical activity [1]. In this framework, PFSA materials such as Nafion® remain the benchmark, although their cost, fluorinated chemistry and environmental persistence continue to drive the development of non-fluorinated hydrocarbon-based (HC) alternatives [2]. Recent studies also indicate that optimized processing routes can mitigate interfacial limitations in mixed HC/PFSA systems; therefore, the key challenge is not only avoiding polymer mismatch, but identifying HC polymers able to operate effectively in both membrane and catalyst-layer environments [3]. Sulfonated poly(phenylene oxide), sPPO, is a suitable platform because the same sulfonated aromatic backbone can be exploited as membrane and ionomer,

enabling chemically coherent catalyst-coated membranes (CCMs). Here, an in-house optimized sPPO membrane is combined with an sPPO catalyst-layer ionomer to assess its potential for fluorine-free PEMFCs.

Objectives

The objective of this study was to evaluate an in-house sPPO polymer as a dual hydrocarbon platform for PEMFC CCMs, using it both as proton-exchange membrane and as catalyst-layer ionomer.

Material and methods

sPPO membranes with a thickness of 70 µm were produced in house by blade casting and solid-state sulfonation, following a previously optimized protocol, and used to fabricate a series of MEAs by the CCM approach. Nafion®, Pemion®, and in-house sPPO were employed as catalyst-layer ionomers. The sPPO ionomer was prepared by solution sulfonation, while commercial Nafion® and Pemion® were used as references. Materials were characterized by WAXD, FTIR-ATR, ^{1}H-NMR and TGA, while IEC, WU and dimensional stability were also evaluated. Electrochemical performance was assessed and compared with fully Nafion®- and Pemion®-based MEAs prepared using the same experimental approach.

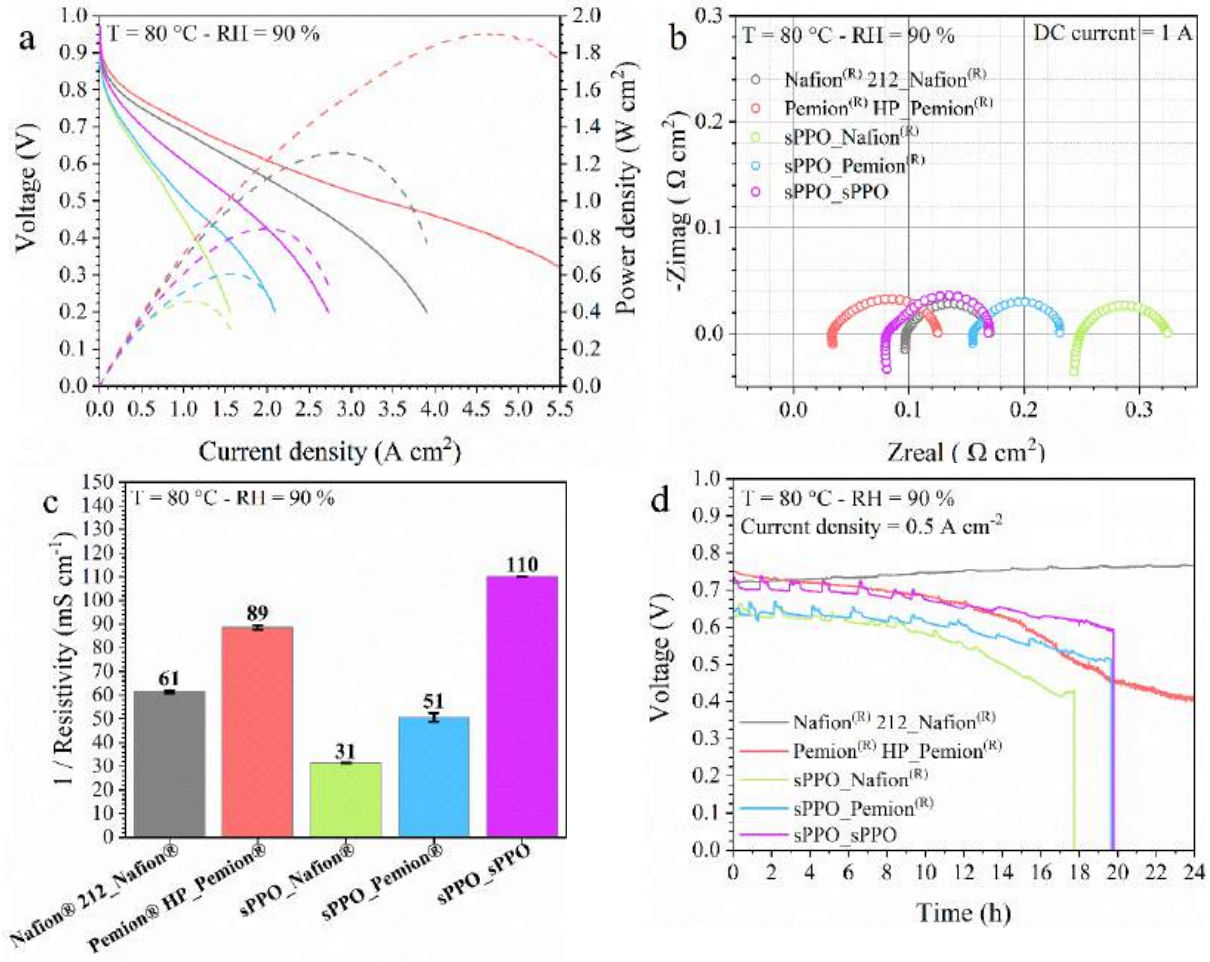
Results

The in-house optimized sPPO membrane showed an IEC of 2.07 meq g^{-1}, comparable to Pemion® HP and significantly higher than Nafion® 212. Its WU was intermediate, although hydration induced relevant dimensional deformation, indicating that unreinforced sPPO films remain mechanically vulnerable under humidified operation. At 80 °C and 70% RH, all sPPO-based CCMs showed similar H_2 fluxes of about 16 nmol s^{-1} cm^{-2}, lower than those of the fully Pemion®- and Nafion®-based MEAs tested under the same conditions. Thus, gas crossover was mainly governed by the membrane and was not penalized by the catalyst-layer ionomer. In fuel-cell operation at 80 °C and 90% RH, peak power density increased from 0.46 W cm^{-2} for sPPO_Nafion® to 0.61 W cm^{-2} for sPPO_Pemion® and 0.85 W cm^{-2} for sPPO_sPPO. Since the membrane and Pt loading were unchanged, this improvement highlights the effective use of sPPO as catalyst-layer ionomer in direct spray-coated CCMs. GEIS confirmed the trend: corrected HFR decreased from 0.22 Ω cm^2 for sPPO_Nafion® to 0.14 Ω cm^2 for sPPO_Pemion® and 0.06 Ω cm^2 for sPPO_sPPO, while the corresponding apparent HFR-derived through-plane ionic conductivity increased from 31 to 51 and 110 mS cm^{-1}. The fully chemically matched architecture between membrane and ionomer therefore provides the most continuous proton-conducting pathway across the catalyst layer–membrane interface. Durability remains limiting, since all sPPO-based MEAs failed before 24 h due to loss of mechanical integrity.

Conclusions

This work demonstrates the potential of in-house sPPO as a dual hydrocarbon platform for PEMFC catalyst-coated membranes. Using the same sPPO backbone as both membrane and catalyst-layer ionomer reduced ohmic and interfacial losses, improving the HFR-derived ionic transport and

polarization performance without changing membrane type or Pt loading. The observed benefit can be attributed to more effective membrane–electrode integration and enhanced ionic continuity at the catalyst layer–membrane interface. However, the premature failure shows that electrochemical performance must be coupled with dimensional robustness, controlled swelling and optimized HC catalyst-layer design.



Figures: (a) Polarization and power density curves, **(b)** GEIS Nyquist plots, **(c)** Apparent HFR-derived through-plane ionic conductivity and **(d)** galvanostatic stability at 0.5 A cm^{-2}.

Acknowledgements

CALIPSO - Celle A combustibiLe innovatIve ad alta Potenza in Sistemi stazionari e di mObilità progetto n. RSH2A_000021 – CUP F57G25000200006 is grateful acknowledged.

References

[1] Deng, X. *et al.*, 2025, *Catalysts*, 15(1),74. [2] Nguyen, H. *et al.*, 2022, *Advanced Energy Materials*, 12(12), 2103559. [3] Weber, K. A. *et al.*, 2025, *ECS Advances*, 4, 034501.



Safe, Fast and Efficient Hydrogen Refuelling for Heavy-Duty Vehicles via a Multiphysics and Data-Driven Approach

M. Genovese[a,*], F. Piraino[a], L. Andaloro[b], I. Belviso[b], L. Pagnotta[a], P. Fragiacomo[a]

* corresponding author: matteo.genovese@unical.it

[a] Department of Mechanical, Energy and Management Engineering, University of Calabria, Arcavacata di Rende, 87036 Cosenza, Italy

[b] National Research Council of Italy, Institute of Advanced Energy Technologies, Via Salita S. Lucia Sopra Contesse, 5, 98126, Messina, Italy

Keywords: dynamic simulation, hydrogen refuelling station, multiphysics modelling, validation

Abstract

Hydrogen refuelling stations (HRS) for heavy-duty (HD) vehicles operate under significantly more demanding conditions than light-duty systems, due to higher hydrogen mass flow rates (up to and beyond 120 g/s), larger onboard storage (10–180 kg H_2), and frequent back-to-back refuelling cycles. Current protocols (e.g., SAE J2601-2) are not fully prescriptive for HD applications and typically enforce conservative operating limits, especially with respect to tank temperature (T_max = 85°C), resulting in underutilized thermal margins (>10–15°C in most cases) and inefficient station design. Compression and precooling dominate the energy consumption of refuelling, contributing approximately 2.2 kWh/kg and 1.4 kWh/kg respectively, leading to a total station energy demand of about 5 kWh/kg H_2 in current configurations. These constraints highlight the need for optimized, data-driven refuelling strategies.

Introduction

Hydrogen refuelling stations (HRS) are complex, multi-component energy systems in which compression, thermal management, and control strategies strongly influence performance and safety. While light-duty refuelling protocols (e.g., SAE J2601) are well established, heavy-duty (HD) applications introduce significantly different operating conditions, including higher hydrogen mass flow rates, larger onboard storage systems (up to 180 kg), and frequent back-to-back refuelling events [1-3]. These factors result in increased thermal loads and stricter requirements for station recovery and throughput. This work presents the methodology and results of the SaFE H2D project, aimed at

developing a data-driven framework for safe, fast, and energy-efficient hydrogen refuelling tailored to heavy-duty vehicles.

Objectives

The objective of this work is to develop a quantitative framework for safe, fast, and energy-efficient hydrogen refuelling of heavy-duty vehicles, based on validated multiphysics modelling and generalized performance metrics. The specific targets include:

- hydrogen mass flow rate > 7.2 kg/min;
- refuelling time comparable to diesel (fossil parity);
- final tank state of charge (SoC) > 90%;
- compliance with thermal constraint T_tank ≤ 85°C..

Material and methods

The methodology is structured into an integrated workflow combining metrics definition, modelling, and design optimization. A classification based on compressed hydrogen storage system (CHSS) capacity is introduced, covering ranges from 10–30 kg up to 120–180 kg. The concept of fossil parity is defined through an energy equivalence factor (k ≈ 0.298 kgH_2/L_diesel), linking hydrogen refuelling requirements to diesel flow rates (60–120 L/min). This results in required hydrogen ramp rates of approximately:

- 17.9 kg/min (equivalent to 60 L/min diesel),
- 35.8 kg/min (equivalent to 120 L/min diesel).

A modular multiphysics simulator is developed to model the refuelling process, including: real gas thermodynamics, transient heat transfer between hydrogen and tank walls, pressure ramp control strategies, station-side components (compressors, cascade storage, precooling systems). The model has been ad-hoc developed in Matlab/Simulink environment. The model is validated and applied to back-to-back refuelling scenarios and different pressure levels (35, 50, 70 MPa). A parametric CAD-based design tool, developed also in Matlab/Simulink, is used to evaluate station layouts and optimize footprint and multi-dispenser configurations.

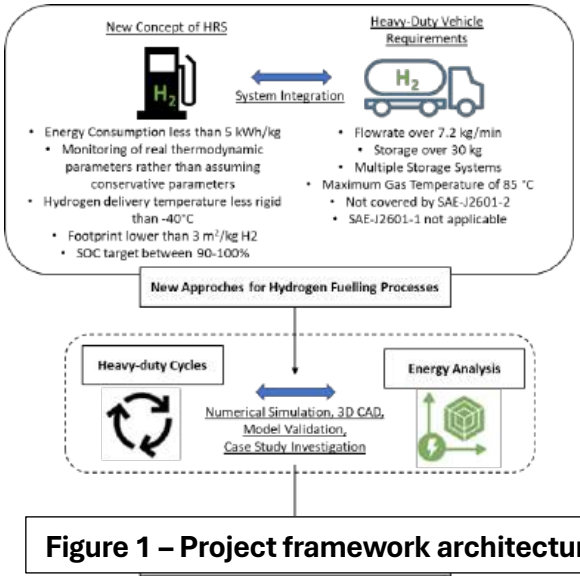


Figure 1 – Project framework architecture

Results

The modelling framework enables the identification of safe operating corridors and quantifies the impact of key parameters on refuelling performance. Results show that increasing precooling temperature from −40°C to −20°C (or higher) is feasible while maintaining T_tank ≤ 85°C,

reducing cooling energy demand and improving system efficiency. This allows reducing total refuelling energy consumption from approximately 5 kWh/kg to about 3 kWh/kg H_2 (−40% reduction). For large storage systems (CHSS 120–180 kg), fossil parity analysis yields:

- required hydrogen mass: 130–170 kg,
- equivalent diesel volume: 438–569 L,
- refuelling time: 7.3–9.5 min at 60 L/min equivalent, or 3.6–4.7 min at 120 L/min equivalent,
- required ramp rates: 17.9–35.8 kg/min.

Conclusions

This study presents a comprehensive framework for improving hydrogen refuelling of heavy-duty vehicles through the integration of multiphysics modelling, system design, and protocol optimization. The results demonstrate that significant improvements in efficiency and infrastructure utilization can be achieved by transitioning from conservative, one-size-fits-all protocols to data-driven approaches based on real operating conditions and vehicle characteristics. The proposed methodology supports the development of generalized protocol guidelines and provides a clear pathway toward standardization, improving interoperability and reducing ambiguity in heavy-duty refuelling operations. Overall, the SaFE H2D approach contributes to enabling safe, fast, and energy-efficient hydrogen refuelling at scale, supporting the decarbonization of heavy transport sectors.

Acknowledgment: This work is part of the SaFE H2D: Safe, Fast and Efficient Hydrogen Refuelling for Heavy-Duty Vehicles; project, funded under the National Recovery and Resilience Plan (PNRR) - Mission 4 - Component 2 - Investment 1.1, within the framework of the National Research Program and Projects of Significant National Interest (PRIN) - PRIN 2022 PNRR, under project reference CUP H53D23008740001 P2022YHME9.

References

[1] Poudel S, Tun H, Reddi K, Elgowainy A. Investigation of precooling unit design options in hydrogen refueling station for heavy-duty fuel-cell electric vehicles. Int J Hydrogen Energy 2024;61:493–502. https://doi.org/10.1016/j.ijhydene.2024.02.197 .

[2] PRHYDE project on heavy-duty hydrogen refueling protocol. Fuel Cells Bulletin 2020;2020:8–9. https://doi.org/https://doi.org/10.1016/S1464-2859(20)30112-7.

[3] Hong Lv, Ying Su, Gangqi Huang, Qianyi Zhang, Cunman Zhang, Research on rapid refueling of Type-IV hydrogen storage tanks for hydrogen-powered heavy-duty commercial vehicles, Renewable Energy,Volume 253,2025,123673,ISSN 0960-1481,

https://doi.org/10.1016/j.renene.2025.123673.



Nanostructured Pt Catalyst Layers for Low-Loading PEMFCs by Pulsed Laser Deposition and Inverse MAPLE

A. Occhicone[a,*], G. De Marino[a], E. De Gregorio[a], C. Ferone[a], G. Ausanio[b], Valentina Naticchioni[c], Viviana Cigolotti[c], Elio Jannelli[a], O. Tarallo[d], G. Roviello[a]

* corresponding author: alessio.occhicone@assegnista.uniparthenope.it

[a] Department of Engineering, University of Naples "Parthenope", Centro Direzionale, Isola C4, 80143 Naples, Italy

[b] Department of Physics "E. Pancini", University of Naples Federico II, Piazzale Vincenzo Tecchio 80, 80125 Naples, Italy

[c] ENEA—Italian National Agency for New Technologies, Energy and Sustainable Economic Development, Via Anguillarese 301, 00123 Rome (Italy)

[d] University of Naples Federico II, Department of Chemical Science, Complesso Universitario di Monte Sant'Angelo, 80126 Naples (Italy)

Keywords: inverse MAPLE, low Pt loading, PEMFC, pulsed laser deposition.

Abstract

Reducing Pt loading while preserving catalytic accessibility is a key challenge for cost-effective proton exchange membrane fuel cells. In this work, pulsed laser deposition (PLD) and inverse matrix-assisted pulsed laser evaporation (iMAPLE) were investigated as laser-assisted routes for preparing nanostructured Pt catalyst layers for low-loading PEMFC electrodes. PLD was used as a top-down process based on direct ablation of a metallic Pt target. In contrast, inverse MAPLE was explored as a bottom-up strategy for transferring preformed surfactant-free Pt nanoparticles from a frozen colloidal matrix. PLD produced crystalline metallic Pt deposits with fcc Pt(111) reflections, coherent-domain sizes of 3.6–5.6 nm, and Pt loadings below the nominal 200 μg cm^{-2} of commercial Pt/C electrodes. The optimized polyol synthesis yielded concentrated Pt colloids mainly in the 2–4 nm range, suitable for iMAPLE transfer. Overall, these results support laser-based processing as a flexible approach to engineer Pt loading, nanocrystalline size, and catalyst-layer morphology beyond conventional ink deposition.

Introduction: PEMFCs are key devices for efficient hydrogen-to-electricity conversion, but their large-scale deployment is still limited by the cost and criticality of platinum-group-metal catalysts [1]. Pt remains the benchmark ORR electrocatalyst in acidic media, although its effective utilization in MEAs

is strongly governed by catalyst-layer morphology, nanoparticle dispersion, ionomer distribution and mass-transport limitations. Since ORR performance depends critically on Pt particle size, typically favoured in the few-nanometre range, advanced deposition methods able to reduce Pt loading while preserving accessible nanostructured surfaces are required [2]. In this framework, PLD and iMAPLE offer complementary thin-layer fabrication routes: PLD through direct ablation of a metallic Pt target, and iMAPLE through the transfer of preformed colloidal Pt nanoparticles from a frozen, weakly absorbing matrix.

Objectives: This work investigates laser-assisted routes for preparing low-loading Pt catalyst layers for PEMFCs. The study correlates PLD parameters with Pt loading and crystalline domain size, develops surfactant-free Pt colloids for iMAPLE, compares PLD and iMAPLE deposits in terms of structure, morphology, coverage and contamination, and identifies the most suitable route for future benchmarking against a commercial Pt/C electrode with 200 μg cm^{-2} Pt loading.

Material and methods: Surfactant-free Pt nanoparticles were synthesized by an alkaline polyol route from $H_2PtCl_6 \cdot 6H_2O$ in ethylene glycol, using NaOH as stabilizer at an optimized NaOH/Pt ratio of 6.2. The colloid was adjusted to ~1 wt% Pt to ensure iMAPLE absorption without polymeric or surfactant additives. PLD was carried out with a 1064 nm Nd:YAG laser on a high-purity Pt target, varying laser power, pulse number and pressure to control Pt loading and morphology [2]. Glass/mica substrates were used for characterization, while Sigracet 22 BC GDLs served for preliminary electrode fabrication. iMAPLE deposits were obtained from the frozen Pt colloid in an ethylene glycol/ethanol matrix. Samples were characterized by XRD/WAXD, SEM/EDX, AFM and FTIR, and Pt coherent-domain size was estimated from the Pt(111) peak using the Scherrer equation.

Results: PLD yielded crystalline Pt deposits showing the characteristic fcc Pt(111) reflection at 39.6–39.8°, with no evident crystalline Pt oxide phases under the investigated conditions. The Scherrer-derived coherent-domain size was tunable within the nanometric range. Earlier high-pressure PLD/MAPLE samples showed Pt domains of 4.62 nm on mica, 5.61 nm on glass and 6.06 nm for MAPLE-transferred commercial Pt nanoparticles. In the new low-pressure PLD depositions on glass, 10,000 pulses produced smaller domains of 4.78 nm at 180 W and 3.64 nm at 200 W. The latter condition delivered approximately 90 μg cm^{-2} Pt, below the nominal 400 μg cm^{-2} loading of the commercial Pt/C benchmark. PLD on carbon paper using 6000 + 6000 pulses at 200 W gave mass increments of about 170–200 μg, while maintaining Pt coherent domains around 4–5 nm, indicating that deposition on a porous GDL did not significantly compromise nanocrystallinity (Figure 1).

The surfactant-free polyol route produced a concentrated Pt colloid mainly composed of ultrasmall nanoparticles, with most particles in the 2–4 nm range. This size window is relevant for PEMFC cathodes because it provides high Pt surface exposure while avoiding the instability typical of sub-nanometric species. The iMAPLE confirmed the feasibility of transferring Pt in nanoparticulate form, but also revealed process limitations. XRD showed a weak broad reflection at 39.8°, corresponding to

an approximate Scherrer size of 1–2 nm. SEM of the 5000-pulse sample showed isolated Pt-rich agglomerates on a largely uncovered glass surface.

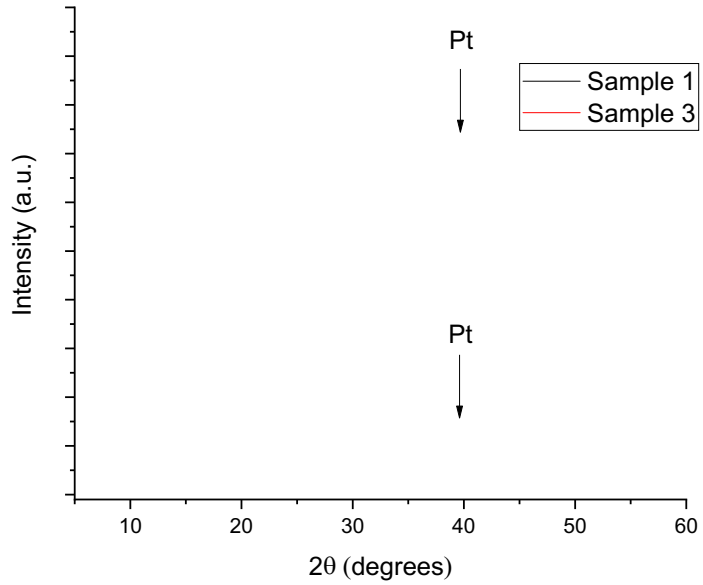


Figure 1: XRD of PLD samples on carbon paper.

Conclusions: The combined PLD/iMAPLE study demonstrates two complementary routes for low-loading nanostructured Pt layers. PLD currently provides the most robust pathway, producing crystalline metallic Pt with coherent domains of 3.6–5.6 nm and controllable sub-200 μg cm^{-2} loadings. iMAPLE offers a bottom-up strategy based on 1 wt% surfactant-free Pt nanoparticles, but remains limited by discontinuous coverage and uncertain yield. Future work will focus on GDL deposition with controlled ionomer integration, and ECSA/ORR benchmarking. Overall, laser-based fabrication appears promising for engineering Pt loading, nanocrystalline size and catalyst-layer morphology beyond conventional ink-deposition.

Acknowledgment: The authors acknowledge the CALIPSO (Celle A combustibiLe innovatIve ad alta Potenza in Sistemi stazionari e di mObilità progetto n. RSH2A_000021 – CUP F57G25000200006) project for the framework support.

References

[1] Debe, M.K. Electrocatalyst approaches and challenges for automotive fuel cells. Nature 2012, 486, 43–51.

[2] Ausanio, G.; Califano, V.; Costantini, A.; Pepe, G.P.; Vicari, C.; Vicari, L.R.M. Laser deposition from a lava stone cup. Optics & Laser Technology 2020, 131.



Deep learning model of PEMFC stack degradation under CO contamination

Luca Pratticò*[a], Francesca Torazzi[a], Gregorio Casagrande*[a], Andrea Gobbi*[b], Johannes Lehmuskoski [c], Lius Daniel [c], Jari Ihonen [c], Matteo Testi [a]

* Corresponding authors: prattico@fbk.eu, gcasagrande@fbk.eu

[a] HyRES unit, Sustainable Energy centre, Bruno Kessler Foundation, Via Sommarive 18 Trento, Italy.

[b] DSIP unit, Digital Industry centre, Bruno Kessler Foundation, Via Sommarive 18 Trento, Italy.

[c] Hydrogen Applications, VTT Technical Research Centre of Finland Ltd., Tietotie 4C Espoo, Finland.

Keywords: Degradation, Deep learning, industrial grade hydrogen, PEMFC

Abstract

Introduction: Proton Exchange Membrane Fuel Cells (PEMFCs) have emerged as one of the most promising electrochemical energy conversion technologies, producing only water as a by-product through a non-combustion process. However, their large-scale deployment remains constrained by durability concerns given by several aspects. In this work, the focus is particularly on the sensitivity of the platinum catalyst to contaminants, specifically carbon monoxide, present in the hydrogen supply. Industrial-grade hydrogen, without expensive purification steps, may contain trace impurities such as CO_2, H_2S, NH_3 and CO [1]. Among these, carbon monoxide has received the most attention in literature, as even sub-ppm concentrations can cause rapid and partially reversible poisoning of the anode catalyst, directly reducing the electrochemically active surface area and cell performance [2]. Developing accurate models of PEMFC behavior is therefore essential to better understand degradation mechanisms and identify optimal operating strategies that extend cell lifetime. However, this is a challenging task: high-fidelity models are already complex for healthy cells and become substantially more demanding when CO contamination dynamics must also be captured [3]. An increasingly explored alternative is the use of data-driven, black-box models trained on experimental data. These approaches offer fast inference after training, the ability to capture complex nonlinear relationships without requiring detailed physical knowledge, and competitive predictive accuracy. Their main limitations lie in data requirements and poor cross-domain generalization: a model trained on one cell or operating regime typically cannot be transferred to a substantially different configuration without retraining them.

Objectives: This work investigates the predictive capability of two recurrent deep learning architectures, Long Short-Term Memory (LSTM) networks and Gated Recurrent Units (GRU), in modelling the temporal evolution of PEMFC stack voltage under CO contamination across different operating regimes.

Material and methods: The models here developed are trained employing experiments already presented in [4]. Two recurrent architectures were implemented and compared: LSTM and GRU, both configured with four layers (32 hidden units each). Both networks forecast a single step ahead by being fed with a sliding window of a fixed length across all training experiments. In addition to the given experimental sensor measures, two other configurations were evaluated: (i) the inclusion of a $CO\ accumulated$ variable, capturing the time-dependent CO exposure at the anode, and (ii) a loss coefficient β that progressively assigns higher importance to post contamination voltage measures via an hyperbolic tangent profile. Also, a third model was introduced, i.e. a simple polynomial regression model which served as a static baseline. First, all models were trained among all twelve experiments with a leave-one-out methodology: for each of the twelve experiments one was used in test and the remaining eleven as training set. Secondly, the training was performed excluding all the experiments related to a single purging regime and using them as test set (e.g. in train all experiments with 5 s and 60 s of purge time and only 400 s in test).

Results: Both recurrent architectures substantially outperformed the polynomial baseline. The GRU consistently achieved the highest and most stable accuracy, with R^2 values typically between 0.83 and 0.94 and RMSE rarely exceeding $0.35\ V$, accurately reproducing both the pre-CO and post-CO contamination phases. The LSTM showed comparable performance in many conditions but also showed a greater sensitivity to signal variability, tending to over smooth rapid transients. The input configuration analysis revealed that the *CO accumulated* variable is the dominant driver of predictive accuracy: its inclusion alone, even without β-weighting, was sufficient for the recurrent networks to reconstruct degradation trajectories with high fidelity. Conversely, the β-weighting scheme provided only marginal benefit when CO information was already present and was insufficient to compensate for its absence when applied alone. In the following pictures, an example for all three models is reported with the presence of the feature $CO\ accumulation$.

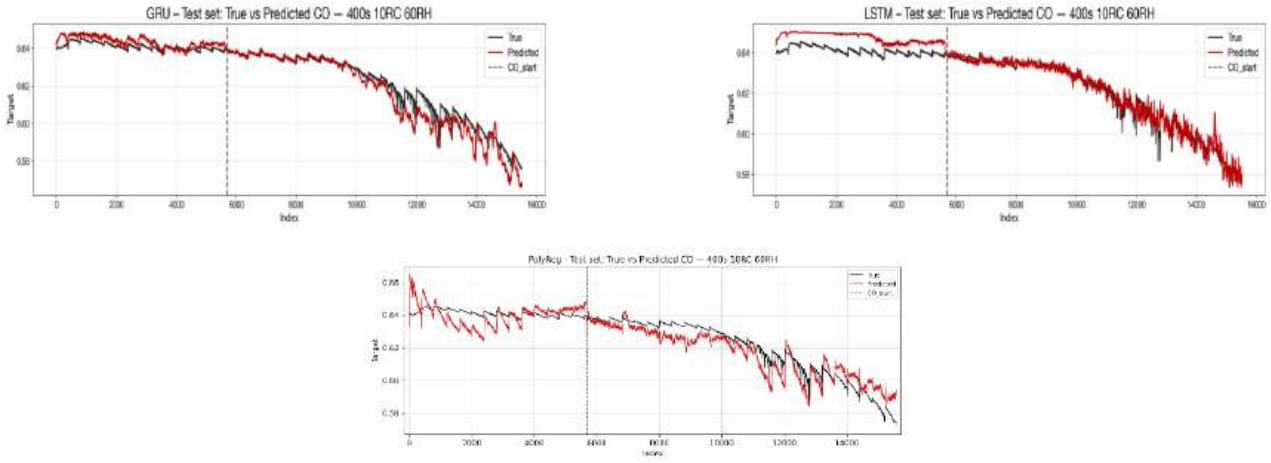


Figure 1- Predicted vs. true average stack voltage for the 400s 10RC 60RH test experiment under the CO accumulated only input configuration. Top left: GRU predictions in red (real value in black), top right: LSTM predictions in red (real values in black), bottom: Polynomial Regression predictions in grey (real values in red). The dashed vertical line marks the onset of CO injection.

Critically, when evaluated on 400 s purge experiments after training exclusively on 5 s and 60 s data, both GRU and LSTM collapsed toward flat predictions, indicating that the temporal structures associated with long purge intervals were entirely unrepresented in the training distribution. Results were less severe when the intermediate 60 s regime was held out, since its dynamics lie between those of the two trained regimes; however, the networks still failed to reproduce the gradual degradation characteristic of that condition.

Conclusions: This study demonstrates that recurrent deep learning models, particularly GRU, can accurately predict PEMFC voltage degradation under CO contamination when training data adequately covers the relevant operating conditions. However, both architectures fail to generalize when entire purge-time regimes are absent from training, highlighting the critical dependence of data-driven prognostic models on training set diversity. Future work should focus on expanding the experimental dataset to cover a wider range of operating regimes and on exploring domain adaptation strategies to improve robustness under distribution shifts.

Acknowledgment: The development of the degradation model was supported by CLEANER project. The CLEANER project is supported by the Clean Hydrogen Partnership and its members. The project is co-funded by the Research Council of Norway and the UK Research and Innovation (UKRI) under the UK government's Horizon Europe funding guarantee. Co-funded by the European Union. Views and opinions expressed are, however, those of the author(s) only and do not necessarily reflect those of the European Union or Clean Hydrogen JU. Neither the European Union nor the granting authority can be held responsible for them.

The datasets were acquired during MetroHyVe 2 project. This project "Metrology for Hydrogen Vehicles 2" (MetroHyVe 2) has received funding from the EMPIR programme co-financed by the Participating States and from the European Union's Horizon 2020 research and innovation programme under Grant agreement No [19ENG04]

References

[1] «Global Hydrogen Review 2023 – Analysis», IEA. Consultato: 12 marzo 2025. [Online]. Disponibile su: https://www.iea.org/reports/global-hydrogen-review-2023

[2] V. F. Valdés-López, T. Mason, P. R. Shearing, e D. J. L. Brett, «Carbon monoxide poisoning and mitigation strategies for polymer electrolyte membrane fuel cells – A review», *Progress in Energy and Combustion Science*, vol. 79, p. 100842, lug. 2020, doi: 10.1016/j.pecs.2020.100842.

[3] T. Jahnke *et al.*, «Performance and degradation of Proton Exchange Membrane Fuel Cells: State of the art in modeling from atomistic to system scale», *Journal of Power Sources*, vol. 304, pp. 207–233, feb. 2016, doi: 10.1016/j.jpowsour.2015.11.041.

[4] L. Pratticò *et al.*, «Study on experimental parameters of PEMFC stack under CO contamination with Machine Learning Technique», in *Conference Proceedings*, ENEA, set. 2025.

EFCH2 2026 European Fuel Cells and Hydrogen
PIERO LUNGHI CONFERENCE
September 15th-17th 2026
Capri / Italy

Advanced Electrochemical Characterization Methods of Solid Oxide Fuel Cells

F. BRUNET-COY, S. FOURCADE, F. MAUVY

CNRS, Univ. Bordeaux, Bordeaux INP, ICMCB, UMR 5026, F-33600 PESSAC, France

Corresponding author: Mauvy Fabrice

Affiliation: ICMCB, CNRS, Univ. Bordeaux

Keywords: SOFC, Oxygen electrode, Impregnation, Electrochemical Impedance Spectroscopy, Tafel plot, Single cell measurements, reference electrode.

Abstract: The development of new, reliable, and robust oxygen electrode materials remains a crucial challenge in the field of solid oxide fuel cells. Building on recent advances in electrode materials and microstructures, the present study focuses on the fabrication of new architectured oxygen electrodes as well as on innovative electrochemical measurements methods[1]. First, the electrochemical characterization of the oxygen electrode has been performed in a symmetrical half-cell geometry. In such two-electrode configuration, only the polarisation resistance values can be determined under air. Under current, a specific sample and a more advanced characterization method are requiring and involves inserting a reference electrode (RE) (i.e. three electrodes configuration)[2,3]. To implement this type of advanced electrochemical diagnosis, the fabrication of symmetrical half-cell consisting of an PrO_{2-x} impregnated porous $Ce_{0.9}Gd_{0.1}O_{2-\delta}$ (GDC) scaffold was carried out by screen-printing on both sides of a GDC electrolyte. The Area Specific Resistance (ASR) of the sample was determined by Electrochemical Impedance Spectroscopy (EIS) as a function of temperature. Using the reference electrode, the overpotential versus current density (Tafel plot) of this oxygen electrode was measured at different temperatures. On the other hand, complete single cells have been elaborated in order to characterize and compare the electrochemical performances of the oxygen electrode under real working conditions. To achieve this, a complete single cell consisting of NiO–6ScSZ/6ScSZ/GDC/PrO_{2-x} was measured in classical two electrodes configuration. Then, reference electrodes positioned on each side make possible to characterize independently the oxygen and hydrogen electrodes under working conditions. This strategy allows for the validation of the experimental setup and the measurement methodology for a complete cell incorporating two reference electrodes. Monitoring the overvoltage and resistance of each component during ageing tests makes it possible to identify the limiting component and better understand the degradation phenomena.

Materials and methods: The fabrication of symmetrical half-cells consisting of a porous (GDC) scaffold was carried out by screen-printing on both sides of a dense GDC electrolyte. This scaffold was impregnated with a praseodymium nitrate solution to obtain the architectured GDC/PrO_{2-x} electrode. Finally, a current collector layer based on $LaNi_{0.6}Fe_{0.4}O_{3-\delta}$ is deposited, as represented in Figure 1.

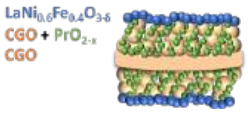


Figure 61: Schematic representation of the elaborated symmetrical half-cell with the architectured oxygen electrode.

Then, regarding the three electrodes configuration, reference electrode based on platinum was placed in a transverse groove machined on the edge of the half-cell and fixed using a platinum ink. By applying a current and performing EIS

measurements, the overpotential (η) of the oxygen electrode in cathodic and anodic modes at different temperatures and atmospheres has been deduced using relation 1:

$$\eta = E_{DC} - R_s \times I_{DC} \quad (1)$$

Where E_{DC} and I_{DC} are respectively the voltage and the current and R_s the electrolyte resistance.

The exchange current density value has been determined for each temperature under different atmospheres. Two methods were used to determine this parameter. The first method is based on the intersection of the Tafel slope, using Equation (2). The second calculation method is based on EIS measurements, where the polarization resistance is related to the exchange current density parameter by Equation (3)[4].

$$i_0 = \frac{RTi}{nF\eta_{act}} \quad (2)^5 \qquad\qquad i_0 = \frac{RT}{nF} \times \frac{1}{R_p} \quad (3)$$

A single cell consisting of NiO–6ScSZ/6ScSZ/GDC/GDC/PrO2-x was used to compare the half cell measurements. In a first step, this sample have been characterized in classical two electrodes configuration to evaluate the overall response of the single cell. Then, reference electrodes positioned on each side make possible to characterize independently the oxygen and hydrogen electrodes under SOFC working conditions. Then, E–I measurements were carried out using "2RE" configuration in order to determine the response of each electrode individually. This approach makes it possible to separate the contributions of the two electrodes and thus provides a more in-depth electrochemical characterization.

Results:First, the oxygen electrode characterization in symmetrical half cell configuration has been performed under air to obtain the Area Specific Resistance (ASR). These results are reported in Figure 2. Concerning the architectured electrode, the ASR value is close to 54 mΩ.cm^{-2} at 700 °C. Thanks to the literature, it can be considered that this oxygen electrode has promising performances compared to others referenced materials[1,6].

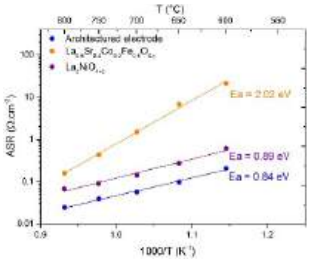
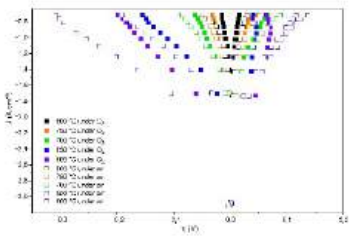


Figure 62: Comparison of the ASR oxygen electrode with materials mentioned in the literature.

The second part of this electrochemical study is dedicated to deeper electrochemical characterization of the architecturated oxygen electrode using three electrodes configuration. For this purpose, EIS measurements were performed under I_{DC}. The overpotential of the oxygen electrode in cathodic and anodic modes at different temperatures and atmospheres is represented in Figure 3.



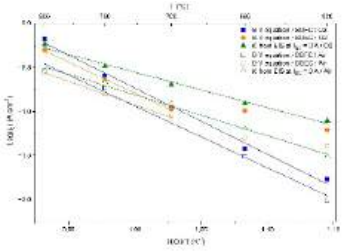


Figure 64: Polarization curves at different temperatures and atmospheres.

Figure 63: i_0 values versus temperature and different atmospheres, using two calculation methods.

As waited, the overvoltage decreases when the temperature increases. Furthermore, measurements in cathodic and anodic modes clearly show that the oxygen electrode performs better in anodic mode (similar as SOEC mode). Furthermore, the overvoltages are lower during measurements in O_2 than in air. These data make it possible to compare the exchange current density values obtained in cathodic and anodic modes at different temperatures and under different atmospheres as shown in Figure 4. A good consistency is observed between the two methods used to determine i_0. For both atmospheres, the values determined from Tafel plots remain close to those determined from the polarization resistance measured by EIS, supporting the reliability of both methods. In addition, the i_0 values measured under air remain lower than those obtained under pure oxygen. Regarding single cells, polarization measurements were performed under SOFC working conditions in order to realize an electrochemical diagnosis using "2RE configuration" enables the polarization values to be measured. Combining the I_{DC} and EIS measurements under steady state conditions makes it possible calculate the anodic (η_A) and cathodic (η_C) overvoltage as represented in figure 5.

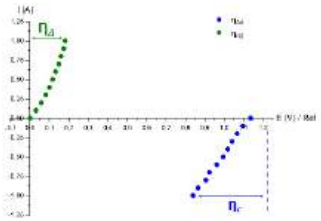


Figure 65: Electrodes polarization curves for both electrodes.

It is then possible to determine the exchange current density for each electrode. Another important point is to determine the specific contribution of the anode, cathode, and electrolyte to the voltage drops across the entire cell. This makes it possible to identify the main losses associated with the cell components and thus to identify the limiting electrode.

Conclusion: The present study highlighted the development of a new structured oxygen electrode, which yielded a favourable polarization resistance value. The experimental method using a three-electrode configuration allowing for the calculation of exchange current density values. Finally, regarding single cells, the "2RE configuration" allows these electrodes to be characterized independently.

Acknowledgement : *This work was supported by a French government grant managed by the Agence Nationale de la Recherche under the France 2030 program, under the reference "ANR-22-PEHY-0003". The author declares no competing interests.*

References

(1) Nicollet, C.; Flura, A.; Vibhu, V.; Fourcade, S.; Rougier, A.; Bassat, J.-M.; Grenier, J.-C. Preparation and Characterization of Pr2NiO4+δ Infiltrated into Gd-Doped Ceria as SOFC Cathode. *J Solid State Electrochem* **2016**, *20* (7), 2071–2078.

(2) Cimenti, M.; Co, A. C.; Birss, V. I.; Hill, J. M. Distortions in Electrochemical Impedance Spectroscopy Measurements Using 3-Electrode Methods in SOFC. I – Effect of Cell Geometry. *Fuel Cells* **2007**, *7* (5), 364–376.

(3) Finklea, H.; Chen, X.; Gerdes, K.; Pakalapati, S.; Celik, I. Analysis of SOFCs Using Reference Electrodes. *J. Electrochem. Soc.* **2013**, *160* (9), F1055–F1066.

(4) Esquirol, A.; Brandon, N. P.; Kilner, J. A.; Mogensen, M. Electrochemical Characterization of La0.6Sr0.4Co0.2Fe0.8O3 Cathodes for Intermediate-Temperature SOFCs.

(5) Chan, S. H.; Khor, K. A.; Xia, Z. T. A Complete Polarization Model of a Solid Oxide Fuel Cell and Its Sensitivity to the Change of Cell Component Thickness. *Journal of Power Sources* **2001**, *93* (1–2), 130–140.

(6) Perry Murray, E. Electrochemical Performance of (La,Sr)(Co,Fe)O3–(Ce,Gd)O3 Composite Cathodes. *Solid State Ionics* **2002**, *148* (1–2), 27–34.



Impact of High-Energy Neutron Radiation on PEM Fuel Cells in Aviation

Nadine Mohamed [a], Till Lennart Kösters [a,b], Benjamin Lutz [c], Michael Heere [a]

* Corresponding author: Michael Heere

[a] Institute of Internal Combustion Engines and Fuel Cells (ivb), Technische Universität Braunschweig, Braunschweig/Germany

[b] SE²A Sustainable and Energy Efficient Aviation, Technische Universität Braunschweig, Braunschweig/Germany;
[c] Physikalisch-Technische Bundesanstalt (PTB), Braunschweig/Germany;

Keywords: Cosmic Radiation, Degradation, PEMFC, Neutrons

Abstract: Proton exchange membrane fuel cells (PEMFCs) are considered a promising alternative power source for future aviation systems due to their high efficiency and low emissions. Several degradation mechanisms still need to be addressed, as current PEMFC technologies are typically limited to approximately 25,000 hours of operation. Yet, their long-term reliability under exposure to cosmic radiation, encountered at cruising altitude, has not been sufficiently investigated. In our study, commercial PEMFC membrane electrode assemblies (MEAs) were exposed to monoenergetic neutrons relevant to extended aircraft operation and comparable to one part of the cosmic radiation. Fuel cell degradation was evaluated using polarization curve measurements before and after irradiation, together with post-irradiation gamma spectrometry analysis. All irradiated MEAs showed noticeable performance deterioration compared with the non-irradiated reference sample.

Introduction: PEMFCs are a promising technology for future civil aviation, particularly because they can contribute to lower emissions, reduced noise, and improved aircraft energy efficiency. The key functional component of a PEMFC is the membrane electrode assembly (MEA), and its long-term stability is essential for reliable and safe fuel cell operation in aircraft applications. One potential challenge is the exposure of fuel cell components to cosmic radiation during flight, which includes secondary particles such as neutrons, protons, and charged pions. Neutrons can interact strongly with hydrogen-rich materials, including water and hydrogen gas [1], both of which are present in PEMFC systems. Therefore, internal fuel cell components may be exposed to repeated neutron interactions during long-term aircraft operation. In addition, previous studies have shown that high-energy radiation can damage polymer structures [2,3]. Since the PEMFC membrane is polymer-based, radiation-induced structural changes could directly affect cell performance and durability. Based on these considerations, neutron radiation may represent a relevant degradation factor for PEMFCs in aviation applications. However, because exposure to cosmic radiation at ground level is comparatively low [4], this effect is usually not considered in conventional PEMFC performance studies. As a result, experimental data on the radiation tolerance of PEMFCs under aviation-relevant neutron exposure remain limited.

Objectives: This study evaluates the stability of PEMFC MEAs under aviation-relevant neutron-radiation conditions. It investigates performance changes after exposure to 1.2 MeV and 14.8 MeV neutrons at fluences representative of extended aircraft operation, supporting the assessment of PEMFC durability at cruising altitudes.

Material and methods: Commercial MEAs with an active area of 45 cm^2 were used for the irradiation experiments.

Neutron irradiation was performed at the Physikalisch-Technische Bundesanstalt (PTB) accelerator facilities in Braunschweig, Germany, where monoenergetic neutrons of 1.2 MeV and 14.8 MeV were generated using the Tandetron accelerator. Neutron fluences of 2.5×10^8 n/cm^2 and 1×10^9 n/cm^2 were applied at both energy levels to represent accumulated exposure at aircraft cruising altitudes, corresponding to approximately 25,000 h and 100,000 h of flight time

During irradiation, three MEAs were placed back-to-back in a hydrogen-rich polymer housing to ensure stable positioning and to approximate the hydrogen-rich environment of a fuel cell system. Polarization curves were measured before and after irradiation using a Horiba Fuel-Con C600 low-temperature fuel cell test bench with a single-cell Baltic Fuel Cells holder. Post-irradiation activation of MEA elements was investigated using a high-purity germanium detector.

Results: Neutron irradiation lead to measurable performance degradation in all exposed MEAs, while the non-irradiated reference sample remains stable during the same experimental period. The small performance increase observed for the reference in Figure 1 is within the uncertainty of the test bench and measurement procedure, indicating that storage, handling, and characterization effects did not significantly influence the results.

All irradiated MEAs show a decrease in cell voltage compared with the reference. The polarization data therefore indicate a clear, current-density-dependent degradation caused by neutron exposure. Differences between the two neutron energies were relatively small and remained within the overall

variation of the dataset. In contrast, the applied fluence and the sample position within the holder had a stronger influence on the observed voltage losses.

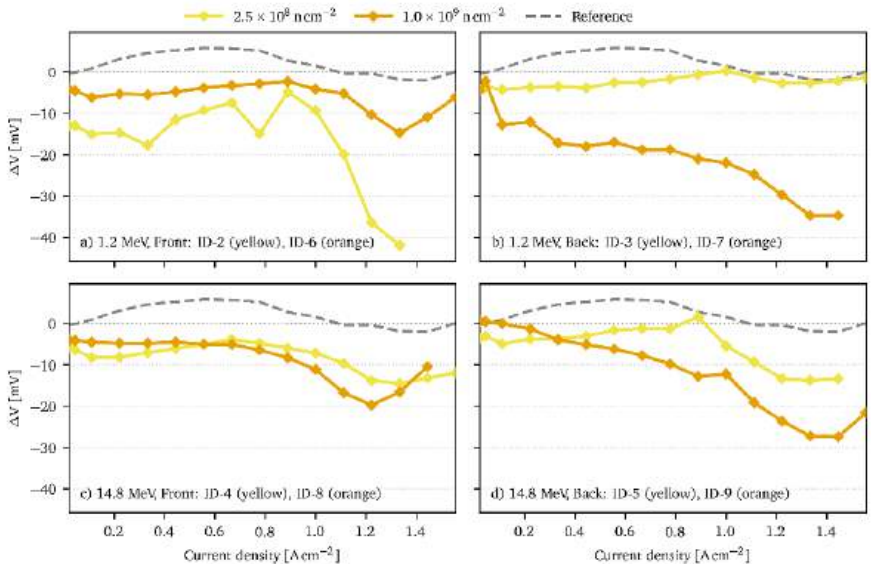


Figure 66: Point-wise voltage difference, ΔV = After − Before, as a function of current density for irradiated PEMFC single cells. The panels compare neutron energy and sample position: 1.2 MeV front, 1.2 MeV back, 14.8 MeV front, and 14.8 MeV back. Curves represent fluences of 2.5 × 10⁸ n/cm² and 1 × 10⁹ n/cm². Negative ΔV values indicate voltage loss after irradiation.

Conclusions: Neutron irradiation caused measurable performance losses in the PEMFC MEAs, while the non-irradiated reference remained stable. The degradation was mainly reflected in reduced cell voltage, with fluence and sample position showing a stronger influence than neutron energy. These results indicate that aviation-relevant neutron exposure may contribute to PEMFC degradation and should be considered in future durability assessments.Further work will include cyclic voltammetry (CV), linear sweep voltammetry (LSV), and electrochemical impedance spectroscopy (EIS) to identify which MEA components are most affected by irradiation and contribute to the observed performance loss. These analyses will be complemented by scanning electron microscopy (SEM) to detect possible irradiation-induced microstructural or interfacial changes within the MEA.

Acknowledgment: This work was supported in part by the Deutsche Forschungsgemeinschaft (German Research Foundation, DFG) through Germany's Excellence Strategy-EXC 2163/1-Sustainable and Energy Efficient Aviation under Grant 390881007.

References

[1] W. Rarita and J. Schwinger, *Physical Review* 59, 436–452, 1941. doi: 10.1103/PhysRev.59.436.

[2] T. Adachi et al., *Journal of Nuclear Materials* 329–333, 2004. doi: 10.1016/j.jnucmat.2004.04.244.

[3] A. Rivaton et al., *Radiation Research* 174, 2010. doi: 10.1667/RR2215.1.

[4] M. M. Meier et al., *Atmosphere* 11, 1358, 2020. doi: 10.3390/atmos11121358.



Ejector Scaling for Marine PEMFC: CFD Modelling and Semi-Empirical Bias Correction from 5 to 200 kW

C. Antetomaso*, G. Cecere, A. Irimescu, S. S. Merola, B. M. Vaglieco

* corresponding author: christian.antetomaso@stems.cnr.it

CNR STEMS, Naples, Italy

Keywords: PEMFC, ejector, hydrogen recirculation, geometric scaling

Abstract

Introduction: Ejector-based anodic recirculation systems (ARS) passively entrain unreacted hydrogen by exploiting the momentum of the primary supply, with no moving parts and no auxiliary power demand. This makes them particularly attractive for marine PEMFC applications, where reliability and efficiency are critical. Validated design and scaling methodologies for medium and high power levels, however, remain scarce in the literature [1]. This work develops a multi-scale framework for ejector scaling from 5 to 200 kW, targeting marine PEMFC propulsion.

Material and methods: The design framework starts from the 5 kW ejector of Nikiforow et al. [2] as geometric reference. All key dimensionless ratios, nozzle throat diameter, mixing chamber geometry, nozzle axial position, and diffuser angle, are preserved across scales, with absolute dimensions set by a choked-flow sizing rule that links the throat area directly to the target stack power. This yields throat diameters of 1.67, 2.36, and 3.73 mm for the 40, 80, and 200 kW levels respectively. Prototypes at 40 and 80 kW were 3D-printed in ABS and tested on dedicated air bench rigs, measuring primary and secondary flow rates over 35 operating points per scale. Figure 1 shows the fluid domain and the printed components. CFD simulations (ANSYS Fluent, 2D axisymmetric RANS) were run in parallel across the same operating maps. Comparing simulations against experimental data revealed a systematic overestimation of the secondary mass flow rate, a known limitation of the axisymmetric assumption [2,3]. A semi-empirical correction coefficient $k = ER_{exp}/ER_{sim}$ was therefore regressed as a linear function of primary inlet pressure p_1 and pressure differential ΔP, independently for each scale. The functional form proved consistent across all three geometries, with regression quality improving with scale, supporting the generalisation of this correction within the ejector family.



Figure 67. Fluid domain of the ejector (left) and printed components (right) used during the experimental campaign.

Results: The corrected CFD shows good agreement with experimental data across all validated scales. The correction coefficient follows the form $k = a - b \cdot \Delta P + c \cdot p_1$ at each power level, with coefficients refitted independently on each experimental dataset:

$k_{5k}W = 0.668 - 1.065 \cdot \Delta P + 0.017 \cdot p_1$

$k_{40k}W = 0.354 - 2.224 \cdot \Delta P + 0.088 \cdot p_1$

$k_{80k}W = 0.267 - 0.910 \cdot \Delta P + 0.045 \cdot p_1$

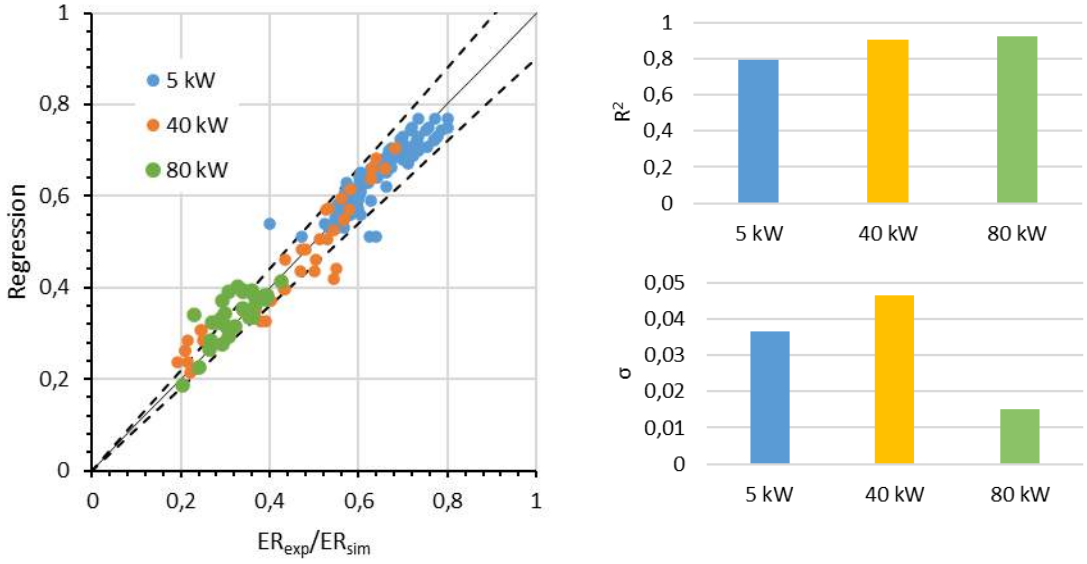


Figure 68. Semi-empirical correlation wrt experimental datasets (left) and R2 and standard deviation for the tested scales

Regression quality improves consistently with scale, confirming that the correction becomes more reliable as absolute flow rates increase and manufacturing tolerances become relatively less significant. The 200 kW CFD campaign is currently underway; prototype fabrication and experimental validation represent the immediate next steps.

Conclusions: A multi-scale framework for ejector-based H_2 recirculation has been validated at 40 and 80 kW (200 kW under characterisation), resting on: (i) dimensionless geometric scaling with the choked-flow rule $D_n \propto \sqrt{P\_stack}$; (ii) 2D axisymmetric CFD validated on air bench data; and (iii) a semi-empirical $k = f(p_1, \Delta P)$ that corrects the inherent axisymmetric overestimation of secondary flow. The correction generalises consistently across all validated scales, with regression quality improving from $R^2 = 0.794$ to 0.926, supporting its use as a reliable design tool without resorting to expensive full 3D simulations.

Acknowledgment

This research was supported in part by PNRR M2C2 – Next Generation EU, Project STAND UP – "Soluzioni Tecnologiche A idrogeNo heavy Duty Per la mobilità", Prog. RSH2B_000022, CUP F59J25000250004.

References

[1] Liu, Y., Tu, Z., & Chan, S. H. (2021). Applications of ejectors in PEMFC: A review. Fuel Process. Technol., 214, 106683.

[2] Nikiforow, K. et al. (2016). Designing a H_2 ejector for 5 kW PEMFC–CFD and experimental validation. Int. J. Hydrogen Energy, 41(33), 14952.

[3] Mazzelli, F. et al. (2015). Computational and experimental analysis of supersonic air ejector. Int. J. Heat Fluid Flow, 56, 305–316.



Europy: a modular pemfc multiphysics framework in python/jax/petsc

Gilmar Nogueira Junior *[a], Pascal Schott[a], Sébastien Kawka[a]

* corresponding author: gilmar.nogueirajunior@cea.fr

[a] CEA LITEN

Keywords: multiphysics simulation, PEMFC modelling, PETSc

Abstract

High-fidelity PEMFC models are valuable for design and diagnosis, but they become limiting when the research question is no longer only the fuel-cell physics, but also the numerical workflow used to solve it. EUROPy was developed to expose a through-plane PEMFC multiphysics model in a fully programmable Python environment, with JAX and PETSc used for efficient residual evaluation and nonlinear solution. The objective is to provide a flexible, license-independent platform where physical assumptions, continuation strategies, solver settings, calibration procedures and future AI-assisted initialization methods can be tested directly. In this work, EUROPy is benchmarked against EuROPIUM Fuel Cell, the in-house CEA modelling platform used as the reference implementation. The current model reproduces the one-dimensional AME_1D configuration, coupling electronic and protonic conduction, gas and dissolved-species transport, membrane and catalyst-layer water transport, heat transfer and electrochemical kinetics. For the baseline case, EUROPy reproduced the full polarization curve from 1.00 V to 0.30 V, completing the 71-point sweep in 124.7 s. The same current-density criterion was then satisfied on five additional EuROPIUM-derived parameter cases. Comparisons of through-plane profiles confirmed that the remaining differences are smooth, localized and physically interpretable. The benchmark indicates that EUROPy preserves the predictive behaviour of the reference workflow while making the PEMFC model available for numerical experimentation, including solver benchmarking, automated calibration, surrogate modelling and future PINN or AI-assisted convergence strategies.

Introduction: *Proton-exchange membrane fuel cell (PEMFC) modelling often relies on robust multiphysics workflows, but these workflows are less convenient when the scientific question is to modify the model, test another solver strategy, couple an optimizer, or use machine learning to improve initialization. EUROPy was developed for this purpose as a license-independent Python/JAX/PETSc framework.*

Objectives: EUROPy is designed to reproduce, inspect and extend a reference PEMFC model while keeping the numerical workflow programmable. EuROPIUM Fuel Cell [1-2], the in-house CEA PEMFC modelling framework, is used here as the reference physics and validation benchmark. EUROPy

translates its one-dimensional through-plane workflow into a modular implementation where physical modules, studies, datasets, diagnostics and solver settings can evolve independently.

Material and methods: The current implementation focuses on the one-dimensional through-plane AME_1D configuration, the fast EuROPIUM use case for parameter studies and electrochemical fitting. EUROPy uses a finite-volume formulation on a EuROPIUM-equivalent through-plane mesh, coupling electronic and protonic conduction, gas and dissolved-species transport, membrane and catalyst-layer water transport, heat transfer and electrochemical kinetics. The nonlinear systems are solved with PETSc/SNES, while JAX accelerates residual and Jacobian-related computations. The solution workflow preserves the staged activation of the reference study before the fully coupled polarization sweep. After discretization, each voltage point solves $R(u; V_{cell}, p) = 0$, where u collects potentials, gas/dissolved species, water/Nafion state, temperature and electrochemical source terms.

Results: EUROPy was benchmarked against EuROPIUM reference exports at global and local levels. For the baseline operating case, it reproduced the full polarization curve from 1.00 V to 0.30 V over the official 71-point sweep, completed in 124.7 s in a fresh verification run. The current-density comparison satisfies the documented agreement criterion over the full curve: either an absolute error below 3 mA cm^{-2} or a relative error below 0.5% once current density exceeds 0.5 A cm^{-2}. In the high-current region, the maximum relative error remains below 0.33%.

Validation was also performed on through-plane profiles, including potentials, temperature, gas species, water activity, proton activity and electrochemical source terms. Five EuROPIUM-derived operating/parameter cases were then simulated with a sequential parameter-homotopy protocol matching the reference export procedure. Across 3905 internal profile comparisons, the remaining differences were smooth and physically interpretable; no branch, sign or equation-translation failure was detected.

Conclusions: The benchmark positions EUROPy as a programmable counterpart to the reference EuROPIUM workflow: close enough for rigorous comparison, but open enough to modify the model and the solver strategy. With a runtime compatible with routine parametric use, EUROPy opens the PEMFC model to constitutive testing, solver benchmarking, automated calibration, custom continuation and future AI/PINN-assisted initialization.

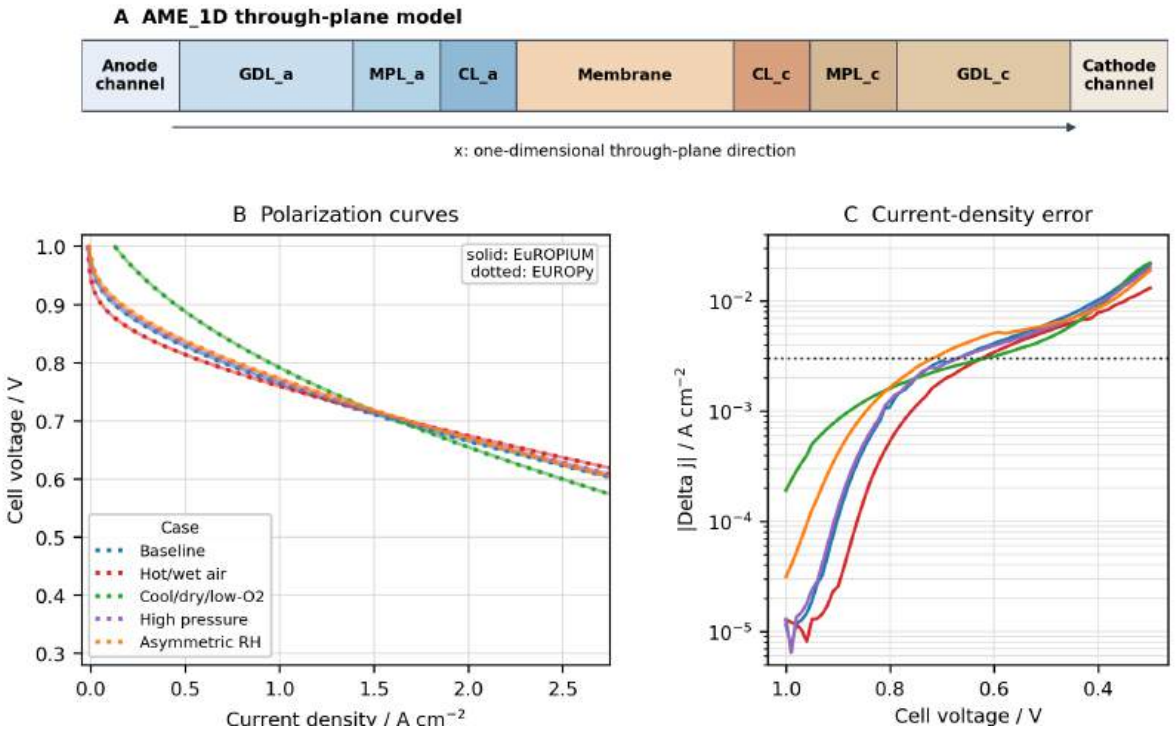


Figure 69 *- EUROPy validation against EuROPIUM reference exports for five parameter cases; the error panel shows absolute current-density error over the same 1.00-0.30 V sweep Panel A: AME_1D through-plane stack.*

Table 11 *- Operating conditions used in the EuROPIUM/EUROPy validation campaign.*

Case	Temperature (C)	RH anode (%)	RH cathode (%)	Pressure anode (bar)	Pressure cathode (bar)	Cathode O_2 mole fraction
Baseline	73	90	90	2.25	2.05	0.15
Hot/wet air	80	100	100	2.25	2.05	0.21
Cool/dry/low-O2	60	50	50	2.25	2.05	0.10
High pressure	73	90	90	2.50	2.30	0.15
Asymmetric RH	73	70	100	2.25	2.05	0.15

References

[1] B. Randrianarizafy, P. Schott, M. Chandesris, M. Gerard, Y. Bultel, "Design optimization of rib/channel patterns in a PEMFC through performance heterogeneities modelling," International Journal of Hydrogen Energy 43 (2018) 8907-8926. https://doi.org/10.1016/j.ijhydene.2018.03.036

[2] F. Vandenberghe, F. Micoud, P. Schott, A. Morin, C. Lafforgue, M. Chatenet, "Low-loaded catalyst layers for proton exchange membrane fuel cell dynamic operation Part 2: Modeling study," Electrochimica Acta 535 (2025) 146542. https://doi.org/10.1016/j.electacta.2025.146542



Degradation modelling of the PEMFC system for heavy-duty long-haul applications using semi-empirical modelling approach

Utkarsh Sodagar*[a], Peter Wahl [a], Krishan Talukdar [a], Tatiana Morosuk [b]
* corresponding author: utkarsh.sodagar@daimlertruck.com
a Daimler Truck AG, Stuttgart, Germany
b Technische Universität Berlin, Berlin, Germany

Keywords: Degradation, Fuel cell electric vehicle, PEMFC, Physics-based modelling

Objectives: Owing to their low operating temperature, clean operation, high power density, long driving range and fast start-up capability, PEMFCs are widely regarded as the most suitable fuel cell technology for heavy-duty long-haul applications to meet EU CO_2 standards (Regulation (EU) 2019/1242) [1]. However, their widespread deployment is constrained by limited lifetime, driven by mechanical and electrochemical degradation whose dependence on real-world operating conditions is not well understood.

Material and methods: This contribution presents a semi-empirical modelling approach for degradation prediction of PEMFC system. The model is developed using a few thousand hours of time-resolved data from system-level test bench operation under representative heavy-duty duty cycles, including dynamic load profiles, start-up and shut-down events, off-time periods, and state-of-health (SoH) assessments of a closed-cathode twin PEMFC system. Relevant thermophysical operating parameters such as current, power, temperature, reactant pressures, relative humidity, and stoichiometry ratio are used as model inputs to capture the influence on degradation behaviour. The model predicts the temporal evolution of cell voltage and implicitly accounts for the combined effects of multiple degradation mechanisms across different operating regimes.

- Data collection and pre-processing:
  - Approximately 2700 hours of 1 Hz of time-series test data for the relevant operating parameters of the twin Fuel Cell System (300 kW total system power, 150 kW per fuel cell system) are collected.
  - Outliers were identified and removed based on deviations from the typical polarization curve of Fuel Cell. The resulting refined dataset from Fuel Cell System 2 (FCS 2) was selected for the subsequent step of model calibration due to its stable operation throughout test period.
- Model calibration:

- Identify and activate degradation mechanisms corresponding to observed test data: Irreversible and reversible catalyst aging, Membrane degradation, Break-in behaviour
- Define a subset of sensitive parameters for calibration
  Manual adjustment of the parameters to bring the model output in the correct trend region of the polarization curve.
- Application of the gradient descent algorithm to minimize the error between simulation and test data.
- Objective function: Root mean squared error (RMSE) between predicted and measured voltage

- Model validation:
  - Refined dataset of FC System 1 (FCS 1) is used as an independent reference.



Figure 70: Mercedes-Benz GenH2 Truck

Results: As shown in *Figure 71,* marker 1 represents calibration process carried out using test data from FCS2, while marker 2 represents the validation performed using test data from FCS1. The comparison between the test data and simulation results show good agreement for both FCS1 and FCS2 of the twin FC System. The model successfully reproduces both the time-dependent and current-dependent voltage behaviour. The RMSE values over the entire test campaign are ~6 mV/Cell and 4.7 mV/Cell for FCS2 and FCS1 respectively.

From a scientific perspective, the proposed approach enables system-level lifetime prediction with explicit degradation mechanism formulations, thereby addressing the complexity and coupling of multiple aging phenomena under realistic operating conditions. Validation against the unseen data of FCS 1 demonstrates that the approach can accurately reproduce both short-term performance variations and long-term degradation trends.

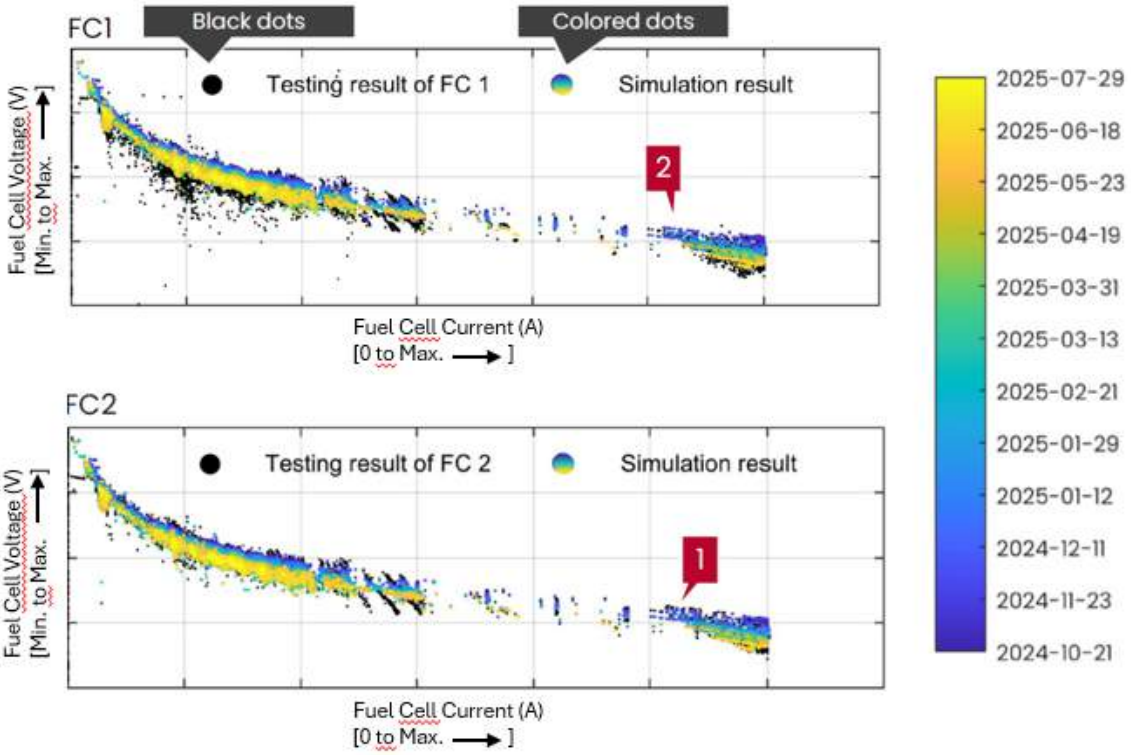


Figure 71: Simulation results of FCS1 and FCS2
(Due to confidentiality clause, the quantities of current and cell voltage cannot be disclosed)

Conclusions: The proposed methodology complements physics-based degradation models, providing a practical tool for durability evaluation and operating strategy optimization of PEMFC systems in heavy-duty applications.

Acknowledgment :The authors gratefully acknowledge that the proposed work was carried out in collaboration with an external partner, whose support and technical contributions are sincerely appreciated.

References

[1] European Commission, CO_2 emission standards for heavy-duty vehicles, Regulation (EU) 2019/1242 and its 2024 amendment, European Union, 2019–2024.



Computational Model-based Performance Assessment of PFAS-Free Membrane-Electrode Assemblies in PEM Fuel Cells

Andreas Podias*[a], Thomas Dankers [a]

* Corresponding author: andreas.podias@tno.nl

[a] TNO – Netherlands Organisation for Applied Scientific Research

Mobility & Built Environment Unit, Powertrains Research Department

Automotive Campus 30, 5708 JZ, Helmond, the Netherlands

Keywords: PEM fuel cell, PFAS-Free fuel cell components, macro-homogeneous physic-based model, membrane transport phenomena

Abstract: This work extends an open-source macro-homogeneous one-dimensional membrane-electrode assembly (MEA) model by incorporating membrane transport parameterisations for two alternatives to Nafion™: Aquivion® and sulfonated poly(ether ether ketone) (sPEEK), as a PFAS-free PEM. The results quantify the performance sensitivity to ionomer water uptake and proton conductivity, and identify the principal transport limitations intrinsic to the specific PFAS-free membrane considered in the current work.

Introduction: PFAS, the chemical class to which Nafion™ and other PFSA ionomers belong, are under regulatory restrictions in the European Union (EU), the United States, and other jurisdictions due to their environmental persistence, bioaccumulation potential, and documented toxicological effects. The EU's REACH regulation and the US Environmental Protection Agency's PFAS Strategic Roadmap signal a trajectory towards broad restriction of PFAS in manufactured products, with potential ramifications for PEMFC commercialisation timelines, driving urgent demand for fluorine-free alternatives that can deliver comparable electrochemical performance under realistic operating conditions.

Objectives: This work's objective was to extend the open-source macro-homogeneous one-dimensional MEA model of Vetter & Schumacher (2019) [1], to incorporate membrane transport parameterisations for Aquivion® PFSA, a short-side-chain PFSA membrane, and sulfonated sPEEK, as a PFAS-free alternative. Furthermore, to compare polarisation curves and key performance indicators across Nafion™ NR-211 (baseline), Aquivion®, and sPEEK under EU harmonised automotive test conditions [2, 3].

Material and methods: Two candidate membrane classes are of particular interest in the current work:

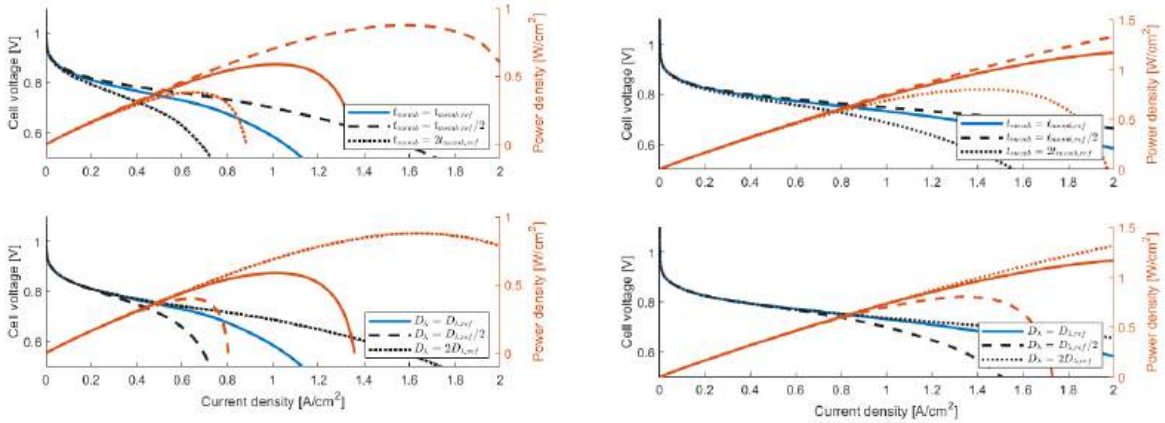
Aquivion® PFSA, with equivalent weight (EW) typically in the range 700-890 g/mol, offering higher crystallinity and improved high-temperature stability compared to Nafion™.

sPEEK, a hydrocarbon ionomer entirely free of fluorine, with tunable ion exchange capacity (IEC) through the degree of sulfonation (DS). sPEEK offers a promising combination of low cost and PFAS-free chemistry, but exhibits fundamentally different water uptake, swelling and transport characteristics relative to PFSA membranes.

Computational domain and governing equations: The present work builds directly on the open-source one-dimensional Master MEA Model (MMM1D) framework of Vetter & Schumacher [1], which provides a steady-state, non-isothermal, two-phase model of coupled transport of charge, heat and mass in the through-plane direction of a five-layer MEA, i.e., anode gas diffusion layer (AGDL), anode catalyst layer (ACL), PEM, cathode catalyst layer (CCL), and cathode gas diffusion layer (CGDL). The governing equations, i.e., Ohm's law for electrons and protons, Fourier heat conduction, dissolved water transport with electro-osmotic drag, Fickean gas diffusion, and Darcy-law liquid water transport, are retained unchanged. Eight coupled second-order PDEs are solved simultaneously using MATLAB's bvp4c boundary value problem solver (see [1]). Butler-Volmer kinetics govern the hydrogen oxidation reaction (HOR) in the ACL and the oxygen reduction reaction (ORR) in the CCL; source terms for heat, water sorption/desorption, and liquid-vapour phase change are retained as specified in the original model [1]. Material-specific parameterisations are substituted for the membrane types under investigation [4-8].

Results: Simulations are conducted under the EU harmonised automotive conditions and selected stress tests (T1–T7) [3]. Simulated polarisation curves at typical operating conditions (T = 70 °C, P = 1.5 bar, RH = 90% anode and cathode), referred to as the base case (see [1]), are depicted in figure 1, where the impact of the PEM thickness and water diffusivity on polarisation performance is highlighted.

Aquivion® outperforms Nafion™ NR-211 at the base case, primarily due to higher water uptake at elevated humidity and improved proton conductivity at the reference temperature. Under dry stress tests (T3–T5), however, the higher EW sensitivity of Aquivion® conductivity to water content reduces this advantage. sPEEK exhibits a significantly higher ohmic membrane resistance under all test conditions, driven by the intrinsically lower proton mobility in hydrocarbon channels. Performance at high current densities is further constrained by the lower water diffusivity, which intensifies the water concentration gradient across the membrane and exacerbates anode drying under electro-osmotic drag.



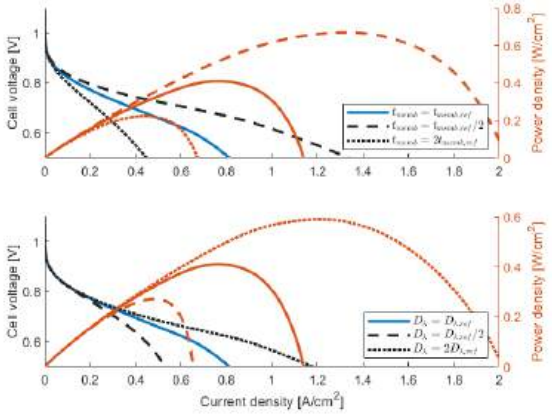


Figure 1. *Impact of PEM thickness (top) and water diffusivity (bottom) on polarisation performance - (Top left) Nafion™ NR-211, (Top right) Aquivion®, (Bottom) sPEEK*

Conclusions and outlook: The extended MMM1D framework demonstrates that Aquivion® PFSA membranes can exceed Nafion™ NR-211 performance under typical automotive operating conditions. sPEEK, while fully PFAS-free, currently suffers from substantially higher ohmic losses and restricted high-current-density performance that must be addressed through membrane engineering, e.g., via composite structures, acid–base blends, or nano-channel alignment, before it can be considered a viable replacement. Future work will extend the model, in line with the PROMISERS project, to include PEMs being developed of fluorine-free proton exchange ionomers based on hydrocarbon polymers, hyperbranched mesoporous polybenzimidazole polymers and cellulose nanofibers. Additionally, (i) temperature-dependent swelling and mechanical stress, and (ii) degradation kinetics relevant to the PFAS-free MEAs will be considered in future model extensions.

Acknowledgment: This work is prepared in the context of the PROMISERS project (Promisers Project - PFAS-FREE HYDROGEN TECHNOLOGY) with Grant Agreement number 101192151.

References

[1] Vetter, R., Schumacher, J.O., Computer Physics Communications, 234 (2019), 223.

[2] Friberg, R, Winkel, R, Smokers, R, Foster, D, Joerissen, L, Tsotridis, G, Winkler, W, Podias, A, & Voigt, C., "A Proposal of a Harmonized Testing Format for Fuel Cell Technology: FCTESTNET." *Proceedings of the ASME 2005 3rd International Conference on Fuel Cell Science, Engineering and Technology*. Ypsilanti, Michigan, USA. May 23-25, 2005. pp. 753-761. https://doi.org/10.1115/FUELCELL2005-74068.

[3] Tsotridis, G., Pilenga, A., De Marco, G., Malkow, T., EU Harmonised Test Protocols for PEMFC MEA Testing in Single Cell Configuration for Automotive Applications, JRC Science for Policy report, EUR 27632 EN, 2015, https://doi.org/10.2790/54653.

[4] Ise M., Kreuer K. D. and Maier J., Solid State Ionics 125 (1999) 213.

[5] Pivovar B.S., Y. Wang, E.L. Cussler, J. Membr. Sci. 154 (1999) 155.

[6] Kreuer, K.D., J. Membr. Sci. 185 (2001) 29.

[7] Pivovar, B.S., Polymer 47 (2006) 4194.

[8] Kusoglu A., Weber A.Z., Chem. Rev., 117 (2017) 987.



Dimethyl sulphide as a biogas contaminant in SOFCs: experimental characterisation and degradation modelling

Lucia Pera*[a], Marta Gandiglio[a], Paolo Marocco[a], Hangyu Yu[b], Cédric Frantz[b], Davide Pumiglia[c], Jan Van Herle[b], Massimo Santarelli[a]

* corresponding author: lucia.pera@polito.it

[a] Department of Energy, Politecnico di Torino, Corso Duca degli Abruzzi 24, 10129 Torino, Italy

[b] Group of Energy Materials, Swiss Federal Institute of Technology in Lausanne (EPFL), Rue de l'Industrie 17, Sion, 1950, Valais, Switzerland

[c] ENEA - Italian National Agency for New Technologies, Energy and Sustainable Economic Development, Research Centre Casaccia, Roma, Italy

Keywords: 0D modeling, Dimethyl sulphide, SOFC, sulphur coverage

Abstract

This work investigates the impact of biogas-derived sulphur compounds beyond the widely studied hydrogen sulphide (H_2S). Anode-supported Ni-YSZ/YSZ/LSCF cells are operated in reformed biogas mixtures at 0.4 A cm^{-2} under fixed temperature, fuel/air flow rates and gas composition, while dimethyl sulphide is added at controlled concentrations.

The extracted parameters and experimental trends are used to build and calibrate a 0D degradation model. The model relates the rate of voltage loss to the level of sulphur contamination under steady operation. After validation against the experimental dataset, it is applied to predict cell lifetime for different contamination scenarios.

Introduction: High-temperature SOFCs are a promising pathway for decarbonised power generation, particularly when coupled with renewable feedstocks such as biogas. However, the trace contaminants inherently present in biogas pose a significant challenge to long-term cell durability [1].

The majority of published degradation studies have used H_2S as a model contaminant [2], leading to a relatively mature body of mechanistic knowledge and semi-empirical correlations for this species. In contrast, the electrochemical effects of other sulphur compounds relevant to real biogas streams remain far less understood.

This work addresses this gap by presenting a dedicated experimental and modelling study of dimethyl sulphide (DMS) induced degradation in SOFCs operating on reformed biogas. A multi-level diagnostic approach is applied to isolate and quantify the electrochemical effects of DMS, and the results are used to develop a compact 0D model capable of predicting cell performance under different contamination levels.

Objectives:

- Quantify the performance decay of Ni-YSZ/YSZ/LSCF cells under DMS contamination.
- Develop and calibrate a 0D electrochemical degradation model.
- Validate the model against an independent experimental dataset.

Material and methods: Anode-supported Ni-YSZ/YSZ/LSCF cells (SolydEra) are operated at 750°C in a reformed biogas mixture at a fixed current density of 0.4 A·cm^{-2}. Gas flow rates and composition are kept constant throughout all tests. After one week of stabilisation in clean biogas, DMS is introduced at 1, 3 and 5 ppm. The experimental protocol and test workflow are illustrated in Figure 1.

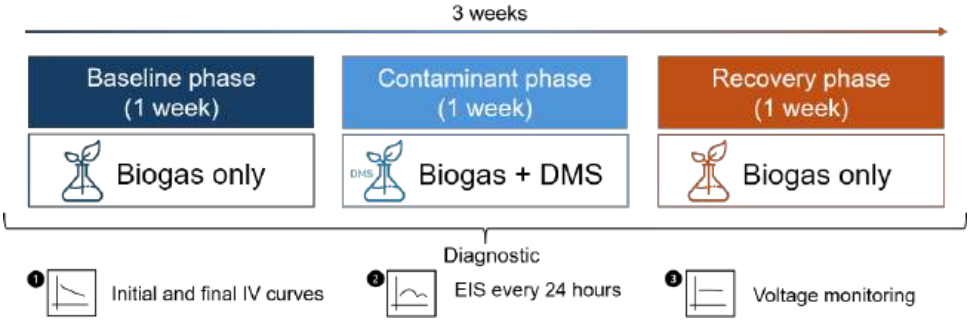


Figure 72. Work flow for each experimental test with different DMS concentration.

The 0D model reconstructs the cell voltage via a full overpotential balance (Nernst + Butler-Volmer + multicomponent diffusion including Knudsen terms). Degradation is introduced through a modified Temkin adsorption isotherm [3] for DMS surface coverage θ_{eq}, calibrated on the 1 and 5 ppm experimental datasets. The coverage reduces the anodic exchange current density linearly through $i_{0,a}^{deg} = i_{0,a}^{clean} \cdot (1 - \theta_{eq})$, and the contaminated IV curve is reconstructed accordingly.

Results: DMS introduction produces an immediate and sustained voltage decay under galvanostatic operation at all concentration levels. A clear dose-response relationship is observed: at 1 ppm DMS the cell voltage drops by approximately 73 mV from the initial clean-fuel value, while the degradation is progressively more severe at 3 and 5 ppm. This behaviour is consistent with an increasing occupation of active Ni surface sites as the contaminant partial pressure rises.

EIS result confirms that DMS acts primarily by inhibiting anodic electrochemical kinetics and water-gas shift activity at the Ni-YSZ anode, with no measurable impact on electrolyte conductivity or cathode behaviour.

In the clean-fuel baseline, the 0D model accurately reproduces the experimental IV curve across the full range of current densities. Under contaminated conditions, a single corrective factor is calibrated from the 1 and 5 ppm datasets and used to adapt the classical H_2S-based Temkin isotherm to DMS adsorption. The resulting equilibrium coverage θ_{eq} increases monotonically with DMS concentration.

The 3 ppm case, used as an independent validation point, yields a reconstructed IV curve in close agreement with the experimental data (Figure 2), demonstrating the interpolation consistency of the modified isotherm within the calibrated range.

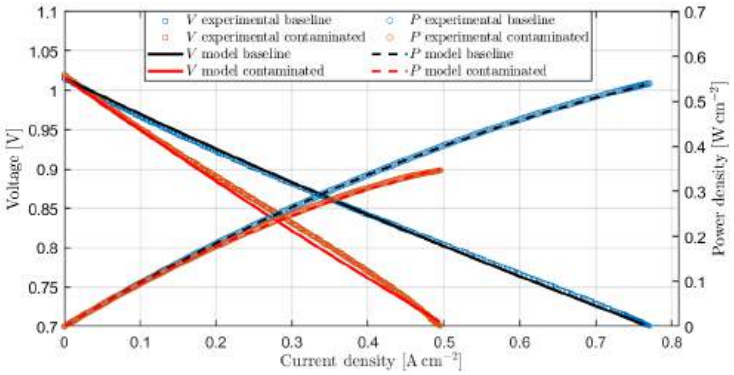


Figure 73. Experimental and modelled iV curve before and after contamination exposure with 3 ppm DMS.

Conclusions: This work presents a combined experimental and modelling study of the impact of dimethyl sulphide on SOFC performance under reformed biogas operation.

A compact 0D degradation model has been developed and calibrated using a modified Temkin adsorption isotherm adapted for DMS. The isotherm parameters are identified directly from the experimental voltage decay data via an inverse procedure. The model successfully reproduces the clean-fuel IV characteristic and the contaminated cell behaviour, and is validated at 3 ppm DMS as an independent test case.

References

[1] L. Pera, M. Gandiglio, P. Marocco, D. Pumiglia, M. Santarelli, Trace contaminants in biogas: Biomass sources, variability and implications for technology applications, J. Environ. Chem. Eng. 12 (2024). https://doi.org/10.1016/j.jece.2024.114478.

[2] A. Hagen, J.F.B. Rasmussen, K. Thydén, Durability of solid oxide fuel cells using sulfur containing fuels, in: J. Power Sources, 2011: pp. 7271–7276. https://doi.org/10.1016/j.jpowsour.2011.02.053.
[3] I. Alstrup, J.R. Rostrup-Nielsen, S. Røen, High temperature hydrogen sulfide chemisorption on nickel catalysts, Appl. Catal. (1981).



Advanced In-situ Oxygen Transport Diagnostics for Large Format PEM Fuel Cells

Mehran Afra*[a], Oliver Curnick[a]

* corresponding author: Mehran Afra

[a] Centre for E-Mobility and Clean Growth (CECG), Coventry University, Coventry, CV12TL, England, United Kingdom

Keywords: Instrumented membrane, in-situ oxygen sensing, PEM fuel cells, spatial diagnostics

Abstract

Introduction: As Proton Exchange Membrane Fuel Cells (PEMFCs) are scaled for high-power applications including heavy-duty transport, aerospace, marine, and stationary power generation, their larger active areas can promote non-uniform oxygen distribution across the cathode. Such non-uniformity can reduce performance, increase susceptibility to local starvation, and contribute to degradation, while conventional measurements such as cell voltage provide only limited insight into the local conditions inside the cell. In response to this diagnostic gap, this work explores the use of instrumented membranes for in-situ oxygen sensing at the cathode catalyst layer (CL)/membrane interface, with the aim of improving local understanding of oxygen behaviour in large-format PEMFCs and supporting future development toward spatially-resolved and stack-relevant diagnostics.

Objectives: The objective of this work was to develop a minimally invasive instrumented membrane platform for in-situ oxygen sensing in PEMFCs under realistic operating conditions. The specific aims are to:

- assess oxygen behaviour at the cathode CL/membrane interface;
- demonstrate the sensing concept in large-format PEMFC hardware;
- refine calibration and interpretation of the sensor response;
- extend the approach beyond single-location sensing toward spatially-resolved measurements;
- and support future progression toward stack-level implementation.

Material and methods: The sensing approach is based on an instrumented membrane incorporating thin-film Pt/C-based sensing elements incorporated into a 250 cm^2 PEMFC (Fig. 1). Local oxygen concentrations were derived from DC chronoamperometric measurements combined with simultaneous high-frequency impedance measurements on the sensor, using model-based calibration to correct for hydration- and temperature-dependent effects. The initial implementation demonstrated local oxygen sensing at a single position, and the approach was subsequently extended

to multiple sensing locations distributed along the cathode flow direction. This enabled comparison of oxygen concentration at different positions in the cell under controlled changes in cathode conditions and air stoichiometry. The platform is now being developed for application in stack-relevant configurations.

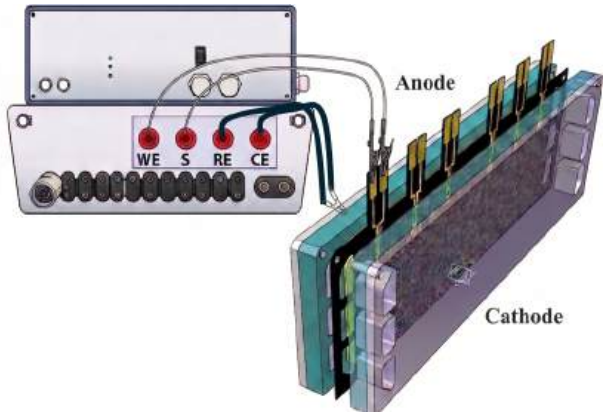


Figure 74 - Schematic of the instrumented membrane oxygen-sensing concept integrated into a 250 cm^2 PEMFC.

Results: The instrumented membrane approach enabled in-situ sensing of oxygen at the cathode CL/membrane interface in large-format PEMFC hardware. The combination of sensor current, high-frequency impedance, and model-based calibration provided continuous measurement of local oxygen concentration during operation. A representative sensor response to step changes in cathode inlet oxygen concentration is shown in Fig. 2.

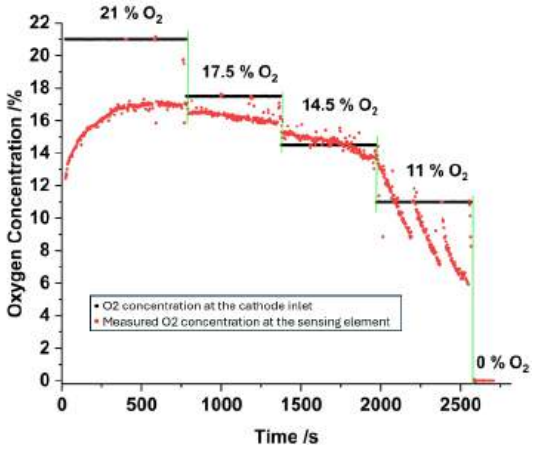


Figure 75 – Measured oxygen concentration at the catalyst layer/membrane interface over time during operation.

Expanding the sensing concept to multiple locations revealed clear spatial variation in oxygen availability along the cathode flow path, with oxygen concentration decreasing both with increasing distance from the cathode inlet and with decreasing air stoichiometry. In the downstream region, local oxygen concentration was observed to approach zero even while the overall cell voltage remained

above 0.4 V, a range generally considered safe for avoidance of air starvation during PEMFC operation. This highlights the value of local oxygen measurements for identifying non-uniformities that are not visible through bulk diagnostics alone.

Conclusions: This work demonstrates the potential of instrumented membranes as a practical platform for in-situ oxygen diagnostics in PEMFCs. The approach enables local oxygen concentration to be assessed at the cathode CL/membrane interface in large-format hardware, and extension to multiple sensing locations shows that it can capture spatial oxygen non-uniformity within the cell. By providing local insight into oxygen transport and availability, instrumented membranes can support prognostics and future optimisation of operating strategies in high-power PEMFC systems, with strong potential to contribute to improved performance and durability.

Acknowledgment

The authors gratefully acknowledge the support of Coventry University's Centre for E-Mobility and Clean Growth (CECG) during this work. This research was partly funded by FEV UK Ltd and supported the European Union's Horizon Europe research and innovation programme under grant agreement number 101096598 (ESCALATE).

References

[1] M. Afra, J. Klütsch, C. Ozyalcin, J. Fleming, O. Curnick, *In-situ measurements of oxygen concentration at the PEMFC cathode catalyst layer/membrane interface*, Journal of Power Sources, 658 (2025) 238275.



1D - 3D heat transfer model for air cooling of hydrogen proton exchange membrane fuel cell

Pierpaolo Martini*[a], Enrico Corti[b], Giacomo Silvagni[b] , Stefano Pesaresi[c] ,

Alessandro D'Adamo[a], Carla Menale[d]

*corresponding author: Pierpaolo Martini

[a] University of Modena and Reggio Emilia, Dept of Engineering "Enzo Ferrari", Modena, 41125, Italy

[b] University of Bologna, Dept of Industrial Engineering, Forlì, 47121, Italy

[c] SPEI s.r.l. Engineering, Modena, 41126, Italy

[d] ENEA – The Italian National Agency for New Technologies, Energy and Sustainable Economic Development, Rome, 00164, Italy

Keywords: air cooling sub-system of fuel cells, heat transfer, multi-physics CFD fuel cell model, small drone's PEMFCs stack testing

Abstract

Air cooling of hydrogen proton exchange membrane fuel cell (PEMFC), mainly in the range of 100 W to 2 kW [1], presents a challenge to balance light weight, ease of manufacturing, reliability and performance of the cooling subsystem. To address this challenge, a 1D-3D heat transfer model is presented, aiming to predict the performance of air cooled fuel cells and design a novel air cooling plate. The 1D model was validated with a 3D multi-physics CFD fuel cell model including a water cooling plate [2]. Once validated, the 1D model was used to design and predict the performance of a new air cooling plate, while validation was performed again with the same 3D multi-physics CFD fuel cell model. Furthermore the model results have been compared to experimental tests on air cooled drone PEMFCs.

Introduction: The development of air-cooled fuel cells is mainly oriented towards small Unmanned Aerial Vehicles (UAVs) and light aviation, starting from a range of 100 W to 2 kW, 100-300 cm^2 FC, to optimize lightness and performance. Much larger H_2 Fuel Cell stacks for light aircraft are currently under development. Consequently, propulsion systems utilizing fuel cells are of great interest in the low-power sector (drones) to increase range, and more generally, in the R&D phase, as a solution for decarbonizing the aviation sector. In both areas, Fuel Cells plays a crucial role: hence the interest in analyzing heat exchanges in detail, with a particular focus on air cooling systems, which are not only the standard for low-power systems (drones), but are also of great interest for large systems (stacks of hundreds of kW).

Objectives: This study aims to develop a 1D-3D heat transfer model with two main objectives: to predict the air cooling performance of fuel cells and to design a high-performance, lightweight, easy-to-manufacture, and reliable air cooling plate that can be developed initially for small drone and subsequently for aircraft environments. Furthermore, the study aims to demonstrate a preliminary validation of the 1D-3D heat transfer model, using test bench experimental data from an air-cooled fuel cells stack (IE SOAR 800).

Material and methods: The methodology adopted in this study involves the creation of a 1D model and the use, for model validation, of both a 3D multi-physics CFD model and experimental data collected from an air-cooled fuel cell stack (IE SOAR 800):

1. 1D heat transfer model was created (using a spreadsheet and Python code), based on the fundamental heat transfer equations (Newton's convection law and energy flow) and the numerical integration of temperature as a function of the cooling duct length. Assumption: a constant surface temperature as the calibration parameter (Ts), to obtain the air output temperature (Tout) and the heat flux. Modeling with variable Ts is currently under investigation.
2. 3D multi-physics CFD fuel cell model (SIMCENTER STAR-CCM+ 2021.2) of water-cooled PEMFCs (25 cm^2, 0.6 V, 0.704 A/cm^2, Pe 10.56 W, serpentine pattern: D 1 mm, L 1.2573 m, laminar flow) was used with a novel air-cooling plate (33 parallel ducts of L 50 mm: 31 square, D 1.45 mm, 2 rectangular on the sides, h x l: 1.45 mm x 0.7 mm, all still laminar flow), aiming to validate the 1D heat transfer model in both water-cooled and air-cooled configurations.

The design method for the new air cooling plate (CAD SOLID*WORKS*), also inspired by commercial fuel cells, features the following characteristics: ease of manufacture and compact size thanks to the use of thin and cost-effective sheet metal, just one-tenth of a millimeter thick, obtained by stamping and punching into a corrugated shape and assembled by welding into a structure of the same thickness. The external structure serves both as a structural element and as a connection between the lower bipolar cathode plate and the upper bipolar anode plate. The trade-off between temperature uniformity and pressure drop was carefully considered in the design of the geometry and mass flow rate, ensuring suitability for mass production.

Results: Preliminary validation results of the 1D model against 3D-CFD model and experimental results can be detailed as follows.

1) The 1D model was validated with the 3D multi-physics CFD model of a water-cooled PEMFCs, providing the coolant output temperature and cathode/anode heat flux in agreement with the CFD simulation.
   The 1D model assumes as calibration parameter the constant surface temperature (Ts) of 356.31 K at the cathode and 355.50 K at the anode, almost equal to the reasonable estimated value (from the 3D CFD model) of the average between the average temperature and the maximum temperature of the catalytic layer at the cathode and anode: under these conditions the 1D model leads to the same outlet air temperature (Tout) as the 3D model at both the cathode (356.25 K) and the anode (355.45 K).

   Furthermore heat flux values across the exchange surfaces estimated by the 1D model were very close to those of the 3D model: 1626 W/m^2 vs 1616 W/m^2 at cathode and 1229 W/m^2 vs 1215 W/m^2 at anode, corresponding to 14.36 W/cell (1D model) and 14.24 W/cell (3D model), according the overall heat generation rate of 15.49 W/cell [i = 17.6 A/cell (0.704 A/cm^2 x 25 cm^2), V_{tn} = 1.48 V, V_c = 0.6 V). The scalability of such model will be discussed, as a contribution to the general knowledge on air-cooled PEMFC stacks.

2) Once validated, the 1D model was used to design an air-cooled PEMFCs; validation of 1D model was performed again with the same 3D multi-physics CFD fuel cell model, assembled with the new air cooling plate over the cathode side (no forced air cooling on the anode side).
   The 3D model selected the temperature as the thermal specification (353 K) of the upper part (Top) of the cooling plate (lower anode side: convection). The 1D model assumed as calibration parameter a constant surface temperature (Ts) of 361 K at the cathode, for the square ducts (as in point 1) and air speed of 3.8 m/s: under these conditions the output temperature (Tout) estimated by the 1D model and 3D CFD model resulted the same: 347 K.
   Furthermore heat flux values, across the exchange surfaces, estimated by the 1D model were close to those of the 3D model: 2016 W/m^2 vs 1849 W/m^2 at the cathode (square ducts), corresponding to 18 W/cell (1D model) and 16.6 W/cell (3D model), according the overall heat generation rate of 14.3 W/cell [i = 16.25 A/cell (0.65 A/cm^2 x 25 cm^2), V_{tn} = 1.48, V_c = 0.6].
3) Finally the following experimental data gathered on an air-cooled fuel cell stack (IE SOAR 800) allowed a preliminary validation of the 1D – 3D model with the new air-cooling plate design:

- the polarization curve for power up to 500 W (Figure 1), extrapolated up to 800 W (max power of IE SOAR 800);

- estimated fuel cell characteristics; number of fuel cells: 37, surface of each fuel cell: 115 cm^2 (estimated 195 mm x 59 mm); number of ducts: 125, length of each duct: 59 mm
- the polarization curve of the single fuel cell has been obtained dividing the overall voltage by the estimated number of cells;
- testing temperature of 323 K assumed as thermal specification of the Top of the new air cooling plate on board of 3D multi-physics CFD Fuel Cell model (Bottom anode FC convection), calibration parameter the constant surface temperature (Ts) of 328.7 K (point 1), air speed of 3.8 m/s, allows to meet cooling requirements, in agreement with 1D model: T out 320.49 K (3D) vs 320.69 K (1D) (Figure 2), heat flux 1005 W/(m^2*K) [3D] vs 1104 W/(m^2*K) [1D];
- the extrapolated maximum stack current allowed the calculation of the cooling requirement for a single fuel cell of IE SOAR 800 stack (at full Pe = 800 W), thanks to the overall heat generation rate of stack of 37.6 W/cell [(with i = 40 A, V_{tn} = 1.48, V_c = 0.541 (20 V/37 FC)], in agreement with 1D model (42.5 W/cell), using the new air cooling design with 125 parallel ducts, L 59 mm: Ts calibration 328.66 K, air speed 3.8 m/s, Tout 322.71 K (Figure 2).

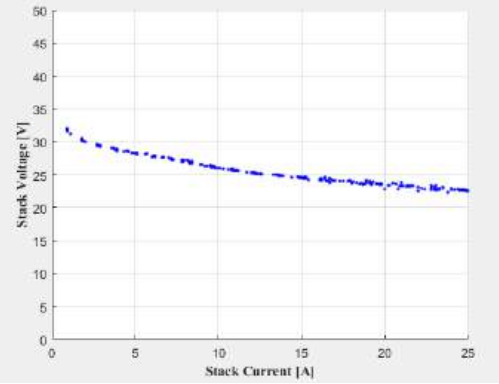


Figure 1 IE SOAR 800 polarization curve test

Voltage-current trend : tested up to 500 W
UNIBO Dept of Industrial Engineering (LEGO project)

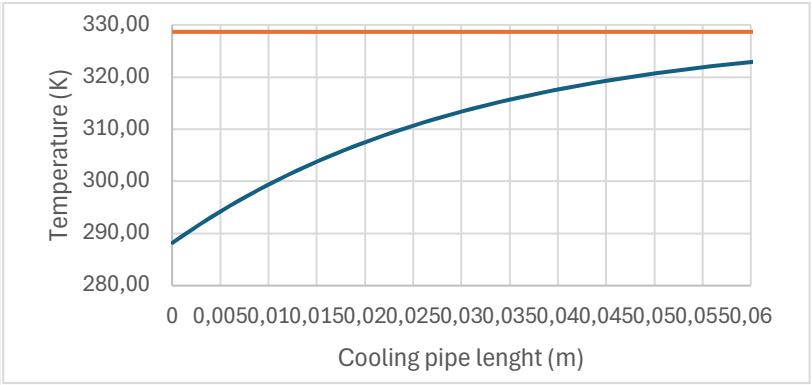


Figure 2 Temperature-square duct length trend - 1D air cooling model

Ts: 328.6 K, D: 1.45 mm, air velocity: 3.8 m/s, L: 50 mm (3D multi-physics CFD model), L: 59 mm (IE SOAR 800 fuel cells modules), mass flow: 9.78e-6 kg/s.

Conclusions: Using a 1D heat transfer model, validated against a 3D multi-physics CFD fuel cell model, a cooling plate structure for air-cooled PEMFCs was designed, achieving cooling performance in line with the extrapolation of experimental data gathered on an air-cooled fuel cell stack for drone up to 500 W (IE SOAR 800).

Acknowledgment: The authors would like to thank ENEA for supporting the first author and his doctoral project, the Engineering Department "Enzo Ferrari" of the University of Modena and Reggio Emilia (UNIMORE), in particular Prof Alberto Muscio and Prof Enrico Mattarelli for supporting the doctoral student's research and the University of Bologna (Forlì Campus) for the laboratory tests of the PEMFCs (LEGO project: learning by doing among students). The authors would also like to thank Eng Davide Romano (PhD student at Engineering Department "Enzo Ferrari" of UNIMORE), Eng Michele Arena and Eng Stefano Bergamini (former students of Engineering Department "Enzo Ferrari" of UNIMORE) for their valuable contribution to the 3D CFD modeling.

References

[1] S. Zhang, S. G. Kandlikar, "A critical review of cooling techniques in proton exchange membrane fuel cell stack" , International Journal of Hydrogen Energy 37 (2012), Department of Mechanical Engineering, Rochester Institute of Technology, NY, USA, 2011.

[2] G. Corda, S. Fontanesi, A. D'Adamo, "Numerical comparison of the performance of four cooling circuit designs for proton exchange membrane fuel cells (PEMFCs)", University of Modena and Reggio Emilia, Dept of Engineering, SAE International, Technical Paper, 2022.



Efficient pseudo 2D PEM fuel cell model for integration in multi-stack system

Noé Labeyrie*[a], Georges Salameh [a], David Chalet[a], Michael Deligant[b]

* corresponding author: noe.labeyrie@ec-nantes.fr

[a] Nantes Université, Ecole Centrale Nantes, CNRS, LHEEA, UMR 6598, F-44000 Nantes, France

[b] Arts et Métiers Institute of Technology, Cnam, LIFSE, F-75013 Paris, France

Keywords: Automotive, Multi-stack, OpenModelica, PEM fuel cell model

Abstract

Introduction: Fuel cell-powered heavy-duty and commercial vehicles will likely rely on multi-stack architectures to meet power requirements while enabling stack modularity and standardization. Such multi-stack systems present new opportunities, notably the design of specific thermofluidic architectures and the possibility of placing certain stacks in standby mode during prolonged periods of low power demand. However, the impact of these architectures and energy management strategies on performance and degradation remains insufficiently understood, particularly regarding the influence of the balance of plant on the stacks. [1].

Objectives: This work aims to develop a PEM fuel cell model suitable for integration into multi-stack systems to investigate system control strategies over driving cycles. The model must be designed to exhibit realistic behavior under dynamic conditions, with special attention paid to the influence of auxiliary components, particularly the pressure and temperature controlled by the compressor and the cooling loop. The stack behavior must also remain realistic at low power under standby conditions. Simultaneously, the model must maintain a reasonable computational time to enable simulation and optimization over a large number of driving cycles.

Material and methods: The model is developed using the OpenModelica software, an open-source implementation of the Modelica language, thus enabling acausal modeling that can be easily integrated into complex energy systems with different control strategies. It is a pseudo-2D macro-homogeneous model with a discretization along the flow channels and the various transport phenomena implemented between each layer, particularly for water vapor. There is no internal discretization within each individual layer; every state variable is considered constant within a single layer: flow channels, catalyst layers, and membrane.

The gas and coolant flows are modeled using the pipe component from the Modelica Standard Library. The electrochemical kinetics are described using the Butler-Volmer formulation, taking into account temperature, pressure and platinum-oxide coverage through their impact on the exchange current density. Kulikovsky's analytical approximation, under the assumption of ideal gas transport through

the thickness of the catalyst layer, is used to avoid explicit discretization within the catalyst layer thickness while preserving accuracy regarding activation and ohmic losses [2].

Hydrogen and nitrogen crossover is also included. Combined with the platinum oxide coverage dependence of the activation model, this allows for a relatively accurate calculation of the voltage at very low power. This aspect is essential for standby control.

Results: The model has been validated for several platinum loadings of the cathode catalyst layer under pure oxygen as well as air, using experimental data from Owejan et al. [3]. At high current and low platinum content, due to liquid water accumulation which is not included in the model, diffusion effects are underestimated. However, the model is intended to be used under conditions without liquid water formation, where the model agreement is good as shown in figures 1 and 2.

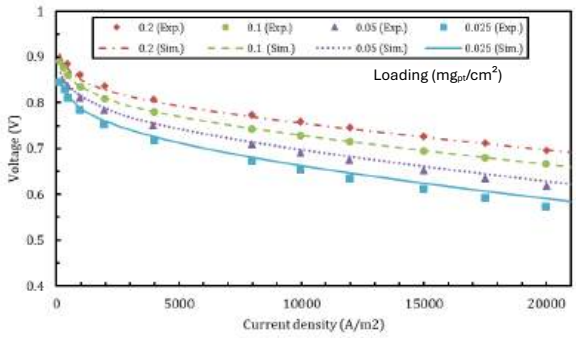


Figure 1: Model validation for several platinum loading under pure oxygen, 100% RH, 80°C and 150 kPa

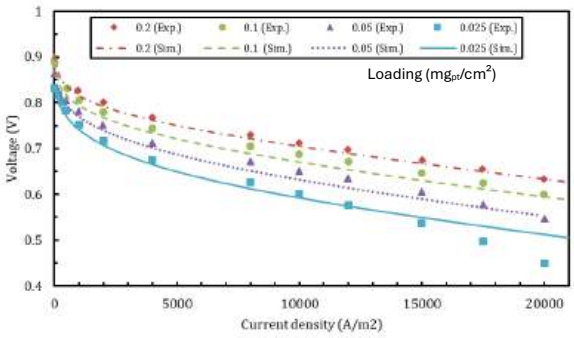


Figure 2: Model validation for several platinum loading under air, 100% RH, 80°C and 150 kPa

The model is integrated into a system with anode recirculation and without cathode humidification. The pressure is fixed at 150 kPa on both sides, and the cathode stoichiometry is set to 2. The current is fixed at 1 A/cm^2, the purge valve is controlled to maintain a nitrogen molar fraction of 0.2 at the anode, air and water inlet flows temperatures are at 70 °C. The cathode air composition is that of atmospheric air at 50% relative humidity and 20 °C. As shown in Figure 3, the anode recirculation flow rate improves the uniformity of the relative humidity distribution. Figure 3 also shows that, in addition to inlet temperatures and pressures, an increase in the temperature gradient along the cell can improve uniformity, but at the cost of overall humidity. Due to the interaction of both parameters, anode recirculation needs to be controlled depending on the temperature gradient along the cell to avoid the risks of drying out or flooding.

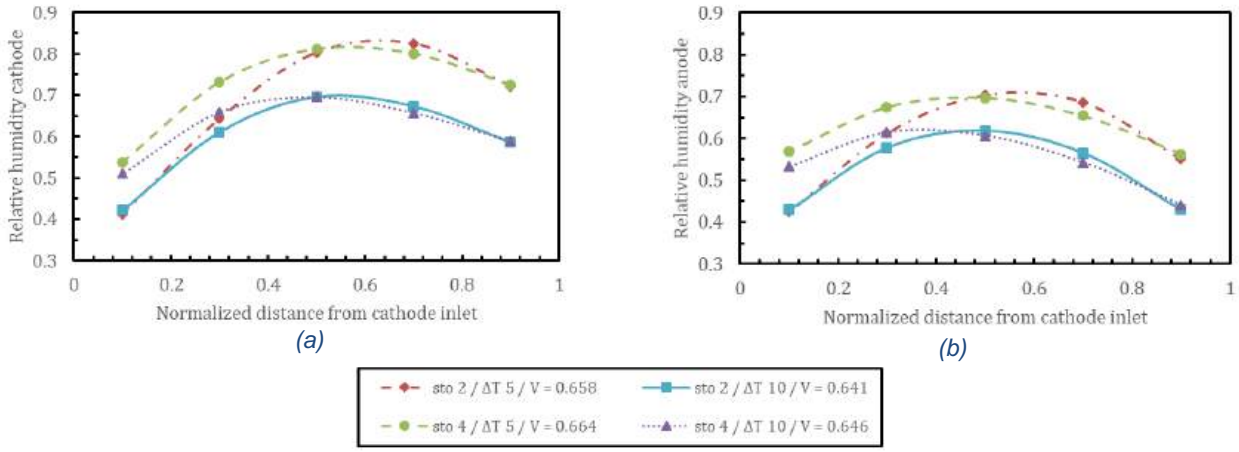


Figure 3: Relative humidity distribution along the cell for several anode stoichiometries and coolant temperature variations between the inlet and outlet. (a) Cathode. (b) Anode.

Conclusions: The proposed pseudo-2D model provides a good trade-off between representativeness and computational time for integration into a system. It thus allows studying the influence of the thermofluidic architecture and control strategies for systems with one or several stacks. In future work, the fuel cell model will be integrated into a complete vehicle system with the compressor(s), the heat exchanger(s), and the battery to study the control and energy management strategies.

Acknowledgment The work in this article is done with funds from ALTOS - a National Research Agency (ANR) project - and the Region des Pays de la Loire.

References

[1] R. Ma et al., « Recent progress and challenges of multi-stack fuel cell systems: Fault detection and reconfiguration, energy management strategies, and applications », Energy Conversion and Management, vol. 285, p. 117015, juin 2023, doi: 10.1016/j.enconman.2023.117015.

[2] A. A. Kulikovsky, « The regimes of catalyst layer operation in a fuel cell », Electrochimica Acta, vol. 55, nº 22, p. 6391-6401, sept. 2010, doi: 10.1016/j.electacta.2010.06.053.

[3] J. P. Owejan, J. E. Owejan, et W. Gu, « Impact of Platinum Loading and Catalyst Layer Structure on PEMFC Performance », *Journal of The Electrochemical Society*, 2013, doi: 10.1149/2.072308jes.

EFCH2 2026 European Fuel Cells and Hydrogen PIERO LUNGHI CONFERENCE
September 15th-17th 2026 Capri / Italy

Large-scale 3D HTPEM stack simulations: single-cell thermal extrapolation vs. full electrochemistry modelling

V. K. Krastev*[a], L. Bartolucci[b], F. Donato[c], M. Kheir Rouz[b] and V. Mulone[b]

*Corresponding author: krastev@dii.uniroma2.it

a Enterprise Engineering Department, University of Rome "Tor Vergata", 00133 Rome, Italy

b Industrial Engineering Department, University of Rome "Tor Vergata", 00133 Rome, Italy

c Energy Technologies Department, ENEA, 00123, Rome, Italy

Keywords: CFD, Cooling Channels, HTPEM, Stack

Abstract

Introduction: Three-dimensional CFD modelling is a common approach for the accurate simulation of electrochemistry, fluid dynamics and heat transfer in HTPEM fuel cells [1], [2]. Most studies in the scientific literature focus on single-channel or single-cell [3] simulations for the following reasons: i) modelling complexity – the need for a large number of governing equations and sub-models adds CPU load and RAM usage intensity (~3 GB for each million of computational cells); ii) geometric complexity – the presence of very thin layers and small channels in the fuel cell assembly often requires large computational meshes, especially if cooling channels need to be included in the simulation. Thus, a research gap clearly emerges in the application of large-scale models for full-stack CFD simulations.

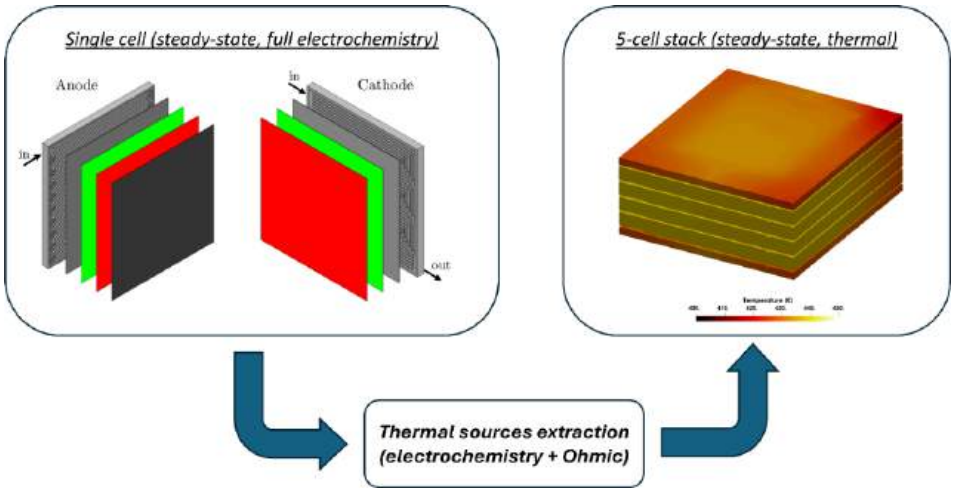


Figure 76 - *Schematics of thermal sources extrapolation from the single-cell towards the 5-cell stack model.*

Objectives: The present work starts from a validated 3D single-cell CFD model and extends it to a 5-cell stack configuration. The main goal is to compare a simplified thermal extrapolation method (Fig. 1) with full electrochemistry modelling, gaining insights for more efficient large-scale simulation approaches.

Materials and methods: For the full-chemistry fuel cell modelling assumptions, governing equations and model validation, the reader is redirected to [3]. The 5-cell stack domain is discretized using a hybrid unstructured grid with a total number of ~100M elements, including BP-integrated cooling channels. The thermal extrapolation method requires mapping of electrochemistry-related heat sources from a converged single-cell simulation towards the same 5-cell stack domain. Fluid flow and heat transfer are then solved, without considering electrochemistry and thus reducing the CPU load. In both cases, governing equations are solved numerically through the Ansys® Fluent commercial CFD code [4]. This simplified thermal (ST) model is here compared with a full-chemistry (F-C) one, where the electrochemistry is considered and fully coupled to the reactive fluid dynamics in the stack flow fields and cooling channels.

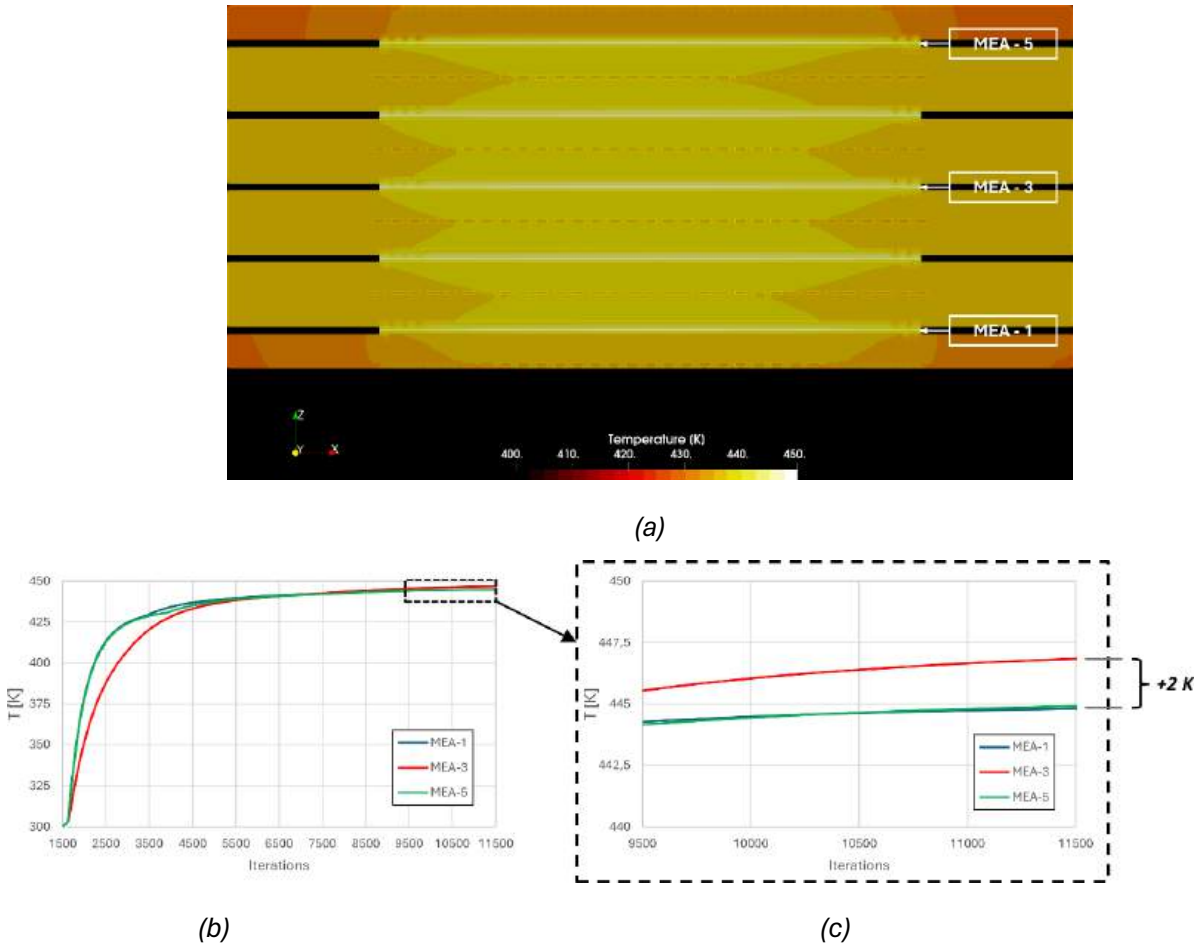


Figure 77 – *Temperature distribution results for the simplified thermal stack simulation: a) middle-section temperature contour with MEA numbering; b) MEA max. temperature convergence trends; c) detail of the last 2000 iterations.*

Results: An initial comparison is made between simplified thermal (ST) and full-chemistry (F-C) runs, with a reference single-cell voltage of 0.4 V (equivalent to a stack voltage of 2V). In both cases coolant flow enters at 433 K, while fuel and oxidant flows enter at 393 K. Figure 2 shows temperature distribution results from ST, highlighting a temperature difference of ~2 K between the central and external MEAs. Notably, the same temperature difference drops to ~1 K in the F-C simulation (Fig. 3). Furthermore, the maximum temperature

absolute value is ~8 K lower in the F-C case. Notably, the ST run requires 4 times less iterations to converge, while the overall CPU time is reduced by one order of magnitude. It is thus demonstrated that full stack simulations require coupling between electrochemistry and fluid dynamics to give accurate predictions of the thermal response.

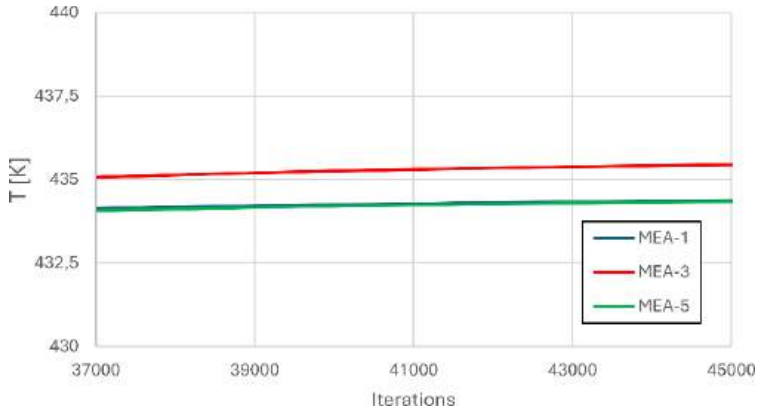


Figure 78 – *Mea max. temperature trends for the 2V full-chemistry simlations, detail of the last 8000 iterations.*

Conclusions: The present work demonstrates the feasibility of liquid-cooled full-stack CFD simulations of the order of ~100 M cells. Using a simplified thermal extrapolation approach allows for CPU time reduction by one order of magnitude and returns a similar temperature difference across the modelled stack domain, compared to full-chemistry modelling. A significant deviation in the maximum absolute temperature value is detected among the two simulation methods, thus requiring further investigations for a comprehensive modelling performance assessment.

Acknowledgments: This research has been funded by the European Union – NextGeneration EU and by the Italian Ministry of Environment and Energy Security, POR H2 AdP MEES/ENEA with involvement of CNR and RSE, PNRR - Mission 2, Component 2, Investment 3.5 "Ricerca e sviluppo sull'idrogeno" WP 3.1 LA 3.1.4 "Gestione e validazione dell'ingegneria di stack di celle a combustibile a membrana polimerica".

References

[1] R. K. Abdul Rasheed, Q. Liao, Z. Caizhi, and S. H. Chan, "A review on modelling of high temperature proton exchange membrane fuel cells (HT-PEMFCs)," *Int. J. Hydrogen Energy*, vol. 42, no. 5, pp. 3142–3165, Feb. 2017, doi: 10.1016/j.ijhydene.2016.10.078.

[2] H. Edwards, M. P. Pereira, S. Gharaie, R. Omrani, and B. Shabani, "Computational fluid dynamics modelling of proton exchange membrane fuel cells: Accuracy and time efficiency," *Int. J. Hydrogen Energy*, vol. 50, pp. 682–710, Jan. 2024, doi: 10.1016/j.ijhydene.2023.09.004.

[3] V. K. Krastev, M. Baldelli, L. Bartolucci, F. Donato, M. Kheir Rouz, and V. Mulone, "Optimal cathode design of a single high temperature PEM fuel cell: A computational study," *Int. J. Hydrogen Energy*, vol. 142, pp. 80–89, Jun. 2025, doi: 10.1016/j.ijhydene.2025.05.346.

[4] Ansys Inc., *ANSYS® Academic Research CFD, Release 2024 R1, Fluent User's Guide*. 2024. [Online]. Available: http://www.ansys.com

European Fuel Cells and Hydrogen
PIERO LUNGHI CONFERENCE
EFCH2 2026
September 15th-17th 2026
Capri / Italy

Fault-Tolerant Operation of a Stacked Interleaved DC-DC Buck Converter for PEM Electrolyzers

S. Okba[a], G. La Tona*[a], G. Marsala[a], M. C. Di Piazza[a], M. Luna[a]

* corresponding author: giuseppe.latona@cnr.it

[a] National Research Council, Institute of Marine Engineering. Italy

Keywords: fault tolerance, PEM electrolyzer, power electronic converter, ripple

Abstract

Introduction: The Stacked Interleaved Buck Converter (SIBC) presented in [1] is an advantageous DC-DC converter topology for PEM electrolyzers, since it exhibits zero output-current ripple, which helps extend electrolyzer lifetime. It features a conversion bridge with a main leg for power transmission and an auxiliary leg for ripple compensation. The semiconductor devices of the auxiliary leg are driven with complementary signals to those of the main leg. Continuity of service is an important requirement for industrial applications, since the occurrence of faults implies production downtime, equipment damage, safety risks, and significant economic losses. Therefore, the adoption of fault-tolerant converters is highly recommended to enhance system reliability and availability.

Objectives: This work aims to make the SIBC capable of fault-tolerant operation in presence of many faults of its semiconductor switches. An open circuit fault of the main leg's bottom device only determines increased losses since the current starts flowing through the parallel-connected diode. With regard to other faults, thanks to the modularity of this conversion topology, a standard single-phase bridge can be used for the SIBC, so the roles of the main and auxiliary legs can be reassigned when needed. This way, the converter can maintain its operation, although with non-null output current ripple and possibly increased losses.

Material and methods: To enable fault-tolerant operation of the SIBC converter, some hardware modifications must be performed, and suitable control logic must be devised. The proposed technique will be described referring to a SIBC that interfaces a PEM electrolyzer (modeled with a linear characteristic) with an active rectifier connected to the national grid. The rated electrolyzer voltage is $V_n = 86.4\ V$, whereas the DC link voltage is $V_{DC} = 630\ V$. Thus, the rated duty cycle is $d^* = 0.1371$. Fig. 1 shows the schematic of the fault-tolerant SIBC. Three mechanical switches (contactors) must be used to isolate the main and aux inductors or connect them to the main and auxiliary legs (*SW_Lp_Main, SW_Lp_Aux,* and *SW_Ls_Aux*). If connection of the main inductor to the auxiliary branch is required, the two signals that are generated by the PWM modulator for the top and bottom devices must be swapped issuing the *swap_PWM_signals* command. Each inductor must be

disconnected when its current is zero to prevent overvoltage and arcing at the switch contacts. Thus, the PWM operation must be stopped by deasserting the corresponding enable signal (*Main_Leg_en* and *Aux_Leg_en*), so that the current will naturally decay to zero. Even with zero current on the auxiliary inductor, the top capacitor remains charged at $V_{DC}(1 - d^*) - V_n = 457.2\ V$. Thus, a suitable discharging circuit must be used, which is activated with signal *SW_Disch* and is based on a suitably driven MOSFET that behaves as a constant-current load. Finally, two additional diodes (D6 and D7) must be included to avoid negative voltage on the top and bottom capacitors during the reconfiguration transients. During normal operation, such diodes are reverse biased, so they do not introduce additional losses.

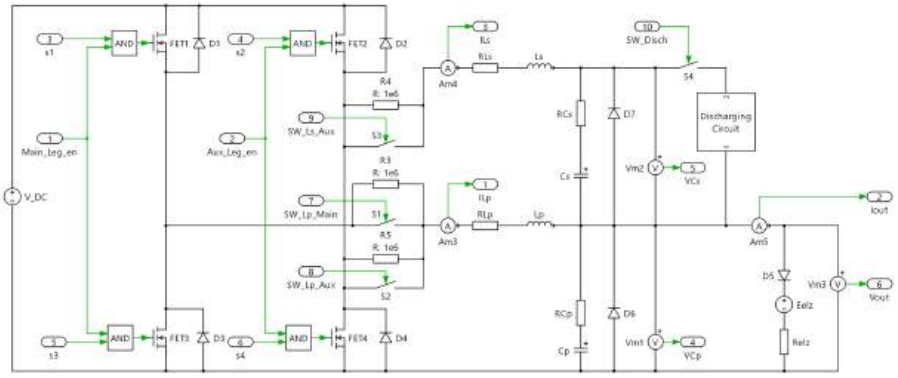


Figure 1. Schematic of the fault-tolerant SIBC.

According to Table 1, faults are classified according to their type and the location of the affected semiconductor device: open circuit (OC) or short circuit (SC); main or auxiliary leg; top or bottom device. In addition, faults that produce similar effects can be grouped. Overall, five fault groups are identified. The reconfiguration procedure consists of several sequential steps defined through a finite state machine (FSM), whose state transition diagram is shown in Fig. 2. The diagram is self-explanatory, since it follows the FSM principles described in [2]. The fault management can be summarized as follows. Fault_1 is the only irrecoverable fault group. Fault_2 impairs the main leg, so the converter operation is briefly suspended (for hundreds of microseconds), the main inductor is disconnected from the main leg and connected to the auxiliary one, and the operation resumes with non-null current ripple. Fault_3 requires no intervention and only implies increased losses. Finally, Fault_4 and Fault_5 impair the auxiliary leg, so the main leg operation continues, and the converter exhibits non-null ripple and possibly increased losses if Fault_3 happens at the same time.

Results: The proposed approach was assessed through simulations in the MATLAB/Simulink environment. As an example, Fig. 3 shows the management of Aux_Top_SC_fault, resulting in non-null current ripple after the fault. Other simulation results are omitted for lack of space.

Conclusions: The SIBC converter can exhibit fault-tolerant operation for 7 out of the 8 possible fault types of its semiconductor switches thanks to suitable hardware modifications and an FSM-based

fault management logic. Simulations showed that the proposed approach is effective for managing all 6 faults, enhancing the reliability and availability of the SIBC.

Acknowledgment: This research was funded by NextGenerationEU, POR H2 AdP MEES/ENEA with involvement of CNR and RSE, PNRR – Miss. 2, Comp. 2, Invest. 3.5.

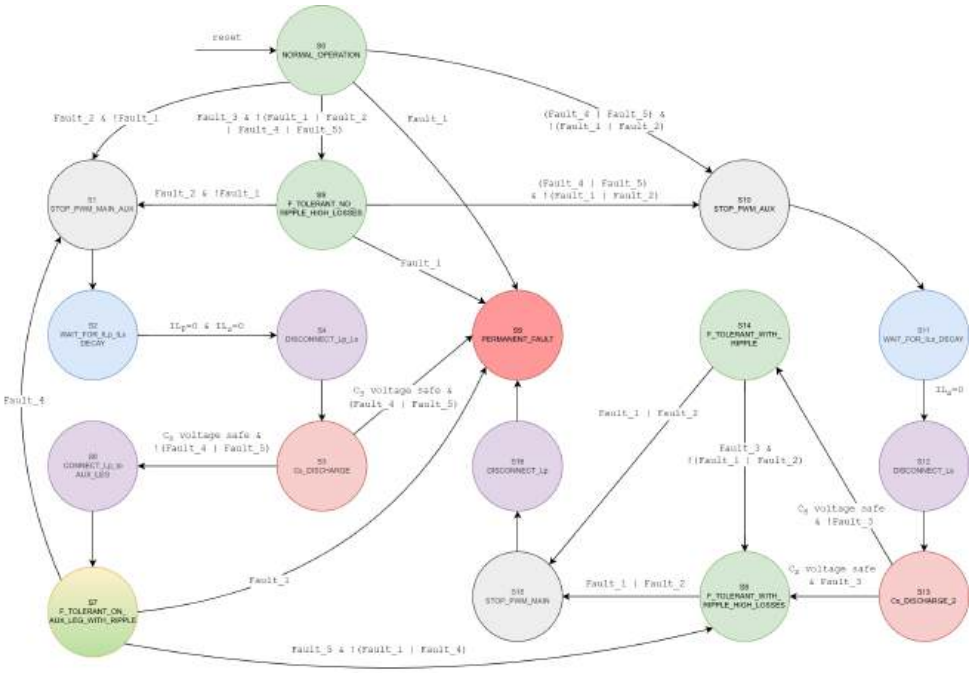


Figure 2. State transition diagram of the FSM used for fault-tolerant operation of the SIBC.

Fault Group	Fault signals	Notes
Fault_1	Main_Top_SC_fault	Irrecoverable fault
Fault_2	Main_Top_OC_fault | Main_Bot_SC_fault | (Main_Bot_OC_fault & !Tolerate_Losses)	Main Leg must be disabled
Fault_3	Main_Bot_OC_fault & Tolerate_Losses	Losses on Main Leg increase
Fault_4	Aux_Top_OC_fault | Aux_Bot_SC_fault | Aux_Top_SC_fault	Aux Leg must be disabled
Fault_5	Aux_Bot_OC_fault	Aux leg cannot cancel ripple but can replace Main leg

Table 1. Fault groups

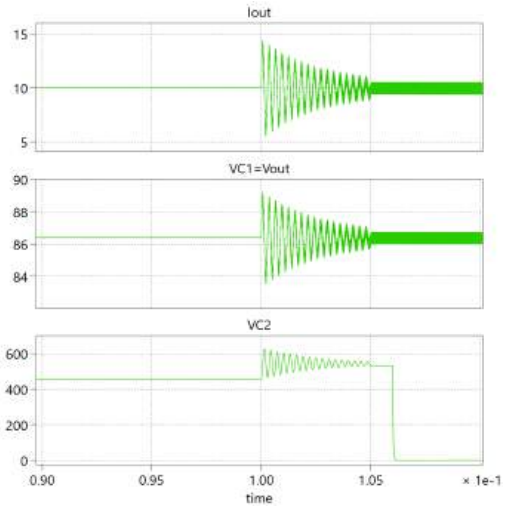


Figure 3. Simul. results for sample fault management

References

[1] D. Guilbert, D. Sorbera, G. Vitale, "A stacked interleaved DC-DC buck converter for proton exchange membrane electrolyzer applications: Design and experimental validation", International Journal of Hydrogen Energy, vol. 45, no. 1, pp. 64-79, 2020.

[2] F. Wagner, R. Schmuki, T. Wagner, P. Wolstenholme, "Modeling Software with Finite State Machines", Auerbach Publications, Boston, MA, United States, 2006, ISBN:9780849380860.

Fuel-Flexible SOFC-CHP for a Just Hydrogen Transition

R. Santagata*[a], G. Di Florio[a], A. Agostini[a]

* corresponding author: remo.santagata@enea.it

[a] ENEA - Italian National Agency for New Technologies Energy and the Environment, Via Anguillarese 301, 00123 Roma, Italy

Keywords: fuel flexibility, social life cycle assessment, SOFC-CHP, sustainable energy

Abstract

Introduction: Hydrogen and fuel cell technologies are increasingly discussed as part of the transition towards low-carbon and renewable energy systems. However, recent literature stresses that hydrogen should not be treated as a universal decarbonization solution, but rather as a context-dependent energy carrier whose environmental, economic and social value depends on production route, energy source, end-use sector and system integration [1]. The adoption of green hydrogen technologies is influenced by heterogeneous actor behaviour, market conditions, policy support, environmental concerns, social visibility and economic feasibility. This is particularly relevant for distributed energy systems, where adoption cannot be understood only through techno-economic optimization, but must also consider local actors, governance arrangements, perceived legitimacy and broader sustainability outcomes [2]. However, sustainability assessments of hydrogen technologies remain uneven [3]. Social impacts and energy justice concerns are increasingly recognized as key dimensions of hydrogen supply chains [4], highlighting the relevance of employment and working conditions, health and safety, democratic participation, access to information, protection of local communities, and fair distribution of benefits and burdens.

Within this context, this work analyzes a fuel-flexible solid oxide fuel cell (SOFC) combined heat and power (CHP) system designed as a future-ready solution for distributed electricity and heat generation.

Objectives: The project targets the infrastructure analysis of a modular SOFC-CHP architecture able to operate with natural gas, hydrogen-enriched natural gas, purified biogas and up to pure hydrogen. It represents a relevant case study for assessing not only the environmental and economic performance of fuel-flexible SOFC-CHP systems, but also their broader sustainability implications in a transition pathway where fuel composition, infrastructure compatibility, local energy resilience and social acceptability are closely connected.

Material and methods: The case study is a fuel-flexible SOFC-based CHP unit designed to operate with variable fuel compositions. The life cycle inventory includes construction-related flows, i.e. stack-related materials, metallic components, insulation, gaskets, etc. The Social LCA is structured according to the Guidelines for Social Life Cycle Assessment of Products and Organisations [5].

Results: Table 1 and Figure 1 show respectively the obtained results for selected categories and the contributions to the results.

Table 1 – Social Impacts Weighting Method for the Stack Module

Child Labour, total	**5.7**	**CL** med risk hours
Goods produced by forced labour	56.7	GFL med risk hours
Frequency of forced labour	37.8	FL med risk hours
Fair Salary	42422.2	FS med risk hours
Health expenditure	1878.2	HE med risk hours
Trade unionism	1396.3	TU med risk hours
Indigenous rights	498.3	IR med risk hours
Minerals consumption	39694.6	MC med risk hours

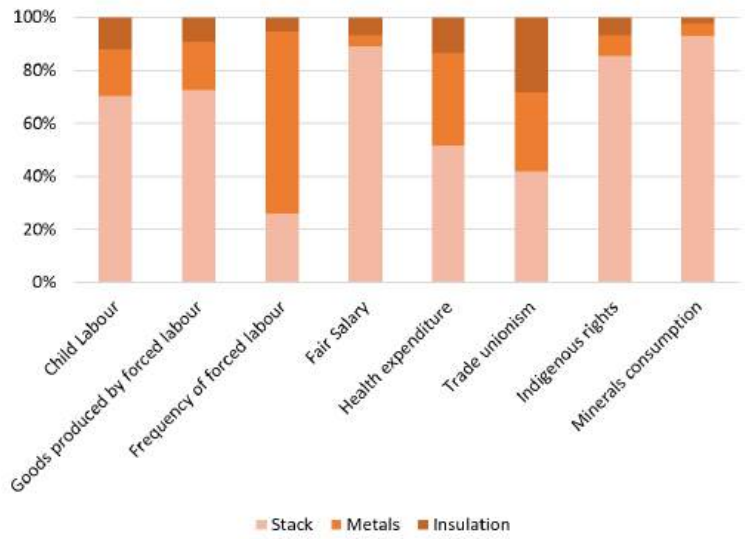


Figure 1 – Percentage contribution to the selected impact categories.

Considering the SOFC stack only, the most relevant social hotspots are associated with the upstream supply chains of critical and strategic raw materials, as well as with occupational health and safety during processing and manufacturing. The EC considers critical raw materials and “rare earths” as materials with high economic importance and high supply risk. The IEA’s Global Critical Minerals Outlook 2024 links nickel, cobalt and rare earths to energy-transition supply chains and assesses

supply-chain risks, geographical concentration, ESG risks and geopolitical vulnerabilities [6]. These considerations guided the choice of indicators used.

The percentage contributions confirm that most of the social impacts are due to the Stack itself (average 64%), confirming the importance of the most complex component, containing delicate materials from a social point of view.

Conclusions: The component level sLCA highlights that, even when the assessment is limited to the SOFC stack module, social risks are not marginal and are mainly driven by the upstream supply chains of critical and strategic materials. These findings confirm the need to integrate supply-chain due diligence, safer manufacturing practices and end-of-life recovery strategies into SOFC-CHP development, so that fuel-flexible hydrogen-ready systems can contribute not only to decarbonization, but also to a more socially responsible energy transition.

Acknowledgment

This research received funding from the Fuel Cells and Hydrogen 2 Joint Undertaking (now Clean Hydrogen Partnership) under grant agreement No 101006667.

This research was also funded by the European Union – NextGeneration EU from the Italian Ministry of Environment and Energy Security POR H2 AdP MMES/ENEA with involvement of CNR and RSE, PNRR - Mission 2, Component 2, Investment 3.5 “Ricerca e sviluppo sull'idrogeno”.

References

[1] R. Flores, M. Al Moubasher, J. Brouwer, and J. Reed, “The social value of electrolytic hydrogen,” *Joule*, 2026, doi: 10.1016/j.joule.2026.102427.

[2] L. Cricelli, S. Ianniello, P. Pragliola, and S. Strazzullo, “Sustainability impacts of green hydrogen production technology: An agent-based model simulation,” *J. Environ. Manage.*, vol. 408, May 2026, doi: 10.1016/j.jenvman.2026.129910.

[3] I. Bulfaro, A. Sánchez, G. Benveniste, B. Amante García, and V. J. Ferreira, “Environmental, economic, and social impacts of methane cracking for hydrogen production: A comprehensive review,” Aug. 08, 2025, *Elsevier Ltd*. doi: 10.1016/j.ijhydene.2025.150310.

[4] J. Bindi, F. Bartolomei, G. Pellegrini-Masini, A. Agostini, and D. Padovan, “Assessing social impacts and Energy Justice along green hydrogen supply chains: a capability-based framework,” Aug. 01, 2025, *Elsevier Ltd*. doi: 10.1016/j.erss.2025.104149.

[5] UNEP, “Guidelines for Social Life Cycle Assessment of Products and Organisations,” 2020, *United Nations Environment Programme (UNEP)*.

[6] IEA, “Global Critical Minerals Outlook 2024,” 2024.

European Fuel Cells and Hydrogen
PIERO LUNGHI CONFERENCE
EFCH2 2026
September 15th-17th 2026
Capri / Italy

Thermally Integrated Hydrogen and Electricity Co-generation in a Direct Ammonia-Fueled Solid Oxide Fuel Cell System

Mihyun Kim[a], Suhyun Woo[a], Hyangsoo Jeong[a], Minseok Bae[a], Sukwoo Nam[a],

Kwan-young Lee[a], Yongmin Kim*[a], Keunsoo Kim*[a], and Hyuntae Sohn*[a]

* corresponding author: sohn@kist.re.kr

[a] Center for Hydrogen and Fuel Cell Research, Clean Technology Research Division,

Korea Institute of Science and Technology (KIST), Seoul 02792, Republic of Korea

Keywords: Ammonia, Hydrogen co-generation, Solid oxide fuel cell, Thermal integration

Abstract

Introduction: Ammonia has attracted increasing attention as a carbon-free hydrogen carrier because of its high hydrogen density and well-established transportation infrastructure [1]. Direct ammonia-fueled solid oxide fuel cells (DA-SOFCs) enable efficient electricity generation through the internal decomposition of ammonia without requiring an external cracking unit [2]. Furthermore, the high operating temperature of SOFCs provides an opportunity to recover waste heat for additional ammonia decomposition, allowing simultaneous production of electricity and hydrogen with significantly improved overall energy utilization. Despite these advantages, experimental demonstrations of thermally integrated hydrogen and electricity co-generation based on direct ammonia-fueled SOFCs remain limited.

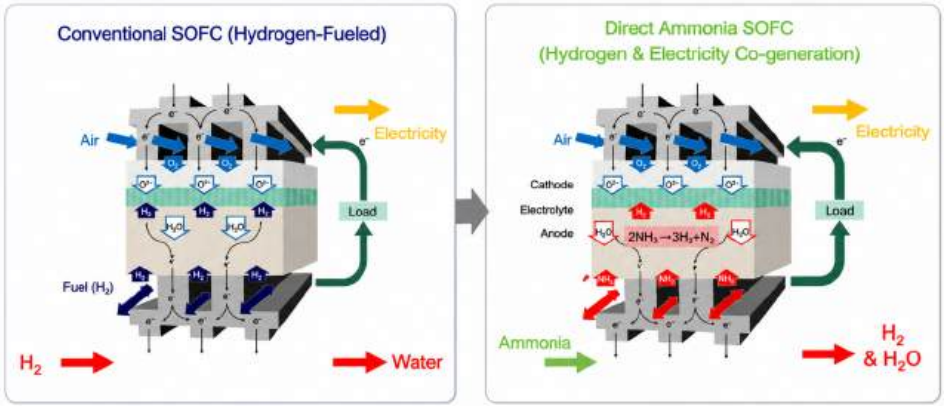


Figure 1. Conceptual illustration of thermally integrated hydrogen and electricity co-generation using a direct ammonia-fueled solid oxide fuel cell (DA-SOFC).

Objectives: The objective of this study is to experimentally demonstrate a thermally integrated direct ammonia-fueled SOFC system capable of simultaneously producing electricity and hydrogen. Particular emphasis is placed on validating the performance enhancement enabled by endothermic ammonia decomposition, identifying the thermal operating limit of the system, and demonstrating practical hydrogen and electricity co-generation under various operating conditions.

Material and methods: A commercial anode-supported SOFC stack (1.5 kWe, Fuel Cell Innovations (FCI), South Korea) was modified by incorporating an anode-off gas recovery module for hydrogen co-production. Ammonia was directly supplied to the SOFC without an external reformer, while excess ammonia was internally decomposed using the thermal energy generated during SOFC operation. The outlet gas was subsequently cooled to condense and remove residual ammonia and water, producing a hydrogen-rich gas mixture containing hydrogen and nitrogen. The total outlet gas flow rate was directly measured using a flow meter, while the hydrogen production rate was calculated from the measured total flow rate and the fuel utilization factor (U_f). Stack temperatures were monitored using K-type thermocouples installed at the stack inlet, stack outlet, and burner to characterize the temperature distribution of the integrated system during operation. Electrochemical performance, stack temperature distribution, hydrogen production rate, energy consumption, and overall system efficiency were experimentally evaluated as functions of ammonia feed rate and electrical load.

Results:

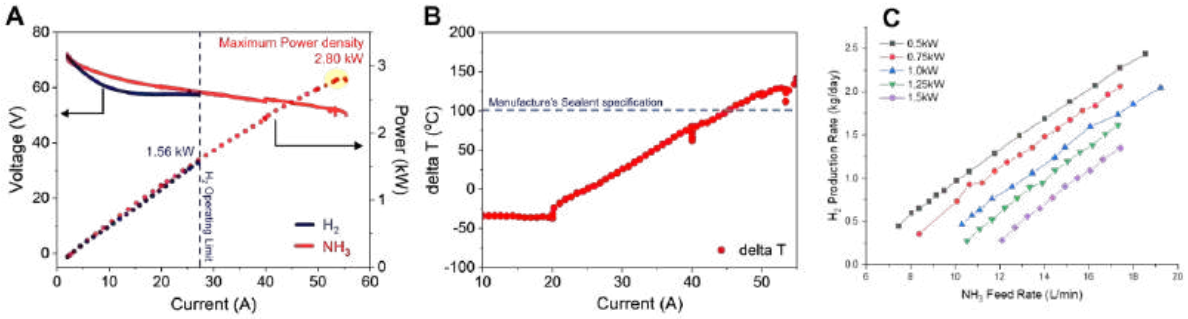


Figure 2. Experimental validation of the thermally integrated direct ammonia-fueled SOFC system: (a) polarization curves, (b) stack inlet-outlet temperature difference, and (c) hydrogen production under different electrical loads.

The endothermic ammonia decomposition effectively absorbed the heat generated by the electrochemical reaction, enabling the commercial 1.5 kWe SOFC stack to operate beyond its nominal power rating. As shown in Figure 2a, the stack achieved stable operation up to a maximum current of 53.4 A with a peak electrical output of 2.80 kW. However, further increases in operating current resulted in a rapid increase in the temperature difference between the stack inlet and outlet

(Figure 2b). This indicates that although thermal coupling between ammonia decomposition and the SOFC effectively enhanced the allowable operating range, operation above approximately 50 A approached the manufacturer's recommended thermal limit, eventually leading to stack degradation. Within the stable operating range, the integrated system successfully demonstrated simultaneous production of approximately 1 kWe of electricity and 2 kg-H_2 day^{-1} of hydrogen. As shown in Figure 2c, the hydrogen production rate increased almost linearly with ammonia feed rate under different electrical loads, demonstrating flexible hydrogen and electricity co-generation. The system achieved an energy consumption of 5.92 kWh kg-H_2^{-1} together with an overall combined efficiency of approximately 94%, substantially higher than that of a conventional hydrogen-fueled SOFC system.

Conclusions: A thermally integrated direct ammonia-fueled SOFC system for simultaneous hydrogen and electricity co-generation was successfully demonstrated. Endothermic ammonia decomposition enabled the commercial SOFC stack to operate beyond its nominal power rating while simultaneously producing hydrogen. To the best of our knowledge, this study represents the first experimental demonstration of thermally integrated hydrogen and electricity co-generation using a direct ammonia-fueled SOFC system. These findings demonstrate the potential of DA-SOFC technology as an efficient and flexible platform for distributed hydrogen and power generation.

Acknowledgment

This work was supported by the Global TOP Strategic Research Program for High-Efficiency and High-Safety Clean Hydrogen Storage and Utilization funded by the Ministry of Science and ICT (MSIT), Republic of Korea.

References

[1] Lan, R.; Irvine, J. T. S.; Tao, S. Ammonia and related chemicals as potential indirect hydrogen storage materials. International Journal of Hydrogen Energy, 37 (2012) 1482–1494.

[2] Valera-Medina, A.; Xiao, H.; Owen-Jones, M.; David, W. I. F.; Bowen, P. J. Ammonia for power. Progress in Energy and Combustion Science, 69 (2018) 63–102.



Estimating Hydrogen, Methanol, and Ammonia Demand for the Deployment of Green Corridors in the Maritime Sector.

Mariagiovanna Minutillo[a], Simona Di Micco[b], Aniello Cappiello[b*]

* corresponding author: aniello.cappiello@phds.uniparthenope.it

[a] Department of Industrial Engineering, University of Salerno, Fisciano, Italy

[b] Department of Engineering, University of Naples "Parthenope", Naples, Italy

Keywords: maritime decarbonization, hydrogen carriers, SOFC, PEMFC, green maritime corridors

Abstract: This study presents a preliminary demand assessment for hydrogen, methanol, and ammonia along the Oslo–Rotterdam and Australia–East Asia Iron Ore Green Maritime Corridors. By analyzing operational load profiles and alternative fuel volumes, the research evaluates the technical feasibility of SOFC and PEMFC systems onboard selected vessels.

Introduction: Green Maritime Corridors (GMCs), introduced through the Clydebank Declaration at COP26 in 2021, have emerged as a promising framework to accelerate the deployment of low- and zero-carbon fuels along specific maritime routes [1]. Currently, despite the increasing number of initiatives, only four corridors have reached the realization stage, with vessels and bunkering infrastructure currently under development [2].

Objectives: This study provides a preliminary assessment of hydrogen, methanol, and ammonia demand for two vessels operating along the Oslo–Rotterdam and Australia–Asia Iron Ore Green Maritime Corridors [3].

Methodology: The preliminary analysis is based on the characterization of the selected vessels in terms of installed power, operational requirements, and load profiles along the two investigated Green Maritime Corridors. The Australia–East Asia Iron Ore Corridor has been selected as a representative case of long-haul deep-sea bulk transport, while the Oslo–Rotterdam Corridor has been considered representative of short-sea container shipping, as shown in Figure 1. For the Australia–East Asia corridor, a solid oxide fuel cell system (SOFC) supplied by either ammonia or methanol is considered. Conversely, for the Oslo–Rotterdam corridor the analysis assumes the use of a proton exchange membrane fuel cell system (PEMFC) powered by onboard liquid hydrogen. The main technical characteristics of the considered vessels are reported in Table 1, while the corresponding load profiles along the two routes are summarized in Table 2.

Table 1. Technical characteristics of the vessels

	Vessel 1	Vessel 2
Corridor	Oslo - Rotterdam	Australia – Est Asia Iron Ore
Round-Trip Travelled Distance (nm)	650	4,230
Ship Size / Type	9,300 DWT (Small Feeder)	200,000 DWT (Bulk Carrier)
Main Engine Installed Power (MW)	8	15.5
Aux. Engines Total Installed power (MW)	2.4 (3x0.8)	3.9 (3x1.3)
Fuel Tank Capacity (m^3)	855 m^3	3,000 m^3



Figure 1. Green Maritime Corridors and different bunkering in posts

		Vessel 1		Vessel 2	
		Time (h)	Power (MW)	Time (h)	Power (MW)
Main Engine operation profile	Port Loading	20	0	72	0
	Outbound Maneuvering	2.5	1.60	6	3.10
	Laden Cruising	36	6.80	336	13.20
	Port Unloading	20	0	72	0
	Inbound Maneuvering	2.5	1.20	6	2.33
	Ballast Cruising	30	4.00	324	7.75
Auxiliary Engines operation profile	Port Loading	20	0.60	72	0.97
	Outbound Maneuvering	2.5	1.36	6	2.20
	Laden Cruising	36	0.68	336	1.10
	Port Unloading	20	0.60	72	0.97
	Inbound Maneuvering	2.5	1.36	6	2.20
	Ballast Cruising	30	0.68	324	1.10

The fuel consumption assessment has been carried out by considering load-dependent conversion efficiencies for the selected fuel cell technologies. In particular, the hydrogen consumption of the PEMFC-based system has been estimated using the efficiency curve reported in Ref. [4], while the ammonia- and methanol-fed SOFC systems have been evaluated according to the corresponding efficiency curves reported in Ref. [5]. This approach allowed the fuel demand to be calculated as a function of the vessel load profile along each corridor.

Results: For the long-haul Australia–East Asia Iron Ore Corridor, the total energy required for propulsion along a round-trip voyage amount to 7,860 MWh. This energy demand translates into a fuel consumption of 3,024 t for the ammonia option and 2,526 t for the methanol option, corresponding to volumes of 4,966 m^3 (density 609 kg/m^3) and 3,190 m^3 (792 kg/m^3), respectively. Considering also the fuel tank space requirement, the total needed storage volume increases to 5,198 m^3 for ammonia,

while no additional tank volume must be considered for methanol storage. Comparing these requirements with the vessel's original conventional fuel storage capacity of 3,000 m^3, it can be concluded that, due to the vast transoceanic distance and the volumetric impact of these alternative fuels, the vessel must be refueled every single leg. For the short-sea Oslo–Rotterdam Corridor, the total energy required for propulsion over a round-trip voyage is 447.5 MWh, requiring the consumption of 26.85 t of liquid hydrogen. Despite the low mass of the fuel, it occupies a physical volume of 371.6 m^3 (with a density of 72.2 kg/m^3), which requires a total onboard storage volume of 637 m^3 once the high-performance cryogenic tank and containment systems are integrated. Because this volume does not exceed the ship's original conventional fuel capacity of 855 m^3, refueling is not needed at each voyage, but rather every 1 round-trip voyages.

Conclusions: The transition to zero-carbon fuels along the investigated corridors highlights the necessity of thoroughly evaluating operational requirements against bunkering constraints, taking into account differing fuel energy densities and route scales. While the short-sea route offers higher operational flexibility, allowing the vessel to complete a full round-trip voyage before its refueling with liquid hydrogen, the transoceanic leg imposes a strict refueling schedule at the end of every single leg. Consequently, while short-sea shipping can effectively adapt to volume constraints within conventional ship dimensions, long-haul corridors remain critically dependent on the development of specialized port infrastructure and advanced alternative storage optimization.

References

[1] UK Department for Transport, COP 26, Clydebank Declaration, 2021, available online: https://www.gov.uk/government/publications/cop-26-clydebank-declaration-for-green-shipping-corridors/cop-26-clydebank-declaration-for-green-shipping-corridors

[2] Getting to Zero Coalition - Global Maritime Forum, At a Crossroad Annual Progress Report on Green Shipping Corridors 2025 Edition, 2025, available online: https://globalmaritimeforum.org/getting-to-zero-coalition/

[3] GREEN SHIPPING CORRIDOR MODELING AND OPTIMIZATION Available online: https://ww2.eagle.org/content/dam/eagle/publications/whitepapers/outlook-green-shipping-corridors.pdf

[4] Lohse-Busch H, Duoba M, Stutenberg K, Iliev S, Kern M, Richards B, Christenson M, Loiselle-Lapointe A. Technology assessment of a fuel cell vehicle: 2017 Toyota Mirai. Report No. ANL/ESD-18/12. Argonne, IL: Argonne National Laboratory; 2018. https://doi.org/10.2172/1463251

[5] Di Micco, S., Sztrinko, P., Cappiello, A., Cigolotti, V., & Minutillo, M., 2025, Multi-Fuel SOFC System Modeling for Ship Propulsion: Comparative Performance Analysis and Feasibility Assessment of Ammonia, Methanol and Hydrogen as Marine Fuels. Journal of Marine Science and Engineering, 13(10), 1960. https://doi.org/10.3390/jmse13101960



From natural gas to hydrogen: experimental performance characterization of a solid oxide fuel cell system installed in an airport environment

M. Gandiglio*[a], D. Trapani[a], L. Pera[a], P. Marocco[a], M. Santarelli[a], G. Restaldo[c], E. Zera[b]

* Corresponding author: marta.gandiglio@polito.it

[a] Department of Energy, Politecnico di Torino, C.so Duca degli Abruzzi 24, 10129 Torino (IT)

[b] SolydEra SpA, Viale Trento 115/117, 38017 Mezzolombardo (IT)

[c] SAGAT SpA – Turin Airport, Strada San Maurizio 12, 10072 Caselle Torinese (IT)

Keywords: SOFC, solid oxide fuel cell, hydrogen blending, fuel flexibility, hydrogen

Abstract

This work presents the experimental performance characterization of a commercial solid oxide fuel cell (SOFC) system operated with natural gas, pure hydrogen, and hydrogen-natural gas blends, installed and tested in a real airport environment within the European project TULIPS. Two BlueGen SOFC units, integrated into a power-to-power configuration with on-site electrolysis and hydrogen storage, were operated over more than 10,000 hours (about 22 MWh produced) across their full electrical modulation range and the full 0-100% hydrogen blending range, using two different control strategies. The system, originally designed and certified for natural gas, operated stably on hydrogen-blended mixtures without hardware modification, providing experimental evidence of the opportunities and limitations of retrofitting commercial SOFC units for hydrogen operation.

Introduction: SOFCs are high-efficiency, fuel-flexible electrochemical devices capable of producing electrical and thermal energy with limited environmental impact. While commercial SOFC systems are typically operated on natural gas, their inherent fuel flexibility also enables operation with hydrogen-enriched blends and pure hydrogen, supporting progressive decarbonization of distributed energy generation. Despite this potential, experimental characterizations of commercial SOFC systems across a wide range of fuel compositions remain limited in the literature, particularly at system level and under real operating conditions rather than laboratory benches.

Hydrogen-natural gas co-fueling of SOFC systems has also been investigated in other application contexts, including marine power systems [1], integrated PV-electrolyser-SOFC plants [2], and system-level SOFC-CHP modelling [3], consistently reporting a trade-off between the benefits of hydrogen enrichment and the associated efficiency and cost penalties – further motivating the experimental validation presented here.

This work presents the experimental characterization of a commercial SOFC unit operated with natural gas, pure hydrogen, and blended mixtures, with the aim of assessing how fuel composition affects stack- and system-level performance across the full modulation range.

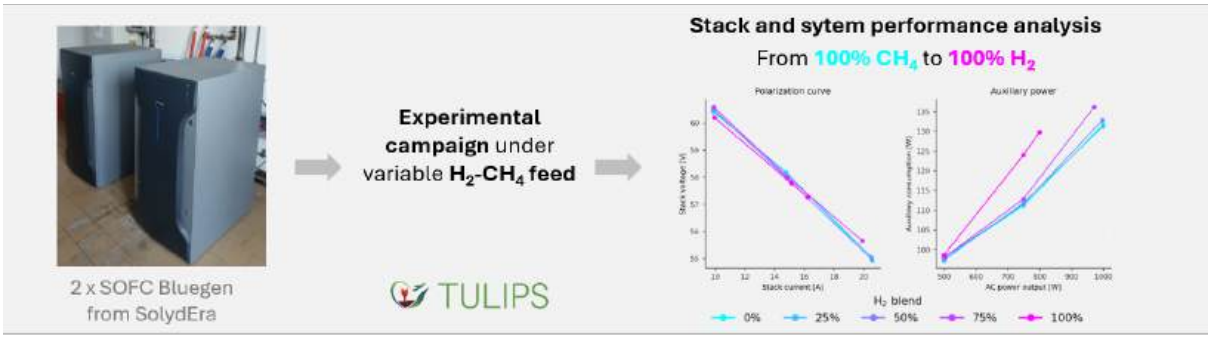


Figure 79. SOFC hydrogen-blending campaign at Turin Airport.

Material and methods: The SOFC systems (2 × BlueGen, nominal power 1.5 kW each), provided by Solydera, are integrated into a power-to-power configuration that includes an anion exchange membrane (AEM) electrolyzer (1 Nm^3/h) and an on-site hydrogen storage unit (0.4 m^3 at 30 bar), enabling flexible fuel management. The system is installed and operated at Turin Airport (managed by SAGAT S.p.A.) within the European project TULIPS [4], at the airside fire station, supported by an 83.6 kW PV plant. The experimental campaign covered the SOFC operating range between nominal power and minimum load (approximately 500-1500 W), with each operating point held for a minimum duration to ensure steady-state conditions. This protocol was applied across fuel compositions ranging from 100% natural gas to 100% hydrogen, including intermediate hydrogen blends tested in either 10% or 25% steps depending on the campaign. During testing, fuel and air flow rates, stack voltage, current, DC and AC power output, and stack temperature were continuously monitored. Two distinct fuel control strategies were adopted over the course of the campaign – an initial blend-based fuel flow control, and a subsequently introduced temperature-based control.

Results: Over more than 6,500 hours of operation across the two fuel cell stacks, results indicate a consistent influence of fuel composition on both electrochemical behaviour and thermal management of the system, in line with expected trends: stack voltage increases with the hydrogen content of the fuel blend, while the reduced methane fraction limits the internal reforming reaction and, consequently, affects the thermal balance and auxiliary power demand of the system. At high hydrogen concentrations, the system underwent power de-rating, limiting output to a maximum of 0.8-1.0 kW due to thermal management constraints. System-level efficiency remained stable up to a blend of approximately 50% H_2, beyond which a reduction was observed. Increasing hydrogen content was found to influence both cell voltage and the electrochemical response of the stack, as well as air and auxiliary power demand at system level, reflecting the system's original design and calibration for CH4 operation. The full dataset was used to derive polarization curves and stack- and system-level efficiency trends as a function of electrical load and fuel composition, together with an assessment

of the measurement uncertainty associated with the fuel flow metering system under hydrogen-enriched conditions.Despite being originally designed and certified for natural gas operation, the SOFC system operated stably and reliably on hydrogen-blended mixtures without hardware modification, although managing a CH4-designed SOFC to run on H2 highlighted that additional flow measurement/control instrumentation would be beneficial, at the cost of increased system complexity.

Conclusions: The results include quantified stack- and system-level performance trends across the investigated fuel compositions and operating conditions, together with a discussion of the practical implications of thermal management and control strategy on hydrogen-blend operability. The derived efficiency curves are intended to constitute a robust input for future techno-economic assessments of fuel-flexible SOFC deployment.

Acknowledgment

This study was part of the EU project TULIPS (https://doi.org/10.3030/101036996) project which received funding from the European Union's EU Horizon 2020 research and innovation program under Grant agreement ID: 101036996. The work was also part of the AMPS (Automated Mass Production of SOC Stack) project (https://www.amps-project.eu/). The project is supported by the Clean Hydrogen Partnership and its members (GA: 101111882).

References

[1] S. Seyam, I. Dincer, M. Agelin-Chaab, An innovative study on a hybridized ship powering system with fuel cells using hydrogen and clean fuel blends, Appl. Therm. Eng. 221 (2023) 119893. https://doi.org/10.1016/J.APPLTHERMALENG.2022.119893.

[2] A. Saberi Mehr, M. Ilkhani, S. Sabernia, S. Nooshmand, A. Ebrahimpour, B. Heydari, Thermodynamic modelling and optimisation of a green hydrogen-blended syngas-fueled integrated PV-SOFC system, Appl. Therm. Eng. 236 (2024) 121506. https://doi.org/10.1016/J.APPLTHERMALENG.2023.121506.

[3] S. Bharati, B.S.M. Reddy, S. Purohit, I. Kalita, D.J. Shendage, P. Tiwari, S. Subbiah, Modelling and simulation of H2-blended NG powered SOFC for heat and power generation applications, Appl. Energy 390 (2025) 125867. https://doi.org/10.1016/J.APENERGY.2025.125867.

[4] CORDIS - EU research results, DemonsTrating lower pollUting soLutions for sustaInable airPorts acrosS Europe, (2022). https://doi.org/10.3030/101036996.



Innovative Manufacturing Processes for Low-Cost, High-Performance SOCs: From Laboratory Results to Industrial Deployment

Gualandris Fabrizio*[a]
* corresponding author: Gualandris Fabrizio
[a] Hydrospark Srl

Keywords: Solid Oxide Cells, Hydrogen, Fuel Cells, Electrolysis

Abstract: Solid Oxide Cells (SOCs) play a crucial role in the green hydrogen transition, yet current manufacturing methods struggle to balance electrochemical performance, durability, and cost-efficiency. This study presents a scalable manufacturing paradigm developed by Hydrospark to produce high-performance SOCs aligned with European Union 2030 cost targets (€8–11.3 per cell). Validated at laboratory scale, our technologies are being deployed in a commercial-scale facility designed for an annual capacity of 1 million cells by 2028, supported by joint industrial investments from SIAD and Brembo Ventures.

Introduction: The European Union is aiming for a substantial reduction in greenhouse gas emissions—between 80% and 95% compared to 1990 levels—by the year 2050. This ambitious target hinges largely on the increased incorporation of renewable energy sources into the EU's energy systems. Efficient harvesting of renewable energy is one of the most important challenges humanity is facing. The impending need of reducing greenhouse gas emissions combined with the constant world population growth requires the use of several alternative technologies for responding to the increasing energy demand. Although batteries are conquering the general consensus of valuable storage technology for the future, they still manifest noteworthy challenges and the problem of storing big amounts of energy remains. The creation of a new economy linked to the use of hydrogen or synthetic fuel is gathering importance. Many different synthetic fuels have been individualized such as methanol, methane, ammonia, specific hydrogen liquid carriers and dimethyl ether are the simples and cheapest to produce. All these different carriers need hydrogen to be produced. Therefore, the need of producing cheap, reliable and high-quality hydrogen is fundamental to facilitate the next upcoming energy transaction. The SOCs are a fuel cell technology and a promising device that converts electrical energy to chemical energy. Due to its unique characteristics this technology serves as vital enablers, efficiently connecting power, gas, and heat sectors. As a result, SOCs stands poised to play a pivotal role in driving the transition towards a more sustainable energy landscape. In order to increase their market adoption, production costs have to be further decreased. Another disadvantage of SOCs is the higher rate of cell and electrolyser system deterioration. This is inherently linked to the more severe operating conditions that put a strain on the materials of the cell and stack. The cause of stack failure is almost always (>90%) attributable to cell failure. The latter has a durability that can

vary between 20,000 and 30,000 hours of operation within a running system. The minimum target is to reach approximately 40,000 hours (5 years at 90%) of operation. Among several failure causes, the durability of the cell is strongly influenced by the electrolyte's ability to prevent the permeation of gases that populate the two adjacent electrodes. Any mixing of these gases would lead to the formation of micro-combustions which, over time, would degrade the electrode-electrolyte interface leading to cell failure.

Objectives: Hydrospark' main objective is to produce SOCs with the best performance while ensuring the lowest price on the market. To achieve these results, we have developed an innovative production process that allows them to obtain more efficient and durable cells. Our business plan focuses on producing and selling 13,000 cells in the first year, 200,000 in the second year, and 1 million cells in the third year. Furthermore, we continue to develop new technologies to optimize and streamline our manufacturing processes.

Material and methods: Hydrospark aims to produce SOCs with the highest performance at the lowest cost. To this end, we have developed innovative processes that enhance both efficiency and durability. A patented method enables the production of a denser electrolyte than the state of the art. This ensures high ionic conduction and impermeability to gases, preventing micro-porosities that typically cause gas mixing, micro-combustions, delamination, and premature stack failure. Such improvements have a decisive impact on cell lifetime. However, performance alone is not enough: the market requires drastic cost reductions. Today, cells in Europe cost much more than the EU 2030 targets for electrolysers, that implies a cost of only €8–11.3 per cell. Traditional manufacturing, even at scale, cannot bridge this gap. Most costs derive from half-cell production, where the fuel electrode and electrolyte are sequentially tape cast. This process is slow (0.6 m/min) and CAPEX-intensive. Hydrospark has developed and patented a new method, achieving ≥5 m/min (8.3× faster) and reducing CAPEX by 2.5×, while preserving essential microstructural properties such as porosity and percolation. The process has been validated on a small scale and is ready for industrial deployment. To accelerate this transition, we are building a new manufacturing plant fully based on these innovations, enabling production of 1 million cells/year by 2028, fully aligned with EU targets.

Results: We currently hold three proprietary patents: two covering advanced manufacturing technologies for SOC production, and one specifically dedicated to stack design. Construction of our state-of-the-art manufacturing facility commenced in September 2025, reaching full operational readiness in June 2026.

We are actively manufacturing initial production batches, undergoing internal cell characterization and testing while fine-tuning key processing steps to optimize yield and efficiency. The performance

of our initial cells fully aligns with current state-of-the-art benchmarks, providing a solid baseline as we progressively scale up production capacity.
Driven by a dynamic and highly motivated team, we are actively participating in several national and EU-funded research programs aimed at accelerating the development and validation of our proprietary stack technology.

Conclusions: The path toward complete European energy independence relies on our determination to push boundaries and achieve unprecedented results. We must shift existing paradigms and advance cutting-edge technologies to eliminate our dependence on fossil fuels. Our mission is to prove that this transformation is possible

Acknowledgment
We would like to thank Brembo Ventures, SIAD SpA, and Petroceramics SpA for their support.



Hot Gas Conditioning and SOFC Systems Coupled to a Steam/Oxygen Fluidized Bed Gasifier Plant

D. Barisano[1,a], P. Garzone[1,a], F. Nanna[1,a], E. Fanelli[1,a], C. Freda[1,a], A. Villone[1,a], A. Giuliano[1,a], U. Pasqual Laverdura[1,b], A. Di Carlo[2], A. Vitale[2], A. A. Papa[2], E. Bocci*[3], Y. Ferruzzi[3], J. D. Palacios Aparicio[3], F. Basile[4], A. Fasolini[4], E. Tosi Brandi[4], G. Balestra[4], A. Messineo[5], M. Volpe[5], A. Picone[5], E. Catizzone[6], A. Dell'Era[7], J. Sitzmann[8], C. Tregambe[9].

* corresponding author: e.bocci@lab.unimarconi.it

[1] ENEA, Italian National Agency for New Technologies, Energy and Sustainable Economic Development, Lungotevere Thaon di Revel 76, 00196 Rome, Italy (a Trisaia Research Center; b Casaccia Research Center); [2] University of L'Aquila, Department of Industrial and Information Engineering and Economics, Piazzale Pontieri 1, Monteluco di Roio, 67100 L'Aquila, Italy; [3] Guglielmo Marconi University, Department of Engineering Sciences, Via Plinio 44, 00193 Rome, Italy; [4] Alma Mater Studiorum University of Bologna, Department of Industrial Chemistry "Toso Montanari", Via Gobetti 85, 40129 Bologna, Italy; [5] University of Enna "Kore", Department of Engineering and Architecture, Cittadella Universitaria, 94100 Enna, Italy; [6] University of Calabria, Department of Environmental Engineering, Via P. Bucci - Cubo 44A, 87036 Arcavacata di Rende, Italy; [7] Sapienza University of Rome, Piazzale Aldo Moro 5, 00185 Rome, Italy; [8] Calida Cleantech GmbH, Adlerstraße 2, 91560 Heilsbronn, Germany; [9] ICI Caldaie S.p.A., Via Giovanni Pascoli 38, 37059 Campagnola di Zevio (VR), Italy.

Keywords: biomass gasification; hot gas conditioning; solid oxide fuel cell (SOFC); syngas purification

Abstract

Introduction: Coupling Solid Oxide Fuel Cells (SOFC) to biomass gasification enables sustainable, high-efficiency combined heat and power (CHP) production, yet the combination of biomass feedstocks with gasifier, gas-conditioning and SOFC technologies has not been fully proven at pilot scale. This work presents the ongoing upgrade of a steam/oxygen fluidized-bed gasification plant, operated by ENEA at the Trisaia Research Centre (Basilicata, Italy), towards its integration with a Hot Gas Conditioning (HGC) unit and a SOFC cogeneration system, within a 36-month project ("Biomass gasification for electricity production via SOFC") funded by the Italian Ministry of the Environment and Energy Security (MASE) under the National Electric System Research programme (RdS), 2025–2027.

Objectives: The project aims to: (i) upgrade the existing 1 MWth internally circulating fluidized-bed (ICFB) gasification plant to allow a 1 MW slip-side coupling with HGC and SOFC units; (ii) define a

technically feasible HGC-SOFC architecture able to feed a 5 kWe SOFC system with clean syngas; (iii) improve syngas purification through high-temperature filtration and catalytic upgrading; (iv) widen the range of usable feedstocks through hydrothermal carbonization (HTC) pretreatment of critical biogenic residues; (v) support the plant upgrade with CFD modelling of the gasifier and its filtration elements; and (vi) develop catalytic metal foams for tar and light-hydrocarbon reforming compatible with SOFC operation.

Material and methods: The ENEA gasification plant is based on a steam/O2 fluidized-bed gasifier (150–160 kg/h biomass) equipped with high-temperature ceramic candles and a tar catalyst for particle filtration and first tar reforming, housed directly in the gasifier freeboard and developed under the FP7 project UNIfHY [2]. The HGC system, developed under the H2020 project GICO [3], comprises CO2, sulphur and chlorine absorbers together with a tar-reforming reactor; the SOFC system, developed under the H2020 project SO-FREE [1,4], comprises an autothermal reforming (ATR) reactor with associated heat exchangers and valves. A functional survey of the existing plant was carried out to identify the hardware and software modifications required for the coupling, covering process and service lines, installed equipment, and electrical and instrumentation systems. In parallel, a 10 kWth bubbling fluidized-bed pilot plant was used to test high-temperature filter candles and catalytic syngas conditioning on real syngas, while citrus-derived residues (lemon, orange and mandarin peel) were characterized for HTC pretreatment via proximate and ultimate analysis. A three-dimensional model of the 1 MW reactor was built for CFD simulation (ANSYS Fluent) of the ceramic candle, using the Darcy-Forchheimer model to describe viscous and inertial resistance across the porous filtering element. Finally, cylindrical nickel foams were coated with a Ni-based oxyhydroxide catalyst by potentiostatic and potentiodynamic electrodeposition, using a nickel working electrode, a platinum-gauze counter electrode and a saturated calomel reference electrode, to obtain structured catalysts for tar and CH4 reforming.

Results: The functional survey identified four main upgrades: the data-acquisition, monitoring and control system; the electrical system for powering and controlling the HGC and SOFC units; a temperature-control system for the biomass feed screw; and a new feed line connecting the gasifier to the HGC, SOFC and auxiliary flare units. A syngas flow rate of about 5 Nm3/h was found sufficient to power the 5 kWe SOFC system and is readily obtainable from the HGC blower as a slip-side of the UNIfHY plant. A reconfiguration of the HGC train was identified as most promising: the reactor originally designed for CO2 polishing can be repurposed for HCl removal, H2S removal is more effective using ZnO rather than BaO owing to the significant CO2 content of the syngas, and the existing catalytic reactor for tar reforming can be adapted by increasing the catalyst mass while remaining within its available volume. Chemical-physical characterization of the citrus-waste

feedstocks confirmed their suitability for HTC pretreatment, with high volatile-matter content (72.5–76.7 wt%) and higher heating values of 17.2–18.7 MJ/kg. CFD simulation of the empty ceramic candle provided the Darcy-Forchheimer parameters (porosity 0.3; viscous resistance 1.4×10^{11} m^{-2}; inertial coefficient 3.77×10^{8} m^{-1}) and the corresponding pressure-drop and velocity fields, establishing the baseline for further simulations with the catalyst-filled candle. Electrodeposition trials produced homogeneous Ni-oxyhydroxide coatings on nickel foam supports under both potentiostatic (−1.1 V, 3000 s) and potentiodynamic (0 to −1.4 V, 20 cycles) conditions, indicating good control over coating coverage and mass loading.

Conclusions: The results obtained indicate the technical feasibility of integrating the ENEA Trisaia gasification plant with the HGC and SOFC units on a 1 MW slip-side, confirming that the syngas produced, once purified from organic and inorganic contaminants, can sustain stable operation of a 5 kWe SOFC system. The parallel activities on syngas purification, feedstock flexibility through HTC pretreatment, CFD-based reactor characterization and catalytic-foam development provide the technical basis needed to move from the current prototype configuration towards a reliable, high-efficiency CHP demonstration based on biomass gasification coupled with SOFC technology.

Acknowledgment

The work presented here is part of the “National Electric System Research (RdS)” programme funded by MASE (Italian Ministry of the Environment and Energy Security), triennium 2025–2027. The authors gratefully acknowledge the support received.

References

[1] E. Bocci, A. Dell’Era, C. Tregambe, G. Tamburrano, V. Marcantonio, F. Santoni, “The Development and Evaluation of a Low-Emission, Fuel-Flexible, Modular, and Interchangeable Solid Oxide Fuel Cell System Architecture for Combined Heat and Power Production: The SO-FREE Project,” Energies, vol. 18, no. 9, art. 2273, 2025.

[2] UNIfHY – UNIQUE gasifier for hydrogen Production, FP7-FCH JU Grant Agreement No. 299732, CORDIS, European Commission.

[3] GICO – Gasification Integrated with CO2 capture and conversion, H2020 Grant Agreement No. 101006656, CORDIS, European Commission.

[4] SO-FREE – Solid Oxide Fuel Cell Combined Heat and Power: Future-ready Energy, H2020 Grant Agreement No. 101006667, CORDIS, European Commission.



STAND UP: Fuel cell–battery power units for heavy-duty applications

Andrea Altomonte*a, Elio Jannellia

* corresponding author: Andrea Altomonte

[a] University of Naples Parthenope, Naples, Italy

Keywords: fuel cell–battery hybrid power unit; heavy-duty vehicles; terminal tractor; hydrogen storage; duty-cycle analysis; supervisory control

Abstract

Heavy-duty vehicles combine sustained energy demand with repeated acceleration, braking and variable payload, a duty profile that a zero-emission power unit must reproduce through the coordinated use of several energy sources. This work reports the design rationale, architecture and modelling framework of a fuel cell–battery hybrid power unit developed within the STAND UP project for heavy-duty terminal-tractor applications. Telemetry acquired from diesel terminal tractors in operational service, covering approximately 580 operating hours, provides the empirical basis for reconstructing representative duty cycles and deriving mission-based sizing requirements. The proposed architecture couples a proton exchange membrane fuel cell (PEMFC) system with a battery through a common DC distribution, complemented by separate high- and low-temperature cooling circuits and a supervisory control layer that allocates power according to battery state of charge, subsystem states and operating limits. Analysis of a high-resolution reference power series yields a mean load of 34.7 kW against a peak of 183 kW, that is, a peak-to-mean ratio in excess of five. This separation between average and peak demand indicates that the sustained power source and the transient power buffer are subject to different sizing criteria, and supports a replicable method for sizing zero-emission power units for heavy-duty mobility applications.

1. Introduction: Decarbonisation of heavy-duty mobility requires power units capable of reproducing the duty profile of diesel drivetrains while eliminating tailpipe emissions. The mission characteristics that define these requirements – continuous power, peak power, operating range, installation volume, mass and environmental conditions – vary substantially between vehicle classes and duty cycles. In terminal tractors, where continuous low-speed manoeuvring is combined with frequent acceleration, braking and coupling events under variable payload, generic sizing assumptions are therefore inadequate, and representative operating data are required in order to translate application demand into fuel cell, battery and hydrogen-storage specifications [1].

Within the STAND UP project, telemetry was acquired from diesel terminal tractors in operational service in order to reconstruct representative duty cycles. The campaign spanned 25 working days, 196 work shifts and 580 operating hours, yielding a dataset of sufficient extent to be regarded as operationally representative [3]. These records characterise the application demand and link vehicle dynamics and duty-cycle analysis to the sizing of the fuel cell system, the battery and the hydrogen storage. The present work reports the mission-based requirements derived from this evidence, the hybrid power-unit architecture developed to satisfy them, the modelling and test environment adopted to support control design, and a quantitative duty-cycle analysis in which sustained and transient power demand are treated separately. The activity is carried out by ATENA Scarl in partnership with ARCO FC, CNR-STEMS and ENEA within the STAND UP project (Project no. RSH2B_000022).

2. Materials and methods: The hybrid power unit couples a proton exchange membrane fuel cell (PEMFC) system and a battery through a common DC distribution. The FC system supplies the sustained mission demand, whereas the battery supplies transient power and recovers braking energy. System integration comprises hydrogen storage and pressure regulation, electrical conversion, traction, vehicle auxiliaries and the associated high- and low-voltage interfaces. Thermal management employs separate high- and low-temperature circuits, serving the FC system and the electrical and auxiliary components respectively, so that subsystems with dissimilar operating temperature ranges remain decoupled. Power allocation is governed by a supervisory control layer on the basis of the instantaneous power request, the battery state of charge (SOC) and the applicable operating limits, thereby relating continuous power, peak capability and stored energy within a single design [1].Control and sizing are supported by zero-dimensional (0D) energy balances and one-dimensional (1D) subsystem models, arranged in a modular structure representing the FC system, the battery, the traction motor and the auxiliaries. The supervisory strategy allocates power according to battery SOC, subsystem states and operating limits; mission inputs and component parameters relate this behaviour to vehicle demand, while fuel cell control unit (FCU) requirements complete the control framework. Experimental verification is performed in a dedicated dynamic test room, in which the FC installation and an electric motor mechanically coupled to a dynamometer provide a hardware environment for assessing the modelled control strategies against the physical behaviour of the subsystems [5].The quantitative duty-cycle analysis is based on a reference power series, denoted 4×2, comprising 577,701 samples acquired at 20 ms intervals over 3.21 h of operation; the fuel cell reference channel spans 0–85 kW [4]. Sixty-second means are employed for graphical representation only, whereas all reported statistics are computed from the full-resolution data, so as to avoid the underestimation of peak demand introduced by smoothing.

3. Results and discussion: Analysis of the full-resolution reference power series yields a mean load of 34.7 kW and a peak load of 183 kW, corresponding to a peak-to-mean ratio of 5.27. The magnitude of this ratio quantifies the rationale for hybridisation: the sustained power source (the FC system) and

the transient power buffer (the battery) are subject to different sizing criteria, and neither can be sized efficiently against the complete duty cycle in isolation.

Taken together, the application requirements derived from telemetry, the integrated architecture and the modelling and supervisory-control framework constitute a coherent design method, in which the distinction between sustained and transient demand is related to the electrical, hydrogen and thermal interfaces of the power unit. Battery sizing is governed by both the transient power and the energy exchanged over the mission, whereas hydrogen-storage sizing additionally requires that conversion losses and auxiliary consumption be accounted for. A power trace alone is therefore sufficient for mission-specific component sizing but does not, in itself, determine fuel consumption or overall system efficiency [2].

4. Conclusions: Three conclusions may be drawn from the present work. First, mission requirements, hybrid architecture and supervisory control can be combined into a single design framework applicable to heavy-duty fuel cell–battery power units. Second, the reference case, reaching 183 kW against a mean load of 34.7 kW, confirms that sustained and transient power paths must be sized separately. Third, the electrical, hydrogen and thermal interfaces defined by the architecture relate subsystem-level design choices to vehicle-level performance demand. Future work will address experimental validation of the supervisory control strategy in the dynamic test room and extension of the sizing method to additional duty cycles.

Acknowledgements

This work was supported by the Italian Ministry of Environment and Energy Security (MASE), under the National Recovery and Resilience Plan (PNRR): Mission 2, Component 2, Investment 3.5 – Hydrogen – type b, funded by the European Union – NextGenerationEU, within the STAND UP project (Project no. RSH2B_000022; CUP: F59J25000250004). The authors thank project partners ARCO FC, CNR-STEMS and ENEA for their contribution to this work.

References

[1] STAND UP Consortium. Updated Development Plan – power unit requirements, architecture and control, pp. 31–34.

[2] STAND UP Consortium. Final Technical Report, 30 June 2026.

[3] STAND UP Consortium. Terminal-tractor technical deliverable, rev. AA, sect. 3–4.

[4] STAND UP Consortium. Reference power dataset, 4×2 worksheet.

[5] STAND UP Consortium. Dynamic test room, photographic documentation.



TOPIC 4. HYDROGEN END-USE APPLICATIONS



Electrolyzer Model Detail in Energy System Optimization: Implications for Dispatch and Waste Heat Availability

Simon Dübell*[ab]

*corresponding author: simon.duebell@rl-kolleg.de

[a] RLS-Graduate School, Rudower Chaussee 12, Berlin, 12489, Germany

[b] Technical University Dresden, Helmholtzstraße 10, Dresden, 01069, Germany

Keywords: electrolyzer modelling, energy system optimization, part-load operation, waste heat recovery.

Abstract

Introduction: In many energy system optimisation models, electrolyzers are represented using simplified constant-efficiency or piecewise linear formulations. These approaches neglect the electrochemical dependence of performance on operating conditions such as current density and temperature, which affect efficiency and heat generation (Sánchez et al., 2018). At the same time, electrolysis converts a considerable share of electrical input energy into heat, which may be relevant for sector coupling and waste heat utilisation (Frassl et al., 2024). This raises the question to what extent detailed electrochemical representations are required in optimisation-based energy system modelling.

Objectives:

- Compare electrolyzer formulations with different levels of electrochemical detail based on the models of Ulleberg (2003) and Sánchez et al. (2018) combined with operational state models following Varela et al. (2021) and Matute et al. (2021).
- Quantify the impact of model formulation on dispatch behaviour, part-load operation, annual revenue and computational feasibility.
- Assess implications for hydrogen production and recoverable waste heat.

Materials and methods:

The study compares three electrolyzer surrogate formulations within a generic mixed-integer linear programming (MILP) case study. The system comprises a renewable-supplied scale-able alkaline electrolyzer with thermal management and hydrogen storage, optimised at hourly resolution using historical day-ahead electricity market data for 2022 and 2024.

Three surrogate representations of the electrolyzer performance map P(I,T) are derived from the semi-empirical model of Sánchez et al. (2018) and combined with operational state constraints following

Varela et al. (2021) and Matute et al. (2021): (i) a piecewise-linear formulation along the current axis at fixed nominal temperature (PWL); (ii) a tangent-plane approximation following Zheng et al. (2022) that linearises performance around a reference operating point (TAN); and (iii) a triangulated performance map (p-formulation) based on Delaunay triangulation of the (I,T) domain to capture temperature-dependent behaviour across the full operating range. Heat generation is modelled consistently with the electrochemical balance to enable a thermodynamically coherent assessment of recoverable waste heat.

The model is implemented in Python using the Pyomo framework and solved with Gurobi. Comparison across formulations is based on the following indicators: annual hydrogen output, dispatch-weighted mean efficiency, full-load hours and part-load distribution, recoverable waste heat (both annual total and its temporal availability), stack temperature distribution, annual revenue from hydrogen sales and computational solving time as an indicator for model tractability.

Results

Across the three formulations, aggregated annual indicators such as total hydrogen production and annual revenue differ only marginally, confirming that simplified surrogate models remain adequate for techno-economic system sizing and dispatch optimization for hydrogen production. However, the underlying operational behaviour diverges substantially: the more detailed electrochemical formulations lead to distinctly different part-load distributions and dispatch patterns (Fig. 1), particularly during periods of intermediate electricity prices and partial renewable availability. Computational solving times remain tractable for all three formulations on annual hourly horizons.

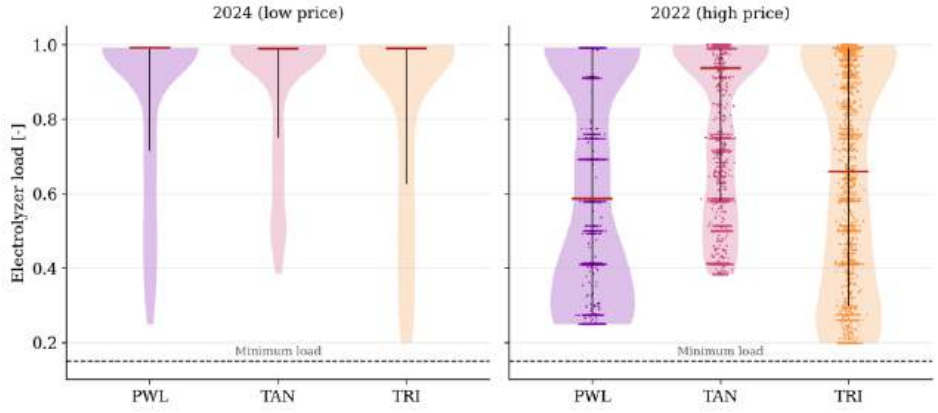


Figure 1: Part-load distribution of all three electrolyzer surrogates in high (2022) and low (2024) price scenarios. PWL is a fixed temperature (90 °C) surrogate and overestimates performance since stack temperature (cold/warm start) trajectories are neglected.

Conclusions

- Simplified electrolyzer models are sufficient for hydrogen production, aggregated techno-economic assessments and design optimization, but not for waste heat utilization.
- Electrochemically informed models become relevant when analysing part-load behaviour, operational flexibility and thermal integration.

Acknowledgment

This research was conducted within the doctoral research activities of the Reiner Lemoine Institut, Berlin. S.D. gratefully acknowledges the financial support of the Reiner Lemoine Foundation through a doctoral scholarship, as well as the initial scholarship provided by the Berlin University of Applied Sciences (BHT) during 2024–2025, during which a substantial part of this work was conducted.

References

[1] Sánchez, M., Amores, E., Rodríguez, L., Clemente-Jul, C., 2018. Semi-empirical model and experimental validation for the performance evaluation of a 15 kW alkaline water electrolyzer. *International Journal of Hydrogen Energy* 43, 20332–20345. https://doi.org/10.1016/j.ijhydene.2018.09.029

[2] Frassl, N., Sistani, N.R., Wimmer, Y., Kapeller, J., Maggauer, K., Kathan, J., 2024. Techno-economic assessment of waste heat recovery for green hydrogen production: a simulation study. *e+i Elektrotechnik und Informationstechnik* 141, 288–298. https://doi.org/10.1007/s00502-024-01231-y

[3] Ulleberg, O., 2003. Modeling of advanced alkaline electrolyzers: a system simulation approach. *International Journal of Hydrogen Energy* 28, 21–33. https://doi.org/10.1016/S0360-3199(02)00033-2

[4] Varela, C., Mostafa, M., Zondervan, E., Zhou, Y., 2021. Modeling alkaline water electrolysis for power-to-X applications: A scheduling approach. *International Journal of Hydrogen Energy* 46, 9303–9313. https://doi.org/10.1016/j.ijhydene.2020.12.111

[5] Matute, G., Yusta, J.M., Beyza, J., Correas, L.C., 2021. Multi-state techno-economic model for optimal dispatch of grid connected hydrogen electrolysis systems operating under dynamic conditions. *International Journal of Hydrogen Energy* 46, 1449–1460. https://doi.org/10.1016/j.ijhydene.2020.10.019

[6] Zheng, Y., Zhang, X., Li, J., Lin, J., Song, Y., 2022. Optimal day-ahead dispatch of an alkaline electrolyser system concerning thermal–electric properties. *International Journal of Hydrogen Energy* 47, 31627–31641. https://doi.org/10.1016/j.ijhydene.2022.07.077



Hierarchical predictive control for coordinated operation of smart prosumers in an energy community

Lorenzo Bartolucci [a], *Edoardo* Cennamo [a], *Stefano* Cordiner [a], *Vincenzo* Mulone [a], *Alessandro* Polimeni *,[a]

* corresponding author: alessandro.polimeni@uniroma2.it

[a] Department of Industrial Engineering, Tor Vergata University of Rome, via del Politecnico 1, 000133, Rome, Italy

Keywords: Energy Communities, Hydrogen Systems, Model Predictive Control

Abstract

Introduction: The increasing penetration of distributed renewable energy sources is progressively transforming traditional passive consumers into active agents [1]. In this context, energy communities represent a promising paradigm for improving system flexibility, increasing renewable self-consumption and reducing the interaction with the external electricity grid [2]. The operation of such systems becomes significantly more complex with the integration of multiple controllable components, including Battery Energy Storage Systems (BESSs) and hydrogen-based technologies such as Proton Exchange Membrane Fuel Cells (PEMFCs) [3]. In these configurations, coordinated control strategies are required to exploit the flexibility of individual members while achieving optimal performance at the community level [4].

Model Predictive Control (MPC) represents a well-established framework for energy management of multi-energy systems, given its ability to handle forecasts, system constraints and multi-objective optimization [5]. However, most existing works either optimize individual prosumers in isolation or rely on fully centralized architectures that require complete knowledge of each member's internal model [6], an assumption that breaks down when community size scales beyond a handful of nodes or when members operate heterogeneous, proprietary technologies. Hierarchical MPC architectures that decouple local optimization from community-level coordination, exchanging only flexibility bounds rather than full system models, have received comparatively limited attention [7] and represent the approach pursued in this work.

Objectives: The aim of this work is to develop and evaluate a hierarchical predictive control framework for the coordinated operation of an energy community composed of heterogeneous members with different flexibility levels. The analysis focuses on the capability of the proposed architecture to exploit distributed flexibility to maximize external electrical grid independence while maintaining feasible operating conditions for individual members. Three different coordination strategies are investigated to quantify the impact of the central controller on community performance.

Material and methods: The considered energy community is located in Rome, Italy; photovoltaic generation profiles are derived from meteorological measurements collected at the on-site weather station of the Department of Industrial Engineering, University of Rome "Tor Vergata". The community consists of three residential members: two prosumers and one consumer. Each prosumer integrates photovoltaic generation (4 kWp), residential electrical demand with a peak load of approximately 7 kW (including EV charging at 3.7 kW), a 5.2-kWh BESS and a 1.5-kW PEMFC. The consumer is characterized only by electrical demand (base load and electric vehicle charging) and therefore does not provide operational flexibility. The control architecture is hierarchical, with a local MPC associated with each community member and a central coordination controller. Each member sends its operational state to the local MPC, which optimizes every 15 minutes over a 48-hour prediction horizon. The local MPC solves a constrained optimization problem in which the decision variables include BESS charging/discharging power, PEMFC output power and grid exchange. The objective function minimizes the expected energy exchange with the external grid over the prediction horizon, based on forecasts of photovoltaic generation and electrical demand, while respecting component operating limits and state-of-charge

dynamics. At the end of the optimization, each member communicates to the central controller the desired exchange profile and the flexibility range within which such profile can be modified without violating internal constraints; the consumer only transmits its expected demand. The central controller receives targets and flexibility bounds from all members, treated as black-box systems, and determines the community-level power exchange profile minimizing total grid interaction subject to the provided flexibility bounds. The resulting targets are sent back to local controllers, which perform a final MPC optimization with the community-imposed exchange as an additional constraint, and the resulting control actions are applied to the controllable components of each prosumer. The energy community model is implemented in MATLAB/Simulink, the control algorithms in Python, interfaced via a Transmission Control Protocol (TCP)-based bridge.

Results: Three different Energy Management Strategies (EMSs) are investigated. In Member Mode (MM) the central controller does not modify the local targets, resulting in independent member operation. In Central Mode (CM) the central controller fully determines the grid exchange of each member within the available flexibility range to minimize overall community grid interaction. In Balanced Mode (BM) the objective function combines the total community grid exchange and the deviation from local targets, with equal weights enforcing a 50/50 trade-off between coordination and preference preservation. Results refer to a seven-day simulation period. Figure 80 summarizes the overall performance of the energy community under the three EMSs, showing both the total energy exchanged with the external grid and the resulting community-level performance indicators.

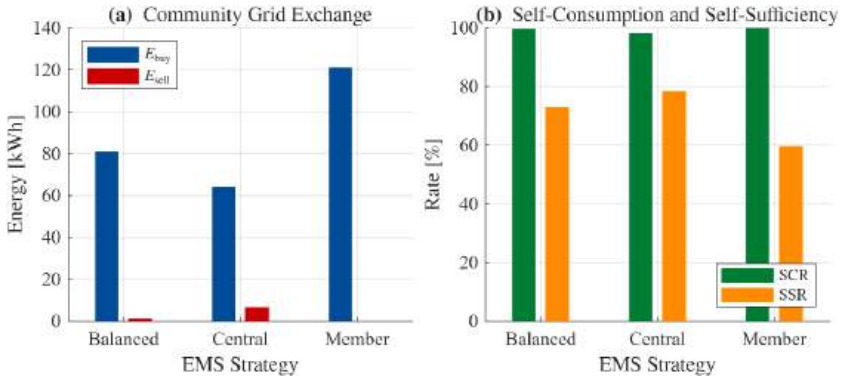


Figure 80. Community-level performance comparison for the three EMSs: total grid energy exchange, SCR and SSR indicators.

In the MM configuration, each prosumer optimizes its operation independently while the consumer lacks controllable resources. Therefore, most of the consumer demand must be supplied by the external grid, resulting in the highest grid dependency with approximately 120 kWh purchased during the simulation period. This behavior is reflected in the corresponding performance indicators, with the lowest Self-Sufficiency Rate (SSR) of about 60%, despite a Self-Consumption Rate (SCR) close to 99%. When coordination is introduced, the central controller exploits the flexibility available within the prosumers to redistribute locally generated energy across the community. This significantly reduces the energy imported from the external grid, which decreases to approximately 65 kWh in CM and 80 kWh in BM. As a direct consequence, the SSR increases to about 78% and 72%, respectively, while the SCR remains nearly unchanged.

Figure 81 disaggregates the community-level results at member level. In MM, the consumer imports the entirety of its electrical demand (≈ 103 kWh) from the external grid, while prosumers partially rely on grid purchases to cover residual load peaks, without exporting electricity. Under coordinated operation (CM and BM), the prosumers begin exporting part of their locally generated energy, which is partially redistributed within the community to supply the consumer demand – thus increasing community SSR— and partially injected into the external grid. Moreover, both prosumers transition from

net importers to net exporters, illustrating that community coordination can reverse the individual grid exchange direction of a member –an effect invisible at the aggregate level shown in Figure 80.

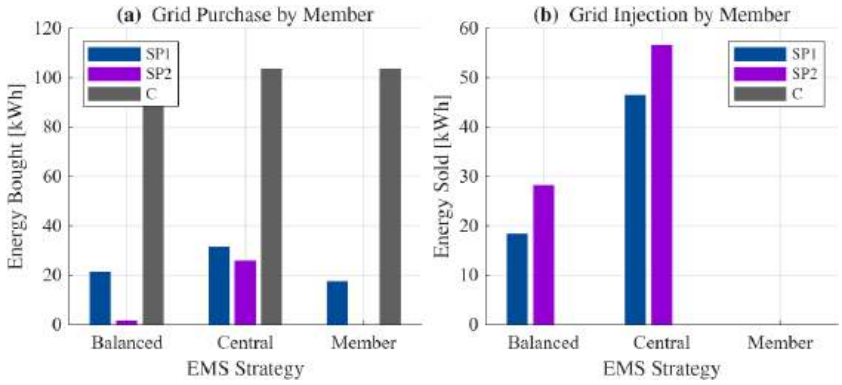


Figure 81. Grid energy exchanges for each community member under three EMS strategies.

Conclusions: This work presents a hierarchical MPC-based control architecture for the coordinated operation of heterogeneous members within an energy community, relying on flexibility exchange between local controllers and a central coordinator without requiring access to internal component-level models.Simulation results over a seven-day operating period show that coordinated operation increases community self-sufficiency by approximately 25%, while reducing grid energy imports by about 40%. These improvements are achieved through the redistribution of locally generated energy from flexible prosumers to an inflexible consumer, demonstrating the capability of the proposed architecture to exploit distributed flexibility at community level. The control cycle of approximately 20 ms confirms the suitability of the framework for real-time supervisory energy management and future Hardware-in-the-Loop implementation. Future developments will extend the architecture to multi-energy coordination including hydrogen production and HT-PEM fuel cell thermal recovery, enabling management of coupled electrical, thermal and hydrogen flexibility at larger community scale.

Acknowledgement: This research was funded by CETPartnership, the Clean Energy Transition Partnership under the 2023 joint call for research proposals, co-funded by the European Commission (GA N°101069750) and with the funding organizations detailed on https://cetpartnership.eu/funding-agencies-and-call-modules.

References

[1] W. Tushar *et al.*, "Peer-to-peer energy systems for connected communities: A review of recent advances and emerging challenges," *Appl. Energy*, vol. 282, p. 116131, Jan. 2021, doi: 10.1016/j.apenergy.2020.116131.

[2] A. C. Lazaroiu, M. Roscia, G. C. Lazaroiu, and P. Siano, "Review of Energy Communities: Definitions, Regulations, Topologies, and Technologies," *Smart Cities*, vol. 8, no. 1, p. 8, Jan. 2025, doi: 10.3390/smartcities8010008.

[3] Z. Ji, H. Zhang, and P. Wang, "Model Predictive Control Scheduling Strategy for Hydrogen-doped Integrated Energy System Considering Ladder Carbon Trading," *J. Therm. Sci.*, vol. 34, no. 2, pp. 337–351, Mar. 2025, doi: 10.1007/s11630-024-2075-0.

[4] K. Basaran *et al.*, "A comprehensive survey of distributed optimization methods and technological enablers for sustainable energy communities," *Energy*, vol. 344, p. 139983, Feb. 2026, doi: 10.1016/j.energy.2026.139983.

[5] S. Lim, J. Lee, and S. Lee, "Model Predictive Control-Based Energy Management System for Cooperative Optimization of Grid-Connected Microgrids," *Energies*, vol. 18, no. 7, p. 1696, Mar. 2025, doi: 10.3390/en18071696.

[6] M. F. Zia, E. Elbouchikhi, and M. Benbouzid, "Microgrids energy management systems: A critical review on methods, solutions, and prospects," *Appl. Energy*, vol. 222, pp. 1033–1055, Jul. 2018, doi: 10.1016/j.apenergy.2018.04.103.

[7] M. Y. A. Khan, H. Liu, Z. Yang, J. Wang, and Y. Zhang, "Hierarchical control of microgrid: a comprehensive study," *Electr. Eng.*, vol. 107, no. 10, pp. 13681–13712, Oct. 2025, doi: 10.1007/s00202-025-03230-4.

EFCH2 2026 European Fuel Cells and Hydrogen PIERO LUNGHI CONFERENCE
September 15th-17th 2026 Capri / Italy

Enhancing e-Biomethanol Synthesis from Biomass-Derived Syngas via a LTA-Zeolite Catalytic Membrane System

N. Cerone[a], L. Contuzzi[a], C. Florio[a], G. Santilli[a], G. Zito[a,b], A. Caivano[a]

C. Ragone[a], A. Romanelli[a], F. Zimbardi[a*]

* corresponding author: francesco.zimbardi@enea.it

[a] ENEA, Dip. Tecnologie e Fonti Energetiche Rinnovabili, ss 106, 75026 Rotondella (MT), Italy

[b]Dip. di Meccanica, Matematica e Management, Politecnico di Bari, 70125 Bari, Italy

Keywords: Methanol, Biomass, Membrane Reactor, Zeolites

Abstract

Introduction: The conversion and valorisation of syngas derived from biomass gasification is key to sustainable energy production. This pathway serves as a fundamental pillar in defossilizing challenging industrial and transportation sectors. Specifically, hard-to-abate industries like heavy manufacturing, maritime shipping, and aviation find in biomass-derived fuels a viable, carbon-neutral alternative to traditional petroleum-based energy sources. By shifting to renewable biomass, these sectors can significantly reduce their environmental footprint while maintaining operational integrity. Within this portfolio, biomethanol has emerged as a versatile and significant green commodity. Its prominence is rooted in an exceptional range of applications that bridge the gap between current infrastructure and future energy requirements. One compelling attribute is its role as a superior hydrogen carrier. Unlike molecular hydrogen, which faces logistical hurdles due to low volumetric energy density and the need for cryogenic storage, biomethanol remains liquid at ambient conditions. This makes it simpler to handle, transport, and store using existing infrastructure. Furthermore, it serves as a high-performance biofuel for internal combustion engines (ICE) and acts as a chemical platform. As a precursor, it is essential for synthesizing value-added products like formaldehyde, acetic acid, and olefins, the building blocks of modern plastics and textile industries.

Objectives: In this paper we considered as an objective the integration of green hydrogen obtained from water electrolysis in methanol synthesis. Despite its clear potential, the industrial-scale synthesis of biomethanol from biomass-derived syngas is complicated by several significant technical and thermodynamic barriers. The first major issue involves the chemical composition of the raw syngas itself. To achieve efficient methanol synthesis, the feed gas must meet a specific stoichiometric ratio of hydrogen to carbon oxides, often quantified by the "Module" value, M= (H_2

$-CO_2)/(CO+CO_2)$. Unfortunately, syngas produced from typical gasification processes rarely meets the ideal ratio of approximately 2.0, usually being deficient in hydrogen. This imbalance necessitates additional hydrogen produced by processing steps such as the Water-Gas Shift (WGS) reaction or the external injection of renewable hydrogen to achieve the required specifications.
The second objective is inherent to the thermodynamics of the methanol synthesis reaction. The conversion of syngas into methanol is an exothermic process that is limited by chemical equilibrium, which results in a relatively low single-pass yield. In a standard reactor setup, only a fraction of the incoming gas is converted into methanol before the mixture reaches a state where no further reaction can occur under those specific conditions. To achieve high overall conversion rates and ensure the process remains economically competitive, industrial facilities must implement complex and energy-intensive recycling loops. The facility we have tested for this research separate the produced methanol and water from the unreacted syngas through the innovative use of membrane reactors that can remove products in situ to shift the equilibrium [1].

Material and methods: The research details the testing and implementation of a cutting-edge membrane reactor (MR) architecture, specifically engineered to optimize the synthesis of biomethanol from renewable feedstocks. The process begins with syngas simulating the gasification of biomass, which inherently lacks the ideal chemical balance for efficient conversion [2]. To address this, the raw syngas is enriched with supplemental hydrogen to precisely calibrate the stoichiometric H_2/CO_x ratio, ensuring the feed gas is thermodynamically primed for the subsequent catalytic reactions. The experimental setup was designed at a meaningful pre-pilot scale, capable of processing a continuous syngas flow of 0.25 Nm^3/h, providing a robust dataset for assessing the system's industrial potential. At the heart of the reactor is a bed containing, commercial-grade $CuO/ZnO/Al_2O_3$ (CZA) catalyst. This specific formulation is widely recognized in the chemical industry for its superior activity and selectivity in methanol synthesis. Within the reactor, the catalyst facilitates the hydrogenation of carbon oxides, a process that is traditionally limited by the buildup of reaction products. By housing this catalyst within a LTA zeolite membrane-integrated environment, the system moves beyond the constraints of conventional fixed-bed reactors, allowing for a more dynamic control of the chemical environment at the molecular level.

Results: The results gathered during the test period of 75 minutes demonstrated high efficiency and operational stability as shown in Figure 1. A mixture of 0.25 Nm^3/h of H_2-enriched air-steam biomass gasification syngas meeting the M value of 2 was introduced in the MR at temperature of 250 °C and pressure of 35 bar. A little flow of N_2 was also introduced from the lumen of the membrane as sweep gas to facilitate the water removal during the methanol synthesis. The system achieved a mean conversion rate of 28.1% for CO_2 and a significantly higher conversion of 68.6% for CO. When combined, these figures represent an overall CO_x conversion efficiency of 53.5%. These metrics provide a compelling proof of concept, establishing a robust foundation for future investigations.

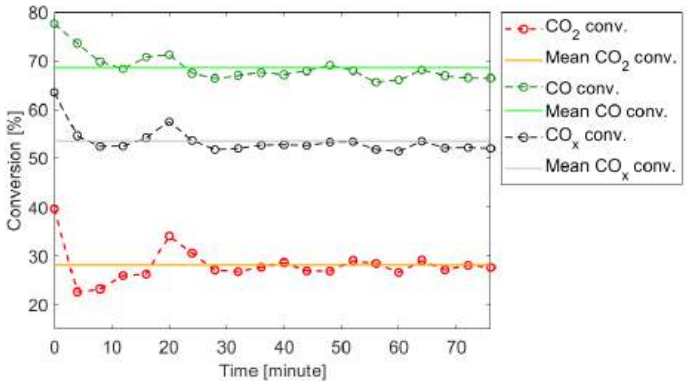


Figure 1: CO, CO_2 and CO_x conversions over test period.

Conclusions: The evidence generated during this initial experimental phase serves as a significant milestone in the development of membrane reactor technology. Subsequent studies will likely focus on subjecting the membrane reactor to a broader spectrum of process variables and significantly longer operational durations to fully characterize its long-term durability and performance envelope under varying industrial syngas compositions. These results can be used as roadmap designed to bridge the gap between laboratory success and industrial implementation.

Acknowledgment

Work funded by the Italian Ministry of the Environment and Energy Security, program agreement MiTE_ENEA, PNRR - Hydrogen Research - Mission M2-C4 - Investment 3.5: Research and development on hydrogen.

References

[1] Inorganic Membrane Reactors for Methanol Synthesis. Galluci 2018 https://doi.org/10.1016/B978-0-444-63903-5.00018-2

[2] Production of hydrogen-rich syngas from biomass gasification by double step steam catalytic tar reforming. Cerone et. al, 2022, https://doi.org/10.1016/j.ijhydene.2024.07.290

EFCH2 2026 European Fuel Cells and Hydrogen PIERO LUNGHI CONFERENCE
September 15th-17th 2026 Capri / Italy

Predictive Energy Management for Hydrogen Fuel Cell Hybrid Trains

Yosef B Jember*[a], Gabriele Peyrani[a], Paolo Marocco[a], Massimo Santarelli[a], Marta Gandiglio[a], Giuseppe Santangelo[b], Clemente Mirko[b]

* corresponding author: yosef.jember@polito.it (Yosef B Jember)

[a]Department of Energy, Politecnico di Torino, Corso Duca degli Abruzzi 24, 10129 Torino, Italy.

[b]Alstom Ferroviaria S.p.A., Via O. Moreno, 23, 12038, Savigliano (CN), Italy

Keywords: Hybrid Multiple Unit Train (HMU), Hydrogen Fuel Cell, Machine Learning, Optimization-Based Energy Management.

Abstract

Introduction: The transport sector is a major source of greenhouse gas emissions and needs to be decarbonized through the adoption of fossil-free energy sources. Fuel cell-and-battery-powered hybrid train (HMU) technology emerges as a viable option for the energy transition to clean heavy-duty transport.

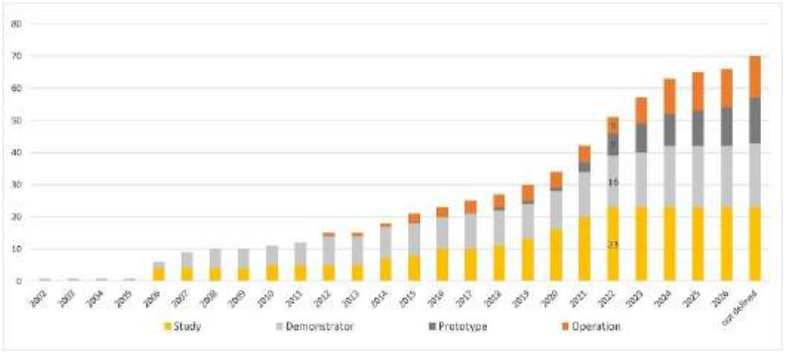


Figure 82:Hydrogen rail projects worldwide trend [1]

However, it requires proper design and analysis to achieve energy-efficient, scalable hydrogen trains for wide adoption [2].

Objectives: This study aims to develop an effective simulation model and an optimal energy management system (EMS) for an HMU train, focusing on the ALSTOM Coradia Stream H train operating along the Brescia-Iseo-Edolo railway line (H) in Italy.

Material and methods: An energy-based simulation is built in MATLAB and Simulink that represents longitudinal train dynamics and powertrain propulsion, the fuel cell stack, the storage battery, and auxiliaries. Physics-based techniques are mainly used in accordance with the train's specifications, using the train's running resistance, the fuel cell's polarization curve, and the battery's state-of-charge (SOC) models, as well as model predictive control (MPC) for power splitting. The MPC was designed based on the SOC model, taking into account operational constraints and the capacities of power components, using primary manufacturer data and the literature. Quadratic programming is used as

the optimization strategy. It can perform online optimization using an active-set solver to minimize the objective function. The cost function and constraint equations used are given below:

$$J = \sum_{i=0}^{p-1} \left[W_{soc} \left(SoC(i+1) - SoC^{ref}(i+1) \right)^2 + W_{Pbat} P_{bat}(i)^2 + W_{Pfc} P_{fc}(i)^2 + Wstress \right] + pen \quad (1)$$

Where W_{soc} weight for SOC control, W_{Pbat} weight for battery power cost, and W_{Pfc} weight fuel cell power.

The following constraints are applied, including DC-link power balance and component stress limits:

$$P_{batMIN} \leq P_{bat} \leq P_{batMAX},\ P_{fcMIN} \leq P_{fc} \leq P_{fcMAX},\ SoC_{MIN} \leq SoC \leq SoC_{MAX} \quad (2)$$

Two machine learning approaches were utilized: a two-stage ensemble predictor for determining regenerative power, and a long short-term memory (LSTM) network to forecast total power demand and enhance MPC performance, with the train's kinematics as features.

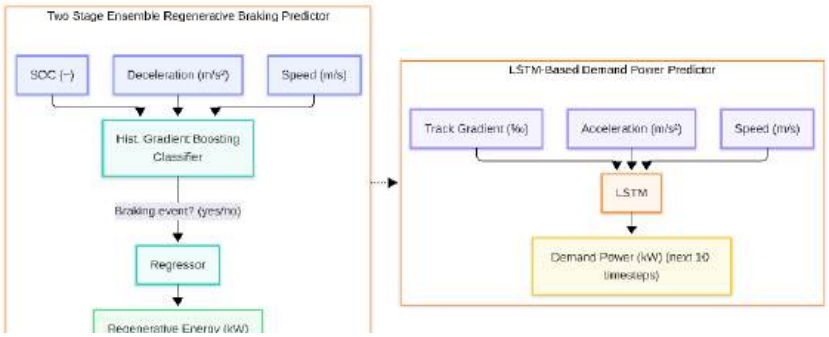


Figure 83: Schematic diagram of the proposed ML models

Results: Training these models yields R^2 values of 0.99 and 0.89 for the ensemble and LSTM, respectively.

The EMS gains were also evaluated at the MPC's optimal weight settings, which minimized the objective function. Introducing LSTM-predicted inputs to the MPC achieves up to a 7% reduction in hydrogen consumption compared to the standard MPC after a round-trip simulation.

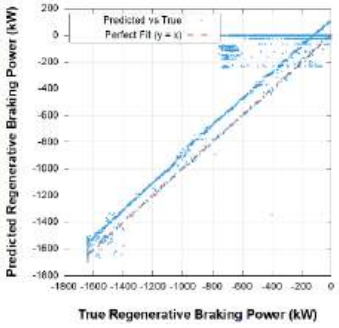


Figure 84: Ensemble based predictor

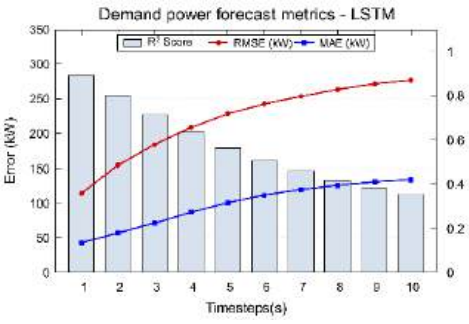


Figure 85: Evaluation metrics for LSTM demand predictor

From the fuel cell lifetime perspective, cumulative power fluctuation was treated as total stress and was found to be 57.9 MW with LSTM-MPC, 2 MW lower than with standard MPC. Furthermore, battery charge sustaining was among the desired objectives, and the enhanced MPC maintained the SOC more precisely throughout the train's round-trip journey.

Table 12: Total stress (cumulative absolute variation in output power)

Fuel Cell	Standard MPC	ML - MPC	Battery	Standard MPC	ML - MPC
	59.8 MW	57.9 MW		23.8 MW	18.1 MW

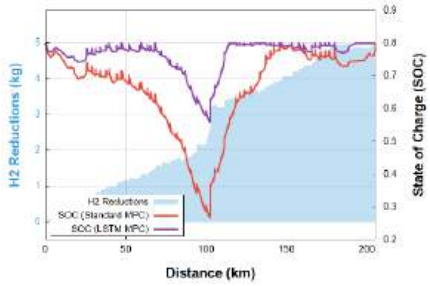


Figure 86: Comparison of EMS in fuel consumption and SOC curve

Conclusions: This paper discussed machine learning-based simulation features and predictive EMS for power splitting in hybrid hydrogen fuel cell battery trains. As part of the simulation system, a two-stage machine-learning ensemble approach is proposed to forecast the occurrence of regenerative braking and the amount of power. Model predictive control is designed for power splitting and is further enhanced by an LSTM model that forecasts near-future power demand. Evaluation of the ML models using relevant metrics indicates an adequate performance in agreement with the traction system. Finally, the proposed EMS is run for the BsEd round trip, and it shows that the LSTM-based MPC saves more hydrogen, maintains an optimal SOC path, and results in lower total stress in the fuel cell and battery.

Acknowledgment

This work was supported by the European Union, Next Generation EU - IPCEI Hydrogen 1 Hy2tech, Project ID: IPCEI-I1_0000003 CUP: B19J23000490004, coordinated by Alstom Ferroviaria S.p.A.

References

[1] M. Böhm et al., Review and comparison of worldwide hydrogen activities in the rail sector with special focus on on-board storage and refueling technologies, International Journal of Hydrogen Energy, 47 (2022) 38003-38017

[2] Q. Li et al., An energy management strategy for multi-stack fuel cell hybrid locomotives with integrated optimization of system service life, IEEE Transactions on Transportation Electrification, 10 (2024) 7954-7970



Integrated Autonomous Hydrogen Energy Systems for Resilience and Humanitarian Crisis Response: A Techno-Economic Assessment

Emmanuel Stamatakis *[a] & Athanasios Stubos [a]

* corresponding author: manos@ipta.demokritos.gr

[a] National Center for Scientific Research DEMOKRITOS (NCSRD), Integrated Hydrogen Laboratory (H2Lab), 15341 Agia Paraskevi, Athens, Greece

Keywords: Cell on Wheels; hydrogen refueling station; containerised systems; resilient energy systems; dual-use

Abstract

The increasing frequency and intensity of climate-related disasters place growing pressure on emergency energy, telecommunications and mobility infrastructure. The September 2023 Thessaly flooding in Greece provides a representative crisis case in which power, transport and communications disruption highlighted the need for rapidly deployable, low-emission energy systems. Green hydrogen integrated with renewable power can function both as an energy-storage medium and as a clean fuel for specialized vehicles.

This work assesses a single-container hydrogen-based Cell on Wheels (H2CoW) architecture combined with a 350 bar emergency refueling function for humanitarian and dual-use civil-defence response, using the Thessaly flooding as the reference deployment scenario. The proposed demonstrator is a road-mobile 20 ft ISO standard container integrating a 20 kWp compact fold-out photovoltaic array, a 12 kW PEM electrolyzer, a 5 kW heat pump supporting thermally driven metal-hydride compression to 350 bar, 40 kg of pre-filled 350 bar hydrogen storage, a 10 kW PEM fuel cell, a 60-80 kWh battery buffer and a certified 350 bar slow-fill dispensing interface. The deployed footprint is approximately 90-100 m2 and the assumed preliminary gross mass is 7-9 t.

Under Thessaly high-solar deployment conditions, represented by 8 equivalent full-load hours per day and a 0.90 photovoltaic derating factor, the 20 kWp array can generate approximately 144 kWh/day. The system is configured for one week of operation at approximately 2.5-3.0 kW average critical electrical demand while supporting one hydrogen-compatible emergency vehicle with two 5 kg refuelings per week, equivalent to approximately 1,100 km of supported emergency mobility.

Introduction: Climate-related disasters, grid outages and security-related disruptions expose common vulnerabilities in emergency communications, field power supply and vehicle-fuel logistics. Cell on Wheels platforms are routinely deployed to restore mobile connectivity when fixed telecommunications infrastructure is damaged. During the September 2023 Thessaly flooding caused by Storm Daniel, extensive damage to roads, energy infrastructure and communications networks underlined the difficulty of sustaining diesel-based emergency assets when access and fuel delivery are constrained. Photovoltaic-hydrogen-fuel-cell systems can extend the autonomy of mobile base stations used in disaster areas [1].

The concept considered here integrates hydrogen-based telecommunications support with limited mobile refueling, creating a dual-use energy hub for civil-protection missions, emergency medical or rescue operations, remote communities, island infrastructure and defence applications. Autonomy, low acoustic signature and zero direct exhaust emissions are valuable in humanitarian response and in defence scenarios where fuel-convoy exposure and operational detectability are critical constraints [3].

Objectives: The objective is to present a compact assessment of an autonomous hydrogen-based Cell on Wheels architecture integrated with a mobile 350 bar hydrogen refueling function for a Thessaly-type flood response scenario. The work defines a road-mobile 20 ft ISO container configuration, quantifies the hydrogen and electricity balance for one-week autonomy with pre-filled storage, estimates footprint and gross mass, and outlines a pilot-deployment pathway involving H2Lab hydrogen technology capabilities.

Material and methods: The proposed architecture consists of a standard 20 ft ISO container integrating a 20 kWp compact fold-out PV array, a 12 kW proton-exchange-membrane electrolyzer, a 5 kW heat pump supporting thermally driven metal-hydride compression to 350 bar, 40 kg of pre-filled compressed hydrogen storage, a 10 kW proton-exchange-membrane fuel cell, a 60-80 kWh battery buffer and a certified 350 bar slow-fill dispensing module. The metal-hydride compression option is motivated by low noise, absence of moving compression parts and suitability for thermally driven operation [2,4]. The energy balance was evaluated for a 2.5-3.0 kW average critical load under representative Thessaly solar conditions, using 8 equivalent full-load hours per day and a 0.90 photovoltaic derating factor. This gives 144 kWh/day, or 1,008 kWh/week, from the 20 kWp array. Hydrogen consumption was calculated using 39.4 kWh/kg as the higher heating value and 55% fuel-cell efficiency. Hydrogen production was calculated at 75% electrolyzer HHV efficiency; with the 5 kW heat pump included during thermal compression, the combined electrolyzer/compression chain requires approximately 17 kW and about 75 kWh/kg H2 produced and compressed to 350 bar. Refueling demand was set at two 5 kg H2 events per week.

Results: For a 3 kW average critical load, weekly electrical demand is approximately 504 kWh. The 20 kWp photovoltaic system produces about 1,008 kWh/week under the assumed high-solar condition, leaving about 504 kWh/week for hydrogen production and compression. With the 12 kW electrolyzer and 5 kW heat pump, this surplus corresponds to roughly 6.7 kg H2/week.



The emergency vehicle requires 10 kg H2/week; therefore, net storage drawdown is approximately 3.3 kg H2/week at the 3 kW design point and about 2.2 kg H2/week at 2.5 kW average load. The 40 kg pre-filled storage provides reserve for poor weather, start-up losses and auxiliary loads.

The single-20 ft ISO container concept can offer the key resilience functions required in a Thessaly-type flood response. The transport footprint is 6.06 m x 2.44 m, or about 15 m^2, while the deployed footprint is approximately

90-100 m2, under a compact fold-out PV arrangement enabling 20 kWp. The assumed gross mass is 7-9 t, supporting truck or military-logistics transport and potential heavy-lift helicopter mobilization subject to certification.

Compared with diesel generation, the system offers zero direct local emissions, very low acoustic signature, reduced fuel-logistics dependence and transferability between civil-protection and defence missions. The assumed 7-9 t gross mass supports both road transport and heavy-lift helicopter mobilization (eg. by a CH-47D Chinook), subject to certified lifting-frame design, centre-of-gravity verification and aircraft-specific sling-load approval.



Conclusions: The proposed single-container hydrogen-based Cell on Wheels and emergency refueling architecture is technically feasible as a dual-use civil-defence resilience demonstrator for various crisis scenarios. A 20 kWp fold-out photovoltaic array deployed over approximately 90-100 m2, 40 kg of pre-filled 350 bar H2 storage, a 10 kW PEM fuel cell, a 12 kW PEM electrolyzer, a 5 kW heat pump supporting metal-hydride compression and a 60-80 kWh battery buffer form a realistic basis for a compact 20 ft ISO-container pilot. Future work should address detailed packaging, weight optimization, photovoltaic deployment mechanisms, seasonal solar variability, emergency dispensing protocols and experimental validation under realistic loads, refueling pilot tests and start/stop cycles. Further priorities include safety certification and permitting templates for mobile hydrogen assets, operator training for civil-protection and defence users, modular scaling of photovoltaic and storage capacity, and lifecycle and techno-economic sensitivity analysis. Demonstrations with emergency services, telecommunications operators and armed-forces logistics units are required to assess the platform as an operational resilience tool. A pilot demonstrator combining NCSRD/H2Lab expertise, CYRUS-type compression and certified 350 bar dispensing hardware would bridge laboratory capability and operational deployment [5,6].

Acknowledgement: *The authors would like to acknowledge the financial support of the European Union's European Defence Fund under the Grant Agreement No. 101168041.*

References

[1] E. Erturk et al., International Journal of Hydrogen Energy 75 (2024) 515-528.

[2] N. Chalkiadakis, A. Stubos, E.I. Zoulias, E. Stamatakis, E3S Web of Conferences 334 (2022) 06002.

[3] A. Soboń, D. Słyś, M. Ruszel, A. Wiącek, Energies 14 (2021) 7089.

[4] G. Tzamalis, E.I. Zoulias, E. Stamatakis, E. Varkaraki, E. Lois, Renewable Energy 36 (2011) 118-124.

[5] H2Lab, https://inrastes.demokritos.gr/laboratories/integrated-hydrogen-laboratory-h2lab/

[6] CYRUS S.A., www.h2cyrus.eu

EFCH2 2026 European Fuel Cells and Hydrogen PIERO LUNGHI CONFERENCE
September 15th-17th 2026 Capri / Italy

Nutrient management in biological methanation reactors: experimental optimization of nutrient formulations and CSTR-TBR comparison

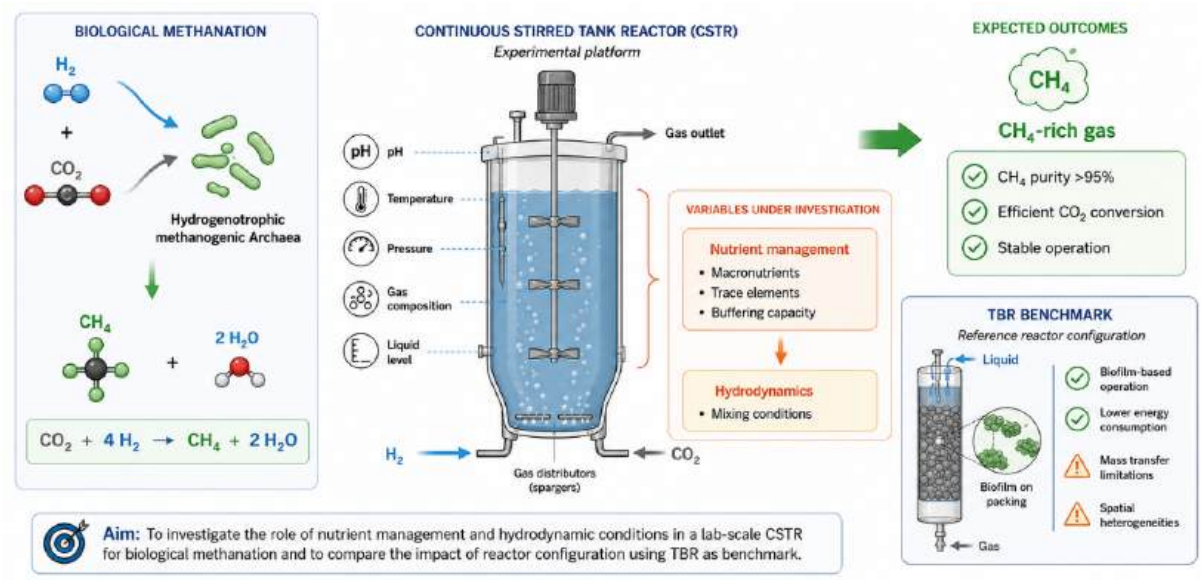
G. Soggia[1]*, M. Nordio[1], M. Mastroleo[1], S. Rossi[1], A. Rossetti[1]

*Corresponding author: gabriele.soggia@rse-web.it

[1] RSE S.p.A. – Ricerca sul Sistema Energetico, Via R. Rubattino 54, 20134 Milan, Italy

Keywords: biological methanation, Continuous Stirred Tank Reactor (CSTR), gas-liquid mass transfer, nutrient management, Trickle Bed Reactor (TBR).

Abstract



Introduction: Biological methanation is a key technology for renewable gas production, enabling the conversion of CO_2-rich streams into methane by hydrogenotrophic methanogenic Archaea. Among the available reactor configurations, Continuous Stirred Tank Reactors (CSTRs) are widely adopted due to their operational flexibility, simple design and compatibility with existing biogas infrastructures[1,2]. Mechanical mixing ensures homogeneous conditions, supporting stable microbial activity[3]. Alternative systems such as Trickle Bed Reactors (TBRs) have attracted increasing interest because of their potentially higher gas conversion efficiencies and lower energy demand. However, biofilm-based operation may introduce mass transfer limitations and spatial heterogeneities. Despite the technological maturity of biological methanation, important knowledge gaps remain regarding nutrient requirements and microbial community dynamics. In addition, process performance is strongly influenced by gas–liquid mass transfer, which affects hydrogen availability and conversion

efficiency. The role of nutrient composition in sustaining microbial activity and optimizing reactor performance remains only partially understood[4].

Objectives: The aim of this work is to investigate the role of nutrient management in biological methanation and evaluate its impact on reactor performance. Particular attention is devoted to assessing whether nutrient composition exerts a greater influence on process performance than reactor design through comparison between CSTR and TBR systems.

Material and methods: Experiments are carried out in a lab-scale CSTR available in a dedicated RSE laboratory facility for biological methanation. The facility was designed to investigate bioprocess optimization across different reactor configurations, with particular focus on nutrient management in the liquid phase. Insights from previously investigated TBRs are used as a benchmark for comparison. The CSTR is a vertical cylindrical vessel, with a total volume of approximately 20 L, of which about 15 L are occupied by the liquid phase. The geometry (H = 1.2 m, D = 0.15 m, H/D = 8) was selected according to previous literature to enhance gas residence time and gas–liquid interaction. Gas substrates (H_2 and CO_2) are injected from the bottom through dedicated distributors, with two independent feeding points enabling flexible gas injection strategies. Mixing is ensured by a multi-impeller system, designed to improve gas dispersion, increase interfacial area and avoid stagnant zones, which are key factors governing gas–liquid mass transfer. The plant is equipped with advanced instrumentation allowing high-frequency monitoring of process performance, including thermodynamic parameters (temperature, pressure, gas composition, liquid level) and biological indicators (pH, nutrient availability and process stability). The reactor operates under strictly anaerobic conditions and is equipped with temperature and pressure control systems (35–80°C, up to 10 bar). The experimental activity focuses on the effect of nutrient composition, which is analysed through systematic variation of macronutrients, trace elements, and buffering capacity. Secondly, the hydrodynamic behaviour is investigated by varying mixing conditions and gas injection strategies, with the aim of improving gas–liquid transfer and H_2 availability. Experiments are conducted with either gaseous substrates only (H_2 and CO_2), or with simulated biogas (i.e., also including inert CH_4).

Expected results: Nutrient composition is expected to play a central role in determining reactor performance. A reduction in macronutrient concentration may still sustain stable operation, while trace elements remain essential for microbial activity. Simplified media may enable cost reduction without compromising reactor performance within a defined operating window, although excessive nutrient limitation could negatively affect methane production or promote competing pathways[2]. Under optimized conditions, the reactor is expected to achieve stable operation, with high CH_4 purity in the off-gas (>95%) and efficient CO_2 conversion. The comparison with TBR systems will assess whether reactor configuration or biological/nutritional management has the strongest influence on process performance. CSTR systems are expected to show greater flexibility and faster response, while TBR systems may exhibit lower energy consumption but different mass transfer limitations due to biofilm-based operation. Improved mixing conditions are also expected to enhance hydrogen

transfer to the liquid phase, resulting in higher methane production rates, although at the expense of higher energy consumption and potential shear stress on the biomass, highlighting the need for process optimization. Gas injection strategies are also expected to play a key role, as they directly influence bubble size, gas distribution and overall mass transfer efficiency.

Conclusions: CSTR reactors represent a mature and flexible solution for biological methanation. This work highlights that, despite the technological maturity of CSTR systems, biological methanation still requires significant optimization from a nutritional and microbial perspective to improve reactor and process performance. The experimental activity carried out at the RSE facility will support the identification of optimized nutrient strategies and help clarify the relative importance of biological and reactor-related parameters in determining process performance.

Acknowledgment: This work was supported by the Italian National Recovery and Resilience Plan (PNRR), funded by the European Union – NextGenerationEU.

References:

(1) Bassani, I.; Kougias, P. G.; Treu, L.; Porté, H.; Campanaro, S.; Angelidaki, I. Optimization of Hydrogen Dispersion in Thermophilic Up-Flow Reactors for Ex Situ Biogas Upgrading. *Bioresource Technology* **2017**, *234*, 310–319. https://doi.org/10.1016/j.biortech.2017.03.055.

(2) Lecker, B.; Illi, L.; Lemmer, A.; Oechsner, H. Biological Hydrogen Methanation – A Review. *Bioresource Technology* **2017**, *245*, 1220–1228. https://doi.org/10.1016/j.biortech.2017.08.176.

(3) Colelli, L.; Segneri, V.; Verdone, N.; Bassano, C.; Deiana, P.; Vilardi, G. Analysis and Modelling of the Biological Methanation Process for Power to Gas Applications. *Biomass and Bioenergy* **2026**, *209*, 108964. https://doi.org/10.1016/j.biombioe.2026.108964.

(4) Yörüklü, H. C.; Kamravamanesh, D.; Köroğlu, E. O.; Patel, G. H.; Havukainen, J.; Karjunen, H.; Sillman, J.; Kokko, M. A Comprehensive Review on Biological Methanation Processes: From Gaseous Feedstocks to Biomethane. *Energy Conversion and Management* **2025**, *341*, 120075. https://doi.org/10.1016/j.enconman.2025.120075.



Fuel properties and composition of green diesel produced via catalytic deoxygenation of rapeseed oil

Sonia Dell'Aversano*[a], Katia Gallucci [a], Giuseppina Vanga [b], Carlo Villante [a], Andrea Di Giuliano [a], Giuseppe Di Vito Nolfi [c], Leucio Rossi [c], Davide Faedo [d], Angelo Lunghi [d], Vittorio Occhipinti [d]

* corresponding author: Sonia Dell'Aversano

[a] Department of Industrial and Information Engineering and Economics, University of L'Aquila, Monteluco di Roio, 67100 L'Aquila, Italy

[b] ENEA, Italian National Agency for New Technologies, Energy and Sustainable Economic Development, via Anguillarese 301, 00123, Rome, Italy

[c] Department of Physical and Chemical Sciences, University of L'Aquila, via Vetoio (Coppito), 67100 L'Aquila, Italy

[d] Innovhub—Stazioni Sperimentali per l'Industria S.r.l., Via G. Galilei 1, San Donato Milanese, 20097 Milan, Italy

Keywords: Green diesel, Catalytic deoxygenation, Rapeseed oil, GC-VUV analysis

Abstract

Introduction: The increasing demand for sustainable drop-in fuels has intensified interest in renewable production pathways capable of reducing dependence on fossil resources [1]. Among the available conversion routes, catalytic deoxygenation (DO) of vegetable oils represents a promising approach for producing paraffinic green diesel fully compatible with existing infrastructures and compression ignition engines [2-5].

In the DO process, triglycerides (TGs) are converted in the presence of hydrogen to produce linear n-alkanes and by-products. Following hydrogenation and hydrogenolysis reactions, the resulting free fatty acids are transformed into hydrocarbons through three competing pathways: hydrodeoxygenation (HDO), decarbonylation (DCO) and decarboxylation (DCO_2) [6]. As part of a research activity focused on green diesel production from rapeseed oil, a paraffinic product was obtained through catalytic deoxygenation in batch reactors. An extensive characterization campaign was carried out to evaluate its composition, physicochemical properties and overall quality.

Objectives: Following preliminary catalyst screening and process optimization activities previously carried out in a smaller-scale reactor [5'6], this work focused on the characterization of the paraffinic green diesel obtained under the selected operating conditions.

The study addressed hydrocarbon composition, main physicochemical properties, combustion behaviour, cold-flow performance and safety-related characteristics. It also aimed to verify the

effective removal of catalyst residues and assess the suitability of the product with respect to the typical parameters used for paraffinic diesel fuels.

Material and methods: Green diesel was produced through catalytic deoxygenation of rapeseed oil using hydrogen and hexane as solvent in 450 and 600 mL PARR batch reactors. A Ni-Mo-Al-based catalyst previously developed at the University of L'Aquila was employed. Reactions were carried out at 320 °C for 6 h with an initial hydrogen pressure of 40 bar. Multiple experimental runs were preliminarily analysed by GC-FID to verify product reproducibility and compositional consistency. After confirming their similarity, the liquid products were combined to obtain representative samples for characterization.

Conversion, diesel yield, selectivity and residual FAME content were determined by GC-FID. Product characterization was performed using standard analytical methods, including GC-VUV compositional analysis, density and viscosity measurements, cold-flow property evaluation, ICP-OES elemental analysis, derived cetane number (DCN), calorimetric analysis, CHN elemental analysis, flash point and autoignition temperature measurements.

Results: The deoxygenation process achieved conversion values between 80 and 100%, with diesel yields ranging from 70 to 83%. Residual FAME content remained below 0.2%, while no oxygenated compounds were detected, indicating an almost complete deoxygenation of the feedstock. Higher conversions were generally observed in the 450 mL reactor compared to the 600 mL reactor, suggesting a possible influence of reactor scale and operating configuration on deoxygenation performance.

The obtained fuel exhibited a highly paraffinic composition, consisting of approximately 99% linear paraffins with minor amounts of isoparaffins and traces of naphthenes. No olefins or aromatic compounds were detected. GC-VUV analysis revealed a predominant presence of C17 paraffins (>70%), while C18 hydrocarbons accounted for approximately 20% of the product distribution. The relatively low C18/C17 ratio suggested that decarboxylation/decarbonylation pathways were favoured over hydrodeoxygenation under the adopted operating conditions.

The produced green diesel showed properties consistent with paraffinic renewable fuels, including a DCN up to 85.5, low water content (14 ppm), density and viscosity within the typical diesel range, and a high heating value of 11256 cal/g. ICP-OES analysis revealed no catalyst-derived metal contamination. Flash point and autoignition temperature were measured at 62 °C and 291 °C, respectively. However, the fuel exhibited poor cold-flow behaviour, appearing partially solid at room temperature and showing CFPP, Cloud Point and Pour Point values around 20 °C, due to the high concentration of long-chain linear paraffins.

Conclusions: The produced green diesel exhibited the main characteristics of a high-quality paraffinic renewable diesel, including high ignition quality, high purity and high energy density. The predominant formation of linear paraffins strongly influenced the final fuel properties. Although the obtained product exhibited excellent combustion-related characteristics, unfavourable cold-flow behaviour was observed due to the high concentration of long-chain n-paraffins.

Overall, the characterization campaign provided a comprehensive evaluation of the obtained paraffinic fraction, highlighting both its potential as a renewable diesel component and the need for further upgrading strategies or cold-flow improving additives.

Acknowledgment

This research was funded by the European Union - NextGenerationEU from the Italian Ministry of Environment and Energy Security, POR H2 AdP MEES/ENEA with involvement of CNR and RSE, PNRR - Mission 2, Component 2, Investment 3.5 "Ricerca e sviluppo sull'idrogeno", CUP: 510 I83C22001170006

References

[1] Energy Institute. (2025). *Statistical review of world energy 2025* (74th ed.). Energy Institute. https://www.energyinst.org/statistical-review

[2] Lucantonio, S., Di Giuliano, A., Rossi, L., & Gallucci, K. (2023). Green diesel production via deoxygenation process: A review. *Energies, 16(2),* 844. https://doi.org/10.3390/en16020844

[3] Mahdi, H. I., Bazargan, A., McKay, G., Azelee, N. I. W., & Meili, L. (2021). Catalytic deoxygenation of palm oil and its residue in green diesel production: A current technological review. *Chemical Engineering Research and Design, 174,* 158–187. https://doi.org/10.1016/j.cherd.2021.07.009

[4] Douvartzides, S. L., Charisiou, N. D., Papageridis, K. N., & Goula, M. A. (2019). Green diesel: Biomass feedstocks, production technologies, catalytic research, fuel properties and performance in compression ignition internal combustion engines. *Energies, 12(5),* 809. https://doi.org/10.3390/en12050809

[5] Di Vito Nolfi, G., Gallucci, K., & Rossi, L. (2021). Green diesel production by catalytic hydrodeoxygenation of vegetables oils. *International Journal of Environmental Research and Public Health, 18,* 13041. https://doi.org/10.3390/ijerph182413041

[6] Lucantonio, S., Di Vito Nolfi, G., Courson, C., Gallucci, K., Di Giuliano, A., & Rossi, L. (2025). Repurposing of propane oxidative-dehydrogenation catalysts to deoxygenation of vegetable oils for green diesel production. *Fuel Processing Technology, 267*, 108173. https://doi.org/10.1016/j.fuproc.2024.108173

EFCH2 2026 European Fuel Cells and Hydrogen PIERO LUNGHI CONFERENCE
September 15th-17th 2026 Capri / Italy

Novel hydrogen-based technologies for green iron and steel making

Alfonso Chinnici*[a]

* corresponding author: alfonso.chinnici@adelaide.edu.au

[a] Adelaide University, Adelaide, Australia

[b] Heavy Industry Low Carbon Transition CRC, Adelaide, Australia

Green iron, hydrogen direct reduction, iron ore beneficiation, hydrogen combustion.

Abstract

Introduction: the iron and steel industry is responsible for approximately 7-9% of global anthropogenic CO_2 emissions [1] and is considered one of the most challenging sectors to decarbonise due to its dependence on carbon-intensive thermal and reduction processes. The transition toward green iron and steel production is therefore a major international priority, with hydrogen-based (H_2) direct reduction and electrified thermal processing emerging as key enabling technologies. However, large-scale deployment of H_2 ironmaking requires significant advances in ore beneficiation, H_2 reduction reactor design, and renewable-compatible high-temperature processing systems.

In Australia, the Heavy Industry Low-carbon Transition Cooperative Research Centre (HILT CRC) is playing a critical role in accelerating the development and commercialisation of low-emission technologies for heavy industry sectors including iron and steel, alumina, cement, and minerals processing. Through collaboration between universities, industry partners, technology providers, and government stakeholders, HILT CRC is supporting the development of integrated pathways for green metals production using renewable electricity, H_2, and advanced thermal technologies.
This work presents recent research undertaken within the HILT CRC ecosystem on novel H_2-based technologies for green iron and steel making, including: (i) high-flux radiation moving-bed technologies for rapid iron ore beneficiation and upgrading, (ii) H_2-based direct reduction using an electrically heated drop-tube reactor platform, and (iii) novel H_2 combustion systems for low-emission pellet induration. These technologies aim to enable the utilisation of lower-grade Australian iron ore resources while supporting future net-zero iron and steel value chains (Figure 1).

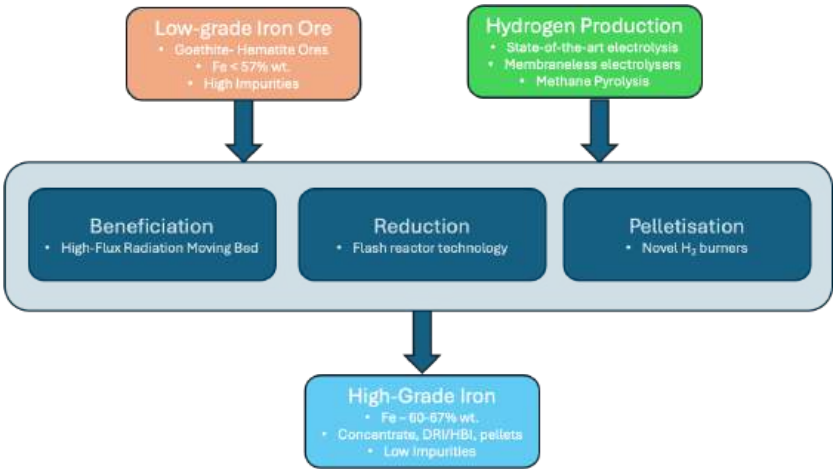


***Figure 1**: Some green ironmaking technologies utilising lower-grade Australian iron ore resources and H_2 as a fuel or reductant under development within HILT CRC*

Objectives: *the objectives of this work are to:*

- *investigate rapid thermal beneficiation approaches for upgrading lower-grade iron ores suitable for H_2-based ironmaking;*
- *evaluate H_2 reduction behaviour and kinetics under intensified reactor conditions relevant to future green DRI production;*
- *develop low-NO_x H_2 combustion technologies for pellet induration and high temperature processing; and*
- *assess the integration potential of these technologies within future green iron and steel value chains.*

Material and methods: high-flux radiation beneficiation studies were conducted using concentrated radiative heating systems capable of delivering ultra-high heating rates to moving packed beds of iron ore materials [2-4]. Experimental investigations examined phase transformations, goethite dehydration, microstructural evolution, magnetic enhancement, and downstream beneficiation performance under controlled thermal histories.

H_2 direct reduction pilot-scale experiments and advanced modeling were performed in collaboration with industry partners using electrically heated drop-tube reactor technology to achieve intensified H_2 reduction environments with rapid heating and short residence times. Reduction behaviour of hematite and upgraded iron ore feedstocks was evaluated under varying H_2 concentrations and operating temperatures [5,6]. Complementary work on H_2 combustion systems investigated novel burner configurations for pellet induration applications [7]. Experimental and modeling studies focused on flame stability, heat transfer characteristics, combustion efficiency, and NO_x mitigation strategies under high-H_2 firing conditions relevant to green pellet production.

Results: High-flux radiation treatment demonstrated substantial enhancement in beneficiation performance for lower-grade iron ores through rapid dehydration and phase transformation pathways that improve downstream magnetic separation and grindability characteristics [2-4]. The intensified thermal approach enables significantly shorter treatment times compared with conventional furnace-based processing while offering potential compatibility with renewable electricity and concentrated solar thermal systems.

H_2 reduction experiments in the drop-tube platform demonstrated rapid reduction kinetics under intensified heating conditions, highlighting the feasibility of compact electrified reactor concepts for future green DRI production [5,6]. Results indicate strong coupling between thermal history, ore morphology, and reduction performance, with upgraded ores exhibiting improved reducibility and metallisation behaviour. H_2 burner development demonstrated stable combustion and effective heat transfer under conditions relevant to pellet induration processes [7]. Novel burner concepts showed potential for reducing NOx emissions while maintaining high thermal efficiency and operational flexibility. These results support the transition from fossil-fuel-fired induration systems toward H_2-compatible green pellet production technologies.

Conclusions: this work demonstrates the potential of integrated H_2-based technologies to support the transition toward low-carbon iron and steel production. Together, these technologies contribute toward the development of future green iron value chains compatible with renewable energy systems and net-zero industrial production.

Acknowledgment

The author acknowledges support from the Heavy Industry Low Carbon Transition CRC (HILT CRC), Adelaide University, and collaborating industry and research partners.

References

[1] International Energy Agency (2023). *Steel - Tracking Clean Energy Progress*. IEA, Paris.

[2] O'Hara et al (2026). Metallurgical and Materials Transactions B, 1-17

[3] Lin et al (2026). Metallurgical and Materials Transactions B, 1-17

[4] Lin et al (2026). Metallurgical and Materials Transactions B, 56 (5), 5045-5059

[5] O'Hara et al (2025). Metallurgical and Materials Transactions B, 56 (6), 6348-6367

[6] Mokhtarani et al (2025). Metallurgical and Materials Transactions B, 56 (2), 1928-1941

[7] Chishty et al (2025). Applications in Energy and Combustion Science 26, 100475



Integration of green hydrogen production for transport decarbonization into the italian electricity grid: a numerical analysis

F. Buzzi*[a], S. Ubertini [a], A. Facci[a]

* Corresponding author: fulviopaolo.buzzi@unitus.it

[a] Dipartimento di Economia, Ingegneria, Società e Impresa (DEIM), University of Tuscia, Viterbo VT 01100, Italy.

Keywords: Green hydrogen production, Italy transports decarbonization, Numerical model, Renewable energies

Abstract

This study evaluates the infrastructural and energetic impact of generating green hydrogen via water electrolysis to support the decarbonization of the Italian transport sector. Following the Italian long-term strategy guidelines, a fleet of 4 million Fuel Cell Electric Vehicles (FCEVs) is assumed by 2050, requiring a total electrical supply of 23.55 TWh/year. Utilizing a numerical model developed in MATLAB, this paper analyzes the amount of photovoltaic (PV), wind and batteries power required to cover this electrical load. The results show that in order to cover 87% of the energy demand 20 GW of PV with 4 GW of wind and 3.3 GW of batteries are required. Moreover, the curtailed energy is 6 TWh with 3 TWh of energy deficit. Conversely, pushing the system toward a 99% direct coverage target drastically reduces the grid deficit to 0.36 TWh, but triggers a massive seasonal overproduction, with annual energy curtailment soaring to 19.5 TWh.

Introduction: The decarbonization of the transport sector represents one of the most critical challenges to achieve climate neutrality by 2050, as highlighted by both the European Green Deal and the Italian Long-Term Strategy (LTS) published by national ministries [1]. While light-duty vehicles are undergoing a rapid transition towards battery electric configurations, hydrogen-fuelled vehicles are expected to capture a strategic share of the market, particularly in specific sub-sectors or heavy-duty equivalent applications. According to the Italian LTS decarbonization scenario, a target of 4 million FCEVs is envisioned by 2050 [1]. However, producing green hydrogen through water electrolysis introduces massive electrical loads onto the national power grid. Understanding the hourly dynamics between this new demand and the volatile nature of non-programmable renewable energy sources, such as solar and wind power, is fundamental to guarantee grid stability and optimize infrastructure investments.

Objectives: The primary objective of this work is to determine the precise amount of additional renewable energy capacity required to fully cover the electrical load generated by green hydrogen production required to feed a fleet of 4 million FCEVs.

Material and methods: A lumped-parameter model is developed using the software Matlab to realize an hourly energy balance of the electrolyzers electrical load and renewable generation. First, the annual hydrogen demand for the 4 million FCEV fleet is determined using an average mileage of 12000 km/year per vehicle, which aligns with the historical statistical indicators for the Italian passenger car fleet reported by ISPRA and ACI [2]. A baseline consumption of 1 kg of H_2 per 100 km (0.01 kg/km) is assumed based on current commercial FCEV benchmarks. The electricity required by the electrolyzers is calculated assuming an average specific energy consumption of 53 kWh per kg of H_2 produced, reflecting the current state-of-the-art and future targets for large-scale PEM electrolyzers, as detailed by the Joint Research Centre (JRC) of the European Commission [3]. Additionally, 7 kWh/kg are accounted for compression (up to 350/700 bar), localized refueling station storage, and distribution losses, following the international supply chain energy expenditure figures validated by the International Energy Agency (IEA) [4] (totaling 60 kWh/kg). This results in a total cumulative load of 23.55 TWh/year. To evaluate grid integration, this total annual demand is distributed equally across the 8760 hours of the year, yielding a flat, constant power load (about 2.7 GW). Choosing a steady-state operation is a strategic engineering decision: operating the electrolyzers at a constant power drastically reduces the required nominal electrolyzer capacity, while fluctuations in vehicle refueling demand are entirely decoupled from production via local and centralized gaseous hydrogen storage buffers.

On the generation side, the model strictly considers photovoltaic (PV) and wind power as the source of electricity. This choice is justified by the fact that solar and wind are the only non-programmable renewable sources characterized by the massive scalability required to sustain such a large-scale transition. Official hourly production profiles for PV and wind in Italy during the year 2025 were retrieved from Terna's database [5]. To avoid an unfeasible oversizing of wind and solar installations, the model integrates a BESS framework to shift daytime solar overproduction to night hours.

Results: The results show that installing 20 GW of PV, 4 GW of wind and 3.33 GW of BESS, the system can directly cover 87% of the electrolyzers' total annual electricity energy demand. Under these conditions, there are 6 TWh of curtailed energy and 3 TWh of energy deficit requiring external grid support. To achieve a 99% self-sufficiency target for green hydrogen production, the required capacity increases to 32 GW of PV, 6.4 GW of wind and 5.33 GW of BESS. This setup virtually eliminates grid dependence, reducing the annual missing energy to just 0.36 TWh. However, the generation leads to a relevant seasonal overproduction, with 19.5 TWh of excess energy being curtailed, as can be seen in Figure 1.

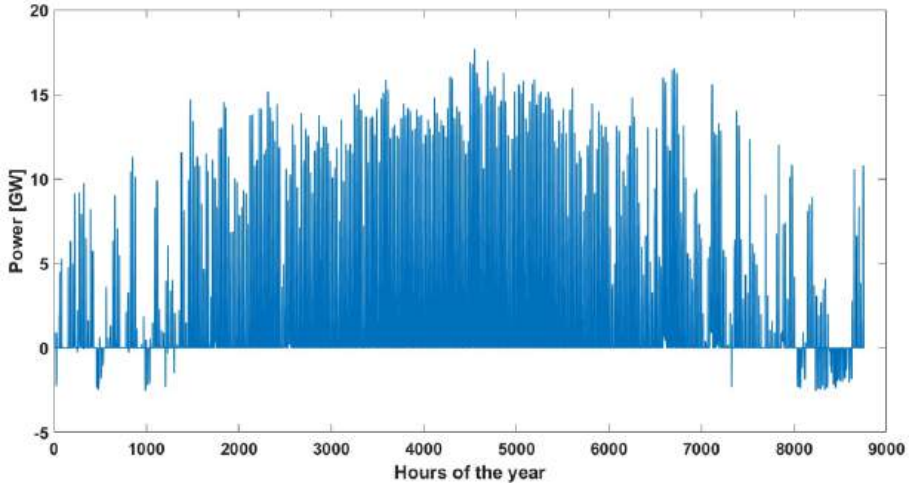


Figure 87: Hourly difference between the renewable generation and the electrolyzers electrical load in the year.

Conclusions: This study quantified the power grid infrastructure required to support 4 million fuel cell electric vehicles in Italy, demonstrating a total electricity demand of 23.55 TWh/year. The MATLAB simulations revealed that installing 20 GW of photovoltaic capacity with 4 GW of wind power and 3.33 GW of battery storage achieves a balanced configuration, directly covering 87% of the electrolyzers' demand while causing 6 TWh of energy curtailment and 3 TWh of grid deficit. Conversely, forcing a 99% self-sufficiency target requires 32 GW of photovoltaic capacity with 6.4 GW of wind power and 5.33 GW of battery storage; this setup virtually eliminates grid dependence (0.36 TWh deficit) but generates a relevant seasonal overproduction, with annual energy curtailment soaring to 19.5 TWh.

References

[1] Ministero dell'Ambiente e della Tutela del Territorio e del Mare, Strategia Italiana di lungo termine sulla riduzione delle emissioni dei gas a effetto serra, Gennaio 2021.

[2] ISPRA, "Rapporto sui fattori di emissione dei gas a effetto serra dal settore trasporti in Italia", Roma, 2024, "Annuario Statistico: percorrenze medie del parco circolante nazionale".

[3] Joint Research Centre (JRC) - European Commission, "Assessment of Hydrogen Production Costs from Electrolysis: Technical and Economic Benchmarks", Publications Office of the European Union, Luxembourg, 2023.

[4] International Energy Agency (IEA), "The Future of Hydrogen: Seizing today's opportunities", Energy Technology Policy Report, OECD/IEA, Paris.

[5] Terna Dati Statistici, Fabbisogno e Generazione Oraria in Italia, 2025.



Hydrogen Energy Storage for Long-Duration Energy Shifting in a Remote Off-Grid Microgrid

Robert Flores*[a], Jack Brouwer[a]

* corresponding author: rjf@apep.uci.edu

[a] Clean Energy Institute, University of California, Irvine, Irvine, CA 92617, USA

Keywords: hydrogen energy storage, long-duration storage, off-grid microgrid, hydrokinetic generation, mixed-integer linear programming

Abstract: Remote off-grid communities rely on costly diesel generation but seek self-sufficiency for cost, safety, and fuel-delivery reasons; renewable alternatives are hindered by strong seasonal mismatches between load and resource availability. This work determines the least-cost pathway to take Igiugig, Alaska off diesel and identifies where hydrogen (H_2) energy storage fits within it. Using mixed-integer linear programming, we optimize selection and dispatch of hydrokinetic turbines (HKT), solar PV, battery, and H_2 technologies. Results show H_2 storage becomes economically necessary only once diesel is removed, providing firm, long-duration supply that shifts surplus hydrokinetic generation from fall into the winter/spring resource gap. This avoids high-cost battery capacity cycled only a few times yearly, reserving batteries for daily load shifting with solar PV. Allowing H_2 storage to operate across seasonal, weekly, and daily timescales rather than a single annual cycle reduces total system cost by $0.22/kWh, enabling affordable, 100% renewable, diesel-free electricity.

Introduction: Remote off-grid communities rely on diesel generation for its reliability, energy density, and availability, but fuel price volatility and the cost, safety, and logistical burdens of remote fuel delivery have motivated a shift toward self-sufficient, locally generated renewable energy. Solar PV, wind, and battery storage are well established for these applications, where hybrid systems pairing complementary resources with efficient storage perform best. However, reaching fully renewable, diesel-free operation in communities with strong seasonal resource mismatches may require long-duration storage. H_2 storage is attractive for this role because it decouples power and energy scaling with minimal self-discharge, enabling seasonal energy shifting, though high capital cost and low round-trip efficiency keep real-world use largely confined to pilot projects. This work determines the least-cost pathway to take the remote community of Igiugig, Alaska off diesel and identifies where H_2 storage fits within that solution, in a hybrid microgrid combining hydrokinetic generation, solar PV, and battery storage. This work is described in greater detail in [1].

Objectives: This study aims to quantify the value of hydrogen energy storage for fully renewable off-grid microgrids and to identify the conditions under which it is adopted. Using optimization, the work determines when H_2 storage is economically justified, how it interacts with hydrokinetic, solar PV, and

battery resources across seasonal, weekly, and daily timescales, and what role it plays in enabling cost-effective, diesel-free electricity supply.

Material and methods: A modified Distributed Energy Resource optimization (DERopt) model is used to identify the least-cost combination of generation and storage assets that meets the hourly electrical load of Igiugig over a full year (8,760 hours). The modeled microgrid includes existing diesel generation and battery storage, with options to adopt and expand solar PV, hydrokinetic turbines, additional battery capacity, and a hydrogen energy storage system comprising an electrolyzer, H_2 compression and storage, and a proton exchange membrane fuel cell. The problem is formulated as a mixed-integer linear program Optimizations are run with and without legacy diesel generation and across a range of hydrokinetic generator costs to test the robustness of H_2 adoption.

Results: When diesel generation is available, the cost-optimal designs adopt no H_2 technologies and add negligible battery capacity, relying on hydrokinetic generation with limited solar PV to displace diesel. H_2 storage is adopted only in diesel-free designs, where it provides firm, long-duration supply alongside HKT, solar PV, and battery storage. Figure 1 summarizes the results. The hydrokinetic resource (A) is strongest in late summer and fall and weakest in late winter and early spring, when solar PV (B) has only begun to recover, producing a pronounced winter/spring resource gap. Surplus fall generation charges H_2 storage through the electrolyzer (C, D), which discharges through the PEMFC to cover the gap—seasonal shifting clearest in the annual state of charge (E), which fills through fall and draws down into spring. This avoids high-cost battery capacity that would otherwise be sized for peak storage demand but cycled only a few times per year, reserving batteries for daily load shifting paired with solar PV. The state-of-charge profile (E) also shows short-duration daily and weekly cycling in late winter. Constraining H_2 storage to a single annual cycle increases the levelized cost of electricity by $0.22/kWh, confirming that this intra-seasonal flexibility matters for cost-optimal diesel-free operation.

Conclusions: Hydrogen energy storage is a key enabler of affordable, fully renewable, diesel-free electricity for remote communities. Its value emerges only once diesel is removed, where it bridges the winter/spring resource gap through seasonal shifting—storing surplus hydrokinetic generation from fall for winter discharge. This avoids high-cost battery capacity sized for peak demand but rarely cycled, reserving batteries for daily load shifting with solar PV. Despite low round-trip efficiency, operating H_2 storage across seasonal, weekly, and daily timescales lowers total system cost, underscoring that long-duration storage and reliable renewables are complementary.

Acknowledgment: Funding was provided by the U.S. DOE Office of Energy Efficiency and Renewable Energy Hydrogen and Fuel Cell Technologies Office and Water Power Technologies Office. The views expressed do not necessarily represent those of the DOE or the U.S. Government.

References

[1] Flores R, McGilton B, Laviguer B, Prabakar K, Gjestvang K, Rezaei S, Brouwer J. Optimizing Hydrokinetic, Solar, Battery, and Hydrogen Storage Technologies for Resilient Microgrids in Remote Regions. Submitted to Energy Conversion and Management X. (2026)

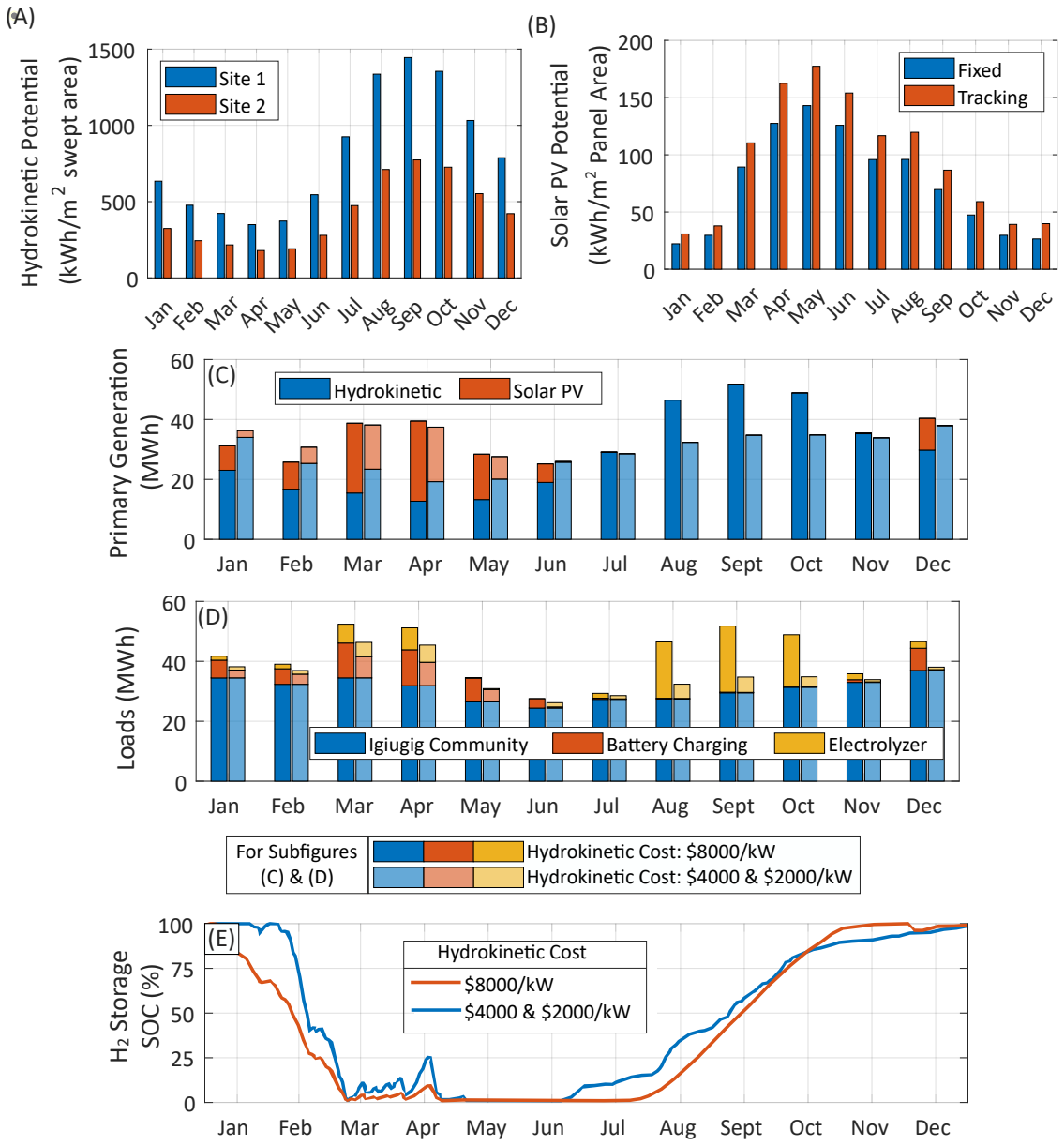


Figure 88: Summary of resource potential and monthly optimization results for the diesel-free Igiugig microgrid. (A) Hydrokinetic resource potential at two Kvichak River sites and (B) fixed-rack and single-axis tracking solar PV potential. (C) Monthly electricity generation by source and (D) corresponding loads, including battery and hydrogen storage charging, shown for hydrokinetic costs of $8,000/kW and $4,000 to $2,000/kW (E) Hourly hydrogen storage state of charge over the year, showing seasonal energy shifting from summer/fall into winter, followed by daily and weekly shifting in spring.



Green hydrogen-driven *in-situ* biomethanation for methane-enriched biogas production in hybrid PtG configurations

Giuseppe Lembo[*a], Antonio Bozzelli [a,b], Antonella Marone[a], Antonella Signorini[a]

* corresponding author: giuseppe.lembo@enea.it

[a] Casaccia Research Center, Italian National Agency for New Technologies Energy and Sustainable Economic Development (ENEA), Rome, Italy

[b] Department of Civil, Building and Environmental Engineering (DICEA), University of Naples "Federico II", Via Claudio 21, 80125, Naples, Italy

Keywords: Hybrid biomethanation, Hydrogenotrophic archaea, In-situ biomethanation, Power to Gas,

Abstract

Power-to-Gas (PtG) technologies based on biological methanation represent a promising route for renewable energy storage and coupling between electricity and gas infrastructures. In this process, hydrogenotrophic methanogens reduce CO_2 to CH_4 using green H_2 produced via water electrolysis, increasing energy recovery from waste biomass while offering a potentially more sustainable and cost-effective alternative to conventional physicochemical upgrading. Among PtG strategies, *in-situ* biomethanation, based on direct H_2 injection into anaerobic digesters, is attractive for its lower capital cost but remains constrained by H_2 mass-transfer limitations, metabolic imbalance, pH increases due to CO_2 depletion, and inhibition at elevated H_2 partial pressures. This study assessed the *in-situ* stage of a hybrid PtG (*in-situ*+*ex-situ*) configuration in which intermediate gas storage separates methane enrichment in the anaerobic digester from subsequent *ex-situ* upgrading. A bulk–pulse H_2 injection strategy was applied during anaerobic digestion to improve gas–liquid transfer while preserving process stability. Two industrial digestates, mesophilic and thermophilic, were screened as inocula under increasing H_2:CO_2 ratios up to 4:1 (v/v). Methane production did not differ between inocula, but, mesophilic trials showed greater performance variability, suggesting lower process stability than thermophilic operation. Therefore, thermophilic digestate was selected for a further scale-up validation experiment in a 3 L continuously stirred tank reactor (CSTR). Based on screening results, an H_2:CO_2 ratio of 2:1 (v/v) was used. CSTR reactor showed stable biogas production with CH_4 content of 69.3±3.6%, representing 17% increase compared to the control. The methane production rate was 0.25±0.07 $L_{CH_4}L_R^{-1}d^{-1}$ with an H_2 conversion efficiency of 81%. The additional methane generated through H_2 conversion (MER) was 0.074 $L_{CH_4}L_R^{-1}d^{-1}$. The pH remained stable at 7.20 ± 0.02, indicating a balanced process. These results show controlled *in-situ* biomethanation can reliably enrich biogas maintaining process stability, supporting its strategic potential role in hybrid PtG systems for scalable renewable energy storage.

Introduction: Power-to-Gas (PtG) technologies enable the conversion and storage of surplus renewable electricity as synthetic natural gas, contributing to decarbonization and facilitating the integration of renewable energy into existing gas infrastructures. Indeed, renewable electricity can be converted into H_2 via water electrolysis, which is then used to reduce CO_2 to CH_4 through catalytic or biological processes. Among these, biological methanation, driven by specialized microorganisms, namely hydrogenotrophic methanogens, offers

lower energy requirements and higher sustainability than conventional physicochemical upgrading techniques. Biological methanation can be implemented in two configurations: *in-situ* in which H_2 is injected directly into the anaerobic digester, offering lower capital costs and straightforward integration into existing plants [1]; and in *ex-situ* configuration in which H_2 is injected into a dedicated downstream reactor enriched with hydrogenotrophic cultures. However, *in-situ* biomethanation is still limited by H_2 mass transfer constraints, for which several strategies have been proposed in literature, i.e. gas diffusion devices, hollow fiber membranes, gas recirculation, and venturi-based injection systems. Nonetheless, the lack of standardized H_2 delivery strategies remains a key bottleneck for full-scale application. Moreover, *in-situ* biomethanation faces key challenges: metabolic imbalances from excess H_2, pH rise caused by CO_2 depletion and inhibition linked to high H_2 partial pressures. Compared with *ex-situ* methanation, the *in-situ* methanation offers the possibility of reducing the investment costs since only one reactor is necessary [2].To mitigate these issues, hybrid concepts combining *in-situ* partial upgrading with downstream *ex-situ* have been proposed. In hybrid systems, a controlled amount of H_2 is added into the digester (*in-situ)* to partially reduce CO_2 and increase the methane content of biogas. The resulting methane-enriched biogas is transferred to an intermediate gas storage unit prior to downstream *ex-situ* methanation, where residual CO_2 is converted into high-purity biomethane (CH_4 > 98%). This intermediate storage step enables temporal decoupling between *in-situ* and *ex-situ* upgrading, improving process flexibility and facilitating integration with intermittent renewable H_2 production [3].

Objectives: Within this hybrid framework, the present study aimed to optimize the *in-situ* biomethanation stage to produce a stable methane-enriched biogas suitable for downstream *ex-situ* upgrading. During anaerobic digestion of cheese whey (CW), a combined strategy based on organic substrate feeding and bulk–pulse H_2 injection under mild overpressure and controlled mixing was applied to enhance gas–liquid mass transfer while preserving process stability. The experimental investigation was carried out in two phases with the following objectives: (i) to evaluate different inocula for *in-situ* biomethanation; (ii) to assess increasing H_2:CO_2 molar ratios up to the stoichiometric value of 4:1 in order to identify the optimal operating ratio; and (iii) to perform a scale-up validation experiment to evaluate process feasibility and stability under more representative operating conditions.

Material and methods: For the screening phase, batch trials were conducted in serum bottles with 70 mL of working volume, operated in semi-continuous mode. Two digestates were used as inocula, one from a mesophilic plant treating agrozootechnical biomass (DB) and one from a thermophilic dairy wastewater treatment plant (DFB). Reactors were fed with CW at an organic loading rate (OLR) of 0.5 $g_{VS}L^{-1}day^{-1}$, a hydraulic retention time (HRT) of 30 days and a continuous mixing at 150 rpm. Biogas production was monitored daily using a pressure transducer and H_2 was injected directly into the headspace after feeding. Based on preliminary batch trial results, the thermophilic dairy-derived inoculum was selected for scale-up experiments, conducted in a 3 L CSTR, with 1.5L working volume, under the same operating conditions (HRT 30 days, OLR 0.5 $g_{VS}L^{-1}day$) and an H_2:CO_2 ratio of 2:1 (v/v). Process performance was evaluated in terms of methane production rate, methane content in biogas, H_2 conversion efficiency, residual H_2 concentration, pH stability and methane evolution rate (MER).

Results: No statistically significant differences in methane production were observed between the two inocula, indicating a limited influence of inoculum origin under the tested conditions. Both inocula exhibited an increase in methane production rates up to an H_2:CO_2 ratio of 3:1, with improvements of 45% and 38% compared to the

control under thermophilic and mesophilic conditions, respectively. Notably, the highest H_2-to-methane conversion efficiency (94 ± 2.5 %) was observed at an H_2:CO_2 ratio of 2:1 (v/v) for both inocula, indicating the best compromise between methane enhancement and process stability. However, the mesophilic process showed greater variability, suggesting lower operational stability. Therefore, thermophilic inoculum was selected for the scale-up validation experiment. In the scale-up reactor, stable anaerobic digestion process was achieved, with a methane production rate of 0.25 ± 0.07 $L_{CH_4}L_R^{-1}d^{-1}$, and a average methane content of 69.3 ± 3.6%, corresponding to a 17% increase compared to the control without H_2 addition. H_2 was almost completely consumed (0–7% residual), with an overall conversion efficiency of 81%. The MER was 0.074 $L_{CH_4}L_R^{-1}d^{-1}$. Stable pH values (7.16 ± 0.02) confirmed the robustness of the process under thermophilic conditions.

Conclusions: These results highlight the potential of optimized *in-situ* biomethanation as a reliable strategy for enhance methane content while preserving process stability under thermophilic conditions. Controlled H_2 addition at optimized H_2:CO_2 ratio (v/v) proved effective in improving gas-liquid mass transfer, maximizing H_2 conversion efficiency and maintaining process stability. The production of a stable methane-enriched biogas suitable for downstream upgrading supports the feasibility of integrating *in-situ* biomethanation into hybrid PtG systems. Overall, this approach represents a promising pathway toward more efficient and scalable renewable energy storage and utilization

Acknowledgment: This research was funded by the European Union–NextGeneration EU from the Italian Ministry of Environment and Energy Security POR H2 AdP MMES/ENEA with involvement of CNR and RSE, PNRR—Mission 2, Component 2, Investment 3.5 “Ricerca e sviluppo sull’idrogeno” CUP: I83C22001170006.

Finanziato dall'Unione europea NextGenerationEU

References

[1] G. Lembo, S. Rosa, A. Marone, and A. Signorini, “In Situ Biogas Upgrading in a Randomly Packed Gas-Stirred Tank Reactor (GSTR),” *Energies*, vol. 16, no. 7, 2023, doi: 10.3390/en16073296.

[2] Y. Rafrafi, L. Laguillaumie, and C. Dumas, “Biological Methanation of H2 and CO2 with Mixed Cultures: Current Advances, Hurdles and Challenges,” *Waste and Biomass Valorization*, vol. 12, no. 10, pp. 5259–5282, 2021, doi: 10.1007/s12649-020-01283-z.

[3] M. A. Voelklein, D. Rusmanis, and J. D. Murphy, “Biological methanation: Strategies for in-situ and ex-situ upgrading in anaerobic digestion,” *Appl. Energy*, vol. 235, no. October 2018, pp. 1061–1071, 2019, doi: 10.1016/j.apenergy.2018.11.006.



Advanced biorefinery platform for renewable h2-based fuels production

E. Cruz*[a], E. Nieto[a], A. Cánovas[a], C. Montes[a], J. J. Azañón[a], P. J. Martínez[a], N. García-Mancha[a]

* corresponding author: encarnacion.cruz□cnh2.es

[a] Centro Nacional del Hidrógeno, Fernando El Santo S/N, 13500, Puertollano, Ciudad Real (España)

Keywords: biomass, CO2, e-fuels, hydrogen

Abstract

Introduction: Electricity demand and, therefore, demand for fossil fuels is constantly growing worldwide as a result of industrial progress and population growth. Fossil fuels (coal, natural gas, and oil) currently account for over 80% of the energy consumed [1]. Their use has given rise to significant concern due to the negative impact that the relentless emission of greenhouse gases is having on the environment [2]. For this reason, one of the challenges facing society today is to shift energy dependence away from traditional fuels towards renewable ones, a new carbon-free energy sources and technologies that are sustainable, cost-effective, and non-polluting. There are various technological pathways for producing renewable fuels, each with different levels of maturity and specific limitations. In this regard, it is worth noting that the resources required to produce these fuels (sustainably sourced crops, agricultural waste, organic waste, and renewable electricity) are more widely available than fossil fuels in many countries. In addition to the many benefits these fuels can offer, such as reduced emissions and energy security, they can support the circular economy by reducing waste and improving soil health, water and air quality creating economic opportunities for farmers [3].

Objectives: With the aim of promoting the circular economy and generating solutions to mitigate current energy supply, the National Hydrogen Center is working on an advanced biorefinery platform for renewable H2-based fuels production, focusing on the recovery of CO2 and waste valorization to obtain renewable fuels and high-added-value products.

Material and methods: The advanced biorefinery consists of different interconnected pilot plants that host the following processes:

- Oxy-gasification: allows synthesis gas to be obtained from lignocellulosic biomass waste. The use of oxygen as a gasifying agent allows a gas with higher calorific value to be produced. This gas can supply the Fischer-Tropsch and methanol production processes, thus promoting the production of renewable fuels and methanol (e-fuels). In this facility, lignocellulosic biomass could be treated such

as: lignocellulosic waste from agriculture (straw, husks, olive leaves, etc.), forestry waste (wood chips, branches, sawdust), and industrial waste such as sludge from the paper industry or sawmill waste.

- Fischer-Tropsch: It is based on the catalytic synthesis of hydrocarbons of industrial interest (gasoline, diesel, kerosene, etc.). Waxes are also obtained, which can be transformed into products with added value.

- Methanol production: this pilot plant produces methanol from the hydrogenation of CO2. Its use as an alternative fuel and hydrogen carrier is being promoted.

These catalysts used in both facilities will be characterised using XRD, adsorption isotherms, XPS, TPR, TPD and SEM. In addition, the influence of the main operational parameters of the different processes will be studied: temperature, pressure, residence time, feed composition (CO2/H2 ratio), catalyst loading and distribution. To this end, the conversion of CO2, the selectivity towards the e-fuel under study, the production of each fuel, the deactivation of the catalyst and its possible regeneration will be evaluated.

- Anaerobic digestion + biogas upgrading: The anaerobic digestion plant, together with the biogas treatment stage, will enable biogas and biomethane to be obtained from different waste, such as livestock and agro-industrial waste, sludge from urban wastewater treatment plants (WWTPs) and the organic fraction of municipal solid waste (MSW). The biomethane produced could be used in electricity generation and in heat and power systems. In this regard, this pilot plant could become a source of energy for other facilities. Not only could the anaerobic digestion of organic waste be studied, but so-called 'dark fermentation' could also be carried out to produce bioH_2. At these facilities, the valorization of different types of waste could be tested, and various waste pre-treatment, co-fermentation, and co-digestion strategies could be evaluated.

Furthermore, this project will include an electrolyzer to meet the H2 requirements of the Fischer-Tropsch, methanol, and biogas upgrading plants, as well as the oxygen required for the oxy-gasification process. It is a 100-kW alkaline electrolyzer powered by a photovoltaic system.

The core strategy for integrating the plants involves using renewable H2 as feedstock for the FT, MeOH, and biogas upgrading plants, as well as O2 from the electrolyzer as feedstock for the oxy-gasification plant. The syngas produced in the oxy-gasification process would also supply FT and MeOH plants for the production of renewable fuels. The processes involved in this biorefinery platform are well-established. The main innovation of this system lies in the integration of these processes. The goal is to evaluate various factors at each plant separately (operating conditions, more efficient catalysts, fuel characterization, etc.) and to determine the optimal integration strategies that ensure both technical and economic feasibility.

Results: The fundamental objective is to optimize processes for subsequent scaling up to demonstrate that this advanced "biorefinery" concept is a sustainable and technically and economically viable alternative for the production of renewable fuels and energy generation from the recovery of widely available waste or by-products in the surrounding area. A significant reduction in CO_2 emissions is expected as a result of biomass recovery, the use of waste gases (synthesis gas from the oxygenation unit) as a feedstock for the methanol and Fischer-Tropsch processes, and the use of biomethane as an energy source.

According to the research lines established in agreement with the different capacities of the pilot plants, the goal is to generate 1.5 kg/h of gasoline and up to 1.5 kg/h of methanol. This will be the result of the recovery of 50 kg/h of forest biomass in the entrained flow reactor of the gasification plant. Also, the anaerobic digestion plant will process 100 kg/day of different types of organic matter (agri-food industry waste, municipal solid waste fractions, sewage sludge, etc.), obtaining 0.13 Nm3/h of biogas and biomethane.

It should also be noted that by-products such as digestates, wastewater, waxes, char, and ash will be characterized and processed for recovery in a way that has a direct impact on the population, such as the development of fertilizers that can be applied to the surrounding land.

Conclusions: The main innovation of this advanced biorefinery platform lies in the integration of different renewable H2-based fuel production processes. The Fischer-Tropsch processes for liquid fuels production, methanol production, biomethane generation by means of anaerobic digestion and upgrading unit, oxy-gasification for syngas obtention, and electrolysis are included. The gas obtained from an oxy-gasification plant, together with a supply of renewable H2 from an electrolyzer, could be used to feed the Fischer-Tropsch and MeOH plants. This idea therefore supports a technological system that constitutes a new concept of advanced biomass biorefinery.

Acknowledgment

Funding from Planes Complementarios de I+D+I from Junta de Comunidades de Castilla-La Mancha, Ministerio de Ciencia e Innovación and the European Union under Plan de Recuperación, Transformación y Resiliencia.

References

[1] Bhukta, A., & Hazra, S. (Eds.). (2025). Economics of the Energy Crisis: Environment, Policy and Security in the Indian Subcontinent (1st ed.). Routledge.

[2] Md. Biplob Hossain, Md. Rabiul Islam, Kashem M. Muttaqi, Danny Sutanto, Ashish P. Agalgaonkar (2023). Advancement of fuel cells and electrolyzers technologies and their applications to renewable-rich power grids, Journal of Energy Storage, Volume 62, 2023, 106842.

[3] IEA (2025), Delivering Sustainable Fuels, IEA, Paris https://www.iea.org/reports/delivering-sustainable-fuels, Licence: CC BY 4.0.



Mapping Hydrogen Supply Opportunities for Aluminium Decarbonization: Development of a GIS-Based Decision Support Tool

Stefano Barberis*[,a,b], Otto Feltges[c], Jörn Benthin[c], Luca Daceva[b], Lorenzo Di Fresco[b], Manuel Anselmo[b]

* corresponding author: Stefano Barberis – sbarberis@bluenrev.com

[a] Thermochemical Power Group – DIME - Università di Genova – Via Opera Pia 15 – 16145 Genova – Italy

[b] BluEnergy Revolution Soc. Coop. – Via Greto Di Cornigliano 6 – 16152 Genova - Italy

[c] Gas- und Wärme-Institut Essen e.V. - Hafenstraße 101 45356 Essen-Stadtbezirke IV, Germania

Keywords: aluminium decarbonization, GIS, hydrogen infrastructure, hydrogen supply chains

Abstract

This contribution introduces a new GIS based tool where all EU Aluminium foundries are geo-referred together with currenly available potential hydrogen supply sources (existing electrolysis plants, existing hydrogen valleys, future EU Hydrogen backbone) as well as local Renewable Energy Sources (RES) power plants, in order to easily identify and preliminarily assess the potential of hydrogen exploitation in secondary aluminium production plants.

Introduction: The decarbonization of energy-intensive industries is one of the major challenges associated with the achievement of European climate neutrality targets. Among hard-to-abate sectors, aluminium production plays a strategic role within European industrial value chains and requires innovative solutions to reduce greenhouse gas emissions associated with energy-intensive and high-temperature processes. Renewable and low-carbon hydrogen is increasingly recognized as a promising option to support this transition. However, effective deployment of hydrogen-based solutions depends on the availability of reliable information regarding industrial demand, hydrogen production assets, transport infrastructures and territorial development initiatives. The lack of integrated spatial information often limits the ability of stakeholders to identify viable hydrogen supply opportunities and prioritize investments.

Objectives: This work presents the development of a Geographic Information System (GIS)-based decision support platform designed to evaluate hydrogen supply opportunities for aluminium production facilities across Europe. The objective is to provide industrial stakeholders, infrastructure developers and policy makers with an integrated tool capable of assessing the spatial relationship between hydrogen demand centres and the emerging European hydrogen ecosystem.

Material and methods: The platform was developed within the H2AL project by integrating and georeferencing multiple datasets relevant to hydrogen production, transportation and industrial consumption. Starting from existing database and geo-referred atlases, the proposed GIS tool includes aluminium production facilities [1], the European Hydrogen Backbone network [2] , Hydrogen Valley initiatives and operational or planned electrolyser projects [3]. Each industrial site is characterized through production-related indicators and estimated hydrogen demand, while hydrogen infrastructures are described using technical and operational information, including production capacities, transport capabilities and project maturity status. Interactive GIS functionalities enable users to select individual aluminium plants and analyse surrounding hydrogen resources through distance-based and proximity assessments.

Results: The developed platform (Sketches in pictures here below) is a web-app that will be integrated into H2AL official project website and it provides an integrated geospatial environment capable of visualizing and analysing the relationship between industrial demand (and related hydrogen demand based on the overall foundry aluminium production) and hydrogen supply infrastructures. Users can rapidly identify nearby hydrogen valleys, electrolyser projects and backbone corridors, enabling a preliminary assessment of supply accessibility and infrastructure readiness as well as to evaluate the distance from the aluminium production plant and different potential hydrogen sources (Hydrogen Backbone, surrounding mapped electrolyser and hydrogen valley projects (Fig.1 above) as well as local renewable power plants that could be exploited for new green hydrogen production facilities (Fig.1 below). The combined visualization and analytical functionalities facilitate the identification of potential synergies between hydrogen producers, transport networks and industrial off-takers. The results demonstrate the value of geospatial decision-support tools in accelerating industrial hydrogen deployment and supporting infrastructure planning activities.

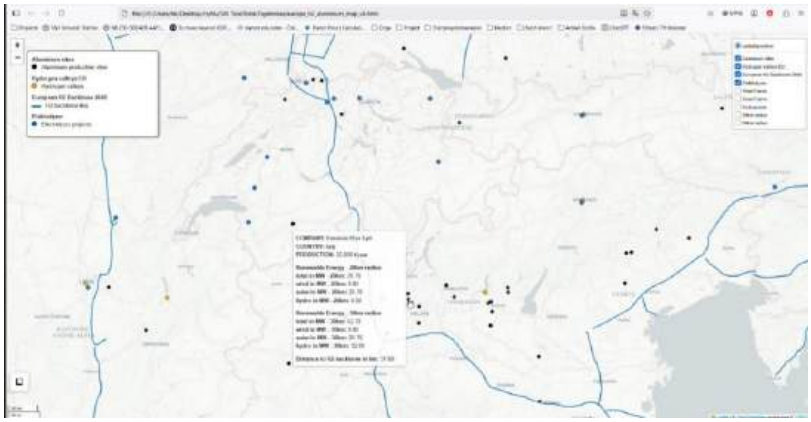




Fig.1 – Sketches from the H2AL GIS Replication tool

Conclusions: The proposed GIS-based platform addresses a critical information gap in the hydrogen transition by integrating demand-side and supply-side information within a common spatial framework. The methodology supports strategic decision-making, infrastructure prioritization and regional hydrogen ecosystem development. Although initially focused on aluminium production, the approach is fully transferable to other hard-to-abate industrial sectors and represents a scalable digital instrument for supporting the development of future hydrogen supply chains across Europe.

Acknowledgment

Co-funded by the European Union

Clean Hydrogen Partnership

This work has been realized in the framework of H2AL project. The project is supported by the Clean Hydrogen Partnership and its members and Co-Founded by the European Union under grant agreement N. 10137610. The project is Co-funded by the European Union. Views and opinions expressed are however those of the author(s) only and do not necessarily reflect those of the European Union or the Clean Hydrogen Partnership. Neither the European Union nor the granting authority can be held responsible for them.

References

[1] https://www.lightmetalage.com/resources-section/secondary-producers/ - – last access 24/6/2026

[2] https://www.h2inframap.eu/#map – last access 24/6/2026

[3] https://observatory.clean-hydrogen.europa.eu/hydrogen-landscape/projects-and-valleys/hydrogen-production-and-consumption-projects – last access 24/6/2026



Green Methanol Production via SOEC Co-Electrolysis Coupled with Solar Energy: Process Design and Analysis

Gianpaolo D'Andrea*[a], Elio Jannelli [a], Alberto Giaconia[b], Massimiliano Della Pietra[b], Simona Di Micco [a], Mariagiovanna Minutillo[c]
* corresponding author: gianpaolo.dandrea@phds.uniparthenope.it

[a] University of Naples Parthenope

[b] ENEA

[c] University of Salerno

Keywords: Co-electrolysis, Methanol Synthesis , Solid Oxide Electrolysis Cell.

Abstract: In the framework of developing efficient hydrogen production supply chains, green methanol has gained significant interest as a versatile energy carrier and sustainable fuel. Within this context, this work is focused on the development a methanol production plant based on the integration of a methanol synthesis section with a high-temperature co-electrolysis plant based on SOEC technology. Data for the SOEC modelling have been obtained by the PROMETEO project. The analysis was conducted by developing a thermo-electrochemical model, which allowed for the evaluation of mass and energy balances. The results show that a single plant module with a SOEC size of 25 kW, a water flow rate of 5.5 kg/h, and a CO_2 flow rate of 4.5 kg/h, can produce about 2.64 kg/h of methanol with a purity of 99.5%.

Introduction: Green methanol is a promising route for decarbonising the energy and chemical sectors, thanks to its role as a fuel, energy carrier, and chemical feedstock. One possible production pathway is catalytic synthesis from syngas generated by H_2O/CO_2 co-electrolysis in solid oxide electrolysis cells (SOECs). Compared to pure CO_2 hydrogenation, the presence of CO in the syngas enhances methanol synthesis and improves overall process performance, while also promoting the Water Gas Shift reaction, which helps reduce water concentration and mitigate catalyst deactivation [1].

Objectives: This work aims to carry out a comprehensive performance and operating conditions assessment of a methanol production plant, where the syngas required for the methanol synthesis section is produced within a high-temperature SOEC co-electrolysis unit.

Material and methods: To evaluate the plant performance, a thermo-electrochemical model was developed within the Aspen Plus environment, built upon previous modelling and analysis activities of the SOEC system [2]. The Peng–Robinson method was adopted for thermodynamic property estimation, as it is widely used for mixtures containing H_2, CO, CO_2, and methanol. To enable co-electrolysis, a CO_2 stream was introduced at the cathode inlet stream, producing a syngas mainly composed of H_2, CO, and CO_2. In the SOEC electrochemical model, CO_2 and H_2O conversions were

set to 64% and 70%, respectively, in agreement with literature data [4]. Figure 1 shows the flowsheet of the developed model. In the red dashed box, the SOEC system model can be noticed, which has been modified compared to the one developed in ref. [2] by introducing an inlet CO_2 stream. In the black dashed box, the SOEC stack is modeled using an RStoic reactor and a separator(*PK-104*). After water removal, the syngas (#SYNGAS), is sent to the methanol synthesis unit where it is compressed through three compression stages (*K-301/3*) to the required pressure of 57 bar, as suggested by the technical literature [3]. Additionally, the reaction temperature has been set to 250 °C in the

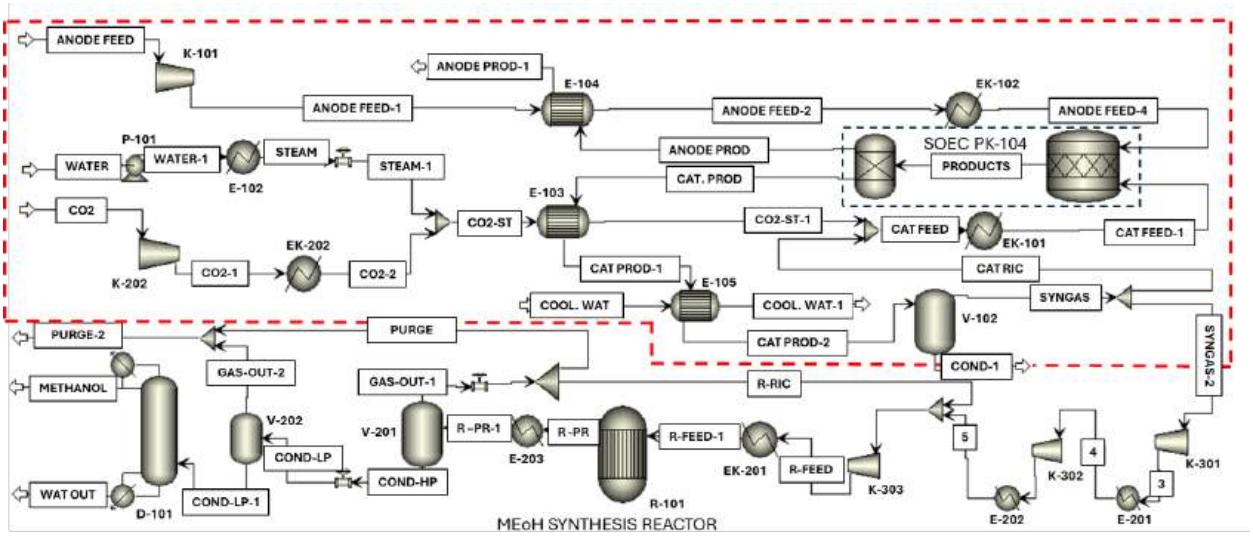


Figure 1 Methanol synthesis plant model flowsheet

MeOH reactor (*R-101*), which has been modelled using an equilibrium reactor (REquil), in which the main methanol formation reactions and the Water Gas Shift reaction are implemented. The reactor effluent (#R-PR) is cooled and sent to a separation train consisting of a high-pressure separator (*V-201)*, followed by a pressure let-down valve and a low-pressure separator (*V-202)*. The gas stream leaving the first separator (#GAS-OUT-1) is partially recycled to the reactor, while the remaining fraction is purged to prevent the accumulation of inert species in the loop (#PURGE-2). The liquid phase (#COND-LP-1) is then purified through a distillation column (*D-101*).

Results: Table 1 summarizes the molar compositions and flow rates of the main process streams, including cathode SOEC outlet (#CAT PROD), compressor inlet(#SYNGAS-2), reactor feed(#R FEED-1), and distillation product(#METHANOL). The equilibrium reactor converts the syngas into crude methanol, which is purified by distillation. The column produces 2.64 kg/h methanol at 99.5 wt% purity, meeting ASTM D1152 fuel-grade specifications, corresponding to an overall plant efficiency of 43.6%.

The efficiency is defined as:

$$\eta_{plant} = \frac{\dot{m}_{MeOH} * LHV_{MeOH}}{P_{SOEC} + \sum P_{aux}}$$

where the denominator includes the electrical power required by the SOEC stack and by all auxiliary units of the methanol synthesis section.

Table 13 Molar compositions and flow rates of the main process streams in the simulated SOEC-based methanol synthesis system.

STREAM		ANODE FEED-1	CAT FEED-1	ANODE PROD	CAT PROD	SYNGAS-2	R FEED-1	COND LP-1	METHANOL	WAT OUT
Description		Anode feed	Cathode feed	Anode Products	Cathode Products	Purified Syngas	Methanol Synthesis Reactor Feed	Condensate from Low-Pressure	Purified Methanol	Water-Rich Bottoms
Operating condiction	**U.o.M.**									
Mass Flow rate	kg/h	28	10,58	32,5	6,06	3,88	11,91	3,07	2,64	0,4
Temperature	°C	733	733	715	715	10	250	50	39	99
Pressure	bar	1,045	1,05	1,038	1,038	1,013	57	1,013	1,013	1,013
Vapor phase fraction		1	1	1	1	1	1	0	0	0
Composiction	**U.o.M.**									
H20	%mol	0	67,00	0	20,00	0,85	0,33	21,38	7,32E-06	99,07
CO2	%mol	0	23,50	0	8,50	10,52	20,36	0,18	0,46	0
H2	%mol	0	7,00	0	54,00	67,10	67,57	4,24E-05	6,34E-05	0
O2	%mol	21,00	0	31,00	0	0	0	0	0	0
N2	%mol	79,00	0	69,00	0	0	0	0	0	0
CO	%mol	0	2,50	0	17,50	21,53	11,44	1,98E-05	3,23E-05	0
CH3OH	%mol	0	0	0	0	0	0,29	78,43	99,54	0,93

Conclusions: This work presnts the main results of a methanol production plant based on the integration of a methanol synthesis section with a SOEC unit; in particular it is highlighted that with a 25kW SOEC system (nominal power in pure hydrogen production mode) , and by using a H_2O/CO_2 feeding ratio it is possible to produce 2.64 kg/h of methanol with a an overall efficiency of 43.6%, in agreement with values reported in the literature[1][3].

Acknowledgment: This project has received funding from the Fuel Cells and Hydrogen 2 Joint Undertaking (now Clean Hydrogen Partnership) under Grant Agreement No 101007194. This Joint Undertaking receives support from the European Union's Horizon 2020 Research and Innovation program, Hydrogen Europe and Hydrogen Europe Research.

References

[1] Andika, et al (2018). Co-electrolysis for power-to-methanol applications. *Renewable and Sustainable Energy Reviews*, *95*, 227-241.

[2] Minutillo, et al (2025). *High-Efficiency SOEC System Coupled with Renewable Sources: Modeling and Energy Analysis at Operating modes variation*. European Fuel Cells and Hydrogen PIERO LUNGHI CONFERENCE.

[3] Zhang, H., et al (2020). Techno-economic optimization of power-to-methanol with co-electrolysis of CO2 and H2O in solid-oxide electrolyzers. *Energy*, *199*, 117498.

[4] Cinti, G., et al (2016). Co-electrolysis of water and CO2 in a solid oxide electrolyzer (SOE) stack. *International Journal of Energy Research*, *40*(2), 207-215.



Hydrogen as a Cross-Sector Vector in Advanced Multi-Energy Networks: Use-Case Framework and NZMES Results for Tertiary Buildings

[a]Salvatore Fabozzi, [a]Maria Valenti*, [b]Sergio Bruno, [b]Francesco Lorusso

[a]Antonio Picarelli, [a]Maria Rosa Fiorillo, [a]Adriano Macaluso, [a]Antonio Ricca

* corresponding author: maria.valenti@enea.it

[a]ENEA – Department of Energy Technologies and Renewable Sources, Smart Grids and Energy Networks Laboratory, Portici Research Centre, Naples, Italy

[b]Politecnico di Bari, Bari, Italy

Keywords: hydrogen vector, multi-energy system, fuel cell CHP, net-zero energy

Abstract

Introduction: The growing penetration of renewable generation and the progressive electrification of end uses are reshaping the operating logic of contemporary energy systems. In this context, hydrogen is increasingly regarded not only as a standalone technology, but as a cross-sector energy vector able to connect electricity, thermal demand, transport and storage within a common operational framework. Its relevance therefore lies less in the performance of one conversion device than in its ability to coordinate multiple carriers and temporal scales under variable renewable generation and non-coincident load profiles [1]–[3].

Five complementary use cases are considered, covering grid-scale flexibility, local fossil-fuel replacement, hydrogen-to-mobility chains, laboratory-scale emulation of hydrogen refuelling infrastructure, and multi-energy self-consumption in buildings. Together, these applications support the interpretation of hydrogen as a networked flexibility resource rather than as a single-purpose option. Quantitative results are reported here, only for the NZMES (Net-Zero Multi-Energy System) case study [2], [4].

Objectives: This work aims to assess hydrogen as an integrating vector in advanced multi-energy networks, to define a common methodological framework across five use cases, and to quantify the contribution of hydrogen storage to self-consumption and self-sufficiency in a tertiary-building net-zero multi-energy system.

Material and methods: A common structure was adopted across the five use cases. Each application was first defined in terms of system boundaries, functional architecture, energy carriers, control variables and performance indicators, and was then analysed through simulation or emulation models selected according to scale and purpose. This harmonised approach supports comparison among heterogeneous hydrogen applications while preserving their specific technical features and maintaining consistency with the broader literature on multi-energy and sector-coupled systems [1], [3], [4].

For the NZMES application, the system includes renewable generation, a battery energy storage system, an electrolyzer, a hydrogen tank, a CHP fuel cell and a heat pump. The hydrogen subsystem operates as a Hydrogen Energy Storage System able to absorb renewable surplus, shift energy over longer time horizons than the battery, and later return energy to both the electrical and thermal domains. The control problem is formulated as a finite-horizon predictive optimization problem and linearized into a mixed-integer linear programming model that minimizes imported electricity while preserving electrical and thermal balances [1], [5].

This formulation is relevant when multiple flexibility resources coexist and may either complement or compete with each other. Batteries mainly provide short-duration balancing, whereas hydrogen storage integrated with a CHP fuel cell enables medium-duration shifting and coordinated electric-thermal support [3], [5], [6].

Results: Quantitative validation was carried out on a tertiary-building case study based on hourly public data from the Building Data Genome Project 2. The selected dataset refers to an educational building in Cardiff and includes electricity and gas demand for 2016. After conversion of thermal demand through a heat pump with a coefficient of performance equal to 3, the system exhibits an annual electrical demand of about 78.16 MWh and an annual thermal demand of about 177 MWhth, corresponding to an equivalent total electrical requirement of roughly 137.20 MWh. Photovoltaic generation was represented by a 137 kWp system, while the reference NZMES configuration includes a 50 kW heat pump, a 50 kW electrolyzer, a 50 kW fuel cell, a hydrogen tank up to 500 Nm^3 and a 50 kW/kWh battery [5], [7].

Without storage, strong temporal mismatch between photovoltaic production and load profiles keeps both self-consumption and self-sufficiency close to 35%, with large renewable exports and significant grid imports. When storage is introduced, hydrogen capacity immediately improves both indicators, with the sharpest gains occurring for tank sizes of about 50-100 Nm^3. Weekly trajectories show a differentiated use of storage: the battery smooths short fluctuations, while hydrogen is charged during prolonged surplus periods and later converted back through the CHP fuel cell to support both electrical and thermal balances. Under the longest optimization horizon, the system reaches SCI = 0.703 and SSI = 0.509, whereas a 24 h horizon yields SCI = 0.499 and SSI = 0.438, confirming the importance of predictive optimization over wider horizons [5], [6], [8].

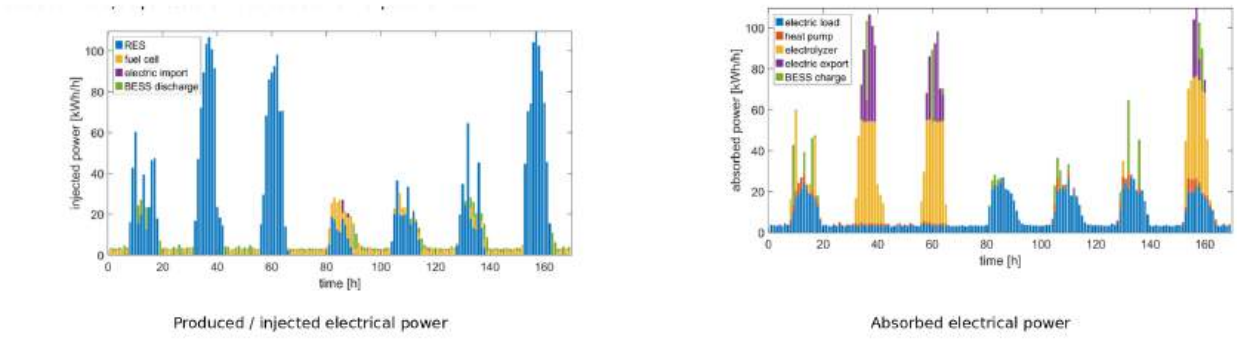


Figure 1. Weekly electrical power trajectories in the tertiary-building NZMES case study: produced/injected power (left) and absorbed power (right).

Overall, the results indicate that HESS has a stronger impact than BESS on self-consumption because it can absorb renewable surplus over longer durations and later support both electricity and heat. BESS and HESS should therefore be interpreted as complementary storage options acting on different time scales [5], [6], [8].

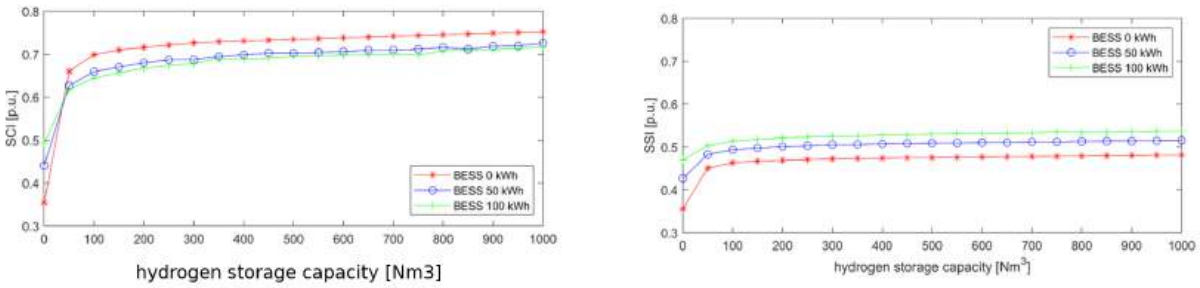


Figure 2. Evolution of the self-consumption index (SCI) and the self-sufficiency index (SSI) as hydrogen storage capacity increases.

Conclusions: The main innovation of this work lies in analysing hydrogen penetration through a coordinated use-case framework rather than through a single-technology perspective. Across the five use cases, hydrogen is treated as a cross-sector vector whose value emerges from the way it reconfigures architectures, control logics and performance trade-offs across advanced energy applications [2], [3], [4].

For the NZMES case study, hydrogen proves most effective when embedded in predictive control strategies and combined with CHP fuel cells, improving electric-thermal coupling, renewable utilization and imported-energy reduction. The findings are relevant for energy communities, campus microgrids and tertiary districts, where integrated multi-vector strategies can outperform purely electrical storage [5], [6], [8].

References

[1] P. Mancarella, "MES: An overview of concepts and evaluation models," Energy, vol. 65, pp. 1–17, 2014.

[2] I. Staffell et al., "The role of hydrogen and fuel cells in the global energy system," Energy Environ. Sci., vol. 12, no. 2, pp. 463–491, 2019.

[3] J. Ramsebner et al., "The sector coupling concept: A critical review," WIREs Energy Environ., vol. 10, e396, 2021.

[4] H. Lund et al., "Smart energy and smart energy systems," Energy, vol. 137, pp. 556–565, 2017.

[5] S. Bruno et al., "Optimal sizing and operation of electric and thermal storage in a net-zero multi-energy system," Energies, vol. 12, no. 17, p. 3389, 2019.

[6] J. Li et al., "Hydrogen and battery synergy in a net-zero smart system," Energy Convers. Manag., vol. 263, p. 115717, 2022.

[7] C. Miller et al., "Building Data Genome Project 2," Sci. Data, vol. 7, p. 368, 2020.

[8] F. Lorusso et al., "Improving self-sufficiency of a NZMES through CHP fuel cell and hydrogen storage," IFAC-PapersOnLine, vol. 59, no. 9, pp. 145–150, 2025.



Hydrogen Demand Projections and Renewable Power System Sizing for Hard-to-Abate Sectors in the Italian Energy Transition.

M. Minutillo[a], A. Perna[b], C. Bassano[c], E. Jannelli[a], S. Di Micco*[a]

* corresponding author: simona.dimicco@uniparthenope.it

[a] Department of Industrial Engineering, University of Salerno, Fisciano, Italy

[b] Department of Civil and Mechanical Engineering, University of Cassino and Southern Lazio, Cassino, Italy

[c] ENEA - Italian National Agency for New Technologies, Energy and Sustainable Economic Development

[d] Department of Engineering, University of Naples "Parthenope", Naples, Italy

Keywords: Hard-to-Abate industries, decarbonization, green hydrogen, renewable sources

Abstract: This paper assesses decarbonization scenarios based on the progressive replacement of fossil fuels used in industrial processes with green hydrogen (H_2) produced by PV-powered electrolysis. Different H_2 penetration levels have been analyzed to evaluate the corresponding energy requirements and potential environmental benefits.

Introduction: *Green hydrogen has emerged as a strategic energy carrier within the European energy transition, particularly for the decarbonization of hard-to-abate industrial sectors.*

Objectives: This study aims at evaluating the penetration of hydrogen in hard-to-abate sector and its production by means of renewable energy source in accordance with the additionality principle.

Material and methods: The analysis has been carried out starting from the data provided by Confindustria [1], including the annual production of the specific product and the yearly thermal energy demand (Table 1) required by different production processes of the energy-intensive industrial sectors such as: cement plants, steelworks, paper mills, glass factories, refineries, ceramics plants and chemical plants.

Table 1: Hard to Abate Industrial Sectors Characterization [1].

	Cement	Steel	Paper	Glass	Refineries	Ceramics	Chemical
Production Volumes (Mt/Year)	19.2	23.35	8.53	5.9	77.6	-	-

Thermal Energy Demand (TWh/Year)	12.33	22.56	27.78	10.78	15.12	16.67	21.33

Starting from these data, a sensitivity analysis has been performed to assess different levels of H_2 penetration in the selected sectors. The penetration level has been defined as the percentage of annual thermal energy demand assumed to be supplied by green H_2. Three scenarios have been considered: i) 3% penetration, according to the PNIEC 2024 target for 2030 [2]; ii) 20% penetration, in line with the National Hydrogen Strategy target for 2050 [3]; and iii) 100% penetration, representing the full replacement of the thermal energy demand [4]. As concern the green H_2 production, it has been assumed an alkaline electrolysis unit (AEL) powered by renewable electricity from dedicated PV plant according to the additionality principle.

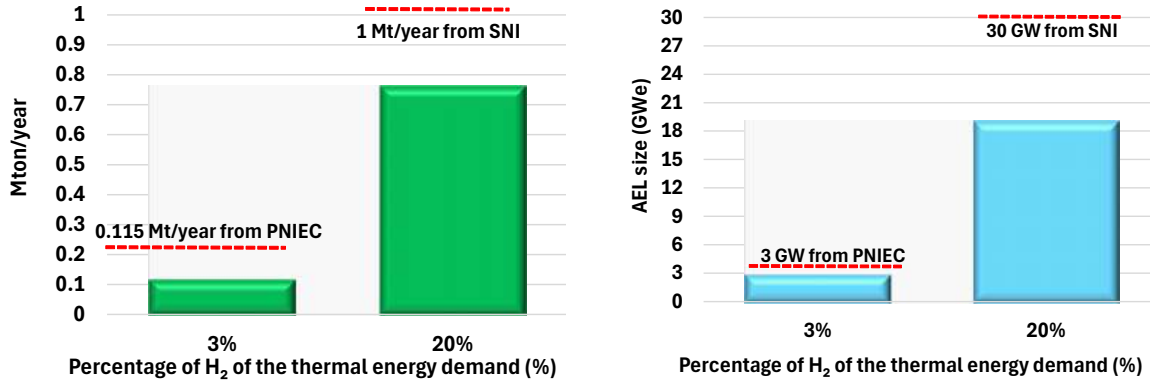
Results: For each industrial sector and H_2 penetration scenario, the annual H_2 demand and the main sizing parameters of the renewable power system have been evaluated. Table 2 summarizes the obtained results in terms of H_2 amount for satisfying the thermal demand in each penetration scenario, the electrolyzer capacity, the electricity demand to supply the electrolyzer, the PV capacity and its corresponding land occupation. The calculations have been performed by assuming that the electrolyzer (energy consumption of 50 kWh/kg H_2) works at its nominal power and, consequently, the annual operating time is set equal to 2,000 h/year.

Table 2: Hard to Abate Industrial Sectors Characterization.

	Cement	Steel	Paper	Glass	Refineries	Ceramics	Chemical
3% H_2 Penetration							
Covered Thermal Demand [TWh/year]	0.36	0.68	0.83	0.32	0.46	0.50	0.64
H_2 amount (Mt/year)	0.011	0.02	0.03	0.010	0.014	0.015	0.019
AEL size (GWe)	0.273	0.51	0.63	0.24	0.34	0.38	0.48
PV size (GWe)	0.46	0.85	1.04	0.4	0.57	0.63	0.8
PV land occupation (m^2)	6.8	12.7	15.6	6.1	8.5	9.4	12
20% H_2 Penetration							
Covered Thermal Demand [TWh/year]	2.43	4.51	5.56	2.16	3.03	3.33	4.27
H_2 amount (Mt/year)	0.073	0.135	0.17	0.065	0.091	0.10	0.128
AEL size (GWe)	1.82	3.38	4.17	1.62	2.28	2.50	3.20
PV size (GWe)	3.03	5.64	6.94	2.69	3.79	4.17	5.33
PV land occupation (m^2)	45.5	84.6	104.2	40.4	56.9	62.5	80.0
100% H_2 Penetration							
Covered Thermal Demand [TWh/year]	12.13	22.56	27.78	10.78	15.17	16.67	21.33
H_2 amount (Mt/year)	0.364	0.677	0.83	0.323	0.455	0.500	0.64
AEL size (GWe)	9.1	16.92	20.83	8.08	11.38	12.50	16.0
PV size (GWe)	15.17	28.19	34.72	13.47	18.96	20.83	29.33

PV land occupation (m^2)	227.5	422.9	520.8	202.1	284.4	312.5	400.0

According to these data, an overall results have been evaluated in terms of total H_2 requirement and electrolyzer installed capacity under the 3% and 20% H_2 penetration scenarios (Figure 1).The obtained results have been compared with the reference values reported by the PNIEC and the National Hydrogen Strategy.



(a) (b)

Figura 1: (a) H_2 amount for satisfying the total industrial energy demand; (b) AEL size

Figure 1a shows that the 3% scenario requires about 0.115 Mton/year of H_2, in line with the PNIEC reference value, while the 20% scenario reaches about 0.75 Mton/year, below the 1 Mton/year target of the National Hydrogen Strategy. As shown in Figure 1b, the corresponding electrolyzer capacity increases from about 3 GWe to 18 GWe, within the 15–30 GWe range indicated for 2050. Regarding PV sizing, the scenarios analysed require a significant installed PV capacity to supply the electrolyzers, ranging from approximately 4.7 GWp to 31.6 GWp. This highlights that domestic hydrogen production may need to be complemented by H_2 imports or hydrogen-derived carriers.

Conclusions: Results confirm that Green H_2 can reduce CO_2 emissions in hard-to-abate sectors of about 0.93 and 6.48 Mton/year under the 3% and 20% penetration scenarios, respectively.

Acknowledgment: This research was funded by the European Union – NextGeneration EU from the Italian Ministry of Environment and Energy Security POR H2 AdP MMES/ENEA with involvement of CNR and RSE, PNRR - Mission 2, Component 2, Investment 3.5 "Ricerca e sviluppo sull'idrogeno", CUP: I83C22001170006.

References

[1] PIANO D'AZIONE PER L'IDROGENO Politiche Industriali https://www.confindustria.it/

[2] PIANO NAZIONALE INTEGRATO PER L'ENERGIA E IL CLIMA (PNIEC2024). https://www.mase.gov.it/portale/documents/d/guest/pniec_finale_17012020-pdf

[3] Strategia Nazionale Idrogeno https://www.mase.gov.it/portale/documents/d/guest/strategia-nazionale-idrogeno-pdf

[4] Hydrogen Innovation Report 2024. https://www.rinnovabili.it/wp-content/uploads/2024/07/HIR_Short-Report-2024.pdf



Preliminary Assessment of a Hydrogen-Powered Pushback Tractor for Ground Handling Decarbonization at Milan Malpensa Airport

S. Di Micco*[a], G. Matteo[b], E. Branchini[b], A. Angiolini[b], V. Cigolotti[c], M.Minutillo[d], G. Leo[b]

* corresponding author: simona.dimicco@uniparthenope.it

[a] Department of Engineering, University of Naples "Parthenope", Naples, Italy

[b] SEA Milano, Italy

[c] ENEA - Italian National Agency for New Technologies, Energy and Sustainable Economic Development

[d]Department of Industrial Engineering, University of Salerno, Fisciano, Italy

Keywords: Hydrogen-powered mobility; Pushback tractor; Airport ground handling operations; Decarbonization.

Abstract: This paper presents a preliminary study of hydrogen-based pushback operations as a decarbonization pathway for airport operations at Milan Malpensa Airport. Real operational data from a TBL 400 pushback tractor are used to characterize the duty cycle and estimate energy demand, hydrogen consumption, and fossil fuel reduction compared with the conventional diesel configuration.

Introduction: *Hydrogen is gaining increasing relevance as a strategic energy carrier for decarbonizing airport ground operations, particularly in the context of ground support equipment and airside mobility [1].*

Objectives: This study focuses on hydrogen potential role in reducing fossil fuel use and supporting low-emission ground support equipment at Milan Malpensa Airport.

Material and methods: The analysis has been carried out starting from real operational data collected for a TBL 400 towbarless pushback tractor (Figure 1) operating at Milan Malpensa Airport. The vehicle characteristics are summarized in Table 1. Figure 2 shows its representative operating profile, which has been reconstructed by dividing the vehicle activity into three main phases: i)approach to the aircraft stand, ii) pushback operation from stand to taxiway, and iii) return trip to the parking area.



Figure 1: TBL 400 towbarless pushback tractor

Table 1: Main technical characteristics of the TBL 400 pushback tractor

Parameter	Value	Unit
Vehicle type	Towbarless	
Engine	Deutz TCD 12.0 V6	
Max power	390	kW
Max torque	2130	Nm
Gross weight	28600	kg
Tow capacity	400	t
Transmission	Automatic (3 gears)	
Drive	FWD	
Aggregated data		
Travelled distance	2.46	Km/mission
Avg mission/day	9	n/day

Figure 2: Representative mission profile of the pushback operation at Milan Malpensa Airport.



Starting from these data, the diesel consumption for each mission has been assessed, together with the average daily diesel demand and the corresponding CO_2 emissions. Then, a hydrogen-based fuel cell configuration has been considered as a potential solution for emissions savings.

Results: Based on the diesel consumption estimated for each mission phase (Figure 3), the overall diesel consumption per mission has been calculated. By considering an average of 9 missions per day (as shown Table 1), the total daily diesel demand of the pushback tractor hes been then obtained. It is worth noting that the total diesel demand per mission, including all operating phases, has been calculated as 4.18 L/mission, corresponding to a daily demand of 37.64 L/day. However, when also considering tractor repositioning operations, which account for an additional daily consumption of 6.96 L/day, the total diesel demand increases to 44.60 L/day. The equivalent hydrogen consumption has been estimated by assuming the same useful energy demand, equal to 137.8 kWh/day (derived from the daily diesel consumption and diesel lower heating value). Considering a hydrogen-based fuel cell configuration with an average system efficiency of 45% [2], the corresponding hydrogen

consumption amounts to 9.19 kg/day. Table 2 compares the main results obtained for the diesel and hydrogen-based configurations.

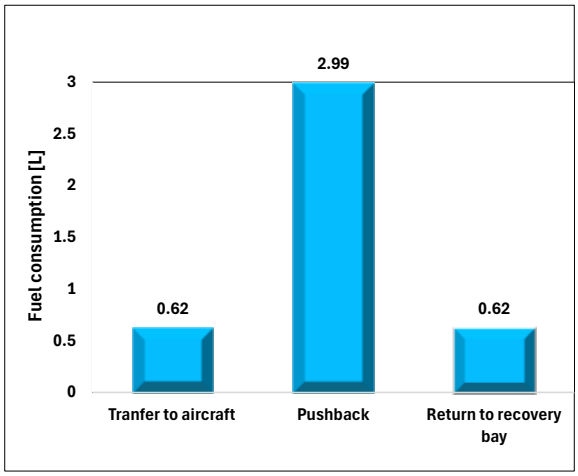


Figure 2: Diesel consumption by mission phase

Table 2. Diesel vs hydrogen energy assessment

Metric	Diesel TBL400	Hydrogen TBL400	Unit
Daily fuel consumption	44.6	9.19	L/day — kg H_2/day
Lower heating value	10.3	33.33	kWh/L — kWh/kg
Average system efficiency	30	45	%
Daily primary energy input	459.4	306.2	kWh/day
Useful energy demand of the operational cycle	137.8		kWh/day

Conclusions: The hydrogen-based configuration reduces the daily fuel energy input by approximately 33.3% compared with the diesel configuration, while ensuring the same useful operational energy demand. Assuming a diesel emission factor of 2.61 kg CO_2/L [3], this scenario would avoid about 116.4 kg CO_2/day, highlighting the potential role of hydrogen-powered ground support equipment in airport decarbonization.

Acknowledgment

Funded by the European Union under grant agreement No 101138105. Views and opinions expressed are however those of the author(s) only and do not necessarily reflect those of the European Union (EU) or European Climate, Infrastructure and Environment Executive Agency (CINEA). Neither the EU nor CINEA can be held responsible for them.

References

[1] Zhang, Y., Li, S., Blythe, P., Edwards, S., 2025. Accelerating airport decarbonisation: Qualitative investigation of stakeholders' perceptions and requirements towards hydrogen-powered ground support equipment. Journal of the Air Transport Research Society, 6, 100097. doi: 10.1016/j.jatrs.2025.100097.

[2] Petrecky, J., 2017. Fuel Cell Powered Airport Ground Support Equipment Deployment. U.S. Department of Energy, Hydrogen and Fuel Cells Program Annual Merit Review and Peer Evaluation Meeting, Project MT011.

[3] Zheng, Z., et al., 2021. The Energy Consumption and CO_2 Emission Impacts of Different Driving Conditions and Policy Implications. E3S Web of Conferences, 268, 01005.



H2SCORE: An Integrated Hydrogen-Based Architecture for Complex Local Multi-Energy Microgrids

M. Gandiglio*[a], P. Marocco [a], M. Santarelli [a]

* Corresponding author: marta.gandiglio@polito.it

[a] Department of Energy, Politecnico di Torino, C.so Duca degli Abruzzi 24, 10129 Torino (Italy)

Keywords: hydrogen, renewable energy community, multi-energy microgrid, fuel cell, electrolyser, rSOC

Abstract

This work presents H2SCORE, a Horizon Europe demonstration project developing an integrated hydrogen-based architecture for community-scale, multi-energy microgrids. The proposed system combines a low-temperature domain – a PEM electrolyser, metal hydride hydrogen storage and a PEM fuel cell – with a high-temperature domain based on a reversible Solid Oxide Cell (rSOC) operating in both SOEC and SOFC modes, further coupled with a biomass gasification unit supplying syngas to the SOFC. While hydrogen-based storage has already shown its potential in off-grid contexts, this work focuses on extending and adapting this architecture to a grid-connected Renewable Energy Community (REC), where interaction with the electrical grid and district heating network introduces additional complexity in terms of dispatch, self-consumption maximisation and multi-vector integration. The modelling and analysis framework developed for the Valsesia (Italy) demonstration case is presented, together with the replication strategy for Spain, Switzerland and Canada.

Introduction: RECs and local multi-energy microgrids are increasingly recognized as key enablers of the energy transition, promoting decentralised generation, increased self-consumption and active participation of end users. Their operation, however, is strongly constrained by the variability of renewable sources and by the difficulty of matching generation with consumption in a way that maximises self-consumption. Multi-vector approaches, capable of jointly addressing electrical, thermal and other energy needs, can substantially increase the flexibility, efficiency and resilience of these systems.

In this context, hydrogen technologies are emerging as strategic enablers of long-duration energy storage and sector coupling, complementing short-term storage with batteries and demand-side flexibility solutions. Their value as a flexibility and storage asset has already been demonstrated in off-grid and isolated systems (REMOTE EU project [1–3]); extending this potential to grid-connected, multi-vector microgrids is the specific challenge addressed by the H2SCORE project [4,5]. The project involves a consortium of industrial technology providers (BluEnergy Revolution, PowerCell Sweden, Zeppelin Power Systems, H2B2, BIO2CHP),

research institutions (Politecnico di Torino, CARTIF, VTT, NTNU) and local stakeholders (Environment Park, ENGREEN, Municipality of Quarona), jointly supporting system modelling, integration, optimisation, environmental and social assessment, and stakeholder engagement. The consortium is further extended by three replication partners – University of Burgos (Spain), AEM (Switzerland) and Yukon University (Canada) – which will lead the adaptation and assessment of the H2SCORE concept in their respective national contexts.

The demonstration is implemented in a REC in Valsesia (Italy), characterised by photovoltaic power generation and an existing biomass-based district heating network. The project started in December 2025 and targets Technology Readiness Level (TRL) 7 during the demo phase.

Objectives: This work aims to present the hydrogen-based architecture developed within the H2SCORE project for complex local multi-energy microgrids, describing its dual hydrogen domain design and its integration with the local electrical grid and district heating network. Building on the promising indications already available from off-grid hydrogen applications, the objective is to outline the methodology and modelling framework currently being developed to assess the same technologies in a grid-connected REC context, and to describe how this framework will be applied to the Valsesia demonstration case and its planned replication sites.

Material and methods: The H2SCORE architecture relies on a dual hydrogen system. A low-temperature domain – based on a PEM electrolyser, metal hydride hydrogen storage and a PEM fuel cell – is combined with a high-temperature domain centred on a reversible Solid Oxide Cell (rSOC), operating in both SOEC and SOFC modes. A biomass gasification unit supplies syngas to the SOFC, further enhancing fuel flexibility and enabling the valorisation of local biomass resources. Hydrogen-based components are embedded within the local electrical grid and the district heating network, enabling multi-vector sector coupling and the provision of flexibility and balancing services to the grid.

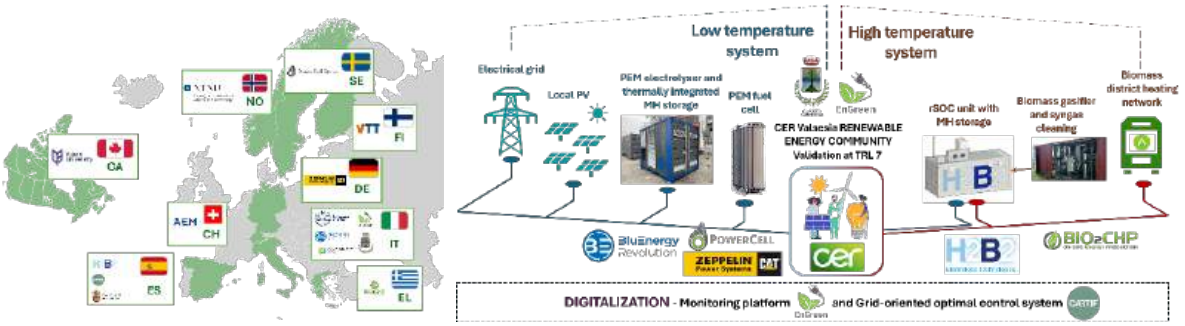


Figure 89. H2SCORE general layout.

Results: Evidence from off-grid hydrogen-based systems has already shown the potential of hydrogen as a long-duration storage and flexibility asset, particularly where no grid backup is available. Building on this, the analysis currently being carried out within H2SCORE extends

this role to the grid-connected microgrid/REC case, where hydrogen retains its function as a long-term storage vector while also being assessed for its additional contribution to self-consumption maximisation, flexibility provision, multi-vector sector coupling with the district heating network, and the overall resilience and robustness of the local grid. The modelling and techno-economic optimisation framework being developed will be used to identify optimal system layouts and sizing rules under different boundary conditions, and to support the comparison between the Valsesia case and the planned replication sites in Spain, Switzerland and Canada.

Conclusions: H2SCORE proposes an integrated and replicable approach to hydrogen-enabled multi-energy microgrids, combining short- and long-duration hydrogen storage, combined heat and power generation, and biomass valorisation. Building on results already demonstrated in off-grid applications, this work highlights the additional challenges and opportunities arising when the same technologies are integrated into a grid-connected RECs.

Acknowledgment: This study was part of the EU project H2SCORE (https://doi.org/10.3030/101251551) project. The project is supported by the Clean Hydrogen Partnership and its members and co-funded by the European Union.

References

[1] P. Marocco, D. Ferrero, A. Lanzini, M. Santarelli, The role of hydrogen in the optimal design of off-grid hybrid renewable energy systems, J. Energy Storage 46 (2022) 103893. https://doi.org/10.1016/J.EST.2021.103893.

[2] P. Marocco, D. Ferrero, M. Gandiglio, M.M. Ortiz, K. Sundseth, A. Lanzini, M. Santarelli, A study of the techno-economic feasibility of H2-based energy storage systems in remote areas, Energy Convers. Manag. 211 (2020) 112768. https://doi.org/10.1016/j.enconman.2020.112768.

[3] CORDIS - EU research results, Remote area Energy supply with Multiple Options for integrated hydrogen-based TEchnologies, (2018). https://doi.org/10.3030/779541.

[4] H2Score - Hydrogen and fuel cells for resilient energy communities, (n.d.). https://h2score.eu/ (accessed April 12, 2026).

[5] CORDIS - EU research results, Hydrogen Storage and Fuel Cells for Optimised Renewable Energy Communities, (2025). https://doi.org/10.3030/101251551.



Real-Time Optimization of a Hydrogen Based Multi Energy System Using Machine Learning

F. Sadeghi*[a], G. Loreti*[b], A. Facci[a], S. Ubertini[a], M. Della Pietra[b], V. Cigolotti[b]

* corresponding authors: fatemeh.sadeghi@unitus.it, gabriele.loreti@enea.it

[a] Department of Economics, Engineering, Society and Business Organization (DEIM), University of Tuscia, 01100 Viterbo, Italy

[b] Department of Energy Technologies and Renewable Sources (TERIN), ENEA C.R. Casaccia, 00123 Rome, Italy

Keywords: distributed energy systems, genetic algorithm, machine learning, neural networks

Introduction: Machine Learning (ML) can be crucial for the optimization of energy systems operation. However, optimization is often a hard problem, being nonlinear and subject to dynamic and power balance constraints [1]. Specifically, ML can support the real-time operation and optimization of multi-energy systems [2] and optimally operating systems with generators and storage units [3]. Despite these advances, many of these studies mainly focus on electricity-driven operation, while thermal and cooling loads have been less frequently considered within a unified machine-learning-based management framework. Therefore, using machine learning to optimize multi-energy systems while considering electrical, heating, and cooling loads is still not widely studied and could significantly improve energy efficiency. In this regard, this study proposes a neural-network-based method for learning optimal operational decisions in a distributed energy system. The main idea is that, instead of solving the optimization problem, the model learns from previously obtained optimal results and predicts the appropriate setpoint of each machine under different operating conditions. When the heavy calculations are transferred to the offline stage, the neural networks can quickly predict the machines' setpoints during online operation and make the optimization results usable in real time. For the individual with the lowest cost difference, this metric, which is defined as the difference between the individual's profit and that of the Offline Optimization Method (OOM) [4] per OOM's profit, is 0.408.

Material and methods: The studied system is a distributed multi-energy system designed to supply electricity, heating, and cooling demands. In this project, the OOM, which is based on backward dynamic programming, is used as the reference source of operational decisions. The training and validation datasets contain the machine setpoints previously obtained from this method for each time step. These optimal setpoints are then used for training and validating the neural-network models. Therefore, the goal of the machine-learning model is to learn the relationship between the system conditions and the decisions previously generated by the OOM. Specifically, a separate neural network is trained for each machine, that are the mechanical chiller, combined heat and power unit

(CHP), fuel boiler, and thermal storage. The inputs include electricity, heating, and cooling demands, temperature, pressure, hour of the day, mean temperature over the previous 10 days, and holiday status, while the outputs are the predicted setpoints for the corresponding machines. In addition, a genetic algorithm is used to select a suitable set of neural-network hyperparameters based on the mean validation accuracy of the setpoint predictions.

The neural network does not generate a free continuous setpoint value; instead, it selects one of the allowed setpoint classes. The possible output classes are taken from the setpoints observed for that machine in the reference dataset. The neural-network models are built using a DNNClassifier. These hyperparameters range explored from the genetic algorithm include the learning rate, ranging from 10^{-5} to 10^{-1}, the two regularization strengths, ranging from 0 to 10, and the tolerance, ranging from 10^{-5} to 1. The batch size ranges from 16 to 1024, the number of steps per period from 50 to 1500, and the maximum number of periods from 10 to 1000. The optimizer is selected between FtrlOptimizer and AdagradDAOptimizer, while the number of hidden layers ranges from 1 to 2 and the number of nodes from 1 to 20. The genetic algorithm is implemented using the PyGAD library. Parent selection is performed using rank selection, while crossover is applied as uniform crossover with a probability of 0.9, and random mutation is applied to 20% of the genes.

For each evaluation of the genetic algorithm, four neural networks are first trained using the proposed hyperparameter settings, one for each machine. The data from the first year are divided into training, validation, and test datasets and are used for neural-network development and hyperparameter selection. Then, the accuracy of each model is calculated on the validation dataset. After the best hyperparameter setting is selected, the final neural-network models are trained using that setting, and raw setpoint predictions are generated for the second year dataset, which is used as an independent evaluation period. Since the setpoints are predicted independently for each machine, they may not directly satisfy the system constraints. These constraints include the electricity, heating, and cooling energy balances, the operating limits of the equipment and grid exchange, and the dynamic constraints of the thermal storage. The predicted setpoints are then passed to the dispatch and heuristic post-processing step to evaluate their performance at the energy-system level. In this step, the final setpoints, grid exchange, state of charge of the thermal storage, operating cost or profit, primary energy consumption, CO_2 emissions, and performance indicators such as the cost difference are calculated for the second year.

Results: The genetic algorithm selects the neural-network hyperparameters based on the mean validation accuracy of the four machine-specific models. The results show that the best prediction performance is obtained for the mechanical chiller and the fuel boiler, while CHP and thermal storage show lower prediction performance. The same pattern can also be observed in the validation accuracy values. This suggests that CHP and thermal storage have more complex reference setpoint patterns than the mechanical chiller and fuel boiler. Their operation includes stronger switching behavior and a wider variation between low and high setpoint values, which makes the classification

task more difficult for the neural networks. Figure 1 presents the final raw accuracy of the four machine-specific models across the evaluated GA individuals, with maximum values of 0.97 for the mechanical chiller, 0.29 for thermal storage, 0.85 for the fuel boiler, and 0.45 for the CHP, while the corresponding validation accuracies were 0.99, 0.37, 0.86, and 0.43, respectively.

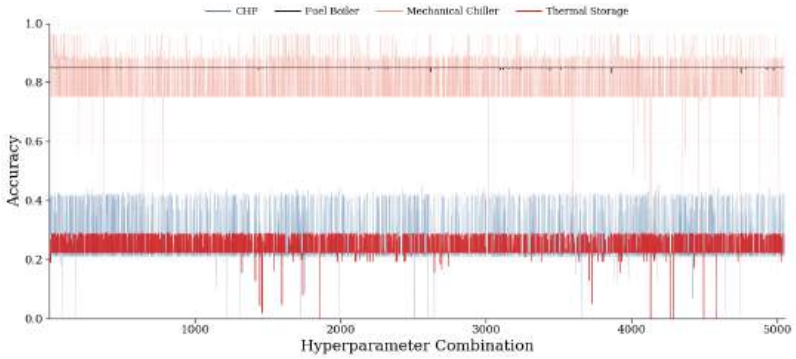


Figure 1. Final raw accuracy values across the evaluated NN-GA hyperparameter combinations.

Conclusions: The proposed method learns the decisions of the OOM and moves the main computational effort to the offline stage, supporting real-time operation. Since the raw predictions do not always satisfy system and storage constraints, the dispatch and heuristic correction step remains necessary for the final evaluation.

Acknowledgement:

Hydro-HT – Project funded by the European Union – NextGenerationEU – NRRP, M2C2.3.5 Ministerial Decree No. 438 of 13 December 2024, Article 1, Paragraph 1, Letter (d) – Approved for the full amount – Project No. RSH2C_000015

References

[1] P. L. Donti, J. Z. Kolter, Machine learning for sustainable energy systems, Annual Review of Environment and Resources 46 (2021) 719–747.

[2] P. Siano, C. Cecati, H. Yu, J. Kolbusz, Real time operation of smart grids via fcn networks and optimal power flow, IEEE Transactions on Industrial Informatics 8 (4) (2012) 944–952.

[3] T. Otani, R. Tanabe, Y. Koyanagi, S. Iwamoto, Cooperative load frequency control of generator and battery using a recurrent neural network, in: TENCON 2017-2017 IEEE Region 10 Conference, IEEE, 2017, pp. 918–923.

[4] A. L. Facci, S. Ubertini, Meta-heuristic optimization for a high-detail smart management of complex energy systems, Energy Conversion and Management 160 (2018) 341–353.



Hydrogen in pathways towards a climate-neutral, circular and competitive European process industry: the AMIGDALA scenario framework

Vittoria Battaglia*[a], Livio De Chicchis, Francesco Gracceva [a], Wouter Nijs, Pieter Valkering[b]

* corresponding author: vittoria.battaglia@enea.it

[a] Agenzia nazionale per le nuove tecnologie, l'energia e lo sviluppo economico sostenibile (ENEA), IT

[b] VITO, BE

Keywords: energy-intensive industries; hydrogen; industrial decarbonisation; scenario analysis

Abstract

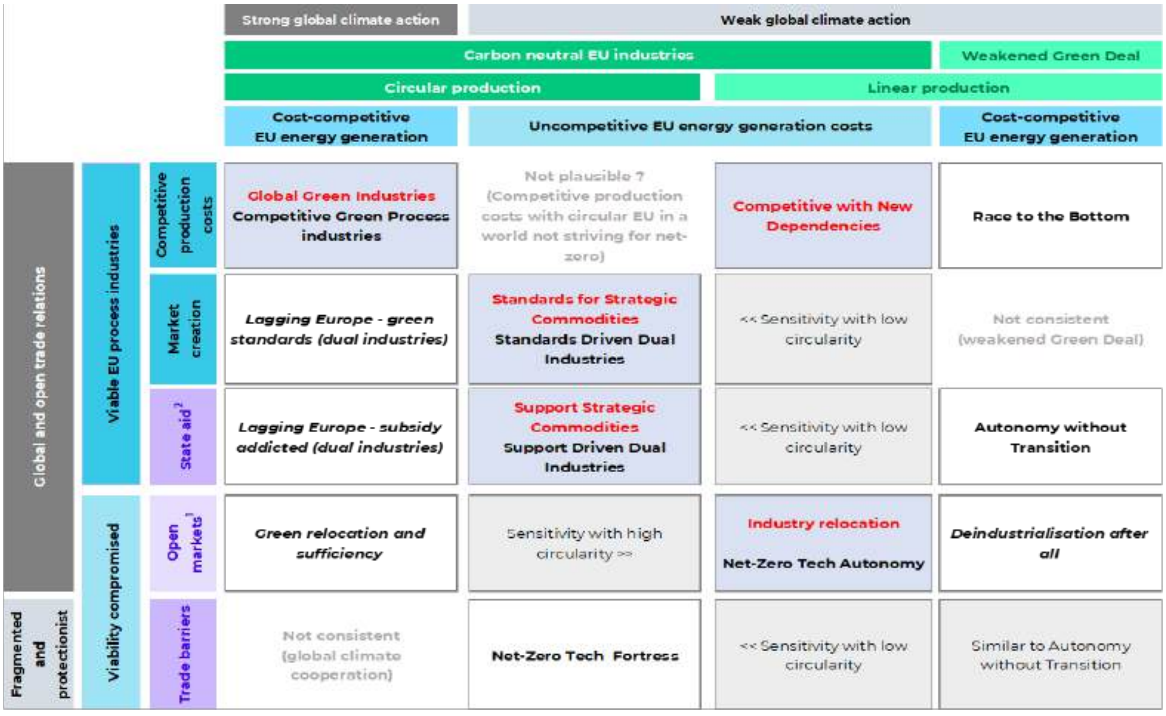
Introduction: European energy-intensive industries face the dual challenge of achieving deep decarbonisation while maintaining competitiveness, security of supply, and resilience in an increasingly constrained energy and materials system. Hydrogen is expected to play an important role in this transition, particularly in sectors where direct electrification is technically or economically challenging, and as a feedstock, reducing agent, energy carrier, and enabler of low-carbon industrial processes. However, the future role of hydrogen in European industry remains highly uncertain. Hydrogen demand will depend not only on technological choices at the plant level, but also on the evolution of electricity and hydrogen supply, energy prices, industrial production, international trade, material efficiency and circularity, carbon management, and EU industrial and climate policies. Consequently, hydrogen deployment cannot be assessed independently from the wider transformation of the European industrial system.

Objectives: The Horizon Europe AMIGDALA project—*Alliance for Modelling Industries towards the Green Deal's objectives And circuLArity*—is developing a model-based decision-support framework to explore pathways towards a climate-neutral, circular, competitive, and resilient European industry. This contribution presents the AMIGDALA scenario framework, with a particular focus on how different future conditions and policy choices may shape the role, demand, and infrastructure requirements of hydrogen in European process industries.

Material and methods: Scenario narratives are developed as structured inputs to quantitative modelling of alternative industrial pathways. The framework distinguishes between exogenous background drivers, such as global economic developments, technological progress, geopolitical dynamics, resource availability, and environmental constraints, and controllable policy levers, including carbon pricing and CBAM, strategic industrial policies, clean-technology support, infrastructure development, and the availability of low-carbon hydrogen. Hydrogen availability is therefore treated not simply as an outcome of industrial decarbonisation, but as a potentially influential policy lever that can affect technology selection, investment decisions, industrial competitiveness, and the spatial distribution of future production.

The framework combines insights from academic literature, policy documents, and stakeholder consultations, complemented by AI-supported factor selection to enable a transparent and systematic prioritisation of scenario drivers and policy levers. The main innovation is the connection of a decision-oriented scenario architecture with an integrated modelling framework spanning global, European and industrial-cluster scales.

Results: Around twenty scenario archetypes are generated by combining alternative assumptions about these factors and subsequently clustered according to the dominant EU ambition—climate neutrality, competitiveness, or strategic autonomy. For each archetype, the potential role of hydrogen is qualitatively assessed, considering its relevance across industrial applications, possible levels of demand, interactions with electrification and other decarbonisation options.



A particular focus is placed on the policy-infrastructure nexus. Different assumptions regarding hydrogen availability and accessibility can lead to substantially different industrial pathways, while infrastructure investment itself can influence the feasibility and attractiveness of hydrogen-based technologies. The key finding is that policy infrastructure and hydrogen availability has a high impact on most of the scenario archetypes assessed.

Conclusions: The resulting scenarios provide internally consistent datasets and boundary conditions for subsequent modelling exercises, while also supporting stakeholder dialogue on the strategic role of hydrogen in Europe's industrial transition. By embedding hydrogen within a broader assessment of industrial production, material flows, circularity, carbon utilisation, energy systems, and EU policy objectives, the framework provides a more comprehensive basis for evaluating when, where, and under which conditions hydrogen can contribute to a sustainable, competitive, and strategically autonomous European industry.

References

[1] Amigdala project website: Alliance for modelling industries



TOPIC 5. HYDROGEN ECONOMY AND SUSTAINABILITY



Fe-phthalocyanine-derived Fe-N-C electrocatalysts for the Nitrate Reduction Reaction (NO_3RR)

S. Lombardi[a]*, M. Muhyuddin[a], N. Lisi[b], V. Ficca[b], F. Paparoni[c], L. Codega[a], J. Rezvani[d], R. Viscardi[b], C. Santoro[a]

* Corresponding author: s.lombardi22@campus.unimib.it

[a] Department of Materials Science, University of Milano-Bicocca, U5, Via Cozzi 5, 20125, Milano (Italy)

[b] Casaccia Research Center, ENEA, Department of Energy Technologies and Renewable Sources, Via Anguillarese 301, 00123 Santa Maria di Galeria, 00123, Rome, Italy

[c] SAMBA beamline, Synchrotron SOLEIL, Dep. 128, 91190 Saint-Aubin, France.

[d]Physics department, University of Camerino, via Madonna delle carceri 9, 62032, Camerino, Italy.

Keywords: Fe-N_x active sites; Iron phthalocyanine; pyrolysis; nitrate reduction reaction; platinum group metal-free electrocatalysts.

Abstract

Introduction:The electrochemical reduction of nitrate to ammonia (NO_3RR) is emerging as an efficacious method to remove nitrates from contaminated water and to synthesize ammonia under ambient conditions, offering a green alternative of the energy-intensive Haber-Bosch process.However, the sluggish kinetics of NO_3RR and competitive hydrogen evolution reaction (HER) are the main bottlenecks of the given technology and demand urgent scientific endeavors. Therefore, the development of efficient electrocatalysts with specific structures capable of suppressing competitive reactions is the need of the hour.

In this context, Fe-Nx-C electrocatalysts have shown great potential for NO_3RR[1]. These electrocatalysts are typically synthetized via high temperature treatments (pyrolysis). The fundamental relationships between pyrolysis conditions, the resulting active site and the NO_3RR performance are a vital area of investigation to develop efficient electrocatalysts.

Objectives: This study presents a methodical investigation to evaluate how pyrolysis temperature dictates the formation, evolution, and structural transformation of iron-based

active sites, and how these changes correlate with electrochemical performance toward NO_3RR.

Material and methods: A mixture of iron phthalocyanine (FePc) supported over carbon black (KJB) was pyrolyzed at different temperatures (in the steps of 100°C) from 200°C to 1000°C for 1 h under a continuous N_2/H_2 gas flux.

XAS was selected as the primary analytical tool to provide unique insights into the electronic structure, local symmetry, and coordination environment of iron.

These spectroscopic findings were integrated with complementary ex-situ characterization techniques (XRD, Raman spectroscopy, HR-TEM, STEM, EDX and XPS) to obtain a comprehensive structural overview of the developed electrocatalysts (ECs).

The electrochemical performance were then tested in Argon saturated phosphate-buffered solution (PBS) through Linear Sweep Voltammetry (LSV) using a rotating disk electrode (RDE), and by Chronoamperometry (CA) in a H-type cell configuration.

Following the chronoamperometric tests, the concentrations of NO_3^-, NO_2^-, NH_4^+ formed during the electroreduction were quantified by ion chromatography (IC).

Results: XAS analysis showed that in the low-temperature range (RT – 400 °C), iron maintains an atomically dispersed Fe-N_x coordination, preserving the nature of the original single-atom sites. Starting from 500 °C, a structural reorganization phase is observed, and the samples starts to lose their N and C ligand coordination, resulting in formation of reduced, yet isolated metallic Fe atoms, with no long-range order. From 600 °C there is the coalescence of Fe atoms into Fe nanoparticles, which rapidly increases as the temperature increases toward 1000°C. XRD and HR-TEM confirmed this trend, while STEM coupled with EDX allowed for a compositional map with a better visualization of elemental distribution. Raman spectroscopy endorses the higher degree of graphitic imperfections and disorders in the carbon matrix, which is consistent with the XRD outcome. XPS analysis further elucidated the surface chemistry evolution, showing a progressive shift in the nitrogen speciation. At lower temperatures (< 400 °C) a high concentration of nitrogen-based moieties was observed, with a prevalence of pyridinic and Fe-Nx structures. As the pyrolysis temperature increased, a systematic depletion of total nitrogen occurred, accompanied by a redistribution toward more stable graphitic nitrogen. To assess the electrocatalytic activity toward NO_3RR and its competition with the HER, LSV was performed in two different conditions: PBS and PBS + 0.16 M NO_3^-. Across all ECs, a significant increase in current density was observed upon NO_3^- addition, contrasting with the negligible current recorded in the NO_3^--free electrolyte.

Quantitative performance was further evaluated through one-hour CA at -0.6, -0.8 and -1.0 V vs. RHE. (Fig.1) At -1.0 V the ECs exhibited ammonia yield rates between 90 and 120 μmol h^{-1}

cm $^{-2}$ with Faradic Efficiencies (FE) reaching 80-90%. At -0.8V, yield rates ranging from 30 to 60 μmol h^{-1} cm $^{-2}$ (FE 60-80%), while at -0.6 V, the yields were measured between 5 and 15 μmol h^{-1} cm $^{-2}$ (FE 60-70%).

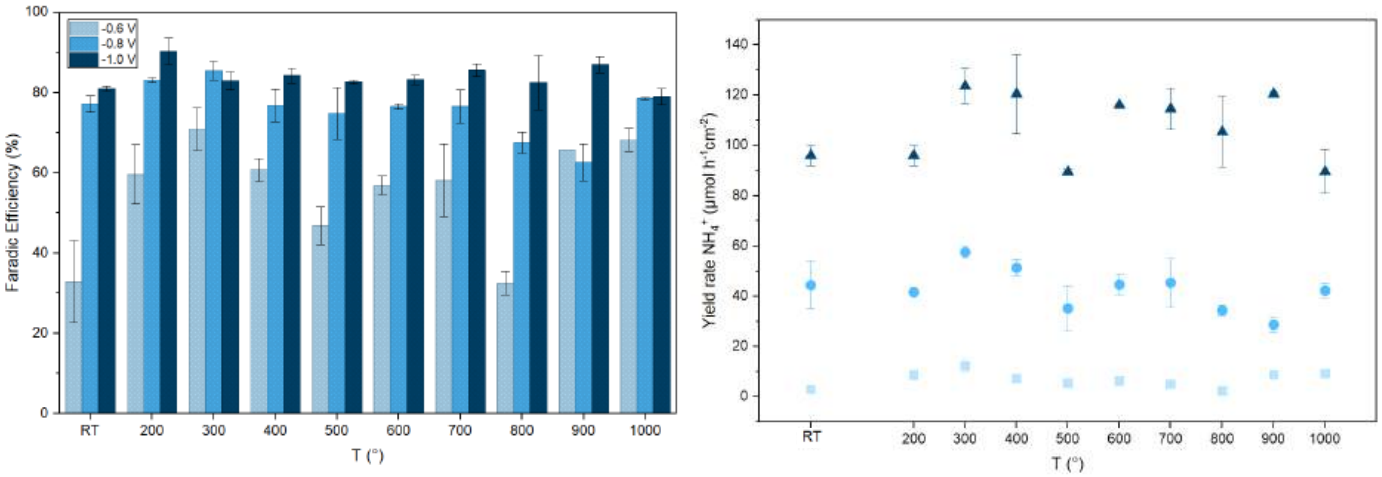


Fig.1. Faradic efficiency (on the left) and ammonia yield rate (on the right) of the ECs obtained at different pyrolysis temperatures at three different potentials: -0.6 V (light blue), -0.8 V (blue) and -1 V (dark blue) vs. RHE.

Conclusions: In this work, we comprehensively evaluated how pyrolysis temperature dictates the formation, evolution, and structural transformation of iron-based active sites derived from Fe-phthalocyanine.

The data reveal a clear potential-dependent performance; however, for any given potential, no definitive trend was observed in relation to the pyrolysis temperature. This indicates that both the atomically dispersed Fe-N_x sites (prevalent at low temperatures) and the Fe nanoparticles and oxides (dominant at high temperatures) are highly effective in promoting NO_3RR.

Acknowledgment: This work was supported by ENEA and the Department of Materials Science of the University of Milano-Bicocca. We would like to thank Alessandro Lavacchi and Enrico Berretti (CNR-ICCOM) for TEM images and characterization.

References

[1] E. Murphy *et al.*, "Elucidating electrochemical nitrate and nitrite reduction over atomically-dispersed transition metal sites," *Nat. Commun.*, vol. 14, no. 1, Dec. 2023, doi: 10.1038/s41467-023-40174-4.

European Fuel Cells and Hydrogen
PIERO LUNGHI CONFERENCE
EFCH2 2026
September 15th-17th 2026
Capri / Italy

HyMantovalley – A Case Study from Italy

Marcello Romagnoli*[a], Nicola Galli [b]

* corresponding author: marcello.romagnoli@unimore.it

[a] Centro Interdipartimentale di Ricerca e per i Servizi nel settore della produzione, stoccaggio ed utilizzo dell'Idrogeno-Università di Modena e Reggio Emilia - Italy

[b] A.G.I.R.E. Srl (Energy Agency of the Province of Mantova)



Keywords: Hydrogen Valley, Research and formation, Sustainable Development, Transportation

Abstract

HyMantovalley is a European initiative addressing environmental and socio-economic challenges in Italy's Po Valley by promoting a localized hydrogen (H_2) ecosystem. The project integrates technological transition and education to support decarbonization and reduce air pollution. It includes the conversion of existing facilities from "blue" to "green" hydrogen using photovoltaic-powered electrolysis and its deployment within a tri-modal transport system (waterways, rail, and road). In parallel, a regional research and education hub is established to train a skilled workforce. The project aims to create a scalable and replicable model, with preliminary expectations indicating reduced emissions, subject to validation through ongoing pilot testing and field measurements.

Introduction: The deployment of hydrogen-based technologies is widely recognized as a critical step toward achieving European decarbonization and mitigating climate change. The Po Valley region of northern Italy, and specifically the province of Mantua, represents a critical case for this transition; while the area is historically rich in industrial activity, it simultaneously suffers from critical levels of air pollution (Fig.1) and severe environmental challenges. To address this, the HYMANTOVALLEY project emerges as a strategic effort to improve regional air quality and stimulate green economic growth by creating a localized H2 ecosystem. However, a significant barrier to this transition is the current "skills gap," as the success of a H2-based economy depends on a workforce trained in both fundamental sciences and hands-on technical applications.

HYMANTOVALLEY intends to resolve these environmental and educational challenges through a dual strategy of technical infrastructure transition and specialized education. Technically, the project aims to transition existing facilities from low-carbon ("blue") H2 to renewable ("green") H2 via an electrolysis unit powered by dedicated photovoltaic installations. This production is integrated into a

unique tri-modal logistics system, encompassing inland waterways (Mantua-Venice corridor), rail, and road to demonstrate zero-emission transport solutions.

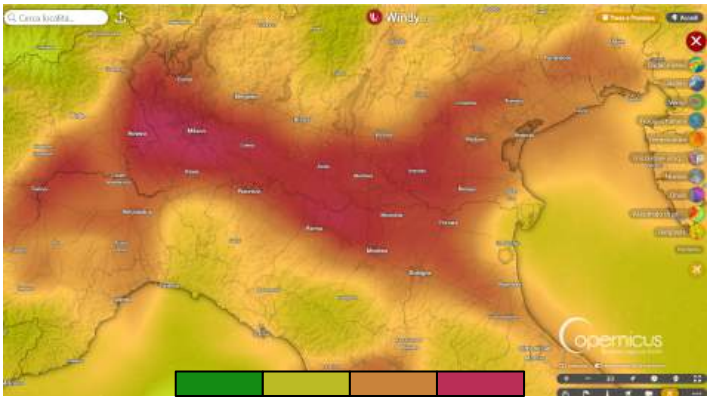


Fig.1 Air Quality Index across the Po Valley 10/03/2026.

Educationally, the project establishes a regional Applied Research and Education Hub to train the technicians essential for this new economy. This local initiative is designed to act as a living laboratory capable of using educational resources already produced in other European projects, free to use and "teach the teacher" methodologies. The European project HyMantoValley has a duration of 4 years and involves 22 partners from 4 European nations: Italy, Austria, Belgium, and the Netherlands. It has received investments of around €9 million and is co-financed at 70% by the European Union through the I3 Interregional Innovation Investments Program – Investments for interregional innovation.

Objectives: HYMANTOVALLEY's integrated approach aims to:

- Establish a scalable framework for green H2 production by transitioning existing facilities from "blue" to "green" via electrolysis powered by photovoltaics
- Implement zero-emission tri-modal logistics, focusing on the decarbonization of maritime transport (Mantua-Venice corridor), rail freight, and heavy-duty road transport
- Pilot innovative H2 applications for studying district heating application, testing pilot-scale heating and cooling systems
- Foster public-private synergies and regional development to bridge the gap between academic research and real-world industrial and vocational applications
- Implement pilot training programs that exploit educational materials and innovative methodologies, also developed within other European projects on this topic, to prepare a highly-skilled local workforce and close the "skills gap"
- Create a replicable blueprint for integrated H2 valleys, providing transferable lessons for other high-pollution industrial regions across the continent

Results: Preliminary considerations suggest that integrating H2 in local transport and industry could cut carbon and nitroxide emissions. Further pilot tests are needed to validate these projections. Key areas for verification include:

- Maritime and inland shipping: The expected shift to H2-powered vessels along the Mantua-Venice corridor, which could reduce reliance on diesel, requires thorough quantitative assessments of emissions and operational performance.
- Rail and road transport: While H2 locomotives and mobile refuelling stations are under development, actual operational data needs to be collected to confirm the viability and scalability of these solutions.
- Production and storage: Although initial simulations of local H2 production coupled with renewable energy suggest stable operation, real-time measurements will be essential to validate energy yield, storage efficiency and cost effectiveness.
- Small scale H2 application in the aquaponic field and related logistic and H2 bicycles

The project includes systematic field measurements, stakeholder feedback and environmental impact assessments. These efforts will verify whether the predicted benefits match real-world outcomes and provide definitive insights into the potential of H2 to drive a sustainable energy transition in regions such as the Po Valley - and beyond.

Conclusions: The transition to H2 as a cornerstone of sustainable energy systems is an increasingly urgent priority, both at national and European levels. As demonstrated by the HYMANTOVALLEY Project, well-coordinated public-private partnerships, robust technical strategies, and proactive stakeholder engagement underpin the successful development of integrated H2 ecosystems.

Future work will focus on:

- Scaling Up current pilot demonstrations to larger fleets of hydrogen-powered maritime vessels, trains, and heavy-duty vehicles.
- Refining Business Models to ensure sustained economic viability and broader stakeholder uptake in diverse regions.

Acknowledgment: Funded by the European Union. Views and opinions expressed are however those of the author(s) only and do not necessarily reflect those of the European Union or EISMEA. Neither the European Union nor the granting authority can be held responsible for them.

Co-funded by
the European Union

References

[1] https://hymantovalley.agirenet.it/en/



Environmental performance assessment of catalysts for water electrolysis in the context of the X-SEED project

Martí Aliaguilla[a], Sandra Martínez-Crespiera[a], Alexandru Tanase[a], Marian Garcia-Montolio[a], Pau Bosch-Jimenez[a], Leonardo Cognini[b], Inma Sanchez[a].

*corresponding author: maliaguilla@leitat.org

[a] Leitat Technological center, Terrassa, Spain

[b] Particular Materials SRL, Cadoneghe, Italy

Keywords: Life cycle assessment, HER / OER catalysts, supercritical water electrolysis.

Abstract

The X-SEED project aims to develop a membrane-less supercritical electrolyser. The scope of the project includes developing the key components required by the technology such as the hydrogen evolution reaction (HER) and oxygen evolution reaction (OER) catalysts. To support decision-making on the selection of perovskite-based catalysts, the environmental performance of five catalysts produced using two synthesis methods was assessed using Life Cycle Assessment (LCA). Continuous flow hydrothermal synthesis (CHFS) method presented 40% lower environmental impact than electrospinning nanofiber-based perovskites (ENP). Electricity consumption was identified as the main hotspot, accounting for nearly 94% of the environmental footprint. Process optimization scenarios indicate that overall impacts can be reduced by up to 34%, underscoring the importance of integrating environmental criteria into catalyst development.

Introduction:

The transition towards climate-neutral energy systems requires cost-effective and efficient green hydrogen production technologies. Within the EU X-SEED project (GA 101137701) a novel membrane-less electrolyzer operating under supercritical water conditions (≥374°C and ≥220 bar) is being developed to overcome the efficiency, durability, and cost limitations of conventional electrolyzers. In this context, the development of robust and efficient catalysts for the HER and OER with high durability and low environmental impact is essential. Consequently, environmental criteria should be systematically integrated into materials development. An LCA based eco-design approach, as proposed by Magnaval *et al*. [1] can provide significant benefits in minimizing the environmental impact of key components in H_2 technologies. The environmental impacts of hydrogen production with the X-SEED supercritical electrolyser are assessed through LCA methodology. Although the project is still generating data for the final electrolyser, LCA has already been applied in early project stages as optimization tool for the development of environmentally friendly catalysts.

Objectives:

This study aims to determine the environmental footprint (EF) of catalyst production processes, identify environmental hotspots to optimise catalyst production, and thereby support decision-making regarding the selection of perovskite-based HER and OER catalysts.

Material and methods:

Within X-SEED, more than 25 perovskite-based catalysts were investigated, and the EF of the top-performing catalysts from each synthesis method (CHFS and ENP) was evaluated by conducting a preliminary LCA. ISO 14040 [2] and 14044 [3], together with the recommendations from the commission on the Environmental Footprint method (PEF) [4] were followed as reference documents. In Addition, specific recommendations for hydrogen production technologies (e.g. LCA checklist tool from the Joint Research Centre [5]) were also considered. The goal of the preliminary LCA was to compare 5 catalysts produced by the two mentioned synthesis methods. The scope of this work encompasses a cradle-to-gate study in an attributional life cycle assessment approach. The system boundaries include two catalysts synthesis methods: CHFS and ENP. CHFS is a patented process producing monodispersed nanoparticles taking advantage of the sharp drop in water's dielectric constant under supercritical conditions, enabling instantaneous precipitation. ENP were produced by the electrospinning of a precursor salt/polymer solutions, followed by thermal treatment in air or controlled atmosphere to remove the polymer and form crystalline perovskites. The functional unit considered was 1 kgH_2. As the catalysts electrochemical characterization is still ongoing, the results presented in this document used 1 kg of catalyst as reference flow for the comparison. The Life Cycle Inventory was conformed mainly of primary data from catalyst producers for the foreground and secondary data was utilized to model the substances non present in the Ecoinvent 3.11 database. The catalyst production processes were modelled using Simapro (10.2.0.2) software and the EF 3.1 environmental footprint method was applied for the impact assessment (16 impact categories).

Results:

The environmental footprint (normalised results) associated with the production of 1 kg of catalyst for the two CHFS and three ENP catalysts studied is presented in Figure 1. The LSCOF and LCO catalysts, i.e., those produced via the CHFS method, exhibited approximately 40% lower environmental impacts compared with ENP catalysts. In CHFS process the main hotspots identified were the drying and the calcination step accounting for 55% and 39% of the total production process impact, respectively, for both LCO and LSCOF catalyst. In both steps electricity consumption was the main contributor to the environmental

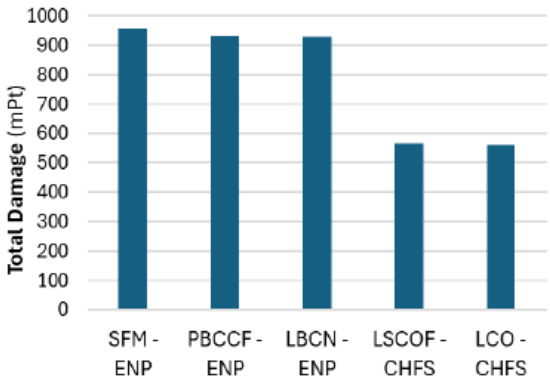


Figure 1. Catalyst EF comparison. Total damage

impact. In ENP production process the main hotspots identified were the Electrospinning and the Thermal treatment steps, responsible for 32% and 62% of the total production impacts, respectively. Similarly to the CHFS method, electricity consumption was the main contributor to the EF of both the electrospinning and thermal treatment steps. In both cases, the ENP and CHFS methods, the two identified hotspots together accounted for approximately 94% of the total impacts. The dominance of electricity consumption in both cases explains the consistent impact pattern observed across the different impact categories. Mitigation strategies have been implemented optimizing both CHFS and EPN production processes resulting in a significant reduction of the overall environmental impact of 34%.

Conclusions:

Perovskite catalysts produced by CHFS present around 40% lower environmental impacts compared with ENP catalysts. The analysis identifies drying and calcination of CHFS method and electrospinning and thermal treatment of ENP method as the main hotspots. In both synthesis methods, electricity consumption during key processing steps dominates the environmental footprint highlighting the potential for significant reductions through process optimization and low-carbon electricity supply. This study will be completed once the electrochemical characterization data is available, enabling the development of a functionalized environmental comparison based on hydrogen production.

Acknowledgment

This work has been done in the context of the X-SEED project, with Grant Agreement number 101137701. The project is supported by the Clean Hydrogen Partnership and co-funded by the European Union. Views and opinions expressed are however those of the author(s) only and do not necessarily reflect those of the European Union or the Clean Hydrogen Partnership.

References

[1] Magnaval, G., Debonnet, T., Margni, M., 2025. Integrated LCA and eco-design process for hydrogen technologies: case study of the solid oxide electrolyser. *The 35th European Symposium on Computer Aided Process Engineering*, Ghent, Belgium, pp. 674–680. https://doi.org/10.69997/sct.171756

[2] International Organization for Standardization, 2006. ISO 14040:2006 Environmental management — Life cycle assessment — Principles and framework. Geneva, Switzerland.

[3] International Organization for Standardization, 2006. ISO 14044:2006 Environmental management — Life cycle assessment — Requirements and guidelines. Geneva, Switzerland.

[4] European Commission, 2013. Product Environmental Footprint (PEF) Guide. European Commission, Brussels, Belgium.

[5] European Commission, Joint Research Centre, 2024. LCA checklist: a tool to improve the communication of the environmental sustainability of the Clean Hydrogen Joint Undertaking projects. Publications Office of the European Union. https://doi.org/10.2760/529754



The Best Uses of Green Electrolytic Hydrogen

Robert Flores*[a], Mariam Al Moubasher[a], Jack Brouwer[a], Jeff Reed[a]

* corresponding author: rjf@apep.uci.edu

[a] Clean Energy Institute, University of California, Irvine, Irvine, CA 92617, USA

Keywords: electrolytic hydrogen, industrial decarbonization, monetized life cycle analysis, transportation decarbonization

Abstract: Renewable electrolytic hydrogen is commonly described as a jack-of-all-trades solution for decarbonizing tough industrial and heavy-duty transportation end uses. In reality, green hydrogen faces major challenges associated with cost, handling and distribution, and limited supply. To succeed as a decarbonization tool, green hydrogen must be deployed where it generates the greatest value. This work examines green hydrogen from a social value perspective, applying monetized life cycle analysis to estimate where the highest social value is generated through reduced impacts on human health, environmental degradation, and resource depletion. Results show that the highest social value, up to \$8/kg H_2, is achieved when hydrogen displaces inefficient coal, oil, and diesel processes, and when decarbonization enables the introduction of energy efficiency improvements. Steelmaking and ocean-going vessels are prime examples. Green hydrogen also performs well for heavy-duty trucking, though greater social value can be achieved by reserving hydrogen for the longest-range applications and decarbonizing shorter-range trucks with battery-electric drivetrains. Social value diminishes for applications that already rely on efficient fossil processes, particularly those using natural gas, such as electricity generation, industrial heating, and some chemical production.

Introduction: Renewable electrolytic hydrogen is increasingly proposed as a versatile solution for decarbonizing industrial processes and heavy-duty transportation. However, green hydrogen faces substantial real-world barriers including high production costs, limited supply, and challenges associated with storage, handling, and distribution. Given these constraints, hydrogen cannot realistically serve as a universal decarbonization tool, and indiscriminate deployment risks displacing more cost-effective alternatives such as direct electrification. Strategic prioritization of green hydrogen toward its highest-value applications is therefore essential for maximizing decarbonization outcomes. This work addresses that need by evaluating green hydrogen through a social value lens, identifying where its deployment generates the greatest societal benefit relative to fossil fuel and direct electrification alternatives. This work is detailed in greater detail in [1].

Objectives: This study aims to quantify and compare the social value of renewable electrolytic hydrogen across major industrial and heavy-duty transportation sectors. By identifying applications

where hydrogen generates the greatest reduction in societal costs, the work provides a framework for prioritizing green hydrogen deployment to maximize decarbonization impact.

Material and methods: A monetized life cycle analysis (LCA) framework is applied to compare renewable electrolytic hydrogen, direct electrification, and conventional fossil fuel pathways across eight industrial and transportation sectors: steelmaking, transoceanic shipping, heavy-duty trucking (classes 3, 6, and 8), industrial heating, electricity generation, and chemical and fuel production (hydrogen, ammonia, methane, and methanol). Social costs are estimated on a cradle-to-grave basis using damage cost factors from Ecoinvent, monetizing impacts across three categories: human health, environmental degradation, and resource depletion. The social value of hydrogen is defined as the reduction in monetized social cost achieved by substituting hydrogen for incumbent fossil processes, normalized per kg of H_2 used. Four U.S. electricity supply scenarios are evaluated, ranging from the current grid (2025, ~40% fossil) to a fully renewable 60% wind/40% solar mix.

Results: Primary outputs from this work is the social cost of different industrial and heavy-duty transportation activities. These results are used to derive the social value of hydrogen by comparing the social cost of a process using fossil fuel versus hydrogen. This difference is divided by the amount of hydrogen used in the process, producing the social value of hydrogen. Key results are summarized in Figure 88.

Conclusions: This study demonstrates that the social value of green hydrogen varies significantly across industrial and heavy-duty transportation sectors. The highest social value is achieved in applications that displace carbon-intensive coal, oil, and diesel processes while enabling energy efficiency improvements, with steelmaking, transoceanic shipping, and long-haul trucking emerging as priority end uses. In sectors dominated by efficient natural gas systems, social value is comparatively low. Electricity supply mix is found to be a critical determinant of hydrogen's social value, underscoring the importance of pairing hydrogen production with renewable energy sources.

Acknowledgment: The authors gratefully acknowledge financial support from Plug Power Inc. and technical feedback from Tim Cortes and Luke Wentlent. The authors also gratefully acknowledge Julie Schoenung and the WISDOM Institute at UC Irvine for their feedback and technical support.

References

[1] Flores R, Al Moubasher M, Brouwer J, Reed J. The social value of electrolytic hydrogen. Joule 2026. https://doi.org/10.1016/j.joule.2026.102427.

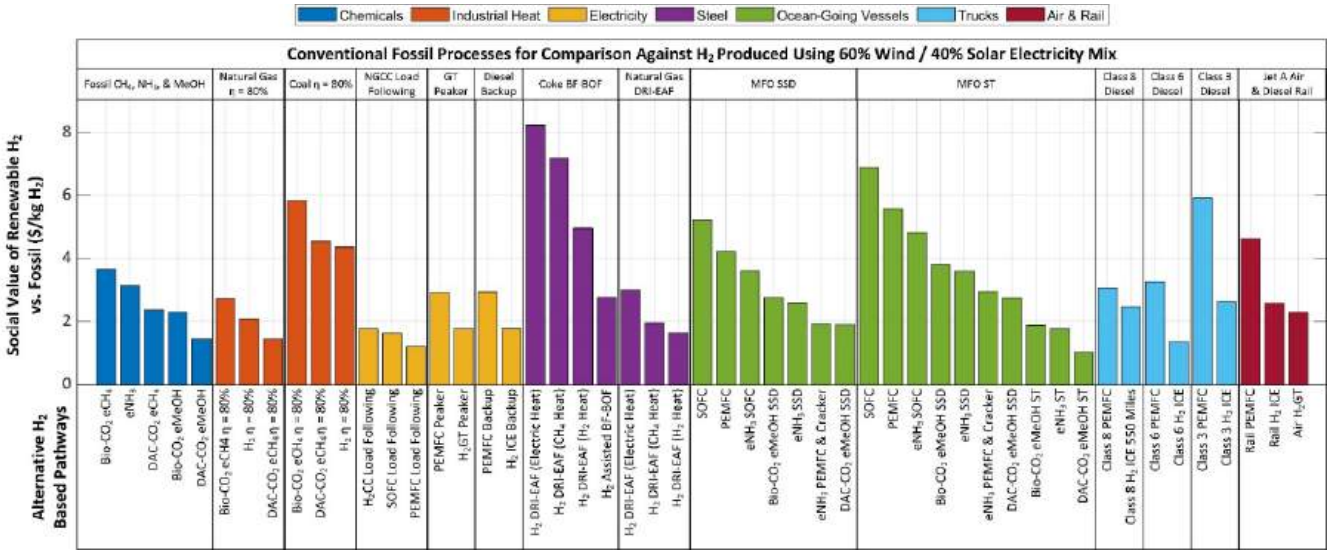


Figure 90: Social value of renewable hydrogen relative to conventional fossil pathways across industrial and transportation sectors. Values represent the monetized reduction in social cost per kg of renewable electrolytic H_2 used, assuming H_2 is produced using a 60% wind / 40% solar electricity mix and delivered via pipeline. Higher values indicate greater societal benefit from displacing fossil fuels with the renewable electrolytic H_2 produced.



Closing the Hydrogen Emissions Knowledge Gap: the NHyRA Approach

V. Palmisano[a], A. Agostini[a], V. Troisi, M. Robino.

* corresponding author: V. Palmisano

[a] ENEA, Rome, Italy

[b] SNAM, Milan, Italy

Keywords: greenhouse effect, hydrogen emissions, hydrogen economy, mitigation strategies.

Abstract

Introduction: Hydrogen (H_2) is set to play a key role in supporting climate neutrality as an energy carrier enabling large-scale integration of renewable sources. Although hydrogen is not a direct greenhouse gas, its atmospheric release can indirectly contribute to climate forcing through well-known mechanisms [1,2]: prolonged methane lifetime, enhancement of tropospheric ozone, and increased stratospheric water vapor. Recent studies confirm that H_2 has a non-negligible climate impact, with estimated GWP100 around 12 and GWP20 approaching 40 [3, 5]. Minimizing hydrogen emissions across the entire value chain remains therefore essential for ensuring both environmental sustainability and system safety.

Despite increasing attention, the understanding of real-world hydrogen emissions is still fragmented, with reported dispersion rates ranging from 0.3% to 20% depending on technologies, operating conditions, and measurement methods [6]. The lack of standardized datasets and validated measurement protocols has hindered robust quantification of hydrogen's climate impact and the development of effective mitigation strategies. The NHyRA project was launched to fill these gaps [7].

Objectives: The NHyRA project, funded under the call HORIZON-JTI-CLEANH2-2023-05-03, aims to create a comprehensive scientific and technical foundation for assessing hydrogen emissions across the European hydrogen value chain. Its objectives include:

1. Establishing an inventory of expected H_2 emissions along the value chain.
2. Identifying critical archetypes in terms of emission potential.
3. Developing and validating measurement methodologies and monitoring frameworks.
4. Creating tools to simulate, quantify, and compare hydrogen emission scenarios.
5. Proposing mitigation options and recommendations to support EU and international standardization.

The project is aligned with the goals of the Horizon Europe Work Programme, aiming to support a sustainable and safe hydrogen economy. Thus, it is strongly connected to EU-projects funded under

HORIZON-CL5-AWP23-D1-01-03: *Climate impacts of a hydrogen economy*, addressing the indirect forcing effect of H_2 emissions on the greenhouse effect.

Material and methods: The project defined and mapped all key components of the hydrogen value chain, identifying typical operating conditions and potential emission sources. An open-access inventory has been progressively populated with data from experiments, literature, industrial partners, and simulation models. In parallel, the project developed and validated multiple measurement strategies—including component-level detection, quantification protocols, and area-level monitoring techniques—tested both in laboratory conditions and through field campaigns. Furthermore, experimental, theoretical, and simulation-based methodologies are being developed and validated, allowing for accurate measurements in both laboratory and field settings. Critical elements of the hydrogen value chain will undergo experimental testing to assess their emission profiles. Looking ahead, the NHyRA project aims to provide a comprehensive understanding of H_2 emissions by evaluating scenarios for the mid-term (2030) and long-term (2050) European hydrogen economy. These evaluations will help decision-makers quantify hydrogen's environmental impact, identify effective risk mitigation strategies, and prioritize actions for achieving a sustainable energy transition. Finally, the project will formulate recommendations for standards and technical specifications to guide the hydrogen industry in minimizing emissions and ensuring safety.

Results: As NHyRA project approaches its conclusion, most of the planned objectives have been achieved. The open-access inventory of H_2 emission archetypes has been completed and is being continuously expanded. A first operational version of the NHyRA emission quantification tool, integrating measurement data, archetype modelling, and scenario analysis capabilities, has been successfully developed. Experimental campaigns addressing key elements of the hydrogen value chain are nearly completed, and initial results have been incorporated into the tool's datasets. Collaboration with sister projects focused on the climate impacts of H_2 has strengthened the scientific basis of the work and ensured alignment with ongoing Horizon Europe initiatives. Several H_2 release scenarios for 2030 and 2050 have been fully developed and validated. A summary of the key results is provided in Table 1.

***Table 1**. Overview of key outcomes of the NHyRA project*

Outcome area	Description	Status
Emission inventory	Open-access database of H_2 emission archetypes across the value chain	Completed and continuously expanding
Measurement methodologies	Component-level and area-level monitoring techniques for H_2 emissions	Validated under laboratory and field conditions

Experimental campaigns	Testing of representative components across the hydrogen value chain	Near completion
Quantification tool	Integrated platform for emission modelling, data integration, and scenario analysis	First operational version available
Scenario analysis	Assessment of H_2 emissions under future deployment scenarios (2030, 2050)	Developed and validated

Conclusions: By systematically addressing critical knowledge gaps and delivering robust, validated methodologies, the NHyRA project significantly advances the quantification and understanding of hydrogen emissions across the European value chain. The project provides a unique combination of experimental datasets, validated measurement protocols, and an operational emission quantification tool, enabling a consistent and science-based assessment of hydrogen's environmental impact. NHyRA also supports informed decision-making by enabling the evaluation of future hydrogen deployment scenarios and the identification of effective mitigation strategies, guiding policymakers, industry stakeholders, and the scientific community toward harmonized approaches for emission monitoring and reporting. Ultimately, the project contributes to the development of future standards and technical specifications, strengthening the basis for a safe, transparent, and environmentally sustainable hydrogen economy in Europe.

Acknowledgments: *This project has received co-funding from the European Commission and the Clean Hydrogen Partnership under Grant Agreement No 101137770. This Partnership receives support from the European Union's Horizon Europe Research and Innovation program, Hydrogen Europe and Hydrogen Europe Research.*

References

[1] Arrigoni, A., and Diaz, B. L. (2022). Hydrogen emissions from a hydrogen economy and their potential global warming impact. Belgium, Germany: European Commission, JRC

[2] Ocko, I. B., and Hamburg, S. P. (2022). Climate consequences of hydrogen emissions. Atmos. Chem. Phys. 22, 9349–9368. doi:10.5194/acp-22-9349-2022

[3] Warwick, N.J., Archibald, *et al.* (2023). Atmospheric composition and climate impacts of a future hydrogen economy. Atmos. Chem. Phys. Prepr., doi:10.5194/acp-2023-29

[4] Sand, M., Skeie, R.B., Sandstad, M. *et al.* A multi-model assessment of the Global Warming Potential of hydrogen. *Commun Earth Environ* **4**, 203 (2023).

[5] Arrigoni, A., Dolci, F., *et al.* (2024). Environmental life cycle assessment (LCA) comparison of H_2 delivery options within Europe. Luxembourg: European Commission, JRC

[6] Esquivel-Elizondo, S.; Hormaza Mejia, A.; Sun, T.; Shrestha, E.; Hamburg, S. P.; Ocko, I. B. Wide Range in Estimates of Hydrogen Emissions from Infrastructure. Front. Energy Res. 2023, 11, 01–08

[7] https://nhyra.eu/



A methodological framework for mapping hydrogen value chains: the case of friuli venezia giulia and the north adriatic hydrogen valley

Favot Marinella*[a], Longato Enrico [a], Soraci Alberto [ab], Guaiana Marcello[a] , Graditi Giorgio[a]

*corresponding author: Favot Marinella

[a] Area Science Park, 99 Padriciano, Trieste, Italy; [b]Università degli Studi di Messina

Hydrogen Valley, Companies mapping, Industrial Policy, Web scraping

Abstract

This paper presents a methodological framework for mapping and segmenting the renewable hydrogen value chain in Friuli Venezia Giulia (Italy), developed within the North Adriatic Hydrogen Valley (NAHV)[1] initiative. The methodology combines industrial classifications, regional innovation databases, and web-based text mining techniques to identify companies potentially active in the hydrogen economy. Eight value chain segments were defined, ranging from renewable energy production to hydrogen-ready transport systems. NACE codes, web scraping, TF-IDF indicators, topic detection algorithms, and qualitative validation were integrated to identify firms with strong and potential signals of belonging to the value chain. The application provides a first structured regional mapping of the hydrogen supply chain.

Introduction: Hydrogen (H_2) is increasingly recognized as a strategic energy vector for decarbonizing hard-to-abate industrial sectors and heavy mobility systems [1]. In Europe, Hydrogen Valleys (HVs) integrate production, storage, and multiple types of end uses of hydrogen in limited geographical areas [2]. Despite growing policy and industrial interest in hydrogen, identifying and characterizing regional industrial ecosystems remains challenging. This study presents a methodology combining industrial classifications, innovation databases, and web-based semantic analysis to map the regional hydrogen ecosystem and identify firms with different levels of involvement in hydrogen-related activities.

Objectives: The main aims of the study are to: define a theoretical regional hydrogen value chain articulated into industrial, services and technological segments; provide a methodological framework for mapping actual and potential companies active in the segments; identify companies with strong and weak signals of belonging to the ecosystem; highlight regional industrial strengths, gaps, and potential development trajectories for the hydrogen economy.

Material and methods: The methodology was developed through a multi-step process integrating quantitative and qualitative approaches. First, the hydrogen value chain was structured into eight industrial segments: (1) renewable energy production and distribution, (2) H_2 production and commercialization, (3) H_2 storage, (4) H_2 transport and distribution, (5) final use in H2A industries and

[1] https://www.nahv.eu/

mobility, (6) H_2 transversal services, (7) H_2-related components and equipment, and (8) H_2-ready transport systems. For each segment, relevant NACE economic activity codes were selected to identify potentially relevant firms. Companies with registered headquarters or local units in FVG were extracted from the Innovation Intelligence FVG database[2], resulting in an initial universe of more than 2,800 firms. The second phase involved web scraping activities applied to company websites considered the main source of information for identifying technologies, competencies, products, certifications, H_2-related activities. The analysis adopted the methodology developed by Blasi and colleagues [3] based on text mining techniques such as Bag of Words (BoW), TF-IDF (Term Frequency–Inverse Document Frequency), and topic detection algorithms (LSA and LDA). Specific bilingual (Italian and English) keyword baskets were developed for each segment of the value chain. An additional phase integrated other sources of information (such a data of financed H2 projects). The methodology combined automated semantic analysis with manual qualitative validation to identify:

1. firms with *strong signals* of belonging to the hydrogen value chain;
2. firms with *medium or weak signals* but potentially relevant;
3. firms without detected signals or below the threshold (only for Segment 5).

For Segment 5 ("Final use"), additional selection criteria were applied to refine the large pool of potentially relevant firms. Companies were assessed according to the enterprise size criteria defined by the European Commission [4], using company size as a proxy for the investment capacity and innovation propensity required for hydrogen adoption.

Results: The study developed and tested a methodology for value chain mapping applied to the hydrogen sector in a region within the North Adriatic ecosystem. The methodology identified 103 companies in the segments characterized by strong indicators of belonging to the hydrogen ecosystem and 311 firms with medium or weak signals of potential relevance.

Supply chain segment	Strong signals (S)	Medium/weak S.	No S./ below threshold
1 - green energy production	37	4	46
2 - H2 production	11	21	44
3 - H2 storage	1	3	6
4 - H2 transport and distribution	4	14	21
5 - H2 final use (H2A and transports)	18	182	559
6 - cross-cutting services	13	34	183
7 - components and equipment for H2	14	31	48

[2] https://www.areasciencepark.it/project/innovation-intelligence-fvg/

8 - means on transport H2-ready	5	22	54
Total	103	311	961

Table 1. Hydrogen value chain mapping results

The analysis highlighted the strong presence of companies operating in downstream Segments (5) as well as in Segment 8, suggesting the existence of a significant potential demand base for hydrogen technologies. Conversely, the storage segment (Segment 3) appeared significantly underrepresented with only 4 companies in total, revealing structural gaps in the regional value chain.

Conclusions: The proposed methodology provides an innovative framework for mapping industrial ecosystems through the integration of industrial classifications (NACE), company databases, web scraping based on Bag of Words (BoW), and topic detection algorithms. The methodology identifies both firms with strong signals of being active in H_2-related sectors and companies potentially ready for future hydrogen market development. The case of Friuli Venezia Giulia highlights a diversified industrial base capable of supporting the development of a regional hydrogen economy, while revealing critical weaknesses in storage and transport infrastructure segments, suggesting the need for targeted industrial and policy interventions. The proposed methodology also has limitations related to the availability and quality of company website content, the selection of NACE codes, and the construction of BoW dictionaries, However, these limitations were partially mitigated through expert validation. The mapping outcomes may support policymakers, regional development agencies, and industrial stakeholders in designing evidence-based strategies for hydrogen ecosystem development and industrial decarbonization.

References

[1] European Commission. (2020). *A Hydrogen Strategy for a Climate-Neutral Europe*. COM(2020) 301 final. Brussels: European Commission.

[2] Bonafé, E., Conte, M., & Bouchaar, K. (2023). Hydrogen Valleys: Assessing the EU Legal and Financial Frameworks that Enable the Hydrogen Economy. *Global Energy Law and Sustainability*, 4(1–2), 96–114. https://doi.org/10.3366/gels.2023.0095

[3] Blasi, S., Fano, S., Sedita, S.R., & Toschi, G. (2024). *A network perspective of cognitive and geographical proximity of sustainable tourism organizations: evidence from Italy*. International Journal of Contemporary Hospitality Management, 36(2), 478–504. https://doi.org/10.1108/IJCHM-03-2022-0366

[4] European Commission. (2003). Commission Recommendation 2003/361/EC of 6 May 2003 concerning the definition of micro, small and medium-sized enterprises. *Official Journal of the European Union*, L 124, 36–41.

Acknowledgment: This study received funding from the European Union's Horizon Europe research and innovation programme under grant agreement No [101111927 - NAHV]). The views and opinions expressed in this paper are solely those of the author(s) and do not necessarily reflect the official positions of the EU or the Clean Hydrogen Joint Undertaking.



The role of hydrogen in Italy's energy transition: effects of carbon budget and of the introduction of nuclear power plants

Matteo Catania[a], Paolo Colbertaldo[a], Fabrizio Fattori[b], Mario Motta[a], Stefano Campanari[*,a]

[*]Corresponding author: stefano.campanari@polimi.it

[a]Department of Energy, Politecnico di Milano - Milan, Italy

[b]Dipartimento di Scienze Teoriche e Applicate, Università degli studi dell'Insubria - Varese, Italy

Keywords: Hydrogen; Energy transition; carbon budget; nuclear power

Abstract: Decarbonisation of the energy system entails deep changes in how energy is generated, exchanged, and converted. Through an integrated energy system model, the paper presents a selection of results of an activity of long-term optimisation of the Italian energy system, analysing the implications of alternative cumulative CO_2 budgets and of the possible future deployment of nuclear power plants on the overall energy mix and on the role of hydrogen.

Introduction: Energy system modelling is a recognized tool to assess the best strategies to cope with a fast and yet realistic energy transition [1], in presence of an expanding role of intermittent renewable energy sources (RES) and considering the possible introduction of other resources such as nuclear power, the use of hydrogen as clean energy vector and of energy storage techniques. This work reports selected outcomes of the research activity "*Integrated Energy System Modeling and H2 Role in Italy for Net-Zero CO2*" developed for this purpose at the H2 Joint Research Partnership of Politecnico di Milano.

Objectives: The work analyses (i) the implications of alternative cumulative CO_2 budgets on the evolution of Italy's generation capacity, hydrogen systems and carbon capture, highlighting their effects on the overall energy mix and on the CO_2 balance; and (ii) how the possible deployment of nuclear power plants in the future Italian energy mix is modified by different techno-economic and infrastructure assumptions, and how the role of hydrogen changes in the different cases.

Material and methods: The analysis is based on the *Future Energy traNsition multI-seCtor modEl* (FENICE), an integrated energy system model developed in the open-source framework *oemof* with a "Multi[4]"approach: the representation is multi-node, multi-vector, multi-sector, and multi-period, including accurate tracking of CO_2 flows to account for fossil and biogenic contribution and cope with given carbon budgets [2-3].

The model minimizes the total system costs over the transition timespan; it simulates years clustered with 24 typical days per year, hourly resolution and a 5-year gap between representative years. Assumptions include operation data in each node and period (e.g. hourly profiles of renewable power generation and energy vectors consumption) and techno-economic data for each technology in each representative period, elaborated in parallel analyses (based on historical data, national datasets of the TSOs, dedicated analyses on technology evolution, forecasts by IEA, IRENA and relevant institutions).

Results: The analysis on cumulative carbon budget (CO_2 budget) considers three options, which arise from the equality and fairness concepts highlighted by Pelz et al. [4]: the Baseline scenario assumes a linear trend between today, the Fit-for-55 targets for 2030, and the Net-Zero goal by 2050, with a carbon budget of 5.64 GtCO2 computed for Italy. The AR6-E scenario is based on the IPCC sixth assessment report considering equality criterions, to limit

global warming to 1.5°C, allocated on a population basis (2.29 GtCO2); the AR6-R scenario adds responsibility criterions, adjusting for historical emissions since 1990 (null carbon budget, 0 GtCO2), and serves as an example of extremely strict conditions.

Results confirm that the transition of the Italian energy system towards carbon neutrality depends also on the cumulative CO_2 budget allowed along the way and on the characteristics of key technologies which can be progressively implemented.

Across all investigated cases, large-scale deployment of variable renewables, hydrogen, and carbon capture is not optional, but structural. Even in the Baseline scenario, the system eventually needs substantial hydrogen production from electrolysis, sizeable underground hydrogen storage, and a combination of CO_2 capture on biomass plants and direct air capture, complemented by CO_2 export, to reach a Net-Zero CO_2 target (Fig.1).

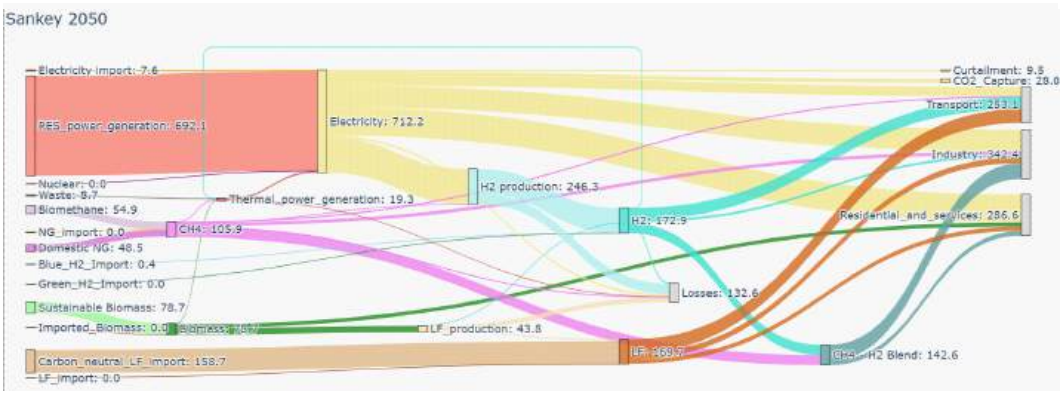


Fig. 91 -. Italy's energy flows (TWh) in the Baseline scenario for 2050 (Carbon budget 5.64 Gt_{CO2}).

As the cumulative CO_2 budget is tightened (Fig. 2), these elements appear earlier and at larger scale: from an investment perspective, long-lived assets (renewable clusters, electrolysers, storage facilities, H2 pipelines, and CO_2 storage) are therefore likely to have a central role under a wide range of climate policy assumptions, and hydrogen-related investments should be considered not as niche options but as core components of long-term strategies. Results highlight the importance of including a representation of the energy infrastructure networks (electricity grid and gas grid) and their evolution, as well as using a sufficiently refined spatial and time detail in the simulations. The model consistently identifies southern regions and the islands as preferred locations for renewable generation and hydrogen production, due to favourable resource conditions, while northern regions confirm as major demand centres and preferred access points to the domestic underground CO_2 storage capacity currently foreseen in the North Adriatic area of Ravenna.

The analysis of the potential role of nuclear shows strong variability of results. Depending on costs, construction times, as well as much depending on the reinforcement of the energy vector transport infrastructures (considering an expansion of both electricity and hydrogen networks and the possibility to allow a higher H2 fraction in the natural gas grid, Fig. 3), the optimised nuclear capacity ranges from negligible to substantial.

Indeed, all assets with long construction times and high investment costs as nuclear plants interact with hydrogen, carbon capture use and networks expansion, and are sensitive to the allowed CO_2 budget; calling for other types of strategical and policy evaluations beyond pure costs.

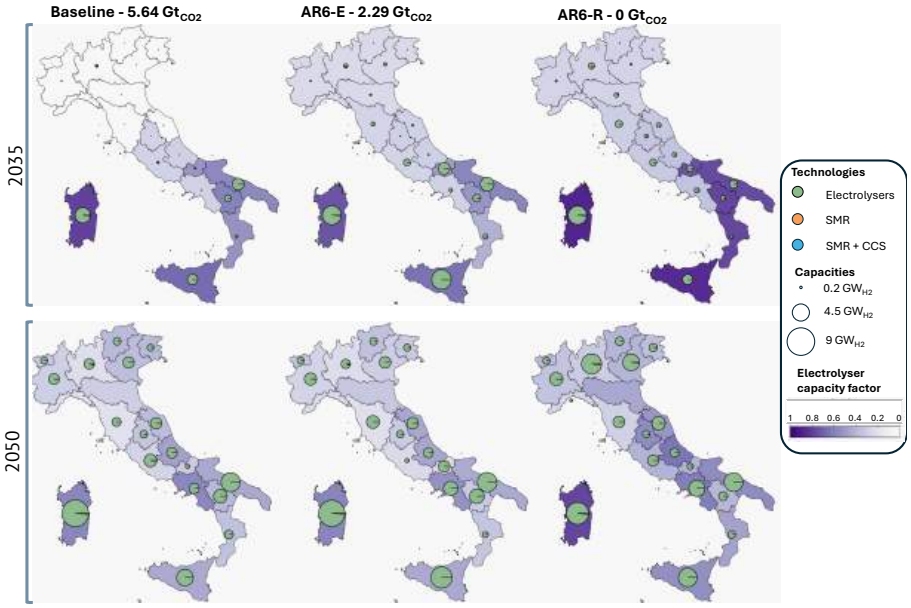


Fig. 2 - Regional H_2 production capacity in 2035 (top) and 2050 (bottom) for the three

Conclusions

This work provides insights on the role of hydrogen in the context of long-term decarbonisation pathways for Italy, for different scenarios of cumulative carbon budget, infrastructure expansion and presence of nuclear power.

Across the investigated set of scenarios, hydrogen always maintains a significant role as an energy vector and as a flexibility tool. The possible inclusion of nuclear may support a wider approach to a low carbon system, where strong RES, hydrogen, storage, and carbon capture are also needed.

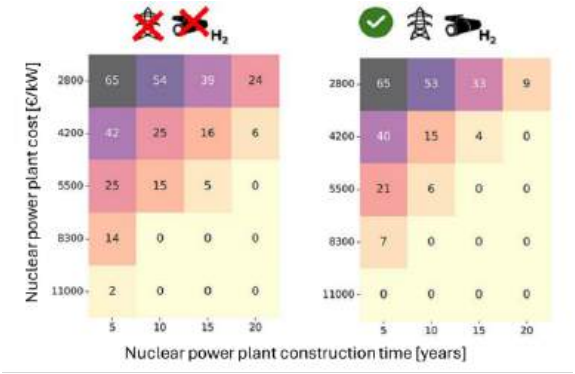


Fig. 3 - Nuclear capacity (GW) by 2050 in scenarios with limited or increased electricity interconnections

Acknowledgements: The work has been funded by the H2 JRP of Politecnico di Milano [5].

References

[1] IEA, "Global hydrogen review 2024", 2024
[2] M. Catania et al., Appl. Energy. doi.org/10.1016/j.apenergy.2025.126354, 2025
[3] M. Catania et al., Energy Conv. Manag. doi.org/10.1016/j.enconman.2025.120663, 2026
[4] S. Pelz et al. Estimates of fair share carbon budgets for Italy, (2024) 1–24.
[5] Hydrogen JRP, www.fondazionepolitecnico.it/progetti/hydrogen-jrp/., 2026



H-PORT: An Integrated Simulation, Safety and Techno-Economic Framework for Hydrogen-Powered Smart Ports

M. Genovese[a], F. Piraino [a,*], P. Fragiacomo[a]

* corresponding author: francesco.piraino@unical.it

[a] Department of Mechanical, Energy and Management Engineering, University of

Calabria, Arcavacata di Rende, 87036 Cosenza, Italy

Keywords: green hydrogen, smart ports, discrete-event simulation, techno-economic optimization, hydrogen safety, digital twin

Abstract

Ports are strategic nodes for the energy transition, yet the deployment of hydrogen requires the joint assessment of operational performance, energy infrastructure, safety and staff preparedness. This paper presents H-PORT (Hydrogen-Powered Port Optimization and Resilience Technology), an integrated framework for designing and evaluating hydrogen-powered port ecosystems. The framework combines a modular port-hub concept, discrete-event simulation of terminal operations, annual techno-economic optimization of renewable-to-hydrogen pathways, regulatory and risk analysis for gaseous and liquid hydrogen, and immersive training tools. Two reference terminal scales, 287,500 and 584,000 TEU/year, were examined. In the modelled high-renewable scenario, the optimizer selects an approximately 5 MW electrolyser, 250 t of gaseous H2 storage and a 754 kW fuel cell, reducing CO2 emissions by 99.87% relative to the baseline and reaching 7.36 kg CO2/TEU at the minimum simulated annual cost of 14.61 MEUR/year. A target configuration retains a 99.78% reduction with lower fuel-cell capacity. The results indicate that integrated modelling can support safe, scalable and economically informed hydrogen transition pathways for Mediterranean and European ports.

Introduction: Port decarbonization involves a tightly coupled system of vessels, yard equipment, trucks, rail interfaces, refrigerated containers and stationary loads. Hydrogen can provide a flexible energy carrier for heavy-duty mobility, backup or combined heat-and-power applications, and future maritime bunkering; however, its adoption modifies both energy flows and operational constraints. A credible design process must therefore connect demand generation, renewable electricity, hydrogen production and storage, layout design, risk barriers and operator training. H-PORT was conceived to close this gap through a modular hydrogen hub concept that can evolve from gaseous hydrogen refuelling for landside equipment to liquid hydrogen and bunkering-oriented applications [1]. The project develops an integrated digital workflow rather than a single component model, enabling comparison between an existing fossil-dependent port configuration and alternative hydrogen-based configurations [2].

Objectives: The objective of this work is to provide a replicable decision-support framework for hydrogen-powered ports. The specific objectives are to:

- define a modular architecture for onsite renewable hydrogen production, storage, distribution and end-use integration;
- link terminal operational demand to energy-system sizing through interoperable simulation modules;
- quantify cost and emissions performance under alternative renewable availability scenarios;
- embed regulatory compliance, risk mitigation and immersive safety training within the design process.

Material and methods: The H-PORT workflow integrates four interoperable components [2]. First, a discrete-event simulation module implemented in AnyLogic represents ship calls, container movements, equipment utilization, refuelling demand, electricity consumption and environmental outputs for the baseline terminal. Second, a MATLAB-based technological and energy module performs an hourly annual simulation (8760 h) and multi-objective optimization of renewable generation, hydrogen production, storage and fuel-cell utilization.

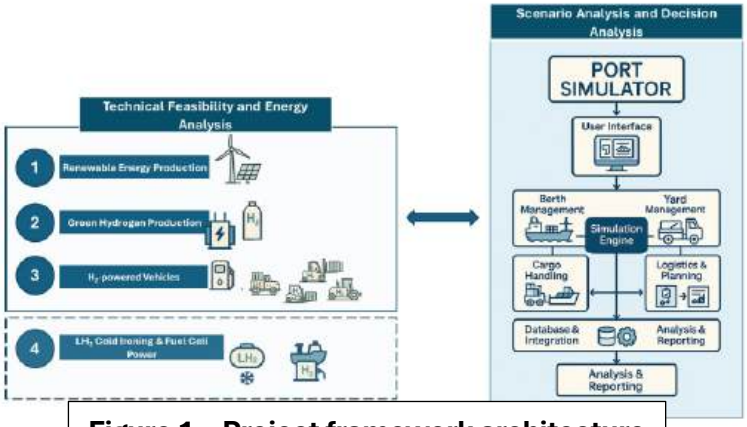


Figure 1 – Project framework architecture

Third, a virtual-reality safety module reconstructs operating environments and procedures for gaseous hydrogen (GH2) and liquid hydrogen (LH2). Fourth, a technical VR module supports interactive exploration of hydrogen production, storage, refuelling, bunkering and control-room functions.

The techno-economic study compares low, mid, full and target renewable-energy scenarios against a conventional baseline. The optimization considers an electrolyser capacity up to 5 MW, GH2 storage up to 250 t and variable fuel-cell sizing, while evaluating annual cost, residual CO2 emissions, unmet hydrogen demand and CO2 intensity per TEU. The safety workstream maps applicable ATEX, PED, ADR/IMDG and Seveso-related requirements and applies hazard-identification and layered-protection logic to release, ignition, cryogenic and interference scenarios. Design measures include physical segregation, ventilation, hydrogen detection, emergency shutdown, passive protection, access control and emergency procedures.

Results and discussion: Across all optimized scenarios, the model drives electrolyser and GH2 storage capacity to the allowed upper bounds, showing that local green-hydrogen availability is central to both emissions reduction and system economics. Fuel-cell integration becomes advantageous in the more renewable-rich scenarios, where excess hydrogen can be converted into useful electricity and heat. Selected outputs of the techno-economic assessment are:

- Full scenario: 14.61 MEUR/year, 4.30 million kg CO2/year, 7.36 kg CO2/TEU, 754 kW fuel cell and 99.87% CO2 reduction relative to the model baseline;

- Target scenario: 15.39 MEUR/year, 7.42 million kg CO2/year, 12.71 kg CO2/TEU, 177 kW fuel cell and 99.78% CO2 reduction;
- Green-H2 production exceeds internal demand in the full and target configurations, indicating the potential evolution of the port from consumer to hydrogen prosumer;
- Safety-by-design requirements include ATEX zoning, detection and ESD systems, protected layouts, and a temporary exclusion area of at least 25 m for naval bunkering/debunkering operations.

Conclusions: H-PORT provides an integrated methodology for evaluating the transition from fossil-dependent port operations to renewable hydrogen ecosystems. The results show that operational simulation, energy optimization and safety engineering must be treated as interdependent elements: the operational model establishes realistic loads; the energy model determines feasible technology sizing and emissions performance; and the regulatory-risk framework transforms technology options into implementable layouts and procedures. Under the studied assumptions, the full scenario delivers the lowest simulated annual cost and the greatest decarbonization, while the target scenario represents a less fuel-cell-intensive option with similarly high emissions reduction. Immersive training and digital interfaces extend the framework from design to operational readiness and dissemination.Future deployment should include site-specific authorization, detailed engineering and controlled validation before full-scale operation.

Acknowledgment: This work was carried out within the H-PORT - Hydrogen-Powered Port Optimization and Resilience Technology project, ECS 00000035, CUP D33C22000970006, developed under the cascading call of Spoke 4 "Smart and Sustainable Ports" of the RAISE innovation ecosystem within the Italian National Recovery and Resilience Plan (PNRR).

References

[1] Baratta, A., Fragiacomo, P., Genovese, M., Longo, F., Manfredi, K. A., Pagnotta, L., ... & Solina, V. (2026). Modeling Hydrogen Integration in Port Logistics. Procedia Computer Science, 277, 3899-3904.

[2] Baratta, A., Fragiacomo, P., Genovese, M., Longo, F., Manfredi, K. A., Pagnotta, L., ... & Solina, V. (2025). Hydrogen-Powered Transformation of Conventional Ports in Europe and the Mediterranean. Procedia Computer Science, 274, 1206-1212.



Decarbonization of a hard-to-abate process in steel making: effects of measured hydrogen plant performances on the techno-economic feasibility study

Beatrice Bulzacca*[a], Alessandro Guzzini[a], Emanuela Marzi[b], Giuseppe Nigliaccio[b], Marco Pellegrini[a], Cesare Saccani[a]

* corresponding author: Beatrice Bulzacca

[a] Department of Industrial Engineering, University of Bologna, Viale del Risorgimento 2, 40136 Bologna (BO), Italy.

[b] ENEA, TERIN-DEC-H2V, via dei Mille 21, 40121, Bologna, Italy.

Keywords: energy transition, hydrogen, steelmaking industry, techno-economic assessment

Abstract

The present study focuses on the decarbonization of the batch annealing process in the steel making industry, currently supplied by grey hydrogen from steam methane reforming. While techno-economic studies usually evaluate feasibility based on reference performances, few attempts have been made to adopt real renewable hydrogen plants' performances. This is due to the lack of open-source data about real plants' performance in dynamic conditions. This study aims to cover this gap and to evaluate the sensitivity of techno-economic results from the selected parameter. For the purpose, a model validated by using the experimental data obtained in a lab scale research facility was applied to a real Italian case study. A previous analysis optimized the size of the plant considered in this study by minimizing the Levelized Cost of Hydrogen (LCOH) through a Mixed Integer Linear Programming (MILP) algorithm. As a result, the implications of plant's real performances and relevant parameters on the economy of the investment and the use of resources were discussed.

Introduction: In energy transition, hydrogen-based technologies are considered as key solvers for the iron and steel industry (ISI). However, questions about sustainability still arise at their current state-of-the-art performance. Grey hydrogen (H_2) produced by steam methane reforming (SMR) is currently used in the annealing process. One possible short-term decarbonization solution is its substitution with renewable H_2. A multiplicity of studies assesses the techno-economic feasibility of investments on green H_2 production plants in ISI case studies. Techno-economic analyses are usually based on the assumption of a constant H_2 production efficiency of the plant [1,2]. Nonetheless, the plant efficiency varies with the load and the integrated operation of the system, which can include a compressor and a storage section.

Objectives: The current study presents a techno-economic evaluation of the investment on the substitution of grey H_2 with renewable H_2 in the reducing atmosphere of the highly convective batch

annealing plant of rolls products. The case study focuses on an Italian ISI plant aiming at covering the following research gaps: what is the impact of integrated hydrogen plant's dynamic behavior on the techno-economic assessment? What suggestions can be provided on the design and operation of the production plant connected to fluctuant and intermittent renewable sources to maximize the profit from the investment?

Material and methods: An experimental campaign was carried out on the dynamic behavior of an alkaline electrolyzer (AWE) connected to a buffer, a diaphragm compressor and a high-pressure storage. The experimental campaign has two objectives: (i) evaluation of the dynamic behavior of the electrolyzer to be used as input to model its performances in dynamic conditions, and (ii) modeling and assessment of the integration of different components on the whole plant performance. Starting from the optimal size of the green hydrogen production plant identified through MILP optimization algorithm, the study simulates the plant through a validated model developed in MATLAB/Simulink. The hydrogen demand of the batch annealing plant has been used as data input to run the simulation. LHV- and HHV-based hydrogen production efficiencies are considered, according to the definition of the JRC [3]. The techno-economic implications of the integrated plant performances are calculated and reported as incremental levelized cost of hydrogen (LCOH).

Results: Focusing on the experimental results of electrolyzer startup, the switch-on time progressively decreases with outside temperature. Hydrogen production efficiencies were normalized on the maximum value reached by HHV-based production efficiency. During the switch-on time (Figure 19) the electrolyzer efficiency progressively increases. In addition, when power is increased with a step function, the normalized H_2 production efficiency decreases temporarily due to the system inertia. Figure 20 highlights the dependency of H_2 production efficiency on the operation of the compressor. At the start of the compressor, the electrolyzer undergoes a temporaneous peak in the production efficiency. Once stabilized, the production efficiency is slightly higher during compression operation. The initial peak is due to the decrease of upstream pressure, that favors the discharge of hydrogen build-up in the filters present between the electrolyzer and the compressor.

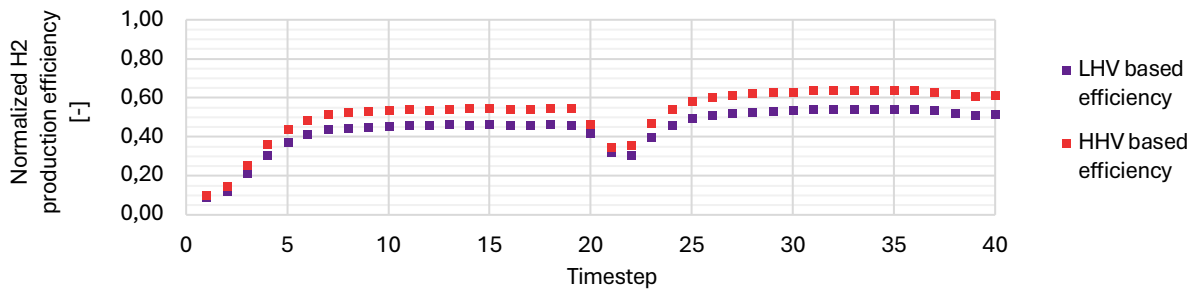


Figure 92. LHV- and HHV- based normalized efficiencies during hot startup and power step increase.

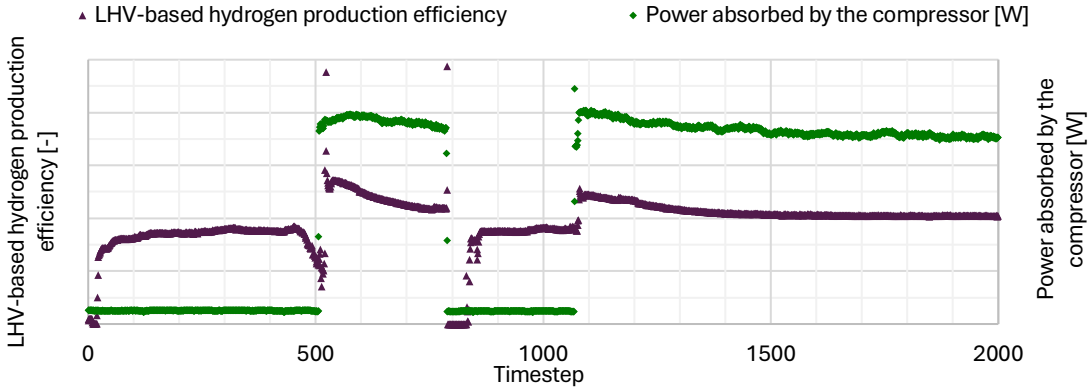


Figure 93. Compressor power and its influence on LHV-based hydrogen production efficiency.

Conclusions: To conclude, the hydrogen production and compression integrated plant undergoes performance variation when considering dynamic conditions and fluctuant renewable electricity, i.e., start and stop cycles, operating condition and load variations. Consequently, the preliminary techno-economic assessment of LCOH should be corrected by accounting for such variations. The validated model allows to investigate which parameters need attention for accurate feasibility studies. Then, recommendations on how to perform testing activities can be provided. Further steps of the study will include techno-economic assessment related to the real operation of other hydrogen production and compression integrated plant.

Acknowledgment

This work has been carried out in the framework of i) the Operational Research Plan (ROP) on green hydrogen developed by ENEA and funded by the Italian Ministry of Ecological Transition (project code: I83C22001170006) under the National Recovery and Resilience Plan (Mission 2. Investment 3.5) funded by the European Union under the Next Generation EU program, ii) the National Recovery and Resilience Plan (NRRP), Mission 4 Component 2 Investment 1.3—Call for tender No. 1561 of 11.10.2022 of Ministero dell'Università e della Ricerca (MUR); and by the European Union—NextGenerationEU. Award Number: Project code PE0000021, Concession Decree No. 1561 of 11.10.2022 adopted by Ministero dell'Università e della Ricerca (MUR), CUP I53C22001450006, according to attachment E of Decree No. 1561/2022, Project title "Network 4 Energy Sustainable Transition—NEST". The Authors also acknowledge Fores Engineering s.r.l for the support and the collaboration in the research activity.

References

[1] N. Usman, A. Javed, A. Ullah, R. Iftikhar, and M. O. Chaudhry, "Deployment of a green hydrogen-based energy solution for the hard-to-abate steel sector," *Int J Hydrogen Energy*, vol. 207, Feb. 2026, doi: 10.1016/j.ijhydene.2026.153540.

[2] A. Bhaskar, R. Abhishek, M. Assadi, and H. N. Somehesaraei, "Decarbonizing primary steel production: Techno-economic assessment of a hydrogen based green steel production plant in Norway," *J Clean Prod*, vol. 350, May 2022, doi: 10.1016/j.jclepro.2022.131339.

[3] G. Tsotridis and A. Pilenga, "EU harmonised protocols for testing of low temperature water electrolysers," 2021. doi: 10.2760/58880



Optimal green hydrogen generation design for the decarbonization of the steel industry: an Italian case study

Emanuela Marzi*[a], Beatrice Bulzacca[b], Alessandro Guzzini[b], Giuseppe Nigliaccio[a], Alberto Giaconia[a], Giulia Monteleone[a]

*corresponding author: emanuela.marzi@enea.it

[a]ENEA, Department of Energy Technologies and Renewable Sources (TERIN), via dei Mille 21, 40121, Bologna, Italy.

[b]Department of Industrial Engineering, University of Bologna, Viale del Risorgimento 2, 40136, Bologna, Italy.

Keywords: green hydrogen; MILP; optimal sizing; steel industry decarbonization.

Abstract

The steel industry is a major hard-to-abate sector, due to its high carbon dioxide emissions and high enthalpy energy demand. This study investigates an immediate decarbonization pathway by targeting the batch annealing stage, a process that already operates using 100 % hydrogen atmospheres. An Italian steel industry is taken as a case study, where the hydrogen is currently supplied to the process via on-site Steam Methane Reforming. Various decarbonization scenarios are analyzed, focused on the optimal sizing of a green hydrogen production plant aimed at minimizing the Levelized Cost of Hydrogen (LCOH), integrating an electrolyzer, a photovoltaic system and energy storage facilities. The findings demonstrate that by implementing strategically sized energy systems it is possible to achieve a fully decarbonized process with an LCOH of approximately 11.5 €/kg.

Introduction: The decarbonization of hard-to-abate sectors is pivotal to achieving global climate goals, with the steel industry standing out as one of the primary sources of anthropogenic greenhouse gas emissions within the heavy manufacturing sector. According to the International Energy Agency, the industry is responsible for 10 % of total global energy sector emissions [1]. Since steel is a fundamental material for global development, decarbonizing this sector poses unique challenges. In the steel refinery process, pure hydrogen (usually gray H_2) is already used in the batch annealing process, that consists of a cold rolling plant for steel refining, which uses hydrogen for the annealing process in bell furnaces [2].

Objectives: This study evaluates the optimal sizing of a hydrogen generation plant (photovoltaic system (PV), PEM electrolyzer, and storage units) for the batch annealing process decarbonization at Acciaierie d'Italia in Taranto (Italy). The process currently uses 100 % hydrogen, which is generated through on-site Steam Methane Reforming (SMR). The objective of this study is to assess the economic and technical feasibility of decarbonizing this process by determining the optimal size and operation of components using a Mixed-Integer Linear Programming (MILP) algorithm. Even though

the batch annealing detailed chemical process modeling is out of scope of this work, actual hydrogen demand profile is used for the analysis.

Material and methods: An optimal sizing algorithm based on MILP was used to perform the optimization of the test case over one year (8760 hourly time-steps), considering the hydrogen demand profile of the process. Figure 94 presents a schematic comparison between the actual baseline system and the proposed configuration (BES = Battery Energy Storage, HS = Hydrogen Storage, PEM = PEM electrolyzer).

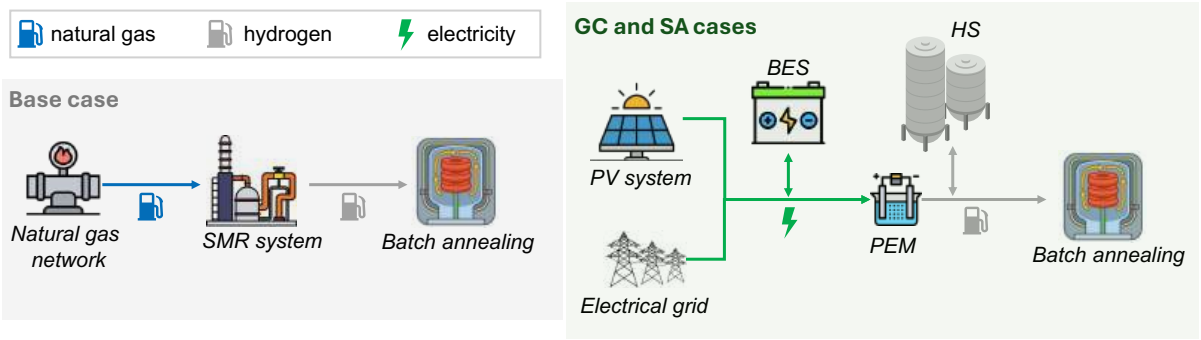


Figure 94: layout of the energy systems considered.

Based on the layout of the system, different case studies are investigated:

- **Base case**: the current plant (with hydrogen generated through SMR);
- **Case GC**: grid-connected (GC) system composed of PV and PEM electrolyzer, BES and HS;
- **Case SA**: Stand-alone (SA) system composed of PV, PEM electrolyzer, BES and HS;
- **Case SA – HS** and **Case SA – BES**: SA systems in which only one kind of storage is allowed: HS and BES, respectively.

The techno-economic parameters for the energy system components are sourced from literature [3,4], with water and natural gas prices taken from [5]. To account for market volatility, a sensitivity analysis was carried out to evaluate different electricity purchase and selling prices. The objective function minimizes the Levelized Cost of Hydrogen (LCOH), encompassing investment, replacement, maintenance, and network operating costs.

Results: An LCOH of 2.9 €/kg was obtained for the base case, while the sizing configurations and LCOH obtained for the other cases are summarized in Table 1, normalized to the peak thermal power of the hydrogen demand. The base case scenario has the lowest LCOH, followed by grid-connected cases, in which electricity price is varied between 50 and 250 €/MWh: nonetheless, in both cases the hydrogen generated is not entirely green hydrogen, as part of the

	Case GC	Case SA	Case SA – HS	Case SA – BES
PV (-)	0.9 ÷ 4.1	6.5	6.7	11.3
PEM (-)	0.7 ÷ 1.9	2.2	2.9	1.7
BES (h)	0.0 ÷ 1.8	6.0	-	81.2
HS (h)	6.1 ÷ 12.6	73.3	87.3	-
LCOH (€/kg)	**4.2 ÷ 8.7**	**11.5**	**11.9**	**29.2**

Table 14: optimal nondimensional sizes and LCOH obtained in the three simulations.

electricity comes from the grid. It is worth noting that carbon taxes of CO_2 emissions were excluded from this analysis; incorporating them would inevitably increase the LCOH in these scenarios. Comparing the stand-alone systems, the most convenient in terms of cost and efficiency is the system with both storages, allowing an LCOH of about 11.5 €/kg. Figure 95 shows how the components CAPEX and OPEX influence LCOH in the two case studies with the lowest and highest electricity price considered, and the SA case study.

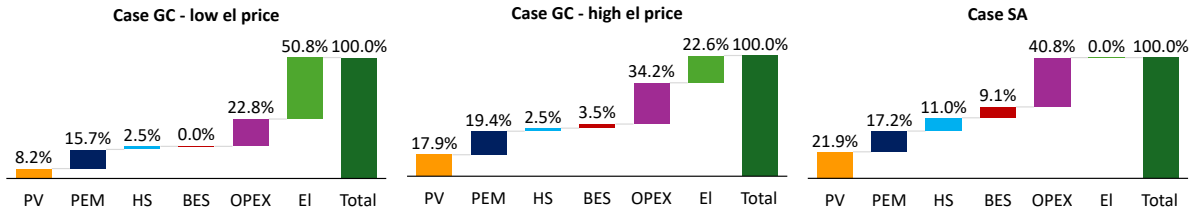


Figure 95: Impact of components and OPEX on LCOH (El = electricity bought).

Conclusions: The work at hand analyzes different pathways to take the first step towards for the decarbonization of steel industries. The batch annealing process of a steel industry located in Italy was considered. The process already uses hydrogen, which is currently produced by methane steam reforming. By integrating a PV system, a PEM electrolyzer, battery and hydrogen storage units, a fully decarbonized process can be achieved with an LCOH of about 11.5 €/kg. The cost is not yet competitive with that grey hydrogen, but effective policy support and technologies innovation could bridge this gap.

Acknowledgment: *This work has been carried out in the framework of the Operational Research Plan (POR) on green hydrogen developed by ENEA and funded by the Italian Ministry of Ecological Transition (project code: I83C22001170006) under the National Recovery and Resilience Plan (Mission 2. Investment 3.5) funded by the European Union under the Next Generation EU program.*

References

[1] IEA (2020), *Iron and Steel Technology Roadmap*, IEA, Paris https://www.iea.org/reports/iron-and-steel-technology-roadmap, Licence: CC BY 4.0.

[2] Pivetta, D.; Dall'Armi, C.; Taccani, R. Multi-Objective Optimization of a Hydrogen Hub for the Decarbonization of a Port Industrial Area. J. Mar. Sci. Eng. 2022, 10, 231.

[3] Marocco, Paolo, Marta Gandiglio, and Massimo Santarelli. "Optimal design of PV-based grid-connected hydrogen production systems." *Journal of Cleaner Production* 434 (2024): 140007.

[4] Gandrik, A.M., Wood, R.A., Patterson M.W., Mills P.M., HTGR-integrated Hydrogen Production via Steam Methane Reforming Process Analysis, Idaho National Laboratory, Idaho Falls (ID), 2010 September, p. 49. Technical Evaluation Study TEV-954 Project No. 23843.

[5] Arera website (Autorità di Regolazione per Energia Reti Ambiente), Dati e Statistiche (https://www.arera.it/)



Mechanical Recovery of Platinum-Based Cathode Catalysts: A Circular Economy Approach for Sustainable and Cost-Effective PEM Technologies

Nerea López García *[1], Irene Peñas Fuertes[1], Juan Carlos Carmona Pulido[1], Jesús Serrano-Jiménez[1], Francisco Javier Patiño[1], Ana Belén Megías[1], Julia Isidro Elvira[1], Jesús Rodríguez Ruiz[1]

* nerea.lopez@cnh2.es

[1] National Hydrogen Center (CNH_2), Puertollano, Spain

Keywords: PEM electrolysis, PEM fuel cells, platinum recycling, circular economy, catalyst recovery, electrochemical characterization, techno-economic assessment

Introduction*:* The large-scale deployment of proton exchange membrane (PEM) technologies is considered essential for the development of a sustainable hydrogen economy. However, platinum group metals (PGMs) remain one of the main contributors to system cost and supply risk [1]. While significant efforts have focused on reducing catalyst loading, catalyst recovery and reuse offer an additional pathway to improve both sustainability and economic competitiveness.

Despite recent advances in platinum recycling, most reported recovery strategies rely on hydrometallurgical treatments involving catalyst dissolution and re-synthesis, which increase process complexity, reagent consumption and environmental impact. Typical approaches include acid leaching followed by platinum separation through solvent extraction, precipitation or electrochemical recovery, and subsequent catalyst re-synthesis on fresh carbon supports [2–4]. In contrast, direct mechanical recovery routes seek to preserve a significant fraction of the original catalyst structure, while avoiding platinum dissolution and extensive chemical processing. However, limited information is available regarding the direct mechanical recovery and reuse of Pt/C catalysts from exhausted PEM electrolyzer components and its potential benefits from both electrochemical and techno-economic perspectives. Addressing this gap is essential for developing practical circular economy strategies capable of reducing the dependence on virgin platinum resources while maintaining the performance of PEM technologies.

Objective: The objective of this work is to develop and validate a direct mechanical recovery route for Pt/C catalysts from exhausted porous transport layers (PTLs) of PEM electrolyzers and to compare its performance with conventional platinum recycling methodologies, such as hydrometallurgical routes based on catalyst dissolution, platinum separation and catalyst re-synthesis [2–4], through electrochemical characterization in a three-electrode cell and in a PEM fuel cell, as well as through techno-economic assessment.

Materials and methods: As illustrated in *Figure 1,* Pt/C (with residual Nafion) catalyst was mechanically recovered from end-of-life titanium PTLs through a combination of surface brushing, ultrasonic-assisted cleaning and subsequent drying steps, enabling the detachment of catalyst

particles from the titanium substrate, thereby avoiding the platinum dissolution and catalyst re-synthesis steps typically involved in conventional hydrometallurgical recycling routes. The recovered material was reformulated into catalyst inks (Pt/C and Nafion) and redeposited onto new carbon-based substrates by spray coating.

Morphological characterization was performed by SEM–EDS and Pt content was quantified by ICP, while electrochemical performance was evaluated through cyclic voltammetry (CV), linear sweep voltammetry (LSV) and electrochemically active surface area (ECSA) determination in a three-electrode cell using a glassy carbon rotating disk electrode (RDE), a 0.5 M H_2SO_4 electrolyte, an Ag/AgCl reference electrode and a platinum counter electrode. Recycled catalyst was also integrated into PEM fuel cell assemblies and assessed through polarization curves and electrochemical impedance spectroscopy (EIS). Catalyst inks for both RDE characterization and PEM fuel cell testing were prepared from the same recovered catalyst and contained the same components (Pt/C, Nafion and solvent mixture), although their relative proportions were adapted to the requirements of each deposition method.

A preliminary comparative techno-economic assessment was conducted considering catalyst recovery efficiency, process complexity and expected cost reduction potential. The overall catalyst recovery, reformulation and validation workflow is summarized in *Figure 1*.

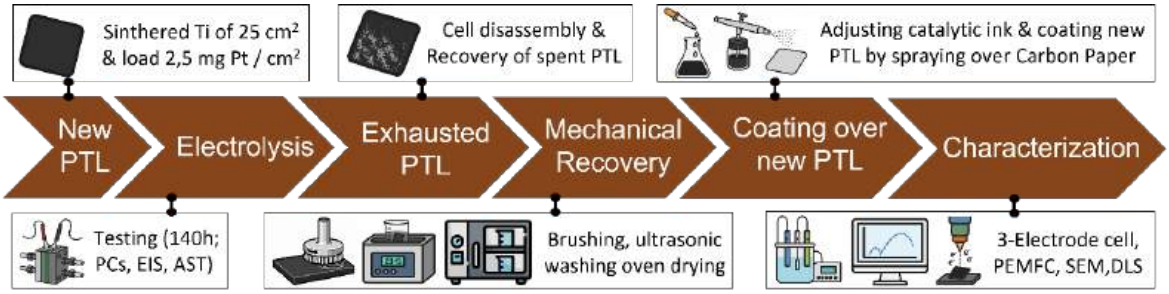


Figure 1. Mechanical recovery workflow for Pt/C catalyst recycling from exhausted PEM electrolyzer PTLs.

Results: Recovery efficiencies of up to 95% were achieved using the proposed methodology. Following electrochemical activation, mechanically recovered catalysts exhibited ECSA values approaching those obtained with fresh commercial Pt/C catalysts, indicating preservation of a significant fraction of the active platinum surface. As shown in *Figure 2a*, progressive electrochemical activation resulted in a substantial improvement of the recovered catalyst response. SEM–EDS analyses revealed differences in catalyst morphology and platinum distribution between fresh and recycled materials, although electrochemical characterization confirmed that the recovered catalyst retained relevant catalytic activity.

As shown in *Figure 2b*, PEM fuel cell testing further demonstrated the technical feasibility of catalyst reuse under realistic operating conditions. However, despite the promising ex situ electrochemical activity observed through ECSA measurements, the performance of the recycled catalyst in the fuel cell remained significantly below that of the fresh catalyst reference. This result may suggest that the electrochemical activation procedure currently applied ex situ does not directly translate into optimal

catalyst utilization within the membrane electrode assembly. Nevertheless, increasing catalyst loading partially compensated for these losses and enabled operation closer to reference values, confirming the potential of the proposed recovery strategy.

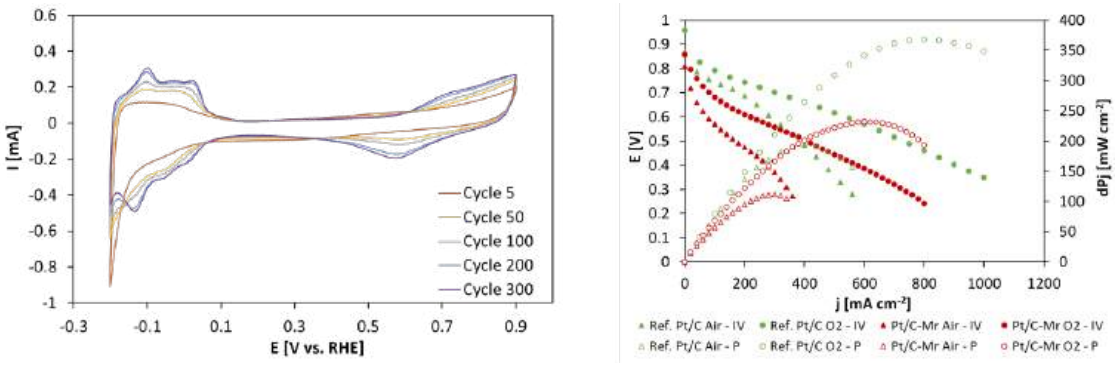


Figure 2. (a) Electrochemical activation and ECSA evaluation of mechanically recovered Pt/C catalysts. (b) PEM fuel cell performance comparison between fresh and mechanically recovered catalysts.

Preliminary results suggest that eliminating catalyst dissolution and re-synthesis steps may reduce reagent consumption, process complexity and associated costs, while simultaneously improving resource circularity and reducing environmental impact.

Conclusions: A direct mechanical recovery route for platinum-based cathode catalysts from exhausted PEM electrolyzer PTLs has been successfully demonstrated. The recovered catalyst retained relevant electrochemical activity and was successfully validated in PEM fuel cell operation.

This approach offers a simpler and more sustainable alternative to conventional recycling routes, with potential benefits in catalyst cost reduction and circularity. Future work will focus on optimizing catalyst activation to improve platinum utilization and cell performance.

References

[1] U.S. Department of Energy. *Hydrogen and Fuel Cell Technologies Office Multi-Year Program* Plan (MYPP) 2024. Washington, D.C., USA, 2024.

[2] Staudacher, M. et al. *Recycling*, 10 (3), 121, 2025.

[3] Montiel, M.A. et al. *Applied Catalysis B: Environmental*, 327, 122414, 2023.

[4] Jha, M.K. et al. *Hydrometallurgy*, 133, 23–32, 2013.



Techno-economic modelling of a hydrogen valley in Italy: a multi-scenario analysis of the Levelised Cost of Hydrogen

Andrés Yáñez*[a], Claudia Bassano[b], Christian Aragón-Briceño[a], Carlos Camacho[a], Mónica Calero[c], María Ángeles Martin-Lara[c]

* corresponding author: ayanez@fcirce.es

[a] CIRCE Foundation. Dinamiza Business Park, Ranillas Avenue Building 3D 1st Floor, 50018 Zaragoza Spain

[b] Department of Energy Technologies and Renewable Sources, Energy and Sustainable Economic Development Research Centre of Casaccia, ENEA, Italian National Agency for New Technologies, Santa Maria di Galeria, 00123 Rome, Italy

[c] Department of Chemical Engineering, Faculty of Sciences, University of Granada, 18071 Granada, Spain

Keywords: electrolysis, hydrogen valley, levelised cost of hydrogen, techno-economic assessment

Abstract

Introduction: Hydrogen valleys are a key element to support the deployment of a decarbonized and independent European energy system, creating local and regional ecosystems that cover the full hydrogen value chain. The EU is currently the frontrunner for the implementation of these hydrogen ecosystems, which are mainly supported through the Clean Hydrogen Joint Undertaking (JU), which has supported to date 22 hydrogen valleys across 20 European countries. These valleys can create the basis for a wider hydrogen economy by laying out the necessary infrastructure. So, the long-term economic sustainability of the valleys is key to their success and expansion. However, the roll-out of hydrogen valleys may be limited in multiple EU regions due to factors aspects, such as high electricity prices, grid congestion, low renewable energy penetration and lack of demand, which would make them unfeasible to sustain in the long run. So, to accelerate hydrogen valleys implementation, it is necessary to better understand the factors affecting their economic feasibility, as well as to develop tools that support effective evaluation and planning.

Objectives: The main objective of the present study is to develop a techno-economic model of a potential hydrogen valley in the region of Emilia-Romagna (Italy) by presenting a design of a hydrogen production system tested under different scenarios to understand the main parameters affecting the LCOH.

Material and methods: A techno-economic hourly model of the hydrogen valley was developed in Python, integrating electrolytic hydrogen production (ALK/PEM), methanation, hydrogen storage, and

renewable electricity production from PV. The data for modelling the hydrogen production and storage were extracted from Clean Hydrogen JU SRIA, considering the state-of-the-art data of 2020 [1]. The typology of the hydrogen valley has been selected to be representative for the Italian industrial and energy landscape, characterized by high energy prices, low RES penetration (despite a relatively high solar resource potential) and an extensive capillary natural gas grid. So, this typology can be used as blueprint that could be replicated into other Italian and EU regions. Three end-uses have been considered: (i) production of synthetic natural gas (SNG) to be injected into the gas grid; (ii) use as a fuel in a ceramic industry; (iii) supply a Hydrogen Refueling Station (HRS) for buses and trucks. The annual valley demand was considered constant, with the following considerations for each individual demand. SNG: based on existing CO_2 flows from a local biomethane plant. Ceramic: average natural demand for a ceramic furnace [2]. HRS: set at 6 trucks and 6 city buses to recharge daily. The hydrogen production system and the RES plant were then designed to ensure that at least 99.5% of the expected annual demand is covered. Three scenarios have been considered: Scenario 1: all the electricity needs are imported from the grid; Scenario 2: the electrolyser is fully disconnected from the grid, and all electricity is provided by the RES plant; Scenario 3: a hybrid scenario where the electricity is supplied by both the electricity grid and the RES plant.

The electricity price was calculated as the 5-year average of non-household electricity prices in Italy and was maintained constant at 17.54 c€/kWh [3]. The project duration was set in 30 years, while the Weighted Average Cost of Capital (WACC) was set at 6%. In all three scenarios, a sensitivity assessment has been done to find the minimum LCOH in each of them. Once the optimal factors are found for each scenario, a sensitivity assessment on the effect of the electricity prices on the LCOH was performed. Finally, for the most favorable scenario, a tornado diagram has been performed to find the most relevant factors affecting LCOH.

Results: The characteristics of the hydrogen production system in each of the scenarios, together with the expected LCOH are shown in Table 1. The most favourable scenario with the electricity prices considered is the hybrid one (Scenario 3), with a LCOH of 12.41 €/kg.

Table 1. Summary of the hydrogen production system design parameters

Scenario	Electrolyser size (MW) and type	PV size (MW)	BESS capacity (MWh) and power (MW)	Hydrogen storage capacity (h of valley demand)	LCOH (€/kg)
Scenario 1	7.5 – ALK	-	-	72 h	14.63
Scenario 2	42.5 – ALK	80	250 MWh /35 MW	480 h	20.18
Scenario 3	7.5 - ALK	19	-	72 h	12.41

Figure 2 shows the results of the tornado diagram for different parameters affecting the LCOH for Scenario 3. Electricity price is by far the most relevant factor. A change in 20% of the electricity price is translated into a variation of around 10% of the LCOH, showing a significant impact. The capex of

the PV plant and the WACC also have a relevant impact, but in both cases is only around 2% of the LCOH.

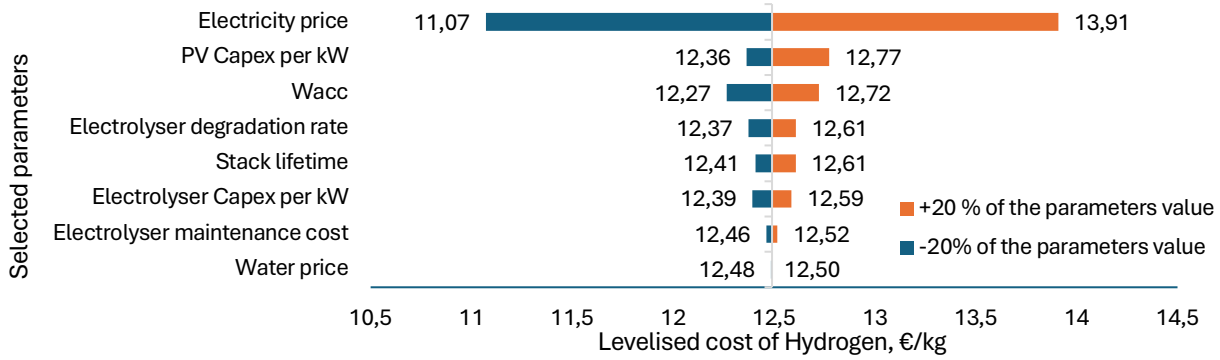


Figure 2. Impact of selected factors on the estimated Levelised Cost of Hydrogen for the Scenario 3

Conclusions: The preliminary results of this study indicate that hydrogen is not competitive in the studied scenarios due to high electricity prices. Still, the combination of a local PV-plant and supply via electric grid seems to be the most favorable option. Electricity prices have a significant impact on the overall feasibility of the valley, so efforts should focus on reducing their cost. So, the next step will involve the assessment of the financial feasibility for different business cases and assets property model in the valley, as well as of different subsidies schemes. The goal will be to select the most suitable managerial and financial option for setting-up the valley and to support public entities in the design of an effective and sustainable subsidies scheme to stimulate its development.

Acknowledgment: The author acknowledges the support provided by the European Union's Horizon Europe programme, through the projects TH2ICINO (GA: 101138473) and H2B:IMPACT (GA: 101138473) and the Mission Innovation Italy through the ENEA Hydrogen demo Valley.

References

[1] Strategic Research and Innovation Agenda (SRIA) 2021-2027 of the Clean Hydrogen JU

[2] G. Graditi, C. Bassano, N. Cerone, P. Deiana, G. Monteleone, M. Beccarello, A. Andreuzzi. Piano d'azione idrogeno focus tecnologie industriali: Potenzialità dell'industria nazionale nella prospettiva della transizione ecologica e mappatura dei potenziali Off-Takers, ENEA/Confindustria, 17 Gennaio 2022

[3] Eurostat, Electricity prices for non-household consumers, https://doi.org/10.2908/NRG_PC_205, 23/12/2025



Social Life Cycle Assessment of green hydrogen technologies: a systematic review and commentary from a social science perspective

Francesco Bartolomei * [a, c], Jacopo Bindi [b], Giuseppe Pellegrini Masini [b], Alessandro Agostini [b], Dario Padovan [a], Viviana Cigolotti [b], Giulia Monteleone [b]

* Corresponding author

[a] University of Turin - Department for Cultures, Politics and Society | IUSS Pavia, PhD Program in Sustainable Development and Climate Change (SDC)

[b] ENEA – Italian National Agency for New Technologies, Energy and Sustainable Economic Development

[c] IUSS Pavia - School for Advanced Studies Pavia

Keywords: green hydrogen, social life cycle assessment, social sustainability, social sciences

Introduction

Green hydrogen has rapidly emerged as a central element of global energy transition strategies, attracting substantial public and private investment and raising questions about its environmental, economic, and social sustainability. While the techno-economic and environmental aspects of hydrogen supply chains are the object of a considerable amount of ongoing research, the associated social impacts remain comparatively under-investigated. The Social Life Cycle Assessment (S-LCA) methodology has established itself over the past decade as the reference framework for evaluating social impacts along product life cycles, building on the UNEP Guidelines [1] and, more recently, on a dedicated ISO standard (ISO 14075). Within the hydrogen sector, S-LCA guidelines have been developed (e.g. in the European SH2E Project concluded in 2024), though key methodological issues remain debated.

Objectives

This paper addresses three interconnected objectives: (1) to map the state of the art of S-LCA studies applied to green hydrogen technologies, documenting operative choices such as functional units, system boundaries, stakeholder categories, impact subcategories and databases used, identifying convergences and differences; (2) to critically examine the internal methodological limitations and uncertainties present in current S-LCA applications, as evidenced by the reviewed literature; and (3) to offer a commentary on S-LCA practice from a social science perspective, discussing the "eloquence" of the methodology - what it can and cannot capture - and its suitability to represent the social pillar of sustainability assessments of emerging socio-technical systems.

Methods

The review covers S-LCA and LCSA studies of green hydrogen technologies published up to May 2026. Relevant literature was identified through a systematic keyword search on two databases, SCOPUS and Web of Science, using a query combining terms related to social life cycle assessment ("social life cycle assessment", "s-lca", "social LCA", "lcsa") and hydrogen technologies ("hydrogen", "electrolyzer", "fuel cell"). The initial SCOPUS search returned 51 documents, refined to 29 peer-reviewed English-language articles; the Web of Science search returned 21 articles. Following the PRISMA protocol we applied a manual screening based on a strict relevance criterion - restricting inclusion to studies directly addressing the social impacts of hydrogen production or of components related to its supply chain. A final corpus of 17 articles was identified consistently across both databases. Purely methodological papers drawing on existing S-LCA data and LCSA studies not performing a dedicated social assessment were excluded. The selected studies were analysed by comparing their operative choices across key dimensions, and the findings were then interpreted through both an internal methodological lens and a broader social science perspective.

Results

The review reveals that the literature is still scarce but the attention on the topic is growing. The majority of studies reviewed analysed hydrogen production systems (over 50%) with a predominantly cradle-to-gate boundary and rarely specified final use. Workers and Society are the most frequently addressed stakeholder categories. Geographically, all but two scenarios are situated in European countries, with Germany, Austria, Spain, and Portugal most commonly represented. The Reference Scale (Type I) impact assessment approach is adopted across all the reviewed studies, while it should be highlighted that no study employs direct assessment through qualitative research (e.g., fieldwork) or the Impact Pathway (Type II) approach. The most consistently identified social risk hotspots are located in upstream supply chains, particularly in the extraction and processing of critical raw materials in geographies characterized for high social risk (e.g., rare earths and Nafion from China; iridium, platinum, titanium from South Africa). A descriptive cross-study finding is that the supply chain complexity can be considered a primary driver of social risks: off-site value chains extending through Global South countries systematically present worse social outcomes than on-site or domestic configurations, with impacts increasing by considerable factors [2] [3] [4]. The few studies extending their scope beyond Europe (to North Africa and Western Asia) confirm this pattern highlighting high social risk profiles related to fair salary and child labour subcategories. The review also points out to significant internal methodological debates such as the system boundary definition and cut-off criteria, the choice of activity variable database dependence and the limited granularity of country-sector average risk indicators. A critical interpretation of findings at a broader epistemic level identifies the methodological risk of considering a weighted average of generic country-sector social risk exposure levels as the actual “social impacts” or “social implications” of a technology during his life cycle. S-LCA origins in environmental LCA methodology raise concerns about the adequacy of the

transposition of the LCA frameworks into the social domain for capturing project- and context-specific social impacts and structural, systemic, and long-term societal dynamics.

Conclusions

S-LCA offers a structured and increasingly standardised approach to screen the social risk embedded in green hydrogen supply chains, and its role in policy and business contexts is expected to grow in the next years. However, the present review highlights that its usual application require significant development to fulfill its epistemological objectives. From the authors' interpretation the methodological priorities identified include: advancing Type II (Impact Pathway) approaches, also exploring the form of qualitative cause-effect mapping; strengthening database granularity to capture territorial and contextual specificity; developing clearer guidance on system boundaries and activity variables for hydrogen systems and, crucially, deepening the integration between S-LCA and the social sciences community, ensuring that social assessment tools orienting policies towards a fairer governance of global supply chains and a just transition are both robust and critically grounded.

Acknowledgment: This research has been developed as a part of a PhD program in Sustainable development and Climate Change founded by ENEA under the PORH2

Key Bibliographical References:

[1] UNEP, 2020. Guidelines for Social Life Cycle Assessment of Products and Organizations 2020. Benoît Norris, C., Traverso, M., Neugebauer, S., Ekener, E., Schaubroeck, T., Russo Garrido, S., Berger, M., Valdivia, S., Lehmann, A., Finkbeiner, M., Arcese, G. (eds.). United Nations Environment Programme (UNEP).

[2] Martín-Gamboa, M., Mancini, L., Eynard, U., Arrigoni, A., Valente, A., Weidner, E., & Mathieux, F. (2025). Social life cycle hotspot analysis of future hydrogen use in the EU. The International Journal of Life Cycle Assessment, 30(6), 1379-1396.

[3] dos Reis, R. A., Rangel, G. P., & Neto, B. (2024). Social life cycle assessment of green hydrogen production: Evaluating a projected Portuguese industrial production plant. *Renewable Energy*, *235*, 121293.

[4] Akhtar, M. S., Khan, H., Liu, J. J., & Na, J. (2023). Green hydrogen and sustainable development–a social LCA perspective highlighting social hotspots and geopolitical implications of the future hydrogen economy. *Journal of Cleaner Production*, *395*, 136438.



From Scrap to Storage: Life Cycle and Circularity Assessment of $TiFe_{0.80}X_{0.20}$ Alloys for Hydrogen Storage

Francesca Garelli,*[a] Claudio Carbone,[b] Alessandro Agostini,[b] Jacopo Bindi,[b] Viviana Cigolotti,[b] Giulia Monteleone,[b] Marcello Baricco,[a] Paola Rizzi,[a] Giuseppe Di Florio[b]

* corresponding author: francesca.garelli@unito.it

[a] Department of Chemistry and NIS, INSTM, University of Turin, Via Pietro Giuria 7, 10125 Torino, Italy

[b] ENEA: Italian National Agency for New Technologies, Energy and Sustainable Economic Development (ENEA), via Anguillarese 301, Rome 00123, Italy

Keywords: Circular economy, Hydrogen storage, Life Cycle Assessment, TiFe-based alloys

Abstract

Introduction:

Hydrogen is increasingly recognized as a cornerstone of the transition toward a low-carbon energy system; however, its efficient and sustainable storage remains a major technological challenge. Among the available options, solid-state hydrogen storage based on metal hydrides offers high volumetric density and improved safety compared with compressed or liquid hydrogen systems [1], [2]. In this context, TiFe-based intermetallic alloys are promising candidates because of their relatively low cost, moderate operating temperature and pressure, and tunable hydrogen sorption properties through elemental substitution [3].

Despite extensive research on their hydrogen storage behavior, the environmental performance and circularity potential of TiFe-based alloys remain only partially explored. This is particularly relevant for substituted TiFe alloys, where used elements may improve activation and reversible capacity, but can also introduce environmental burdens associated with critical raw materials, such as titanium and cobalt. Moreover, the use of secondary raw materials from production or end-of-life scraps is a promising route to reduce environmental impacts, although the final benefit depends on scrap composition, recycling route and the resulting hydrogen storage performance [4].

Objectives:

The purpose of this work is therefore to develop an integrated circularity framework of TiFe-based alloys, linking hydrogen storage performance, alloy chemistry, activation requirements and secondary-material pathways. The proposed approach is built on the use of a service-based environmental assessment, in which TiFe-based alloys are compared according to the actual amount

of hydrogen reversibly stored and delivered, rather than only by their nominal composition or maximum theoretical capacity.

Material and methods:

A cradle-to-gate Life Cycle Assessment (LCA) was performed for TiFe0.80X0.20 alloys (X = Co, Cu, Cr, Al), considering both laboratory-grade and scrap-based production routes. The system boundaries include alloy synthesis by arc melting, optional annealing for Cr- and Al-substituted alloys, and hydride activation, explicitly accounting for hydrogen irreversibly consumed during the activation process. Environmental impacts were assessed within the EF/PEF framework, while circularity was evaluated using the Circular Footprint Formula (CFF) [5].

To reflect the service provided by hydrogen storage materials, two functional units were adopted: 1 kg of stored hydrogen based on (i) maximum storage capacity and (ii) reversible storage capacity under realistic operating conditions. Hydrogen storage and activation data were taken from experimental datasets previously reported for the same alloy compositions [6]. Scrap-based scenarios were defined by varying the recycled content of Ti, Fe and the alloying element X, according to conservative and optimistic assumptions derived from SCRREEN critical raw material reports [7].

Results:

Results show that environmental impacts are governed by the interplay among alloy chemistry, hydrogen storage efficiency and activation requirements. When impacts are normalized to the maximum hydrogen storage capacity, Cr-substituted alloys exhibit the lowest environmental impacts. However, when reversible capacity is used as functional unit, Co-substituted alloys emerge as the lowest-impact option, because of their higher usable hydrogen capacity. This confirms that the environmental ranking of metal hydrides changes substantially when the functional unit is based on the real storage service delivered by the material.

Scrap-based scenarios reveal that impact reductions are not simply proportional to recycled content: the chemical composition of the secondary feedstock is decisive. Chromium-rich steels minimize the need for primary Cr additions, while high recycled titanium fractions consistently lower impacts across all compositions. By contrast, cobalt recycling from spent lithium-ion batteries may provide limited or even adverse benefits in some categories, because current recovery routes can be energy- and reagent-intensive.

Conclusions:

Sustainable design of TiFe-based hydrogen storage alloys requires a holistic approach that simultaneously considers reversible hydrogen performance, activation conditions, alloy chemistry and the specific chemistry of secondary feedstocks and recycling impacts. The main innovation of this work is the integration of LCA, circularity modelling and experimental hydrogen storage data into

a single service-based framework. This approach provides quantitative guidance for designing circular and environmentally efficient hydrogen storage materials suitable for large-scale deployment in future hydrogen and fuel cell systems.

Acknowledgment

This research was funded by the European Union – NextGeneration EU from the Italian Ministry of Environment and Energy Security POR H2 AdP MASE/ENEA with involvement of CNR and RSE, PNRR - Mission 2, Component 2, Investment 3.5 "Ricerca e sviluppo sull'idrogeno", CUP: I83C22001170006.

References

[1] K. T. Møller et al., "Hydrogen - A sustainable energy carrier," Prog. Nat. Sci.: Mater. Int., vol. 27, no. 1, pp. 34–40, 2017.

[2] N. Klopčič et al., "A review on metal hydride materials for hydrogen storage," J. Energy Storage, vol. 72, p. 108456, 2023.

[3] E. M. Dematteis et al., "Substitutional effects in TiFe for hydrogen storage: a comprehensive review," Mater. Adv., vol. 2, no. 8, pp. 2524–2560, 2021.

[4] Y. Shang et al., "Developing sustainable FeTi alloys for hydrogen storage by recycling," Commun. Mater., vol. 3, no. 1, p. 101, 2022.

[5] R. Pant et al., Suggestions for updating the Product Environmental Footprint (PEF) method. Luxembourg: Publications Office of the European Union, 2019.

[6] F. Garelli et al., "Kinetics tuning of TiFe alloys by elemental substitution: Enabling activation under moderate conditions," Int. J. Hydrogen Energy, vol. 162, p. 150720, 2025.

[7] SCRREEN Project Consortium, "SCRREEN – CRMS 2023," 2023. [Online]. Available: https://scrreen.eu/crms-2023/



Lessons learned from the PEFCR development process: the case of the Fuel Cells and Hydrogen PEFCR for hydrogen storage devices

C. Carbone[a*], G. Di Florio[b], S. Maranghi[c], A. Zamagni[c], K. Ben Hnich[d], D. Iribarren[d], S.K.R. Maddula[d], T.M. Bachmann[e], Y.C. Wang[f], A. Agostini[b].

* corresponding author: C. Carbone

[a] ENEA, Bologna, Italy

[b] ENEA, Rome, Italy

[c] Ecoinnovazione, Bologna, Italy

[d] IMDEA Energy, Madrid, Spain

[d] EIFER, Karlsruhe, Germany

[b] Hexagon Purus GmbH, Kassel, Germany

Keywords: PEF, PEFCR, hydrogen supply chain, LCA, hydrogen storage.

Abstract

Introduction: Hydrogen is widely seen as a key pillar of decarbonisation due to its potential across industry, transport and energy systems. However, most current hydrogen production relies on fossil fuels (mainly natural gas and coal), raising significant environmental concerns. Transparent, robust assessment frameworks are therefore needed to quantify impacts of hydrogen technologies and inform policy, market and investment decisions during the energy transition.

At the European level, the demand for transparency and methodological consistency prompted the European Commission's Environmental Footprint (EF) framework (Commission Recommendation 2021/2279); a revised version is expected by the end of 2026. Within this framework, Product Environmental Footprint Category Rules (PEFCR) give product-specific guidance to ensure LCA results are comparable for products delivering equivalent functions.

While PEFCRs have been established and are under development for some strategic sectors, such as tourism and space, they are not available for hydrogen and fuel cell systems, while guidelines for conducting LCA on hydrogen and fuel cells have been developed along the years[3]. This challenge is addressed by the HyPEF project ("Promoting an Environmentally Responsible Hydrogen Economy by Enabling Product Environmental Footprint Studies"; http://hypef.eu), by supporting the development of harmonised rules and the consolidation of high-quality life cycle data. Within this context, a categorisation of hydrogen and fuel cell systems along the hydrogen value chain has been defined to

[3] Recent guidelines have been developed in the framework of the SH2E project (https://sh2e.eu/project/) and eGHOST (https://eghost.eu/)

identify key methodological aspects for supporting the definition of hydrogen PEFCRs (Ben Hnich et al., 2026). The suggested approach begins with the identification of hydrogen and fuel cell (FCH) systems based on a market analysis covering commercially available and pre-commercial products across the entire hydrogen life cycle (Bachmann et al., 2024). This analysis aimed to ensure that the further categorisation reflects current and near-future technologies and products.

Based on this, hydrogen products have been grouped into five families corresponding to the main stages of the hydrogen value chain, encompassing hydrogen production, conditioning, storage, transport, and end use. Following the identification of hydrogen devices, a categorisation process was also applied in accordance with the rules set out by the European Commission Recommendation 2021/2279 (European Commission, 2021), and two levels of product categorisation have been considered (Ben Hnich et al., 2026): Product Categories and Product Subcategories. Within HyPEF, PEFCRs were developed for two product subcategories and one product category: PSC1.2—electrochemical devices for hydrogen production; PSC5.4—tanks for compressed hydrogen storage for heavy-duty mobility; and PC9—hydrogen fuel cells for electricity generation. This work reports the results of case studies conducted to validate the PEFCRs for hydrogen storage devices (product subcategory PSC5.4).

Objectives: The objective of the present work is to provide consistent insights into the methodological aspect that need to be addressed for Environmental LCA Footprint applied to hydrogen storage devices (product subcategory PSC5.4). This includes the functional unit and reference flow, system boundaries, multifunctionality approach, relevant impact categories, all of which allow for a robust characterisation and fair comparison of hydrogen storage systems.

Material and methods: The HyPEF FCH-PEFCRs were tailored to be tested in three life-cycle case studies and the representative product (RP), and were aligned with the EC recommendations 2021/2279, regarding the use of EF methods to measure and communicate the life cycle environmental performance of products and organisations.

The case studies and RP were chosen based on dominant applications and market traits. Heavy-duty mobility is currently the most promising application, with compressed hydrogen tanks as the leading technology. Both Type III and Type IV tanks are used in this sector, but Type IV tanks are considered state-of-the-art: they are lighter than Type III tanks, and Type III—although currently cheaper—are expected to lose favour as mobility markets grow. Type IV costs are expected to decline with large-scale adoption. Reliable market-share data for Type III versus Type IV in heavy-duty applications are not yet available because the market is very small, and Type V tanks remain under development. For these reasons the case studies selected for the draft PEF-RP study of hydrogen storage (PSC5.4) are commercial, Type IV compressed hydrogen tank manufactured by Hexagon Purus (Ben Hnich et al., 2026).

Results: The most relevant impact categories were identified following the guidelines in EC recommendations 2021/2279. First, the normalized and weighted results were organized from the highest to the lowest, then those contributing together to more than 80% of the single score were identified. For each most relevant category, the processes that together contribute more than 80% to the total impact were identified. Figure 1 show the most relevant impact categories. Also the most relevant life cycle stages, processes and elementary flows were identified.

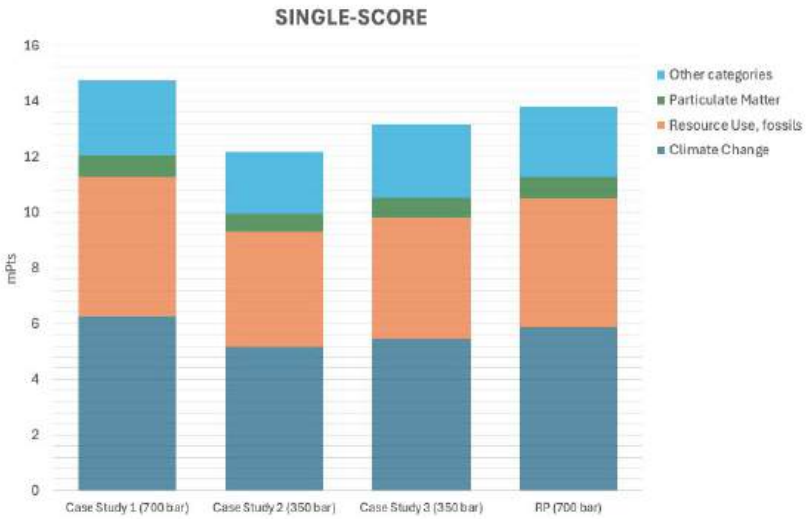


Figure 1. *Results for the case studies and the representative product of Type IV tanks for compressed hydrogen storage PSC 5.4.*

Conclusions: The most relevant impact categories are Climate Change, Resource Use (fossils), and Particulate Matter. The raw materials acquisition and pre-processing phase showed the greatest environmental impact across all relevant categories. Carbon fibres represent the process with the highest environmental impact.

Acknowledgments: *This work has been carried out in the context of the HyPEF project, which is supported by the Clean Hydrogen Partnership and its members. HyPEF is funded by the European Union (Grant Agreement No 101137575). Views and opinions are however those of the authors only and do not necessarily reflect those of the European Union or the Clean Hydrogen Partnership. Neither the European Union nor the granting authority can be held responsible for them.*

References

Bachmann T.M, Van der Kamp J., Ben Hnich K., Maddula S.K.R., Maranghi S., Carbone C., Agostini A., Galvini G., Iribarren D. (2024) Learnings from relevant existing P(EF)CRs, HyPEF project deliverable D2.1, https://shorturl.at/s3g7D

Ben Hnich K., Maddula S.K.R., Bachmann T.M, Maranghi S., Zamagni A., Carbone C., Agostini A., Nawaya T., Bereketidou O., Brière R., Beretta D., Galvini G., Iribarren D. (2026) Laying the ground for product environmental footprint category rules of hydrogen devices through product categorization. Cleaner Environmental Systems, Volume 21, 100420, doi: 10.1016/j.cesys.2026.100420.

European Commission 2021/2279. Commission recommendation on the use of the Environmental Footprint methods to measure and communicate the life cycle environmental performance of products and organisations. https://eur-lex.europa.eu/legal-content/EN/TXT/?uri=CELEX%3A32021H2279



Qualitative Risk Assessment of Hydrogen Transport and Hydrogen-Fuelled Mobility in Road Tunnel

Emanuela Bruno*[a], Valeria Spampinato, Andrea Carpignano, Raffaella Gerboni

* corresponding author: emanuela.bruno@polito.it

[a] Politecnico di Torino, Energy Department

Keywords: HAZID, Hydrogen Valley; Hydrogen Transport; Road Tunnel Safety.

Abstract

Introduction: The development of integrated Hydrogen Valleys is accelerating hydrogen production, storage, distribution, and transport activities across Europe [1]. While hydrogen is expected to play a key role in the energy transition, its increasing use also introduces new technical and safety challenges, particularly when these emerging activities interact with existing critical infrastructures. Road tunnels [2] represent a sensitive context in this regard, as they form part of major transport corridors and may be involved in future hydrogen transport scenarios. Developed within the framework of the IMAGHyNE project [3], this work addresses this safety issue through a qualitative assessment of hydrogen transport and hydrogen-powered mobility within tunnel infrastructures, considering the Fréjus Tunnel cross-border corridor between Italy and France as the case study [2][4]. The present examines plausible future scenarios linked to the expected development of Hydrogen Valleys and the possible increase of hydrogen-related traffic.

Objectives: The primary objective of this study is to perform a rigorous Hazard Identification (HAZID) analysis aimed at identifying potential deviations from expected operating conditions associated with different modes of hydrogen transport. Beyond describing possible hazards, the study systematically compares and assesses three distinct operational scenarios:

- Compressed Hydrogen (CH_2) transport: using high-pressure tube trailers;
- Liquid Hydrogen (LH_2) transport: using cryogenic road tankers;
- Hydrogen-fuelled vehicles (HFCVs): operating within the tunnel environment.

This distinction is relevant because storage state, inventory, and confinement conditions influence accident evolution and consequence severity.

Material and methods: The study adopts a systematic and structured approach that combines technical system knowledge with a brainstorming-based HAZID methodology. A two-step risk evaluation protocol is applied: first, hazardous scenarios are assessed without safeguards to estimate the intrinsic risk; second, existing prevention and mitigation measures, are included to evaluate the residual risk.

Results: The HAZID analysis provided a systematic screening of the hazardous situations that could occur within the Fréjus Tunnel for the three identified configurations: compressed hydrogen transport, liquefied hydrogen transport, and hydrogen-fuelled vehicles. For each case, the analysis linked potential accident scenarios to technical, operational, and traffic-related causes, including road traffic accidents caused by human error, tunnel fires, brake overheating, hydrogen releases from storage systems, mechanical failures, and tunnel-system malfunctions. Existing safeguards were explicitly considered, including vehicle-level systems such as pressure relief devices, shut-off valves, and storage protection systems, with some examples in [5][6], as well as tunnel-level measures such as traffic control, monitoring and incident detection systems, ventilation, emergency exits, evacuation provisions, and emergency management procedures, as in [7]. This allowed the residual risk to be assessed after the application of preventive and mitigative barriers. The results showed different risk profiles. Liquefied hydrogen transport was associated with the most severe consequences, mainly due to the larger inventory and escalation potential associated with cryogenic hydrogen releases in a confined environment. Compressed hydrogen transport showed more persistent residual risks for asset integrity and tunnel operability, particularly in the case of high-pressure release, jet fire, or mechanical burst. Hydrogen-fuelled vehicles showed an overall lower risk level, mainly due to their limited on-board inventory and integrated safety systems.Across all configurations, road traffic accident caused by human error emerged as dominant risk driver, rather than the intrinsic failure of hydrogen components alone. Dedicated Bow-Tie models were developed for CH_2 transport, LH_2 transport, and HFCVs to account for differences in escalation mechanisms and potential impacts on people, infrastructure, and tunnel operability.

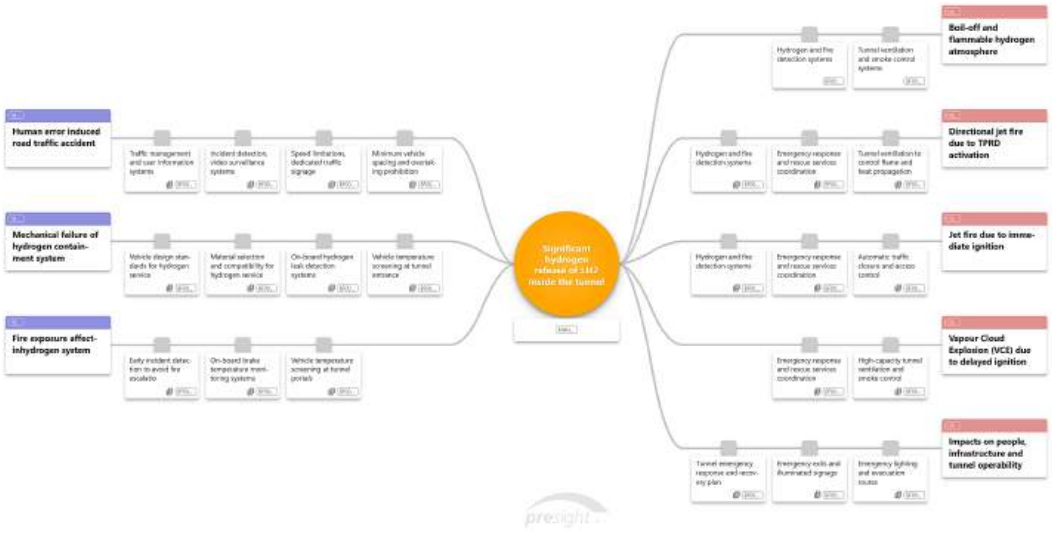


Figure 96 - Bow-Tie model developed for the LH_2 transport case study

The Bow-Tie model reported in Figure 96 refers to the LH_2 transport case study and illustrates the main causal pathways, preventive mitigative barriers, hazardous event, and potential consequences

considered in the assessment.Beyond the identification of critical scenarios, the analysis provides a structured basis for evaluating future operational and technical measures that could support the safe authorisation of hydrogen transport through tunnel infrastructures. Examples include dedicated transit conditions, enhanced monitoring systems, specific emergency procedures, and differentiated access criteria depending on the hydrogen transport configuration considered.

Conclusions: Building on the residual criticalities identified through the HAZID analysis, future work should focus on the priority scenarios, particularly human-error-induced road traffic accidents inside the tunnel, through dedicated Quantitative Risk Analysis. This would allow the qualitative findings to be refined using quantitative safety metrics, with specific attention to residual risk, user exposure, infrastructure resilience, emergency response effectiveness, and possible additional risk reduction measures. The results support the need for differentiated regulatory and operational criteria for hydrogen-fuelled vehicles, compressed hydrogen transport, and liquefied hydrogen transport, accounting for their different inventories, storage conditions, and consequence potential. Hydrogen-fuelled vehicles appear compatible with the current tunnel configuration from a qualitative risk perspective, provided that existing safety systems and operational controls are maintained. Conversely, hydrogen transport, especially in liquefied form, may require specific access and transit conditions, such as dedicated transit rules, enhanced monitoring and detection, specific emergency procedures, spacing or convoy management, and inventory-related limitations. Overall, the methodology developed in this study provides a structured basis for supporting future risk-informed decisions concerning infrastructure adaptation, operational requirements, and authorisation strategies for hydrogen mobility within tunnel environments.

Acknowledgment: The authors acknowledge the support of the IMAGHyNE project, co-funded by the European Union and the Clean Hydrogen Partnership as part of a consortium of public and private organisations.

References

[1] Hydrogen Europe, *Hydrogen Valleys Platform and Insights Report*, Brussels, 2023. Available at: https://hydrogeneurope.eu

[2] European Parliament and Council. Directive 2004/54/EC on minimum safety requirements for tunnels in the Trans-European Road Network. OJ L 167, 30.04.2004.

[3] Région Auvergne-Rhône-Alpes, "IMAGHyNE : la grande vallée hydrogène," *Région Auvergne-Rhône-Alpes*, Jun. 24, 2024. [Online]. Available: http://www.imaghyne.eu/

[4] SITAF S.p.A. Motorway Service Charter – Fréjus Road Tunnel (T4). 2025 Edition.

[5] Ahluwalia, R.K., Roh, H.-S., Peng, J.-K., Papadias, D., Baird, A.R., *et al.* (2023). Liquid hydrogen storage system for heavy-duty trucks: Configuration, performance, cost, and safety. *International Journal of Hydrogen Energy*, 48, 13308–13323.

[6] Toyota Motor Corporation (2020). *Development of the Toyota Fuel Cell System (TFCS)*. Toyota Technical Review, Vol. 66, pp. 4–13

[7] SFTRF (Société Française du Tunnel Routier du Fréjus), 2024. *Fire-fighting equipment and safety systems of the Fréjus Road Tunnel*. Available at: https://www.sftrf.fr/en/nos-valeurs/



Impacts of the Hydrogen Economy on Global Hydrogen and Air Pollutant Emissions: A Scenario Analysis Using the GAINS Model

Thiago Luis Felipe Brito*[a], Peter Rafaj*[a], Anna Pauls[b], Shaohui Zhang[a], Robert Sander[a], Lena Höglund-Isaksson[a] and Zbigniew Klimont[a]

* corresponding authors: brito@iiasa.ac.at; rafaj@iiasa.ac.at

[a] International Institute for Applied System Analysis (IIASA), Schloßplatz 1, 2361 Laxenburg, Austria

[b] BOKU University, Institute of Sustainable Economic Development, Vienna, Austria

Keywords: hydrogen emissions, hydrogen economy, air pollutants, hydrogen leakage

Introduction: Hydrogen is expected to become a major energy carrier in the transition towards climate neutrality and is increasingly considered essential for decarbonising hard-to-abate sectors, including transport, heavy industries, or production of chemicals. However, a large-scale hydrogen economy may also create new environmental challenges. Hydrogen itself is an indirect greenhouse gas because it alters atmospheric chemistry by increasing the lifetime of methane and contributing to tropospheric ozone and stratospheric water vapour formation. Furthermore, hydrogen production, transport, storage and end-use can lead to additional emissions of greenhouse gases and air pollutants, including methane, nitrogen oxides, ammonia, sulphur dioxide, carbon monoxide and particulate matter. Quantifying these emissions is essential for understanding the net environmental implications of future hydrogen deployment strategies.

Objectives: The objective of this work is to develop a comprehensive global inventory of current hydrogen emissions and to evaluate their evolution under alternative energy transition pathways [1]. Specifically, the study quantifies historical and future anthropogenic hydrogen emissions from incomplete combustion and fugitive sources. It also estimates associated emissions of key air pollutants and greenhouse gases across the hydrogen supply and demand chain. The study further investigates the effectiveness of currently available emission-control and leakage mitigation technologies and explores the environmental trade-offs associated with different hydrogen production methods.

Material and methods: The analysis applies the Greenhouse Gas–Air Pollution Interactions and Synergies (GAINS) model extended with a dedicated hydrogen module that represents the entire hydrogen value chain, including production, storage, transport, distribution and end-use sectors. Historical and future emissions were estimated for the period 1990–2050 for approximately 185 world regions. Future projections are based on energy demand scenarios derived from the IEA World Energy Outlook [2] and combine baseline (BL), existing mitigation commitments (MT) and carbon-neutral (CN) pathways with current legislation (CLE) and maximum feasible reduction (MFR) strategies to control hydrogen and other pollutants. Alternative hydrogen production routes include a) maintaining the

current fossils-dominated production mix, b) transitions based on electrolysis and biomass gasification, and c) pathways relying on a combination of electrolysis and steam methane reforming with carbon capture and storage (CCS). Uncertainties associated with hydrogen leakage factors were evaluated using Monte Carlo simulations.

Results: Global anthropogenic hydrogen emissions decreased from approximately 13 Mt H_2 in 1990 to 10 Mt H_2 in 2020, largely because of reduced emissions from incomplete combustion in transport and residential sectors. Under hydrogen-intensive decarbonisation scenarios, total hydrogen emissions (without biomass burning) may increase to 17–20 Mt H_2 by 2050 if current leakage control practices are maintained, while the share of incomplete combustion declines (Figure 1). The analysis indicates that projected hydrogen emissions are increasingly dominated by losses from transmission and distribution infrastructure. The widespread implementation of best available technologies could reduce future emissions by approximately 70%, demonstrating the importance of efficient leakage prevention strategies.

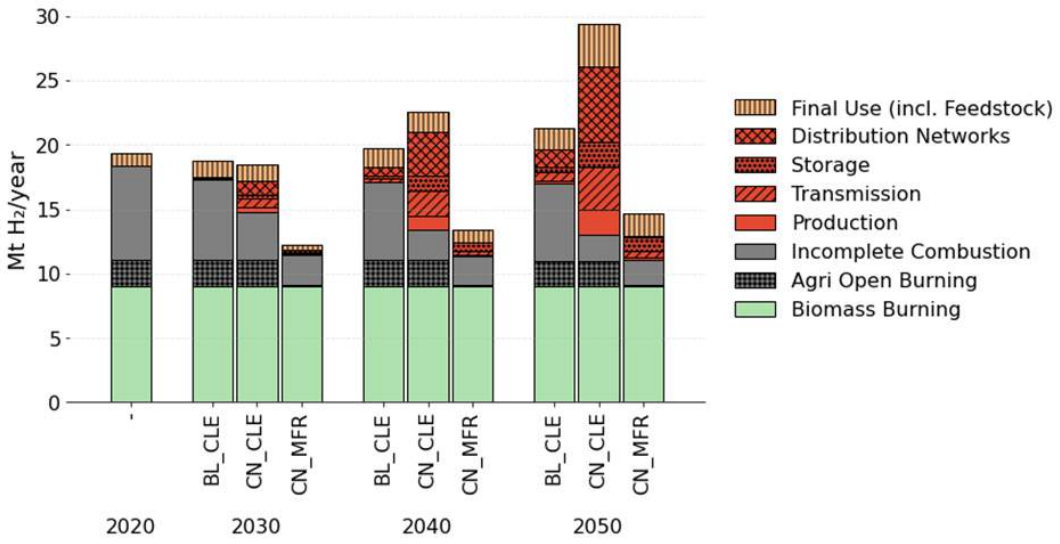


Figure 1: Global emissions of hydrogen by sector and scenario.

Hydrogen deployment also affects conventional air pollutants: combustion of H_2 (pure or blended) leads to higher temperatures and thermal NO_x formation when compared to natural gas. Such incremental emissions could reach 2.5 Mt NO_x by 2050 in the most hydrogen-intensive scenarios, with industrial applications representing around three-quarters of total emissions (Figure 2). Fugitive NH_3 emissions associated with ammonia-based storage and transport may reach 6.5 Mt by 2050. Upstream emissions strongly depend on the selected hydrogen production route. Biomass-based production pathways can significantly increase emissions of CH_4, CO, NO_x, $PM_{2.5}$ and to lesser extent SO_2, whereas production pathways based on electrolysis or steam methane reforming with carbon capture substantially reduce CO_2 emissions. Existing emission-control technologies, including selective

catalytic reduction, dedusters and improved handling practices, can mitigate a large fraction of these pollutants.

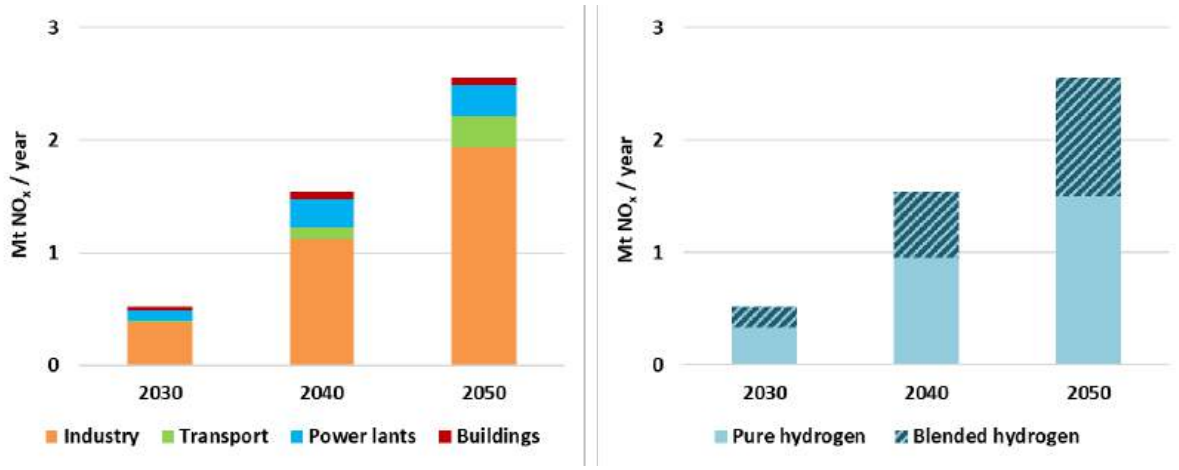


Figure 2: NO_x emissions from hydrogen combustion by sector (left panel) and by fuel type (right panel).

Conclusions: The results demonstrate that a transition towards a hydrogen economy cannot be evaluated solely on the basis of carbon dioxide reductions. Hydrogen leakage and associated air pollutant emissions represent important environmental considerations that may offset some of the expected climate benefits if not properly managed. Nevertheless, the study shows that currently available technologies and operational practices can substantially reduce both hydrogen emissions and co-emitted pollutants. The extended GAINS framework provides a comprehensive tool for integrated assessments of hydrogen-related emissions and supports the design of policies that maximise the environmental benefits of large-scale hydrogen deployment while minimising unintended consequences.

Acknowledgment: This research has been funded from the European Union's Horizon Europe research and innovation programme under Grant Agreement No. 101137582 (HYway). We also acknowledge the International Energy Agency for providing energy scenarios and trends to derive underlying activity projections used in this study.

References

[1] Brito T.L.F., Rafaj P., Pauls A., Zhang S., Sander R., Höglund-Isaksson L., Klimont Z. (2026). Global hydrogen emissions and air pollutants from the hydrogen economy: scenario analysis with the GAINS model. Environmental Research: Energy, 3, 025024.

DOI 10.1088/2753-3751/ae69e3

[2] International Energy Agency (2024). World Energy Outlook 2024. Paris: IEA.



Advancing Social Life Cycle Assessment for Hydrogen Energy Pathways in Italy's 2050 Transition

Giuseppe Cecere[a], Edgar Towa[a], Laura Zanchi[a], Anna Niero[a], Alessandro Agostini[b], Giuseppe Pellegrini Masini[b], Vittoria Battaglia[b], Viviana Cigolotti[b], Giulia Monteleone[b], Alessandra Zamagni[a]

* corresponding author: Alessandro Agostini (alessandro.agostini@enea.it)

[a] Ecoinnovazione srl Spin-off ENEA

[b] ENEA–Italian National Agency for New Technologies, Energy and the Sustainable Economic Development, Rome, Italy

Keywords: Energy scenarios, Hydrogen technologies, Social risk assessment, Social LCA

Introduction: Hydrogen is increasingly considered a key option for achieving long-term decarbonisation, especially in hard-to-abate sectors, selected transport applications and energy system flexibility. However, most hydrogen assessments still focus mainly on environmental and techno-economic performance, while social sustainability remains less systematically addressed [1].

Hydrogen value chains may generate social risks related to raw material extraction, equipment manufacturing, energy supply, imports, labour conditions, governance quality and the geographical distribution of benefits and burdens. Social Life Cycle Assessment (S-LCA) provides a structured framework to assess these issues, but its application to hydrogen technologies and future energy scenarios is still limited. This is particularly challenging because available social risk databases, such as PSILCA, are based mainly on present-day country-sector conditions, whereas hydrogen strategies refer to future energy systems.

Objectives: This study develops and tests a two-level social risk assessment approach for hydrogen pathways in Italy's 2050 energy transition. The first level assesses selected hydrogen production technologies. The second level evaluates hydrogen deployment within national energy system scenarios generated with TIMES-Italy.

The objectives are to identify relevant social topics, stakeholder groups and supply-chain hotspots; compare the social risk profiles of different hydrogen production routes; assess the contribution of hydrogen within future Italian energy scenarios; and examine the usefulness and limitations of current S-LCA databases for prospective energy planning.

Material and methods: The study follows the UNEP S-LCA Guidelines and ISO 14075 and uses the PSILCA database in OpenLCA. Social risks are assessed through the Reference Scale approach and expressed mainly in Medium Risk Hours [2].

At technology level, the analysis considers six hydrogen production routes: alkaline electrolysis, solid oxide electrolysis, steam methane reforming with and without carbon capture, solid biomass gasification, and coal gasification with carbon capture. The functional unit is 1 kg of hydrogen. The system boundary is cradle-to-gate and includes raw material extraction, processing, component manufacturing, assembly and hydrogen production, while end-of-life, transport, storage and distribution are excluded. Technology inventories combine techno-economic data and life cycle inventory information. Physical and monetary inputs are mapped to PSILCA country-sector processes. At scenario level, TIMES-Italy 2050 outputs are used to model energy carrier consumption, hydrogen production mixes, imports and costs under different decarbonisation assumptions.

Results: The technology-level assessment shows that hydrogen production routes have different social risk profiles. Solid oxide electrolysis shows the highest risk values in the baseline modelling, mainly because of its higher uncertainty, lower current maturity and cost-related assumptions. Across technologies, recurrent hotspots include fair salary, public sector corruption, trafficking in persons, violations of employment laws, association and bargaining rights, and trade unionism.

At scenario level, social risks depend on both the scale of energy carrier deployment and the social risk intensity of the related country-sector supply chains. Larger energy and monetary flows generally lead to higher social risk scores, but some imported commodities and country-sector combinations contribute disproportionately to specific risks. In the FIT55 configuration, hydrogen plays a more visible role because of higher hydrogen penetration and the strong contribution of SOEC. Although non-hydrogen commodity sets often remain dominant, hydrogen-related processes contribute significantly to selected indicators, especially those linked to labour rights, material supply chains and geographical sourcing.

Conclusions: The study shows that integrating S-LCA with energy system scenario modelling can support early identification of social risks in hydrogen transitions. The proposed approach is useful as a screening tool for policymakers and energy planners, helping to identify which technologies, supply chains, materials and social indicators deserve closer attention.

The results should not be interpreted as predictions of future social impacts, but as indicative social risk signals based on current country-sector data and future scenario assumptions. Future research should improve data granularity, include uncertainty analysis, update social risk databases over time, and integrate primary data from emerging hydrogen value chains. Overall, the study contributes to the development of prospective S-LCA and supports the inclusion of social sustainability in national hydrogen planning.

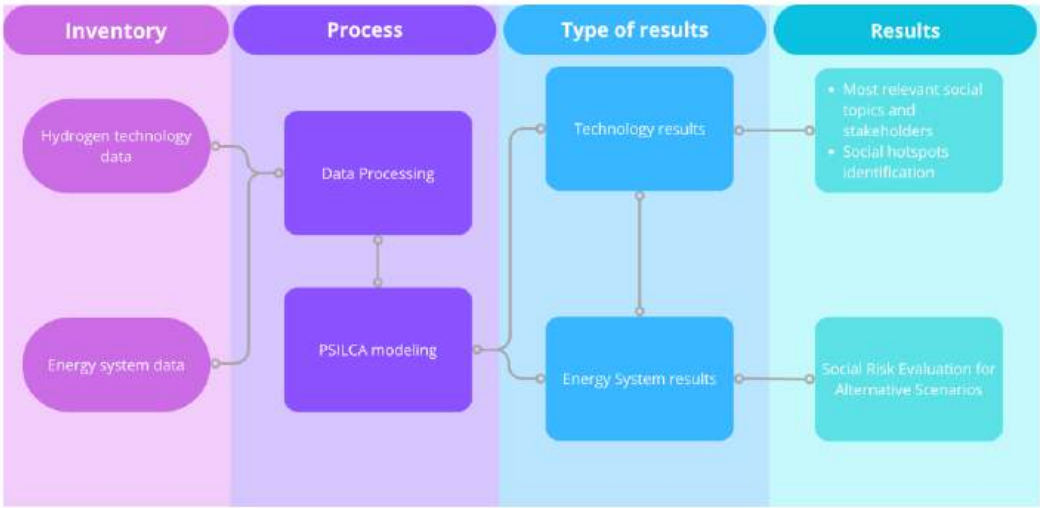


Fig.1: Two-tier methodological framework for the social risk assessment of hydrogen pathways. Hydrogen technology data and energy system scenario data are processed and modelled in PSILCA to generate two complementary outputs: technology-level results, used to identify the most relevant social topics, stakeholder groups and hotspots; and energy-system-level results, used to evaluate the social risks associated with alternative hydrogen deployment scenarios.

Acknowledgment: This research was funded by the European Union – NextGeneration EU from the Italian Ministry of Environment and Energy Security POR H2 AdP MASE/ENEA with involvement of CNR and RSE, PNRR - Mission 2, Component 2, Investment 3.5 "Ricerca e sviluppo sull'idrogeno", CUP: I83C22001170006 and from Horizon Europe research, grant agreement No. 101192503.

References

[1] Manfredi, A., Traverso, M., Manfrida, G., & Fiaschi, D. (2026). Systematic literature review on the application of social LCA to H_2 technology in the energy sector. International Journal of Life Cycle Assessment.

[2] Martín-Gamboa, M., et al. (2025). Social life cycle hotspot analysis of future hydrogen use in the EU. International Journal of Life Cycle Assessment.

[3] Zamagni, A., et al. (2025). A conceptual framework for assessing and monitoring social risks and impacts related to hydrogen technologies and their value chains. Joint Research Centre, European Commission.



Advancing the assessment of climate and environmental impacts of a future Hydrogen Economy with the HYDRA project

R. Urgnani[a,*], N. Ferreras Alonso[b], I. Capellán-Pérez[c], A. Bellucci[d]., O. Wild[e], G. Kardaras[f], P. Marocco[g], V. Crognaletti[h], I. Vicini[i]

*corresponding author: rossella.urgnani@tinextainnovaitonhub.com

[a]Tinexta Innovation Hub, Casalecchio di Reno, Italy

[b]CARTIF Foundation, Valladolid, Spain

[c]University of Valladolid, Valladolid, Spain

[d]Consiglio Nazionale delle Ricerche, Bologna, 40129, Italy

[e]Lancaster University, Lancaster, United Kingdom

[f]Centre for Research and Technology Hellas (CERTH), Thessaloniki, Greece

[g]Politecnico di Torino, Torino, Italy

[h]AUTOMA S.r.l., Ancona, Italy

[i]beWarrant, Etterbeek, Belgium

Keywords: climate change scenarios, hydrogen economy, hydrogen leakages, life cycle assessment

Abstract

Introduction: Hydrogen has the potential to become a major pillar of the low-carbon energy transition, potentially supplying more than 22% of global energy demand by 2050 while avoiding over 80 gigatonnes of CO_2 emissions [1]. As such, H_2 could contribute to a more secure and resilient EU energy system by diversifying both energy sources and supply chains [2]. Despite a 66% increase in installed electrolyser capacity in 2026, the deployment of the hydrogen economy continues to face significant challenges, including high costs, regulatory uncertainty, inadequate infrastructure, uncertain demand [1,2], and safety risks [3]. At the same time, growing awareness of the role of H_2 as an indirect greenhouse gas (GHG) has raised concerns about the potential climate impacts associated with its large-scale deployment. Although H_2 is not itself a greenhouse gas, changes in its atmospheric abundance resulting from increased H_2 emissions may lead to higher concentrations of CH_4, tropospheric O_3, and stratospheric water vapour, all of which are potent GHGs [4]. Recent studies have estimated a 100-year global warming potential (GWP100) for hydrogen of 12 ± 6 [5]. However, more accurate assessment of H_2 emissions and soil uptake processes are needed to reduce uncertainties and improve our understanding of H_2 overall climate impact [4]. In parallel, a fully developed green hydrogen economy based on electrolysers could require substantial water resources (~34,500 GL/year globally [6]), while the associated large-scale deployment of renewable energy sources (RES) could entail significant land requirements (0.09-0.6 million km^2 for solar photovoltaics; 1.9-13.5 million km^2 for wind power depending on the 2050 deployment scenario considered [7]), potentially leading to competition with other land-dependent activities, such as agriculture [7].

Objectives: The Horizon Europe HYDRA project (GA n° 101137758) aims to advance understanding of the integrated climate and environmental impacts associated with large-scale hydrogen deployment. In particular, the project pursues the following objectives:

- to investigate the mid- to long-term diffusion of H_2 technologies at both EU and global levels across different sectors, and to quantify H_2 leakages along the value chain;
- to assess the environmental and climate impacts of the large-scale deployment of hydrogen technologies in the medium to long term;
- to update the life cycle assessment (LCA) methodology for hydrogen technologies by accounting for their potential environmental and climate impacts;
- to develop an innovative sensor for the detection and quantification of H_2 leakages;
- to simulate mitigation scenarios and develop recommendations supporting the sustainable deployment of the hydrogen economy.

Material and methods: HYDRA started its activities by mapping the global landscape of H_2-related policies to identify which technologies are being incentivised and which targets have been established across different countries. In parallel, a comprehensive assessment of H_2 technologies, market dynamics, and leakage emissions was carried out. This preparatory work supported the development of the H_2 sector representation within the Integrated Assessment Model (IAM) WILIAM, and informed the development of future hydrogen deployment scenarios and a KPI framework translating policy targets into measurable indicators for modelling and scenario analysis. WILIAM has now generated a set of future H_2 emission scenarios, which serve as inputs to the FRSGC/UCI Chemical Transport Model (CTM), which will quantify the global and regional impacts of increased atmospheric H_2 concentrations on O_3, CH_4, NOx, VOCs, CO, and other atmospheric oxidants. The SLIMCAT model is being used to assess the corresponding influence of these scenarios on stratospheric composition. Concentration changes generated by these simulations will subsequently be used to estimate the effective radiative forcing associated with H_2 emissions using the EC-Earth climate model. These modelling activities will provide a comprehensive assessment of the benefits and risks associated with large-scale H_2 deployment. They will also support the enhancement of the climate module within WILIAM, enabling the IAM to evaluate the integrated impacts of hydrogen deployment across climate, environmental, and socio-economic dimensions. This enhanced framework will be used to assess mitigation pathways and support the development of sustainability-oriented policy recommendations.

Furthermore, the environmental and climate results generated within HYDRA will contribute to the update of LCA methodology for hydrogen technologies, ensuring that their impacts are adequately captured. Complementing these activities, HYDRA has also focused on the development and test of an innovative hydrogen leakage monitoring tool.

Results: Results delivered so far indicate that: i) the current distribution of policy instruments reflects an early-stage market that relies on rules to reduce uncertainty and on public funding to de-risk large-scale deployment [8]; ii) partnerships, guidance initiatives, and research activities help address capability and knowledge gaps [8]; iii) by 2050, overall H_2 leakage rates across the supply chain could range from less than 2% under optimistic assumptions to nearly 20% in worst-case scenarios [9].

In parallel, uncertainties associated with the soil hydrogen sink have been assessed, and the parameterisation of soil uptake processes has been improved within the CTM framework. LCA activities have also been initiated through a review of existing methodologies and the selection of representative use cases for testing the updated approach (hydrogen building, hydrogen valley). In addition, the hydrogen leakage monitoring tool has been successfully tested under a range of different conditions in a wind-tunnel environment and is currently being prepared for further validation at an operational hydrogen storage facility.

Conclusions: HYDRA is significantly advancing the state of the art not only in the understanding of the impacts associated with the hydrogen economy, but also in the representation of H_2 within IAMs, the parameterisation of H_2 soil sinks in CTMs, the application of Raman spectroscopy for H_2 leakage detection, and the integration of hydrogen-related impacts into the LCA.

Acknowledgment

This research has been supported by the European Union's Horizon Europe research and innovation programme (grant no. 101137758, HYDRA).

References

[1] Humayun, M., et al (2026). Global hydrogen economy and hydrogen technologies: A new path to economic sustainability in the era of renewable energy. Chem. Eng. J. Adv, 101209.

[2] IEA (2026), Global Hydrogen Review 2026, IEA, Paris https://www.iea.org/reports/global-hydrogen-review-2026, Licence: CC BY 4.0

[3] Anekwe, I. M. S., et al. (2025). The hydrogen challenge: addressing storage, safety, and environmental concerns in hydrogen economy. Int. J. Hydrogen Energy, 167, 150952.

[4] Sand, M., et al. (2026) Climate impacts of hydrogen emissions. Nat Rev Earth Environ 7, 359–373.

[5] Warwick, N.J., et al. (2023). Atmospheric composition and climate impacts of a future hydrogen economy. Atmos. Chem. Phys. Prepr.,

[6] Woods, P., et al. (2022). The hydrogen economy-Where is the water?. Energy Nexus, 7, 100123.

[7] Tonelli, D., et al. (2023). Global land and water limits to electrolytic hydrogen production using wind and solar resources. Nat. Commun., 14(1), 5532.

[8] Work Package 2 - Key Results, CARTIF: Analysis of hydrogen-related policies ad targets (2025) https://www.hydraproject.eu/wp-content/uploads/2025/09/WP2-Key-Results.pdf

[9] Trapani, D., et al. (2025). Hydrogen leakages across the supply chain: Current estimates and future scenarios. Int. J. Hydrogen Energy, 145, 1084-1095.



Multi-criteria assessment of green hydrogen value chains for Europe's sustainable transition

Marianna Kama*[a,b], Ilaria Lucentini[a], Damien Evrard[b], Peggy Zwolinski[b], César Valderrama[a]

* corresponding author: marianna.kama@upc.edu

[a] Chemical Engineering Department, Escola d'Enginyeria de Barcelona Est (EEBE), Universitat Politècnica de Catalunya (UPC)-BarcelonaTECH and Barcelona Research Center for Multiscale Science and Engineering (CCEM), Av. Eduard Maristany 16, Campus Diagonal-Besòs, 08019 Barcelona, Spain

[b] Univ. Grenoble Alpes, CNRS, Grenoble INP, G-SCOP, 38000 Grenoble, France

Keywords: green hydrogen, value chains, multi-criteria decision analysis, techno-economic assessment

Abstract

Introduction: Europe has firmly committed to hydrogen as a pillar of its energy transition with the EU Hydrogen Strategy and REPowerEU set ambitious targets of at least 40 GW of electrolysers and 10 Mt of domestic renewable hydrogen by 2030, complemented by a further 10 Mt of imports [1,2]. The political direction is therefore clear, but the practical question of how Europe will actually embrace hydrogen remains open. Green hydrogen can be delivered through a very large number of technically viable production-to-use combinations, yet supply is predominantly fossil-based and deployment is held back by high costs, energy-intensive storage and transport, and immature infrastructure [3]. With limited resources, decision-makers must decide which value chains to prioritise. However, life-cycle and techno-economic studies typically cover complete pathways but address only one dimension, environmental or economic [4,5,6], while multi-criteria studies that combine dimensions are usually applied to a single stage, such as production, carrier selection or storage [7,8]. Assessments combining the full value chain with multiple criteria at once therefore remain scarce, particularly in Europe.

Objectives: This work addresses that gap with two objectives. First, to identify the green hydrogen value chains that are genuinely relevant for deployment in Europe. Second, to develop and apply a multi-criteria decision-analysis methodology that ranks these pathways by simultaneously weighing environmental, economic, technical and safety performance, in order to identify the configurations best suited to the European energy system.

Material and methods: A structured multi-criteria decision analysis (MCDA) framework was applied in four steps: pathway definition, criteria selection and data collection, pathway-level aggregation, and

ranking. Feasible pathways were built by combining a production technology (alkaline, PEM or solid-oxide electrolysis), intermediate processing (compression, liquefaction or carrier conversion such as ammonia, methanol and LOHCs), a storage option (compressed hydrogen, liquid hydrogen, underground storage, or chemical carriers) and a transport mode (pipeline, truck, ship or rail) retaining only technically compatible combinations yielded 28 pathways. Each pathway was evaluated against six criteria spanning environmental, techno-economic and operational performance: GHG emissions (kg $CO_{2\text{-eq}}$/kg H_2), levelised cost of hydrogen (EUR/kg H_2), electricity demand (kWh/kg H_2), efficiency (%), safety (0-1) and technology readiness level (1-9). Data were compiled from European studies published between 2020 and 2025 in two stages: an initial systematic screening of more than 300 publications in Scopus, followed by targeted complementary searches to obtain stage-specific values wherever the initial data was incomplete. Because no standardised, location-independent safety metric exists in the literature, a dedicated qualitative safety indicator was developed in this work and applied to every stage of the chain (production, conversion, storage, transport and reconversion) by scoring operating conditions and intrinsic hazards on a 0-1 scale. All values were converted to a common functional unit of 1 kg H_2 and aggregated along each pathway, summing emissions and costs across non-overlapping stages, combining efficiencies multiplicatively and setting technology readiness by the average stage. The database was built in a structured spreadsheet, and processed by a Python script that computes the pathway metrics and rankings and exports them to a results workbook. Criteria weights were obtained with the Analytic Hierarchy Process (AHP), and pathways were ranked using two independent methods, TOPSIS and PROMETHEE II, with robustness assessed through equal and criterion-focused weighting scenarios, sensitivity analysis and Monte Carlo simulation of both the input data and the criteria weights.

Results: The framework produced a consistent and robust ranking of the 28 pathways. The two independent methods, TOPSIS and PROMETHEE II, were in strong agreement across every weighting scenario (Spearman rho between 0.91 and 0.97), and the relative ordering remained largely stable under Monte Carlo perturbation of both data and weights. Clear structural trends emerge: pathways based on compressed hydrogen with direct delivery consistently outperform carrier-based routes, whereas pathways requiring energy-intensive conversion and reconversion steps, particularly methanol-based chains, rank lowest owing to cumulative energy and cost penalties.

Conclusions: The proposed framework offers a transparent, reproducible screening tool for comparing complete green hydrogen value chains in the European context. Its main innovations are threefold: the simultaneous, whole-value-chain evaluation of multiple integrated pathways rather than isolated segments, a new cross-stage qualitative safety indicator applied uniformly from production to reconversion and a reproducible tool that couples a consolidated European database to a dual-method (TOPSIS and PROMETHEE II) ranking engine. The strong agreement between the two methods and the stability of results under uncertainty support the reliability of the approach, while the findings indicate that minimising energy-transformation steps and favouring direct-use hydrogen

formats improves overall value-chain performance, providing evidence to inform European policy, infrastructure prioritisation and strategic decision-making.

Acknowledgment

The authors gratefully acknowledge funding from the European Union under the Marie Skłodowska-Curie Actions - Doctoral Network "Unite!Energy" (HORIZON-MSCA-2022-DN-01-01, Grant Agreement No. 101119805). The authors also thank Kiane de Kleijne and Alessandro Arrigoni for kindly providing additional data related to Refs. [5,6].

References

[1] European Commission, A Hydrogen Strategy for a Climate-Neutral Europe, COM(2020) 301 final, Brussels, 2020.

[2] European Commission, REPowerEU Plan, COM(2022) 230 final, Brussels, 2022.

[3] A. Ajanovic, M. Sayer, R. Haas, On the future relevance of green hydrogen in Europe, Applied Energy 358 (2024) 122586.

[4] D. Alghool, M. Haouari, P. Trucco, It is not the same green: A comparative LCA study of green hydrogen supply network pathways, International Journal of Hydrogen Energy 140 (2025) 958-970.

[5] Arrigoni, A., D'Agostini, T., Dolci, F., & Weidner, E. (2025). Techno-economic and life-cycle assessment comparisons of hydrogen delivery options. Frontiers in Energy, 19(6), 1129–1142.

[6] K. de Kleijne, M.A.J. Huijbregts, F. Knobloch, R. van Zelm, J.P. Hilbers, H. de Coninck, S.V. Hanssen, Worldwide greenhouse gas emissions of green hydrogen production and transport, Nature Energy 9 (2024) 1139-1152.

[7] O. Oner, K. Khalilpour, Evaluation of green hydrogen carriers: A multi-criteria decision analysis tool, Renewable and Sustainable Energy Reviews 168 (2022) 112764.

[8] C. Acar, E. Haktanır, G.T. Temur, A. Beskese, Sustainable stationary hydrogen storage application selection with interval-valued intuitionistic fuzzy AHP, International Journal of Hydrogen Energy 49 (2024) 619-634.



HySPARK: A Cross-Regional Hydrogen Valley for Airport and Urban Mobility Decarbonization

Alessia Piccolo*[a], Andrea Altomonte[a], Viviana Cigolotti[b] , Elio Jannelli[a]

* corresponding author: alessia.piccolo@phds.uniparthenope.it

[a] University of Naples Parthenope, Naples, Italy

[b] ENEA, Rome, Italy

Keywords: airport decarbonization, fuel cell retrofit, ground support equipment, hydrogen valley

Abstract

Introduction: Every year, Warsaw Chopin Airport serves a large number of passengers, yet behind the scenes its ground operations, feeder trucks and public transport still rely largely on diesel and grid electricity. HySPARK (*Hydrogen Solutions for euroPean Airports & Regional Kinetics*) sets out to change this picture. Funded by the Clean Hydrogen Partnership under Horizon Europe (Grant Agreement No. 101192536, 2025-2029, EU contribution ca. EUR 9 million), the project builds a cross-regional hydrogen valley around Warsaw, turning a renewable and low-carbon hydrogen hub in Włocławek into the backbone of a cleaner airport, city and freight corridor. Coordinated by the Polish Instytut Energetyki, with ORLEN as industrial lead, HySPARK unites partners from Poland, Italy, Great Britan and Ireland around a shared ambition: proving, at real scale, that hydrogen can decarbonise everything from heavy trucks to airport tugs.

ATENA S.c.a.r.l., an Italian technology district specialised in fuel-cell and zero-emission traction, brings this ambition to the tarmac, retrofitting airport ground support equipment with hydrogen powertrains. This abstract offers a general overview of the HySPARK project: its vision, objectives, approach and expected impact with a focus on ATENA's contribution to a hydrogen-ready Warsaw Chopin Airport.

Objectives: HySPARK's ambition is to establish Warsaw Chopin Airport and its surrounding region as a real-world demonstrator of a hydrogen-based ecosystem, moving proven technologies from bench-scale readiness to everyday operation. Rather than testing hydrogen in a single niche, the project

applies hydrogen across multiple mobility applications including long-haul freight trucks, urban public transport, airport ground handling, and an existing ammonia plant, so that one shared hydrogen supply chain serves markedly different users. This diversification is central to the project's logic: it is precisely by connecting several simultaneous demand points that a small-scale hydrogen valley becomes commercially credible rather than a one-off demonstration.

Within this shared ecosystem, ATENA's objective is to prove that hydrogen fuel cells can reliably take over one of the least visible but most demanding jobs on an airport apron: towing aircraft, baggage carts and ground equipment, hour after hour, in all weather, without compromising safety or performance. Concretely, ATENA aims to retrofit three electric towing tractors with hydrogen fuel-cell power packages, define together with airport ground-handling operator LS Airport Services (LSAS) how such a fleet is best deployed and scheduled, and build a monitoring framework able to capture how the retrofitted tractors actually perform once put to work.

Material and Methods: The project follows the classic anatomy of a hydrogen valley: production feeds distribution, which in turn feeds a portfolio of end-uses, held together by a digital planning layer that keeps supply and demand in balance. On the production side, ORLEN is scaling up renewable and low-carbon hydrogen output in Włocławek, combining an existing large chlor-alkali electrolyser with a new dedicated renewable hydrogen unit, and extending refuelling infrastructure toward Warsaw and its airport. This hydrogen then flows into four parallel testbeds: heavy-duty trucks, city buses, airport ground support equipment and a green-ammonia line, each stress-testing hydrogen under different duty cycles and operators, with a dedicated planning tool optimising the whole system and a two-year field campaign generating the data needed to judge its real performance.

ATENA's own approach, within the airport ground-handling strand, is a retrofit rather than a from-scratch design: existing electric towing tractors, with towing capacities to 47 kN, are fitted with a hydrogen fuel-cell power pack of equivalent output and a compact 1.8 kg hydrogen tank, in place of their battery pack, while meeting the safety and technical requirements set by LSAS. Alongside the hardware, ATENA works with LSAS to plan how the retrofitted fleet is deployed, refuelled and maintained day to day, and puts in place a monitoring system that follows every tractor's performance throughout the two-year demonstration: moving the solution from an early, bench-validated concept to a fully proven, airside-tested technology, within a common techno-economic framework built around the cost of hydrogen and safety compliance shared by the whole project.

Expected Results and Impact: As HySPARK entered its implementation phase in January 2025, this overview reports the project's targeted rather than field-validated results. Once fully operational, the Mazovian Hydrogen Valley is expected to generate up to 3,000 tons of renewable and low-carbon

hydrogen demand per year from Włocławek, with a roadmap toward 4,500 tons/year beyond 2030, enough to power a fleet of heavy trucks, two city buses, a retrofitted tractor fleet and a green-ammonia line simultaneously.

For the airport testbed specifically, ATENA's retrofit is expected to prove that hydrogen fuel cells can be a genuine drop-in replacement for batteries in ground handling equipment, matching towing performance while meeting the safety and certification bar of a live airport. Two years of continuous operational data should reveal, in concrete terms, how such a fleet behaves day to day: how much it costs to run, how refuelling logistics hold up, and how reliably it keeps aircraft turnaround on schedule.

Beyond the numbers, HySPARK aims to leave behind a credible, replicable blueprint, already earmarked for further hydrogen-ready-airport initiatives in Italy and Ireland, together with tangible emission reductions and a stronger public case for hydrogen-fuelled transport in cities like Warsaw.

Conclusions: HySPARK is not a laboratory exercise: it is a bet that hydrogen can work, at the same time, across trucks, buses, ammonia and airport ground handling, fed by a single regional supply chain. If that bet pays off, it offers Europe a rare thing, a hydrogen valley whose economics do not depend on a single flagship user.

ATENA's role, quietly retrofitting the tractors that keep an airport apron moving, tackles a corner of airport decarbonisation that has received far less attention than aircraft or terminals themselves, yet touches every flight that departs. As the project unfolds through 2029, its two-year monitoring campaigns are set to become one of the richest available datasets on how hydrogen performs, day in and day out, at the edge of a European hub airport.

Acknowledgment

This research has been supported and funded by the Clean Hydrogen Partnership under Grant Agreement No. 101192536, within the HySPARK initiative.

References

[1] HySPARK Project. Grant Agreement No. 101192536, HORIZON-JTI-CLEANH2-2024-06-02, Clean Hydrogen Partnership.

[2] European Commission, CORDIS. HySPARK – Hydrogen Solutions for euroPean Airports & Regional Kinetics, Project Fact Sheet, 2025.



TOPIC 6. HYDROGEN POLICY, MARKET AND BUSINESS MODELS

EFCH2 2026 European Fuel Cells and Hydrogen PIERO LUNGHI CONFERENCE
September 15th-17th 2026 Capri / Italy

Price-driven optimal grid-connected hydrogen production

Robert R Dickinson*[a,b], Greg Metha [a], Graham (Gus) Nathan [a]

* corresponding author [a] Adelaide University, [b] Dataspace Insight

Keywords: grid-connected, optimal, price-driven, production

Acronyms and definitions

PD-ODTF = Price-driven operational demand-trough filling. *VRE* = Variable Renewable Energy (Wind and Solar production). An *inter-region-capacity-constrained high VRE proportion* (IRC VRE) region is one in which wind and solar production (including rooftop solar) intermittently exceed electricity demand, whilst also having insufficient capacity to export the excess to adjacent regions. *RRP* = Regional Reference Price ($/MWh). *Economic offloading* occurs when a generator is dispatched below its maximum availability because the *RRP* is below its submitted bid price. *Network curtailment* occurs when a generator is dispatched below its availability due to network constraints, even though its bid is below the RRP.

Introduction: Opportunities have been identified for power-to-hydrogen to consume electricity during periods of low demand and high VRE production. This was raised in 2016 during the IEA H2 TCP's Task 38 [1], and highlighted again for the California region at last year's EU FCH2 conference [2]. Until now, what has been missing is a robust market-based system design to harness the opportunity. Hence a method to adapt an existing market operation is presented for *IRC VRE* regions. Price is used to drive economically optimal outcomes for all participants – generators, large-scale and retail consumers, and distribution and network operators.

Objectives: The purpose of this work is to develop an optimal market-based approach that can eliminate e*conomic offloading* in *IRC VRE** regions. This differs from *network curtailment*, which is small relative to economic offloading. *e.g., For the SA Region of the NEM [3], for the 365.25 days ending 31 March 2026, wind and large scale solar supplied 69% of operational demand (demand not supplied behind the meter with roof top solar).

Methods Overview: The price-driven model is the outcome of statistical analysis of RRP(t_i) as a 5-minute time-series function of OpDemand, WindGen, (large-scale) SolarGen, and EcoOffload (see table below), noting that rooftop solar is accounted for as a reduction in operational demand. The method introduces a new TroughFill demand, for which new trough-filling technologies bid, to influence the RRP. In summary, the RRP without a Trough-filling demand is as follows:

$$RRP(t) = \boldsymbol{f}(OpDemand(t) - WindGen(t) - SolarGen(t) - EcoOffload(t)) \quad \textbf{[1]}$$

while the increased RRP associated with a given TroughFill (t_i) is:

$$RRPtf(t) = \boldsymbol{f}(OpDemand(t) - WindGen(t) - SolarGen(t) - EcoOffload(t) + TroughFill(t)) \quad \textbf{[2]}$$

where:

RRP(t_i)	Regional Reference Price, $/MWh
RRPtf (t_i)	The maximum price that trough filling technologies pay for electricity
OpDemand(t_i)	Regional operational demand (a.k.a. Load), MW

TroughFill(t_i)	Sum of consumption side dispatched demand trough fills, MW
WindGen(t_i)	Sum of production of regional wind power generators, MW
SolarGen(t_i)	Sum of production of regional large-scale solar power generators, MW
EcoOffload(t_i)	Sum of economic offload of all wind and solar generators, MW
t_1 , t_n	The times at the beginning and end of the time series

A numerical example: A dedicated zero-in algorithm adapted from [4] is used to find the inverse of the trough-filling function, ***f***. An example of ***f*** is shown in Fig. 1. The additional revenue generated and energy consumed from the application of the price-filling market is presented in Fig 2. The system design shown in equation **[2]** benefits all market participants, with the standout benefit being an increase in the market value of VRE.

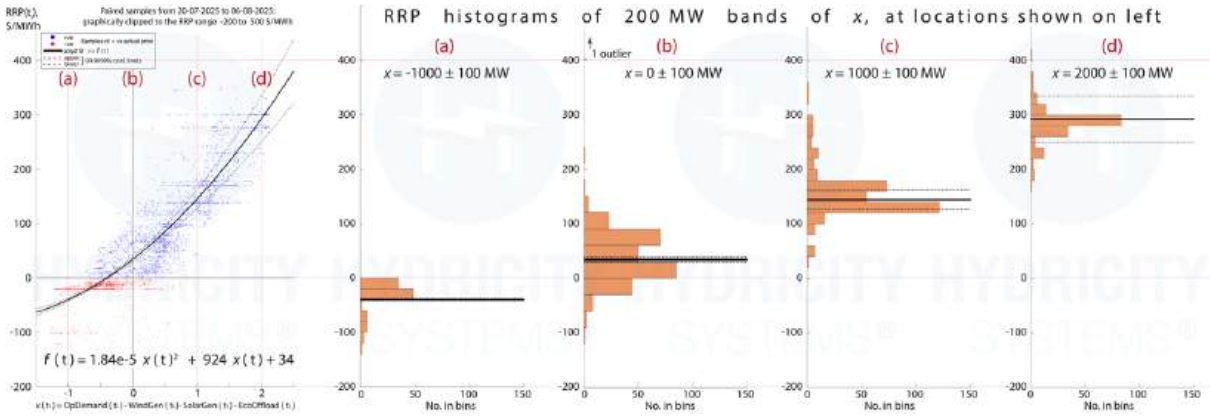


Fig 1: The statistical model ***f*** (*x*) used to compute the results presented in Fig. 2. The data are actual samples from the SA Region of the NEM [3], "zoomed in" for exemplary purposes on 20-07-2025 to 06-08-2025

Note that the increase in market value of VRE production is inaccessible with co-located electrolysis and wind turbine models [5-8]. Additional results to be presented will focus on displacing fossil gas for peak production and on market competition, such as intermittent power-to-industrial-heat [9, 10]. The introduction of multi-technology competitive bidding for demand troughs is expected to be critical to securing broad approval for rule changes from policymakers and market operators.

Limitations: Assessments of the form of ***f*** across moving 2-year spans (t_1 - t_{210384}) have shown that it typically takes over 2 years for substantial changes to be observed due to

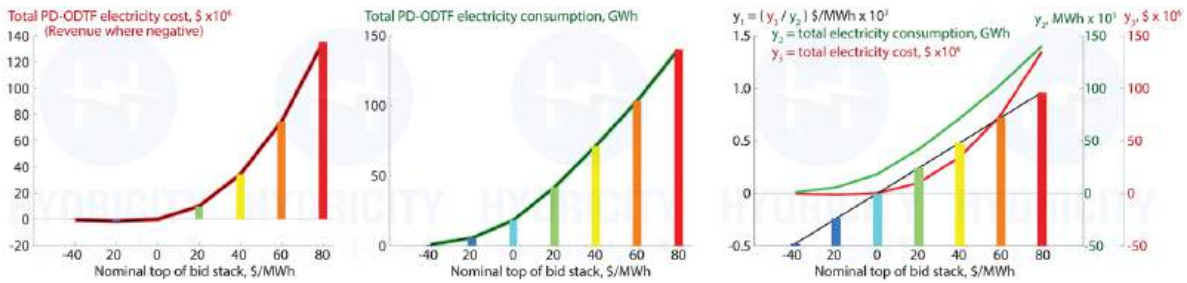


Fig 1: The influence of the top of stack trough filling bid on: **(a)** Total electricity cost, **(b)** Total electricity consumption, and **(c)** total cost / total consumption. While the variations in **(a)** and **(b)** are not linear, the variation of the ratio in **(c)** is linear because cost and consumption are directly related by ***f***.

factors such as inflation. Similar results are expected for any *IRC VRE* region. Conversely, if a high-VRE-proportion region is unconstrained with respect to the export of excess VRE production, then economic offloading will be reduced accordingly. Nevertheless, regardless of such differences, we forecast that any region with an intermittent VRE production proportion exceeding about 75% would be prospective for price-driven trough-filling. Also note that this assessment does not cover CAPEX. The RRPtf for each trough-filling technology will always be a function of the technology's supply and demand for its output, its CAPEX, and its utilisation factor, which is a direct function of RRPtf.

Conclusions: This work shows that a systematic, price-driven market to fill the troughs in operational demand benefits all market participants. Wind and solar electricity producers benefit from increased revenue for the same supply. Power-to-hydrogen producers benefit by being able to set the price at and below which they are willing to consume electricity. Network operators benefit from distributed technologies rather than co-located VRE production and electrolysis. Retail consumers with rooftop solar benefit from the elimination of negative feed-in tariffs. And renewable electricity production targets can be set above "100%".

Acknowledgments: The first author expresses deep gratitude to the co-authors, and to Craig Oakeshott, Australian Energy Market Commission, for the collaboration that led to this outcome.

References

1. Olfa Tlili, C.M., Paul Lucchese, et al. TASK 38 Final Report: Power-to-Hydrogen and Hydrogen-to-X: System Analysis of the technoeconomic, legal, and regulatory conditions. [accessed on: 5 Mar 2020]; Available from: https://eudp.dk/files/media/document/TASK-38-FINAL-REPORT_1_22012021_0856.pdf.
2. Jack Brouwer, *Critical Challenges and Opportunities in Building a Viable Hydrogen Market*, in *European Fuelcells and Hydrogen*. 2025: Capri, Italy.
3. Australian Energy Market Operator (AEMO). National Electricity Market (NEM). [accessed on: May 2026]; Available from: https://www.aemo.com.au/energy-systems/electricity/national-electricity-market-nem.
4. Cleve Moler. Zeroin, Part 3: MATLAB Zero Finder, FZERO. [accessed on: 26 Feb 2015]; Available from: https://blogs.mathworks.com/cleve/2015/11/09/zeroin-part-3-matlab-zero-finder-fzero/.
5. IEA Wind Technical Collaboration Program. Task 61: Variable Renewable Energy to Hydrogen (VRE-H2) [accessed on: 4 Mar 2026]; Available from: https://iea-wind.org/task-61/.
6. IEA Photovoitaic Power Systems Technical Collaboration Program. Task 20: Energy Hubs & Green Hydrogen. [accessed on: 2026]; Available from: https://iea-pvps.org/research-tasks/hydrogen/.
7. Program, I.H.T.C. Offshore Hydrogen Production. [accessed on: May 2026]; Available from: https://www.ieahydrogen.org/task/task-46-offshore-hydrogen-production/.
8. Groenemans, H., et al., *Techno-economic analysis of offshore wind PEM water electrolysis for H2 production.* Current Opinion in Chemical Engineering, 2022. **37**: p. 100828.
9. Rondo Energy. Low-cost, zero-emission industrial heat and power. [accessed on: May 2026]; Available from: https://www.rondo.com/how-it-works.
10. HILT CRC and Rondo Energy. HILT CRC is collaborating with Rondo Energy to advance industrial decarbonization, using high-temperature thermal energy storage. [accessed on: May 2026]; Available from: https://www.google.com/search?q=hilt+crc+%22rondo+energy%22.



Standardization Safety and Analytical Protocols for Biomass Hydrogen: the project START-H2

Nadia Cerone, Luca Contuzzi, Ramona Agostini, Carmine Florio, Fausta Cosentino, Rosario Milanese, Massimo Morgana, Giovanni Santilli, Umberto Calice, Francesco Zimbardi*

** corresponding author: nadia.cerone@enea.it*

[a] *ENEA, Dipartimento Tecnologie e Fonti Energetiche Rinnovabili, ss 106, 75026, Rotondella (MT), Italy*

Keywords: Hydrogen, biomass, purity, standard

Abstract

Introduction: Large-scale hydrogen integration is vital for global carbon neutrality and the decarbonization of hard-to-abate sectors. However, building a resilient and viable value chain faces significant technical bottlenecks and legislative barriers. Current regulatory frameworks struggle to keep pace with innovation, necessitating harmonized international standards and simplified administrative procedures to attract investment and provide operational certainty. Moreover, the shift toward decentralized energy systems, including urban transport and residential use, leads to complex safety challenges. The unique properties of hydrogen, such as metal embrittlement, low ignition energy, and high flammability, needs a deep shift in risk management through advanced mitigation strategies. Rigorous safety protocols are essential not only for operations but as a sociological prerequisite for public trust and social acceptance. Consequently, establishing clear, safety-oriented authorization processes is the *sine qua non* condition for reducing CAPEX, reassuring the public, and facilitating the seamless integration of sustainable hydrogen into the global energy landscape.

This research was carried out under the umbrella of the START-H2 project (Technological Development and Research on Hydrogen in Italy), a flagship project designed to catalyse the national hydrogen economy. Under the leadership and technical coordination of ENEA, the project has served as a critical bridge between laboratory-scale innovation and industrial-scale implementation.

Objectives: In this context, although the international standard ISO 14687:2019 already constitutes a consolidated benchmark for regulating hydrogen fuel quality in the automotive sector, remains a concerning lack of specific protocols for emerging sectors such as thermochemical production pathways. Production routes derived from biomass gasification present unique analytical challenges due to the presence of feedstock-specific contaminants (such as tars, ammonia (NH_3), hydrogen sulfide (H_2S), and organic silicon compounds) which vary significantly depending on the organic raw materials utilized [1]. To date, the absence of rigorous, dedicated guidelines for the certification of bio-derived hydrogen represents a critical bottleneck that prevents industrial scalability. Furthermore, the

state-of-the-art analytical methodologies currently employed to validate gas purity (such as Gas Chromatography-Mass Spectrometry (GC-MS) or Cavity Ring-Down Spectroscopy (CRDS)) are often characterized by prohibitively high costs and an extremely intensive requirement for specialized human and instrumental resources [2,3]. These financial and technical burden act as a high barrier to entry for small and medium-sized enterprises, slowing down large-scale industrial deployment and preventing the technology from achieving the economies of scale necessary to compete effectively with traditional energy carriers.

Material and methods: The primary scientific focus of this specific research segment devoted to the green hydrogen produced from biomass resources, has been the definition and validation of standardized, high-precision, and cost-effective analytical methodologies specifically engineered for the rigorous quantification of hydrogen quality. While traditional electrolysis-based hydrogen has established benchmarks, hydrogen derived from biomass-to-energy pathways has a highly complex impurity profile that is not yet fully addressed by existing international norms. By addressing the technical blind spots in current protocols, this research aimed to develop a robust certification framework that ensures gas purity, crucial for protecting sensitive downstream components like Proton Exchange Membrane (PEM) fuel cells, while simultaneously reducing the CAPEX and OPEX associated with high-end gas analysis. Consequently, the outputs of START-H2 project will contribute to lowering the technical barriers for bio-derived hydrogen, facilitating its seamless integration into the domestic and European energy infrastructure.

The basis for the analytical protocols is the experimental data gathered from pilot and laboratory-scale facilities. Central to this experimental phase is the PRAGA rig (Updraft Gasification Facility), a robust pilot plant capable of the continuous thermochemical conversion of 20–30 kg/h of raw biomass into syngas. This facility provides the necessary industrial-scale environment to stress-test the durability and accuracy of online sensing equipment under realistic operational conditions [4]. Parallel to this, the research utilizes specialized lab-scale facilities for BAE (Biomass-Assisted Electrolysis), an emerging technology that significantly reduces the electrical energy demand for hydrogen production by utilizing organic matter as an anodic feedstock [5].

Results: A primary output of this research is the formalization of a comprehensive draft of standardized protocols and operational procedures, specifically engineered for both real-time online monitoring and high-precision offline laboratory analysis. These rigorous analytical frameworks are designed to characterize the complex chemical composition of high-hydrogen syngas mixtures generated through advanced thermochemical biomass conversion processes, as well as the high-purity hydrogen streams produced via innovative electrochemical biomass conversion pathways. By addressing both thermal and electrochemical routes, the study provides a holistic view of the bio-hydrogen landscape, ensuring that regardless of the production method, the resulting gas meets the stringent quality requirements for advanced energy applications.

Conclusions: The research provides the necessary technical-scientific evidence to inform future legislative standards, ensuring that biomass-derived hydrogen can be safely and legally integrated into the global energy grid.

Acknowledgment

Work funded by the Italian Ministry of the Environment and Energy Security, program agreement MiTE_ENEA, PNRR - Hydrogen Research - Mission M2-C4 - Investment 3.5: Research and development on hydrogen.

References

[1] Biomass gasification for hydrogen production. IEA Bioenergy Task 33, 2025, https://www.ieabioenergy.com/wp-content/uploads/2025/03/IEA-Bioenergy_T33_Bio-H2_Final_v2.pdf

[2] Mass Spectrometry-Based Purity Assessment of Hydrogen from Different Production Pathways: Compliance Evaluation with ISO 14687:2019 Standards. Sinambela, 2025, http://doi.org/10.69855/science.v2i4.272

[3] Cavity Ring-Down Spectroscopy: Recent Technological Advancements, Techniques, and Applications. Mayti et al, 2020, https://doi.org/10.1021/acs.analchem.0c04329

[4] Production of hydrogen-rich syngas from biomass gasification by double step steam catalytic tar reforming, Cerone et. al, 2022, https://doi.org/10.1016/j.ijhydene.2024.07.290

[5] Electro-Reforming of Biomass Gasification Tar with Simultaneous Hydrogen Evolution, Calice at al., 2026, https://doi.org/10.3390/pr14030444



CRM content in PEM water electrolysers: a review of catalyst loading, material intensity and temporal trends

Talukdar Smritirekha [a], Favot Marinella*[a], Sofi Sonia [b], Soraci Alberto [ac], Graditi Giorgio [a]

* corresponding author: Favot Marinella

[a] Area Science Park, 99 Padriciano, Trieste, Italy

[b] Consiglio Nazionale delle Ricerche: Istituto di Tecnologie Avanzate per L'energia "Nicola Giordano", Via S. Lucia sopra Contesse, n. 5, 98126, Messina, Italia.

[c]Università degli Studi di Messina

Critical raw material, Material intensity, PEMEC, Quintuple Helix

Abstract: This study investigates the role of critical raw materials (CRMs) in water electrolysis, with a focus on PEM electrolysers and platinum group metals (Pt, Ir). By combining literature review and data harmonisation, it analyses catalyst loading and material intensity trends over time, highlighting both improvements and persistent variability. Results indicate a reduction in CRM demand at the cell level, but a remaining gap at system scale, underlining the importance of standardised metrics and material-efficient innovation pathways.

Introduction: Climate change demands new decarbonisation strategies, with green hydrogen increasing its importance as a key enabling technology [1]. Beyond its role in reducing emissions, hydrogen represents a broader transformation in production systems, requiring innovation paradigms such as the Quintuple Helix model [2], where technological development is closely linked to policy, industry, and sustainability constraints, including the availability of critical raw materials (CRMs). According to the JRC study, 36 raw materials are used across the four main water electrolyser technologies (alkaline, PEM, SOEC, and AEM), including platinum group metals (PGMs) and titanium for PEM electrolysers, and yttrium and rare earth elements for SOEC technologies [3]. Proton exchange membrane electrolysers (PEMECs) have high current density, fast response to dynamic operating conditions compared to the other available technologies along with having an intrinsic dependence on PGMs such as Pt and Ir [4,5]. The cathode in the PEMECs consists generally of Pt/C and the anode of Ir or IrOx. Some bipolar plates can have Pt coating to ensure high corrosion resistance and durability however, its contribution towards material intensity can remain negligible compared to that of catalyst loadings [6,7]. In this case, we considered the PGM loadings in terms of the catalyst loading in the electrolyser. This was also done since the unit, $g.kW^{-1}$, for material intensity or material input is at the system level. To define, material intensity is the term that quantifies the mass of physical substances required per unit of economic output or function. The catalyst loading, however, is reported at the electrode level in $mg \cdot cm^{-2}$. It makes cross-scale comparison in general challenging.

Objectives: This study investigates the role of iridium and platinum as critical raw materials (CRMs) in PEM electrolysers for green hydrogen production, with a focus on the EU context. Through a systematic literature review, it quantifies CRM content across electrolysis technologies and harmonizes differing units to enable cross-study comparability. It further examines whether technological progress has reduced iridium and platinum demand over time, analysing trends in both catalyst loading and system-level material intensity. Finally, it explores whether these reductions reflect the Quintuple Helix framework, in which technological development responds to constraints in resource availability, thereby linking innovation processes with environmental and material sustainability which are activated by a circulation of knowledge [2].

Material and methods: This study as stated in the objectives, carries out at first a systematic literature review to identify the available electrolyser technologies and identify the materials in them. Each material was mapped against the latest European classification of Critical Raw Materials (CRMs) to assess the level of criticality associated with each technology along with their occurrence as Strategic Raw Materials [8] [9]. Further, PEMECs were selected for in-depth analysis due to their rapid technological development, increasing deployment in green hydrogen systems, and intrinsic reliance on scarce platinum group metals (PGMs), particularly iridium and platinum, which are widely recognised as key constraints for large-scale deployment[10]. Subsequently, literature data on Ir and Pt content in PEMECs were collected and analysed. The data availability varied in peer-reviewed scientific articles in terms of catalyst loading ($mg \cdot cm^{-2}$), whereas in technical reports mostly in material intensity ($g \cdot kW^{-1}$). The lack of standardisation in the reported quantities, let us in this study to implement the below mentioned formulas. By obtaining some crucial information such as the active area per cell (cm^2), number of cells per 1 MW of stack, we can calculate the material intensity from a reported value of catalyst loading.

$$Material\ Intensity(g.kW^{-1}) = \frac{[Catalyst\ Loading(mg \cdot cm^{-2}) * Active\ area\ per\ cell\ (cm^2) * No.\ of\ cells\ per\ MW\ stack]}{1000000}$$

Another way to calculate the equation is as follows

$$Material\ Intensity(g.kW^{-1}) = \left[\frac{Catalyst\ Loading(mg \cdot cm^{-2})}{\{CurrentDensity(A.cm^{-2}) * CellVoltage(V)\}}\right] * 1000$$

Results: Implementing these conversion formulas enable harmonization of the data, however, availability of detailed data can be a constraint. From the available data, a 75% reduction in Ir catalyst loading from 2.00 $mg \cdot cm^{-2}$ [11] to 0.50 $mg \cdot cm^{-2}$ [12] across 2020–2023 can be noted. Yet, projected material intensities of 0.40 $g \cdot kW^{-1}$ [13] for Pt and 0.55 $g \cdot kW^{-1}$ for Ir [13] at GW-scale PEM deployment fall within the mid-range of values reported to date, pointing to a persistent gap between achievable

material efficiencies at the cell level and what is realistically deployable at system scale. The values vary widely. This highlights the lack of harmonized Life Cycle Analysis (LCA) system boundaries for PEM electrolysers and puts constraints on any robust tracking of material efficiency gains over time.

Conclusions: A comparative overview of CRMs, and particularly the use of Pt and Ir in PEM electrolysers have been noted to vary widely across studies, but a clear trend toward reduced catalyst loading over time is evident. At the system level, this translates to lower critical raw material (CRM) demand per unit of installed capacity, though results depend heavily on assumptions around current density, lifetime, and configuration CRM scarcity is increasingly driving innovation in PEM technology, reflecting the interplay between research, industry, and policy. Future work should focus on harmonized metrics, CRM recovery, and sustainable value chains.

References

[1] Algburi S, Munther H, Al-Dulaimi O, et al. Results in Engineering 2025;26. https://doi.org/10.1016/j.rineng.2025.105109.

[2] Carayannis EG, Campbell DFJ Int. J. Soc. Ecol. Sustain. Dev. 2010;1:41–69. https://doi.org/10.4018/jsesd.2010010105.

[3] Carrara S, Bobba S, Blagoeva D, et al. https://doi.org/10.2760/334074.

[4] Babic U, Suermann M, Büchi FN, et al. J Electrochem Soc 2017;164:F387–99. https://doi.org/10.1149/2.1441704jes.

[5] Kiemel S, Smolinka T, Lehner F, et al. Int J Energy Res 2021;45:9914–35. https://doi.org/10.1002/er.6487.

[6] Sarjuni CTA, Shahril AAD, Low HC, et al. Fuel Cells 2024;24. https://doi.org/10.1002/fuce.202300196.

[7] Prestat M. J Power Sources 2023;556. https://doi.org/10.1016/j.jpowsour.2022.232469.

[8] E. Parliament and C. of the European Union, 2024. [Online]. Available: https://eur-lex.europa.eu/legal-content/EN/TXT/?uri=OJ:L_202401252

[9] Eikeng E, Makhsoos A, Pollet BG. Int J Hydrogen Energy 2024;71:433–64. https://doi.org/10.1016/j.ijhydene.2024.05.096.

[10] Group CME. Platinum Group Metals in the Hydrogen Economy: Midstream 2024.

[11] Minke C, Suermann M, Bensmann B, et al. Int J Hydrogen Energy 2021;46:23581–90. https://doi.org/10.1016/j.ijhydene.2021.04.174.

[12] Fu C, O'Carroll T, Shen S, et al.. Curr Opin Electrochem 2023;38. https://doi.org/10.1016/j.coelec.2023.101227.

[13] Duke C, Davies B, Abdul-Manan AFN, et al. Resour. Conserv. Recycl., vol. 226, Elsevier B.V.; 2026. https://doi.org/10.1016/j.resconrec.2025.108687.



Applying Hydrogen Safety Lessons to the 2026 Colton Accident

David Blekhman*[a]

* corresponding author: .blekhman@calstatela.edu

[a] California State University, Los Angeles

Keywords: Hydrogen safety, pressure relief device, trailer, explosion

Introduction: The broader deployment of hydrogen systems requires a safety culture that is grounded not only in codes, standards, and engineering analysis, but also in the best real-world operational experience. Hydrogen has been used for decades in industrial and aerospace applications that contained safety hazards to specific locations and limited practices; however, emerging high-pressure distribution, public-facing fueling, and mobile storage applications place hydrogen systems in new operating environments, where stakeholders, maintenance practices, public interfaces, emergency response considerations, and increasing system complexity. Any accidents can lead to significant system disruptions and limit access to fuel for months affecting everyone in the hydrogen ecosystem.

The February 2026 hydrogen trailer explosion in Colton, California, underscores the need to examine potential root causes for this incident, which involved a high-pressure hydrogen transport trailer, owned by Pilot and manufactured by BayoTech, and resulted in one fatality and one severe injury among technical personnel working with the trailers. The trailers are designed for gaseous hydrogen delivery at pressures up to 520 bar and capacities up to 731 kg, using Type III metal-lined composite cylinders and thermal pressure relief devices (PRD) intended to prevent cylinder rupture during thermal exposure. Although the Colton event remains under investigation, available information and video evidence raise questions about potential pathways toward the failure: trailer enclosure design, venting behavior, maintenance conditions, and pressure-relief operation.

Objectives: Because hydrogen-related accidents can significantly disrupt operations across the ecosystem, this study provides an initial analysis of the incident, identifies possible failure pathways by comparing it with similar occurrences, and examines how lessons learned from prior events may apply to this accident.

Material and methods: Earlier incidents and additional experimental work with containerized explosions provide context for interpreting possible failure pathways. In the 2018 Diamond Bar, California tube-trailer fire, an incorrectly installed pressure relief device opened unexpectedly, released hydrogen, and ignited. The investigation identified wrong CNG pressure relief devices installed during maintenance, inventory-control failures, improperly secured vent tubing, and material-compatibility problems.

The 2019 Sandvika, Norway fueling-station explosion illustrates the contrasting risk of enclosed or modularized systems. An assembly error in the high-pressure storage unit led to a leak, hydrogen accumulation, ignition, and extensive facility destruction. HySEA container experiments similarly show

that confinement, obstruction, vent area, and ignition location strongly influence incident severity. Considering that this incident is relatively recent and a formal report has not yet been finalized, the analysis relies primarily on multiple video sources—both from the incident itself and from controlled containerized explosion tests—which provide visual evidence of similarities in event progression and the resulting damage to the containers.

Results: Let's consider the conditions of the main **Colton Incident, 2026:** Recent incidents illustrate how hydrogen safety outcomes are often shaped by the interaction of technical, procedural, and organizational factors. The February 2026 Colton, California hydrogen trailer incident further reinforces the need to examine hydrogen safety across the full logistics chain. The incident involved a hydrogen transport trailer in a storage yard and resulted in one fatality and severe injury to another individual, both of whom were technical personnel working with the trailers [1]-[2]. The trailer involved was owned by Pilot and originally manufactured by BayoTech. The HyFill hydrogen trailers are engineered up to 520 bar for delivery of gaseous hydrogen, with each unit capable of carrying up to 731 kilograms. While the incident remains under investigation, it underscores the importance of managing safety processes for high-pressure hydrogen trailers not only during transit and fueling operations, but also during maintenance and repair. Similar accidents, along with existing safety research and demonstrations, can provide valuable insights into what may have occurred in Colton.

Diamond Bar Incident, 2018: The February 2018 Diamond Bar, California tube trailer module incident provides a particularly instructive example [3]. In that event, a pressure relief device on a hydrogen tube trailer module opened unexpectedly and released hydrogen, which ignited. A cylinder PRD opened on a 25-cylinder hydrogen tube-trailer module (about 10 kg per unit)., igniting the module. During the fire, 12 PRDs activated and released an estimated 120 kg of hydrogen, which was consumed in the flames. Causes: During December 2017 maintenance, technicians installed four CNG PRDs instead of hydrogen-rated devices; these CNG PRDs activate at 5,833 psi rather than the required 10,000 psi for hydrogen. In addition, the pressure-relief vent tubing on the failed PRD was ejected, allowing the fire to impinge on nearby cylinders; 21 cylinders were damaged, and six additional PRD vent tubes were also ejected due to improperly secured fittings. Material-compatibility issues were also identified, including the use of nickel disks, which are not permitted in hydrogen service.

Notably, although the trailer sustained fire damage, the open top of the trailer allowed the hydrogen flame to vent upward. This helped avoid catastrophic structural failure of the trailer.

Sandvika Incident, 2019: The difference between open-air and enclosed conditions is another recurring safety theme. Hydrogen releases in open environments can disperse rapidly when ventilation is unobstructed. However, in enclosed, semi-enclosed, or congested spaces, gas accumulation can occur, and ignition may lead to rapid pressure rise. Performed by HySEA project, container demonstrations and computational studies of enclosed and vented hydrogen deflagrations [4]-[5] demonstrate these principles.

The Sandvika station was modularized in enclosed containers, a design choice that can concentrate both equipment and risk within a compact footprint. The 2019 hydrogen fueling station explosion was attributed to an assembly error involving a plug in the high-pressure storage unit. The incorrect assembly

led to a hydrogen leak, accumulation, ignition, and significant destruction of the facility. Containerized systems must incorporate ventilation.

TPRD Activation: BayoTech patented Thermal PRD (TPRD), which uses a fast-acting glass-bulb designed for compatibility with hydrogen and activating at elevated temperatures. The Colton incident also provided rare footage of a TPRD operating correctly during an actual accident. The video captures one normal jet-flame release, illustrating proper venting behavior. In another sequence, a hydrogen jet catches a flamelet at its upper tip, after which the flame rapidly propagates down to the orifice of the vent pipe on top of the trailer—consistent with expected behavior. This controlled venting prevented further damage to the affected system and demonstrates the critical role of properly functioning TPRDs in high-pressure hydrogen incidents.

Conclusions: Practical lessons from these incidents include designing trailers for safe hydrogen dispersion, ensuring hydrogen-compatible components and correct configuration, strengthening maintenance and inspection controls, treating leaks and abnormal pressure events as actionable near-misses, providing hydrogen-specific hazard training, and reinforcing a safety culture that uses incident history, questioning, and reporting to support continuous improvement.

Acknowledgment: This material is based upon work supported by the National Science Foundation under Grant No. 2112554 and by the State of California Employment Development Department, with the California Community Foundation (CCF) serving as Fiscal Agent and the Los Angeles County Economic Development Corporation (LAEDC) as Regional Lead.

References

[1] CBS Los Angeles, “Colton truck explosion leaves 1 dead,” YouTube, Feb. 25, 2026. [Online]. Available: https://www.youtube.com/watch?v=kEg2MtYPtb8

[2] KTLA 5, “1 killed, 1 injured in Colton hydrogen truck explosion,” YouTube, 2026. [Online]. Available: https://www.youtube.com/watch?v=yYGPN8Zg1FE

[3] National Transportation Safety Board. (2019). *Air Products and Chemicals, Inc. tube trailer module hydrogen release and subsequent fire, Diamond Bar, California, February 11, 2018* (NTSB/HZM-19/02, PB2019-101398).

[4] Gexcon, “Simulating Vented Hydrogen Deflagrations: Improved Modelling in the CFD Tool FLACS-Hydrogen,” YouTube, n.d. [Online]. Available: https://www.youtube.com/watch?v=KUExNGx5xkg

[5] Gexcon, “HySEA Project Container Experiment #9 — No vent devices,” YouTube, n.d. [Online]. Available: https://www.youtube.com/watch?v=qXlGw6u0F9Q



Linking hydrogen demand for freight transport and power system decarbonization through spatially resolved energy system modelling

Antonio De Padova[a,b*], Claudio Carbone[c], Daniele Salvatore Schiera[a,b], Francesco Demetrio Minuto[a,b], Alessandro Agostini[c], Andrea Lanzini[a,b]

* corresponding author: antonio.depadova@polito.it

[a] Department of Energy, Politecnico di Torino, C.so Duca degli Abruzzi 24, 10129 Torino, Italy

[b] Energy Center Lab, Politecnico di Torino, Via Paolo Borsellino 38/16, 10138 Torino, Italy

[c] ENEA - Italian National Agency for New Technologies, Energy and the Environment, Italy

Keywords: energy system modelling, freight transport, hydrogen refuelling infrastructure, power system decarbonization

Abstract

Introduction: As a response to the growing climate crisis, the decarbonization of the energy system and the reduction of greenhouse gases (GHGs) emissions have become one of the most important global priorities, emerging as a critical target for science-based policy initiatives. In this context, the European Green Deal sets an ambitious objective for the European Union (EU) to achieve climate neutrality by 2050 through a transition towards a Net Zero emissions system, placing the energy sector at the core of mitigation strategies. Furthermore, it aims to reduce emissions in the transport sector by 90% by 2050. It is worthwhile to mention that the transport sector accounts for almost 25% of GHG emissions across Europe. In particular, while representing less than 2% of the overall circulating vehicles in Europe, heavy duty (HD) vehicles account for approximately 27% of CO2 emissions of the whole road transport sector and about 6% of all GHG emissions in the EU. Specifically, among the various categories of HD vehicles, trucks are responsible for about 85% of these emissions, highlighting the urgent need for decisive action on the freight transport to address the environmental impact of the whole sector. However, the decarbonization of this segment remains a critical challenge, due to high energy demand, long-distance operations, and the limited suitability of direct electrification for specific transport services. In this context, hydrogen-based trucks may complement direct electrification, provided hydrogen is supplied through a renewable domestic value chain and its production is coherently integrated with power-system expansion.

Objectives: The study assesses whether freight-related hydrogen demand can act as an anchor load for electrolytic hydrogen production and support the emergence of a domestic hydrogen supply chain. It also evaluates whether this transport-driven demand can create benefits beyond the mobility

sector, especially by enabling hydrogen-derived synthetic natural gas and fuel switching options for dispatchable thermal generation. The analysis compares scenarios with and without exogenous hydrogen demand for heavy-duty freight and identifies the spatial conditions under which hydrogen deployment is beneficial or costly.

Material and methods: The methodological framework combines a transport infrastructure optimization model with a spatially resolved national energy system model. In particular, hydrogen demand for freight transport is obtained from a Node Capacitated Flow Refueling Location Model (NC-FRLM), which identifies the minimum number and location of Hydrogen Refueling Stations (HRS) required to satisfy long-distance freight demand along the Italian TEN-T network subject to technical, regulatory, and policy constraints [1]. The resulting HRS locations and associated hydrogen demand are converted into geographically explicit inputs for an updated version of Calliope-Italy [2], a capacity expansion model based on the Calliope framework [3]. The model represents the Italian power system through 7 bidding zones, 20 NUTS-2 regional nodes connected to their corresponding bidding zones, and 6 neighbouring foreign regions. This structure captures spatial differences in electricity demand, renewable resource availability, existing generation capacity, transmission constraints, and cross-border exchanges. Electrolytic hydrogen is modelled in accordance with the EU framework for renewable fuels of non-biological origin (RFNBOs). Electricity used for electrolysis is therefore subject to additionality, temporal-correlation, and geographical-correlation requirements. Because the analysis refers to 2030, temporal matching between eligible renewable generation and electrolyser electricity consumption is imposed at hourly resolution. Therefore, interzonal hydrogen exchanges and international hydrogen trade are excluded from the analysis to isolate the effects of developing a domestic, spatially constrained supply chain.

Results: When exogenous hydrogen demand from freight transport is introduced, total installed electrolyser capacity reaches 326.3 MW. Most of this capacity is concentrated in the North (200.7 MW), Center-North (53.6 MW), and Center-South (45.4 MW), which together host approximately 92% of the national total. The remaining part is distributed across the South and the Islands. This spatial pattern reflects the combined influence of the geographically distributed demand from HRS and the geographical-correlation requirements applicable to RFNBO production. Compared with the reference scenario, the transport-driven one requires approximately 2 GW of additional renewable generation capacity, while installed BESS capacity decreases slightly, by 6.7%. The EAC consequently increases by approximately 2.5%, from 22.17 to 22.73 b€. Notably, despite the deployment of electrolysers to satisty freight-transport demand, no additional hydrogen is allocated to methanation and synthetic natural gas production. This result indicates that, even when an electrolytic hydrogen supply chain is established through an exogenous transport demand, hydrogen-derived SNG remains uncompetitive under the considered assumptions, even in this latter case, no hydrogen is produced for subsequent methanation and synthesis, showing that even in place of an imposed hydrogen production, this solution is not competitive under the considered conditions, highlighting the need for dedicated policy support to enable its deployment.

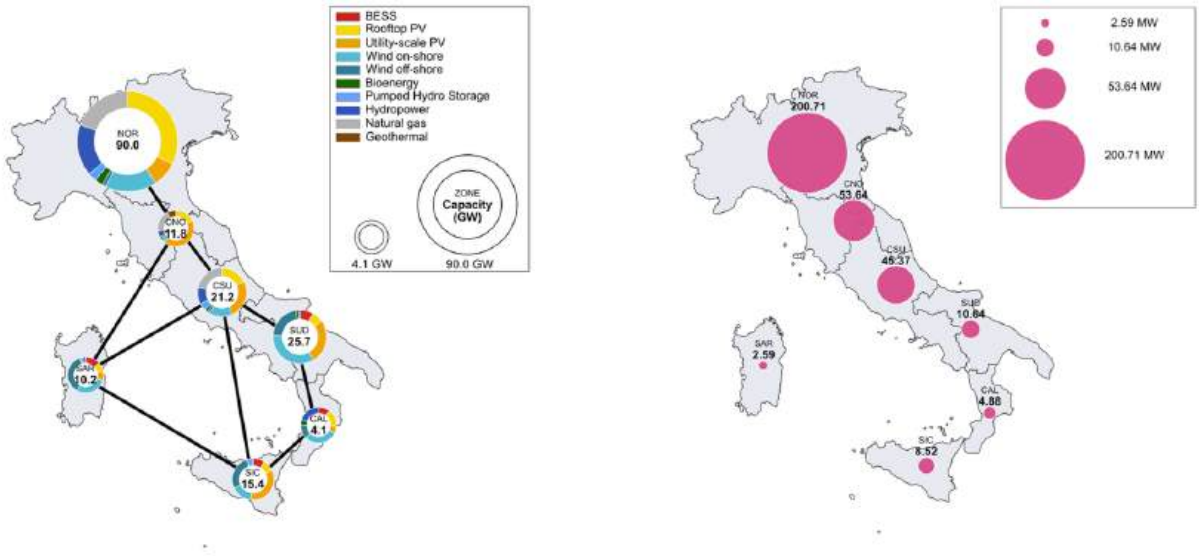


Figure 97 - Least-cost 2030 system configuration in the hydrogen-demand scenario from freight transport (on the left), and spatial distribution of required electrolysis capacity (on the right).

Conclusions: The contribution of this work lies in the integration of spatially explicit freight hydrogen demand into a detailed national energy system model, combined with an explicit representation of repowering, fuel switching, and hydrogen-derived synthetic fuel pathways. Unlike approaches based on aggregate national hydrogen demand, the proposed framework links HRS siting decisions to zonal energy system constraints and evaluates the role of hydrogen across both transport and power sector decarbonization. Overall, the framework provides a decision-support tool for assessing whether hydrogen deployment in Italy is primarily driven by mobility requirements or whether transport demand can trigger a wider domestic hydrogen value chain. By comparing 2030 configurations with and without freight-related hydrogen demand, the study identifies the costs, the infrastructure needs, and the consequences of integrating an exogenous hydrogen demand.

References

[1] A. De Padova, D. S. Schiera, F. D. Minuto, A. Lanzini, Spatial MILP optimization framework for siting Hydrogen Refueling Stations in heavy-duty freight transport, International Journal of Hydrogen Energy, Volume 94, 2024, Pages 669-686, ISSN 0360-3199, https://doi.org/10.1016/j.ijhydene.2024.11.086.
[2] F. Lombardi, B. Pickering, E. Colombo, S. Pfenninger, 'Policy Decision Support for Renewables Deployment through Spatially Explicit Practically Optimal Alternatives', Joule, vol. 4, no. 10, pp. 2185–2207, Oct. 2020, doi: 10.1016/j.joule.2020.08.002.
[3] Pfenninger S., Pickering B. Calliope: a multi-scale energy systems modelling framework. Journal of Open Source Software, 2018, 3(29), 825.



Energy system modelling for hydrogen integration in the italian power grid: benchmarking and 2050 scenario analysis

Punit Kumar[1]*, Antonio De Padova[1], Andrea Lanzini[1], Francesco Gracceva[2], Alessandro Agostini[2], Giulia Monteleone[2], Viviana Cigolotti[2]

* corresponding author: Punit Kumar (punit.kumar@polito.it)

[1] Energy Center, Politecnico di Torino, Italy
[2] ENEA (Italian National Agency for New Technologies, Energy and Sustainable Economic Development), Italy

Keywords: Economic dispatch, Electrolyser integration, Energy Systems Modelling, Hydrogen Systems

Abstract

Introduction: Achieving a net-zero energy system in Italy by 2050 necessitates large-scale integration of Variable Renewable Energy (VRE) sources and the implementation of advanced flexibility solutions. This research presents a high-resolution SAInt-based energy system model of the Italian power grid to assess hydrogen integration, electrolyser flexibility, electric vehicle (EV) participation, and distributed storage within the ENTSO-e TYNDP Global Ambition 2050 scenario.

Objectives: This research develops a high-resolution multi-zonal energy system model of the Italian power grid to evaluate hydrogen integration under high renewable penetration. The study benchmarks the SAInt model against historical ENTSO-e data and assesses the operational role of electrolysers, EV flexibility, and distributed storage in the 2050 ENTSO-e TYNDP Global Ambition scenario.

Material and methods: The SAInt mixed-integer linear programming framework was applied for economic dispatch and multi-vector optimisation. The Italian power system was modelled with seven bidding zones, incorporating both interzonal and cross-border interconnections. Historical datasets from Terna, GME, and ENTSO-e informed the calibration of the 2023 model. The 2050 TYNDP-GA framework incorporates large-scale renewable integration, electrolyser modelling, electric vehicle nodes with Vehicle-to-Grid functionality, battery energy storage systems, and sector-coupling constraints. Electrolyser demand was associated with local renewable generation and prioritised through SAInt custom penalty pricing parameters.

Results: The 2023 benchmarking exercise demonstrated strong alignment between the SAInt simulation and historical ENTSO-e data, with a total annual generation deviation of approximately -2% (Figure 98). This result confirms the model's suitability for scenario analysis. In the 2050 TYNDP Global Ambition scenario (Figure 99), both ENTSO-e and SAInt identify solar photovoltaic (PV) as the primary generation source, with ENTSO-e reporting approximately 310 TWh and SAInt 315 TWh. The solar share, however, decreases from 52–53% in ENTSO-e to 45–46% in SAInt, primarily because SAInt reflects higher system throughput associated with storage and flexibility operations. Battery storage increases substantially from approximately 80 TWh in ENTSO-e to around 150 TWh in SAInt, indicating more intensive charge–discharge cycling to support renewable integration. System-level indicators (Figure 100) also reflect reduced imports, declining from about 72 TWh to

67 TWh, and reduced exports, from approximately 17 TWh to 12 TWh. Renewable curtailment drops significantly from nearly 20 TWh in ENTSO-e to around 5 TWh in SAInt, representing an approximate 75% reduction. Despite these improvements, SAInt reports approximately 35 TWh of demand not served, underscoring the need to further calibrate nodal adequacy, flexibility constraints, and demand-priority assumptions.

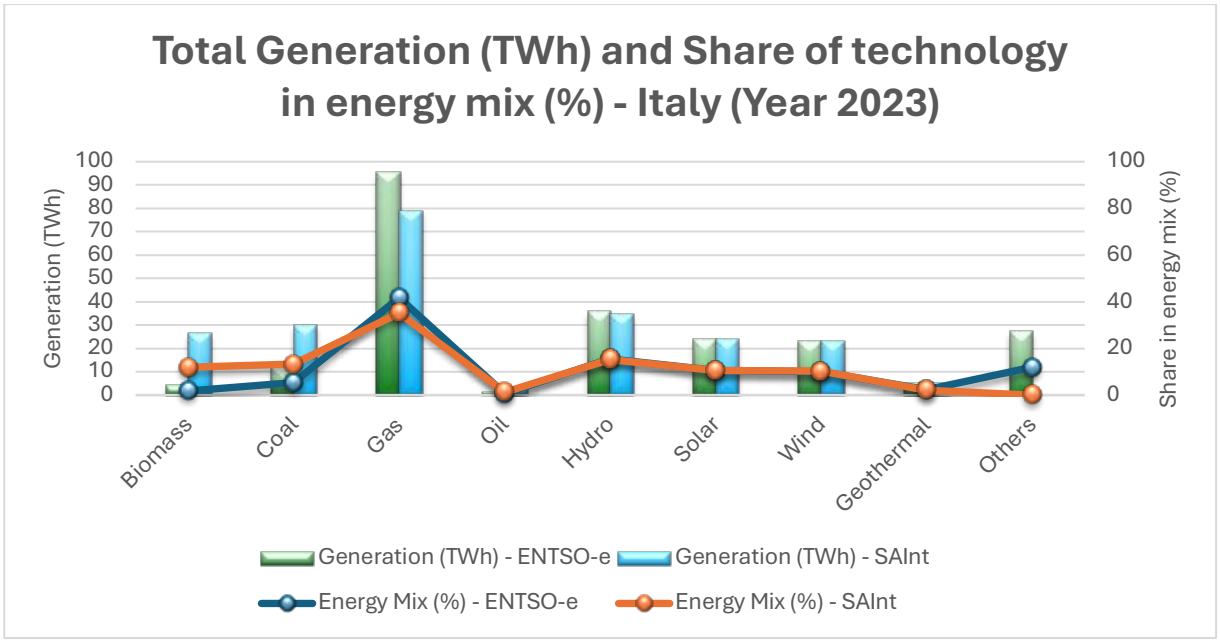


Figure 98: Total Generation (in TWh) and share in energy mix (%) per different technology types (Italy, Year 2023) – ENTSO-e and SAInt

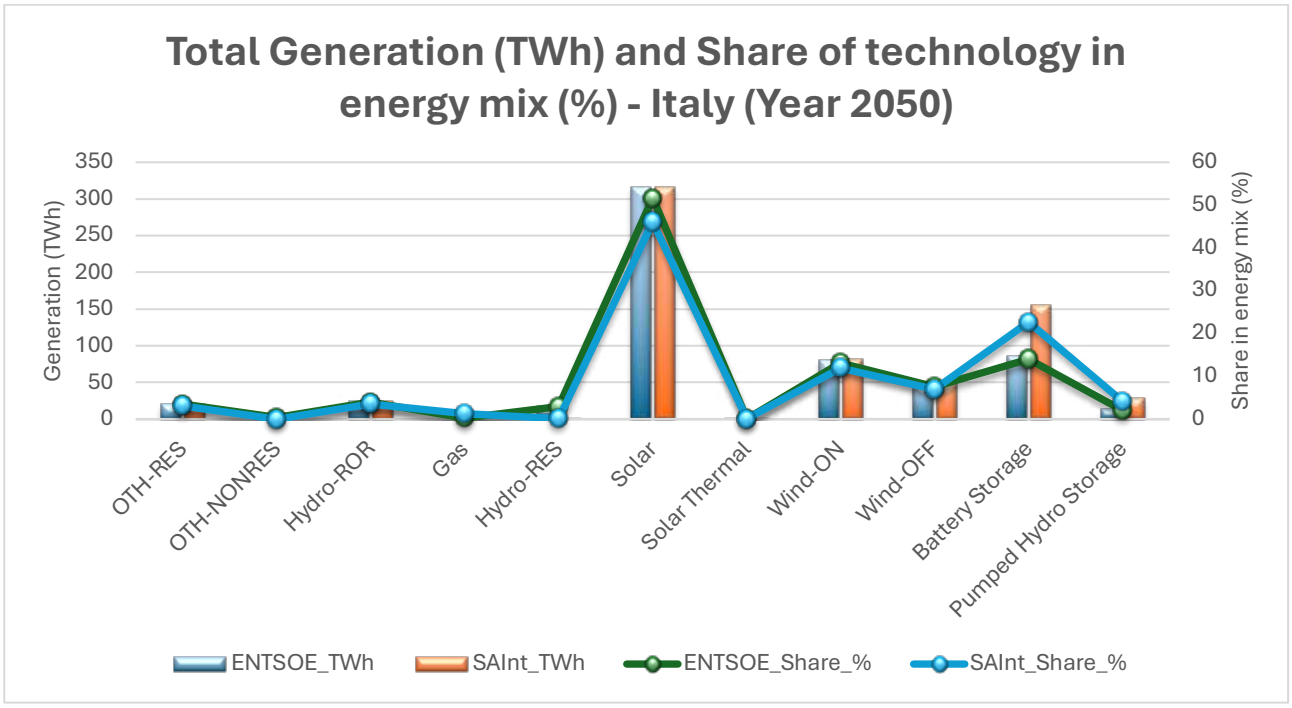


Figure 99: Total Generation (in TWh) and share in energy mix (%) per different technology types (Italy, Year 2050) – ENTSO-e and SAInt

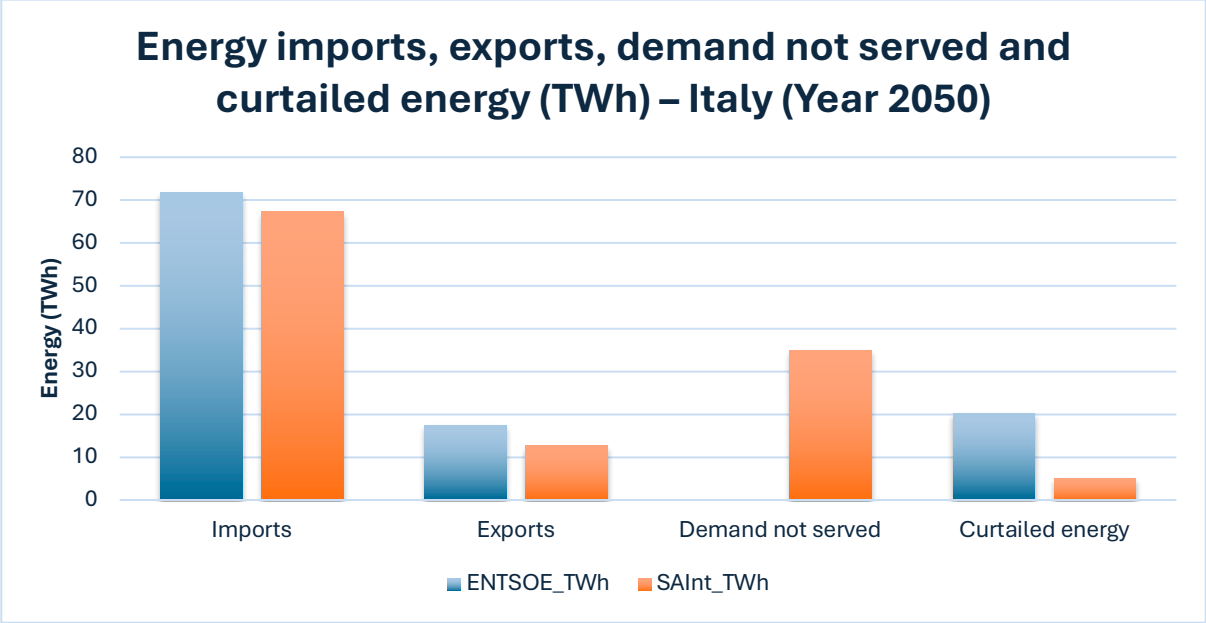


Figure 100: Energy imports, exports, demand not served and curtailed energy (TWh) – (Italy, Year 2050) – ENTSO-e and SAInt

Conclusions: The SAInt framework offers a comprehensive and integrated methodology for the analysis of hydrogen-enabled future power systems. By coupling electrolysers, electric vehicle flexibility, and prosumer storage within a unified optimisation framework, the approach improves the representation of distributed flexibility and renewable energy integration. This methodology facilitates future research on Hydrogen Valleys, sector coupling, and long-term decarbonisation planning for the Italian electricity system.

Acknowledgment: The authors acknowledge the support of Politecnico di Torino and ENEA for providing datasets, modelling support and technical guidance for this research work.

References

[1] ENTSO-e TYNDP 2024 Scenario Report – Global Ambition Framework.

[2] SAInt User Documentation and Modelling Framework References.



Flow measurement traceability for hydrogen in gas networks: an insight into H2FlowTrace project

Remy Maury[a]*, Lucie Dangeon-Vassal[a], Alessandro Guzzini[b], Marco Pellegrini[b], Cesare Saccani[b], Marc de Huu[c], Hans-Benjamin Böckler[d], Menne D. Schakel[e], Marc MacDonald[f]

* corresponding author: r.maury@cesame exadebit.fr

[a] CESAME-EXADEBIT, Route de L Aerodrome 43, 86000, Poitier, France

[a] Department of Industrial Engineering, University of Bologna, Viale del Risorgimento 2, 40136 Bologna (BO), Italy

[c]Federal Institute of Metrology METAS, Bern-Wabern, Switzerland

[d]Physikalisch-Technische Bundesanstalt (PTB), Braunschweig, Germany

[e]National Metrology Institute (VSL), Delft, the Netherlands

[f]TÜV SÜD National Engineering Laboratory, East Kilbride, United Kingdom

Keywords: Hydrogen, Hydrogen transportation, Gas meters, Metrology, Testing benches

Abstract

The sustainability of the hydrogen value chain cannot overlook flow measurement. However, a metrological infrastructure capable of ensuring traceability for flow measurements of pure hydrogen and hydrogen–natural gas blends over the wide range of flow rates and pressures relevant to transmission and distribution networks is still lacking. Among its objectives, the H2FlowTrace project designed the so-called small-scale transfer skid, a metrological infrastructure for hydrogen and, potentially, hydrogen–natural gas blends, intended to provide traceability for master flow meters. The small-scale transfer skid was designed for a maximum mass flow rate of 120 kg/h (1,300 m^3/h at 0.1 MPa or 45 m^3/h at 3.3 MPa) and can be extended up to 720 kg/h (7,800 m^3/h at 0.1 MPa or 270 m^3/h at 3.3 MPa) by means of two different sets of calibrated sonic nozzles, referred to as Set A and Set B, with maximum flow rates of 20 kg/h and 120 kg/h per nozzle, respectively. This paper presents the main characteristics of the small-scale transfer skid and the first results of the calibration of the sonic nozzles.

Introduction: Hydrogen transportation through pipelines is widely recognized as the most suitable solution for long-distance and large-volume delivery [1]. Among the open research questions, no definitive answer has yet been provided regarding the metrological performance of state-of-the-art gas meters when operating with hydrogen [2,3]. To address these challenges, fill existing gaps, and build upon the achievements of previous projects, the H2FlowTrace project is developing the traceability infrastructures that are currently missing in Europe and worldwide for hydrogen and hydrogen–natural gas mixtures (HENG). Within this framework, a Small-Scale Transfer Skid (SSTS)

has been designed, constructed, and commissioned to provide large-scale flow meter calibrations for end users through an integrated service involving European National Metrology Institutes, representing the first infrastructure of its kind in Europe.

Objectives: Once the small-scale transfer skid was realized, the calibration of the six sonic nozzles belonging to the "set A" was necessary since their use together to calibrate the set of large sonic nozzles which go up to 120 kg/h, i.e., the "set B", in turn used for the calibration of industrial master meters. Figure 101 schematically depicts the configuration adopted to calibrate the "set B" with "set A" nozzles in the SSTS (in the right).

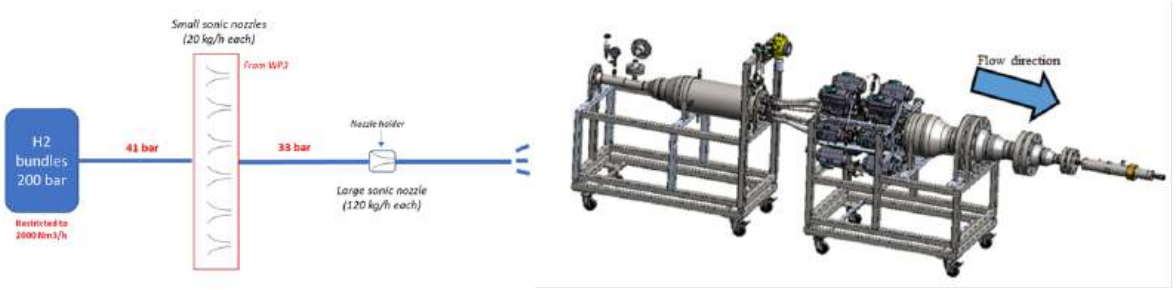


Figure 101. Calibration of the large sonic nozzles through the small sonic nozzles in the small scale transfer skid (in the left) and the SSTS general arrangement (in the right).

Material and methods: The PVTt (Pressure–Volume–Temperature–time) reference standard at CESAME was used for the calibration of the sonic nozzles belonging to Set A. The facility is based on the PVTt method and is characterized by a flow rate range of 0.4–34 kg/h, an operating pressure range of 1–70 bar, and an operating temperature range of 15–65 °C, with an optimal operating temperature of 20 °C. The facility can accommodate sonic nozzles with throat diameters ranging from 0.2 mm to 5 mm and provides a target uncertainty on the discharge coefficient (Cd) of 0.2%. The calibration procedure is as follows. Hydrogen flows through the sonic nozzle and is collected in the pressure vessels of the PVTt reference standard, where pressure, temperature, and filling time are measured. Since the volume of the reference standard is accurately known, the hydrogen mass flow rate can be determined from the measured thermodynamic state variables using established thermodynamic relationships. During the calibration campaign, a single nozzle was installed in the nozzle holder at a time. Set A consisted of six identical toroidal sonic nozzles with a throat diameter of 1.6 mm. The calibration was performed over a flow rate range from 1 kg/h to 20 kg/h by carrying out at least eight calibration points and repeating each measurement a minimum of three times.

Results: The first results of the calibration of the "set A" nozzles and the expected trend for SSTSA-01 calculated in accordance with ISO 9300:2002 are shown in the Figure 102. As shown the Cd values are lower than expected with the standard. The roughness of the inner surface of the sonic nozzles may be the cause.

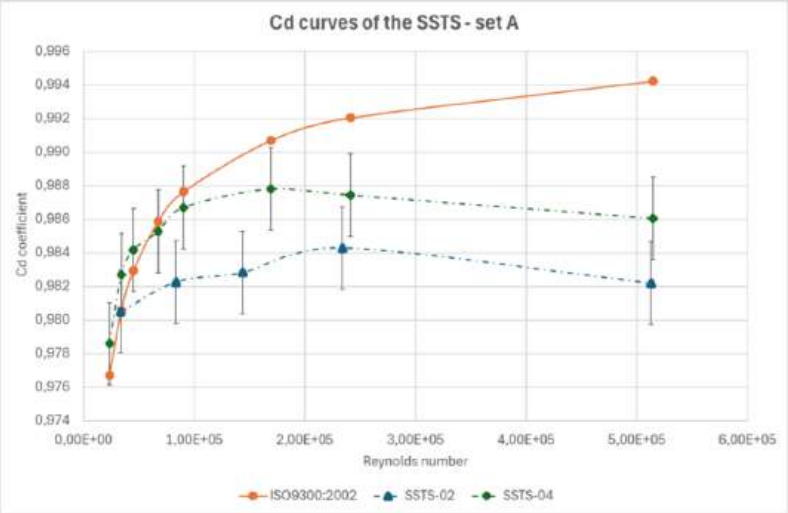


Figure 102. Results of the calibration of two nozzles form the set of the six small sonic nozzles (blue and green dotted plots) compared to the expected trend of the discharge coefficient (Cd) in accordance with ISO 9300:2002 (orange plot).

Conclusions: H2FlowTrace project completed the engineering and the realization of a new transfer skid to ensure hydrogen and HENG flowrate measurement traceability in presence. Aiming to calibrate large sonic nozzles up to 120 kg/h, small sonic nozzles were calibrated in a PVTt testing bench. While researchers are investigating the trends of some of the small nozzles calculated from the measurements, the SSTS is under preparation for the calibration of the larger sonic nozzles.

Acknowledgment

The project (23IND05 H2FlowTrace) has received funding from the European Partnership on Metrology, co-financed from the European Union's Horizon Europe Research and Innovation Programme and by the Participating States.

References

[1] Aghakhani A.; Haque N.; Saccani C.; Pellegrini M.; Guzzini A., Hydrogen transportation and distribution, in: Towards Hydrogen Infrastructure: Advances and Challenges in Preparing for the Hydrogen Economy, Amsterdam, Elsevier, 2023, pp. 187 – 224.

[2] Gislon, P., Cerone, N., Cigolotti, V., Guzzini, A., Pellegrini, M., Saccani, C., Robino, M., Carrubba, T., Cigni, A., Enescu, D., Fernicola, V., Dudek, A., Gajec, M., Kułaga, P., Maury, R., Rayana, F.B., Hydrogen blending effect on fiscal and metrological instrumentation: A review, Int. J. Hydrogen Energy, Vol. 67, pp 1295-1307, 2024.

[3] Guzzini, A., Pellegrini, M., Saccani, C., Dudek, A., Gajec, M., Król, A., Kulaga, P. Gislon, P. Cigolotti, V., Robino, M., Enescu, D., Fernicola, V.C., Smorgon, D., Maury, R., Gaiardo, A., Valt, M., Polak, D., Bissig, H., Hydrogen in natural gas grids: prospects and recommendations about gas flow meters, Int. J. Hydrogen Energy, Vol. 86, pp 343-362, 2024.



Importing Decarbonisation: The Geopolitics of Italy's Hydrogen Hub Strategy in the Mediterranean

Giuseppe Pellegrini-Masini*[a]

* corresponding author. Email: giuseppe.pellegrinimasini@enea.it

[a] ENEA, Agenzia Nazionale per le Nuove tecnologie, l'Energia e lo Sviluppo Economico Sostenibile, Rome, Italy

Keywords: energy justice, energy security, hydrogen geopolitics, Mediterranean hydrogen corridor

Abstract

Introduction: Hydrogen has moved to the centre of Europe's energy-security agenda, reframed after the 2022 gas crisis as both a decarbonisation vector and a hedge against import dependency [7]. Italy's Strategia Nazionale Idrogeno (SNI, November 2024) [6] embraces this dual role and adds a distinctively geopolitical ambition: positioning Italy as the Mediterranean gateway for hydrogen entering the European Union. On the strategy's own projections, domestic demand rises from roughly 0.7 Mtep in 2030 toward a 6 to 12 Mtep range by 2050, and long-run supply is framed as a "make or buy" choice — 70% domestic / 30% import against 80% import / 20% domestic — with a strategic role for the SouthH2 Corridor, ports as entry gateways, and renewable hydrogen and ammonia from North Africa [6]. This paper offers a political reading of that ambition, drawing on energy-security and energy-justice scholarship [1]–[3].

Objectives: The paper asks three questions a techno-economic roadmap leaves implicit: (i) whether substituting Russian gas dependency with North African hydrogen dependency advances strategic autonomy or merely reconfigures it; (ii) who captures the value of a transit corridor whose principal demand poles lie in Germany and Austria; and (iii) whether the socio-environmental burdens of export-oriented production are displaced onto supplier countries. The paper speaks to the conference's themes of global hydrogen supply chains, hydrogen hubs and international trade, bringing a governance and international-justice lens to questions usually treated as purely infrastructural.

Material and methods: The study combines a qualitative content analysis of the SNI [6], benchmarked against international hydrogen-strategy trends [4], [5], with a reading of the European instruments that structure Italy's import-and-transit role: the SouthH2 Corridor and Italian H2 Backbone (Project of Common Interest status under the trans-European energy networks framework), the RePowerEU import targets [7], the European Hydrogen Bank and its first auction, the IPCEI waves, and the H2Global double-auction mechanism explored trilaterally with Germany and Austria. The analysis is organised around three axes adapted from energy-security and energy-justice scholarship

[1]–[3]: dependency and strategic autonomy; the distribution of value and power along the corridor; and recognition of the interests and burdens of exporting regions.

Results: The analysis proceeds along the three axes above. Table 1 separates, for each, the strategy's own framing from the interpretation advanced here; the discussion below develops the political reading.

Axis	What the strategy states	Geopolitical interpretation
Dependency and strategic autonomy	RePowerEU: 20 Mt renewable H2 by 2030, half imported. North Africa costed < 5 €/kg; delivery 0.2–1 €/kg. Domestic route: 15–30 GW electrolysers, ~90 GW added renewables, €8–16 bn (electrolysers) / €13–24 bn (all routes).	Security of supply is invoked, yet the 80/20 case reproduces external dependency in a new vector. Make-or-buy is a strategic-autonomy decision, not merely an economic one.
Corridor value and transit position	SouthH2 Corridor and Italian H2 Backbone (PCI status); principal demand anchors in Germany and Austria. Trilateral H2Global-type intermediary: long-term purchase contracts with producers, short-term sale contracts with off-takers, price gap covered by public funds.	A transit state gains regulatory leverage and infrastructure rents, but structural demand — and bargaining power — sit downstream. The intermediary fixes where standard- and price-setting power accumulates.
Recognition of the exporting periphery	North Africa framed as a low-cost supply basin; ports as ammonia conversion hubs. No provisions on the conditions of production abroad.	Export-oriented electrolysis implies land, water and renewable commitments serving EU rather than local demand — a transfer ("green extractivism") left ungoverned.

Table 1. Key findings: descriptive synthesis and geopolitical interpretation across the three analytical axes.

Dependency. The security-of-supply rationale is internally tension-ridden: an import-prevalence pathway substitutes North African hydrogen for Russian gas without resolving the external vulnerability that motivated post-2022 policy [7], so "make or buy" is best read as a decision about how much strategic autonomy to trade for lower cost.

Corridor value. Because the corridor's demand anchors lie in Central Europe, Italy's hub ambition is more a transit position than one of command: it confers leverage and rents while leaving bargaining power — and, through the proposed intermediary, authority over standards and prices — downstream.

Recognition. Treating North Africa as a supply basin while remaining silent on production conditions risks relocating rather than resolving the burdens of scale-up; extended to the international scale, an

energy-justice lens [1]–[3] shows that import can decarbonise Italy partly by exporting its externalities across the Mediterranean.

Conclusions: The paper proposes four governance principles to make Italy's hub strategy both more resilient and more legitimate: (1) diversification and autonomy safeguards, setting a floor on domestic production and diversifying suppliers so as not to recreate single-source dependency in a new vector; (2) reciprocity and co-development clauses, tying import partnerships to co-investment and local-value conditions in exporting countries; (3) recognitional safeguards in certification, extending guarantees of origin to cover the socio-environmental conditions of production abroad [1]–[3]; and (4) transparent corridor governance, institutionalising transparency over capacity allocation, intermediary auctions and standard-setting. By embedding these principles, Italian hydrogen policy could move from a hub narrative centred on cost and infrastructure toward one that explicitly governs dependency, value distribution and cross-Mediterranean justice — reducing the risk that Europe's import ramp-up reproduces old asymmetries of energy power in a decarbonised guise.

Acknowledgment

This research has been carried out with the financial support of the POR H2 project, financed by the Piano Nazionale di Ripresa e Resilienza – Mission 2.

References

[1] R. J. Heffron and D. McCauley, "The concept of energy justice across the disciplines," Energy Policy, vol. 105, pp. 658–667, 2017.

[2] K. E. H. Jenkins, D. McCauley, R. Heffron, H. Stephan, and R. W. M. Rehner, "Energy justice: A conceptual review," Energy Research and Social Science, vol. 11, pp. 174–182, 2016.

[3] G. Pellegrini-Masini, A. Pirni, and S. Maran, "Energy justice revisited: A critical review on the philosophical and political origins of equality," Energy Research and Social Science, vol. 59, art. 101310, 2020.

[4] IEA, Global Hydrogen Review 2023. Paris: International Energy Agency, 2023.

[5] IRENA, Green Hydrogen Strategy: A Guide to Design. Abu Dhabi: International Renewable Energy Agency, 2024.

[6] Ministero dell'Ambiente e della Sicurezza Energetica, Strategia Nazionale Idrogeno. Rome, Nov. 2024.

[7] European Commission, REPowerEU Plan, COM(2022) 230 final, Brussels, 18 May 2022.



Traceable Humidity Measurements Supporting Hydrogen Quality Assurance and Safety Across the Hydrogen Supply Chain

R. Nobakht*[a], R.Cuccaro [a], V. Fabiani[a,b], D.Smorgan[a],

R. Salerno[a], V. Fernicola[a]

* corresponding author: R. Nobakht

[a] Istituto Nazionale di Ricerca Metrologica, Torino, Italy

[b] Politecnico di Torino, Torino, Italy

Keywords: Hydrogen supply chain quality control, Hydrogen Iso 14687 standards, sensor calibration

Abstract

Introduction: Reliable hydrogen quality monitoring is essential for the safe deployment of hydrogen technologies. Within the Met4H2 project, INRIM developed a Precision Humid Hydrogen Generator (PHG) to provide traceable calibration of humidity sensors under representative hydrogen conditions. Commercial sensors were calibrated in both nitrogen and hydrogen and subsequently deployed during monitoring campaigns at an AEM electrolyser facility at Torino Airport (Caselle) and at the Nippon Gases hydrogen production plant in San Salvo, Italy. The results revealed measurable carrier-gas effects, highlighting the importance of hydrogen-specific calibration procedures. These findings were further supported by activities within the THOTH2 project, where instrumentation for hydrogen and hydrogen–natural gas infrastructures was evaluated under hydrogen service conditions. The work demonstrates the transfer of metrological traceability from laboratory standards to industrial environments, supporting hydrogen quality assurance, safety monitoring and the implementation of international standards.

Objectives: The objective of this work is to demonstrate an integrated metrological framework for hydrogen quality monitoring, linking traceable reference standards, laboratory calibration of humidity sensors, and validation through industrial deployment. The work aims to show how measurement traceability can support hydrogen quality assurance and safety throughout the hydrogen supply chain, from production facilities to future transport infrastructures.

Material and methods: Within the Met4H2 project, INRIM developed a Precision Humid Hydrogen Generator (PHG) to provide traceable humidity measurements in hydrogen. The generator produces humid hydrogen streams with water vapour amount fractions between 0.5 µmol mol^{-1} and 50 µmol mol^{-1} at pressures up to 6 MPa and was used as a reference standard for the calibration of commercial humidity sensors intended for hydrogen service. Calibration campaigns were performed in both nitrogen and hydrogen over the frost-point temperature range from −60 °C to −10 °C and at pressures up to 3 MPa in order to evaluate the influence of the carrier gas on sensor performance.

Following laboratory calibration, selected sensors were deployed during on-site monitoring campaigns carried out within Met4H2. The first campaign was performed at the Torino Airport (Caselle) hydrogen demonstrator, where hydrogen produced by an AEM electrolyser was monitored downstream of the purification and drying stages. Humidity measurements were complemented by oxygen monitoring and gas sampling activities. A second campaign was conducted at the Nippon Gases hydrogen production plant in San Salvo, Italy, where online measurements were performed using traceable instrumentation and analytical systems developed within the project. Additional investigations performed within THOTH2 extended the assessment of humidity sensors to hydrogen and hydrogen–natural gas applications relevant to future transport infrastructures.

Results: Calibration of commercial humidity sensors between −60 °C and −10 °C frost-point temperature and at pressures up to 3 MPa revealed systematic differences between nitrogen- and hydrogen-based calibrations, highlighting the importance of hydrogen-specific calibration procedures. The calibrated sensors were subsequently deployed at the Caselle Airport AEM electrolyser facility and at the Nippon Gases hydrogen production plant, demonstrating the applicability of traceable humidity monitoring under real operating conditions. Consistent observations obtained within the THOTH2 project further confirmed the influence of hydrogen on sensor response. Together, the results demonstrate a complete metrological chain, from traceable reference standards to industrial validation, supporting hydrogen quality monitoring, safety verification and the implementation of standards such as ISO 14687, ISO 19880-8 and ISO 21087.

Conclusions: This work demonstrates an integrated metrological approach for hydrogen quality monitoring, combining a traceable humid hydrogen reference standard, calibration of commercial humidity sensors, and validation at industrial hydrogen facilities. The observed carrier-gas effects confirm the importance of calibration under representative hydrogen conditions, while the field campaigns at Caselle and Nippon Gases demonstrate the practical implementation of traceable measurements in operational environments. The complementary results obtained within Met4H2 and THOTH2 provide technical support for hydrogen quality assurance, safety monitoring and the implementation of standards relevant to the hydrogen supply chain.

Acknowledgment: This work was supported by the European Partnership on Metrology project 21GRD05 Met4H2 – Metrology for the Hydrogen Supply Chain, co-financed by the Participating States and the European Union. Additional support was provided by the THOTH2 project (Grant Agreement No. 101101540), funded by the Clean Hydrogen Partnership and supported by the European Union, Hydrogen Europe and Hydrogen Europe Research.

References

[1] Met4H2 Consortium, Good Practice Guide on Metrologically Traceable Quality Monitoring in the Hydrogen Supply Chain, Deliverable D6, 2025.

[2] R. Cuccaro, R. Nobakht, D. Smorgon, R. Salerno, D. Enescu and V.C. Fernicola, Providing Traceability to Humidity Sensors in the Hydrogen Supply Chain, TEMPMEKO 2026.

[3] M. Robino et al., Experimental Investigation of Metering Device Performance under Hydrogen–Natural Gas Mixtures, SDEWES 2025.

[4] ISO 14687, Hydrogen Fuel Quality — Product Specification.

[5] ISO 19880-8, Gaseous Hydrogen — Fueling Stations — Quality Control.

[6] ISO 21087, Gas Analysis — Analytical Methods for Hydrogen Fuel Quality.



Biogas-Fueled Renewable Peak Power and Renewable Hydrogen and Fuel Generation Using Reversible Solid Oxide Electrolysis Cells – potentials on local and national level in Finland

Robert Weiss*[a], Ville Saarinen[a], Werneri Huhtinen[a], Pyry Mäkinen[a], Olli Himanen[a]

* Corresponding author: robert.weiss@vtt.fi, tel.: +358-40-5381204

[a] VTT Technical Research Centre of Finland Ltd, P.O. Box 1000, FI-02044 VTT, Finland

Keywords: Balancing Power, Biogas Plants, reversible Solid Oxide Electrolysers, RFNBO fuel

Abstract

Introduction: Biogas generated through the anaerobic digestion (AD) of sewage sludge, organic wastes, or sustainably produced biomass represents a significant potential energy source for advancing societal sustainability. This unrefined AD biogas typically consists of 50–65 molar percent methane (CH_4) and 50–35 molar percent carbon dioxide (CO_2). Following its initial production, raw biogas from larger biogas plants may undergo an upgrading process to yield biomethane, which contains more than 98 molar percent CH_4 and possesses energetic characteristics like those of fossil natural gas. Biomethane can even be liquefied for use as transport fuel. Unfortunately, for smaller and mid-sized biogas plants, such upgrading and liquefaction investments are often economically prohibitive. As a result, if utilized at all, raw biogas is typically utilized in many countries for combined heat and power production using combustion engines, which results in low conversion rates to power (typically below 40%) and considerable local emissions. However, at this scale, unrefined biogas can be utilized for flexible peak power production in Solid Oxide Fuel Cell (SOFC) plants, achieving conversion rates as high as 60% with zero local emissions. Such SOFC systems can also be designed as novel high-performance reversible Solid Oxide Electrolysis Cells (rSOC). In addition to operating in SOFC power and heat production mode, rSOC systems can function in the opposite direction as solid oxide electrolyzers (SOE): During periods of surplus renewable power, the SOE mode can convert excess electricity and steam into green hydrogen and other renewable fuels of non-biologic origin (RFNBO) [1], with the necessary steam supplied by a simple boiler using available unrefined biogas. In this way, biogas plants can serve as both balancing power plants as well as daily, weekly, and longer-term energy storage solutions, buffering temporal electrical energy surpluses and producing domestic green hydrogen or other RFNBO for the transport sector or storing hydrogen for later peak power production.

Objectives: This study presents cost (LCOE) and profitability estimates for optimal rSOC investment, dimensioning and operation strategies at small- and midsized biogas plants in Finland, considering market estimates on Finnish fuel and hydrogen markets. rSOC electrolysis mode (SOE) uses intermittent green power, while the fuel cell mode (SOFC) runs on raw biogas. Market operations, renewable source sizes, plant dimensions, scheduling and operational strategies of integrated rSOC and biogas plant sites were assessed using a Power-to-X (P2X) optimization model adapted for this assessment purpose and upscaled to national level results.

Material and methods: A dedicated Power-to-X optimization framework, developed at VTT for hydrogen valley and site-level assessments [2][3][4][5], was refined here for biogas plant integrations. The model optimizes process integration, rSOC and other unit sizing, operating strategy, renewable power sourcing, and balancing and wholesale power trading. Renewable electricity can be directly coupled or contracted through wind and solar PPAs, with hourly trading used to capture market volatility [2]. Large trades affect hourly wholesale prices through modeled price elasticities, limiting surplus power sales into saturated markets [3].

The model represents biogas feed and composition, grid connection, battery, electrolyser, fuel cell or CHP unit, H_2 compressor, H_2 storage, and optional P2X downstream unit. Electrolyser and fuel cell submodels include shutdowns, cold and warm starts, and associated preheating losses and costs [2]. In rSOC cases, both modes are represented as a single reversible unit, including shared investment, lower nominal fuel cell capacity, start-ups, and hot switching between modes. Hourly operation captures renewable intermittency, wholesale and balancing price variation, start-up losses, and process constraints, while storage, unit sizing, and wind and solar PPA volumes are optimized over longer horizons. SmartP2X therefore links detailed hourly operation with investment and contracting decisions [2]. Electrolyser techno-economic parameters are based on 2030 estimates from Hydrogen Europe [6], with additional CAPEX for siting, project work, and contingency estimated by the authors. Parameters for compression, pipeline storage, market power prices, renewable production, and PPA costs are reported in [2], [3], [4], and [5].

Results and Conclusions: Integrating Power-to-Gas and Gas-to-Power operation at small- to mid-scale biogas plants can strengthen their role as renewable fuel producers and providers of power-system flexibility through smart energy buffering.

Reversible solid oxide electrolysis (rSOC) enables bidirectional operation: it produces green hydrogen during periods of surplus renewable electricity and converts raw biogas to electricity when demand exceeds sustainable supply. This supports flexible, bioenergy-based production of both green gas and renewable balancing and peak power. The rSOC pathway also offers near-zero local emissions, with no measurable NO_x, SO_2, HCl, HF, organic compounds, N_2O, or CH_4. Avoiding methane slip is particularly relevant, as CH_4 has a substantially higher global warming potential than CO_2, making rSOC a lower-emission alternative to conventional gas engines.

The results indicate strong profitability in 2024-2025, yielding a net production price of 2.8 €/kg RFNBO-H_2 (at a sales price of 4€/kg) mainly driven by high wind penetration and pronounced electricity price volatility in Finland. For a biogas plant at a 10-20kV/10MW max grid connection with biogas buffer, hydrogen buffer and steady 1 MW production of untreated raw biogas containing 64% CH_4, a rSOC with 4 MW SOFC and 9.3 MW SOEC capacity would optimally integrate 19 MW wind power and 26 MW solar PV power. Both 1100 full load hours (FLH) peak power and 6700 FLH RFNBO-compliant hydrogen would be produced by the same rSOC unit with minimal emissions.

At the national scale, the concept could in 2030 provide substantial ~10% balancing capacity during periods of low wind and solar output, provided that sufficient deployment is achieved.

Acknowledgment

This research was carried out in the HEROES – Heat and Energy Recovery Of Electrolyser Systems - public research project, with funding from Business Finland, VTT and company partners.

References

[1] The European Commission, “Detailed Rules for the Production of Renewable Liquid and Gaseous Transport Fuels of Non-Biological Origin,” 2023.

[2] R. Weiss and J. Ikäheimo, “Flexible Industrial Power-to-X Production as Virtual Hydrogen Storage enabling Large Scale Wind Power Integration: A Case Study of future Hydrogen Direct Reduction Iron Production in Finland,” Appl. Energy, vol. 365, no. July 2024. doi: 10.1016/j.apenergy.2024.123230.

[3] R. Weiss, T. Kanto, K. Kiviranta, J. Ikäheimo, and J. Kärki, “Large scale power-to-X production enabling hydrogen valleys: A case study of future industrial hydrogen valley opportunity in Finland,” Appl. Energy, vol. 388, no. March 2025, doi: 10.1016/j.apenergy.2025.125596.

[4] R. Weiss, J. Ikäheimo, K. Kiviranta, and T. Kanto, “P2X and Hydrogen Valleys Enhancing Wind Power Profitability,” in International Conference on the European Energy Market, EEM, IEEE Computer Society, 2025. doi: 10.1109/EEM64765.2025.11050212.

[5] R. Weiss, T. Kanto, K. Kiviranta, J. Ikäheimo, and J. Kärki. Integration of Green and Turquoise Hydrogen for Blast Furnace Injection and Power-to-X Fuel Production in Industrial Hydrogen Valleys under EU Renewable Fuel Regulation, Journal of Energy Conversion and Management, vol. 336, 2026. doi.org/10.1016/j.enconman.2026.121835.

[6] Clean Hydrogen Joint Undertaking, “Strategic Research and Innovation Agenda 2021 - 2027,” 2022.



The French National Research Program on Low Carbon Hydrogen: Projects and Achievements

Abdelilah SLAOUI[*a], Hélène BURLET

* corresponding author: Abdelilah SLAOUI

[a] CNRS, 3 Rue Michel-Ange, 75016 Paris

[b] CEA, Rue des Martyrs, 38000 Grenoble

Keywords: French Low Carbon Hydrogen Strategy, hydrogen production, fuel cells, hydrogen systems

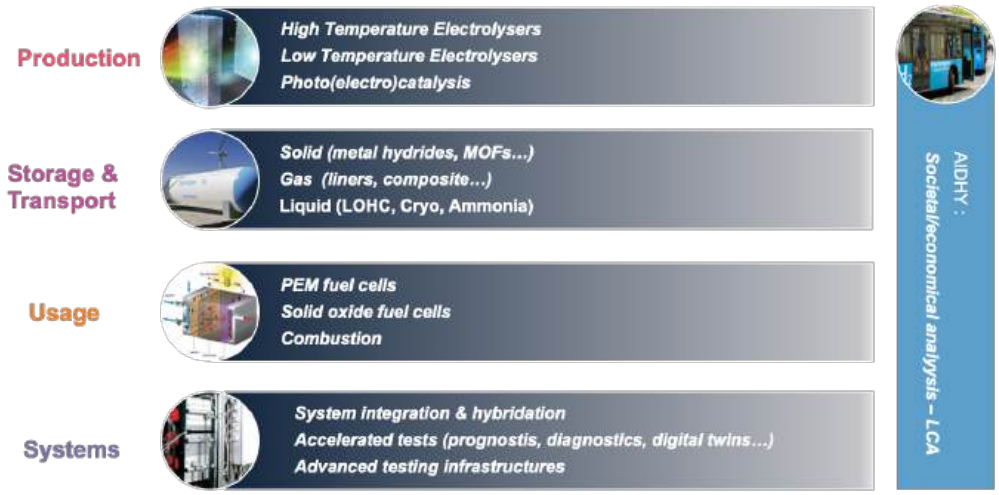
Abstract

The first part of the presentation gives insights on the French Low Carbon Hydrogen Strategy [1]. This strategy aims to enhance industrial autonomy, while focusing on the utilisation of the country's low-carbon electricity. The strategy sets targets for electrolysis capacity, aiming for 4.5 GW by 2030 and up to 8 GW by 2035, with plans to meet domestic hydrogen needs without relying on imports up to 2035. It emphasises the development of various electrolyser technologies, integration with nuclear power to improve efficiency, and substantial financial support for national hydrogen production. Additionally, the strategy focuses on sector-specific hydrogen use in industry, maritime, and aviation, while promoting the export of French equipment and international collaboration through technical expert positions. The development of hydrogen transport networks and storage infrastructure is also a key priority, supported by regulatory frameworks and financial mechanisms.

The second part of the presentation focuses on the research and development activities linked to the strategy on low carbon hydrogen economy. This program, named PEPR-H2, [2] aims to develop upstream research activities, specifically addressing: (i) low-carbon hydrogen production via electrolysis or photo(electro)catalysis; (ii) hydrogen use in heavy-duty mobility—developing a new generation of high-performance, durable fuel cells while also investigating hydrogen combustion for transport; and (iii) hydrogen storage in solid, liquid, or gaseous forms. Research will also be conducted to support the deployment of hydrogen systems through life-cycle assessments, techno-socio-economic studies, and analyses of safety and regulatory aspects.

The program currently comprises 21 R&D projects covering the entire value chain; 19 address technological challenges, while one focuses on developing decision-support tools. The key drivers guiding the PEPR-H2' projects are reaching performances beyond the state of the art for electrolyzers and fuel cells, enhancing their durability, and reducing their cost to facilitate the deployment of

hydrogen systems. Projects took into account constraints regarding access to certain materials deemed critical, prioritize processes with a low environmental footprint, and incorporate eco-design principles. The program also includes the DurabilitHy project dedicated to the updated infrastructures for testing. To date, the projects have resulted in several patents filing and more than 100 journal publications.



Some remarkable results issued from the PEPR-H2' projects will be presented, with a focus on hydrogen production and fuel cells.

Acknowledgment

The authors knowledge the funding of the PEPR-H2 program through France 2030 initiative.

References

[1] https://www.france-hydrogene.org/app/uploads/sites/4/2023/10/France-Hydrogene_National-Hydrogen-Strategy_EN.pdf

[2] https://www.pepr-hydrogen.com/



TOPIC 7. HYDROGEN INNOVATION AND FUTURE TRENDS



Research and Innovation Across the Hydrogen Value Chain: current status, main challenges and Future Perspectives

Julie Mougin*[a]

[a] Univ. Grenoble Alpes, CEA/LITEN, 17 rue des Martyrs, F-38054 Grenoble, France

Keywords: hydrogen technologies; hydrogen value chain; research and innovation; system integration; scale-up; durability and reliability; research and technology infrastructures

Abstract

Hydrogen is expected to play an important role in industrial decarbonisation, energy-system flexibility and the decarbonisation of applications where direct electrification is difficult. Its successful deployment, however, requires the whole value chain—from production to storage, transport and end use—to be developed and optimised in an integrated manner. This presentation reviews the current status of hydrogen research and innovation (R&I) across the value chain and illustrates recent progress through European projects in electrolysis, underground hydrogen storage and fuel-cell applications. It then discusses the main challenges related to robustness, durability, scalability, representative validation, system integration and competitiveness. Future perspectives are finally outlined around predictive technology development, digitalisation, next-generation components and systems, flexible operation, modularity, large-scale demonstration and shared Research and Technology Infrastructures. The central message is that future hydrogen R&I must increasingly connect advances in materials and technologies with system-level optimisation and deployment.

Introduction

Driven both by the urgent need to mitigate CO_2 emissions and by growing concerns over energy security and dependence on imported fossil fuels, low-carbon hydrogen has become a strategic component of the energy transition. Its importance is increasingly reflected in European policies [1-2] and in national energy and industrial strategies. While hydrogen is already widely used in conventional applications such as refining and ammonia and fertiliser production, its future role could extend considerably. In particular, it offers a pathway to decarbonise sectors that are difficult or impossible to electrify directly, including primary steelmaking. Hydrogen and hydrogen-derived fuels can also contribute to long-duration energy storage and to the decarbonisation of heavy-duty and long-distance transport, where direct battery electrification may not be technically or economically suitable. Potential applications include road freight, shipping and aviation, either through the direct use of hydrogen in fuel cells or turbines, or through synthetic fuels produced from low-carbon hydrogen, such as e-kerosene, e-methanol (obtained by combining hydrogen with CO_2) and e-ammonia. The expansion of these emerging applications is expected to substantially increase global hydrogen consumption. According to the IEA Net Zero Emissions by 2050 Scenario, global hydrogen demand could increase from around 100 Mt today [3] to approximately 150 Mt by 2030 and 430 Mt by 2050 [4]. Aviation and maritime transport are expected to become particularly important sources of future demand, together potentially representing around one-third of low-carbon hydrogen consumption by mid-century [4].

A value-chain approach is essential because hydrogen competitiveness and sustainability are not determined by production alone. Production, conditioning, storage, transport, distribution and end use are strongly interconnected. The most appropriate pathway depends on the location of supply and demand, the required scale and the targeted application. R&I must therefore address critical interfaces, infrastructure and safety constraints while minimising total cost, energy losses and environmental impacts.

Current status of R&I across the hydrogen value chain

Hydrogen R&I has progressed from fundamental materials research towards increasingly integrated systems. At materials and component level, advances include new functional materials, reduced critical-material content, improved microstructures and interfaces, and advanced manufacturing. At technology and system level, R&I increasingly addresses durability, reliability, automation, monitoring, diagnostics, prognostics and optimisation. Cross-cutting developments in multiscale modelling, digital twins, in-situ and operando characterisation, safety, eco-design and techno-economic analysis further accelerate development.

Recent European projects illustrate this evolution. MULTIPLHY demonstrates the transition from stack development to a 2.6 MW solid oxide electrolysis system [5-7]. HYPSTER has progressed from modelling and risk assessment to large-scale cyclic operation of hydrogen in a salt cavern, coupled with a 1 MW electrolyser [8]. In end-use applications, REALHYFC combines advanced fuel-cell stack architectures with degradation modelling, virtual sensors and control strategies for durable operation under representative heavy-duty duty cycles [9-10]. STAShH addresses deployment and replication through standardised mechanical, fluidic, electrical and digital interfaces for fuel-cell modules [11]. Together, these examples illustrate the shift from technology performance alone towards scale-up, representative operation, integration and replication.

Main challenges

A first set of challenges concerns making technologies robust and scalable. Long-term performance must be maintained under dynamic and harsh operating conditions. This requires better understanding and mitigation of degradation mechanisms across materials, components and systems, together with scale-up and manufacturing processes ensuring reproducible quality and reliability. Further efficiency improvements must also be maintained under variable operation, while dependence on critical raw materials and harmful substances needs to be reduced.

A second set concerns making complete hydrogen solutions deployable and competitive. This includes integration with electricity, storage, heat and industrial processes; safety and infrastructure reliability; interoperability and standardisation; and the generation of long-term operational data under representative conditions. R&I must ultimately reduce total cost of ownership while enabling successful demonstrations to be replicated at larger scale.

Future perspectives

Future R&I will increasingly move from understanding materials and degradation towards predictive technology development. Digitalisation, advanced monitoring, digital twins and AI-supported operation can support the transition from failure detection to prognostics and predictive maintenance. Multi-scale and multi-physics modelling, advanced characterisation, high-throughput screening, materials-by-design approaches, accelerated stress testing, and efficient Research and Technology Infrastructures will be important enablers for faster and more predictive technology development.

At the same time, the perspective is shifting from standalone technologies to system-wide optimisation. This includes next-generation, higher-efficiency components and systems across the whole hydrogen value chain, through both incremental and breakthrough innovation. Advanced system integration and optimisation tools, together with flexible and intelligent operation, control and management systems, will be needed under

changing energy-system conditions. Modular, standardised and interoperable architectures can facilitate replication, while large-scale integrated demonstrators are required to validate complete value chains under realistic conditions. System-level optimisation should increasingly include infrastructure aspects, supported by shared and networked Research and Technology Infrastructures [12-13].

Conclusion

The next phase of hydrogen R&I is not only about improving individual technology performance: it is about delivering robust, efficient, scalable and sustainable technologies and integrating them into safe, flexible and competitive systems. This will require continued support for both mature and breakthrough technologies, from materials to systems, together with representative testing and demonstration capabilities. Harmonised regulation and standards, permitting, certification, policy and financial support, and responsible use of resources will also be essential to translate R&I progress into large-scale deployment.

References

1. https://energy.ec.europa.eu/topics/renewable-energy/renewable-energy-directive-targets-and-rules/renewable-energy-directive_en; https://transport.ec.europa.eu/transport-modes/air/environment/refueleu-aviation_en;
2. https://transport.ec.europa.eu/transport-modes/maritime/decarbonising-maritime-transport-fueleu-maritime_en
3. IEA Global Hydrogen Review 2026 https://iea.blob.core.windows.net/assets/af4b6218-0311-4963-91ab-903cb18ca0ca/GlobalHydrogenReview2026.pdf
4. https://www.iea.org/reports/hydrogen-2156
5. J. Mougin, et al, International Journal of Hydrogen Energy 141 (2025) 1165-1171, doi: https://doi.org/10.1016/j.ijhydene.2025.02.070,
6. J. Aicart, et al, International Journal of Hydrogen Energy 258 (2026) 156630, https://doi.org/10.1016/j.ijhydene.2026.156630
7. https://multiplhy-project.eu/
8. https://hypster-project.eu/
9. https://realhyfc-project.eu/
10. E. Fensterle et al, International Journal of Hydrogen Energy 250 (2026) 156060; https://doi.org/10.1016/j.ijhydene.2026.156060
11. https://stashh.eu/
12. www.acthyve.eu
13. S. Abermann , et al, International Journal of Hydrogen Energy, 270 (2026), 157061, https://doi.org/10.1016/j.ijhydene.2026.157061



Operando SAXS and XAS analyses for PEM fuel cells and water electrolyzers: time-resolved insights about catalyst degradation at a single cell level

Marco Bogar*[a], Yurii Yakovlev[b], Yevheniia Lobko[b], Heinz Amenitsch[c], Rodolfo Taccani[a], Iva Matolínová[b]

* corresponding author: marco.bogar@dia.units.it

[a] Department of Engineering and Architecture, University of Trieste, Via Alfonso Valerio 6/1, 34127, Trieste, Italy

[b] Charles University, Faculty of Mathematics and Physics, Department of Surface and Plasma Science, V Holešovičkach 2, 18000 Prague 8, Czech Republic

[c] Institute for Chemistry and Technology of Materials, Graz University of Technology, 8010 Graz, Austria

Keywords: catalyst degradation, operando x-ray-based investigation techniques, Proton Exchange Membrane Fuel Cells, Proton Exchange Membrane Water Electrolysers

Abstract

Catalyst stability is a key issue limiting both efficiency and lifetime of electrochemical devices for both hydrogen production (Water Electrolysers, WEs) and use (Fuel Cells, FCs). With the aim of studying degradation kinetics affecting the catalysts in both FCs and WEs, a properly designed electrochemical cell was developed to monitor *in operando* conditions catalyst stability by means of x-ray-based investigation techniques. By complementing obtained results with electrochemical measurements and electron microscopy, morphological and chemical changes affecting both Pt and Pt_3Co catalysts for the oxygen reduction reaction in Proton Exchange Membrane (PEM) FCs were compared, showing how Co leaching affects degradation kinetics from the very initial times of FC operation. Analogously, the stability of novel Ir-supported catalyst materials for the oxygen evolution reaction in PEMWEs (Ir/TiO_2, Ir/TiC_2, Ir/TiN_2), and the stability of standard Ir catalyst with respect to potential switching were studied. Ir-supported catalysts showed promising electrochemical performances, but still need to be optimised in terms of stability to withstand support dissolution.

Introduction: costs and efficiency losses are the main factors limiting the diffusion of hydrogen technologies for decarbonising the so-called hard-to-abate sectors, and both of them can be related to the catalyst composition within the Membrane Electrode Assembly (MEA) [1]. Regarding hydrogen production, Ir NanoParticles (NPs) are currently used as catalysts for the Oxygen Evolution Reaction (OER), and Ti-compounds have been shown constituting a possible novel class of supporting materials for Ir NPs [2], as their effective deployment would allow to reduce the overall Ir content in

Proton Exchange Membrane Water Electrolysers (PEMWEs), reducing costs without affecting performances. Nonetheless, their stability with respect to the operating potentials still needs to be properly studied, as the anodic operating conditions strongly limit the range of materials suitable for this purpose. Concerning catalysts for the Oxygen Reduction Reaction (ORR) in PEM Fuel Cells (PEMFCs), the interest in Pt bimetallic alloys is due to their comparable performance and reduced Pt content with respect to bare Pt NPs [3], but leaching of the less noble metal composing the alloy is expected to affect catalyst stability over time.

Objectives: to properly quantify stability of catalyst materials for PEM FCs and WEs, x-ray-based investigation techniques were used with the aim of monitoring chemical and morphological changes regarding catalyst materials used in both PEM FCs and WEs. In this framework, stability of novel Ti-based compounds supporting Ir NPs for the OER reaction to operating potential was compared. In parallel, the same approach was used to depict changes in degradation kinetics of Pt and Pt_3Co catalysts for the ORR in PEMFCs.

Material and methods: a windowed Electrochemical Cell (EC) was developed for monitoring in *operando* conditions the evolution of catalyst materials by means of Small-Angle X-ray Scattering (SAXS) and X-ray Absorption Spectroscopy (XAS) [4]. SAXS allowed to monitor morphology changes of the catalyst NPs loaded in the MEA by measuring the change in Particle Size Distribution (PSD), while XAS (collected at the Pt L_3- and Co K- absorption edges) provided information about changes in catalyst chemistry, in terms of change of oxidation state of the catalyst of interest. In FC-mode, the evolution of two standard catalyst materials was studied (Pt and Pt_3Co NPs, 0.8mg/cm^2): from pristine conditions, during the break-in (T_{cell}:80°C,ϕ_{H2} :20NmL·min^{-1}/100%RH, ϕ_{O2}:20NmL·min^{-1}/100%RH, V:0.4V/2h), and undergoing Accelerated Stress Tests (ASTs) simulating load cycle operation (potential switching 0.65-0.9V, 3s/step) [4]. Based on previous experiments [5], and due to beamtime temporal constraints, cyclic voltammograms and SAXS patterns were recoded every 250 cycles, while XAS spectra were recorded at specific timepoints of interest. In WE-mode, the EC was used to compare stability of novel Ir-supported catalysts for the OER (Ir/TiO_2, Ir/TiB_2, Ir/TiN_2, 1mg/cm^2), starting from pristine conditions, and under specifically designed AST (T_{cell}:70°C, ϕ_{H2O}:100mL·min^{-1}, potential switch:0-2.0V, 5s/step). Finally, the stability of bare Ir NPs was assessed under square-wave current operation by alternating between *x* A·cm^{-2} and 0V (3s/step, *x*:2,3,4A·cm^{-2}). Electrochemical characterization and SAXS patterns were performed every 50 cycles (as degradation kinetics of the systems studied were unknown but expected to start since the early stages of AST); XAS spectra were recorded at the specific timepoints of interest.

Results: Figure 1 summarises main results. Regarding FCs, by comparing changes in PSD and electrochemically active surface area (ECSA), it was shown as Co dealloying changes degradation kinetics, surprisingly slowing down the onset for Ostwald ripening. Co leaching was detected from the very first steps of FC operation, as confirmed by the formation of Co complexes, revealed by XAS [6]. By referring to WEs, Ir/TiO_2 was found to be the most stabile formulation among the three studied, but

here, growth in Ir NPs size was detected too. While in the other two formulations Ir NP size remained constant, not all of the Ir was found oxidised, potentially limiting the overall performances in terms of charge transfer. Results were supported by electron microscopy and both x-ray and electron spectroscopies [7].

Conclusions: regarding FCs, results highlight as dealloying might be better studied and engineered with the aim of mitigating catalyst degradation in PEMFCs. Concerning WEs, findings show that Ir-supported NPs for the OER need to be further improved to provide satisfying performances for being used in in commercial devices.

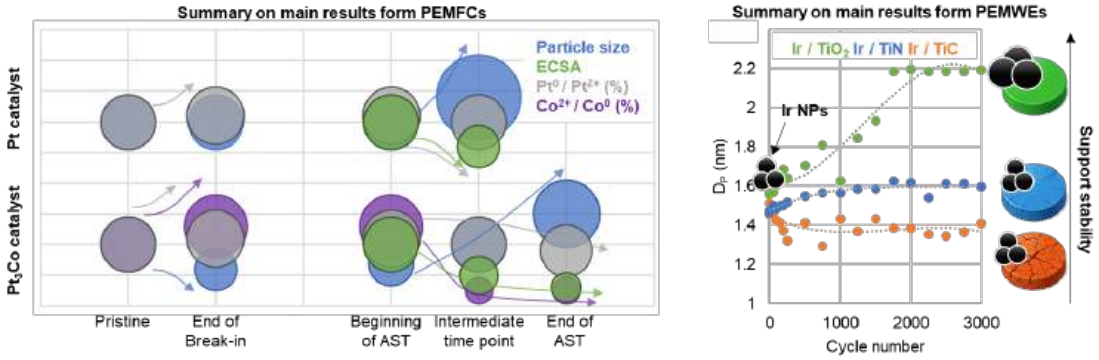


Figure 103. Main results from operando analyses (left) on PEMFCs and (right) on PEMWEs

Acknowledgment

M.B. and R.T. acknowledge the financial support from: Italian Operative Program for Research and Innovation 2014–2020 (Italian Ministry of University and Research) and NAHV project (North Adriatic Hydrogen Valley, HORIZON-JTI-CLEANH2-2022-2, Project ID: 101111927). Y.Y., Y.L., and I.M. acknowledge financial support from project "Energy Conversion and Storage" (Programme Johannes Amos Comenius – Excellent Research; Ministry of Education, Youth and Sports of the Czech Republic, Project ID: CZ.02.01.01/00/22_008/0004617).

References

[1] IRENA (2020), Green Hydrogen Cost Reduction; ISBN:978-92-9260-295-6

[2] Li C., *et al.*, J. Alloys Compd., (2024),979,173576;doi: 10.1016/j.jallcom.2024.173576

[3] Wang Y., et al., Materials Today, (2020),32,178-203; doi: 10.1016/j.mattod.2019.06.005

[4] Bogar M., et al., J.Power Sources, (2024),615,1-8; doi: 10.1016/j.jpowsour.2024.235070

[5] Bogar M., et al., ACS Catal., (2021),11,11360−11370; doi: 10.1021/acscatal.1c01111

[6] Bogar M., et al., Chem.Eng.J.Gr.Sust.,(2026),1,100017; doi: 10.1016/j.cejgas.2025.100017

[7] Lobko E., Bogar M., *et al.*, Journal of the American Chemical Society, (2026), *submitted.*



A Fault Injection Framework for Hydrogen Fuel Cell-Battery Hybrid Trains to Enable Condition-Based Maintenance

Lavinia Gaeta*[a], Marta Gandiglio [a], Paolo Marocco[a], Pierpaolo Cherchi[b], Marco Cocco[c], Massimo Santarelli [a]

* Corresponding author: lavinia.gaeta@polito.it

[a] Department of Energy, Politecnico di Torino, Corso Duca degli Abruzzi 24, 10129 Torino, Italy.

[b] Alstom Ferroviaria S.p.A, Via Ottavio Moreno 23, 12038 Savigliano (CN), Italy

[c] Alstom, Via Fosse Ardeatine 120, 20099 Sesto San Giovanni (MI), Italy

Keywords: Condition-Based Maintenance, Digital Twin, Fault Injection Analysis, Hydrogen Hybrid Train

Abstract

Introduction: The global shift toward zero-emission transport has accelerated the adoption of Hydrogen Multiple Units (HMUs) to decarbonize non-electrified rail lines. By hybridizing hydrogen fuel cells with battery energy storage, HMUs provide a viable alternative to diesel traction, offering long-range autonomy [1]. However, the novelty of these systems poses concerns regarding operational reliability and sustainability. In this context, Condition-Based Maintenance (CBM) plays a pivotal role in minimizing downtime by evaluating the real-time State of Health (SoH) of individual components [2]. Despite its potential, CBM implementation faces a critical bottleneck: the scarcity of historical operational data.

Objectives: To bridge this gap, this study proposes a simulation-based framework centered on the development of a high-fidelity Digital Twin of an HMU, integrating the fuel cell power packs, the traction batteries and hydrogen storage system into a cohesive multi-physics model. Implemented in the Matlab/Simulink environment, the Digital Twin is designed to replicate the exact multi-physics behavior of the hybrid train, including its electrochemical and thermal interactions. The role of this model is twofold: first, to establish a reliable baseline for healthy operations; and second, to serve as a controlled environment for Fault Injection Analysis.

Material and methods: The HMU propulsion system is modeled as three interconnected subsystems, the Fuel Cell Power Pack (FCPP), Traction Battery System (TBS), and Compressed Hydrogen Storage System (CHSS), using a zero-dimensional (0D) approach to balance physical accuracy with computational speed. The FCPP utilizes a dynamic electrochemical model that captures non-linear voltage drops (activation, ohmic, and concentration overpotentials) based on temperature, hydration, and pressure. To manage peak loads, the TBS is modeled via a second-order Equivalent Electric

Circuit (EEC) integrated with a Battery Thermal Management System (BTMS) to regulate module temperatures through water-glycol cooling. Finally, the CHSS simulates the 350-bar hydrogen supply using a real-gas Equation of State and a radial thermal sub-model. This hierarchical structure avoids the complexity of 3D CFD while remaining sensitive to the degradation features required for fault analysis.

With the Digital Twin established as a high-fidelity baseline, the framework is extended to simulate anomalous operations through a systematic Fault Injection Analysis (Figure 104). Based on critical failure modes identified in technical literature, faults are integrated into the model by perturbing physical root causes or simulating their observable system effects. To ensure the resulting datasets are both comprehensive and computationally manageable, a multi-stage simulation strategy is implemented. This process begins with a preliminary sensitivity assessment to isolate parameters with a significant impact on observable states, followed by a propagation analysis to evaluate how localized degradations affect subsystem-wide performance through electrical, thermal, and fluid-dynamic cross-coupling. The methodology concludes with an advanced sampling approach designed to effectively explore the multidimensional space of fault combinations and degradation ranges, providing the robust synthetic data necessary for training future prognostic algorithms.

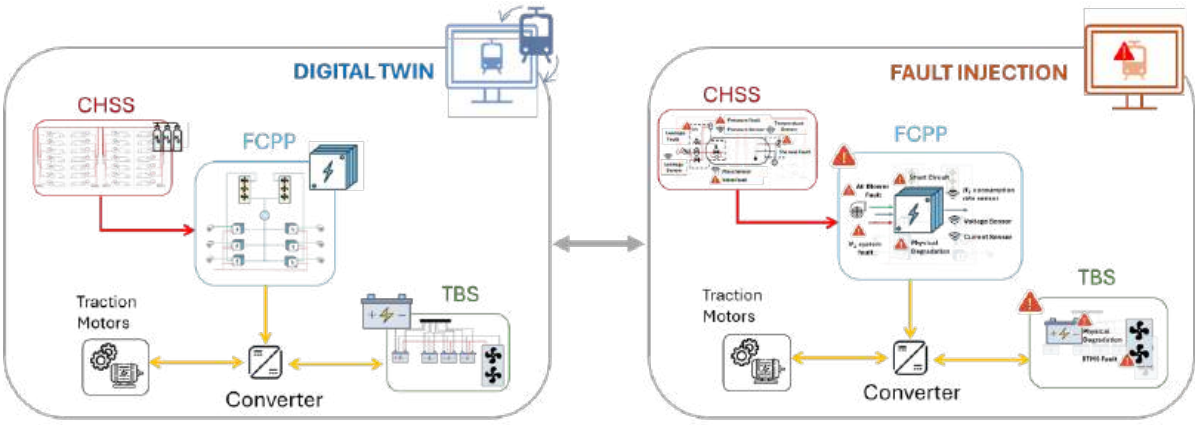


Figure 104.Conceptual workflow of the Fault Injection Analysis: transition from the nominal Digital Twin (left) to the degraded state (right), highlighting the systematic perturbation of CHSS, FCPP, and TBS parameters for diagnostic signature mapping.

Results: The Digital Twin is validated against industrial field data to ensure its fidelity in replicating HMU operations. For the FCPP, the model demonstrates high accuracy, with simulated polarization curves and auxiliary power demands showing a strong correlation with benchmark data (Mean Absolute Error ≈1%). Similarly, the CHSS validation confirms that the real-gas approach accurately tracks pressure and mass evolution. While direct reference data for the TBS are currently unavailable, the model shows high physical consistency in its electrical and thermal responses during simulated missions. The results of the Fault Injection Analysis demonstrate that the Digital Twin accurately replicates the physical phenomena associated with specific failure modes. The model successfully captures electrochemical and fluid-dynamic anomalies in the FCPP, such as those affecting

membrane hydration and reactant supply, as well as thermal and resistive degradations within the TBS and its cooling circuit. However, the analysis also revealed that the model is not suitable for capturing high-frequency transient faults, such as short circuit event. For this reason, these specific events were excluded from the final diagnostic dataset to ensure data integrity. For the remaining valid scenarios, the framework identified critical operational thresholds, such as maximum allowable internal resistance and pressure limits, beyond which system stability is compromised. Beyond identifying failures, the analysis demonstrates that the HMU can often continue to operate safely despite the presence of a fault, even if the overall system response deviates from the nominal baseline. By mapping these performance shifts, the study characterizes the resilience of the HMU powertrain, distinguishing between manageable degradation and incipient failure. This capability is essential for defining safe operating envelopes and creating maintenance triggers that prioritize both operational continuity and passenger safety.

Conclusions: This study validates the Digital Twin as a reliable virtual testbed for the hydrogen rail sector, overcoming the current lack of operational data. By accurately replicating the HMU response to both nominal and faulty conditions, the framework serves as a strategic asset for powertrain design optimization and the validation of safety protocols without the need for costly physical testing. The results confirm that the model can effectively distinguish between manageable degradation and critical failures, providing a foundation for real-time diagnostic tools. Future work will integrate specific physical wear mechanisms, such as catalyst degradation and battery capacity fade, to enable precise Remaining Useful Life (RUL) estimation. Ultimately, this Digital Twin will support the development of degradation-aware Energy Management Strategies (EMS), optimizing power distribution to extend the train's operational life and ensure the economic sustainability of zero-emission mobility.

Acknowledgment

This research was funded by the European Union - Next Generation EU – Project ID: IPCEI-I1_0000003 CUP: B19J23000490004 coordinated by Alstom Ferroviaria S.p.A.

References

[1] G. e. a. Peyrani, «Techno-economic modeling framework to assess the feasibility of hydrogen-powered trains on non-electrified routes.,» *Journal of Power Sources 652,* n. 237677, 2025.

[2] M. e. a. Jouin, «Prognostic and Health Management of PEMFC - State of the art and remaining challenges,» *International Journal of Hydrogen Energy 38.35,* 2013.



Redox properties of Azo Dyes determined via quantum chemical methods

Eleonora Hubenova*[a,b], Nikolay Toshev[c], Yolina Hubenova[a,b,d]

[a]Centre of Competence HITMOBIL, Acad. G. Bonchev Str., bl.10, Sofia 1113, Bulgaria

[b]Institute of Electrochemistry and Energy Systems "Academician Evgeni Budevski", Bulgarian Academy of Sciences, 1113 Sofia, Bulgaria

[c]Medical University of Plovdiv, 4002 Plovdiv, Bulgaria

[d] Plovdiv University "Paisii Hilendarski", 4000 Plovdiv, Bulgaria

Keywords: Azo dyes, DFT, HOMO-LUMO energies, Redox activity

Abstract

Azo dyes are widely used compounds that have recently been explored as exogenous electron transfer mediators in microbial fuel cells (MFCs). In this study, density functional theory (DFT) calculations were performed to evaluate the redox properties of β-Naphthol Violet, Orange G, Orange II, and Methyl Orange. Geometry optimizations and orbital energies were obtained at the B3LYP/6-31G level (gas phase) and B3LYP/6-311++G(d,p) level (aqueous phase). Among the calculated parameters, β-Naphthol Violet exhibited the lowest energy gap of 2.272 eV , indicating the highest redox activity. Conversely, Orange G had the highest energy gap of 3.038 eV.

Introduction: Azo dyes are among the most widely used classes of synthetic dyes. Over the last decade, dyes have found a new application as exogenous mediators (ExMs) of electron transfer in microbial fuel cells (MFCs) [1-4]. The HOMO- LUMO energies are associated with the oxidation and reduction potentials of a donor–π–acceptor structure. Dyes with smaller energy band gaps are expected to exhibit more facile charge-transfer processes and, consequently, enhanced electrochemical activity. In this study, quantum chemical calculations of the frontier molecular orbital energies of four azo dyes - β-Naphthol Violet, Orange G, Orange II, and Methyl Orange were made to establish their redox activities, and to theoretically determine, for the first time, their HOMO–LUMO energy levels and corresponding band gaps.

Objectives: Molecular orbital energies of Azo dyes were estimated by DFT calculations, using the B3LYP/6-31G level in the gas phase and the B3LYP/6-311++G(d,p) level with the polarizable continuum model (PCM) solvent model in the aqueous phase to evaluate solvent effects and the redistributed charge density in both reduction and oxidation states of the conjugated systems.

Material and methods: The applied B3LYP/6-31G method in the ideal gas phase uses the B3LYP functional with the 6-31G basis set to calculate molecular properties for an isolated molecule in vacuum, without considering solvent effects. Whereas, B3LYP/6-311++G(d,p) with PCM in the aqueous phase uses a flexible basis set, including diffuse and polarization functions, together with the PCM to simulate the effect of water as

a solvent. The calculations were carried out with the Gaussian 16 commercial software [5]. The structures were visualized with the ChemCraft software.

Results: The frontier molecular orbitals suggest that redox processes are strongly dependent on the donor-π-acceptor behavior of the molecules. The HOMO energy level observed in ideal gas conditions is predominantly localized in electron-rich donors, whereas the LUMO level is localized in electron-withdrawing acceptors (Fig. 1). In the aqueous phase, solvation stabilizes charged species and makes the redox trends more realistic. The HOMO in all dyes is primarily localized on the azo bond and aromatic rings, indicating that oxidation occurs within the π-electron system (Fig. 1,).

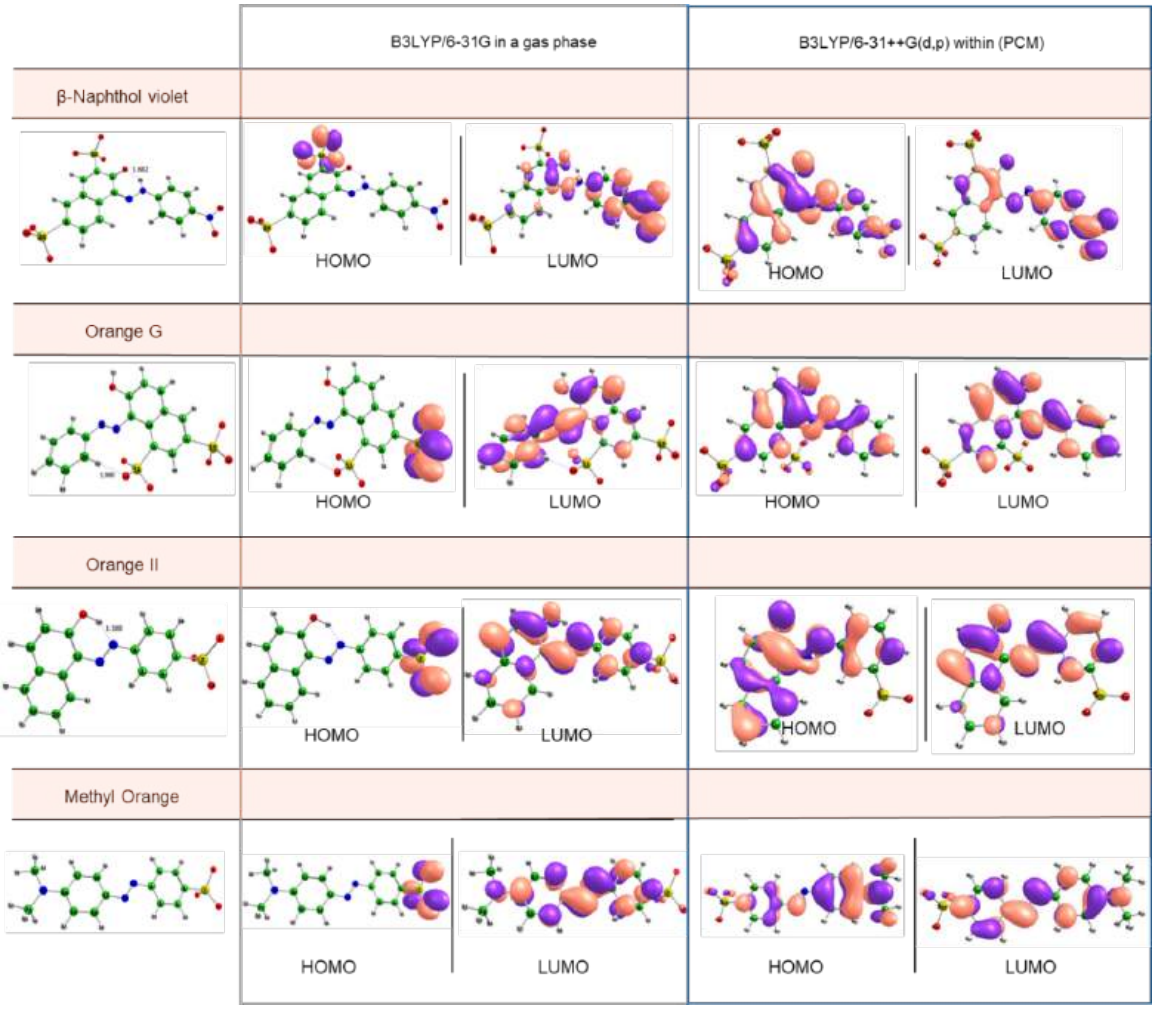


Fig. 1. The structures and the frontier molecular orbitals of the studied dyes obtained by

From the results shown in Table 1, in gas and in aqueous conditions , β-Naphthol Violet can be considered the most prone to oxidation among the studied dyes. Its relatively narrow energy gap suggests enhanced intramolecular charge transfer and increased electronic polarizability, which are typically associated with higher electrochemical reactivity. This arises from its extended π-conjugation and stronger donor–acceptor interaction across the molecule. In contrast, Orange II and Methyl Orange, characterized by more negative HOMO energies, are expected to be more resistant to oxidation, reflecting greater electronic stability. Orange G and Orange II have larger gaps, mainly attributable to the electron-withdrawing sulfonate groups, which reduce

effective π-delocalization and lead to less efficient conjugation across the molecule, resulting in more localized orbitals. Table 1. HOMO and LUMO obtained through quantum chemical calculations using the B3LYP/6-31G theoretical level in a gas phase and the B3LYP/6-31++G(d,p) method within a polarizable continuum model (PCM) simulating the aqueous environment.

	1 mM Dye	B3LYP/6-31G in a gas phase			B3LYP/6-31++G(d,p) within (PCM)		
		HOMO, eV	LUMO, eV	$E_g^{opt} = E_{LUMO} - E_{HOMO}$, eV	HOMO, eV	LUMO, eV	$E_a^{opt} = E_{LUMO} - E_{HOMO}$, eV
1	β-Naphthol Violet	-0.767	0.370	1.137	-5.285	-3.013	2.272
2	Orange G	-0.025	2.699	2.724	-4.935	-1.897	3.038
3	Orange II	-2.422	-0.572	1.850	-4.991	-1.986	3.004
4	Methyl Orange	-2.095	0.218	2.313	-5.541	-2.532	2.847

Conclusions: In conclusion, the aqueous model provides a more realistic description when investigating azo dyes. Solvent stabilization enhances orbital delocalization, corrects energy levels, and yields more reliable predictions of redox behavior, whereas gas-phase results can distort both orbital energies and their spatial distributions, particularly for polar, sulfonated dyes.

From the four azo dyes, β-Naphthol Violet is predicted to be the most redox-active, with the trends governed by orbital energies and HOMO–LUMO gaps, suggesting its potential use as ExM in MFC.

Acknowledgment: This study was supported by the project "Bioelectrochemical Systems for Bioremediation of Organic Pollutants", funded by the Bulgarian Science Fund (contract KP-06-H67/6/2022). It was carried out within the framework of the Integrated Laboratories of the National Scientific Infrastructure "Energy Storage and Hydrogen Energy" (grant DO1-160/2018) and the project "Development and Sustainability of the Centre of Competence HITMOBIL" (grant BG16RFPR002-1.014-0009).

References

[1] E. Hubenova, Y. Hubenova, Bacteria and eukaryotes as anodic biocatalysts in microbial fuel cells – A comprehensive review, J Power Sources 629 (2025) 236002. https://doi.org/10.1016/J.JPOWSOUR.2024.236002 .

[2] Y. Hubenova, R. Bakalska, E. Hubenova, M. Mitov, Mechanisms of electron transfer between a styrylquinolinium dye and yeast in biofuel cell, Bioelectrochemistry 112 (2016) 158–165. https://doi.org/10.1016/j.bioelechem.2016.02.005.

[3] K. Mishra, M.M. Islam, U. Soni et al., Electron transfer mechanism in microbial fuel cells, Discov. Electrochem. 3, 33 (2026). https://doi.org/10.1007/s44373-026-00118-1

[4] C. Santoro, C. Arbizzani, B. Erable, I. Ieropoulos, Microbial fuel cells: From fundamentals to applications. A review, Journal of Power Sources, Volume 356, 2017, Pages 225-244, ISSN 0378-7753, https://doi.org/10.1016/j.jpowsour.2017.03.109.

[5] M. J. Frisch, Gaussian 16, (n.d.).



Anodic biofilm formation under short-circuited conditions of SMFC

Yolina Hubenova*[a,b,c] and Eleonora Hubenova[a,b]

[a]Institute of Electrochemistry and Energy Systems, Bulgarian Academy of Sciences, 1113 Sofia, Bulgaria

[b]Centre of Competence HITMOBIL, Acad. G. Bonchev Str., bl.10, Sofia 1113, Bulgaria

[C]Plovdiv University "Paisii Hilendarski", 4000 Plovdiv, Bulgaria

Keywords: Sediment microbial fuel cell, precious metals recovery, short circuit voltage

Abstract: This study aims to verify rapid biofilm formation by exoelectrogenic bacteria that can be used in a microbial electrochemical snorkel for metal recovery without additional energy input. The performance of the developed bioelectrochemical systems (BESs) was monitored over time by polarization and power curves. Electrochemical activity and charge transfer have also been explored.

Introduction: The precious metals in electronic waste constitute a significant secondary resource for metal recovery. BESs have emerged as highly energy-efficient technologies for this purpose [1]. In these systems, cathodic electrodeposition is coupled with extracellular electron transfer mediated by electroactive microorganisms, enabling metal recovery while maintaining the system's energy balance. At the cathode, target metal species are reduced and deposited, thereby facilitating their recovery [2]. When BESs operate in short-circuit mode, referred to as a microbial electrochemical snorkel (MES), anodic bioelectrochemical activity is maximized [3]. This enhanced anodic process drives the reduction of metal ions at the cathode, promoting their deposition from the electrolyte.

Objectives: This study explores the potential application of the microbial electrochemical snorkel (MES) to recover Group 1B metals from the periodic table. A novel sediment-based microbial electrochemical system was designed, and the conditions required to rapidly form an electrochemically active biofilm from freshwater sediment were established.At this stage, the work focuses exclusively on electrochemical characterization and verification of biofilm formation on the electrode surface and of its charge-transfer capabilities. The investigation of cathodic metal deposition and recovery, without external energy input, is planned for subsequent studies.

Materials and methods: One-chamber microbial fuel cells operating in alternating short-circuit and recovery modes were used in the experimental setup. The anodic bacterial consortium was derived from freshwater river sediment (GPS 42.0659201, 24.6556015). The anodes were fabricated from graphite (surface area of 0.0124 m^2) and buried in the sediment, while the cathodes made from carbonized felt were situated in the water phase. The performance of the BESs and biofilm maturation were assessed using polarization and power curves. The measured cell voltage was used to calculate the generated current, and electrochemical techniques, such as IES and CV, were applied to evaluate the kinetics of adhesion, biofilm formation, and electrochemical activity.

Results: An electrochemically active anodic biofilm formed during alternating periods of short-circuited (SCV) and open-circuited electrodes. After open-circuit operation and stabilization of OCV, polarization and power curves were recorded over time (Fig. 1). The power density increased 20-fold in the first month of incubation and 50-fold after two months, reaching ca. 30 mW/m2. The current density improved by 10-15-fold, reaching a maximum of 155 mA/m2 in the third month of batch operation. The internal resistance ($R_{int.}$) was estimated from the slope of the linear (ohmic) region of the polarization curve. After 5 months of operation, $R_{int.}$ was 474±5Ω. The results show that, after prolonged operation in SCV, both current and power densities decreased, most probably due to increased ohmic resistance. Given that activation losses had reached equilibrium over time, it was suggested that concentration polarization also contributes to SMFC performance. These results indicate that a biofilm formed on the anode after a month and matured over the next two months without additional substrate addition.

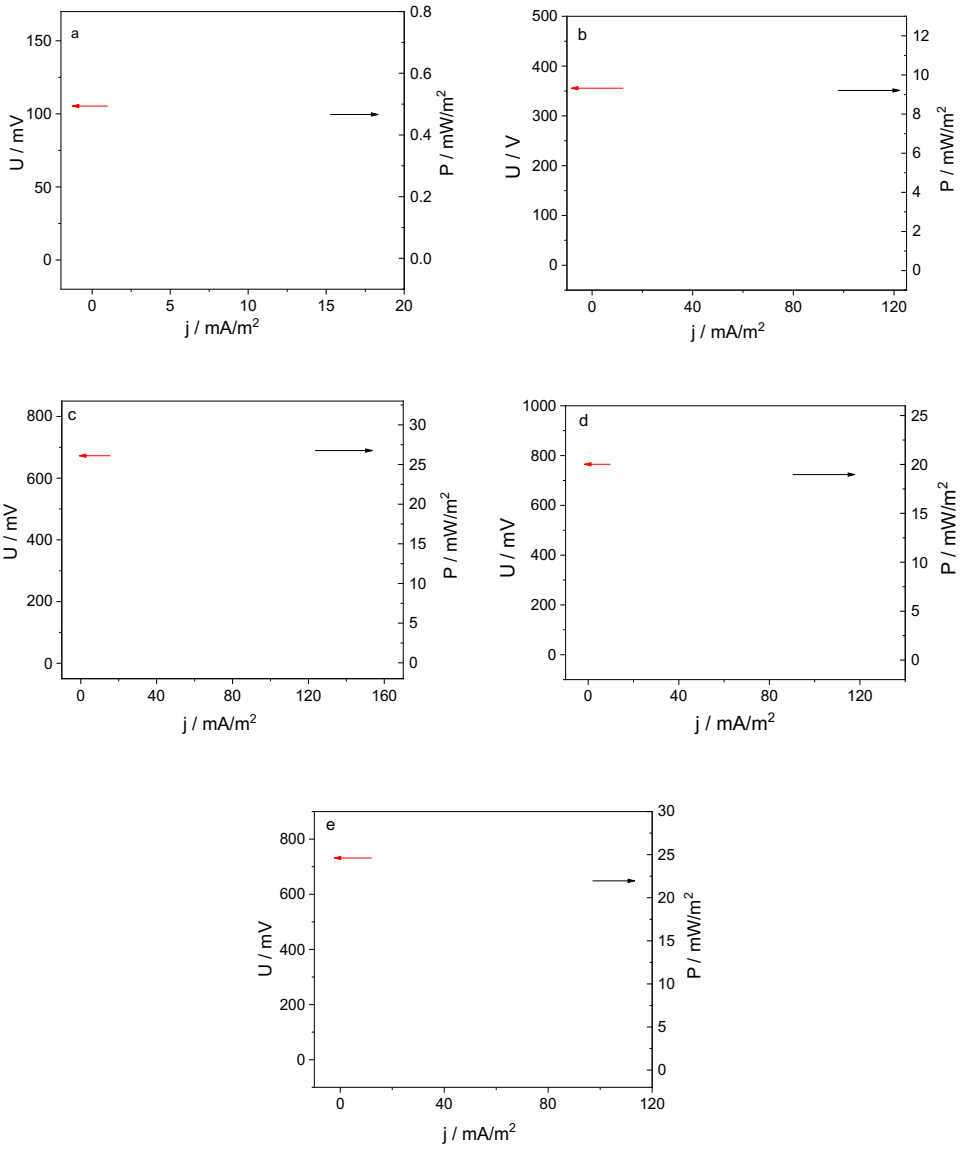


Fig. 1. Polarization and power curves of one-camber sediment microbial fuel cells over time: a) at the beginning; b) after one month; c) after two months; d) after three months; e) after five months.

To assess the biofilm's charge-transfer capabilities, electrochemical impedance spectroscopy (EIS) was conducted at different potentials (Fig. 2a). EIS measurements were performed in a two-electrode configuration; therefore, the fitted equivalent circuit parameters (Randel's) represent the overall cell response rather than individual electrode processes. The results indicate that, at this stage, the system is in equilibrium and the biofilm is electrochemically active (Fig. 2b).

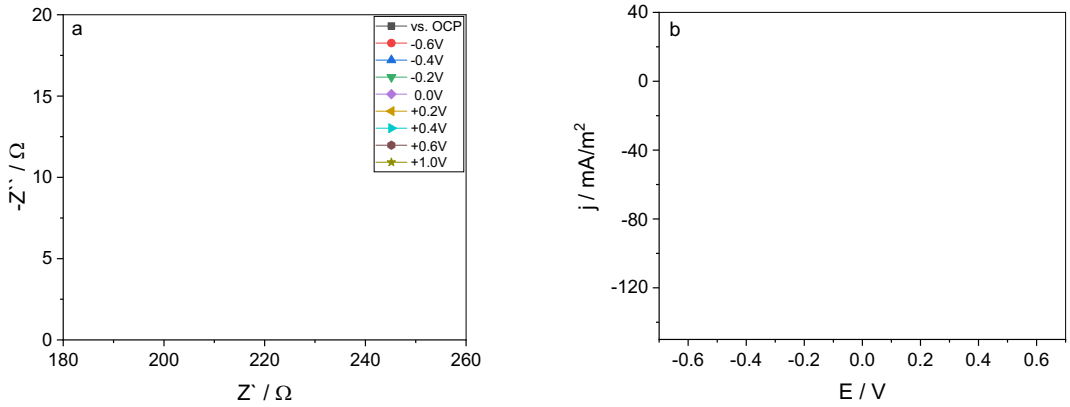


Fig 2. Electrochemical characterization performed in two-electrode mode (WE- bioanode, CE, RE – cathode): a) EIS – Nyquist plots vs. different E_{dc} in V, E_{ac}=0.01 V; b) CV, second scan, scan rate 1 mV/s.

Conclusions: Operating in alternating SCV and OCV regimes stimulates rapid biofilm formation on the anode, promoting the adhesion of exoelectrogenic bacterial species. The generated current density of 100 mA/m2 is an underlying assumption for the conduction of the next phase assays – metal recovery, which is ongoing.

Acknowledgment: This study was supported by the project "Bioelectrochemical systems for bioremediation" by the Bulgarian Science Fund (KP-06-H67/6/12.12.2022) and implemented in the National Scientific Infrastructure "Energy Storage and Hydrogen Energy", project No. DO1-160/2018.

References:

[1] M. Mitov, I. Bardarov, E. Chorbadzhiyska, K. Kostov, Y. Hubenova (2020) First Evidence for Applicability of the Microbial Electrochemical Snorkel for Metal Recovery. Electrochemistry Communications 122, https://doi.org/10.1016/j.elecom.2020.106889

[2] M. Mitov, E. Chorbadzhiyska, I. Bardarov, K. Kostov, Y. Hubenova (2022) Silver Recovery by Microbial Electrochemical Snorkel and Microbial Fuel Cell. Electrochimica Acta 408, 139941, https://doi.org/10.1016/j.electacta.2022.139941

[3] Y. Hubenova, E. Chorbadzhiyska, K. Kostov, M. Mitov (2022) Efficient gold recovery by microbial electrochemical technologies. Bioelectrochemistry 149, https://doi.org/10.1016/j.bioelechem.2022.108311



Feasibility Assessment of Long Short-Term Memory Neural Networks for Electrolyzer Operation Prediction under Start-Stop Conditions

Piergiovanni Domenighini*[a]

* corresponding author: piergiovanni.domenighini@rse-web.it

[a] Ricerca sul Sistema Energetico RSE spa, Via Maresciallo Pilsudski 124,

Roma 00197

Keywords: electrolyzer operation, hydrogen production forecasting, Long short-term memory neural networks, time-series modeling

Abstract

Introduction: Hydrogen is widely recognized as a key energy vector for future low-carbon systems, and water electrolysis is among the most promising pathways for low-emission hydrogen production, especially when coupled with renewable electricity. Nevertheless, improvements are still needed to reduce the levelized cost of hydrogen, enhance efficiency, and better assess long-term operation and maintenance costs. In this context, digital and data-driven methods, including Neural Networks (NNs), offer valuable opportunities for advanced electrolyzer operation and management. Recent studies show that NN-based models can accurately predict hydrogen production, stack voltage evolution, and degradation trends, while reducing the computational burden of detailed multi-physics simulations [1-4]. For instance, ANN-based prediction of transient hydrogen flow in PEM electrolyzers achieved coefficients of determination up to 0.90 with mean squared error as low as 0.00337 [4], while remaining-useful-life studies on PEM water electrolyzer stacks reported mean prediction errors of 0.0372 mL/min under steady-state current and 0.0806 mL/min under dynamic current [2]. In particular, Recurrent Neural Networks (RNNs) and Long Short-Term Memory (LSTM) architectures are well suited to electrolyzer applications because they capture temporal dependencies such as transient effects, load variations, and cumulative degradation phenomena [2-4]. This is confirmed by CNN-LSTM studies, where voltage degradation over datasets of 1140 h under constant load and 660 h under start-stop conditions was predicted with R2 values above 0.98, and degradation after 1000 h was estimated at about 4.5 % and 2.5 %, respectively [3]. These capabilities support more effective operating-condition control, predictive maintenance, and remaining useful life estimation, with benefits in efficiency, durability, and reliability [1-4]. However, important limitations remain, including dependence on training-data quality, limited transferability across electrolyzer technologies, and the need for greater interpretability for industrial deployment [1-3].

Objectives: Despite their advantages, RNN and LSTM architectures are not universally suitable because of their intrinsic structure. As shown in **Figure 1**, the LSTM cell relies on three gates—forget, input, and output—and two internal states, which together regulate information flow and temporal memory. Accordingly, the hidden state and the network output at time step t can be written as:

$$a^{\langle t\rangle} = \Gamma_o^{\langle t\rangle} \tanh\left(c^{\langle t\rangle}\right) \qquad \acute{y}^{\langle t\rangle} = \psi_2\left(W_y\, a^{\langle t\rangle} + b_y\right) \qquad (1)$$

where denotes the updated cell state, the output-gate activation, and are the output-layer weight matrix and bias term, while denotes the output activation function. Under electrolyzer start-stop operation, the resulting large oscillations may hinder LSTM training because of weight saturation and vanishing-gradient or backpropagation-instability effects.

Material and methods: To assess the feasibility of the LSTM neural-network architecture, a literature dataset representative of electrolyzer start-stop (on/off) operation was used for training and testing (**Figure 1**). The prediction target was the hydrogen flow rate in NL/h, selected because it is strongly correlated with the supply current through Faraday's laws of electrolysis. The same Keras-based LSTM architecture, with one hidden layer of 256 neurons and dense input-output layers, was then tested under three different input-output configurations:

- AP: absolute H2-flow prediction;
- NP: normalized H2-flow prediction using MinMaxScaler (scikit-learn);
- DNP: delta normalized H2-flow prediction (lagging, $\Delta y^{<t>} = y^{<t>} - y^{<t-1>}$).

The dataset was organized into sliding windows of 8 samples, with a one-step-ahead prediction horizon. The LSTM model comprised 256 units and was trained using a batch size of 32, the Adam optimizer with a learning rate of $5 \cdot 10^{-4}$, gradient clipping set to 1, and mean absolute error as the loss function.

Results: The results in **Figure 1** show a reasonably good consistency between the AP and NP cases. The best overall performance was obtained in the *DNP* case, where the model was able, in several portions of the profile, to reproduce the oscillatory behavior with good fidelity. In some cases, however, the oscillation was predicted with a slight time advance. The most pronounced spikes were not captured satisfactorily in any of the three configurations. An interesting behavior emerged in the NP case: the LSTM tended to predict an average value, flattening the signal rather than reproducing the oscillations, likely as a strategy to reduce the overall prediction error. The validation losses for AP, NP, and DNP were 12.27, 0.041, and 0.0755, respectively. It is worth noting that the validation loss was higher when the model attempted to follow the oscillatory pattern of the signal than when it converged toward the mean value. These results should be regarded as a first assessment based on preliminary optimization choices. A more complete optimization process would require additional tests on batch size to mitigate data-induced noise, as well as on learning rate and the number of neurons in the dense layers; however, this lies beyond the scope of the present work.

Conclusions: This preliminary analysis shows that standalone LSTM networks can capture the overall hydrogen-flow trend under start-stop conditions, with the best performance obtained for the DNP configuration. However, the main spikes and the most abrupt oscillations are still not satisfactorily reproduced, suggesting that hybrid architectures such as CNN-LSTM may offer a more robust solution for this type of signal [3].

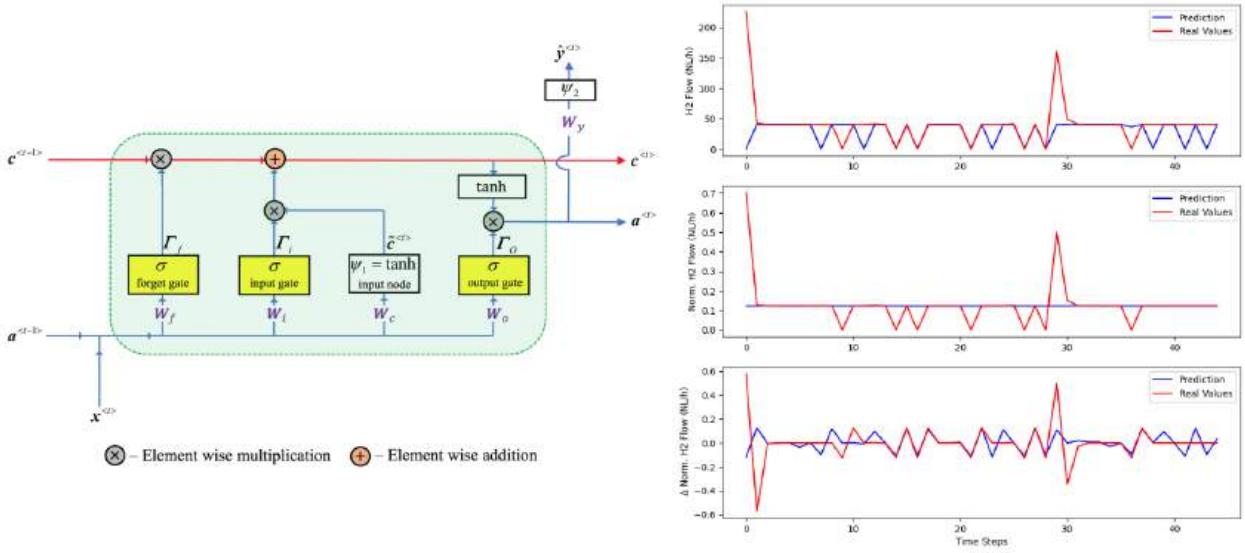


Figure 105 *On the left, schematic representation of the LSTM unit cell; on the right, comparison between measured and predicted hydrogen-flow profiles for the three tested configurations: AP, NP, DNP.*

Acknowledgment Research activities carried out in the context of the national recovery and resilience plan (pnrr) - mission 2 - component 2 - investment 3.5 "research and development on hydrogen", funded by the european union - next generation eu, and performed in implementation of the operative research program (por) approved by the ministry of ecological transition on 06.27.2022

Funded by the European Union NextGenerationEU

References

[1] M. Bahr, A. Gusak, S. Stypka, B. Oberschachtsiek, Artificial Neural Networks for Aging Simulation of Electrolysis Stacks, Chem. Ing. Tech. 92 (2020), DOI: 10.1002/cite.202000089.

[2] Prediction of hydrogen production in proton exchange membrane water electrolysis via neural networks, ACS Omega (2025), DOI: 10.1021/acsomega.5c10432.

[3] B. Xu, W. Ma, W. Wu, Y. Wang, Y. Yang, J. Li, X. Zhu, Q. Liao, Degradation prediction of PEM water electrolyzer under constant and start-stop loads based on CNN-LSTM, Energy and AI 20 (2024) 100420, DOI: 10.1016/j.egyai.2024.100420.

[4] M. Biswas, T. Wilberforce, M. A. Biswas, Prediction of Transient Hydrogen Flow of Proton Exchange Membrane Electrolyzer Using Artificial Neural Network, Hydrogen 4 (2023) 542-555, DOI: 10.3390/hydrogen4030035.



Data-Driven Degradation Forecasting for AEM Water Electrolysis

Marco Veneriano*[a], Ani Gjergji[a], Sebastiano Bellani[b], Andrea Riva[b], Vito Paolo Pastore[a], Matteo Santacesaria[a]

* corresponding author: marco.veneriano@gmail.com

[a] MaLGa Center, Università degli studi di Genova

[b]Antares Electrolysis

Keywords: Anion Exchange Membrane Water Electrolysis, Machine Learning, Voltage degradation curve, Deep Learning for time series

Abstract

This study provides a data-driven analysis of a novel dataset of single-cell Anion Exchange Membrane water electrolyzers (AEMWE), operated under constant current load across multiple heterogeneous experimental campaigns.We train and evaluate a range of machine learning models with different complexity, including LTSMs, foundation models, and vision based architectures, to perform medium-term forecasting of the cell voltage degradation curve. The models are assessed within a rigorous training and evaluation framework specifically designed for heterogeneous industrial data.

Introduction

Green hydrogen production via water electrolysis is widely regarded as a key technology for reducing emissions in both industrial and civilian sectors. Anion Exchange Membrane Water Electrolysis (AEMWE) has recently emerged as a promising alternative to conventional Proton Exchange Membrane (PEM) and alkaline systems. AEMWE offers the potential for lower costs by reducing the reliance on fluorinated polymers and precious metals, while also mitigating their associated environmental impact. However, a major limitation for large-scale deployment is the technological immaturity of the membranes, often limiting system lifetime. In this work, we present the design and evaluation of a data-driven framework, applied to an in-house AEMWE single-cell dataset, with the goal of developing predictive models for degradation dynamics on a budget, and providing insights applicable to industrial settings.

Objectives

Given a heterogeneous dataset comprising multiple experimental runs under different configurations, we aim to model AEMWE degradation by forecasting the future evolution of the voltage curve over medium-term horizons. This differs from most existing studies, which focus primarily on short-term prediction [1–3]. Importantly, the considered time series correspond to the initial phase of operation, characterized by transient dynamics and significantly higher degradation rates compared to steady mid-life conditions. This makes the forecasting task particularly challenging and distinct from typical degradation studies, which often focus on quasi-stationary regimes. Our modeling choices reflect the need for architectures capable of generalization to unseen experimental conditions, robustness to noise, and effectiveness in a data-scarce regime. To this end,

we propose a complete framework for training and evaluation in such settings, including robust validation protocols suitable for industrial deployment.

We compare different machine learning models, ranging from linear baselines to deep learning architectures, and introduce two transfer learning approaches that are novel in this domain: foundation models for time series and vision-inspired representations.

Material and methods

System Description, Dataset and Preprocessing

Data are collected from constant-current experimental campaigns conducted by Antares Electrolysis on a 5 cm^2 AEM single cell under heterogeneous conditions using a custom test station. The dataset comprises 12 runs lasting 40–100+ hours, with a focus on cell voltage as the primary observed variable. Time series are smoothed via Gaussian filtering, interpolated with cubic splines, and resampled at a uniform 5-minute interval. A supervised dataset is constructed dividing the time series in overlapping 24-hour sliding windows with a 1-hour stride; targets are then defined by selecting a prediction horizon $H \in [3,24]$ hours, and averaging the final quartile of the horizon, acting as a low-pass filter to reduce stochastic variability. To address experimental heterogeneity, each window is locally standardized using its own mean and standard deviation.

Models and evaluation

We adopt a leave-one-out cross-validation strategy in which, at each fold, one experimental run is held out for testing and the model is trained on the remaining runs. The reported results are averaged across all hold-out folds. No additional validation split is used, as it results in increased variance without improving results: hyperparameters are therefore selected heuristically, supported by sensitivity analysis.

We evaluate models of increasing complexity, starting from linear baselines (Ridge Regression) and ensemble methods (Random Forests). We then consider neural approaches, including a strongly regularized shallow network and classical time series architectures such as 1D-CNNs and LSTMs, kept deliberately simple due to data limitations. To address data scarcity, we explore two transfer learning strategies. First, the Chronos-2 [4] foundation model is fine-tuned and used in an autoregressive forecasting setting, unlike the direct prediction approach adopted by the other models. Second, a vision-inspired approach encodes time series as two-dimensional representations processed by a pretrained VGG16 [5] network to extract embeddings, which are combined with raw features and fed into a shallow regressor.

Results

Performance is evaluated using Mean Absolute Error (MAE), reported both in normalized units and in centivolts, averaged over multiple runs with standard deviation.

Horizon	Metric	Ridge	Shallow NN	2D-CNN	1D-CNN	LSTM	Chronos
24h	Norm	2.567	*1.816±0.015*	**1.522±0.073**	1.925±0.147	1.977±0.205	2.031±0.059
	cV	1.909	*1.000±0.005*	**0.990±0.040**	1.345±0.226	1.063±0.146	1.358±0.022

18h	Norm	2.127	1.733±0.019	**1.615±0.038**	1.785±0.038	*1.730±0.035*	2.063±0.036
	cV	1.710	**1.150±0.020**	1.195±0.046	1.403±0.026	*1.191±0.059*	1.489±0.018
12h	Norm	1.614	**1.471±0.004**	*1.498±0.019*	1.560±0.013	1.562±0.041	1.587±0.028
	cV	1.393	**1.180±0.010**	1.240±0.010	1.302±0.032	*1.197±0.039*	1.314±0.021
6h	Norm	1.020	*0.970±0.009*	1.044±0.037	1.017±0.006	1.154±0.035	**0.969±0.003**
	cV	0.867	*0.850±0.010*	0.920±0.029	0.870±0.014	0.965±0.028	**0.829±0.004**
3h	Norm	0.644	0.675±0.003	0.712±0.018	*0.657±0.010*	0.790±0.045	**0.541±0.012**
	cV	0.575	0.620±0.000	0.690±0.040	*0.574±0.008*	0.690±0.036	**0.472±0.012**

The Chronos model achieves the lowest MAE over short time horizons, benefiting from its learned internal representations and dataset fine-tuning. Across all horizons, the Shallow Neural Network provides robust results, mirroring the trend of the 1D-CNN but with slightly lower errors. The LSTM yields performance comparable to the 1D-CNN overall, though its accuracy degrades specifically on shorter time frames. For longer horizons, the 2D-CNN delivers the best performance. Notably, the centivolt MAE for both the shallow neural network and the 2D-CNN remains stable over longer time frames, indicating that these architectures avoid overfitting to noise and successfully extract meaningful physical representations.

Conclusions

The proposed framework proves robust in handling heterogeneous and data-scarce conditions, supporting its applicability in industrial settings. The results highlight a clear trade-off in architectural bias: models with a strong temporal inductive bias excel at short-term forecasting, whereas simple models with strong regularization or vision-based models generalize better over long time horizons. Ultimately, the success of the 2D-CNN indicates that transforming data into visual/geometrical representations can effectively capture underlying long-term degradation patterns and yield physically grounded predictions.

References

[1] Zhang, Fan, et al. "Machine learning assisted health status analysis and degradation prediction of aging proton exchange membrane fuel cells." *Applied Energy* 384 (2025): 125483.

[2] Jia, Chunchun, et al. "A performance degradation prediction model for PEMFC based on bi-directional long short-term memory and multi-head self-attention mechanism." *International Journal of Hydrogen Energy* 60 (2024): 133-146.

[3] Xu, Boshi, et al. "Degradation prediction of PEM water electrolyzer under constant and start-stop loads based on CNN-LSTM." *Energy and AI* 18 (2024): 100420.

[4] Ansari, Abdul Fatir, et al. "Chronos-2: From univariate to universal forecasting." *arXiv preprint arXiv:2510.15821* (2025).

[5] Simonyan, Karen, and Andrew Zisserman. "Very deep convolutional networks for large-scale image recognition." *arXiv preprint arXiv:1409.1556* (2014).

EFCH2 2026 European Fuel Cells and Hydrogen
PIERO LUNGHI CONFERENCE
September 15th-17th 2026
Capri / Italy

From Photovoltaics to Integrated PEC Systems: Hybrid Perovskite Photoanodes with Operando H_2 Analysis

Vera La Ferrara* [a], Marco Martino [a], Antonio Marino [a], Giovanni Landi [b], Silvano Del Gobbo [c], Nicola Lisi [c], Rosanna Viscardi [c], Alberto Giaconia [c], Viviana Cigolotti [c] and Giulia Monteleone [c]

[a] *ENEA Portici Research Center, Department of Energy Technologies and Renewable Sources, 80055 Portici, Italy*

[b] *ENEA Portici Research Center, Energy Efficiency Unit Department, 80055 Portici, Italy*

[c] *ENEA Casaccia Research Center, Department of Energy Technologies and Renewable Sources, 00123 Rome, Italy*

* Corresponding author: vera.laferrara@enea.it

Keywords: encapsulation, hydrogen production, perovskite photoanodes, solar water splitting

Abstract

Introduction: Direct solar-to-chemical energy conversion through photoelectrochemical (PEC) water splitting has emerged as a promising strategy for sustainable green hydrogen production. However, major challenges still limit the large-scale implementation of PEC systems, including the difficulty of identifying photoanode materials capable of simultaneously combining high photovoltage, efficient charge transport, catalytic activity, and long-term operational durability. Traditional metal oxide photoanodes (such as $BiVO_4$, WO_3 and Fe_2O_3) exhibit good chemical stability under PEC conditions but suffer from wide bandgaps and slow charge transport. Triple-cation metal halide perovskites have emerged as promising alternatives, delivering high photovoltages (>1.0 V) and photocurrent densities (>12 mA cm^{-2}) [1–3]. The integration of perovskites into aqueous PEC systems remains severely limited by rapid chemical dissolution, photocorrosion, and phase instability under extreme pH stress. In this work, encapsulated triple-cation perovskite photoanodes operating in both photovoltaic-assisted outside (OS) and immersed (IS) PEC configurations are investigated for efficient solar-driven hydrogen production in alkaline media. Conductive and catalytic interfaces were integrated as functional bridges between the perovskite absorber and the aqueous environment, providing physical protection against direct chemical attack while enabling efficient hole extraction and oxygen evolution reaction (OER) activity. Through optimized device integration and encapsulation, favourable energetic alignment and reduced interfacial recombination losses can be achieved. In addition to electrochemical and photovoltaic characterization, quantitative hydrogen evolution is being investigated through operando mass spectrometry coupled with mass-flow measurements and calibrated using hydrogen generated from a commercial electrolyzer. The results are further compared with state-of-the-art perovskite-based PEC systems reported in the recent literature in order to

compare the proposed architecture and evaluate its positioning in terms of Applied Bias Photon-to-Current Efficiency (ABPE), photocurrent density, stability and Solar-to-Hydrogen (STH) efficiency.

Objectives: The main objective of this work is to demonstrate the transition from photovoltaic-assisted operation toward integrated PEC hydrogen production using encapsulated triple-cation perovskite photoanodes. Particular attention is devoted to understanding how device architecture affects photovoltage delivery, PEC charge-transfer kinetics, and operando hydrogen evolution under alkaline conditions.

Material and methods: Triple-cation perovskite solar cells based on $Cs_{0.1}(MA_{0.17}FA_{0.83})_{0.9}Pb(I_{0.83}Br_{0.17})_3$ were fabricated by spin coating in a glass/ITO/SnO_2/Perovskite/Spiro-OMeTAD/Au n–i–p architecture and integrated with nickel-foil based electrodes, acting as OER catalysts (Fig. 1a). The nickel electrodes provide a versatile platform for future catalytic coatings and protective interlayers aimed at improving charge-transfer kinetics and long-term stability. The devices were encapsulated using a PET/EVA multilayer polymer barrier and tested in 1 M KOH under AM 1.5G illumination (100 mW cm^{-2}). The perovskite films and catalytic layers were investigated through crystallographic, vibrational, and optical characterization (such as X-ray diffraction, Raman spectroscopy, and UV–VIS absorption spectroscopy), in order to correlate material properties with PEC hydrogen evolution performance. Device performance was evaluated using cyclic voltammetry, chronoamperometry, and electrochemical impedance spectroscopy.

Results: Both OS and IS configurations demonstrated unassisted photoelectrochemical water splitting, i.e. under zero external electrical bias. Due to the photovoltage supplied by the perovskite device, the OER onset shifted from 1.32 V vs. RHE (recorded for the standard

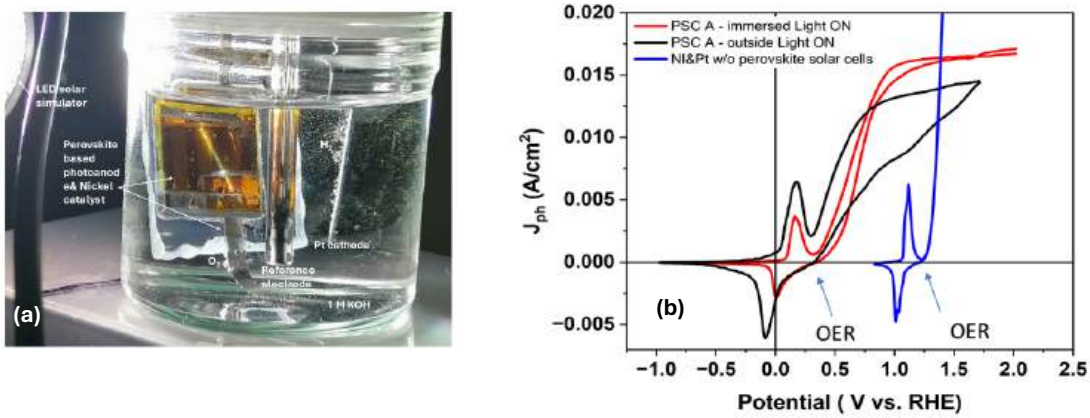


Figure 1. *(a) encapsulated perovskite-based photoanode with Ni electrode in 1M KOH electrolyte, reference electrode and Pt as the cathode (b) Cyclic voltammetry curves of the encapsulated perovskite in both OS and IS configurations (dark and red curves), and w/o perovskite solar cells, i.e standard Ni/Pt cell (blue curve) [3]*

Ni/Pt cell) to 0.34 V vs. RHE (Fig. 1b). The immersed configuration exhibited accelerated charge-transfer kinetics, suppressed voltammetric hysteresis, and superior photocurrent densities compared to the outside configuration. Preliminary results show a maximum ABPE of approximately 20% achieved in the immersed configuration, assuming an ideal Faradaic efficiency of 100%. Operando hydrogen quantification through calibrated mass spectrometry and mass-flow analysis is expected to provide a direct correlation between photocurrent generation and hydrogen evolution, enabling experimental estimation of STH efficiency.

Conclusions: This work demonstrates that device architecture is a key parameter governing the efficiency of perovskite-based PEC systems. Direct immersion of the encapsulated PSC into the electrolyte significantly improves photovoltage utilization and PEC performance compared to conventional photovoltaic-assisted configurations. Furthermore, the combined methodology based on electrochemical characterization and calibrated mass spectrometry enables a reliable experimental determination of STH efficiency in integrated PEC systems.

Acknowledgment

This work was funded by the European Union – NextGenerationEU through the Italian Ministry of Environment and Energy Security, POR H2 AdP MASE/ENEA with involvement of CNR and RSE, PNRR – Mission 2, Component 2, Investment 3.5 “Ricerca e sviluppo sull’idrogeno”, CUP: I83C22001170006.

References

[1] Fehr, A.M.K.; Agrawal, A.; Mandani, F.; Conrad, C.L.; Jiang, Q.; Park, S.Y.; Alley, O.; Li, B.; Sidhik, S.; Metcalf, I.; et al. Inte-grated halide perovskite photoelectrochemical cells with solar-driven water-splitting efficiency of 20.8%. Nat. Commun. 2023, 14, 3797. https://doi.org/10.1038/s41467-023-39290-y .

[2] Hansora, D.; Yoo, J.W.; Mehrotra, R.; Byun, W.J.; Lim, D.; Kim, Y.K.; Noh, E.; Lim, H.; Jang, J.W.; Seok, S.I.; et al. All-perovskite-based unassisted photoelectrochemical water splitting system for efficient, stable and scalable solar hydrogen production. Nat. Energy 2024, 9, 272–284. https://doi.org/10.1038/s41560-023-01438-x .

[3] La Ferrara, V.; Martino, M.; Marino, A.; Landi, G.; Del Gobbo, S.; Lisi, N.; Viscardi, R.; Giaconia, A.; Monteleone, G. Triple-Cation Perovskite Photoanodes for Solar Water Splitting: From Photovoltaic-Assisted to Immersed Photoelectrochemical Operation. Micromachines 2026, 17, 431. https://doi.org/10.3390/mi17040431



H2-SimNet: A Simulation-Based Framework for Data-Driven Monitoring of Hydrogen Networks

Andrea Senese *[a], Saverio De Vito [b] ,Elena Esposito [b] ,Giovanni Acampora [a] ,Girolamo Di Francia [b] ,Antonia Longobardi [c] ,Giulia Monteleone [d]

* corresponding author: Andrea Senese

[a] Department of Physics "Ettore Pancini", University of Naples Federico II, Via Cinthia, 21 (Building 6), Naples, 80126, Italy

[b] TERIN-SSI-EDS Laboratory - ENEA CR-Portici, Piazzale Enrico Fermi, 1, Portici, 80055, Italy

[c] Department of Civil Engineering, University of Salerno, Via Giovanni Paolo II, Fisciano, 84084, Italy

[d] ENEA, Lungotevere G.A. Thaon di Revel, 76, Rome, 00196, Italy

Keywords: Anomaly detection, Digital twin, Hydrogen networks, Quantum optimization

Purpose of Study:

The integration of hydrogen into existing natural gas infrastructure is a key strategy for the energy transition but introduces significant safety and monitoring challenges [6,7]. Digital twin development is currently limited by the lack of realistic data for validating data-driven models [8]. This study proposes a simulation-informed framework toward a future digital twin for hydrogen transport networks, leveraging high-fidelity synthetic data generated in MATLAB Simscape Fluids to support machine learning and optimization for network monitoring. The proposed framework integrates anomaly detection and sensor placement optimization [1–5]. A high-fidelity simulator generates synthetic datasets under nominal conditions, anomalies, and measurement noise [1,3,4], enabling controlled modeling of transient and abnormal operational states. Anomaly detection is performed using neural models for multivariate time series, with classical machine learning [1] and hybrid quantum-classical approaches based on quantum kernels [2] used as baselines. Sensor placement is formulated as a combinatorial optimization problem [5], where a surrogate neural model estimates anomaly detection performance via a Delta-loss relative to a baseline configuration. The resulting objective is expressed as a QUBO and optimized using the Quantum Approximate Optimization Algorithm (QAOA), incorporating sensor utility, redundancy, and a soft cardinality constraint. Overall, the framework provides a simulation-driven step toward digital twins for hydrogen transport systems.

Methodology: The framework relies on a simulation environment for hydrogen transport networks generating multivariate time-series data under nominal and anomalous conditions with measurement

noise and operational variability. Data are preprocessed via filtering and segmentation into overlapping windows for neural training. Anomaly detection is performed by a neural network learning nominal system dynamics and detecting deviations in observed signals [4], with classical machine learning [1] and hybrid quantum-classical quantum kernel methods [2] used as baselines. For optimal sensor placement [5], a surrogate-assisted pipeline estimates anomaly detection performance across configurations. The objective, capturing sensor utility and redundancy, is formulated as a QUBO and optimized via QAOA, enhanced by EVOVAQ [9], as shown in Fig. 1.

Results: Experimental evaluations were conducted across the main modules of the framework under different simulated scenarios and realism levels. The anomaly detection system shows stable and robust performance under noise and operational variability, indicating that network temporal dynamics provide sufficient information to distinguish nominal from anomalous states. For optimal sensor placement, preliminary results show consistent identification of highly informative sensor subsets in the first topology, while increasing noise produces greater variability in selected configurations, particularly in more realistic scenarios. Experiments on additional topologies are ongoing.

Conclusions: This study presents H2-SimNet, a simulation-informed framework for data-driven monitoring of hydrogen transport networks integrating anomaly detection and optimal sensor placement. Results demonstrate that combining high-fidelity simulation with machine learning enables robust anomaly detection under noisy and variable conditions. Furthermore, the surrogate-assisted QUBO formulation optimized via QAOA and the EVOVAQ framework enables effective sensor selection strategies. Overall, the proposed approach represents a step toward scalable digital twins for hydrogen infrastructure monitoring.

Acknowledgements: This work was supported by the EU PhD scholarship in Computational Intelligence (39th Cycle), funded under the MiTE–ENEA POR-H2 program and supervised by Dr. Elena Esposito at the ENEA Portici Research Center. The authors thank Giulia Monteleone, Giovanni Acampora, Saverio De Vito, Antonia Longobardi, and Michele Villari for their support and contributions.

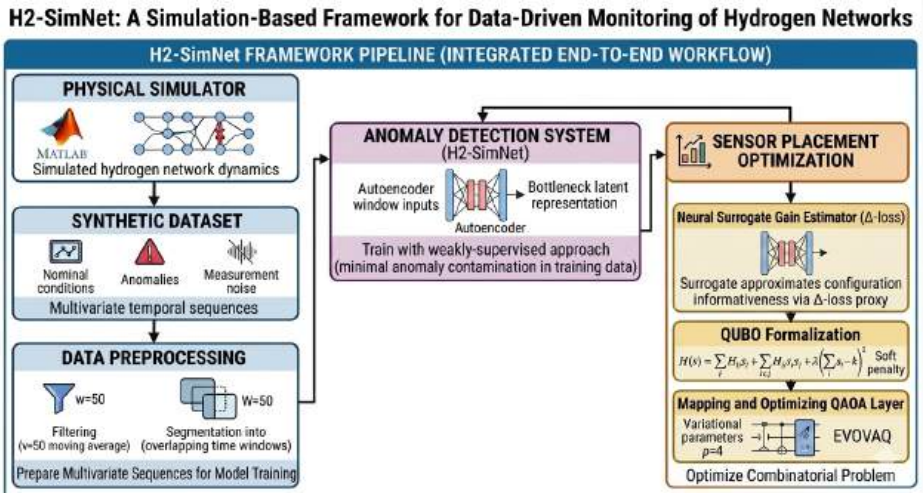


Fig 1. Workflow of the H2-SimNet Framework.

References

[1] Villari, M., De Vito, S., Esposito, E., Senese, A., Longobardi, A., Di Francia, G. (2025). Digital Twin Development for Hydrogen Transport Network with Machine Learning-Based Anomaly Detection.

[2] Senese, A., Esposito, E., De Vito, S., Acampora, G., Di Francia, G. (2025). Hybrid-Quantum Machine Learning Approach for Anomaly Detection in Complex Industrial Systems.

[3] Senese et al. (2026). A Simulation-based Dataset for Anomaly Detection in Hydrogen Blend Transport Networks. Data in Brief.

[4] Senese et al. H2-SimNet: A Simulation-Based Framework for Data-Driven Monitoring of Hydrogen Networks. To be submitted.

[5] Senese et al. Neural Surrogate–Driven Constrained QUBO Formulation for Optimal Sensor Placement. To be submitted.

[6] Xie, Z., Jin, Q., Su, G., Lu, W. (2024). A Review of Hydrogen Storage and Transportation: Progresses and Challenges. Energies, 17, 4070.

[7] Kappes, M. A. and Perez, T. (2023). Hydrogen blending in existing natural gas transmission pipelines: a review of hydrogen embrittlement, governing codes, and life prediction methods. Corrosion Reviews, 41(3), 319–347.

[8] B. Gerard, E. Carrera, O. Bernard, and D. Lun, “Smart Design of

Green Hydrogen Facilities: A Digital Twin-driven approach,” E3S Web

of Conferences, vol. 334, p. 02001, 2022.

[9] Giovanni Acampora, Carlos Cano Gutierrez, Angela Chiatto, Jose Manuel Soto Hidalgo, Autilia Vitiello, EVOVAQ: EVOlutionary algorithms-based toolbox for VAriational Quantum circuits, SoftwareX, Volume 26, 2024, 101756, ISSN 2352-7110.



Electrochemical characterisation of Electrospun Nitrogen-Doped PVDF Hybrid Nanofibers for Bifunctional Metal-Free Electrocatalysts

Claudio Mele*[a], Maria Federica De Riccardis[b], Marilena Re[b], Carmela Tania Prontera[b], Daniela Fico[a], Sonia Bagheri[a]

* claudio.mele@unisalento.it

[a] Department of Engineering for Innovation, University of Salento, Lecce, Italy

[b] ENEA - Italian National Agency for New Technologies, Energy and Sustainable Economic Development, Department of Energy Technologies and Renewable Sources, Brindisi, Italy

Keywords: Electrocatalysts, Electrospinning, Polyaniline, ECSA

Abstract: The development of low-cost and efficient electrocatalysts for the oxygen reduction reaction (ORR) and oxygen evolution reactions (OER) is essential for advancing fuel cells, electrolyzers, and metal-air batteries. In this work, the electrochemical properties of electrospun nanofibrous mats based on poly(vinylidene) fluoride (PVDF), functionalized with polyaniline (PANI) and mesoporous carbon (mC) coated with manganese oxide (MnO_x) as bifunctional noble-metal-free electrocatalysts were analysed. The materials were prepared through a combination of thermal treatment and electrospinning to enhance the activity of nitrogen-containing sites and increase the electrochemically active surface area (ECSA). PANI powders were thermally treated under a nitrogen atmosphere at temperatures ranging between 300 and 750 °C. Raman spectroscopy and electrochemical analyses revealed that the treatment at 350°C provided the best compromise between structural preservation and enhancement of C–N functionalities. Different contents of mC@MnO_x powder were added to a PVDF suspension, then used to produce electrospun PVDF nanofibres. Self-supported porous catalytic mats with fibre diameters in the submicrometric range were obtained. Electrochemical characterization by cyclic voltammetry (CV), linear sweep voltammetry (LSV), and electrochemical impedance spectroscopy (EIS) demonstrated enhanced ORR/OER activity, attributed to the increased active surface area and porous nanofibrous architecture. Surface morphology of the catalytic mats was investigated by optical microscopy and atomic force microscopy (AFM). The developed materials represent promising low-cost alternatives to noble-metal-based electrocatalysts for hydrogen and fuel-cell technologies.

Introduction: Electrocatalytic reactions such as the oxygen reduction reaction (ORR) and oxygen evolution reaction (OER) play a key role in fuel cells, electrolyzers, and metal-air batteries. However, state-of-the-art electrocatalysts are typically based on noble metals, such as platinum and iridium, whose high cost and limited availability hinder the large-scale diffusion of sustainable energy technologies. Consequently, carbon-based materials doped with heteroatoms, particularly nitrogen, have attracted significant interest owing their electrical conductivity, chemical stability, and tunable catalytic properties [1].

Among nitrogen-containing precursors, conjugated polymers such as polyaniline (PANI) are particularly attractive because their nitrogen-rich structure can generate catalytically active sites after suitable thermal treatments. Furthermore, electrospinning is a versatile and scalable technique for producing porous nanofibrous structures characterized by high surface area and interconnected pathways that promote efficient mass transport and charge transfer. In this work, electrospun PVDF nanofibrous mats containing thermally treated PANI and mesoporous carbon coated by MnO_x were developed as bifunctional ORR/OER electrocatalysts. Particular attention was devoted to optimizing thermal treatment and enhancing the electrochemically active surface area through the formation of porous three-dimensional nanofibrous structures [2].

Objectives: This work aimed to investigate self-supported electrospun nanofibrous electrocatalysts based on PANI and MnO_x-coated mesoporous carbon for ORR and OER applications. The study focused on (i) optimizing thermal treatment conditions of PANI to enhance nitrogen-related active sites, (ii) investigating on the process parameters for preparing porous electrospun PVDF/PANI-MnOx-coated mesoporous carbon composite mats, (iii) increasing the electrochemically active surface area (ECSA) of electroactive mats, and (iv) evaluating ORR/OER electrocatalytic activity through electrochemical characterization.

Material and methods: MnO_x-coated mesoporous carbon (mC@MnOx) and polyaniline (PANI) powders were used as the active components. Before use, PANI powders were thermally treated under a nitrogen atmosphere at temperatures between 300 and 750°C in order to optimize the structure of nitrogen-doped carbon compounds. Raman spectroscopy was performed to investigate the structural modifications induced by thermal treatment and to evaluate the evolution of carbon- and nitrogen-related functional groups. The thermally optimized PANI powder and mC@MnO_x were dispersed separately in acetone/DMF and ethanol, respectively, and then dispersed in a PVDF solution in different ratios. The composite suspensions were processed by electrospinning, collecting the electrospun fibres on a flat collector. Electrospinning parameters were optimized to obtain uniform nanofibres with diameters in the range of 0.6–0.9 µm. The mats were then dried and subjected to additional post-treatment to improve porosity and accessibility of catalytic active sites.

Electrochemical characterization was carried out using cyclic voltammetry (CV), linear sweep voltammetry (LSV), and electrochemical impedance spectroscopy (EIS) in both acidic and alkaline electrolytes. Measurements were performed using a three-electrode configuration with an Ag/AgCl reference electrode and a platinum counter electrode. Surface morphology was investigated by optical microscopy and atomic force microscopy (AFM).

Results: Thermal treatment significantly influenced the structural and electrochemical properties of PANI. Treatments above 600 °C caused significant degradation of the polymeric structure and a reduction in nitrogen content, whereas treatment at 350 °C preserved the conductive framework and enhanced the concentration of C–N active functionalities. Raman spectroscopy confirmed an increased intensity of nitrogen-related bands for samples treated at 350°C.

Electrospinning enabled the fabrication of homogeneous porous nanofibrous mats in which PANI/mC@MnO_x particles were uniformly distributed throughout the fibres. Compared with electrosprayed samples, the electrospun structures exhibited superior mechanical stability and a significantly larger exposed surface area.

Electrochemical measurements demonstrated bifunctional electrocatalytic activity toward both ORR and OER under acidic and alkaline conditions. Among the investigated formulations, the electrospun suspension containing PANI thermally treated at 350°C, mC@MnO_x at a ratio of 2.5 wt%, and polyvinylidene fluoride (PVDF)(PANI-$C_{2.5}$/PVDF) mats showed the best electrochemical performance. This behaviour can be attributed to the synergistic combination of nitrogen-doped active sites, porosity of mC@MnO_x, and highly porous nanofibrous architecture. CV and EIS analyses evidenced an increase in ECSA area and improved charge-transfer characteristics, while LSV measurements confirmed enhanced catalytic activity for oxygen-related reactions. Furthermore, the three-dimensional porous morphology facilitated electrolyte penetration and improved accessibility of catalytic active sites. An additional advantage of the developed materials lies in their self-supported nanofibrous structure which eliminates the need for polymeric binders or conductive interlayers, thereby reducing ohmic losses and simplifying electrode integration.

Conclusions: Electrospun PVDF nanofibrous mats functionalized with thermally treated PANI and mC@MnO_x were successfully developed as bifunctional noble-metal-free electrocatalysts for ORR and OER reactions. Thermal treatment at 350°C on PANI provided the best compromise between preservation of the polymeric structure and enhancement of nitrogen-related catalytic functionalities. The optimized electrospun PANI-$C_{2.5}$/PVDF mats exhibited increased ECSA and improved electrocatalytic performance in both acidic and alkaline media. The combination of nitrogen-doped carbon active sites and a porous nanofibrous architecture highlights the potential of these materials as low-cost alternatives to conventional noble-metal-based electrocatalysts for fuel-cell and hydrogen-related technologies.

Acknowledgment: This research was partially funded by the European Union Next Generation EU from the Italian Ministry of Environment and Energy Security, POR H2 AdP MEES/ENEA with involvement of CNR and RSE, PNRR- Mission 2, Component 2, Investment 3.5 “Ricerca e sviluppo sull’idrogeno”, CUP: I83C22001170006.

References

[1] K. Perović, S. Morović, A. Jukić, K. Košutić, Alternative to Conventional Solutions in the Development of Membranes and Hydrogen Evolution Electrocatalysts for Application in Proton Exchange Membrane Water Electrolysis: A Review, Materials **2023**, 16, 6319. https://doi.org/10.3390/ma16186319.

[2] L. Tian, X. Wei, Q. Zhuang, C. Jiang, C. Wu, G. Ma, X. Zhao, Z. Zong, S. Sun, Bottom-up synthesis of nitrogen-doped graphene sheets for ultrafast lithium storage, Nanoscale **2014**, 6, 6075. https://doi.org/10.1039/c4nr00454j.



Design and Validation of a Modular Microbial Fuel Cell Stack for Urine Valorization and Energy Harvesting

Andrea Reina[a], Carmine Cava [*a], Angelo Fabbrizi[a], Anna Barra Caracciolo[b], Paola Grenni[b], Gian Luigi Garbini[b], Ludovica Rolando[b], Paolo Marzioli[a], Gabriele Guglielmo Gagliardi[a], Andrea Pietrelli[c], Ioannis A. Ieropoulos[d], Domenico Borello[a]

* Corresponding author

[a]Department of Mechanical and Aerospace Engineering, Sapienza University of Rome, Italy

[b]National Research Council, Water Research Institute (CNR-IRSA), Rome, Italy

[c]Department of Electronic and Telecomunications Engineering, Sapienza University of Rome, Italy

[d]Water and Environmental Engineering Group, University of Southampton SO16 7QF Southampton, UK

Keywords: Water treatment, MFC, aerospace, bioelectricity

Abstract

This work presents the development of a modular microbial fuel cell (MFC) system designed for simultaneous urine treatment and bioelectricity generation in space-oriented applications. The proposed architecture employs low-cost materials in a modular cascade configuration to maximize organic load removal. Preliminary experiments successfully demonstrated biofilm formation, achieving open-circuit voltages up to 0.6 ± 0.01 V and maximum power up to 0.25 ± 0.04 mW per cell. Furthermore, the system reached chemical oxygen demand (COD) reduction ≥ 50%. These promising results highlight the potential of the proposed system for a sustainable circular resource management in space missions.

Introduction: Resource circularity is a crucial aspect in space applications, where the aim is to maximize the use of all in-situ available resources due to the high cost of transport to orbit, as well as the difficulty of supplying certain elements.

The “Bioregenerative Experimentation for Analog Testing and Resource optimization exploiting ISRU, autonomous Cultivation and MFC-based Energy harvesting” Project (BEATRICE), deals with a system capable of exploiting a waste stream, such as astronauts’ urine, to obtain a valorised product suitable for plant cultivation within a space habitat [1]. In this context, MFCs emerge as a promising solution, because they simultaneously make it possible a reduction in COD and a production of bioelectricity [2].

Despite MFC potential, the transition of this system from laboratory-scale studies to practical applications, particularly, a challenge owing to the complexity of scaling up of this technology in the context of space utilization. Therefore, the development of a robust operational methodology and its validation at different scales are necessary steps toward the future deployment of this technology.

Objectives: This study focuses on the development and experimental validation of a modular MFC system designed to treat artificial urine medium (AUM) and produce an effluent suitable for its reuse for plant cultivation. To ensure result reproducibility, the experimental setup consists of two separate and identical stacks, each composed of four individual MFCs electrically connected in parallel.

Material and methods: The individual MFCs were set up using low-cost ceramic cylinders closed at one end following widely established methodologies [3,4]. The experiments were conducted using two small stacks, each consisting of four MFCs electrically connected in parallel, tested inside a temperature-controlled chamber at 20 °C. After an acclimatation phase to promote microbial acclimation and enhance biofilm formation with electrogenic bacteria [5], the systems were refilled and operated under continuous recirculation (4 mL/min) and MFCs were connected to an external circuit of 1500 Ω. Every 7 days, the stacks were drained and then refilled with 750 mL of a 20:80 mixture of the inoculum (from the stacks drainage) and fresh AUM. After 14 days, the resistances were reduced to 75 Ω, and polarization and power curves were recorded weekly. Sensors integrated into each stack monitored internal liquid levels, pH and temperature, while the chamber humidity was also tracked. Liquid samples from the stacks were regularly analyzed using standard spectrophotometric kits to quantify COD, biochemical oxygen demand, ammonium, total nitrogen, and phosphate. Optical density (at 620 nm) and microbial abundance (by DAPI counts) were assessed at the start and end of each cycle.

Results: The tests have demonstrated the proper functioning of the designed MFC configuration. Biofilm formation was observed at about 30 days, confirming the suitability of AUM as a substrate for microbial activity. Furthermore, individual MFCs reached an open-circuit voltage of approximately 0.6 ± 0.01 V. An example of power and polarization curve from the developed system are reported in Figure 106 and Figure 107, respectively. At the module level, the system yielded a power output ranging up to 0.98 ± 0.13 mW (Figure 106), while simultaneously achieving a 56% COD reduction over a one-week period (Figure 108). Interestingly, microbial abundance increased in concomitance with COD decrease, suggesting the role of microorgamisms in urea degradation.

Conclusions: This study has validated a modular MFC configuration, achieving high reproducibility, a power output up to 0.98 ± 0.13 mW, and a 56% COD reduction within one week. These promising results will guide the future scale-up and optimization of this technology.

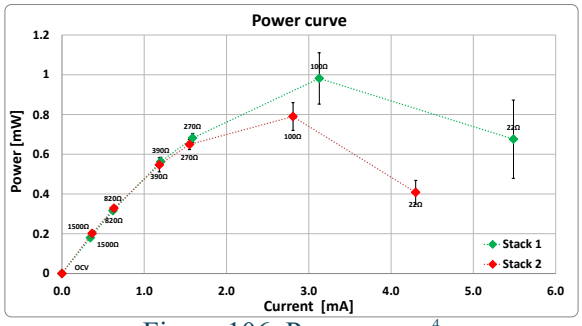


Figure 106. Power curve[4]

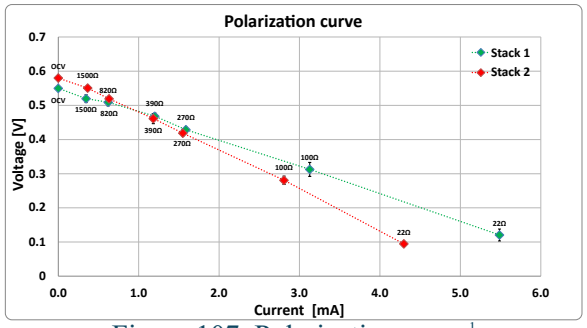


Figure 107. Polarization curve[1]

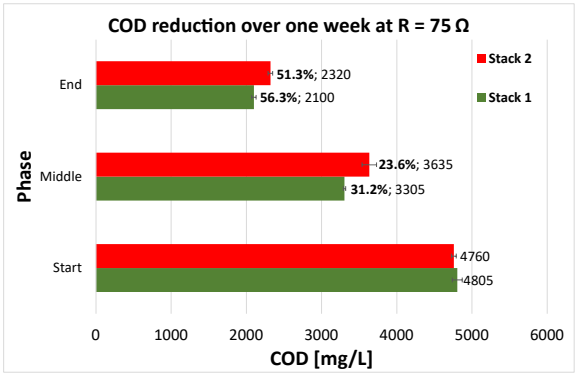


Figure 108. COD evaluation for R = 75 Ω[1]

Bibliography

[1] Marzioli P, Barra Caracciolo A, Grenni P, Ancona V, Cavone C, Balsamo M, et al. Integrated Bioregenerative System for Astronaut Waste Processing and Autonomous Cultivation Exploiting ISRU Techniques: BEATRICE Project, Milan, Italy: International Astronautical Federation (IAF); 2024, p. 476–82. https://doi.org/10.52202/078355-0059.

[2] Gajda I, Obata O, Jose Salar-Garcia M, Greenman J, Ieropoulos IA. Long-term bio-power of ceramic microbial fuel cells in individual and stacked configurations. Bioelectrochemistry 2020;133:107459. https://doi.org/10.1016/J.BIOELECHEM.2020.107459.

[3] Gajda I, Greenman J, Melhuish C, Ieropoulos I. Simultaneous electricity generation and microbially-assisted electrosynthesis in ceramic MFCs. Bioelectrochemistry 2015;104:58–64. https://doi.org/10.1016/J.BIOELECHEM.2015.03.001.

[4] Gajda I, Stinchcombe A, Merino-Jimenez I, Pasternak G, Sanchez-Herranz D, Greenman J, et al. Miniaturized ceramic-based microbial fuel cell for efficient power generation from urine and stack development. Front Energy Res 2018;6. https://doi.org/10.3389/fenrg.2018.00084.

[5] Obata O, Salar-Garcia MJ, Greenman J, Kurt H, Chandran K, Ieropoulos I. Development of efficient electroactive biofilm in urine-fed microbial fuel cell cascades for bioelectricity generation. J Environ Manage 2020;258:109992. https://doi.org/10.1016/J.JENVMAN.2019.109992.

[4] The results presented in this work should be considered preliminary, as the experiment is currently ongoing. Additional long-term tests and experimental replicates are being conducted to improve the statistical robustness and reproducibility of the collected data.



Development of a BioH_2-Biorefinery Through the Integration of Dark Fermentation and Microbial Electrolysis Cells

Clara Marandola[a,b], Gaia Salvatori[b], Costanza Arvigo[a,b], Federico Scopetti[a,b], Leonardo Di Filippo[a,b], Eleonora De Santis[a], Silvia Rosa[a], Giuseppe Lembo[a], Antonella Signorini[a], Elio Fantini[c], Loretta Daddiego[c], Loredana Lopez[c], Roberto Ciccoli[a], Marianna Villano[b], Antonella Marone*[a]

* corresponding author: antonella.marone@enea.it

[a] ENEA Casaccia Research Center, Via Anguillarese 301, 00123 Roma, Italy

[b] Department of Chemistry, Sapienza University of Rome, P.le Aldo Moro 5, 00185 Rome, Italy

[c] ENEA Trisaia Research Center, strada statale Jonica 75026, Rotondella, Italy

Keywords: Microbial Electrolysis Cell, Bio-H_2, Integrated Technologies, H_2-Biorefinery

Abstract: This study investigates the integration of microbial electrolysis cells (MECs) as downstream process to Dark Fermentation (DF) for enhanced hydrogen production and waste treatment. Electroactive biofilms acclimation strategy was first developed in H- type cells and then validated in a continuous flow MEC using real effluents deriving from DF of cheese whey and orange processing waste. Stable performance was achieved in the MEC fed with both DF effluents, with high coulombic and cathodic efficiencies. Microbial analysis revealed high diversity and a shift toward metabolically flexible and syntrophic species. These results demonstrate that optimized anodic microbial consortia enable efficient DF–MEC integration for sustainable bioH_2 production.

Introduction: Waste and wastewater represent an abundant, cheap and widely available source of biodegradable substrates largely unexploited to produce green H_2 by biotechnological routes [1]. One of the most important biotechnological challenges is the integration of biotechnologies that maximize energy yield and, at the same time, enable complete waste treatment. In this context, the coupling Microbial Electrolysis Cells (MECs) to fermentative H_2 production by dark fermentation (DF) has been proposed as a promising strategy to overcome the limitations of both technologies [2]. Indeed, DF is a specialized bioprocess in which complex organic waste streams are anaerobically degraded by microorganisms to produce bio-H_2 as gaseous output. Nevertheless, due to thermodynamic constraints, most of the carbon substrate (2/3) is accumulated within the liquid stream as metabolic residues. As for the MEC, since it leverages the chemical energy contained in the organic substrate, a theoretical 10 times less voltage than standard water electrolysis to generate H_2 at the cathode is required. The integrated DF-MEC system overcomes the need for substrate pre-treatment, promotes a circular "Biorefinery" approach (waste treatment + energy recovery), and serves as an energy storage solution for surplus renewable electricity.

Objectives: The aim of this work was to develop a continuous-flow MEC as a cascade process integrated with DF to maximize the overall process yield in terms of H_2 generation and depollution of complex organic waste streams. The focus was on the selection and enrichment of efficient exoelectrogenic bacteria to enhance the conversion of DF byproducts in the graphite-packed MEC anode. The selection and optimization of microbial consortia has been monitored using high-throughput molecular methodologies.

Material and methods: To optimize H_2 production, an in-depth investigation was conducted on the growth of Electro-Active Biofilms (EABf) in H-type cells (180 mL each chamber). Specifically, the cells were equipped with a carbon-felt anode and a stainless-steel cathode to facilitate the H_2 evolution reaction. The acclimation of EABf was evaluated using either acetate (as a model substrate) or a synthetic mixture of organic compounds (containing ethanol, lactate, acetate, and butyrate), which was ad hoc designed to simulate the composition of a real effluent deriving from a lab-scale DF reactor fed with Cheese Whey (CW). All experiments were performed in triplicate and operated with the anode poised at +0.20 *vs*. SHE (Standard Hydrogen Electrode). Once EABf were acclimatized on synthetic substrates, the real DF effluent was fed to the H-cell systems to assess the H_2 production performance. Based on the obtained results, a two-chamber MEC (1.5 L total volume) was set up and continuously fed with the synthetic mixture to stimulate the EABf acclimation at the anode and simultaneously allow the H_2 production and recovery at the cathode. The anode consisted of a granular graphite bed, designed to provide a high surface area for the development of an efficient EABf, and was separated by a proton exchange membrane (PEM) from the stainless-steel mesh cathode. The MEC was operated under the same polarized conditions as the H-type cells. Once EABf were acclimatized on synthetic substrate and stable current was reached, the real DF effluents were fed to the MEC to evaluate the performance of the integrated process. Two experimental runs were conducted using effluents derived from the DF of different substrates. The first run investigated cheese whey (CW) as the primary substrate, whereas the second run evaluated the effluent from a DF reactor fed with orange processing waste (OPW). EABf were analyzed by full-length 16S rRNA gene sequencing using Oxford Nanopore technology, allowing species-level taxonomic resolution.

Results: It was demostrated that the acclimation strategy strongly influenced the performance of the EABf in H-type cells. Biofilms acclimatized on a synthetic mixture of fermentation products outperformed acetate-acclimatized biofilms, achieving higher H_2 production (i.e., 5.73 ± 2.40 *vs.* 1.26 ± 0.20 meq H_2, respectively) and Cathode Capture Efficiency (CCE), which accounted for 83 ± 15% vs. 66 ± 22%, respectively. Thus, the enrichment on synthetic mixture resulted in the establishment of an efficient electro-active biofilm. Regarding the continuous flow MEC, it was initially fed with synthetic substrates at an OLR of 2 gCOD/L d for 26 days (corresponding to nearly 107 hydraulic retention times, HRT). The reactor produced a stable current of 41 ± 4 mA, the COD (Chemical Oxygen

Demand) removal efficiency was 70 ± 2% corresponding to a Coulombic Efficiency (CE, which represents the faction of the removed COD converted into current) of 53 ± 4%. The maximum H_2 production rate was 0.54 L/Ld, matching a CCE close to 100%. Then, the MEC anode was fed with the effluent deriving from DF of CW for 48 days (corresponding to 198 HRTs) while maintaining the same OLR. The reactor performance resulted in a current generation of 47 ± 4 mA, a COD removal efficiency of 82 ± 5% and a CE of 94 ± 8%. The H_2 rate reached 0.66 L/Ld, corresponding to a CCE of 87±5%. Finally, to validate the robustness of the developed EABf, a second run was conducted using the OPW DF effluent as substrate for the bioanode. Here, the COD removal efficiency was 51±7% and the CE accounted for 100±1%, demonstrating that the total fraction of oxidized compounds was recovered as electric current. H_2 production rate reached 0.39 L/Ld corresponding to a CCE of 88±7%. These results indicate the resilience of the electroactive biofilm at the MEC anode in the treatment of different waste streams. The microbial community showed high diversity and underwent a significant compositional shift between the acclimation phase and the DF feeding phase. Several species increased significantly, including *Desulfitobacterium hafniense,* known for metabolic flexibility and Extracellular Electron Transfer capability, *Clostridium grantii* and *Acetonema longum*, often involved in syntrophic relationships, while typical electroactive species such as *Geobacter* almost disappeared. Overall, the granular graphite-packed anodes create multiple ecological niches that support a highly diverse microbial community capable of functional adaptation while maintaining stable H_2 production.

Conclusions: Overall, the obtained results clearly indicate the feasibility of integration of DF and MEC biotechnologies to develop circular "BioH_2-Biorefinery". Specifically, we demonstrated that tailored strategies can be applied to optimise energy yield and, at the same time, enable complete waste treatment by developing a highly diverse anodic microbial community capable of functional adaptation while maintaining stable H_2 production.

Acknowledgment: This research was funded by the European Union–Next Generation EU by Italian Ministry of Environment and Energy Security POR H_2

References

[1] Hallenbeck, PC., Int. J. Hydrog. Energy, 2009, 34, 7379-7389.

[2] Marone, A., et al., Int. J. Hydrog. Energy, 2017, 42,3,1609-1621.



Hydrogen-related pathways in NEST++: reversible conversion, biomass-to-syngas routes, storage monitoring and intelligent control

Francesca Santoni*[a], Mario Tucci [b], Gabriele Loreti[a], Maria Valenti[c], Piero De Fazio[d], Isabella De Bari[e], Giulia Monteleone [f]

* corresponding author: Francesca Santoni -*francesca.santoni@enea.it*

[a] Department of Energy Technologies and Renewable Sources, Laboratory for Hydrogen and new Energy Vectors (TERIN-DEC-H2V) ENEA, C.R. Casaccia, Via Anguillarese 301, 00123, Rome, Italy.

[b] Department of Energy Technologies and Renewable Sources, Photovoltaic Industry Engineering Laboratory (TERIN-SPV-IIF), C.R. Casaccia, Via Anguillarese 301, 00123, Rome, Italy

[c] Department of Energy Technologies and Renewable Sources, Smart Grid and Energy Networks Laboratory (TERIN- SSI-SGRE) ENEA - C.R. Portici Piazzale Enrico Fermi, 1 - Località Granatello, 80055 Portici (Napoli), Italy

[d] Department of Energy Technologies and Renewable Sources, Section Processes and Material for Energy Applications (TERIN-PAEN) ENEA C.R. Trisaia, s.s. 106 Jonica km.419,500, 75026, Rotondella (MT), Italy

[e] Department of Energy Technologies and Renewable Sources, Section Bioenergy, Biorefineries and Green Chemistry (TERIN-BBC) ENEA - Italian National Agency for New Technologies, Energy and Sustainable Economic Development, C.R. Trisaia, s.s. 106 Jonica km.419,500, 75026, Rotondella (MT), Italy

[f] Department of Energy Technologies and Renewable (TERIN) ENEA -, C.R. Casaccia, Via Anguillarese 301, 00123, Rome, Italy.

Keywords: Energy storage, Hydrogen, Reversible fuel cells, Smart monitoring

Abstract

This work presents the hydrogen-related pathway developed within NEST++, focusing on reversible electrochemical conversion, smart monitoring of hydrogen storage, biomass-to-syngas routes and intelligent control of multi-energy systems. ENEA contributes through complementary activities based on fibre Bragg grating sensors for composite tank monitoring, MAPPO-based multi-agent reinforcement learning and predictive modelling of syngas-based renewable fuel processes. The proposed approach supports the validation of hydrogen as an enabling vector for renewable integration, long-duration storage, system flexibility and resilient low-carbon energy systems.

Introduction: The energy transition requires systems able to combine high shares of renewable generation with flexibility, reliability and resilience. NEST++ - "Strengthen the research network for a sustainable and resilient energy transition" - builds on the NEST extended partnership to consolidate the national research infrastructure for renewable energy generation, energy conversion and storage, resilient infrastructures, digital twins, artificial intelligence and advanced skills. Within this framework,

hydrogen-related activities are strategic for long-duration storage, sector integration and power-to-power applications. This contribution focuses on the NEST++ hydrogen-related pathway, considering reversible electrochemical conversion, smart monitoring of hydrogen storage components, syngas-based renewable fuel routes and intelligent control of complex energy systems. ENEA contributes through three complementary workstreams: real-time monitoring of composite hydrogen tanks, MAPPO-based multi-agent reinforcement learning for decentralised optimisation in demonstrator environments, and predictive modelling of an integrated microwave gasification and liquid biofuel synthesis system based on the syngas platform. The latter activity is not conceived as a hydrogen storage route, but as a complementary pathway for renewable carbon valorisation and renewable fuel production, where syngas composition and quality are key process parameters.

Objectives and proposed innovations: The main objective of this work is to describe how NEST++ supports the development and future validation of hydrogen-based and hydrogen-related technologies within a broader research and demonstration infrastructure for flexible, resilient and low-carbon energy systems. In this framework, hydrogen is considered as an enabling vector for renewable integration, long-duration storage and power-to-power applications. The activities addressed in the project are not conceived as a single technological chain, but rather as complementary modules contributing to a shared validation ecosystem, where renewable generation, electrochemical conversion, storage, monitoring, digital modelling and intelligent control can be analysed under relevant operating conditions.

The specific objectives are to: i) define the role of hydrogen within the NEST++ strategy for renewable integration and system flexibility; ii) analyse reversible electrochemical systems, including regenerative electrolysers and fuel cell operation, for the conversion of surplus renewable electricity into hydrogen and its reconversion into electricity; iii) consider biomass-derived syngas pathways as a complementary ENEA contribution to renewable fuel production; iv) improve the safety and reliability of stationary hydrogen storage through smart monitoring of composite tanks; and v) investigate MAPPO-based multi-agent reinforcement learning for decentralised optimisation of complex multi-energy systems.

The proposed innovation lies in the coordinated development of these complementary activities within the NEST++ validation ecosystem. Reversible power-to-power concepts support the management of variable renewable electricity, while fibre Bragg grating sensors, predictive analysis and digital twin tools contribute to safer hydrogen storage operation. MAPPO-based control provides an advanced methodology to optimise infrastructures composed of renewable generators, storage units, flexible loads and hydrogen-related components. Finally, the syngas-based activity introduces predictive modelling based on experimental data and artificial neural networks to support the validation and scale-up of microwave gasification and liquid biofuel synthesis processes.

Materials and methods: The methodology is based on the coordinated assessment of distinct workstreams contributing to the NEST++ validation framework. Reversible electrochemical conversion is analysed through power-to-power configurations in which renewable electricity is converted into hydrogen and later reconverted into electricity. The assessment considers operating conditions, dynamic response, cycling capability, system constraints and model calibration using literature and/or experimental data on SOEC/SOFC technologies.

For the syngas-based renewable fuel pathway, experimental data from microwave gasification and liquid biofuel synthesis are organised and used to develop predictive models. Artificial neural networks are applied to describe nonlinear relationships among feedstock properties, process conditions, syngas composition and conversion performance; results will be assessed through RMSE, MAE and R^2 and compared with conventional statistical models.

Hydrogen storage monitoring is addressed through fibre Bragg grating sensors for real-time acquisition of strain, temperature and pressure-related information during loading and unloading cycles of composite tanks. These data support predictive analysis and digital twin development. Intelligent control is investigated by defining agents, constraints and objectives for multi-energy systems including renewable generators, storage devices, flexible loads, grid nodes and hydrogen-related components, enabling comparison between centralised and decentralised strategies.

Expected results: As NEST++ is at an initial stage, experimental results are not yet available. The first expected outcome is a coherent framework for assessing hydrogen-related technologies as modular elements of the NEST++ infrastructure. For reversible conversion, models and validation procedures will support the analysis of operating windows, dynamic behaviour and interaction with renewable generation. For the syngas pathway, the expected output is a predictive tool for pre-feasibility analysis, scale-up and identification of operating conditions required for industrial implementation. For hydrogen storage, the monitoring framework is expected to improve safety, reliability and maintenance strategies for stationary composite tanks. Finally, MAPPO-based control will provide a methodological basis to compare optimisation strategies in terms of efficiency, reliability, operational safety and scalability in demonstrator environments.

Conclusions: The NEST++ hydrogen-related activities address key challenges of the energy transition: renewable integration, long-duration storage, system flexibility, renewable fuel production and safe operation of hydrogen infrastructures. ENEA contributes through complementary activities on storage monitoring, intelligent control and predictive modelling of syngas-based processes. Although validation is still ongoing, the proposed approach establishes a common experimental, digital and methodological framework, supporting hydrogen as an enabling vector for resilient, flexible and low-carbon energy systems and contributing to the NEST++ objective of strengthening the national research and innovation ecosystem for the energy transition.



Characterization and Calibration Protocols for Gas Sensors in Hydrogen Systems: Towards Integrated Environmental Monitoring

E. Massera*, B. Alfano, T. Polichetti, M. L. Miglietta, L.V. Mercaldo, P. Delli Veneri, G. Vanga, C. Bassano

* corresponding author: ettore.massera@enea.it

Department of Energy and Sustainability, Research Center ENEA of Portici, P.le E. Fermi 1, Portici (Napoli)

Keywords: environmental monitoring, hydrogen sensing, IOMS, olfactometry

Abstract

Introduction: Instruments for Odour Monitoring and Assessment (IOMS) are sophisticated tools designed to evaluate and quantify odour-related nuisances across various environments. These devices play a crucial role in monitoring air quality, identifying sources of odour pollution, and addressing community concerns about unpleasant smells or anomalous events to prevent accidents. IOMS leverage technologies such as gas sensors, artificial intelligence, and pattern recognition to emulate human olfactory perception and provide objective measurements of odour intensity and characteristics. Their applications span industries including waste management, food processing, and chemical production. We believe that these instruments can be effectively adapted and integrated into the hydrogen system context, where hydrogen transitions from being merely a process gas for the chemical industry and oil refining to becoming a key energy carrier [1,2]. The Innovative Devices (DIN) laboratory within the Photovoltaic Solar Energy (SPV) division of ENEA's Energy and Sustainability Department (TERIN) is involved in several research areas. These include the development of innovative materials relevant both to the aforementioned scenario and to environmental hydrogen sensing [3,4]. This work is part of the Research Operational Plan (POR), supporting research aligned with the Italian National Recovery and Resilience Plan (PNRR) and the European strategy identifying green hydrogen as a priority for energy system decarbonization. The increasing deployment of hydrogen highlights the need for innovative monitoring technologies, especially considering its potential atmospheric impacts.

Objectives: The objective is to demonstrate how laboratory research activities—focused on hydrogen sensors and olfactometric technologies—can support the adoption of Instrumental Odour Monitoring Systems (IOMS) for environmental monitoring in hydrogen-related industrial sites.

Material and methods: Over the past twenty years, we have been testing chemiresistive films—both heated and unheated—as well as single or array-based gas chemo sensors, including electrochemical sensors, MOX sensors, PID, and IMS, in controlled atmospheric environments. These artificial atmospheres consist of a humidified carrier gas contaminated with precisely controlled amounts of air pollutants. The artificial atmosphere must be carefully tailored to the specific application scenario, and the following upgrades are necessary:

- Enhancing safety measures: Adapt the facility's safety standards by installing ATEX-certified extractors and gas sensors to mitigate risks in hazardous environments.
- Improving validation equipment: Upgrade the tools for validating artificial atmospheres by acquiring a GC-IMS and calibrated solid-state gas sensors.
- Advancing sensor conditioning capabilities: Enhance sensor conditioning equipment by procuring an LCR meter for precise impedance measurements.

The work includes development of innovative materials for hydrogen sensing, experimental testing of prototype sensors, evaluation of IOMS devices as electronic noses, comparison with dynamic olfactometry, and participation in standardization activities (UNI, CEN-ISO, IEEE).

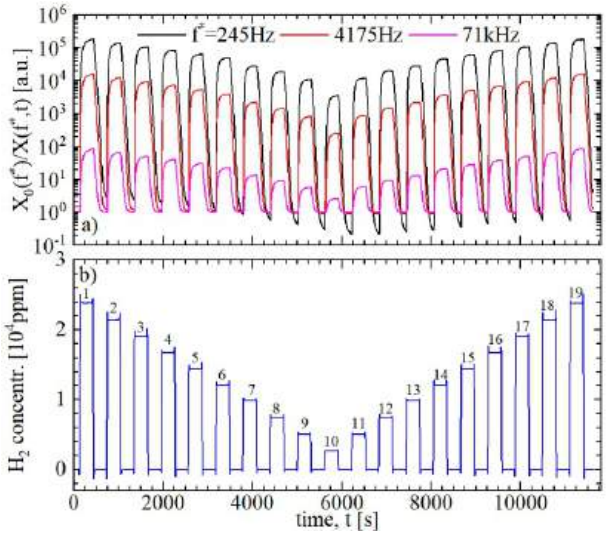


Figure 1: impedance time behaviour to multi step exposure to several hydrogen concentration for the heated chemiresistor based on nanostructured WO3-Pt doped with Graphene.

Results: Regarding the testing and development of innovative materials for Hydrogen Chemi sensing, two classes are considered:

Heated chemo resistive film of WO3-Pt doped with Graphene are tested in controlled environment, studying the response of the impedance when exposed to hydrogen as shown in figure 1

Not heated chemo resistive film of Gr-Pt installed on a Passive RFID antenna are also successfully tested in controlled environment towards hydrogen to demonstrate the possibility of use of pervasive passive solid state sensors in field.

hydrogen can be monitored at ppm-level concentrations relevant for environmental assessment. IOMS enable continuous, real-time monitoring compared to traditional methods. Advanced algorithms enhance sensitivity and reliability. The laboratory is involved in international Standardization and experimental applications of procedures for the use and classification of IOMS for improving reproducibility.

Conclusions: Integration of hydrogen sensing and olfactometric systems is promising for environmental monitoring in decarbonized industrial contexts. Once standardized, IOMS can be deployed effectively in hydrogen production and storage sites.

Acknowledgment

This research was funded by the Operational Research Plan (POR) of the Italian Ministry of Ecological Transition within the Next Generation EU framework (H2 supply chain project).

References

[1] Nam, T. H., Lee, J. H., Choi, S. R., Yoo, J. B., & Kim, J. G. (2014). Graphene coating as a protective barrier against hydrogen embrittlement. International journal of hydrogen energy, 39(22), 11810-11817.

[2] Kumar N, Lee SY, Park SJ. Advancements in hydrogen storage technologies: A comprehensive review of materials, methods, and economic policy. Nano Today. 2024 Jun 1;56:102302.

[3] Alfano B., Miglietta M. L., De Girolamo A., Massera E., Arroyo P., Lozano J. and Polichetti, Comparative Study of Metal Oxide Nanoparticle Composites for Hydrogen Gas Sensing, T. EFC 2023 10th edition of the "European Fuel Cells and Hydrogen Piero Lunghi Conference" Capri (Naples, Italy) 13th- 15th September 2023.

[4] Polichetti T. , Miglietta M.L. , Alfano B. , Massera E. , Arroyo P., Lozano J. Indium tin oxide/metal nanoparticles composite for H2 gas detection 109° CONGRESSO NAZIONALE Società Italiana di Fisica Salerno, 11-15 settembre 2023.



From converter measurements to internal degradation: a converter-oriented method for assessing pem electrolysis cell health

L. Palma[a], J. Núñez[b,c], L. Morán[a], C. Carrasco*[b,c]

* corresponding author: ccarrascoc@udec.cl

[a] Department of Electrical Engineering, University of Concepción, Concepción, Chile

[b] Thin Films and Electrochemical Processes Laboratory (TFep), Departament of Materials Engineering, Universidad de Concepción, Chile

[c] Solar Energy research Center, Chile

Keywords: Degradation diagnostic, health assessment, PEM cells, power converter

Abstract

Introduction: In green hydrogen production systems, power electronic converters regulate PEM electrolysis cells using electrical variables measured at the stack terminals [1]. In contrast, the degradation mechanisms that determine cell lifetime are developed within the membrane electrode assembly and are commonly investigated by electrochemical techniques and post-mortem characterization. Although multidisciplinary studies combining electrical and materials analyses have recently emerged [2,3], identifying converter-accessible electrical variables sensitive to internal degradation remains an open challenge.

Electrochemical impedance spectroscopy (EIS) provides the most comprehensive electrical description of the cell internal state, but its implementation requires dedicated instrumentation and relatively long acquisition times. Recent work demonstrated that the required electrical perturbations can be generated through the power converter during normal operation [4], shifting the challenge toward identifying electrical variables suitable for converter-based degradation assessment. This work addresses that challenge by integrating electrical engineering, electrochemical characterization and post-mortem materials analysis to identify converter-level electrical variables associated with internal degradation in PEM electrolysis cells operated under long-term dynamic conditions.

Objectives: To determine the electrical variables available at the power converter level that remain sensitive to internal degradation in PEM electrolysis cells operated under long-term dynamic conditions, enabling the development of a converter-oriented diagnostic methodology for early health assessment and condition monitoring.

Material and methods: Commercial PEM electrolysis cells (H-TEC R103) were operated under three representative long-term dynamic modes (On/Off, On/Standby and Continuous). Each operating mode comprised 365 cycles, equivalent to one year of operation. After aging, polarization curves, electrochemical impedance spectroscopy and post-mortem characterization of the membrane,

anode and cathode were performed. An equivalent-circuit model was used to determine the characteristic electrochemical time constants together with the ohmic, charge-transfer and interfacial resistance contributions. These parameters were correlated with the degradation features identified by post-mortem analysis to identify the converter-level electrical quantities sensitive to internal degradation, establishing the basis for converter-oriented health assessment and condition monitoring.

Results: Electrochemical characterization and post-mortem analyses demonstrated that different operating modes promoted distinct degradation pathways within the membrane electrode assembly. Representative SEM images of the anodes (Fig. 1) illustrate the corresponding degradation states after long-term operation

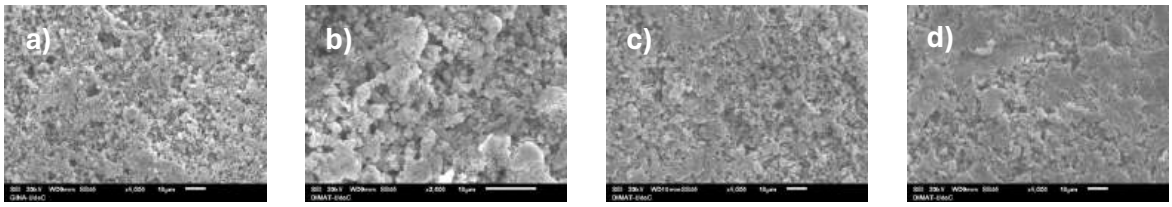


Figure 1: SEM images of anode: a) new cell and cells after operation under b) On/Off, c) On/Standby and d) Continuous modes

Despite these marked differences in degradation, only moderate variations were observed in the conventional electrical variables monitored during operation (Table 1). The initial and final operating voltage remained within a relatively narrow range after 365 operating cycles, regardless of the operating mode. In contrast, the total resistance obtained from EIS clearly differentiated the degradation mechanism of the cells. These results demonstrate that severe internal degradation may develop while the electrical variables conventionally available at the power converter level remain largely unchanged.

Based on these experimentally established relationships, a converter-oriented diagnostic methodology was developed by combining complementary electrical information obtained at different time scales. The voltage-to-current ratio (V/I), continuously available during operation, provides a global measure of the electrolyzer electrical response by reflecting the combined effects of activation, ohmic, interfacial and mass-transport contributions. Cell voltage measured at a reference operating current provides a normalized indicator for tracking degradation independently of operating load. These steady-state variables are complemented by the periodic estimation of the high-frequency resistance through a short converter-generated electrical perturbation, which isolates the

ohmic contribution and provides independent information on membrane proton conductivity and internal electrical connectivity. Together, these complementary electrical quantities establish a physically supported framework for converter-oriented degradation diagnosis that remains compatible with practical implementation in industrial PEM electrolyzer systems.

Table 1: Conventional electrical variables and EIS-derived resistance measured in cells after different long-term operation conditions.

Operation mode	V_{stable} (cycle 20)	V_{final} (cycle 365)	ΔV (%)	τ_2 (ms)	R_T (mΩ)
New	-	-	-	26.7	1030
On/Off	2.3	2.4		19.8	1902
On/Standby	2.7	2.9		24.5	8300
Continuous	2.4	2.6		10.1	2310

Conclusions: This work demonstrates that different long-term operating modes promote distinct degradation pathways in PEM electrolyzers, while the conventional electrical variables available at the power converter level remain largely insensitive to these internal degradation processes. By integrating electrical measurements, electrochemical characterization and post-mortem materials analysis, electrical quantities sensitive to internal degradation were identified and related to the underlying physicochemical aging mechanisms. These findings enabled the development of a converter-oriented diagnostic methodology based on complementary electrical indicators, namely the voltage-to-current ratio (V/I), cell voltage measured at a reference operating current and periodically estimated high-frequency resistance (HFR), providing a practical framework for health assessment of PEM electrolysis cells under long-term dynamic operation.

Acknowledgment

The authors acknowledge the financial support from ANID through projects Fondecyt 1251285 and the Solar Energy Research Center, SERC-Chile (ANID/CIN250043)

References

[1] Majumdar et al., Int. J. Hydrogen Energy (2023) 48(79):30621.

[2] Zaccarine *et* al. *J. Electrochem. Soc.* (2022) 169 064502.

[3] Finger *et* al. *Energy Environ. Sci.* (2025) 18 (22): 9877-9894.

[4] Li *et* al. *Chem. Eng. J.* 526 (2025) 171524.



Smart and Sustainable Ports
Artificial intelligence for cargo logistics and hydrogen terminal tractors

Andrea Altomonte[a*], Giovanni Di Ilio[a], Viviana Cigolotti[b], Elio Jannelli[a]

* Corresponding author: Andrea Altomonte

[a] University of Naples Parthenope, Naples, Italy

[b] ENEA, Rome, Italy

Keywords: port decarbonisation, artificial intelligence, cargo traceability, driving assistance, hydrogen terminal tractors

Abstract

Introduction: Port decarbonisation requires both more efficient cargo movements and the deployment of lower-emission handling vehicles. Digital information and artificial intelligence (AI) can support this transition at complementary operating scales. AI-PORT combines onboard computer vision with georeferenced cargo records to support asset retrieval and future route optimisation. SPOTT equips a hydrogen-battery terminal tractor with perception-based driving assistance and deterministic vehicle supervision. Developed within RAISE Spoke 4, the two projects address operational visibility and assisted vehicle operation. This study presents their respective technical validation and identifies the evidence needed to assess their contribution to port decarbonisation.

Objectives: The objective was to verify the information chain required for cargo traceability and the perception-to-action chain required for assisted manoeuvres, while assessing the hydrogen-battery platform supporting SPOTT. Each project underwent a separate validation programme.

Materials and methods: AI-PORT used cameras, a Global Navigation Satellite System (GNSS) receiver, an inertial measurement unit and local processing on a vehicle-powered edge node. Optical character recognition (OCR) generated candidate identifiers that were associated with position and time, buffered locally and transmitted to a persistent backend. The dashboard supported identifier searches, last known position and movement histories. Laboratory checks and an operational field shift assessed acquisition continuity, communication recovery and retrieval [1,2]. PortRouteOptimizer was formulated using reinforcement learning and a deep Q-network, with field evaluation remaining prospective [1].

SPOTT combined perimeter ultrasonic sensing with front and rear radar. A perception controller qualified sensor data and generated risk states. The Bosch Rexroth BODAS RC27 vehicle control unit (VCU) arbitrated warnings, torque limitation and controlled braking using sensor diagnostics and vehicle-state interlocks. Validation included computer-aided design coverage studies, installation inspection, controlled acquisition, software-in-the-loop checks and hardware-in-the-loop (HIL) tests with the real VCU [3,4]. A representative duty cycle was also replayed on the dynamometer using the real fuel-cell source and high-voltage powertrain [4].

Results: During an approximately five-hour field shift, two AI-PORT acquisition units on one operational vehicle maintained continuous power and local logging. Automatic reconnection, persistent event storage and dashboard retrieval were verified. Dual viewpoints and preprocessing adjustments improved identifier readability qualitatively. Numerical OCR accuracy and operational route-planning benefits were not quantified [2].

SPOTT provided simultaneous range and echo-amplitude data from twelve ultrasonic channels and radar object lists containing position, relative velocity and diagnostic information. In HIL testing, a simulated obstacle trigger propagated through supervisory control and the RC27 commanded motor braking to a complete stop under the test condition. Duty Cycle 15 lasted 4 h 46 min 33 s, with 77.9 kWh electrical energy and 4.2 kg hydrogen consumption. These energy measurements provide supporting evidence for the host platform [4].

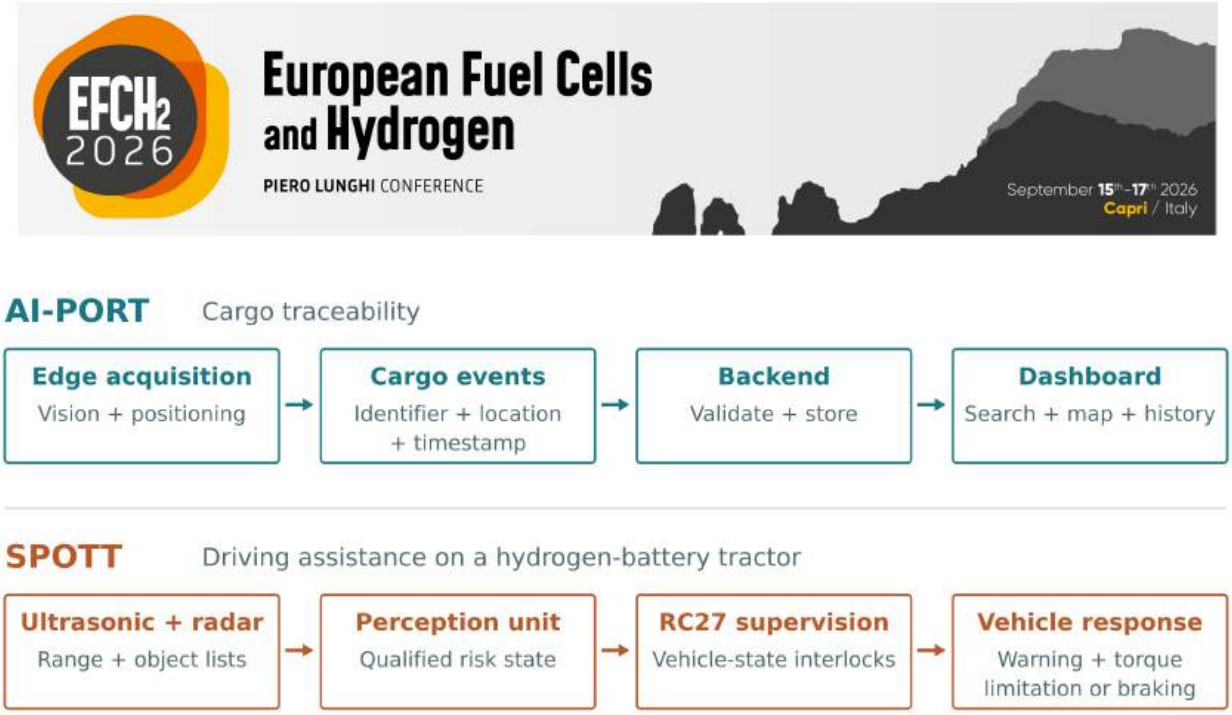


Figure 1. Complementary functional chains for AI-PORT and SPOTT. Cargo traceability and supervised driving assistance were assessed in separate validation programmes [1-4].

Conclusions: The results establish complementary technical capabilities for port decarbonisation: traceable cargo information and controlled driving assistance on a hydrogen-battery tractor. Route optimisation benefits and operational collision reduction remain unquantified, and SPOTT field deployment was pending authorisation. Future comparisons should use equivalent terminal missions, consistent service output and hydrogen-supply carbon intensity to determine whether these technical capabilities translate into lower energy consumption and emissions.

Acknowledgment: This work was carried out within the AI-PORT and SPOTT projects, RAISE Ecosystem, Spoke 4 - Smart and Sustainable Ports, ECS 00000035, CUP D33C22000970006.

References

[1] AI-PORT Project. D1: System architecture and methods.

[2] AI-PORT Project. D2: Testing and results.

[3] SPOTT Project. D1: Design and integration.

[4] SPOTT Project. D2: Controlled validation.

EFCH2 2026

European Fuel Cells and Hydrogen

PIERO LUNGHI CONFERENCE

CAPRI, GRAN HOTEL QUISISANA
15 > 17 September, 2026

ATENA FUTURE TECHNOLOGY

ENEA ITALIAN NATIONAL AGENCY FOR NEW TECHNOLOGIES, ENERGY AND SUSTAINABLE ECONOMIC DEVELOPMENT

Università degli Studi di Napoli Parthenope

CLEAN ENERGY INSTITUTE UNIVERSITY OF CALIFORNIA, IRVINE